BINARY GAS ADSORPTION IN MOLECULAR SIEVES

by

Mark Joseph Heslop, M. Eng. (Hons)

A Doctoral Thesis
Submitted in partial fulfilment of the requirements
for the award of
Doctor of Philosophy of the Loughborough University of Technology

July 1993

ABSTRACT

This thesis is concerned with the development of sorption-effect chromatography as a rapid method for the determination of binary gas-mixture adsorption isotherms. There are many alternative non-chromatographic methods but these have inherent disadvantages: the *direct experimental methods* require excessive equilibration times and the *predictive methods* require the respective pure-component isotherms and an ideal adsorbed phase. A computer simulation has shown that for an *alternative* chromatographic method, good results will only be obtained if both binary isotherms are close to linear.

Sorption-effect chromatography is characterised by the *flowrate retention time* (τ_N) which measures the change in column inventory when a perturbation is made to the system. Along with the standard composition retention time (τ_X), this extra measurement allows the gradient of each binary isotherm to be evaluated. Subsequent integration will give the respective mixture isotherm. Three gas systems (nitrogen-argon, nitrogen-helium and argon-helium) have been investigated over zeolite 5A at different temperatures. The results confirm that the adsorbed phase amounts decrease with increasing temperature and that there are degrees of component interaction.

Experimentally, thermal fluctuations in the oven will cause noise on the flowrate record making τ_N determination difficult. Isolation of the column from direct air flow was seen to reduce the noise level. Also, using a computer simulation model, the heat of adsorption for the above zeolite 5A systems will be easily dissipated preventing any unwanted gas temperature rises; the comparatively small column diameter was found to be a significant factor.

The employment of delay lines (empty tubes) in various locations has been investigated. To directly determine τ_N it is necessary to use delay lines downstream of the column. Also, the chromatographic method has been extended to determine mixture isotherms by considering the *change in average column pressure* rather than the motion of a composition front through the column. Delay lines situated upstream of the column are able to separate these two effects, and preliminary results are satisfactory. However, the use of delay lines anywhere in the system changes the measured retention times and the theory has to be adjusted to account for this.

ACKNOWLEDGEMENT

I would like to thank my supervisor Geoff Mason for his help and encouragement during my time in Loughborough, as well as the part-time employment which has enabled me to complete this thesis. I would also like to thank Bryan Buffham for many helpful suggestions. I am grateful to Paul Addison for his help on computing matters. I would like to acknowledge the financial assistance from the *Science and Engineering Research Council* in the form of a studentship. Finally. I would like to thank my mother for her patience and support during my time in Loughborough.

TABLE OF CONTENTS

LIST OF FIGURES

LIST OF TABLES

Chapter One

INTRODUCTION AND PRELIMINARY INVESTIGATION

1.1 Introduction

This chapter will start by showing how the process of *adsorption* has developed from its main application of gas purification to a larger application of gas adsorption. There are three principles upon which an adsorption separation can be achieved; the most important of these is equilibrium separation. Design of adsorption processes requires equilibrium mixture data. There are many ways of obtaining this data and this thesis is concerned with one such chromatographic method.

Then follows a section reviewing the development of this chromatographic method until the project commencement; this includes the experimental modifications as well as the theoretical advancements. At project commencement, a working apparatus was inherited and a series of experiments was carried out; the next section gives a review of these results. The latter two sections would not normally be contained in the introduction, but they help identify the aims of the thesis which are listed in the final section.

1.2 Development of Adsorption Processes

Over the years, adsorption has become an increasingly important process for *gas separation*. Previously, when the choice of adsorbent was limited, adsorption was mainly limited to *gas purification* where the amounts to be adsorbed are very small and have little or no value. Gas separation refers to the separation of mixtures into two or more valuable components. It has become a serious rival to distillation because of the latter's high energy requirement, especially when the components have similar boiling points. For distillation, the *ease of separation* is defined as the *relative volatility*. This quantity is dimensionless and the higher the quantity, the more feasible distillation would be. However, for values of the relative volatility below 1.2, distillation becomes undesirable; the efficiency becomes very low and the recycle requirements become excessive (Ruthven, 1984a).

For the distillation of two components, the relative volatility can be obtained from the classic *temperature-composition* diagram; this shows the temperature at which a particular liquid mixture composition will start to boil along with the equilibrium vapour composition. The ratio of the ratio of these compositions will give the relative volatility. Typically, there will be a variation in the relative volatility across the composition range due to the equilibrium temperature variation.

For adsorption, the ease of separation is defined as the *separation factor*. However, the separation factor is more complicated than the relative volatility because of three extra considerations. Firstly, separation can be based upon other factors apart from equilibrium; these will be discussed later. Secondly, the separation factor will vary between adsorbent types. The development of adsorption processes has been greatly aided by the introduction of new adsorbents such as zeolite and carbon molecular sieves. Finally, the system temperature and pressure can be specified independently. These quantities are seen to affect the *amounts* adsorbed as well as the separation factor. Often, adsorption processes are carried out at relatively low pressures because the corresponding low coverage leads to a higher separation factor. At higher pressures, which lead to multi-layer formation, the separation factor tends to that of distillation (Kaul, 1984).

Similar to distillation, a high separation factor is required to make an adsorption process feasible. However, although high separation factors are desirable for both adsorption and distillation processes, it is not correct to compare values of separation factor and relative volatility; they are different quantities. That is, if two processes have numerically the same value of separation factor and relative volatility, it does not mean that the processes have equal feasibility. The reason for this is the fundamental difference between adsorption and distillation processes. In a distillation column, at any time separation of the mixture is occurring everywhere (on every plate) in the column. However, in an adsorption column, at any time separation is only occurring at the front where the equilibrium composition is being disturbed. Upstream and downstream of the front, the mixture compositions are not changing with time.

1.3 Classification of Adsorption Processes

1.3.1 Introduction

The previous section showed the fundamental differences between adsorption and distillation equilibrium. With regard to the actual industrial processes, a distillation column will operate at steady-state; everywhere in the column, the temperature and both phase concentrations will not vary with time. However, this is not usually the case for adsorption processes. It is possible to have an adsorption process operating at steady state, although these processes are more commonly characterised by column composition changes with time; that is the motion of concentration fronts through the column. Adsorption processes can be divided into three categories, and these will now be discussed in turn. The following Sections 1.3.2 to 1.3.4 are summarised from Chapters 10, 11 and 12 of the book by Ruthven (1984). In each of the chapters, the process characteristics are described and examples are given of industrial applications.

1.3.2 Chromatographic Separation Processes

As the name suggests, this category is restricted to processes in which the solid phase is contained in a packed column and the mixture to be separated is introduced as a pulse into the carrier. As for an analytical chromatograph, it is necessary that each component pulse will emerge from the column at different times. The column effluent is directed alternately to particular receivers where the products are separated and the carrier is then recycled to the inlet. When the process is scaled up from the analytical scale to the industrial scale, it is termed *preparative scale chromatography*.

1.3.3 Cyclic Batch Systems

This is the most common category and it is basically characterised by an adsorbent bed being alternately saturated (adsorption) and regenerated (desorption) in a cyclic manner. Often, many of these units will be operating at different stages so that the products appear to be produced continuously. These processes differ from each other mainly in the method by which the adsorbent is regenerated during the desorption cycle. The two main categories are *thermal swing adsorption* (TSA) and *pressure swing adsorption* (PSA). In the former, the bed is regenerated by heating with a stream of hot carrier gas. In the latter, desorption is effected by reducing the pressure at constant temperature.

1.3.4 Continuous Countercurrent Systems

This is the only steady-state category, and it involves operating the process with an adsorber unit and a regenerator unit. An extra design complication is that the *adsorbent* needs to be circulated. It is particularly useful for applications in which the selectivity is low or the mass transfer rates are slow; countercurrent contact maximises the driving force for mass transfer.

1.4 Classification of Adsorption Separations

1.4.1 Introduction

As has already been discussed, distillation processes depend upon an equilibrium separation. For adsorption processes, the majority of cases also depend upon an equilibrium separation. However, adsorption processes can also achieve separation by two extra principles; *kinetic separation* and *steric separation*. Examples are given in Chapter 11 of the book by Ruthven (1984). All three of these cases will now be discussed in turn:

1.4.1 Kinetic Separations

By definition, equilibrium data will give no indication of the time taken to reach this state. Indeed, feasibility for an equilibrium process should include the pre-requisite that experimental times are not prohibitive. This brings in the question of mass-transfer rates, which are discussed in Chapter Two. Summarising, if the ratio of component mass-transfer rates is very high, for a range of experimental times, one component will travel through to the active sites preferentially and a separation will be achieved. Of course, if the experimental time is large enough, the slower component will catch up and the adsorbate composition will approach the equilibrium value. Industrial applications include the separation of air by carbon molecular sieves (Nandi and Walker, 1976) and the separation of air to obtain inert gases using 4A zeolite. (Kapoor and Yang, 1989).

1.4.2 Steric Separation

Adsorbents used in industrial separation are *microporous*, that is to say most of the active sites (most of the surface area) are within the solid on the inside of the micropores. In older adsorbents such as activated carbon and silica gel, there is a wide distribution of pore diameter. However, zeolite and carbon molecular sieves have a regular three dimensional pore network which has effectively a zero spread in the pore size distribution; only one or two pore sizes. If an adsorbent can be chosen which only allows one component to enter the network, then a *perfect separation* can be achieved. Industrial separations are rare and include the separation of linear paraffins over 5A zeolite. Of course, the excluded molecules will still have access to the active sites on the exposed surface but these form only a small proportion of the total sites. This type of separation can be thought of as an extreme case of a kinetic separation with one component having a zero mass-transfer rate.

1.4.3 Equilibrium Separation

This is by far the most common separation and has found many industrial applications; air separation is achieved using both 5A and 13X zeolites. However, this type of equilibrium is not totally analogous to that of distillation because the phase diagram will not totally define the system; the amounts adsorbed of each component must also be considered. This brings in the new term of *adsorbent capacity*. Because of the inadequacy of the phase diagram, the absolute way of representing this equilibrium data is by showing the *isotherms*. For just one component, these are termed single/pure component and are conveniently represented by a graph of amount adsorbed against gas concentration or gas pressure. Figure 1.1 shows a typical example of one such isotherm. This type of equilibrium can easily be obtained by the conventional *gravimetric* and *volumetric* methods. These are described in more detail in Chapter Two. Indeed, pure-component data is well tabulated for many systems.

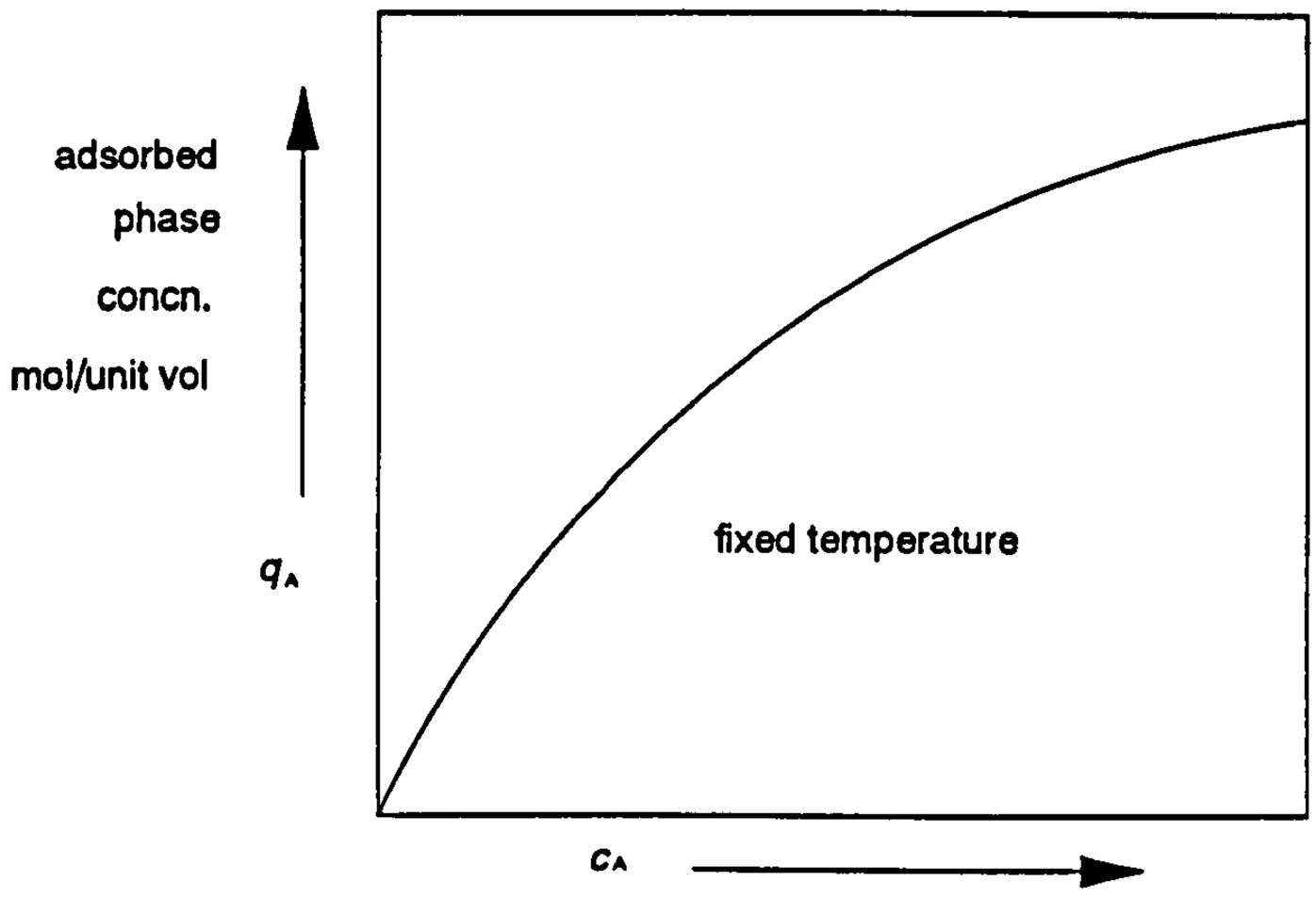

Figure 1.1 General Representation of a Pure-Component Isotherm

For the general multi-component case, a simple graphical representation is not possible because of the many possibilities for gas phase composition; a complete representation would require many tabulations. However, this situation is considerably simplified for two components since both gas phase mole fractions must sum to one. The general representation for a binary system is shown in Figure 1.2.

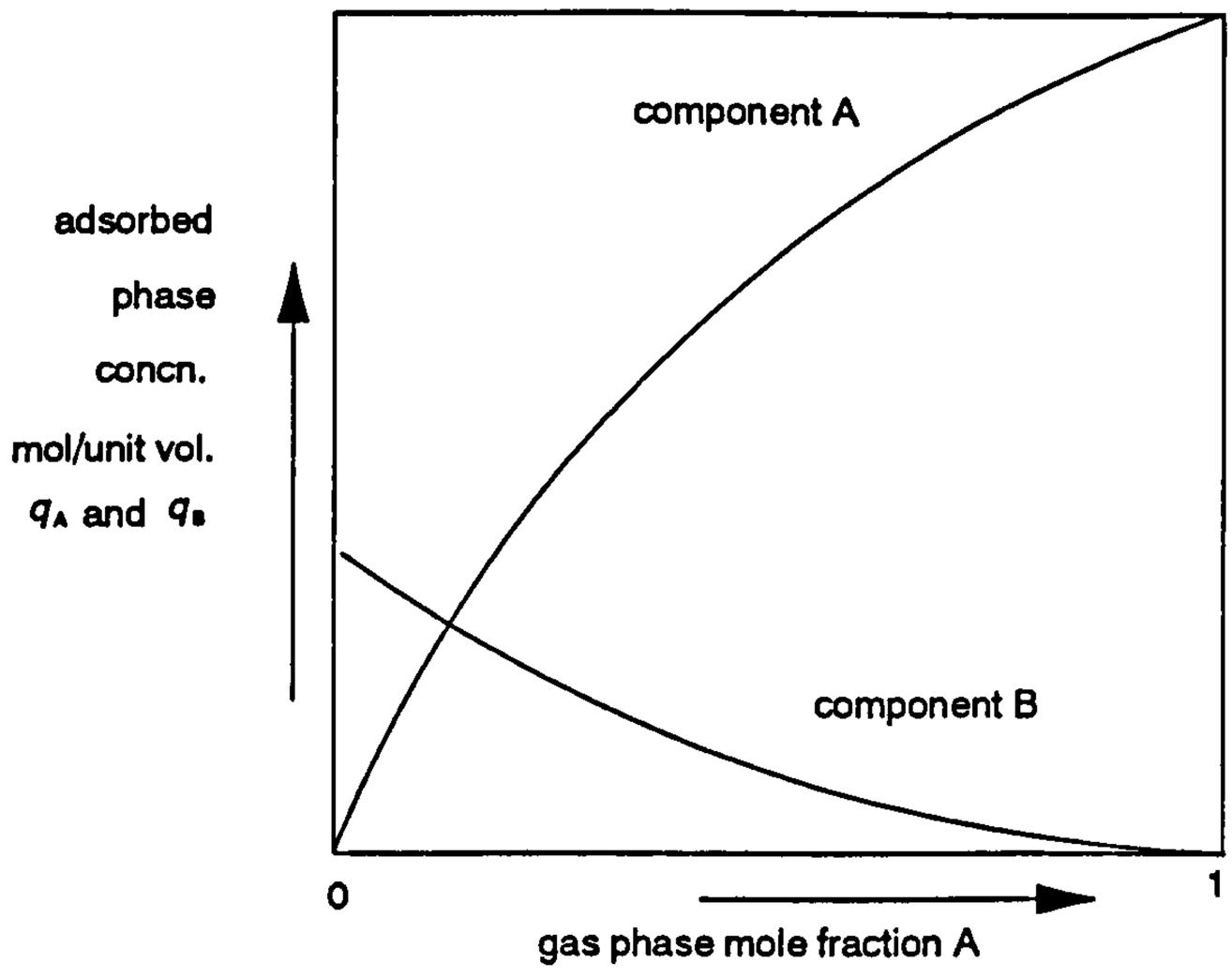

Figure 1.2 General Representation of a Binary System

From this representation, the *total capacity* representation can be obtained by simply adding together the individual component amounts adsorbed. The phase diagram can be obtained by using these amounts to obtain the adsorbed phase compositions and from these compositions an *equilibrium selectivity* graph can be obtained by the following equations:

$$x_A = \frac{q_A}{q_A + q_B} \qquad 1.1$$

$$Y_A = \frac{c_A}{c_A + c_B} \qquad 1.2$$

$$S_{AB} = \frac{\left(\frac{x_A}{Y_A}\right)}{\left(\frac{x_B}{Y_B}\right)} \qquad 1.3$$

where c_A, c_B = individual component gas concentrations

q_A, q_B = individual adsorbed phase concentrations

x_A, x_B = the adsorbed phase mole fractions

Y_A, Y_B = the gas phase mole fractions

S_{AB} = selectivity of component A compared to component B

The phase diagram and selectivity graph are particularly useful since they will indicate the presence of any azeotrope; this is characterised by a selectivity of one and is very undesirable for process design. Thus, adsorbents should be chosen or process conditions employed to avoid this phenomenon. Figure 1.3 shows a typical phase diagram and Figure 1.4 shows an example of a selectivity graph.

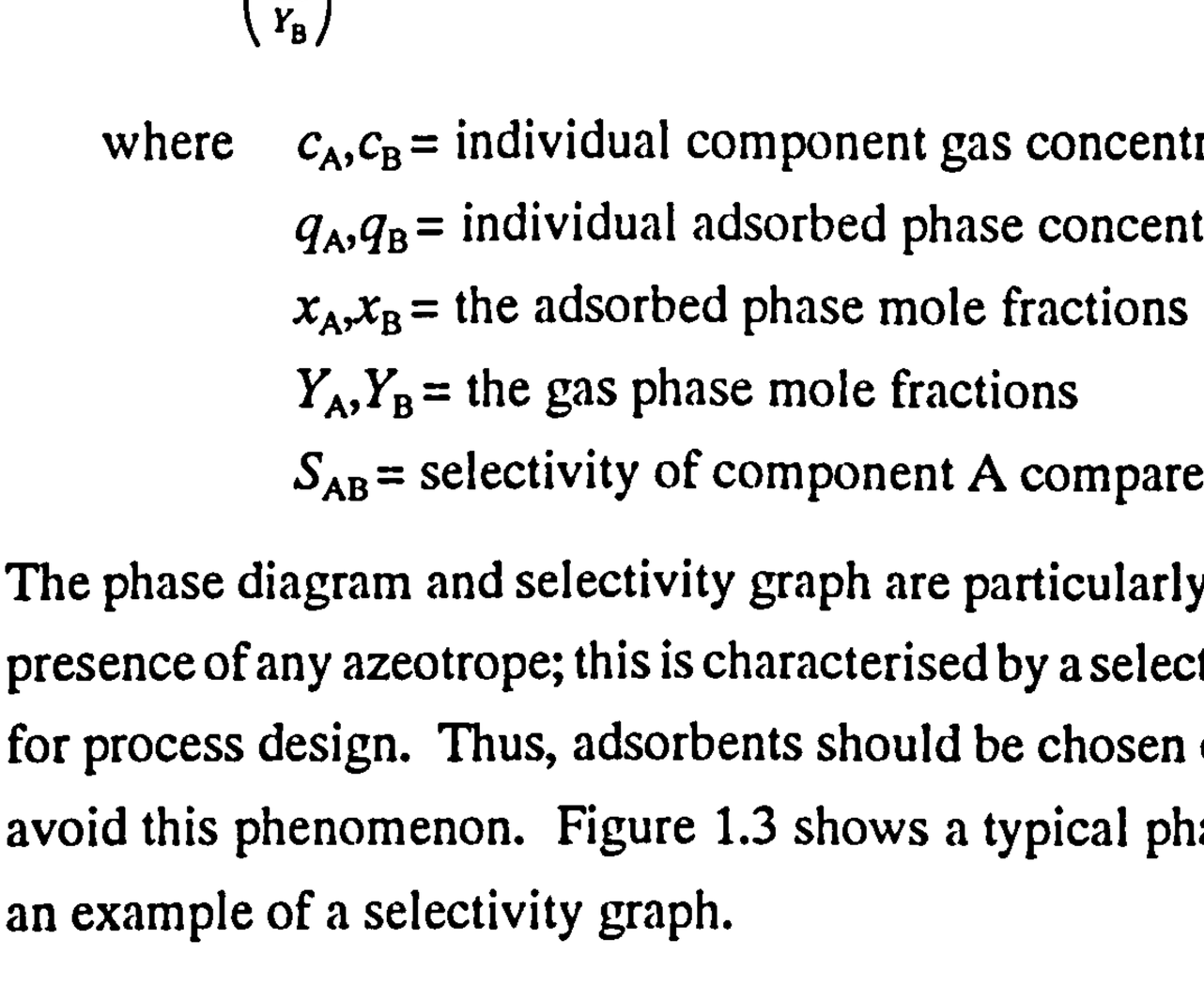

Figure 1.3 Schematic Representation of Phase Diagram

The phase diagram looks similar to that for distillation except that for distillation the equilibrium temperature is not fixed and will vary along the phase diagram.

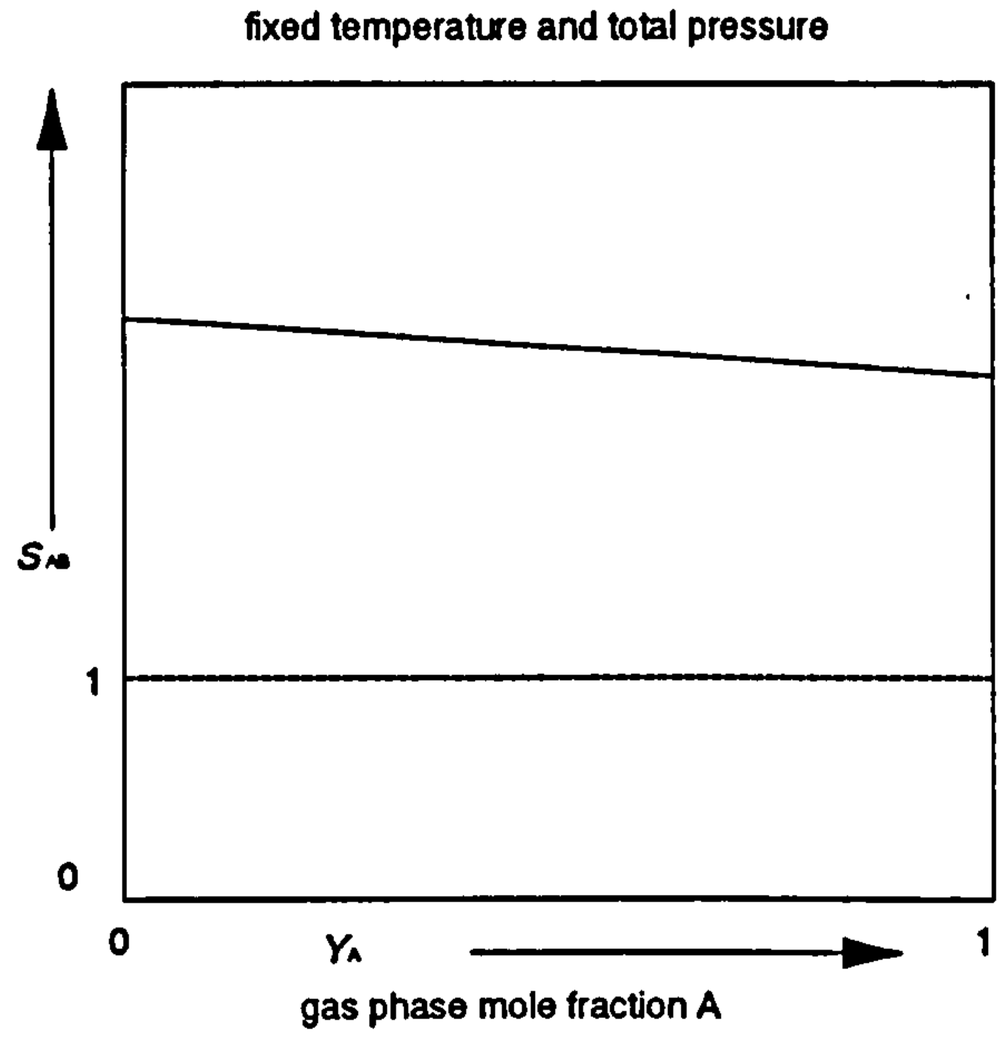

Figure 1.4 Schematic Representation of Selectivity Chart

1.5 Determination of Equilibrium Mixture Data

To investigate a particular separation, there are many possible combinations considering the choice of adsorbent, operating pressure and operating temperature. Thus, a full investigation requires a huge number of data points to be measured. There are many ways of obtaining this equilibrium data and a critical review is contained in Chapter Two. An alternative is to predict the mixture equilibrium data from pure-component data. Summarising, there are two main categories; *predictive* and *chromatographic.*

The former is by far the most popular and basically involves predicting mixture data from pure-component isotherms using a particular theory. The most popular of these is the Ideal Adsorbed Solution Theory (IAST) proposed by Myers and Prausnitz (1965). The success of these theories is mixed, but this has been increased by including the use of a limited amount of binary mixture data; hence the method becomes *predictive/correlative.* Chromatographic methods are especially useful since they are quick and do not suffer from the problem of heat effects. One method is the *tracer-pulse method,* extended by Danner (1980, 1985). However, this requires isotopes for each component and this can be expensive, if indeed isotopes can be found for each component. The other main method is the *polynomial-fitting method* proposed by Van der Vlist and Van der Meidjen (1973). This requires a particular function of the mixture composition retention times to be fitted to a polynomial. In Chapter Nine, a rigorous analysis of this method is carried out and it concludes that the method is only suitable for particular systems. Moreover, the method

requires independently obtained selected pure-component data. It can be seen that there is much need for an improved chromatographic method, and it is the purpose of this project to help develop it.

1.6 Previous Development of Project Method

1.6.1 Introduction and Basic Principles

Previous chromatographic methods have been only concerned with measuring the *composition retention time* (τ_x), the *normal* chromatographic measurement which utilises a composition detector such as a katharometer. This detects composition fronts by detecting the change in thermal conductivity with composition. This caused a problem for previous workers since they were trying to evaluate the slopes of two unknown mixture isotherms using only one measurement. This problem was overcome by Buffham (1973, 1978), who proposed measuring the flowrate variation as well as the composition variation. This was practically achieved by Buffham, Mason and Yadav (1985) who measured the *flowrate retention time* (τ_N). This extra measurement forms the basis of the results reported in this thesis.

The flowrate meter was simply constructed from two matched pieces of capillary tubing, with a pressure transducer upstream; by the Hagen-Poissieulle equation flowrate variation can be detected as pressure variation. The adsorbent under examination is packed as two identical columns, one for each side of the system and both are placed in an oven at the temperature of investigation. A binary gas-mixing system provided the required gas mixture and this flows through the whole system. After equilibrium has been achieved, a small perturbation is made to the system and the resulting composition and flowrate transients are recorded on the chart-recorder. These two retention times can be obtained from the respective transients. The remainder of Section 1.6 will comprise a review of the theory, apparatus and results during project development.

1.6.2 Paper of Buffham, Mason and Yadav (1985)

component gas cylinders

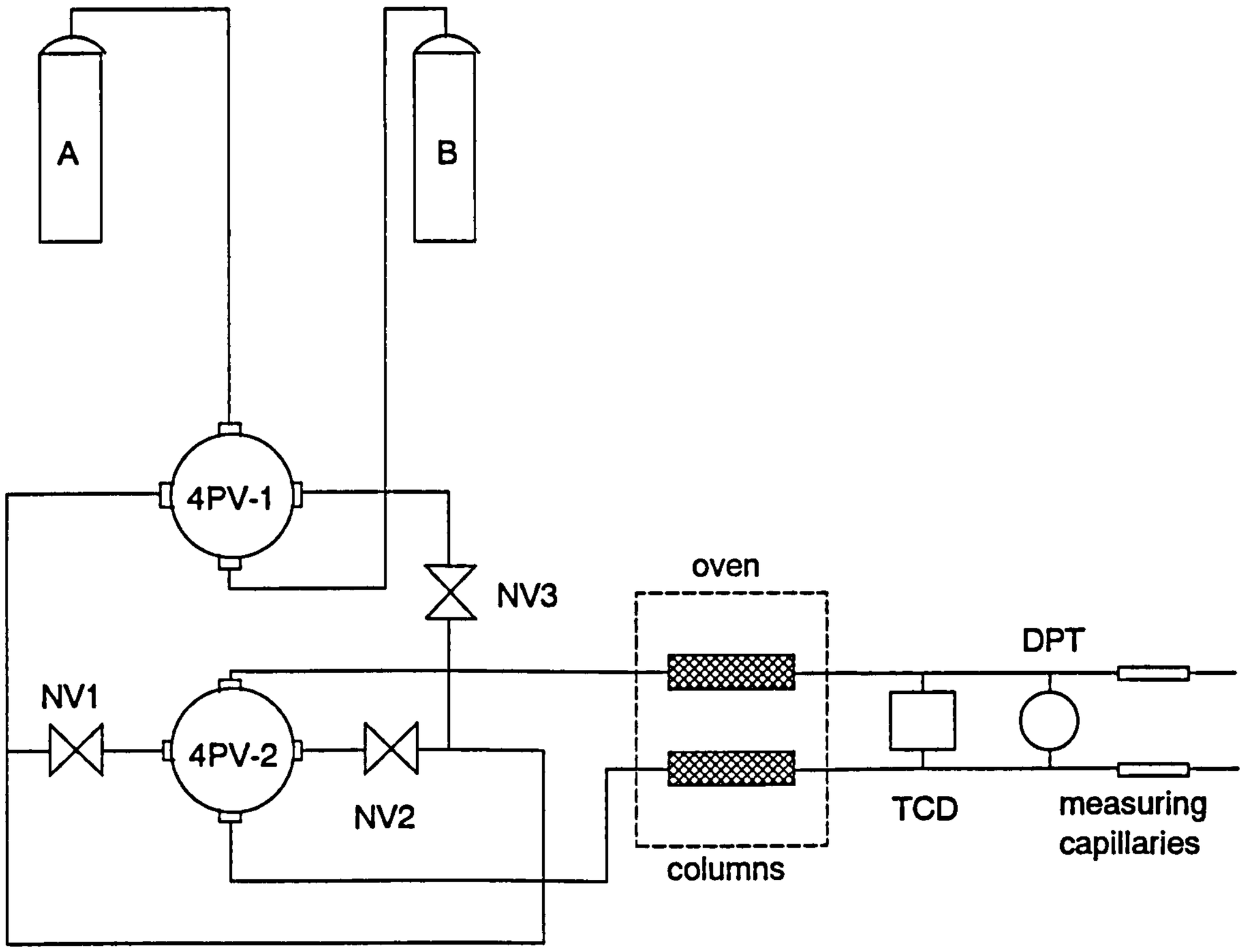

TCD = thermal conductivity detector
DPT = differential pressure transducer

Figure 1.5 Schematic Representation of Apparatus

The carrier gas flowrates were set mainly by the high resistances obtained with the needle valves NV1 and NV2. The valve 4PV-1 allows the carrier gas and the perturbation gas to be selected. According to the diagram, one component will be the carrier gas and the other will be the perturbation gas; it is not possible for both carrier and perturbation gases to be the same component. The perturbation gas flowrate is adjusted by the valve NV3 to be about 1% of each column flowrate. The perturbation was achieved by the valve 4PV-2 which switches the carrier flows between columns. Although the molar flowrates are the same in each column, the compositions are slightly different because of the perturbation gas addition. The idea of employing two columns was to obtain double the deviation; upon switching valve 4PV-2, the gas composition was changing in both columns. Thus the system

was measuring the cumulative effect of two transients; the composition was increasing in one column and decreasing in the other. The equations used to obtain the binary gradients were:

$$\frac{dq_A}{dc_A} = \frac{\tau_X + Y_A\tau_N - \frac{\varepsilon V_C}{Q_{CAV}}}{\frac{(1-\varepsilon)V_C}{Q_{CAV}}} \qquad 1.4$$

$$\frac{dq_B}{dc_B} = \frac{\tau_X - Y_B\tau_N - \frac{\varepsilon V_C}{Q_{CAV}}}{\frac{(1-\varepsilon)V_C}{Q_{CAV}}} \qquad 1.5$$

where τ_X = composition retention time

τ_N = flowrate retention time

ε = column voidage

V_C = column volume

Q_{CAV} = average column volumetric flowrate

dq_A/dc_A = dimensionless gradient of component A isotherm

dq_B/dc_B = dimensionless gradient of component B isotherm

Because of the manner in which the experiments were conducted, the chart-recorder required calibration before the flowrate retention time could be obtained. The authors investigated the system argon-nitrogen-zeolite 5A system at 313 K. There was a lot of *noise* on the flowrate record and there were blips obtained when the columns were switched. Results were presented for the two end-points of each component isotherm; not just the Henry positions. Thus they used mixtures of roughly 99% argon and 99% nitrogen. The gradients were approximately the same as those obtained by Ruthven and Kumar (1980) and confirmed the approximate linearity of both mixture isotherms; Ruthven and Kumar (1980) carried out their investigations at different temperatures and so the results are not directly comparable.

1.6.3 SERC Report by Buffham (1986)

From the findings of some undergraduate projects, many experimental modifications were made. The first set concerned the flowrate record quality and the undesirable noise which sometimes made retention time determination difficult. There were found to be two causes for these fluctuations; room pressure variations and oven temperature variations. Firstly, pressure fluctuations can be caused by the weather (on a stormy day) and opening doors. These fluctuations did not cancel out because it was found difficult to perfectly match all the components. The remedy was to combine the two outlet streams and feed them to atmosphere via a back pressure regulator. This regulator was set to a small back pressure such as 0.1 bar. Temperature fluctuations within the chromatograph were found to cause random adsorption and desorption in the columns, and hence random noise. This problem was particularly bad for nitrogen carrier gas because of its higher extent of adsorption. This problem was reduced by reducing the fan speed and insulating the columns from direct air flow.

The final experimental modification concerned the way in which the perturbation was made. Instead of switching carrier flows between columns, a small flow of pure component was switched between columns. This enabled either of two pure components to be used and so doubled the number of measurements which could be made. For this modification, a five-port valve was employed. The cause of the previous blips was found to be a pressure imbalance upstream of both columns, and so extra trimming valves were added to remedy this problem. Finally, long pieces of capillary tubing were used to provide the main flow resistance as these were found to have a more constant resistance than needle valves

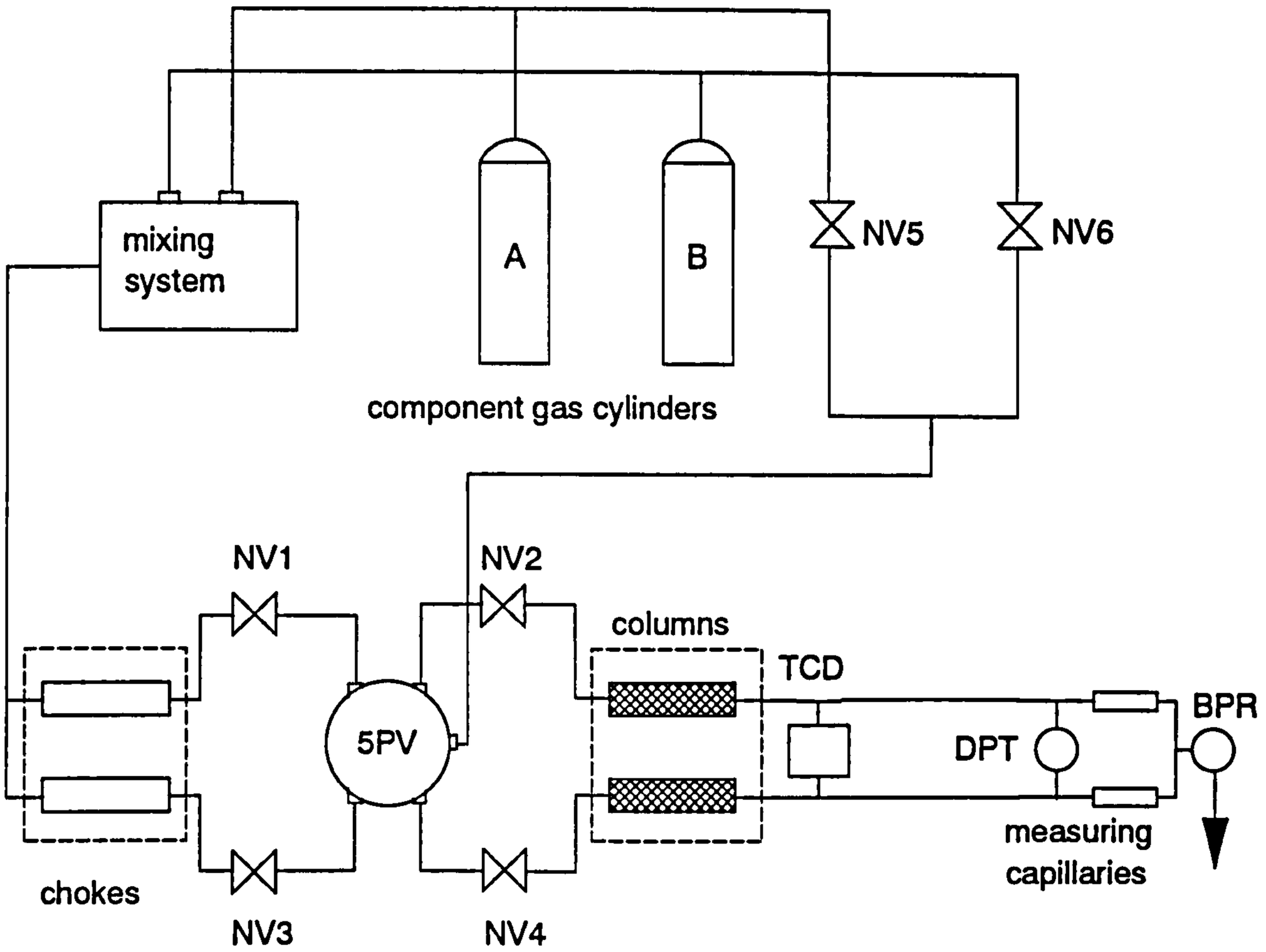

BPR = back pressure regulator
TCD = thermal conductivity detector
DPT = differential pressure transducer
NV = needle valves

Figure 1.6 Schematic Representation of Apparatus

The theoretical developments were very significant and this summary is taken from an unpublished paper by Mason and Buffham. Firstly, consider an adsorption column of volume V_C and voidage ε subjected to a change in gaseous concentration δc_i such that the adsorbed phase concentration changes by δq_i. The resulting change in the total amount of species i is the change in *hold-up*, δH_i. A molar balance on any component gives:

$$\Delta H_i = \varepsilon V_C \delta c_i + (1-\varepsilon) V_C \delta q_i \qquad 1.6$$

$$\frac{\delta q_i}{\delta c_i} = \frac{\frac{\Delta H_i}{\delta c_i} - \varepsilon V_C}{(1-\varepsilon) V_C} \qquad 1.7$$

Thus in order to obtain the required mixture isotherm gradient it is necessary to evaluate the change in hold-up with concentration. This analysis is started by considering the addition

of a perturbation of molar flowrate n and composition Y_{iT} to a carrier of composition Y_{iO}. The change in hold-up is the difference between what goes in and what goes out. This leads to the important equation:

$$\Delta H_i = M \int_0^\infty (x_i(\infty) - x_i(t))dt + Y_{iO} \int_0^\infty (n(\infty) - n(t))dt \qquad 1.8$$

These integrands can be obtained from the composition and flowrate records respectively. This is a general equation and will hold for all conditions. At first it was assumed that the change in concentration was caused solely by the change in composition and this allowed Equation 1.8 to be developed by substitution:

$$\frac{\Delta H_i}{\delta c_i} = Q_{CAV}\left[\int_o^\infty \frac{x_i(\infty) - x_i(t)}{x_i(\infty) - x_i(0)}dt + \frac{Y_{iO}}{Y_{iT} - Y_{iO}} \int_0^\infty \frac{n(\infty) - n(t)}{n(\infty) - n(0)}dt\right] \qquad 1.9$$

The first and second integrals are defined as the composition and flowrate retention times respectively (τ_N and τ_X). By the above definition, these can be obtained by dividing the respective areas by the respective offsets. Thus a major development is the non-requirement of chart-recorder calibration.

When this equation was applied to an argon-nitrogen system, it was found that agreement for the holdup gradients calculated for each perturbation gas was poor for each component at a specific location. Because the error was systematic, it was assumed that Equation 1.9 required modification. It was decided that as the perturbation flow was added, the mean column pressure was being increased and so this would further increase the component concentration. Furthermore, any change in the mixture viscosity would further increase the mean column pressure. The end result was that Equation 1.9 was re-written but with a correction factor:

$$\frac{\Delta H_i}{\delta c_i} = \frac{Q_{CAV}}{F_{PVCi}}\left[\tau_X + \frac{Y_{iO}}{Y_{iT} - Y_{iO}}\tau_N\right] \qquad 1.10$$

$$F_{PVCi} = 1 + \frac{Y_{iO}}{Y_{iT} - Y_{iO}}\left[\frac{1 + \frac{\Delta P_C}{3P_{COUT}}}{1 + \frac{\Delta P_C}{2P_{COUT}}}\right]\frac{\Delta P_C}{2P_{COUT}}(1 + B(\mu)) \qquad 1.11$$

where ΔP_C = column pressure drop

P_{COUT} = absolute outlet column pressure

F_{PVCi} = column correction factor

$B(\mu)$ = system mixture viscosity factor

The term Q_{CAV} is not directly measurable because it is the average column volumetric flowrate. However, it is easier to measure the volumetric flowrate at ambient conditions, Q_M, and use the following equation to relate these flowrates since the molar flowrate everywhere is constant. The factor of 120 arises because the carrier flowrate is measured for both columns in ml per minute whereas the average column flowrate is required in ml per sec for only one column.

$$\frac{P_{AT}Q_M}{T_{AM}} = \frac{120P_{CAV}Q_{AV}}{T_C} \qquad 1.12$$

where P_{AT} = atmospheric pressure
P_{CAV} = average column pressure
T_{AM} = ambient temperature
T_C = column temperature

From the above equations, the flowrate retention time is required to calculate the isotherm holdup gradients. However, from the Hagen-Poissieulle equation, any change in gas mixture viscosity caused by the change in gas mixture composition will obscure the true flowrate variation. Essentially, the *pressure retention time* (τ_p) is obtained from the flowmeter. An equation was derived to try and account for this problem and it was proposed that the introduction of delay line tubing between the columns and the flowmeter would enable direct determination of the flowrate retention time; this is further investigated in Chapter Four. Using these pressure and viscosity correction terms, the agreement for each set of gradients was seen to greatly improve.

1.6.4 Paper by Mason and Buffham (1989)

For this paper, the system studied was the same as that previous. The equipment is very similar in that the perturbation gas was switched from one column to the other, although mass-flow controllers were used to regulate the flowrate and tracer cut-off valves were situated just upstream of the switching valve. It was further demonstrated that the pressure correction gave good agreement between the results for each perturbation gas. Subsequent integration showed the nitrogen isotherm to be slightly curved and the argon isotherm to be virtually straight.

1.7 Preliminary Investigation of Argon-Nitrogen-5A System

1.7.1 Introduction

This section will show how binary mixture isotherms for the argon-nitrogen-zeolite 5A system at 50°C are obtained using the chromatographic method. It is termed preliminary because these were the first results obtained with essentially the inherited apparatus, albeit with two experimental modifications. The columns are of length 150 cm and inside diameter 0.4 cm and are packed each with 14.5g of 22-30 mesh molecular sieve 5A. In this thesis, these column specifications will be referred to as standard.

1.7.2 Experimental Modifications

The major modification to the apparatus described in Section 1.6.3 was that lengths of delay line tubing were inserted between each column and its respective flow measuring capillary; these are termed *downstream delay lines*. From the theory development, these should enable the flowrate retention time to be obtained directly from the chart recorder transient. The minor modification concerns the way that the perturbation gas is selected; previously both perturbation gases were combined and the outlet fed into the five-port valve. The required perturbation gas was selected by closing the other component needle valve. However, this arrangement will cause lengths of tubing to contain stagnant gas; this is termed *dead-volume*. It is better to have these lines flushed out with the selected perturbation gas. To remedy this problem, the line containing the required perturbation gas was connected directly into the five-port valve.

1.7.3 Evaluation of Isotherm Holdup Gradients

Both nitrogen and argon perturbation gases were employed and these flowrates were set to be about 1% of the column flowrate. Table 1.1 shows the measured and adjusted volumetric flowrates. The required values of volumetric flowrate are obtained using Equation 1.12 and the following temperatures and pressures:

$T_{AM} = 293$ K

$T_C = 323$ K

$P_{AT} = 760$ mm Hg

$P_{CAV} = 860$ mm Hg

Table 1.2 gives a summary of all the relevant measurements taken from the chart-recorder. Both retention times are calculated by dividing the appropriate area by the appropriate offset, and the viscosity factor is calculated by simply dividing the two offsets on the flowrate chromatogram when downstream delay lines are employed.

Table 1.1 Calculated and Adjusted Carrier Flowrates

% N_2	$Q_{M/(ml/min)}$	$Q_{CAV/(ml/s)}$
0	35.5	0.287
5	36.4	0.294
10	36.9	0.298
20	37.3	0.301
35	38.6	0.312
50	39.9	0.322
60	41.3	0.334
80	42.9	0.347
90	44.5	0.360
95	44.7	0.361
100	46.4	0.375

Table 1.2 Summary of Chart Recorder Measurements

	nitrogen prtbn			argon prtbn		
% N_2	τ_X/s	τ_N/s	$B(\mu)$	τ_X/s	τ_N/s	$B(\mu)$
0	277	143	-0.2	-	-	0
5	261	131	-0.2	264	-1.3	0.02
10	252	130	-0.18	255	-8.3	0.02
20	231	111	-0.17	234	-17.8	0.05
35	204	82	-0.14	201	-34.5	0.08
50	177	60	-0.13	177	-46.4	0.12
60	162	45	-0.11	162	-53.9	0.15
80	135	29	-0.07	135	-71.3	0.22
90	114	16	-0.03	119	-74.8	0.26
95	111	9.8	-0.02	113	-79.2	0.29
100	-	-	0	105	-80.5	0.33

Figure 1.7 shows the chromatograms obtained for switching a nitrogen perturbation flow between two 95% argon carriers. The top chromatogram is the composition record and the bottom one is the flowrate record. The flowrate record is relatively complicated because it records *any* change in the column flowrate. Before the perturbation flow is switched, the baseline position corresponds to $n(0)$. When the perturbation flow is switched, the column flowrate increases steadily until the composition front reaches the column. Because the perturbation gas is the more highly adsorbed nitrogen, the flowrate is reduced as the front passes through the column; this corresponds to net adsorption in the column. When the front leaves the column, it passes through the downstream delay lines and the plateau baseline increases (because there is no more net adsorption) to a level corresponding to $n(\infty)$. The difference in these baseline positions $n(\infty)$-$n(0)$ is proportional to the perturbation flowrate. Finally, as the composition front passes through the measuring capillaries, the *change in viscosity* caused by the perturbation gas causes a change in the baseline position to $p(\infty)$. According to the theory which is described in Chapter Four, the viscosity factor $B(\mu)$ can be directly obtained by measurement of the two relevant offsets:

$$B(\mu) = \frac{p(\infty) - n(\infty)}{n(\infty) - n(0)} = -\frac{1.4}{7} = -0.2$$

According to Equation 1.9, τ_N can be directly obtained by dividing an area by an offset. From the definition of the integral term, this will be the area bounded by the dotted line and the flowrate chromatogram; it will be termed I_N for convenience. When this area is divided by the offset a distance will be obtained. For this distance to be converted to a retention time, the chart recorder speed is required. For a chart recorder speed of 2 cm per minute, this is equivalent to 30 seconds per cm

$$I_N = \int_0^\infty n(\infty) - n(t)dt = 31\text{cm}^2$$

$$\tau_N = \frac{I_N}{n(\infty) - n(0)}\left(\frac{30\text{second}}{\text{cm}}\right) = 131\text{seconds}$$

The composition record is relatively simple because it only deviates when the composition of the gas in the katharometer is changing. It might be expected that there should only be one deviation in the composition record, corresponding to the composition front leaving the column. According to Equation 1.9, τ_X can be directly obtained dividing an area by an offset. From the definition of the integral term, the required area will be bordered by the dotted line and the composition record; it will be termed I_X for convenience.

$$I_X = \int_o^\infty x(\infty) - x(t)dt = 39\text{cm}^2$$

$$\tau_X = \frac{I_X}{x(\infty) - x(0)}\left(\frac{30\text{second}}{\text{cm}}\right) = 261\text{seconds}$$

Figure 1.8 shows the chromatograms obtained for switching an argon perturbation flow between two 90% argon carriers. The top chromatogram is the flowrate record and the bottom one is the composition record. Once again, the composition record is of a relatively simple shape because the only deviation occurs when the composition front leaves the column. When the perturbation gas is switched, the column flowrate steadily increases until the front reaches the column. Because the perturbation gas is the least adsorbed argon, the column flowrate is increased as the front passes through the column; this corresponds to net desorption in the column. When the front leaves the column, because there is no more net desorption, the flowrate record moves back to the $n(\infty)$ position. As the front passes through the measuring capillaries, the shift to position $p(\infty)$ is smaller than for Figure 1.7 and it is in the opposite direction. From the flowrate chromatogram, there are two distinct areas to consider when calculating τ_N. From the integral definition, one area will be positive and the other will be negative.

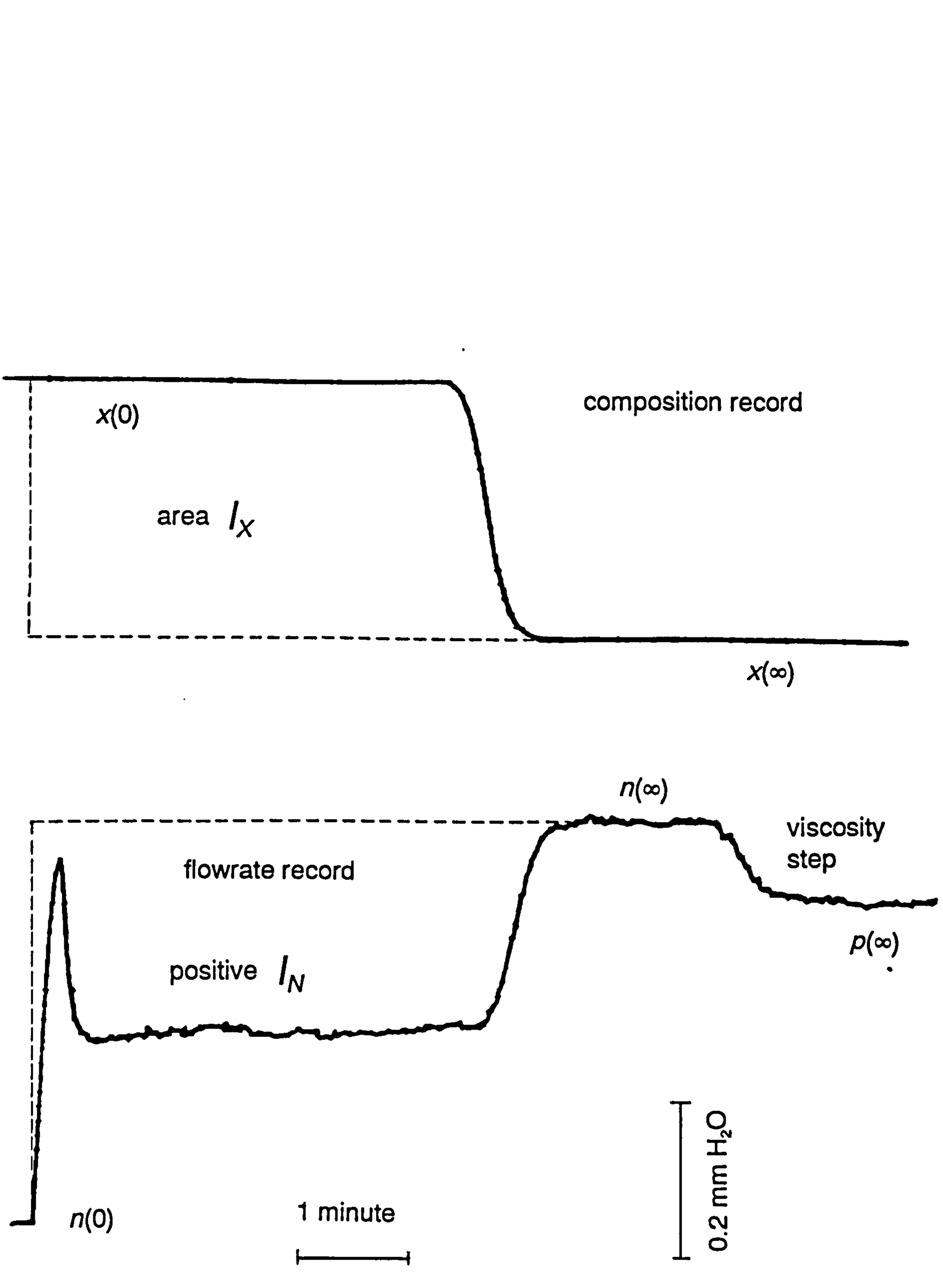

Figure 1.7 Chromatograms for Switching Nitrogen Perturbation Gas Between 95% Argon Carriers at 50°C

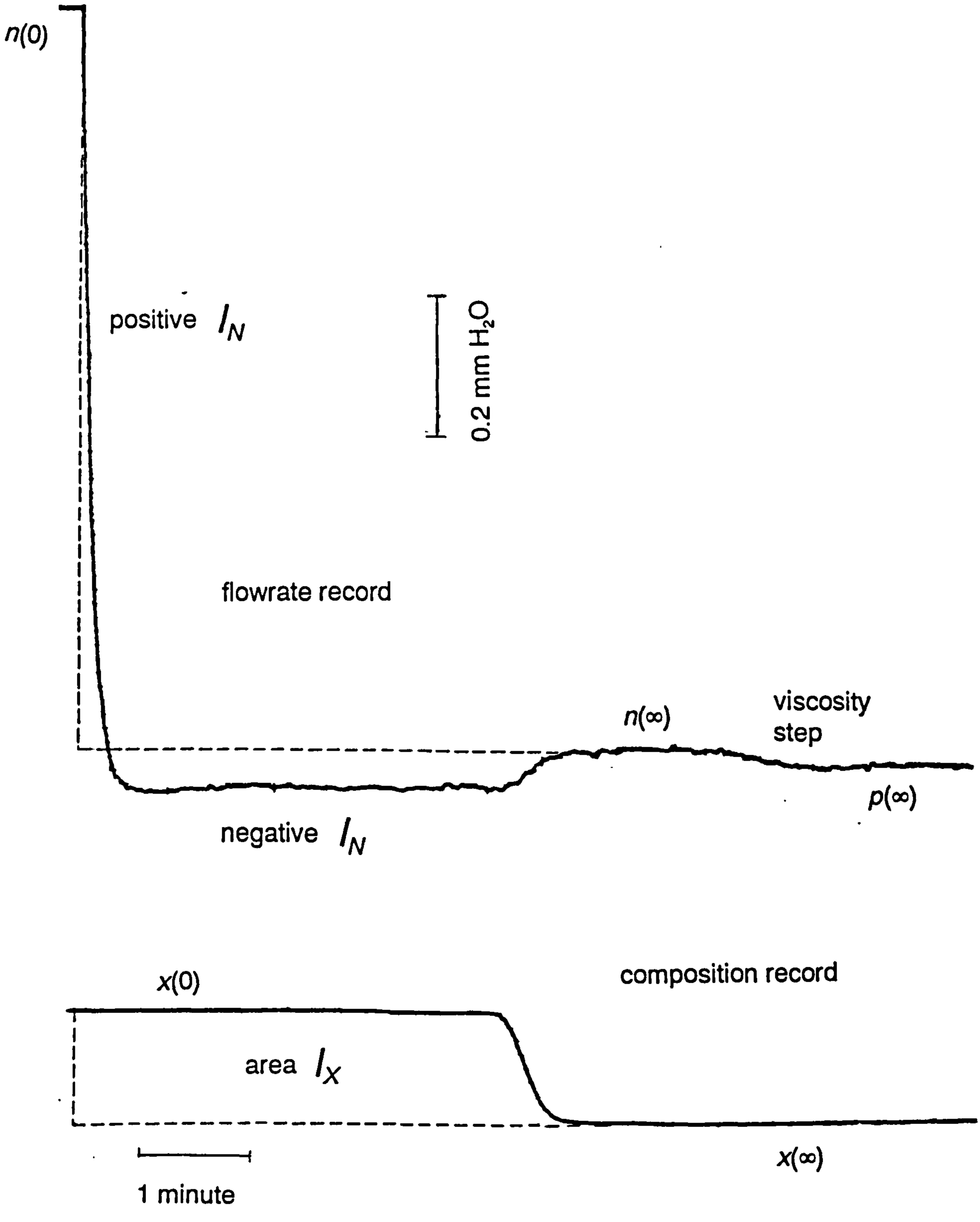

Figure 1.8 Chromatograms for Switching Argon Perturbation Gas Between 90% Argon Carriers at 50°C

It can be seen that the composition retention times are roughly similar for each perturbation gas employed. The flowrate retention times are of different signs since adding a nitrogen perturbation causes net adsorption and an argon perturbation causes net desorption. Firstly, these retention times are processed in the standard way without any correction factors. The isotherm holdup gradients are calculated using Equations 1.10 and 1.12. The results are contained in Table 1.2. For convenience, the holdup derivatives are represented by the symbol G under the respective component heading, with the respective perturbation component as a subscript.

Table 1.3 Calculations of Isotherm Holdups with No Correction Factors

	nitrogen isotherm			argon isotherm		
% N_2	G_{N2p}/ml	G_{Arp}/ml	ΔG/ml	G_{N2p}/ml	G_{Arp}/ml	ΔG/ml
0	78.1	-	-	37.9	-	-
5	78.7	78.0	0.7	38.3	70.3	-32
10	79.4	78.1	1.3	36.3	53.5	-17.2
20	78.2	76.0	2.2	36.2	49.1	-12.9
35	77.5	74.7	2.8	38.1	43.5	-1.4
50	76.4	72.6	3.8	37.6	42.5	-4.9
60	77.2	72.0	1.2	39.5	42.0	-2.5
80	86.6	71.6	11.0	36.3	40.7	-4.4
90	92.5	69.5	23.0	31.3	39.6	-4.3
95	108.6	69.3	39.3	36.9	39.1	-2.2
100	-	69.6	-	-	39.4	-

Similar to previous observations, the largest discrepancies occur in particular regions. The component gradients obtained using the other component as the perturbation gas require small corrections; only a slight shifting upwards. These fit in with previous observations of a roughly linear argon isotherm and a nitrogen isotherm which becomes progressively less steep.

In order to calculate the various correction factors, the column upstream and downstream pressures were measured. The column pressure drop was found to be about 3.8 cm mercury. This was confirmed using a precise pressure gauge. The isotherm holdup gradients were

calculated using Equations 1.10, 1.11 and 1.12. Tables 1.3 and 1.4 show how these correction factors give much better agreement of both isotherm gradients for each trace. The viscosity correction is also included although it makes very little difference.

Table 1.4 Corrected Isotherm Holdups for Nitrogen

	nitrogen prtbn		argon prtbn		
% N_2	$1/F_{PVC}$	G_{N2}/ml	$1/F_{PVC}$	G_{Ar}/ml	ΔG/ml
0	1.00	78.1	-	-	-
5	0.999	78.6	1.03	80.3	-1.7
10	0.998	79.2	1.03	80.4	-1.2
20	0.996	77.9	1.03	78.3	-0.4
35	0.990	76.7	1.03	76.9	-0.2
50	0.981	71.0	1.03	74.8	0.2
60	0.972	71.0	1.03	74.2	0.8
80	0.924	80.3	1.03	73.8	6.5
90	0.859	77.6	1.03	71.6	6.0
95	0.709	77.0	1.03	71.4	1.6
100	-	-	1.03	71.7	-

Table 1.5 Corrected Isotherm Holdups for Argon Isotherm

	nitrogen prtbn		argon prtbn		
% N_2	$1/F_{PVC}$	G_{N2}/ml	$1/F_{PVC}$	G_{Ar}/ml	ΔH/ml
0	1.02	38.7	-	-	-
5	1.02	39.1	0.701	49.3	-10.2
10	1.02	37.0	0.832	44.5	-7.5
20	1.02	36.9	0.915	44.9	-8.0
35	1.02	38.9	0.958	41.7	-2.8
50	1.02	38.4	0.976	41.5	-3.1
60	1.02	40.3	0.983	41.3	-1.0
80	1.02	37.0	0.993	40.4	-3.4
90	1.02	36.0	0.997	39.5	-3.5
95	1.02	37.6	0.999	39.1	-1.5
100	-	-	1.000	39.4	-

Certainly, it can be seen that the correction factors have greatly improved the agreement between the isotherm holdups calculated using both perturbation gases for both components. However, it can be seen that there are certain systematic discrepancies. It can be seen that when the mixture has a high (greater than 75%) composition of the perturbation gas , the values of correction factor have not reduced the high values enough. Of course, these corrections are dependant upon the value of column pressure drop employed; there could be error associated with its measurement.

It would seem that there is an underlying effect of the argon perturbation gas giving increased values of isotherm gradient, superimposed upon the increase associated with adding the perturbation component flow to a mixture rich in the respective component. At these points, there is also the problem of the larger multiplication factor, so that any error in the measurement of the flowrate retention time could be disastrous. From Figure 1.8, it can be seen that the noise level makes this determination more difficult.

1.7.4 Integration of Isotherm Gradients

Of course, once the gradients have been obtained, they must be integrated to obtain the actual mixture isotherms. Figures 1.9 and 1.10 show the calculated isotherm holdup gradients for nitrogen and argon. On each graph are shown the isotherm gradients calculated without using the necessary F_{PVCi} correction term. Also shown are the regression lines for the corrected isotherm holdup gradients (one for each perturbation component). Certainly, these graphs show up rogue points as well as possible trends. Mason and Buffham (1991), suggested that, for this system, both sets of gradients could be fitted to a straight line. For the nitrogen component, the argon perturbation predictions fit in well with the findings of Mason and Buffham (1991); the isotherm becoming progressively less steep with increasing nitrogen composition. The nitrogen perturbation predictions are fine until the nitrogen-rich mixtures, when they become too high. For the argon component, the nitrogen perturbation predictions fit in well with the findings of Mason and Buffham (1991); a virtually straight line. Of course, calculation of the actual isotherm gradients is achieved using Equation 1.7 and this requires values for the following variables:

$\varepsilon = 0.376$

$V_C = 18.5$ cc

Figure 1.11 shows the isotherms obtained by integrating the regression lines for each perturbation gas. For the nitrogen component, the isotherms are very close; compared to what might be expected from comparing the sets of gradients. For the argon component, the regression lines are significantly different and this shows up upon integration. The nitrogen perturbation gas gives much lower values, although, this difference is still less than that which might be expected from comparing the sets of gradients. On these same graphs, the total amounts adsorbed are seen to have roughly the same variation.

These lower nitrogen perturbation values for the argon component cause the differences in the phase diagram shown in Figure 1.12. This difference is very small compared to the difference in selectivities shown in Figure 1.13. Thus the selectivity is seen to be a more severe way of making a comparison. This is not surprising considering the presence of the composition in the denominator as well as the numerator. Finally, comparing gradients is seen to be a much more severe way of making comparisons than the actual isotherms.

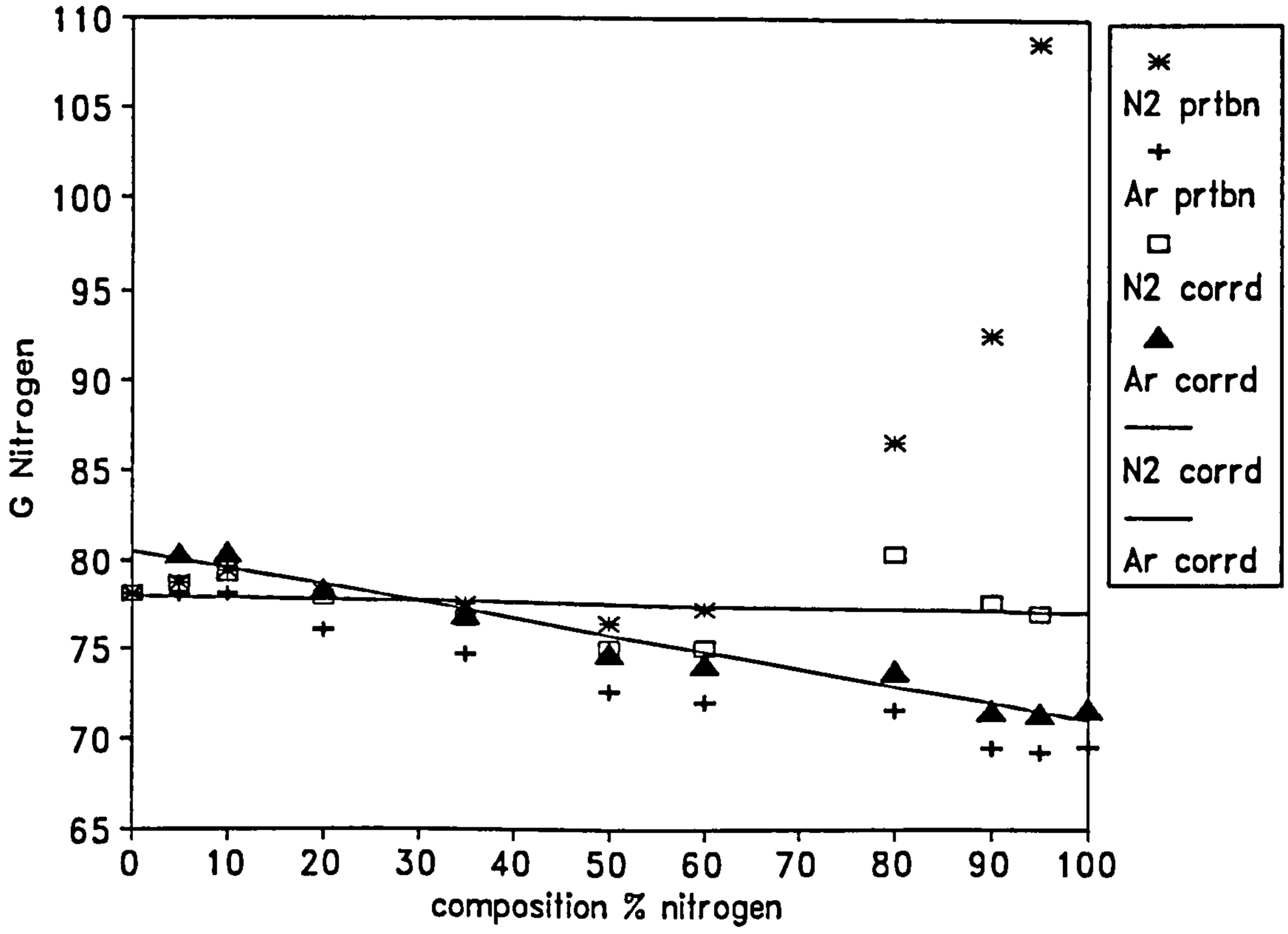

Figure 1.9 Comparison of Nitrogen Gradients for Each Perturbation Gas

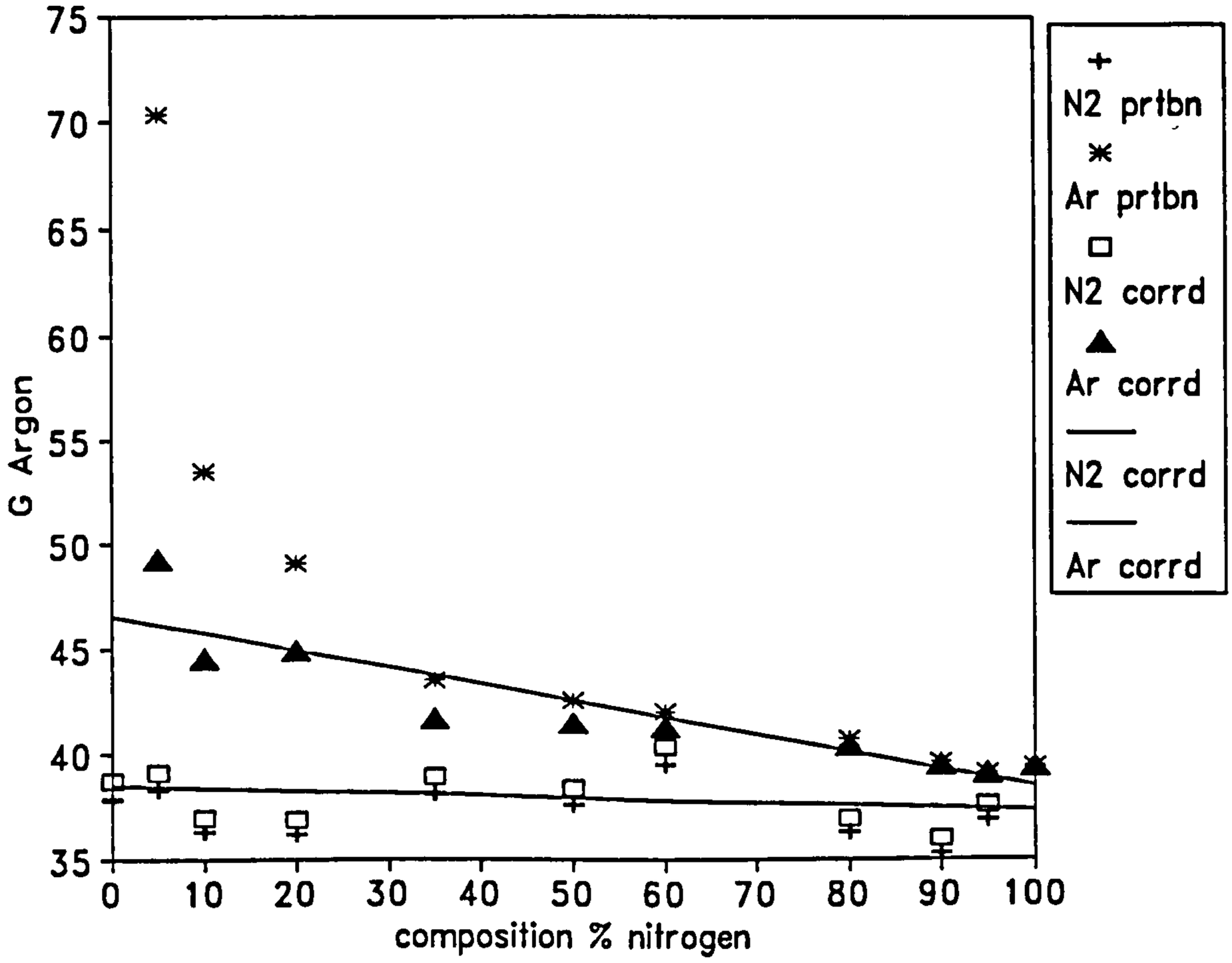

Figure 1.10 Comparison of Argon Gradients for Each Perturbation Gas

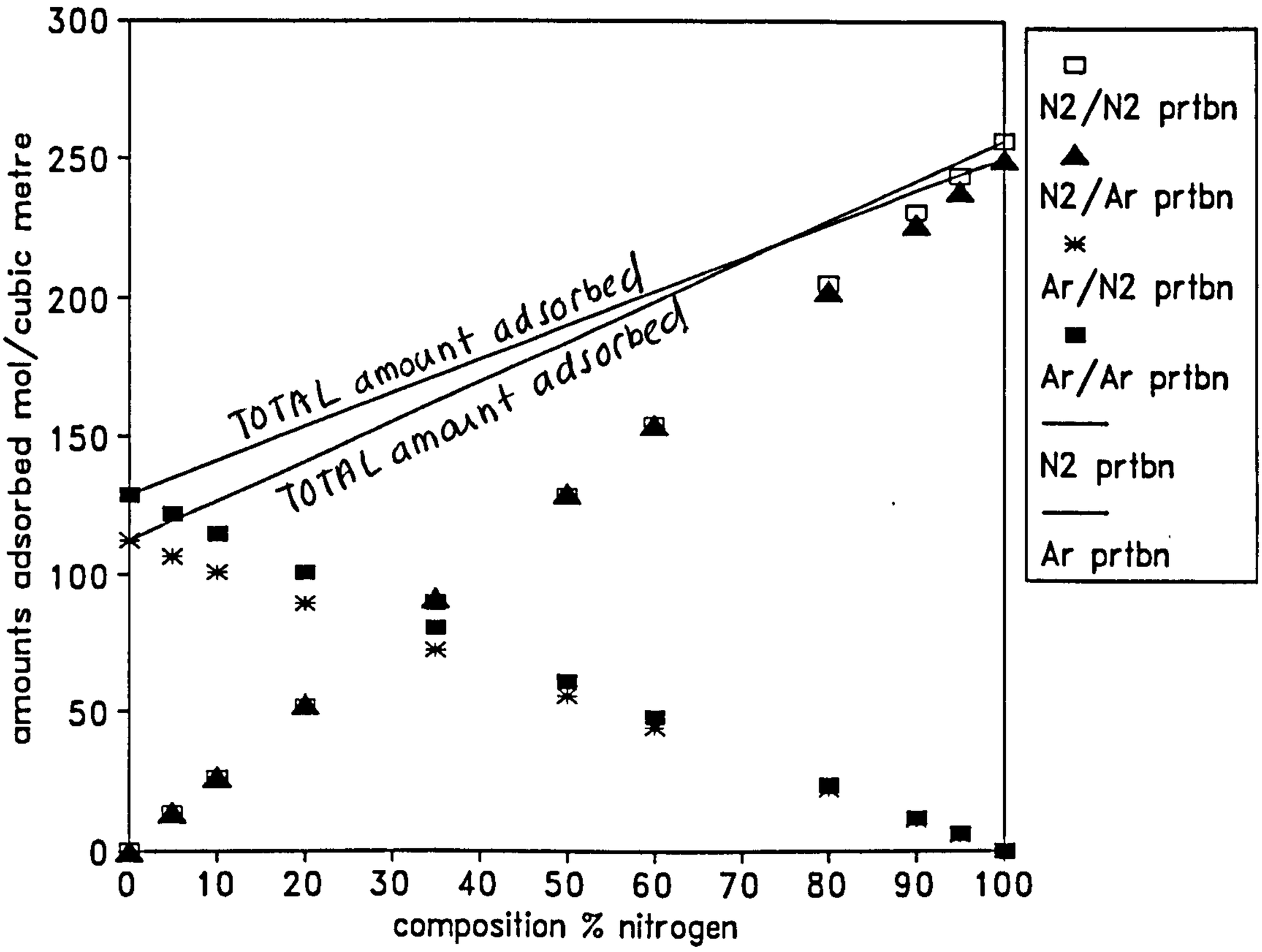

Figure 1.11 Comparison of Binary Isotherms for Each Perturbation Gas

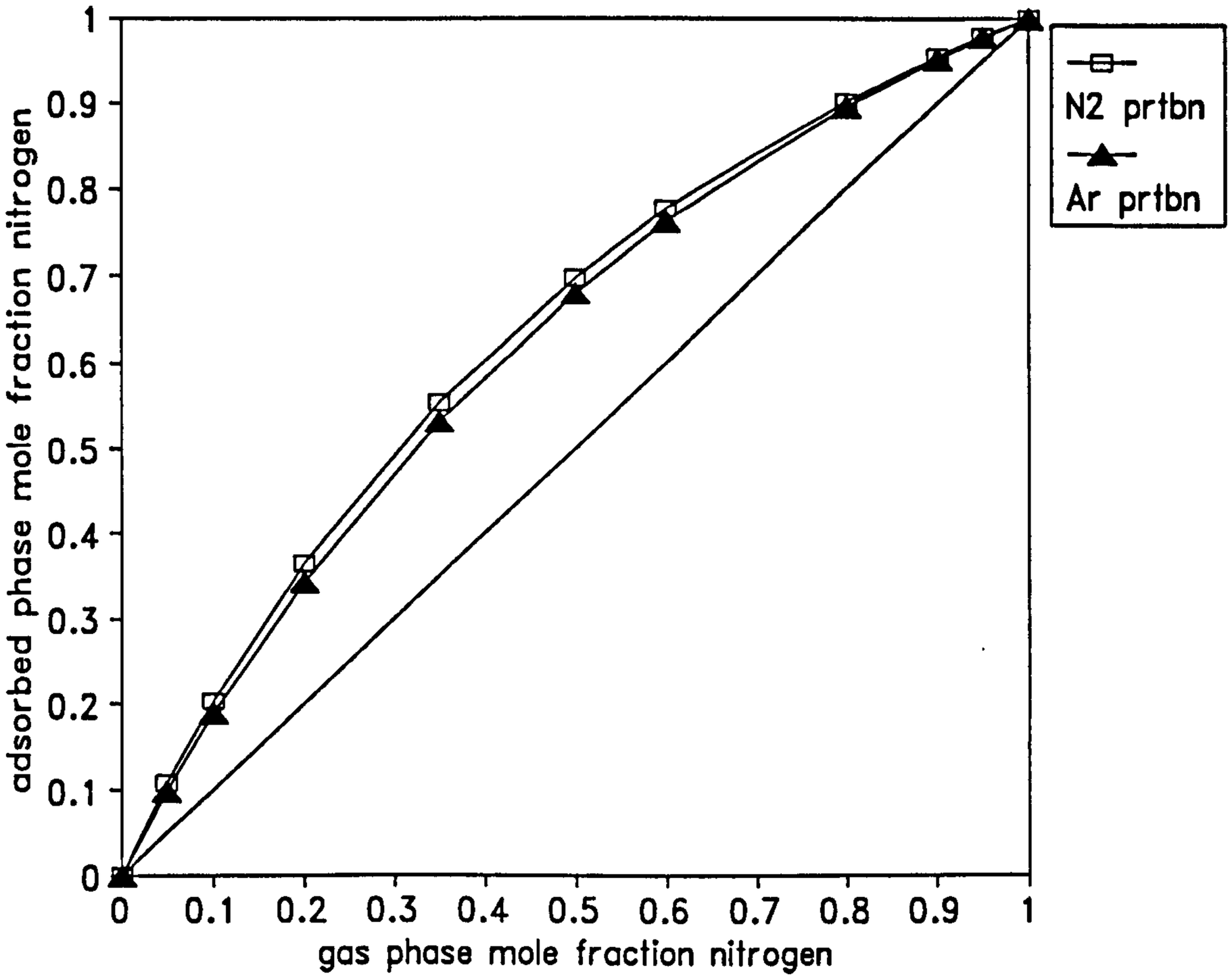

Figure 1.12 Comparison of Phase Diagrams for Each Perturbation Gas

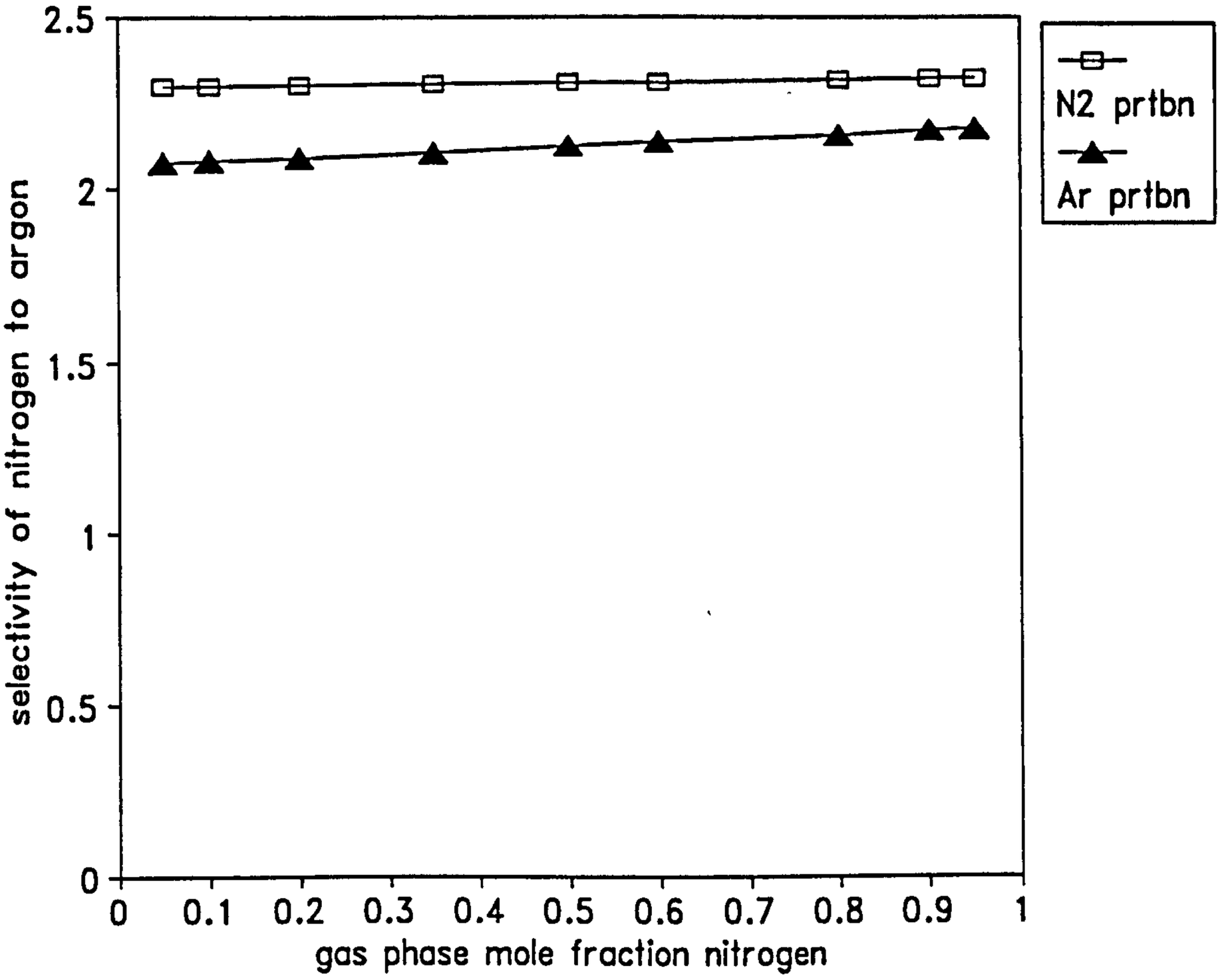

Figure 1.13 Comparison of Selectivity Charts for Each Perturbation Gas

1.7.5 Problem of Column Deactivation

Many more experiments were carried out in which the perturbation gas was changed many times. Eventually, to test the reproducibility, selected mixtures from the argon-nitrogen system were repeated. However, the resulting chromatograms were found to be significantly different from the corresponding previous cases. Figure 1.14 shows the chromatograms obtained for switching a nitrogen perturbation flow between 100% argon carriers. The experimental arrangement includes the usual downstream delay-lines. The top chromatogram is the flowrate record and the bottom one is the composition record. It should be remembered from the experimental arrangement described earlier, that both chromatograms correspond to the *cumulative* effect of the same perturbation being added to one column *and* removed from the other. For explanation purposes, though, it is easier to describe the effects of *adding* the perturbation gas. Once again, the composition record is relatively simple in shape and the only deviation *should* be a smooth sweep from the initial baseline $x(0)$ to the final position $x(\infty)$ as the front leaves the column and enters the TCD. The deviation between these positions corresponds to *twice* the perturbation flow. Comparing with Figure 1.7, it can be seen that the composition retention time will be reduced because the composition front emerges after a shorter time. However, there is also a small unexpected deviation in the composition record when the composition front is still in the column. This might suggest that there is another front passing through the column, although the presence of only two components would preclude this possibility. This behaviour was only noticed around the time of these particular experiments and was not noticed afterwards.

Because of the chart recorder polarity, for the flowrate record the downward direction corresponds to an increasing flowrate. When the perturbation gas is added, the flowrate record moves from the initial baseline *towards* the $n(\infty)$ position. When the front reaches the column, the net adsorption caused by the nitrogen reduces the column outlet flowrate to a position close to $n(0)$. However, unlike Figure 1.7, as the front moves through the column, the column outlet flowrate is not maintained at this level but is seen to increase continually. When the front leaves the column, there is no more net adsorption and the column outlet flowrate increases to the $n(\infty)$ position. The deviation from $n(0)$ to $n(\infty)$ corresponds to twice the perturbation flow. The final deviation is due to the viscosity effect when the front leaves the downstream delay-lines and enters the measuring capillaries, causing the flowrate record to move from the positions $n(\infty)$ to $p(\infty)$. As discussed previously, it should be possible to calculate the viscosity factor $B(\mu)$ by measurement of the relevant offsets using the $n(0)$, $n(\infty)$ and $p(\infty)$ positions. This factor should be unaffected by column deactivation. From the flowrate chromatogram, it can be seen that the required area and hence the calculated flowrate retention time will be reduced. Table 1.5 shows how

the retention times have been affected for switching the perturbation gas between pure carrier flows of the non-perturbation gas. Table 1.6 shows how the subsequent reductions in these retention times have affected the isotherm gradient holdups.

Table 1.6 Effect of Column Deactivation on Retention Times

$\%N_2$	τ_X/s	$\Delta\tau_X$/s	τ_N/s	$\Delta\tau_N$/s
0	228	-50	101	-41
100	102	-3	-63	18

Table 1.7 Effect of Column Deactivation on Holdup Gradients

	nitrogen		argon	
$\%N_2$	G/ml	ΔG/ml	G/ml	ΔG/ml
0	64.1	-14.0	36.4	-2.3
100	63.8	-7.9	38.3	-1.1

Thus the column deactivation has caused a reduction in isotherm gradients and so a reduction in the amounts adsorbed. This is not surprising considering the number of times the perturbation gas was changed; each time a small volume of air would enter the chamber and eventually find its way to one of the columns. Air contains water-vapour and this can occupy sites preventing other gases from doing likewise. Baking out the columns, using a high helium flowrate at 200°C, restores the original retention times. What is particularly interesting is that the nitrogen gradients have been significantly reduced (18% and 13%) whereas the argon gradients have not been so affected (6% and 3%). Thus deactivation is seen to change the *selectivity* as well as the *capacity*.

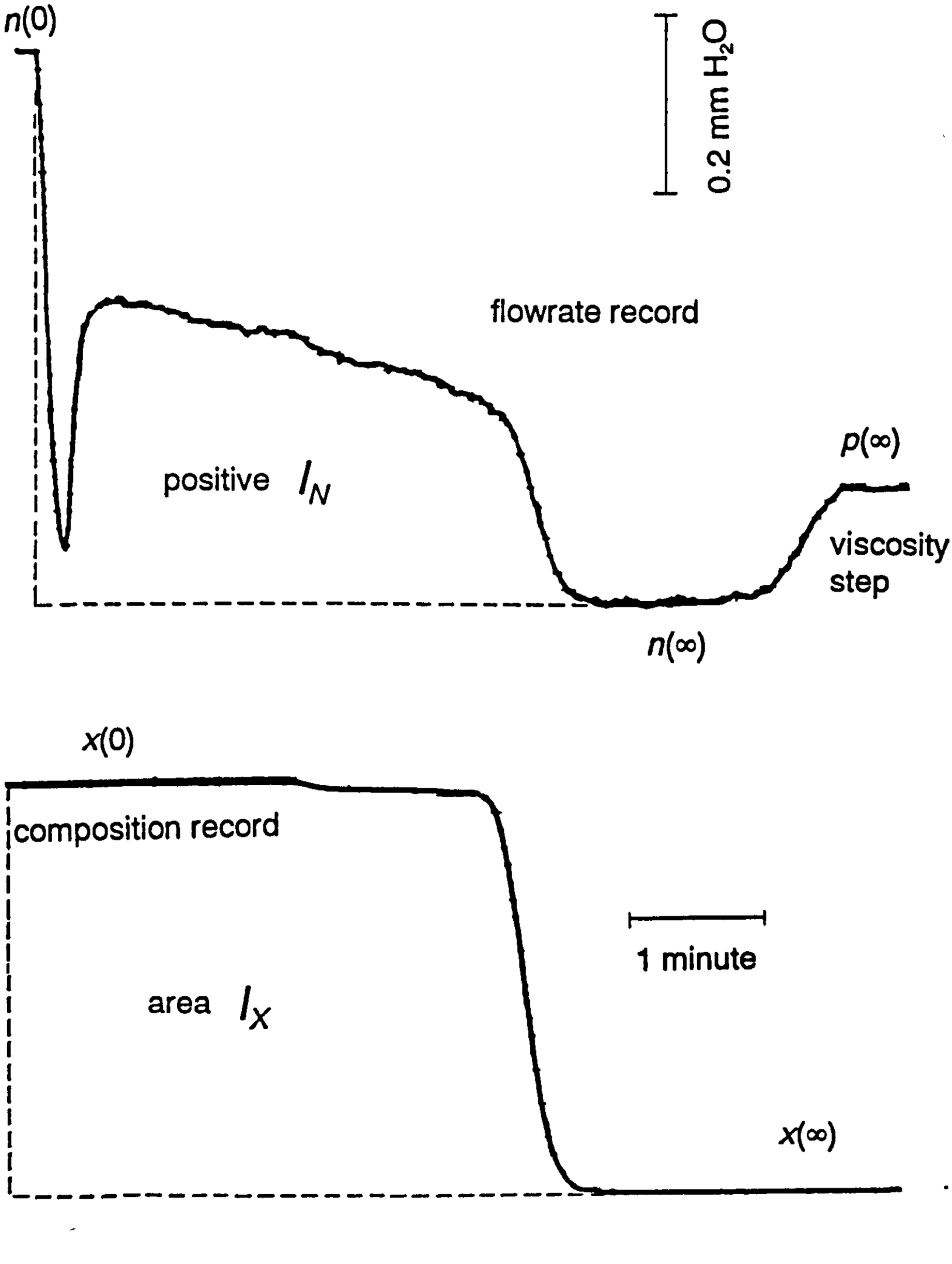

Figure 1.14 Effects of Column Deactivation on Chromatograms for Switching Nitrogen Perturbation between 100% Argon Carriers at 50°C

1.8 Program of Areas to be Researched

From the preliminary investigation, good predictions have been obtained for the argon-nitrogen-zeolite 5A system at 50°C. These results agree qualitatively with those obtained by Ruthven and Kumar (1980) given that they used different column temperatures. The whole procedure was very quick compared to the static methods; complete determination for eleven mixtures took only about two hours and half of this time was due to repeating with the other perturbation gas. The following points will now be made concerning how the project will be developed:

1. From the preliminary results, thermal noise was seen to be a potential problem, and so modifications to the apparatus would be required to reduce this noise. The factors which produce thermal noise need to be identified. Also, the problem of adsorption heat will be considered; equilibrium data is very sensitive to temperature.

2. So far, the perturbation has been initiated by switching a small flow of perturbation gas from one column to the other; the idea being to obtain double the deviation and double the area. However, this requires identical columns with identical packing amounts and identical activities. The preliminary experiments indicated that the apparatus was more than sensitive enough and that the problems produced by having to make matched columns did not give any corresponding benefits in sensitivity. Also, from basic chromatographic theory, there is nothing to suggest that advancing and retreating transients should be the same. So, an improvement would be to separate out these transients; as well as allowing a comparison it will provide double the number of measurements.

3. From Equation 1.9, the flowrate retention time (τ_N) is required for holdup gradient calculation. However, because the flowmeter works by monitoring the pressure drop, the pressure retention time will actually be measured. It will be shown how the introduction of delay lines between the columns and the flowmeter can be used to directly obtain the important flowrate retention time. Also, it will be shown how these delay lines can be used to obtain information about the gas mixture viscosity data.

4. Experiments will be conducted with and without delay lines to enable direct determination of the flowrate and pressure retention times, and so confirmation of the validity of the derived equation above. The possible effects on the retention times of delay lines will be investigated.

5. Clearly, the perturbation gas selection system needs improvement. A system will be developed which allows the perturbation gas to be changed and measured without the problem of column deactivation or the problem of dead volume. Column deactivation is a great problem and extra experimental steps will be taken to avoid this problem.

6. So far, the perturbation gas employed has been either of the pure components. This means that the perturbation gas has always caused an overall change in composition, namely a chart-recorder offset. There exists the possibility of using a perturbation gas having the same composition of the mixture. The theory will be developed to enable the holdup gradients to be evaluated from such a perturbation type. This will involve the important concept of the change in average column pressure caused by the increase in the column flow.

7. Results will also be obtained for argon-helium and nitrogen-helium systems. Also, columns with different packing sizes and different diameters will be employed to see the effect of the column pressure drop.

8. Finally, a computer based simulation will be carried out to examine the suitability of this method for many hypothetical systems. As a comparison, the simulation will also show how a rival chromatographic method will perform for the same systems.

Chapter Two

SUMMARY OF LITERATURE SEARCHING

2.1 Introduction

The project is concerned with a chromatographic method to determine binary gas-mixture adsorption equilibria. Initially, some relevant papers concerning binary gas-mixture adsorption equilibria were supplied; these were concerned with reporting this equilibrium data using alternative methods. One objective of this literature search was to summarise and obtain a basic understanding of the main methods. Also, it is useful to summarise all the data reported for gas-mixture adsorption on 5A molecular sieve, since this is used experimentally in the project. Generally, the literature searching was accomplished by two methods. The first method involved searching the various indexes using particular keywords, namely *subject searching*. The second involved taking particular papers of interest and then using the *citation index* to find out who has cited these papers. Initially, this was done using the relevant papers above. However, the subject searching revealed further interesting papers and these were also used with the citation index.

2.2 Subject Searching

The subject searching was effected in two stages. The first stage was to study the bound volumes, and the second was to conduct an *on-line* computer search. The former was started in late 1989, and has been updated monthly since then. The latter was conducted in the summer of 1991.

2.2.1 Searching Bound Volumes

Three bound volumes were found to be useful, and these are listed along with the years searched. These are all found in the Pilkington Library:

1. ***Theoretical Chemical Engineering Abstracts*** **(from 1966)**
2. ***Engineering Index*** **(from 1950)**
3. ***Chemical Abstracts*** **(from 1947)**

In order to obtain a broad perspective of the area, initially an expanded list of keywords was used resulting in an excessive number of references. Finally references were restricted to the equilibrium adsorption of gas mixtures on a variety of solid adsorbents. Actually, most of these references were for binary mixtures, although some included up to five components. The list of adsorbents consists zeolites, carbon molecular sieves, activated carbon and silica gel. Actually, papers using silica gel have rarely appeared in the last twenty years.

The *Theoretical Chemical Engineering Abstracts* contains very few useful references. Moreover, since 1987 the method of contents indexing has deteriorated. *The Engineering Index* contains many useful references, although some of the science journals are not covered. *Chemical Abstracts* covers the widest range of journals, and the internal subject indexing is the best. Thus, this became the major index. The keywords used for this index were:

A. Adsorption/Desorption with the many subheadings including binary gas, gas mixture, specific gas names and many more.
B. Chromatography,Gas with the subheadings adsorption, frontal and pulse.
C. Molecular Sieves with the subheadings adsorption and carbon.
D. Zeolites with the subheadings adsorption and the various type names.

2.2.2 Computer Searching

This consisted an on-line search of Chemical Abstracts. This index is updated weekly although it only covers papers from 1967. To do a search, a list of keywords is required. Often, the list of keywords is used with combinations of "and" and "or", in order to minimise the number of irrelevant titles. The computer can search on three levels for this final keyword combination. For the present, the computer searched the title and keyword list. Additionally, it can also search the complete abstract. Because the extensive subject search had already been carried out on the bound volumes, the results from the computer search would show how well the keywords had been chosen. The actual combination was to choose one word from each of the following categories A to D:

A. Extensive list of adsorbents
B. sorption or adsorption
C. equilibrium, equilibria or isotherm
D. gas, gaseous or gases

2.3 Citation Index Searching

The Pilkington Library stocks the Science Citation Index from the earliest volume to 1990, but it does not cover 1991. This facility is supposed to be on computer but it has not yet been installed. So, this necessitated a visit to the Nottingham University library. Here is a list of the papers whose citations were checked. The list of papers can be divided into two categories. The first part consists papers concerned with the main chromatographic techniques, and the second part consists the papers concerned with the frequently used prediction techniques.

2.3.1 Primary Papers

1. The paper by **Buffham, Mason and Yadav (1985).**

2. The paper by **Van der Vlist and Van der Meidjen (1973)**, which introduced the concept of polynomial-fitting of a concentration-pulse technique to determine binary adsorption isotherms.

3. The two papers by **Ruthven and Danner (1980)** and **Shah (1988)** which employed the previous technique.

4. Two papers by **Hyun and Danner (1982,1985)** were published giving a critical assessment of the technique proposed in part 2.

2.3.2 Secondary Papers

1. The classic paper proposing the Ideal Adsorption Solution Theory (IAST) by **Myers and Prausnitz (1965).**

2. The paper introducing the Vacancy Solution Theory proposed by **Sunawyuen and Danner (1980)**, which has been cited almost as frequently as the IAST.

3. The Potential Theory was extended to mixtures firstly by **Lewis *et al.* (1950)** and then by **Grant and Manes (1966).**

4. The frequently used, but much criticised multicomponent Langmuir equation **(Markham and Benton, 1931)** which was later modified by **Yon and Turnock (1971).**

5. The semi-empirical method proposed by **Cook and Basmadjian (1965).**

6. Probably one of the first empirical methods devised by **Minkoff (1964)**

7. An exact method, applicable only for binary ideal systems, this was proposed by **Lee *et al.*(1984).**

2.4 Literature Review Summary

There have been many papers on the adsorption of binary gas mixtures on the previously stated adsorbent list. Early on, many of the papers refer to silica gel and activated carbon as adsorbents. However, in recent years, zeolite molecular sieves and, to a lesser extent, carbon molecular sieves have become increasingly studied because of their growing importance in industrial gas separations. The frequency of ternary and higher component mixtures has increased in recent years, although the maximum number of components has not exceeded five. There are similar traits in many of these papers, and four conclusions can now be made regarding the content and purpose of these papers.

1. Often, initially pure-component isotherms are obtained by one of the *direct* techniques. Basically, these techniques are termed such because the adsorbed amounts are obtained directly from simple PVT measurements and a subsequent molar balance. Then, the

technique is repeated to obtain the gas-mixture adsorption isotherms. However, for the latter case the technique is much more complex and time consuming. These techniques can be regarded as *absolute*, the standard by which other techniques are evaluated.

2. For a particular adsorbent-adsorbate system, data may be required over a range of system temperatures and pressures, and over the complete composition range. Because of the time involved, researchers are keen to avoid the use of direct measurements on a routine basis. Alternative methods can be divided int two categories and these will be described in parts 3 and 4.

3. One such way to avoid the direct way is to employ one of the many *chromatographic* methods. However, for some of these the theory is still developing, so the absolute data is sometimes used to test the chromatographic method.

4. The great majority of papers employ one or more of the many *predictive* methods, which require only the pure component data to attempt a prediction of the mixture data. In some of the papers, existing mixture data is used to try and improve the particular predictive method.

5. The literature review will therefore concentrate on giving an up-to-data and critical assessment of these methods. Generally, it will be concerned with binary mixtures, although mention is made of extension to ternary and higher component mixtures.

2.5 Direct Measurement Methods

2.5.1 Introduction

Before considering multicomponent techniques, it is better to describe first the principles behind single-component techniques. These can be divided into two categories, namely *gravimetric* and *volumetric*. Both involve allowing the adsorbent to equilibrate with a fixed amount of gas. In the former, a balance will give the mass adsorbed, and then a knowledge of the molecular weight will give the moles adsorbed. For the latter, the initial and final gas pressures are required as well as the various system volumes. Application of the simple ideal-gas equation will solve the molar balance. For higher system pressures, a suitable equation of state should be employed instead of the ideal-gas equation.

For the multicomponent case, all the techniques should be described as volumetric. However, the calculations are complicated because the adsorbate composition is an additional unknown which must be determined indirectly by a molar balance. For a mixed adsorbate, the average molecular weight varies with composition and so the total moles adsorbed cannot be obtained directly from the mass adsorbed. Hence, the gravimetric data can only serve as a check on the volumetric data, not as an alternative method.

The measurements of the initial and final gas composition are usually determined by gas chromatography. The detectors in gas chromatography are either *differential* or *integral.* Most detectors are of the former type, where the peak area is measured directly from the chromatogram. In the latter type, the area is calculated by the integrator and represented on the chromatogram by an offset or a numerical value. To use these areas for gas composition determination, it is first necessary to *calibrate* the detector. This is achieved by injecting a gas mixture sample of known composition into the gas chromatograph; this allows the *sensitivity factor* of the detector to each component to be evaluated. Knowing these factors, any unknown gas mixture composition can be evaluated from the respective chromatogram. There is one great advantage of these techniques; for the extension to ternary and higher component mixtures there are no additional calculations. The only additional measurements will be the additional peak areas on the chromatograms.

2.5.2 Batch Methods

As the name suggests, these methods involve allowing the adsorbent to equilibrate with a fixed amount of gas mixture. They can be divided into two categories depending upon how the adsorbate-adsorbent contacting is achieved.

2.5.2.1 Simple Two-Chamber System

Basically, this type consists of a mixing chamber connected by a single pipe to the adsorbent chamber. This is typical of the equipment described in the earlier papers on gas mixture equilibria. However, this type of equipment has appeared recently in papers by Miller (1983), Miller *et al.* (1987) and Verelst and Baron (1985). First of all the gases are admitted to the mixing chamber until a particular pressure is attained. Then the valve is slowly opened to admit the mixture to the previously evacuated adsorption chamber. Because some of the mixture will adsorb, the chamber pressure will decrease, so that the inlet valve is opened to admit further pulses of the mixture. When equilibrium is reached, the adsorbed amounts can be obtained according to the procedure described in Section 2.4.

One of the main problems is to determine when equilibrium is reached. This is quite a complex problem and is further described in Section 2.5.4. It usually takes a long time. Actually, Miller (1983) has suggested times of up to 10 hours, and Ritter *et al.* (1987) has suggested times of up to 48 hours. Another problem is the lack of control over the system pressure and temperature. It can be very tricky to obtain a particular pressure and composition because as soon as the mixture is added, one of the components is preferentially adsorbed and the pressure and composition will change. This is a particular problem if data is required at constant pressure or gas composition. One way of solving this problem is to

add an excessive amount of mixture (relative to the adsorbent capacity) so that the gas composition and pressure will effectively remain constant. This will also reduce the equilibration time.

2.5.2.2 Batch with Internal Recycle

With this modification, instead of simple admittance to the chamber, the mixture is continuously pumped through the chamber around a loop. Equilibrium is achieved when the inlet and outlet compositions are the same. These are usually continuously monitored with a katharometer. Most of the volumetric techniques in recent papers employ this variation. With this technique, equilibrium should be reached in a shorter time. Indeed, Loughlin *et al.* (1990) have reported times of one hour, and Veyssiere *et al.* (1981) have reported times of two hours.

2.5.3 Continuous Flow Methods

This differs from the batch methods in that fresh gas mixture is continually flowing through the adsorbent. The adsorbent takes the form of a packed bed so that all the gas mixture flows through the bed. Thus equilibrium should be reached in a shorter time. Once again, equilibrium is determined by the check described in Section 2.5.4. Recently, Chen *et al.* (1990) have reported using such a method although no mention is made of the times involved. Once equilibrium is achieved, the adsorbent container is sealed off. Desorption is facilitated by heating to a sufficiently high temperature. Once again, knowledge of compositions, pressures and volumes will give amounts adsorbed of each component. Another advantage of this system is that the gas composition and pressure in the bed can easily be controlled, although, a good gas mixing system is required.

2.5.4 Rate of Attainment of Equilibrium for Direct Measurement Methods

2.5.4.1 Introduction

The main drawback of the direct methods is the longer times taken to reach equilibrium for each experimental point. These times are excessive for the purely batch methods, although introducing some form of flow re-circulation reduces these times somewhat. This section will discuss all the factors which determine the experimental time, and will show theoretically why introducing a degree of re-circulation is desirable experimentally.

2.5.4.2 Structure of Commercial Adsorbents

Before discussing equilibrium times it is helpful to first consider the sorbent structure. At synthesis, the typical zeolite crystals are very small, typically less than 10 micrometres (Ruthven, 1984a). This size would be too small for gas flow applications since an excessive pressure drop would be required. Thus these crystals are formed into macroporous pellets of practicable size. Such a pellet offers two distinct diffusional resistances to mass transfer: the micropore diffusional resistance of the individual zeolite crystal and the macropore diffusional resistance of the gaps between the crystals. The optimal size of crystal and pellet is a complex problem and will depend upon the gas system employed.

2.5.4.3 Relative Rates of Heat and Mass Transfer

The rate of attainment of equilibrium, or how long equilibrium takes to achieve, will depend upon both the rates of heat and mass transfer. In contrast to trace systems where a relatively small perturbation is made, the addition of comparatively large amounts of gas mixture means that much heat will be evolved. Of course this amount will depend upon the adsorbate-adsorbent system. This heat needs to be conducted away from the bed as quickly as it is produced otherwise the bed temperature will rise. For equilibrium to be reached quickly, both rates need to be high, although the heat rate must be higher. If one rate is low and the other high, then the situation would either be slow isothermal or a high bed temperature rise.

2.5.4.4 Factors Affecting the Above Rates

Many of the following arguments are taken from the book by Ruthven (1984). The various analyses depend upon subjecting a pellet or bed to a step change in sorbate concentration. That is to say, a comparatively large amount of mixture must be added. If this is not the case, then the rates will be even slower, since the sorbate concentration will reduce with time. This will have implications with regard to times required for batch methods.

In a bed of pellets there are three resistances to mass transfer; pellet diffusional resistance, micropore diffusional resistance and, for mixtures, there is a boundary layer around the pellet. The latter two are fixed for a particular system and so only the pellet size is adjustable; reducing this will reduce the macropore resistance. However, this would be pointless if the micropore resistance was limiting. Indeed, Schalles and Danner (1988) have shown that oxygen and nitrogen have such widely differing micropore resistances on CMS 3A that this forms the basis for a *kinetic separation.* Also, Kapoor and Yang (1989) have made the same observation but for carbon-dioxide and methane on CMS 5A.

In a bed of pellets there are two resistances to heat transfer. Firstly, conduction across the bed and secondly convection from the exterior surface. The former is much quicker so that the whole bed can be considered at a uniform temperature. In order to reduce the resistance, the surface area to volume ratio should be as a high as possible. This would normally require long thin beds rather than short fat beds.

2.5.4.5 Application of Above Reasoning to Literature Times

For the basic batch method, the gas mixture is static so that heat is transferred from the exterior of the bed by natural convection. Moreover, the ambient gas might heat up so that the reduction in temperature driving force would further reduce the heat transfer rate. Indeed, Verelst and Baron (1985) have reported that this bed temperature rise is very problematic. However, with the internal recycle the gas mixture is flowing around the bed surface. Thus, heat will be transferred by forced convection for which the Nusselt number indicates much higher heat transfer coefficients. This might explain why this variation yields lower times.

Furthermore, the next variation is to have gas flowing *through* the bed. Considering the mass transfer rate, the pellet boundary resistance should be reduced. For heat transfer, the gas flow will effectively reduce the bed size to that of the pellet. From geometry, the surface area to volume ratio will thus be greatly increased and so the heat transfer resistance will be reduced. Combined, these two facts would explain why the equilibration times for this variation should be even shorter.

2.6 Chromatographic Methods

2.6.1 Introduction

This set of methods can be divided into four categories and each one will be discussed in turn. In all these methods a gas mixture flows through a cylindrical column packed with the required adsorbent. Generally, these methods involve measuring one or more retention times of a front or pulse. The main advantage of these methods over the direct methods is that the experimental times are much shorter. Reduction of column volume and increasing the gas flow-rate will further reduce these retention times. However, in order to obtain accurate residence times, sharp fronts or pulses are required with minimal spreading. This implies a restricted choice of column dimensions and particle size. These requirements are dealt with in any gas chromatography text book, for example Purnell (1967).

2.6.2 Concentration-Pulse and Polynomial-Fitting

Previous to the present research subject, the only conventional chromatographic method to determine binary adsorption isotherms was that proposed by Van der Vlist and Van der Meijden (1973). It is based upon the well known expression relating the retention time of a small concentration in a binary mixture to the gradients of both binary adsorption isotherms (Peterson and Helfferich, 1965). The method involves adding a pulse of perturbation gas to the mixture in question and continually monitoring the column effluent with a thermal conductivity detector. Of course there will only be one retention time.

However, the binary isotherms are unknown so the method involves fitting the binary gradients to polynomials in composition. Then, a third order polynomial is fitted to the retention times and the binary polynomial coefficients are obtained by simultaneous equations. Integration will then produce the binary isotherms. This integration will also require boundary conditions of the pure amounts adsorbed at the system pressure. This method can also be used to obtain single-component isotherms by choosing an inert component, that is one having a zero isotherm gradient.

Ruthven and Kumar (1980) and Shah (1988) have subsequently used this method although they compared their predictions to those obtained by the statistical theory rather than directly obtained data. Also, Hyun and Danner (1982, 1985) have published papers criticising this method. Their conclusion is that this method is better suited to obtaining single-component isotherms. They conclude that although a higher order polynomial would provide a better fit of the residence times, solution of the corresponding simultaneous equations would require independently obtained mixture data; mixture data obtained by one of the direct methods. Considering that the point of these chromatographic methods is to find a viable alternative to the direct methods, this requirement somewhat defeats the object. Chapter Nine of this thesis will be devoted to a novel technique which can qualitatively and quantitatively test this method under a variety of conditions.

2.6.3 Tracer-Pulse Addition

As the name suggests, this method uses a perturbation gas that is a radioisotope of one component. The column effluent then passes through an ionisation cell where the response is recorded. The equations for this method are simple. The great advantage of this method over the concentration-pulse method is that the actual mixture isotherm point can be directly obtained from the residence time (isotherm chord). Of course for the concentration-pulse method this time is dependant on both binary mixture gradients. Helfferich (1964) has eloquently illustrated the fundamental difference between both concentration and tracer residence times.

The idea of using radioisotopes was first proposed by Stalkup and Kobyashi (1963). Initially, only the Henry's law region was investigated but later Danner *et al.* (1980) extended the method over the entire concentration range using mixtures of ethane and ethylene over 13X zeolite. Later, Al-Ameeri and Danner (1984) improved the method even further. Since the residence time for each radioisotope pulse depends only upon the individual mixture isotherm chord, then this method is applicable to multicomponent situations. However, this would require a radioisotope for each component and then the cost would become prohibitive, if indeed a radioisotope was available for each component. The availability would be better for components containing carbon.

2.6.4 Combination of Tracer and Concentration Methods

Realising the inadequacies of the above methods, Hyun and Danner (1985) suggested combining these methods. They considered the highly non-ideal isobutane-ethylene-13X zeolite system for which the concentration-pulse method was shown to fail. They only used the tracer for ethylene since no radioisotope was available for isobutane. They achieved very good results. However, there is no advantage in using this combination for three or more component mixtures because there will be too many unknown partial derivatives.

2.6.5 Breakthrough Curves

2.6.5.1 Introduction

These methods are characterised by the addition of the *whole* mixture to the column rather than just making a small perturbation. From the literature there are two variations and these will now be discussed.

2.6.5.2 Low Binary Concentration in Inert Carrier

Compared to all other methods, the exceptional thing about this variation is that the binary concentration should not exceed about 1% of the total bulk flow. From basic chromatographic theory two breakthrough curves will be obtained. Thus a disadvantage of this method is that many samples of the outlet effluent will be required and these will then will have to be analysed by gas chromatography. A simple thermal conductivity detector cannot be employed because more than one front will be obtained.

The method was first proposed by Huang and Madey (1982) and was later applied to the adsorption of ethane and propane on activated carbon at a total pressure of 7 mm Hg. Despite the comparatively low concentrations, they showed typical breakthrough curves with the components intefering with each other. A great advantage of this method is that it can be extended to three or more components without an increase in equation complexity. Of course when each sample is analysed there will be more peaks in the chromatogram, but this should not cause too much problem.

2.6.5.3 Significant Binary Concentration in Inert Carrier I

This is a very recent modification, and was proposed by Kluge *et al.*(1991). Once again two concentration fronts will be obtained and this will thus necessitate the sampling and analysis of many samples. However, additionally the flowrate will be monitored as well. The assumption of a constant flow-rate is only valid when the concentration of the adsorbed components is less than about 15% of the total bulk-flow.

Isothermal operation is a necessity if the results are to be meaningful, and with this in mind the method is likely to be susceptible to adiabatic behaviour; the large concentration changes will evolve more heat than simply adding a small perturbation flow. This may have implications concerning the column diameter and the column exterior wall. That is to say, a thinner column may be preferred with a high heat transfer coefficient to the surrounding fluid in order that the heat may be dissipated quickly. Kluge *et al.*(1991) applied the technique to the adsorption of methane and carbon dioxide on activated carbon. On comparing their results with those obtained volumetrically, agreement was very good.

2.6.5.4 Significant Binary Concentration in Inert Carrier II

This was proposed by Robinson and Thomas (1980). Once again, many samples of effluent are required allowing the effluent concentrations to be determined for the whole of the breakthrough curve. Additionally, the column outlet flowrate is fixed by a flow control valve. Using the material balance equations, the instantaneous rate of adsorption can be determined for each component as a function of time. Subsequent integration will determine the amount adsorbed of each component and repeating this procedure at different mixture compositions will obtain the complete binary mixture equilibrium. Although this method notes the variation in column outlet flowrate, it is not measured directly but obtained by material balance.

2.6.6 A Direct Chromatographic Method

The present research project is concerned with this method. The method was first formulated by Buffham *et al.*(1985) who applied the method only to the isotherm end points. Later, Mason and Buffham (1991) extended the method to cover the whole concentration range. The method is similar to the previously described concentration-pulse method in that a very small perturbation flow is added to the particular mixture. However, as well as the usual katharometer to monitor the effluent composition, a flowmeter is employed to monitor the small flowrate changes. From the flowrate and composition records, the two retention times can be obtained, and these will give the two binary gradients. Integration of the whole composition range will give the actual binary isotherms. Typical experimental times are around five minutes. Presently, the method has only been applied to binary mixtures. However, there are plans to extend the method to ternary mixtures.

2.7 Predictive Methods

2.7.1 Introduction

The basic requirement of these methods is a knowledge of the pure component isotherms at the system temperature. However, over the years these purely predictive methods have been unable to deal with mixtures exhibiting non-ideality in the adsorbed phase. Consequently, one solution has been to employ independently obtained binary data. The number of points will vary from one method to another and this number can vary from two upwards. In this case, the method will not be purely predictive but will include a degree of correlation.

2.7.2 Simple Empirical Methods

2.7.2.1 Method of Minkoff

One of the first workers to propose a method for prediction was Minkoff (1964). Indeed, this method has received very little attention in the literature and it is included because at the time this was one of the few simple methods around. The paper dealt with the adsorption of alkanes on 5A zeolite. At first glance, the method seems very similar to the principles behind liquid-vapour equilibria. The method was only accurate in certain composition regions and when compared to volumetric data the best agreement was about 20%. Actually, the method may seem similar in structure to the classic IAS theory (Myers and Prausnitz, 1965) but the IAS theory includes the necessary concept of spreading pressure equality. Hence, the lack of accuracy is not surprising. However, at the time this method was suitable as a first approximation.

2.7.2.2 Constant Separation Factor Method

This was proposed by Lee *et al.*(1984). The major requirement is a constant separation factor, that is to say an ideal binary system. Although this may seem a severe limitation, surprisingly many systems have been shown to exhibit such behaviour. Usually, this ideality will require components with similar molecular properties. The separation factor is obtained by integrating the pure component isotherms according to a method proposed by Lewis *et al.*(1950). This method actually requires a thermodynamic consistency test proposed by Broughton (1948). Once the separation factor is obtained, the binary isotherms can be obtained with explicit equations. With the resultant phase diagram, the selectivities can be obtained as a function of composition and these can be compared with the original *Lewis* selectivity. Obviously, agreement of this selectivity with those across the whole composition range will confirm the validity of the binary predictions. However, despite its inherent attractions, this method has received very little attention in the literature, not even as a first approximation.

2.7.3 Pure Component Isotherm Extension

The first requirement for this type of method is that all the pure-component data can be fitted to a particular isotherm by regression. The most frequently cited examples are the Langmuir isotherm (Langmuir, 1918) and the Langmuir-Freundlich isotherm (Sips, 1948). There have been many variations on the Langmuir equation, and these can be found listed in the paper by Abdul-Rehman *et al.*(1990). Once this is achieved the equation is extended to the multicomponent case by keeping the same numerator but adding the terms on the denominator.

2.7.3.1 Extended Langmuir Isotherm

The most widely used extension is that of the Langmuir proposed by Markham and Benton in 1931. This has met with mixed reactions from various workers: Verelst and Baron (1985) have obtained very good predictions for mixtures of oxygen and nitrogen on 5A zeolite whereas Miller *et al.*(1987) report poor predictions for the same system but at lower temperatures. Also, Miller (1987) reports that the method fails for the same system but on 13X zeolite.

2.7.3.2 Loading-Ratio Correlation

This was proposed by Yon and Turnock (1971). It is very similar to the pure Langmuir and Langmuir extension except that the monolayer amount is replaced by the maximum attainable loading. They employed the data of Lederman and Williams (1964) who studied the adsorption of alkanes on 5A zeolite. It has received very little attention in the literature.

2.7.3.3 Inclusion of Binary Interaction Parameters

Schay (1956) extended the Langmuir isotherm to account for molecular interaction (non-ideality). However, this will require some binary data so the approach will become slightly correlative. Ritter and Yang (1987) have shown that up to quaternary data on activated carbon can be successfully predicted at moderate pressures. Chen *et al.*(1990) have stated that up to ternary data on 5A zeolite can be moderately predicted at high pressures. These results are not surprising since higher pressures will increase the degree of non-ideality. Yon and Turnock (1971) also employed interaction parameters but the predictions were still only as good as the IAST theory. Of course this theory assumes an ideal adsorbed phase.

2.7.4 Statistical Thermodynamic Theory

The statistical thermodynamic theory was extended to binary systems by Ruthven *et al.*(1973). This model is only valid for zeolites. For non-polar molecules such as saturated hydrocarbons, this model has been shown to provide a good representation of the pure component isotherms and a good prediction of binary isotherms (Loughlin *et al.*,1976). However the assumptions of this 1973 paper preclude localised adsorption and Holborow and Loughlin (1977) have shown that systems containing carbon-dioxide or unsaturated hydrocarbons will give poor predictions (localised adsorption is more likely for polar molecules). Ruthven and Wong (1985) extended the theory to solve the localisation problem and this improved the predictions.

2.7.5 The Potential Theory

This theory was introduced by Polyani in 1914 and many workers have tried to extend it to gas mixtures. One such method was by Grant and Manes (1966). However, this variation would only work for activated carbon and failed for silica-gel and zeolites. A review by Valenzuela and Myers (1984) utilised binary adsorption data for many adsorbents and gas systems. It compared some of the predictive methods by calculating an average selectivity error. This will be discussed later, but it concluded that the average error for the Potential method was the worst and was 80% The unique thing about this method is due to the fact that the pure component curve is independent of temperature. Thus, having obtained the potential curve at a particular temperature, this should then enable prediction of the mixture equilibria at any other temperature.

2.7.6 The Vacancy Theory

This is the most recent of the predictive theories and was proposed by Suwanyuen and Danner (1980). Basically, the theory is concerned with treating the adsorbed phase as a mixture of adsorbed species and vacancies; a vacancy being a vacuum entity which can occupied by an adsorbed molecule. The equilibrium theory so derived includes these vacancies. Firstly, a particular isotherm was developed to fit the pure component data and then this was extended to mixtures by considering activity coefficients in the calculations. A two-coefficient Margules equation was employed for which Cochran *et al.*(1985) has stated is inappropriate for adsorption equilibria. These authors then used the classic Wilson equation for which the predictions were better. Later variations of this method included using different equations to represent the activity coefficient variation and the predictions were seen to improve.

2.7.7 Gibbs Adsorption Isotherm Development

At first this seems a very clever technique. Van Ness (1969) suggested taking the classic Gibbs Adsorption isotherm, applying it for two components and then obtaining an explicit expression for the adsorbed phase requiring only the total amount adsorbed as a function of composition. There is a case for putting this method under the section for direct methods since gravimetric measurements are required. Of course there is an added complication; the equation requires the moles adsorbed whereas the measurement will be the mass adsorbed and the average molecular weight depends upon the composition. Recently this method was cited by Myers (1986) who represented the calculations as two first order partial differential equations. However, the same author stated that despite the method being rigourous, too many data points would be required. The author then went on to modify the method by involving the classic Wilson equation multiplied by a function of spreading pressure. Although a numerical algorithm is required, the number of data points is considerably reduced. The latest modification was by Ritter and Yang (1989). So far the Gibbs equation has used pressure instead of fugacity. This assumption is only valid if the gas is at low pressure and this is not always possible. These authors extended this method to binary systems at high pressures. Because of the requirement of fugacities, the spreading pressure equation includes the adsorbate composition and so the method becomes iterative.

2.7.8 Adsorbed Solution Theory

2.7.8.1 Introduction

These are by far the most frequently used in the literature. The idea was first formulated by Myers and Prausnitz (1965), when they considered the concept of spreading pressure. The theory was first termed the Ideal Adsorbed Solution Theory (IAST) and since then there have been over 200 citations of the original paper. Also there have been modifications to try and account for non-ideality and heterogeneity.

2.7.8.2 The Ideal Adsorbed Solution Theory (IAST)

As the name suggests, this assumes that the adsorbed phase is ideal, that is to say, the activity coefficients are unity. In spite of this apparent severe limitation, surprisingly many systems have been shown to exhibit such behaviour. For example, sometimes the pure components can be fitted to particular pure component isotherms (for example Langmuir, Freundlich, Dubinin-Raduschkevich) and the predictions can be obtained by solving equations iteratively. However, the success will depend upon a good regression especially in the low pressure region (Richter *et al.*, 1989). However, for two components a graphical method can be employed. One possible drawback of this method is that the pure component data for one or more of the components may be required at pressures far in excess of the mixture pressure. Even for systems that are non-ideal, a comparison between the predictions and the volumetrically obtained data will give a qualitative idea of the adsorbed phase activity coefficients (Myers, 1965). These coefficients can also be obtained quantitatively, although this method has never been repeated; Glessner and Myers (1969) incorporated the Margules activity coefficient equation in their calculations and solved it to obtain the two coefficients and hence obtain the complete range of activity coefficients. They demonstrated the non-ideality of methane and carbon-dioxide on 5A zeolite.

2.7.8.3 The Real Adsorbed Solution Theory (RAST)

This was formulated by Costa *et al.* (1981). This variation allows for non-ideality by incorporating the Wilson equation (Wilson, 1964) into the IAST. However, the Wilson parameters must be obtained by regression of binary data which means the data must be obtained by a direct method. The method thus becomes correlative. At first sight this may seem to defeat the object since the whole point is to *predict.* However, once obtained these parameters can be used to predict multicomponent adsorption equilibria; the Wilson equation only requires binary parameters. Costa *et al.* (1981, 1989) showed the RAST to be superior to the IAST for the adsorption of hydrocarbons on activated carbon. Recently, Costa *et al.* (1991) have obtained adsorption data directly for hydrocarbons on 13X zeolite and they will be discussing the applicability of the RAST in a future paper.

2.7.8.4 The Non-Ideal Adsorbed Solution Theory (NIAST)

The previous method of Costa *et al.*(1981) depends upon an analogy between vapour-liquid and gas-solid equilibria. This assumes that the activity coefficients are a function of pressure whereas they are a function of spreading pressure (Myers and Prausnitz, 1965). Hence the RAST becomes thermodynamically inconsistent. Thus the RAST can only be used if the spreading pressure is constant; this is practicably impossible to achieve since normally the system pressure remains constant while the spreading pressure varies with composition (Talu and Zwiebel, 1986) To overcome this deficiency in the RAST, a spreading pressure dependant (SPD) equation was proposed to evaluate the adsorbed phase activity coefficients. For binary systems it can be used in either a predictive or correlative mode. The latter requires tabulated molecular properties, but the former is much more powerful; it only requires a couple of experimental points from each binary system and then prediction of ternary and higher component systems can be attempted. Talu and Zwiebel (1986) considered highly non-ideal systems on H-mordenite and showed this method to correctly predict the azeotropes much better than the RAST.

2.7.8.5 Heterogeneous Ideal Adsorbed Solution Theory (HIAST)

The latest development has been to try and account for the heterogeneity of the surface. Generally, what is meant by this type of surface is a variation in activation energy. There is still much research to determine the variation function but often a Gaussian function is employed. Valenzuela *et al.*(1988) were the first workers to actually use the term HIAST and they applied the theory to the non-ideal data of Talu and Zwiebel (1986) and showed dramatic improvements over the IAST. Moreover, Valenzuela *et al.*(1988) stated that other factors apart from the actual surface will determine the effects of heterogeneity. Firstly, if each component has roughly the same standard deviation in activation energy, then the method will reduce to the IAST. Secondly, a reduced system pressure will mean that the band of sites occupied will have a small range of activation energies and so the method will also reduce to the IAST. Finally, for components having larger molecules, these molecules will be spread over more sites as opposed to the smaller molecules which will tend to occupy the high energy sites. Thus, for components having large molecules, the predictions will tend towards IAST. Finally, developments in heterogeneous theory have implications concerning the usefulness of activity coefficients obtained from the IAST, RAST and NAST. Neglecting heterogeneity, then this will manifest itself as non-unity activity coefficients. Myers (1983) showed this quantitatively using a simple two-activation energy model, whereas in reality the spread in activation energy will be much greater. Also, the fact that the HIAST gave improvements over the IAST for the "non-ideal" data of Talu and Zwiebel (1986) means that the subsequently obtained "activity coefficients" are not entirely due to non-ideality.

2.7.8.6 Analytical Expressions for Binary Isotherms

This is really a direct application of the IAST, although it is listed separately because of its novelty value. This was proposed by LeVan and Vermeulen (1981). The basic requirement is that the pure components obey either the Langmuir or Freundlich isotherms although presumably this method could also be extended to other isotherms. Once this can be established, the IAST can be used to obtain *explicit* expressions for both binary isotherms. This is the only example of a thermodynamically consistent explicit expression for binary isotherms, and surprisingly this method has received very little attention in the literature.

2.7.8.7 Other Thermodynamic Methods

Thermodynamic methods are so named because they are independent of any particular theory of adsorption. The most cited thermodynamic method is the previously discussed IAST. Sircar and Myers (1973) have demonstrated that the methods of Kidnay and Myers (1968), Lewis *et al.*(1950), Arnold (1949) and Cook and Basmadjian (1965) are based upon the IAST but differ in their choice of standard state. The IAST is based upon all mixture components having equal spreading pressures and this being the same as the mixture. Of the rest of these thermodynamic methods the Lewis correlation has received by far the most citations. Although this method cannot completely define the system it provides an empirical way relating the amount of each component adsorbed to that which would be adsorbed by the pure component at the same total pressure. The original authors first employed this correlation successfully for mixtures of hydrocarbons on silica-gel and activated carbon, although Dorfman and Danner (1975) applied this correlation successfully to mixtures of nitrogen and oxygen on 10X zeolite.

2.8 Papers Concerning Gas-Mixture Adsorption on 5A Zeolite

1. Sorial *et al.*(1983): Volumetric Determination
Pure components and binary mixtures of oxygen and nitrogen.
System temperatures of 273.15, 293.15 and 303.15 K
System pressures of 1.7 and 4 bar
Note: IAST gives very good predictions from pure components.

2. Verelst and Baron (1985): Volumetric determination
Pure components and binary mixtures of nitrogen, oxygen and argon.
(However, argon is considered the same as oxygen and so the binaries containing argon are not investigated)
System temperatures of 298.6 and 319.9 K
System pressures of 1.04, 3 and 4 bar
Note: Multicomponent Langmuir and Ruthven Statistical give good predictions from pure component isotherms.

3. Robinson and Thomas (1980): Breakthrough Curves
Pure components and binary mixtures of methane and ethane.

4. Crosser and Hong (1980): Volumetric Determination
Pure components of propylene, propane and carbon-dioxide; binary mixtures including carbon-dioxide.

5. Danner and Wenzel (1969): Volumetric Determination

Pure components and binary mixtures of oxygen, nitrogen and carbon-dioxide.

System temperatures of -200 F

System pressures of 1 bar

Note: Multicomponent Langmuir gives poor predictions but the IAST gives good predictions for the oxygen-nitrogen binary.

6. Chen *et al.*(1990): Volumetric Determination

Pure component, binary, ternary, and quaternary mixtures of hydrogen, methane, carbon-dioxide and carbon-monoxide.

7. Veyssiere *et al.*(1981): Volumetric Determination

Pure component and binary mixtures of methane, ethane and carbon-dioxide.

8. Ruthven (1976): Volumetric Determination

Pure component and binary mixtures of oxygen, nitrogen, methane and carbon-dioxide.

System temperature of 145 K

System pressure of 1 bar

9. Holborow and Loughlin (1977): Volumetric Determination

Pure component and binary mixtures of ethylene, propane and cyclo-propane.

10. Loughlin *et al.*(1990): Volumetric Determination

Pure component, binary, ternary and quaternary mixtures of methane, propane, ethane and n-butane.

11. Peterson and Redlich (1963): Volumetric Determination

Pure component and binary mixtures of normal paraffins.

12. Loughlin *et al.*(1975): Volumetric Determination

Pure component and binary mixtures of ethylene and cyclo-propane.

13. Lederman and Williams (1964): Volumetric Determination

Pure component and binary mixture of nitrogen and methane.

14. Glessner and Myers (1969): Volumetric Determination

Pure components and binary mixtures of ethane, n-butane and carbon-dioxide.

15. Persichini and Mersmann (1990): Volumetric Determination

Pure component and binary mixtures of ethane, ethylene and carbon-dioxide.

16. Miller *et al.*(1987): Volumetric Determination

Pure component and ternary mixture of nitrogen, oxygen and argon.

17. Ruthven and Kumar (1980): Chromatographic Determination

Many mixtures and pure components are studied; included are the binaries nitrogen-argon and nitrogen-oxygen.

System pressure of 760 torr

System temperature of 298 and 304 K

Note: Results not compared with static data but with statistical data

18. Shah (1988): Chromatographic Determination

Many mixtures and pure components are studied; included is the binary oxygen-nitrogen.

System pressure of 750 torr

System temperature of 298 K

Note: Chromatographic method criticised

19. Van der Vlist and Van der Meijden (1973): Chromatographic Determination

Pure component and binary mixture of oxygen and nitrogen.

System pressure of 1 bar

System temperatures between 10 and 50°C.

Note: No independent comparison of data

20. Mason and Buffham (1990): Chromatographic Determination

Binary mixture of argon and nitrogen

System pressure of 1.2 bar

System temperature of 50°

2.9 Conclusions from Literature Searching and Application to Research Project

1. From the literature there are many actual or possible gas separations which involve only two components. Even in some of the applications involving three components, two of these components can be lumped together. Hence, binary data obtained from the chromatographic method could be useful purely for process feasibility and design.

2. Binary data would also be useful to test the various methods which predict binary data from pure component data. The pure component data would be required over a particular pressure range, and this would have to be obtained from another method.

3. To account for non-ideality the latest predictive methods correlate binary data and use only these binary parameters and the pure-component data to predict ternary and higher order data. So the chromatographic method could provide binary data for correlation purposes.

4. While there is still a reasonable amount of literature data for binary mixtures, data for ternary mixtures is still relatively scarce. There are many processes which involve three components and it is not always possible to lump two components together. When the chromatographic method is extended to three components, it will provide quick data for process feasibility and design. Also, the extended method could provide ternary data for testing the various predictive methods which use only pure-component data. Finally, the extended method could provide ternary data for testing the various methods which correlate the binary data.

5. So far all the attention has been on obtaining mixture isotherms. One of the reasons was that direct methods are very cumbersome when applied to mixtures. However, it would also be desirable for the same method to be adapted to obtain pure component isotherms. Firstly, these could be used in evaluating the various predictive methods and secondly this data could be used to obtain various thermodynamic data. Of course pure component data can be obtained from binary mixture data; the binary isotherm end points will give the amount adsorbed at the system pressure, but these will necessitate experiments across the whole range so that integration can be carried out. Even then this method is restricted to pressures above atmospheric. Experimentally, this would require some form of vacuum arrangement to enable sub-atmospheric pressures to be obtained.

6. The list of papers reporting gas-mixture adsorption data for the 5A zeolite show some interesting facts. Firstly, only one paper reports data for the argon-nitrogen system and no papers report data for the helium binary systems. Furthermore, the data for the argon-nitrogen system is obtained using another chromatographic method and is *not* confirmed independently by a static method. Many papers report data for the oxygen-nitrogen system because of the industrial importance of air separation. It can be seen that for most papers, both the pure-component and binary mixture data is obtained independently by a static method. Then, one or more of the predictive methods is used to try and obtain the binary mixture data. The chromatographic method investigated in this thesis should be able to save much experimental time.

Chapter Three

EXPERIMENTAL ARRANGEMENT AND DESCRIPTIONS

3.1 Introduction and Main Gas Circuits

In Chapter One, the main experimental and theoretical advances were summarised which were current at the time of project commencement. This chapter is concerned with presenting the experimental arrangements and specifications at the project conclusion. Actually, not all the project results were obtained with the latest arrangement; some of the modifications have come about from critical appraisal of the results. Two in particular are mentioned in later chapters. Firstly, the employment of a *chromatography pig* to reduce the oven thermal noise is described in Chapter Five, this chapter being concerned with the heat effects in the oven. Secondly, the development of a mixing device to enable the trace flow to be added to the carrier is described in Chapter Six.

Before describing in detail the various parts of the system, it is helpful to consider the purpose of each part in relation to the gas circuits; Figure 3.1 shows the system block diagram. The three gas cylinders each supply the carrier gas mixing system (CGMS) and the perturbation gas selection system (PGSS). Additionally, the CGMS supplies a perturbation gas having the same composition as the mixture. Thus the PGSS allows one of four gases to be selected. The carrier gas is mixed at the pressure indicated by the upstream back pressure regulator (BPRU). Actually, the carrier gas flowrate is determined by this pressure as well as the main flow resistance, namely the capillary chokes (CC). Before entering the CC, the carrier gas is split into two flows, one for each column. A needle valve (NV) is located downstream of each CC, the purpose being to trim the flowrates in each column to the same value.

Meanwhile, in the PGSS, the required perturbation component and flowrate is selected; this then flows to the modified 3-port valve (M3PV) where it can be added to the required column carrier flowrate. The perturbation gas is actually contacted with the carrier in the mixing device (MD). Both carrier flows then pass through a valve arrangement where the upstream delay-lines (of the column) can be employed (UDL) if required. From this valve arrangement, both carrier flows pass into the oven which contains matched columns packed with the required adsorbent at the required column temperature. After leaving the columns, both carrier flows then pass through the thermal conductivity detector (TCD) which is still located in the oven. From the oven, both carrier flows pass through the downstream delay-lines (DDL) before entering the differential flow measurement arrangement (DFM). Then both carriers are combined and pass through the downstream back pressure regulator

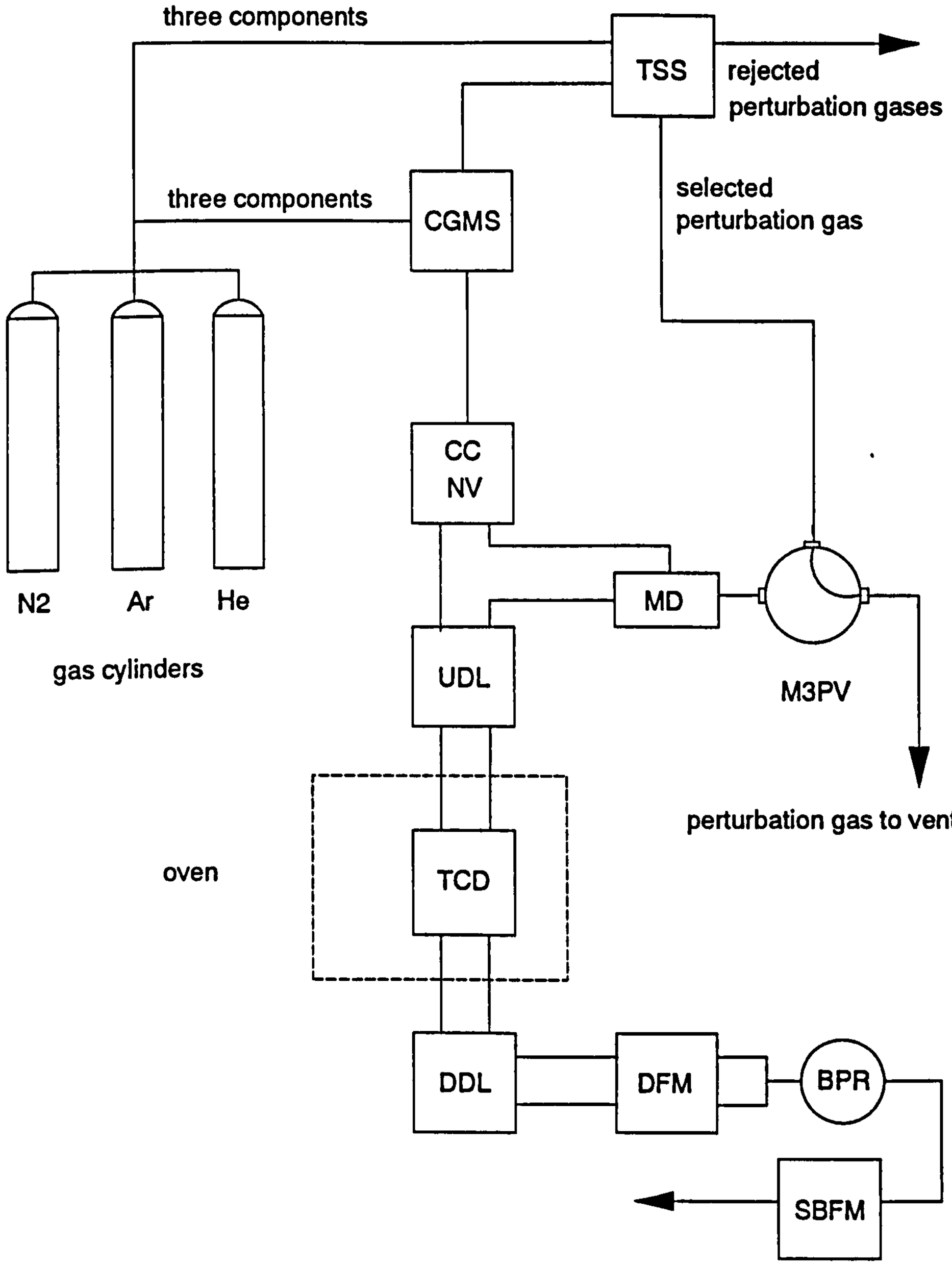

Figure 3.1 Block Diagram Showing Main Components and Gas Routes

(BPRD). This regulator is usually set to some low value, typically 0.1 bar. The output from the regulator vents at atmospheric pressure into a soap bubble flowmeter (SBFM) where the total carrier flowrate is measured.

3.2 Component Descriptions

3.2.1 Introduction

In the previous section, the main functions of the apparatus were described in relation to the main gas circuits. In the following sections, these will be further described. However, in these following sections it will be seen that particular *equipment components* are referred to, some with great regularity. It is the purpose of this section to describe these equipment components in sufficient detail to enable a reasonable understanding of the main functions of the apparatus. Where applicable, acronyms will be employed.

3.2.2 Delay-Lines

A delay-line is simply a length of tubing which will delay the passage of a front through the system; it is effectively dead volume. The position of these delay-lines relative to the other components in the apparatus can vary, and a subscript is employed to specify the location. These locations are further described in Chapters Six and Seven. Nylon tubing having two different external diameters was employed, namely 1/8 inch and 1/4 inch. Various lengths were employed ranging from 10 to 60 metres. Obviously, the internal volume of the tubing will determine the time for the front is delayed. One of the problems of operating such a chromatograph is that of temperature fluctuations: if one of the delay-lines is held, the increase in temperature will cause the gas to expand and this will register as a flowrate change. This can be a problem if these random fluctuations obscure the flowrate variation of interest when a perturbation is made to the system. Hence, it is desirable to place the delay-lines in an insulated box. The subject of heat transfer is further discussed in Chapter Five.

3.2.3 Rotameters

In the carrier gas mixing system, rotameters are used to monitor the flowrate of each component. A rotameter basically consists of a tapered tube with the smallest diameter at the bottom. The tube contains a freely moving float which rests on a stop at the bottom of the tube when there is no flow. When the fluid is flowing, the float rises until its weight is balanced by the upthrust of the fluid, the position of the float indicating the flowrate. The pressure difference across the float is constant and does not depend upon the flowrate. However, the area for flow is the annulus between the float and the tube wall; this will increase with float height. Rotameters are also known as *variable area meters*. From Coulson and Richardson (1982a), the following equation is used to characterise the rotameter:

$$G = C_D A_2 \sqrt{\frac{2g V_F(\rho_F - \rho)\rho}{A_F\left(1 - \left(\frac{A_2}{A_1}\right)^2\right)}} \qquad 3.1$$

where G = mass flowrate

C_D = coefficient of discharge

A_1 = tube cross sectional area

A_2 = area of annulus between the tube and the float

A_F = maximum float cross sectional area

g = acceleration due to gravity

V_F = float volume

ρ_F = specific float density

ρ = fluid specific density

The coefficient of discharge, which depends upon the float shape and the Reynolds number of the fluid flow through the annulus, characterises the frictional losses; the maximum value of one corresponds to zero losses. In Coulson and Richardson (1982a) graphs of C_D are shown for various float shapes. Although, the rotameters used in the project have spherical floats, and this float shape is not covered in the book. For liquids, it is conventional to obtain the rotameter complete with the flowrate scale, albeit for a specified temperature. This is because liquid flow is considered compressible; the density varies negligibly with pressure. However, for gases the scale is simply in terms of the float position. A graph is usually supplied to give the flowrate at ambient conditions. This is because the actual *mass flowrate* is dependent upon the pressure and the temperature. For an ideal gas, the following equation can be written:

$$P = \frac{\rho R T}{M_W} \qquad 3.2$$

where M_W = molecular weight of gas component

P = absolute gas pressure

Also for gases it can be assumed that $\rho_F \gg \rho$ and so Equation 3.1 can be re-written:

$$G = C_D A_2 \sqrt{\frac{2g V_F \rho_F P M_W}{RTA_F\left(1 - \left(\frac{A_2}{A_1}\right)^2\right)}} \qquad 3.3$$

This means that for a given float and float position, G is proportional to $\sqrt{P}$ and inversely proportional to $\sqrt{T}$.

3.2.4 Back Pressure Regulator (BPR)

The purpose of the BPR is to maintain a constant *upstream* (of the regulator) pressure regardless of any variation in flow through the regulator. For the gas to pass through the regulator, it must first push open a diaphragm which is held shut by a spring in compression. The diaphragm is contained in a chamber which is connected to the atmosphere via a small hole. Thus, for gas to escape, it must have a total pressure of atmospheric plus the spring pressure; the gauge pressure will be the spring pressure. The range of back pressures available can be extended by using a spring of increased stiffness. The BPR employed is a Porter Model 9000.

3.2.5 Pressure Regulator (PR)

The purpose of the PR is to maintain a constant *downstream* (of the regulator) pressure regardless of any changes in supply pressure. The PR employed is a Porter Model 8286 which utilises a pneumatic balanced poppet valve to ensure a constant outlet pressure. As for the BPR, a spring arrangement is used to select the outlet pressure. There is a constraint regarding efficient operation of the PR; a minimum pressure drop of ten psi is required.

3.2.6 Needle Valves (NV)

Needle valves are designed to allow fine adjustments to be made to the gas flowrate. In the apparatus, Nupro M Series valves are employed. Flow adjustment is achieved by a variable flow resistance in the form of a needle valve which can be screwed in to restrict the gas flow and increase the NV pressure drop. When adjusting the NV a complication concerns the internal NV volume, which although is minimised, will vary with valve position. As the needle valve is screwed out to reduce the resistance and increase the flowrate, there will be an increase in the internal volume and hence system volume. This extra system volume will require extra gas and so there will be a temporary decrease in the flowrate. Conversely, as the needle valve is screwed in to reduce the flowrate, there will be an overall reduction in system volume and the extra gas will be pushed out leading to a temporary increase in the flowrate. If not accounted for, this volume problem would make it appear that the valve was being incorrectly adjusted.

3.2.7 Mass Flow Controller (MFC)

A MFC is employed to *specify* and *maintain* a constant mass flow regardless of changes in *either* the upstream *or* downstream pressure. These are more complicated than the needle valves already described. A needle valve is simply a flow resistance and the mass flowrate will depend upon both the upstream *and* downstream pressures. The first sentence allows the MFC types to be divided into two categories; *downstream regulating* and *upstream regulating*. For the first category, constant mass flow regulation requires a *constant*

upstream pressure and the selected mass flow will be maintained regardless of any change in downstream pressure. A pressure regulator situated upstream of the MFC would maintain the required upstream pressure. For the second category, a *constant downstream pressure* is required and the selected mass flow will be maintained regardless of any change in the upstream pressure.

Similar to the BPR, the MFC contains a spring which is acted upon by a control stem; this arrangement is used to set the *differential pressure* across the *flow resistance*. This will then set the mass flow which the MFC should maintain. The value of the flow resistance will determine the *maximum* or *span flowrate*; the flowrate obtained when the control stem is rotated to obtain the maximum differential pressure. The form of this flow resistance will depend upon the make of MFC. For the Porter Model 1000, a coloured flow element is selected and screwed in to the controller body. Different colour elements correspond to different flowrate ranges. However, for the Condyne Model 202, a needle valve is adjusted to set the span value; to set a low span value, the needle valve must be screwed in tightly.

3.2.8 Switching Valves

In analytical chromatography, switching valves are usually employed to enable samples to be injected onto the columns. These switching valves can be divided into two categories; *internal sample injector* and *external sample injector*. For the former category, the sample volume is fixed and located within the valve. For the latter category, the sample volume is formed by linking two ports and the total volume between these ports forms the sample volume. In the project, the latter type will be employed, but it will be used to swap streams. Switching valves work by connecting adjacent ports to each other and they are usually *two-position*; in one position each port is connected with *one* of its adjacent ports and in the other position each port is connected to its *other* adjacent port. For analytical chromatography, in one position the sample loop is filled with sample gas and in the second position the carrier gas sweeps away the sample. Figure 3.2 shows the two valve positions for both three-port and four-port valves. In further diagrams, however, these switching valves will be represented without the flow paths.

The company Valco manufactures a wide range of these switching valves. The number of ports can vary from three to ten. The port dimensions are chosen to be either 1/8 inch or 1/16 inch; for switching small perturbation flows the latter port size is used but for switching carrier flows the former port size is used to reduce any pressure drop across the valve. The valve specification also include operating temperature and operating pressure.

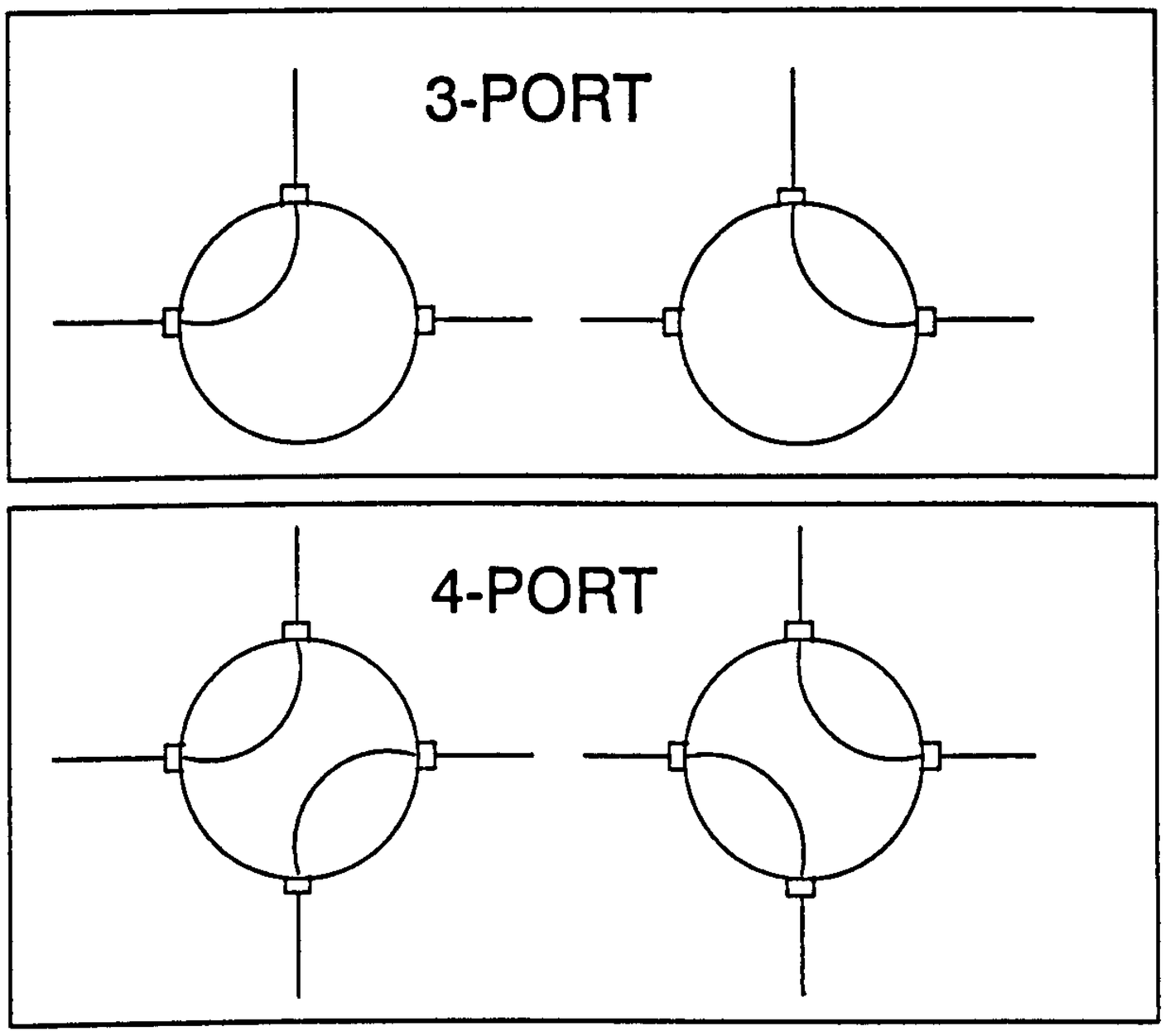

Figure 3.2 Representation of Both Valve Positions for Three-Port and Four-Port Switching Valves

3.3 Carrier Gas Mixing System

Figure 3.3 gives a schematic representation of the gas-mixing system employed. Each gas cylinder is connected directly to the respective MFC which supplies the respective rotameter. The outputs from these rotameters are combined and fed into the inlet port of the upstream back pressure regulator (BPRU). The BPRU is adjusted to give the required system pressure and hence carrier flowrate. It must be ensured that the venting rotameter registers a flowrate to ensure that the system pressure is valid.

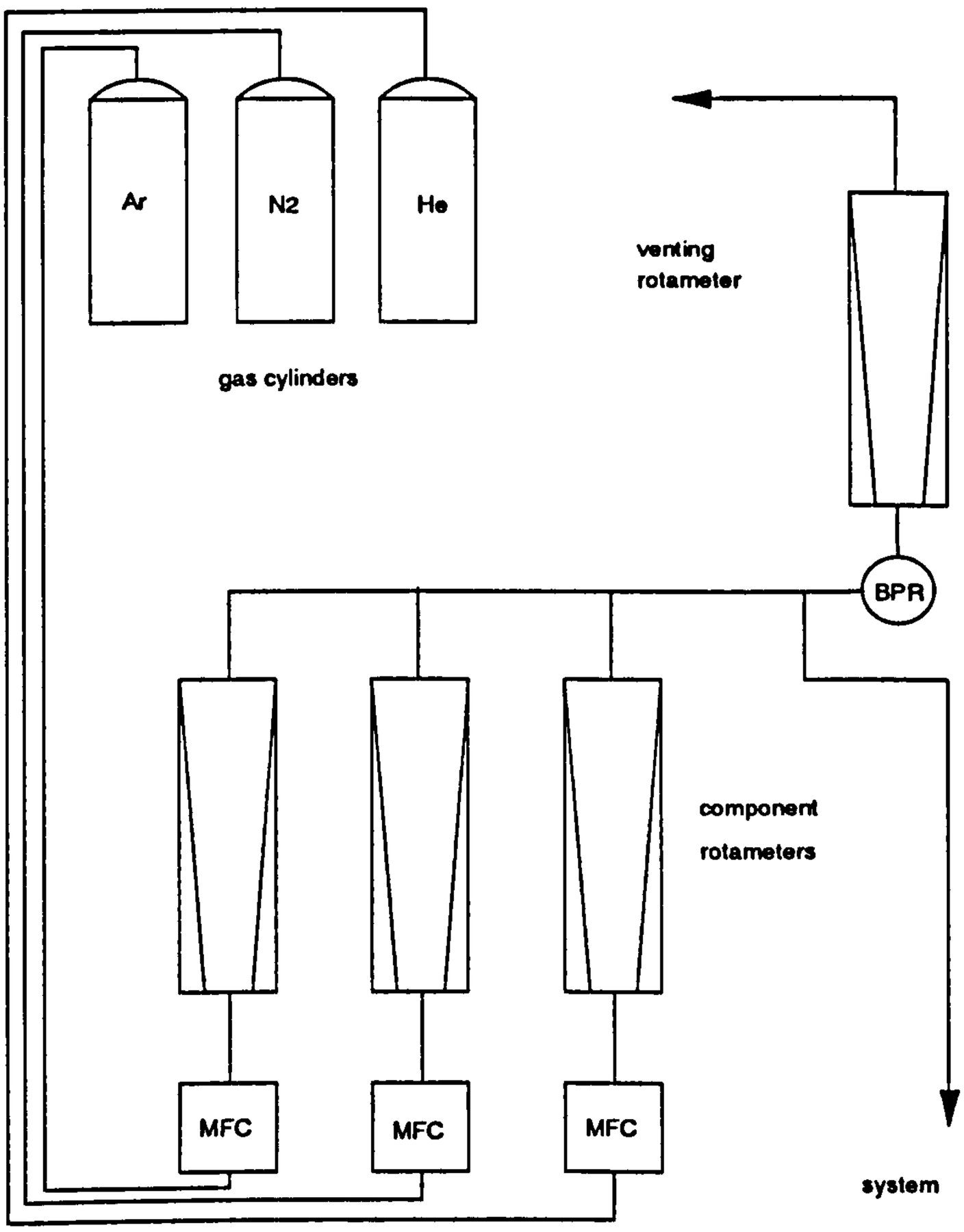

Figure 3.3 Schematic Representation of Gas Mixing System

The required gas mixture composition is set by adjusting each respective MFC to give a required rotameter reading; rotameter readings are pre-selected to give volumetric flowrates in the proportion corresponding to the required gas mixture composition. Thus before use, it is necessary to calibrate each component rotameter by obtaining graphs of volumetric flowrate against rotameter position at constant atmospheric pressure and constant ambient temperature. Although the calibration is carried out at atmospheric pressure, the graphs can be used for any system pressure. Appendix A contains the calibration graphs for nitrogen, argon and helium.

3.4 Flow-Setting Chokes

These simply consist of 150 cm lengths of 1/16 inch stainless-steel tubing with an inside diameter of 10/1000 inch. Because of the high tubing resistance, it was necessary to have both lengths as close as possible. The transducer detects flowrate difference between each side of the system and any difference between the choke lengths (flow resistances) will cause a flowrate difference and shift the effective chart-recorder zero: this is the chart-recorder position when there is no perturbation gas being added to the system. Obviously, if the choke length difference is small enough, the zero can be shifted by slight adjustment of the respective needle valve. However, if the flowrate difference is too large, the zero will be shifted too far and it will not be possible to record the flowrate transient when the perturbation gas is added to the system. A needle valve was positioned downstream of each choke for fine flow adjustment. Originally, each NV was exposed and each CC placed in a water bath. However, because of the NV resistance sensitivity to temperature, each NV and CC were later placed in a large thermostatically controlled oven with a modified door. For convenient adjustment, each NV was attatched to a hole in the plastic door. When using standard columns and standard packing, the chokes were found to account for about 90% of the total pressure drop. Hence, it is important to maintain the chokes at constant temperature; any change in temperature will change the flow resistance and hence the chart-recorder reading.

3.5 Perturbation Gas Selection System

Figure 3.4 gives a schematic representation of how the required perturbation gas is selected, measured and then added to the carrier. All the valves shown are two-position; each port is connected to *either* of its neighbours. The required perturbation gas is selected by appropriate use of the three 4-port valves (4PV). With three valves, any one of four perturbation gases can be selected. Each of the three pure perturbation flows passes through a PR before entering the respective MFC. Each PR is set to 30 psi and ensures that the perturbation flowrate remains constant, assuming that the regulator pressure does not fall below 30 psi. The mixture perturbation flow is tapped off just upstream of the chokes and since this is at constant pressure, there is no need for another PR. If 4PV1 is set to *select*, the mixture perturbation gas will be selected regardless of the position of 4PV2 and 4PV3. Similarly, if 4PV2 is set to *select* and 4PV1 is set to *reject* then the helium perturbation gas will be selected. If both 4PV1 and 4PV2 are both set to *reject*, then either the argon or nitrogen perturbation gas can be selected by switching valve 4PV3. The three rejected perturbation flows are combined and sent through a BPR to atmosphere. One advantage

of this system is that there is no *dead volume*; when a different perturbation gas is selected, the previous perturbation gas is swept away and the new perturbation flow is quickly available.

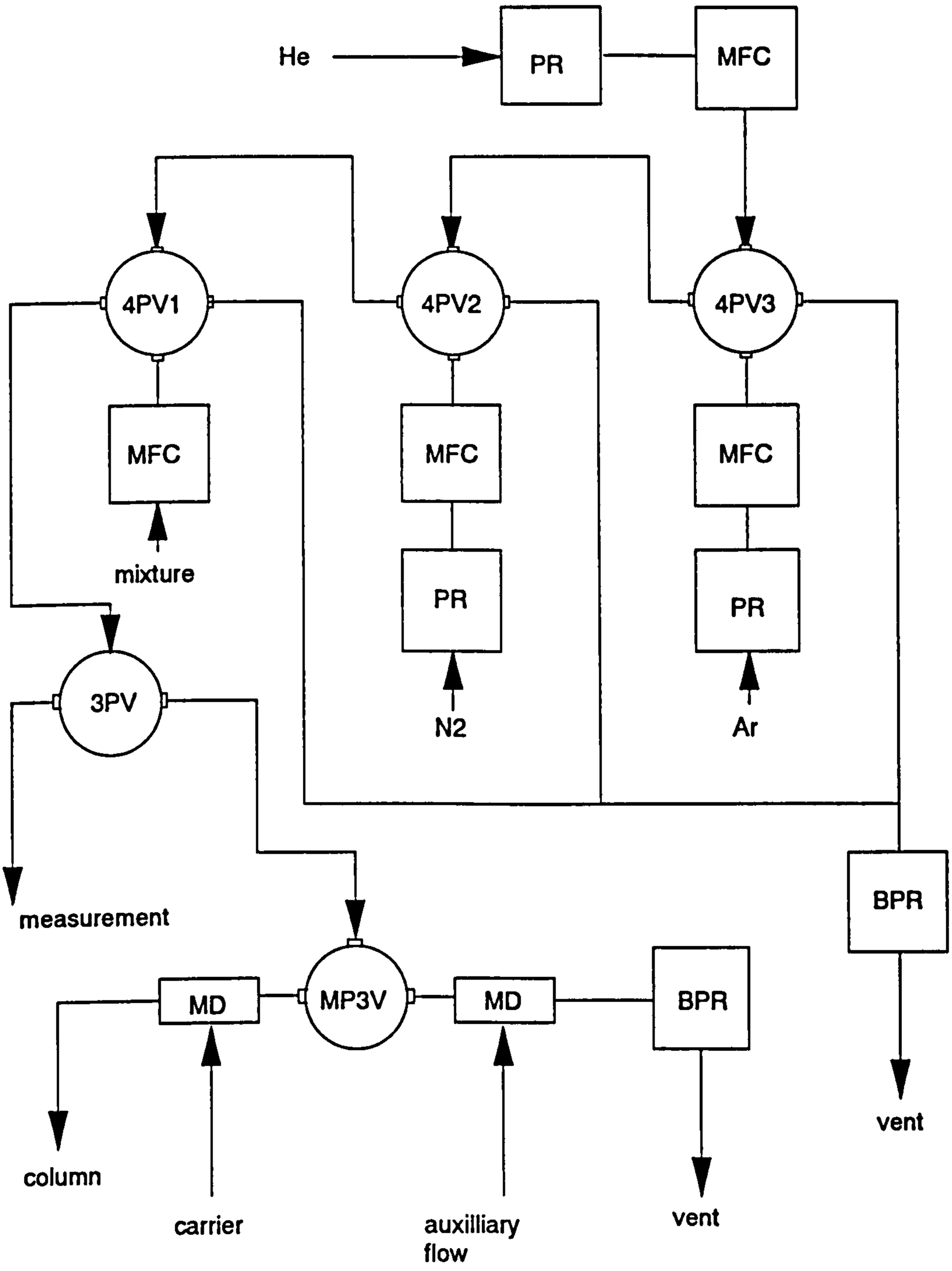

Figure 3.4 Schematic Representation of Trace Selection System

In order to measure the perturbation gas flowrate, the selected perturbation flow passes through a 3-port valve (3PV) from where it can be directed to a measuring pipette. For the experiments, the selected perturbation flow is directed to the modified 3-port valve (M3PV) where it is added, via a mixing device (MD) to the carrier flow. The MD enables addition

of the perturbation flow without any dead-volume effects; the development is described in Chapter Six. The auxiliary flow is a small mixture flow tapped off at the same position as the mixture perturbation flow. When the perturbation flow is vented, it is added to the auxiliary flow via another MD, rather than just venting through a BPR to atmosphere. The purpose of this is that the three-port valve switches the perturbation flow moves between mixtures of the same composition, eliminating any diffusion effects. All the PR are situated inside the oven. The MFC and the various selection valves are bolted to the modified oven door.

3.6 Columns Employed

3.6.1 Column Packing Material

The column packing employed was molecular sieve 5A. This is a form of zeolite A, which is a synthetically produced zeolite. The word zeolite has Greek routes and means "boiling stones", a reference to the visible loss of water observed when natural zeolites are heated. Zeolites (Barrer, 1978) are crystalline metal aluminosilicates with a three-dimensional interconnecting network structure of silica and alumina tetrahedra. This network is open and contains channels and cavities in which are located cations and water molecules. Once this water is removed, the crystal has an enormous surface area and pore volume available for adsorption. In particular, zeolites are of interest because of their capacity to adsorb gases. Calcium is the cation associated with molecular sieve 5A. Molecular sieves 3A and 4A are the potassium and sodium forms respectively. The crystals contain interconnecting cavities of uniform size separated by narrower openings of equal uniformity. Molecular sieve 5A will adsorb many different molecules; from Chapter Two it can be seen that many papers have cited this type with regard to the adsorption of commercially available gases.

3.6.2 Column Packing Size Ranges

With regard to gas flow through packed columns, it is not conventional to use pure crystals in their natural form; the very small size would lead to a high column pressure drop and a small flowrate. Hence it is usual to form these crystals into much larger *pellets*. Actually, the use of pellets can lead to other problems with regard to heat and mass transfer, and these are further discussed in Chapter Five. For the purpose of this project, four grades of pellet will be employed. Table 3.1 gives the relevant mesh ranges along with the respective size ranges.

Table 3.1 Column Packing Size Ranges Employed

mesh	d_p/mm
11-14	1.4-1.2
22-30	0.7-0.5
30-60	0.5-0.25
60-80	0.25-0.2

3.6.3 Glass Column Arrangement

Originally, standard Pye Columns of dimension 1.5m x 6mm o.d. x 4mm i.d. were employed. Because of the problem of thermal noise, these columns were surrounded by a specially constructed box. In Chapter Five, it will be seen that a major development is to coil the columns tightly and to enclose them in a glass envelope for thermal insulation; this structure is termed a *chromatography pig* and a photograph is shown in Chapter Five. Two pig versions were employed; the first was effectively a coiled version of the Pye column and the second contained a shorter, fatter column but having the same column volume. The tight coiling makes the pigs difficult to pack and often a reasonable gas cylinder pressure, namely greater than 50 psi, is required to compact the packing and remove any voids. A void is a gas space where there is no packing and this will affect the results by causing unwanted flowrate deviations.

3.7 Composition Detection

3.7.1 General Detector Requirements

The conventional chromatographic detector works by detecting changes in the carrier gas composition by monitoring a particular property of the gas mixture. The most commonly used types are the thermal conductivity detector (TCD) and the flame ionisation detector (FID). The former works by monitoring the change in thermal conductivity with gas composition, and the latter works by detecting components which produce ions upon combustion. The main requirement of the composition detectors is that there is a *significant* change in the particular property with gas composition. This means that one detector is not suitable for all gas mixtures.

3.7.2 TCD Theory

For this project a TCD was employed because it works over the entire composition range; the FID will only work with dilute mixtures in hydrogen carriers. For many years, the TCD or *katharometer* has been used to detect changes in gas composition to a high degree of accuracy. The TCD basically consists of a heated metal wire mounted coaxially within a metal cylinder; the gas mixture flows through the annulus. The metal cylinder has a high thermal mass and can be considered maintained at a constant temperature. As the gas flows through the annulus, heat is conducted from the filament to the cylinder as well as being swept away by the gas flow. From Purnell (1967), the following heat balance can be written:

$$\frac{i^2R}{J} = \frac{2\pi k_M L (T_F - T_C)}{\ln \frac{r_C}{r_F}} + HL \qquad 3.1$$

where i = filament current

R = temperature dependant filament resistance

J = mechanical equivalent of heat

k_M = composition dependant gas mixture thermal conductivity

L = cylinder length

T_C = cylinder temperature

T_F = filament temperature

HL = sum of heat losses

With a constant i, if k_M varies then so must R. Thus the filament resistance will change in proportion to the thermal conductivity change. Since absolute measurements of thermal conductivity are too tedious and difficult, a differential technique is employed; the *difference* in thermal conductivity is measured between the two column flows. Through one column the carrier alone is flowing, and through the other the carrier plus perturbation gas is flowing. Each column will have its own chamber and filament. Each filament forms one arm of a Wheatstone Bridge; the other two arms are variable resistors. When there is carrier flowing through each column (no perturbation gas added), the bridge is *balanced* to zero the bridge current. Upon adding the perturbation flow to one column, when the front reaches the filament, this filament is heated or cooled with a subsequent change in the arm resistance. The signal is amplified and recorded by the chart recorder. There are a number of possible Wheatstone bridge arrangements for a double channel katharometer and these are discussed by Purnell (1967).

3.7.3 TCD Design Employed

Basically all katharometers are of similar design; they consist of a filament within a chamber. The main difference lies in the gas flow pattern. In the simplest design, the gas flows directly over the filament and this *direct flow* design gives the most rapid response to a concentration change. However, the disadvantage is that the HL term is not negligible due to much heat being swept away before reaching the cylinder. An attempt was made to overcome this problem by locating the filament in a side chamber, so that the composition front had to reach the filament by diffusion. However, because diffusion is slow, the response of the *side-chamber* design is much slower than the previous case. This sluggishness can greatly distort the concentration profile giving a false impression of column performance. A further attempt was made to incorporate the advantages of both designs by splitting the main flow before passing one part through the filament chamber. This *semi-diffusion chamber* type is utilised in the Pye design. According to Purnell (1967), there will still be problems at high column flowrates since the splitting ratio is constant. Touloukian (1968) presented graphs of gas-mixture thermal conductivity against composition for many binary systems including the three of interest in this project; argon-nitrogen, argon-helium and nitrogen-helium. In particular, the TCD would not be applicable to the nitrogen-oxygen system at room temperature because the thermal conductivity-composition profile is virtually horizontal.

3.8 Delay-Line Arrangements

3.8.1 Delay-Line Location

For the downstream delay-lines, it is easy to remove and select the required arrangement by simply disconnecting the previous arrangement. Upon disconnection, the gas simply flows to atmosphere; there is still gas flowing through the columns and thus the columns do not become deactivated. However, for the upstream delay-lines, the situation is more complicated since disconnection will cut off the column flow and allow air to enter the columns causing partial deactivation.

3.8.2 Upstream Delay-Line System

To this end, a new valve arrangement was designed which would allow upstream delay-lines to be selected, removed or changed without stopping the carrier gas flowing through the columns; Figure 3.5 gives a schematic representation of the new valve arrangement for the front column. Because carrier flows rather than perturbation flows will be passing through, valves will be employed with the larger 1/8 inch port fittings; otherwise the pressure drop across the valve would be prohibitive.

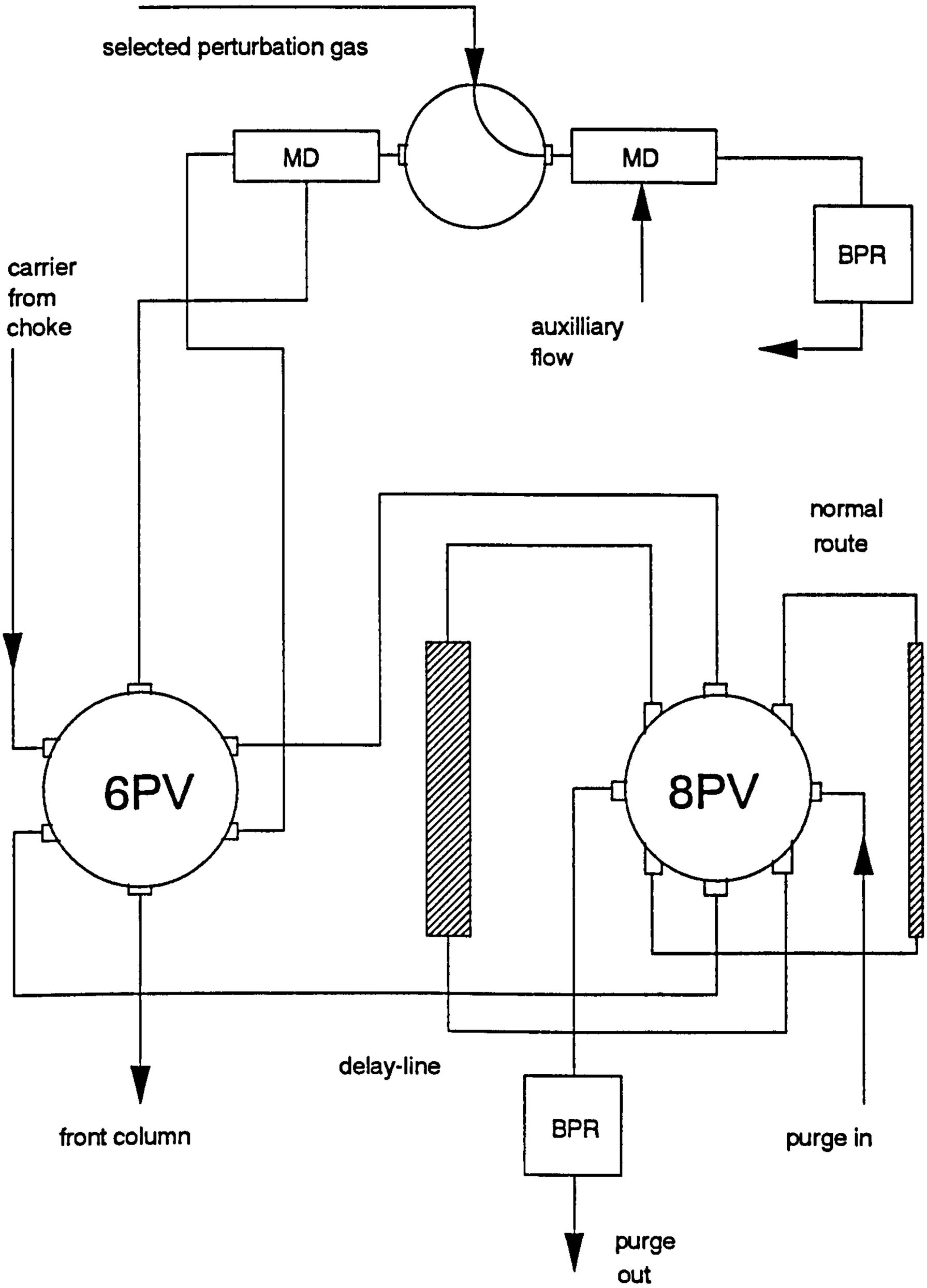

Figure 3.5 Schematic Representation of Delay-Line Selection System

It can be seen that the eight-port valve allows the carrier flow to pass through the upstream delay-lines. The purpose of the six-port valve is to place the selected delay-lines either upstream or downstream of the M3PV. It might appear that the former combination is pointless since the perturbation flow will not then pass through the delay-lines. However, this configuration is investigated in Chapter Seven. Obviously, only one leg of the 8PV can be used and the other leg is continuously purged with a small mixture flow before passing through a BPR set at about 0.1 bar. The purge ensures that when the 8PV is switched,

the selected arm is filled with carrier and *no* water vapour. When it is required to change the delay-line, the 8PV is switched to the *normal* leg and the delay-line can be replaced with the required choice. After a few minutes, all the air will have been purged out and the new delay-line will be "safe" to use. For the rear column, only an 8PV is employed since the extra location choice is not necessary. To maintain system balance, each 8PV is set to the same choice.

3.9 Differential Flowrate Detector

This detector is particular to *sorption-effect chromatography* and its development is fully described in the thesis of Meacham (1990). Basically, the detector consists of two matched pieces (25 cm length) of 1/16 inch stainless-steel tubing with inside diameter 43/1000 inch. A differential pressure transducer (DPT) is connected to both upstream outlets and measures the difference between both upstream pressures. The downstream ends are connected and fed through a BPR to atmosphere. The BPR is set to around 0.1 bar gauge. Previously, both ends were connected directly to atmosphere without the BPR. Employment of the BPR was seen to greatly reduce the ambient pressure fluctuations (Meacham,1990). The downstream pressure is considered constant and so any change in flowrate is registered as a change in the respective upstream pressure at the DPT. For streamline flow through the measuring capillary, the following equation applies:

$$P_{TU}^2 - P_{TD}^2 = M K_T L_T \mu_M R T_{AM} \qquad 3.4$$

where P_{TU} = capillary upstream pressure
P_{TD} = capillary downstream pressure
M = molar flowrate
K_T = capillary tubing type constant
L_T = tubing length
μ_M = gas mixture viscosity
R = ideal gas constant

Differentiating Equation 3.4 at constant P_{TD} gives the following equation:

$$dP_{TU} = \frac{K_T L_T \mu_M}{2} dM \frac{RT}{P_{TU}} \qquad 3.5$$

From Equation 3.5, it can be seen that the change in P_{TU} is proportional to the change in M. The signal due to the difference in the upstream pressures is amplified before being sent to the chart-recorder. Hence, the chart-recorder deviation will be proportional to the change

in M. Actually, P_{TU} appears in the denominator and it might appear that this will violate the linear relationship. However, because the perturbation is small this linear relationship still holds, although this might not be the case for much larger perturbations.

3.10 Soap Bubble Flowmeter (SBFM)

The total carrier flowrate is measured by a soap bubble flowmeter (SBFM). This works by timing a bubble between two levels in a graduated tube. It is better to send many bubbles ahead of the measured bubble since gas may diffuse through the bubble giving incorrect results at low carrier flowrates.

Chapter Four

THE VISCOSITY EFFECT AND EFFECT OF DOWNSTREAM DELAY LINES

4.1 Introduction and Previous Work

In the experimental configuration of the apparatus used by previous workers, the gas leaving the column passes directly into the flowrate measuring part of the system. This part of the system measures flowrate differences by monitoring the difference in the pressure drops down two matched capillaries: when a perturbation is made to one side of the system, the change in flowrate will change the pressure drop down the respective capillary by changing *only* the capillary upstream pressure (the capillary downstream pressure remains constant). However, this change in the capillary pressure drop will also depend upon the change in gas-mixture viscosity; a perturbation gas changing the gas-mixture viscosity would change the capillary pressure drop even if there were no change in flowrate. Strictly speaking, previous arrangements measured the *pressure retention time* (τ_P), which is a combination of flow and viscosity effects indicated by a capillary flowmeter. However, from Chapter One, determination of the isotherm gradients requires the *flowrate retention time* (τ_N).

In the theoretical section, an argument is presented which develops an equation relating these two types of retention time. The theory is only approximate and the best solution is to avoid the problem by inserting lengths of tubing between the columns and the flowrate measuring capillaries; this will give a delay between the flowrate fluctuations and the viscosity change fluctuations. This should enable the required flowrate retention time to be obtained directly. In Chapter Seven, results are presented for four systems, with and without delay lines. Thus sets of both types of retention times can be directly obtained and used to determine the validity of the derived equation relating these retention times.

However, this theoretical equation contains a particular function of the mixture viscosity-composition curve called the *viscosity factor*. It will be shown theoretically that the viscosity factor can be obtained directly from the chromatogram when downstream delay-lines are employed, but there still remains doubt over the accuracy of some of these measurements. Thus alternative ways of obtaining these viscosity factors will be investigated including the many gas-mixture viscosity predictive methods; these predict the whole gas-mixture viscosity curve using only the pure component viscosities and the molecular weights of each component. Finally. a new correlative method is investigated which involves employing accurately measured viscosity factors to try and predict the entire gas-mixture viscosity curve.

4.2 Definitions and Measurements of Relevant Quantities

4.2.1 Definitions and Measurements of Retention Times

The following definitions of retention time are taken from Mason and Buffham (1991). They are similar in that they can easily be obtained from the chart-recorder by measuring a particular area and dividing by the relevant offset. Thus, no calibration is required of the chart-recorder and this is a major method improvement over that of Buffham *et al.* (1986). All that is required is the chart recorder speed. The areas can be measured accurately by a planimeter, although errors can arise in the retention time when the offset is small. This problem can be alleviated by the use of a multi-channel recorder; the same flowrate signal is put into another channel with a higher sensitivity (larger chart deviations). This larger distance can thus be measured more accurately and scaled down appropriately. As has already been discussed in Chapter One, the *composition retention time* (τ_x) is defined by the following equation:

$$\tau_x = \int_0^\infty \frac{x(\infty)-x(t)}{x(\infty)-x(0)}dt \qquad 4.1$$

where $x(\infty)-x(0)$ = overall chart recorder deviation

$x(\infty)-x(t)$ = deviation between actual at time t and final position

This is the standard chromatographic measurement and is obtained using the katharometer. If the fronts are sharp, the area can be approximated as a trapezium and the planimeter is not required. Some mixtures, however, give peculiar shapes and for these the planimeter must be used. The pen colour used to record composition deviations was always red. As has already been discussed in Chapter One, direct measurement of the *flowrate retention time* (τ_N) requires sufficient delay line length between the column and the flowrate measuring capillary to enable the front leaving the column to attain a plateau before entering the flowrate measuring capillary. The flowrate retention time is defined by the following equation:

$$\tau_N = \int_0^\infty \frac{n(\infty)-n(0)}{n(\infty)-n(t)}dt \qquad 4.2$$

where $n(\infty)-n(0)$ = overall chart recorder deviation

$n(\infty)-n(t)$ = deviation between actual at time t and plateau

The term $n(\infty)$ refers to the plateau position mentioned above. Actually, the delay-length required will depend upon the sharpness; the sharper the front the less length required. The pen colour used to record pressure differentials was always blue. As has already been

discussed in Chapter One, the *pressure retention time* (τ_p) will be obtained from the blue pen when there are no delay-lines present. The pressure retention time is defined by the following equation:

$$\tau_p = \int_0^\infty \frac{\delta p(\infty) - \delta p(t)}{\delta p(\infty) - \delta p(0)} dt \qquad 4.3$$

where $\delta p(\infty) - \delta p(0)$ = overall chart recorder deviation

$\delta p(\infty) - \delta p(t)$ = deviation between actual at time t and final position

The term $\delta p(\infty)$ refers to the chart recorder position when the front has completely left the system. Unlike the flowrate retention time, there are no restrictions regarding front sharpness (eventually the pen will reach the final position).

Figure 4.1 shows the flowrate chromatograms obtained by adding an argon perturbation to a helium carrier at 25°C. The top chromatogram is obtained by employing 1/8 inch downstream delay lines of length 30 metres, and the bottom chromatogram is obtained using no delay lines at all. It is helpful to consider what the various parts of the chromatogram represent. Before the perturbation gas is added, the baseline corresponds to $n(0)$ and $p(0)$ respectively. When the perturbation gas is added, the column outlet flowrate steadily increases until the composition front reaches the column. Because the perturbation gas is the more highly adsorbed argon, the flowrate is reduced as the front passes through the column (this corresponds to net adsorption). When the front leaves the column, there is no more net adsorption and with downstream delay-lines, the pen moves to the $n(\infty)$ level. *If* there were delay-lines upstream of the column, it might be expected that the pen would reach this $n(\infty)$ level before the front reached the column. The variable n is used describe the movement of the pen because the gas composition is *constant* in the capillaries and so the differential pressure changes are *solely* due to flowrate changes. Hence the difference in levels $n(\infty)$ and $n(0)$ is proportional to the perturbation flowrate. When the front leaves the downstream delay-lines and enters the measuring capillaries, the pen moves to the $p(\infty)$ position. This final change is not due to a change in flowrate but a change in viscosity. From Equation 4.2, the integral term in τ_N is the area bounded by the dotted line and the chromatogram (this is termed I_N for convenience). If there are no downstream delay-lines present, when the front leaves the column the pen will move straight to the $p(\infty)$ position. From Equation 4.3, the integral term for τ_p is the area bounded by the dotted line and the chromatogram (this is termed I_p for convenience).

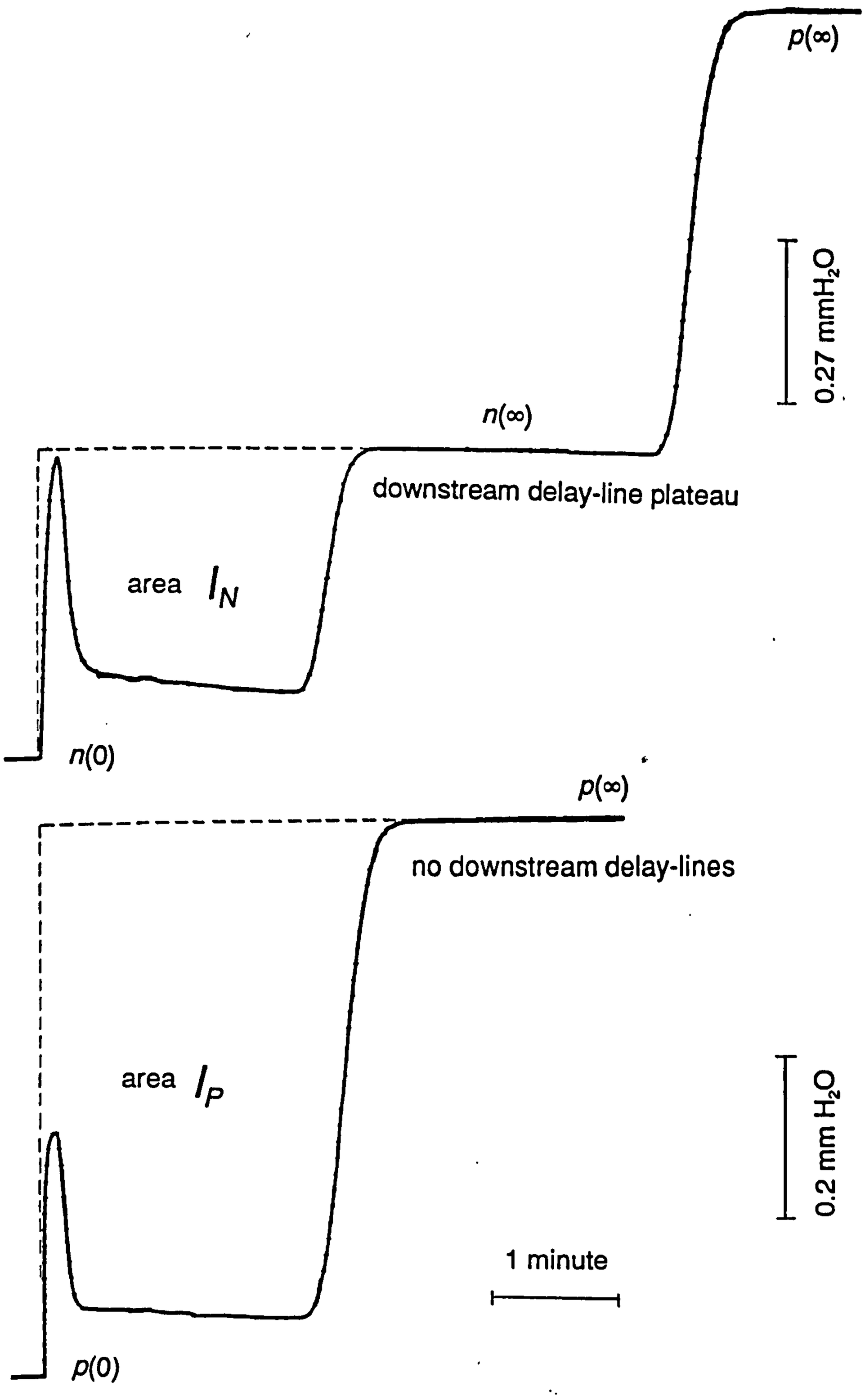

Figure 4.1 Flowrate Chromatograms With and Without Delay-Lines

4.2.2 Definition of $B(\mu)$ Terms

This is the term which will appear explicitly in the derived equation relating τ_N and τ_P . Basically, it is a gradient of the mixture viscosity-composition curve and it involves the fractional change in mixture viscosity when a small perturbation flow is added to a carrier flow.

$$\frac{d\mu_M}{\mu_M} = \frac{n}{M} B(\mu) \qquad 4.4$$

where $B(\mu)$ = viscosity factor
n = molar flowrate of perturbation flow
M = molar flowrate of carrier
μ_M = gas-mixture viscosity
$d\mu_M$ = change in gas-mixture viscosity caused by perturbation

For a binary system this quantity can be related to the viscosity mixture-composition curve (at specified temperature) and the composition only. The equation form is further improved by making the viscosities dimensionless by dividing by the lowest pure-component viscosity, say that of component A. Thus, these dimensionless mixture viscosities will vary from unity upwards to a value equal to the pure-component ratios. Simple molar balances enable these viscosity factors to be re-stated for each perturbation gas:

$$B(\mu)_{\text{A prtbn}} = \frac{1 - Y_A}{\mu_M^*} \frac{d\mu_M^*}{dY_A} \qquad 4.5$$

$$B(\mu)_{\text{B prtbn}} = \frac{-Y_A}{\mu_M^*} \frac{d\mu_M^*}{dY_A} \qquad 4.6$$

where Y_A = gas-mixture mole fraction A
μ_M^* = dimensionless mixture viscosity
$d\mu_M^*/dY_A$ = gradient of dimensionless mixture viscosity curve

By re-arranging the above equations and dividing, the following equation is obtained:

$$\frac{-B(\mu)_{\text{A prtbn}}}{B(\mu)_{\text{B prtbn}}} = \frac{Y_{BP}}{Y_{AP}} \qquad 4.7$$

where Y_{AP} = predicted composition of component A
Y_{BP} = predicted composition of component B

Thus, both viscosity factors for both perturbation gases are related to the composition. In Section 4.7.4 it will be shown how these viscosity factors can be obtained experimentally if downstream delay-lines are incorporated into the equipment. This equation can be used in two ways. Firstly, if both viscosity factors can be obtained accurately, a check is obtained for the composition. Secondly, the form of the equation suggests that towards each end of the composition range, one of the perturbation gas factors becomes very small and so difficult to measure. Thus, by measuring the larger factor and knowing the gas composition, the smaller one can be accurately determined.

4.2.3 Equation Relating Retention Times

The flowmeter consists of two matched pieces of capillary tubing with a differential pressure transducer connected between them upstream. The downstream pressure is fixed and so a changing gas flowrate will register as a changing upstream capillary pressure. However, even if the flowrate is constant, changes in gas viscosity will register as changes in the upstream pressure and so will obscure the true column flowrate variation, the measurement of which is the whole point of the project. The simple solution is to insert a delay line between the column and the measuring capillary. It must be long enough to ensure that the gas composition in the capillary tubing is constant for some time after the front has left the column. Thus use of these delay lines enables the true column flowrate variation to be monitored. The following equations are a summary of an analysis by Mason and Buffham (unpublished). This analysis is based upon the journey of the chromatographic front through the column and capillary tubing. Figure 4.2 gives a schematic representation of the analysis.

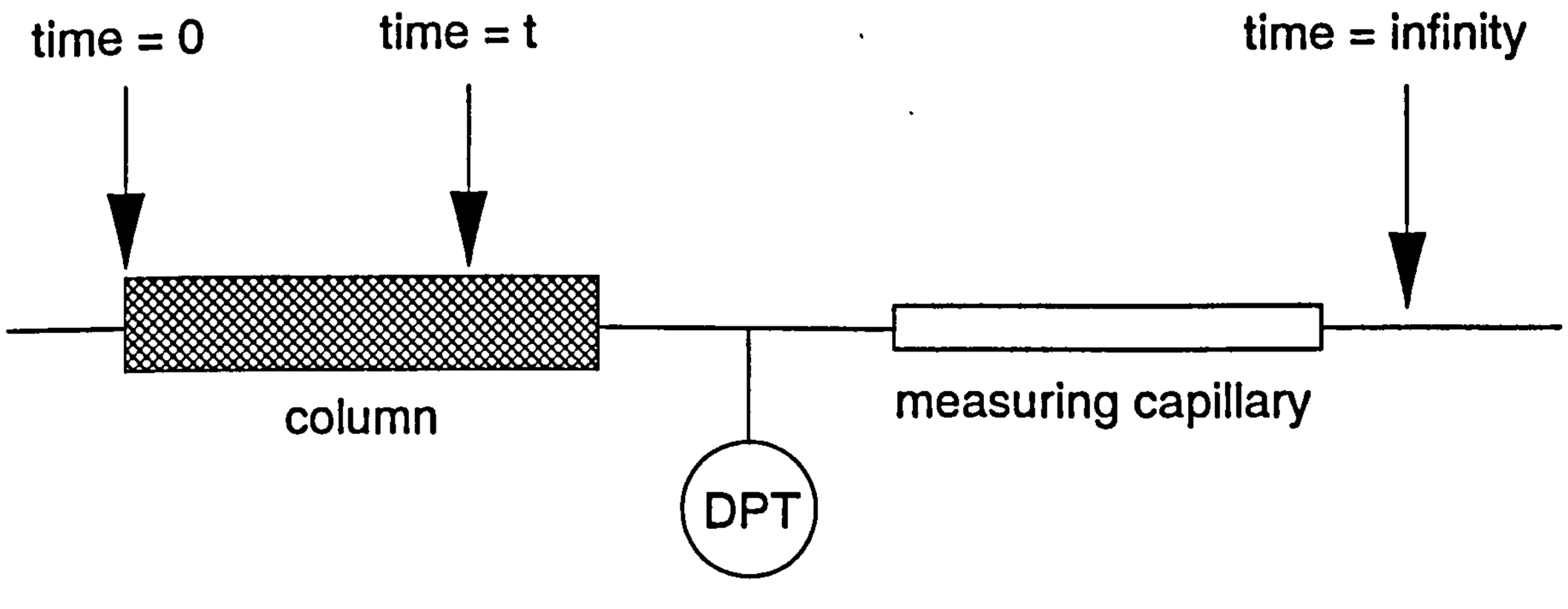

DPT = differential pressure transducer

Figure 4.2 Passage of Front through System

The above diagram shows the position of the front at three particular times. At time zero the front is just about to enter the column. At any intermediate time *t*, the front is still in the column. For both these cases, the gas mixture composition in the capillaries is unchanged at the original value. The time infinity refers to the time after which both chart recorder pens have stopped deviating. For a single capillary tube, the general equation for compressible laminar flow is:

$$\delta P_T\left(P_{AT}+\frac{1}{2}\delta P_T\right)=K_T\mu_M MRTL \qquad 4.8$$

where δP_T = pressure drop down capillary tube

K_T = capillary tube constant

R = universal gas constant

L = tube length

T = absolute gas temperature

Differentiating, the following equation is obtained:

$$\frac{dM}{M}=\frac{d(\delta P_T)}{\delta P_T}\left(\frac{P_{AT}+\delta P_T}{P_{AT}+\frac{1}{2}\delta P_T}\right)-\frac{d\mu_M}{\mu_M} \qquad 4.9$$

The final viscosity term can be substituted for using Equation 4.4. Firstly, considering the time difference from time zero to infinity, Equation 4.9 can be written as:

$$\frac{n(\infty)-n(0)}{M}=\frac{(\delta P_T(\infty)-\delta P_T(0))(P_{AT}+\delta P_T)}{\delta P_T\left(P_{AT}+\frac{1}{2}\delta P_T\right)}-\frac{(n(\infty)-n(0))}{M+n}B(\mu) \qquad 4.10$$

Secondly, considering the time difference from any time *t* to time infinity:

$$\frac{n(\infty)-n(t)}{M}=\frac{(\delta P_T(\infty)-\delta P_T(t))(P_{AT}+\delta P_T)}{\delta P_T\left(P_{AT}+\frac{1}{2}\delta P_T\right)}-\frac{(n(\infty)-n(0))}{M+n}B(\mu) \qquad 4.11$$

Re-arranging Equation 4.11 and substituting into Equation 4.10, the following equation is obtained:

$$\frac{n(\infty)-n(t)}{n(\infty)-n(0)}=\frac{\delta P_T(\infty)-\delta P_T(t)}{\delta P_T(\infty)-\delta P_T(0)}(1+B(\mu))-B(\mu) \qquad 4.12$$

From earlier definitions, integration of both sides of Equation 4.12 from zero to infinity will produce both pressure and flowrate retention times. The final term only has to be integrated over the time the front spends in the column, namely τ_x . The final equation relating these residence times is thus:

$$\tau_{NP} = (1 + B(\mu))\tau_P - B(\mu)\tau_X \qquad 4.13$$

where τ_{NP} = predicted value of flowrate retention time

Alternatively, the equation can be re-stated to obtain explicitly the value of viscosity factor required for equation agreement. This form is especially useful when there is doubt about the value of viscosity factor:

$$B(\mu)_A = \frac{\tau_N - \tau_P}{\tau_P - \tau_X} \qquad 4.14$$

4.2.4 Experimental Measurement of Viscosity Factors

It has already been stated that the viscosity factor $B(\mu)$ can be measured directly if downstream delay-lines are employed. Figure 4.3 shows the schematic shapes of flowrate chromatograms obtained using downstream delay-lines for two systems: the top chromatogram corresponds to adding a nitrogen perturbation gas to an argon carrier and the bottom one corresponds to adding a nitrogen perturbation to a helium carrier. Position A refers to the baseline position *before* the perturbation gas is added. Position B refers to the pen position as the front moves through the column. Because the perturbation gas is the more highly adsorbed nitrogen, position B refers to net adsorption and a subsequent flowrate reduction. When the fronts leave the column and pass into the downstream delay-lines, there is no more net adsorption and the pen rises to plateau C. Finally, when the composition front passes into the measuring capillaries, any change in mixture composition caused by the perturbation will move the pen to plateau D. For the argon carrier it can be seen that there is a reduction in mixture viscosity, but for the helium carrier there is an increase in mixture viscosity.

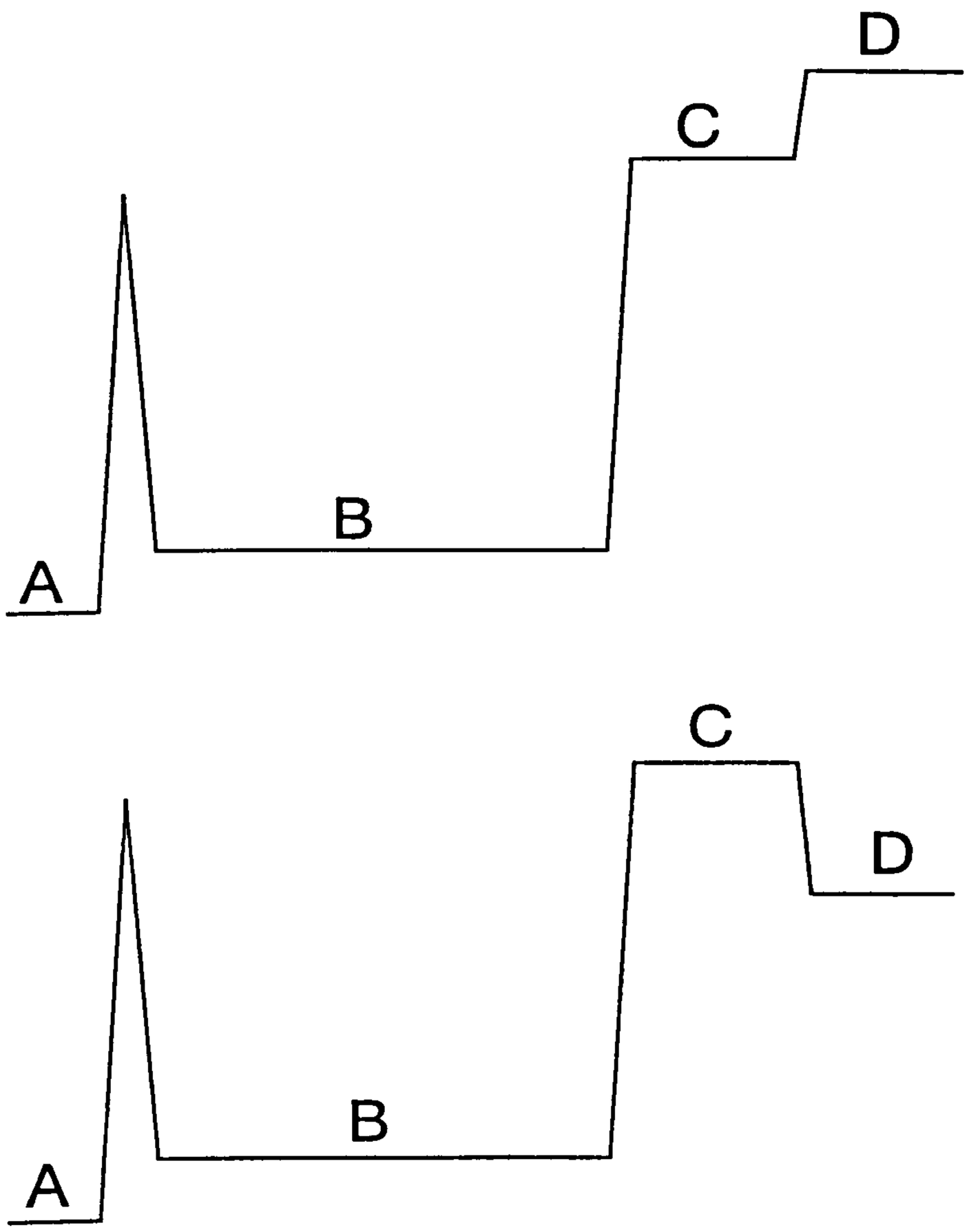

Figure 4.3 Schematic Flowrate Chromatogram With Delay-Lines

By re-arranging Equation 4.9 and separating out the pressure term, the following equation is obtained:

$$d(\delta P_T)\left(\frac{1}{\delta P_T}+\frac{1}{2\left(P_{AT}+\frac{1}{2}\delta P_T\right)}\right)=\frac{dM}{M}+\frac{d\mu_M}{\mu_M} \qquad 4.14$$

From position A to position C there is a change in flowrate but no change in the composition of the gas in the capillary. Thus, Equation 4.14 can be re-stated as:

$$(\delta P_{TC}-\delta P_{TA})\left(\frac{1}{\delta P_T}+\frac{1}{2\left(P_{AT}+\frac{1}{2}\delta P_T\right)}\right)=\frac{n}{M} \qquad 4.15$$

From position C to position D there is no change in flowrate, only a change in the gas composition of the capillary. Thus, Equation 4.14 can be re-stated as:

$$(\delta P_{TD}-\delta P_{TC})\left(\frac{1}{\delta P_T}+\frac{1}{2\left(P_{AT}+\frac{1}{2}\delta P_T\right)}\right)=\frac{d\mu_M}{\mu_M} \qquad 4.16$$

Dividing Equation 4.14 by 4.15 and substituting using Equation 4.4, the following important equation is obtained:

$$B(\mu) = \frac{\delta P_{TD} - \delta P_{TC}}{\delta P_{TC} - \delta P_{TA}} \qquad 4.17$$

Hence, these viscosity factors can be simply obtained from the chart-recorder by simply measuring the two relevant offsets. From Figure 4.3 it can be seen that the viscosity factor can be either negative or positive.

4.3 Required Experimental Modifications

For this case, the modifications are very simple. All that is required is a length of tubing connected between the column outlet and the capillaries. To maintain balance, *both* sides of the system require identical lengths of tubing. Of course there are many tubing diameters available. To provide sufficient delay, a suitable combination is 30 metres of 1/8 inch nylon tubing. The volume of each delay line is about 53 cc compared to an empty column volume of about 18 cc. The measured pressure drop across this combination is about 15 cm of water, which although smaller than the column pressure drop, is certainly not negligible compared to it. Smaller diameter tubing would give too high a pressure drop; in order to provide sufficient delay, a much longer length would be required. Of course, using 1/4 inch tubing, a much smaller length would be required to provide the same delay. However, this wider bore can be detrimental to front sharpness. Overall, 1/8 inch is found to be the optimum tubing diameter.

4.4 Experimentally Measured Viscosity Factors

4.4.1 Introduction and Table Descriptions

The viscosity factors are obtained by measuring the relevant offsets and substituting in Equation 4.17. Although the end points can be measured fairly accurately, some of the other points involve measuring distances of a few millimetres and so the percentage errors in these points becomes undesirable. As for the case of retention time measurement, an improved method would be to employ another chart recorder channel with higher sensitivity and scale down appropriately. As mentioned previously, another way to alleviate this problem of dubious viscosity factors is to employ Equation 4.7 using the other accurately measured viscosity factor. This approach is satisfactory for the argon-nitrogen system where the mixture viscosity curve is fairly linear, but it breaks down for the helium-argon and helium-nitrogen systems since these have maxima where both viscosity factors tend to zero. Around these points, the viscosity factors for both perturbation gases are too small to measure. According to Equation 4.7, it should be possible to use the measured viscosity factors to obtain the mixture composition. Of course, for some mixtures one of the factors

will be small so that the predictions will be unreliable. The fourth column gives the predicted value of the mixture composition and the fifth column gives the error from the true value of mixture composition.

Table 4.1 Measured Viscosity Factors for Nitrogen-Argon System at 25°C

$\%N_2$	$B(\mu)_{N2}$	$B(\mu)_{Ar}$	$100Y_{N2P}$	error
0	-0.19	0	N/A	N/A
5.3	-0.18	0.01	2.7	-2.6
10.0	-0.18	0.02	8.6	-1.4
25.3	-0.16	0.06	26.9	1.6
49.6	-0.12	0.11	46.7	-2.9
74.8	-0.06	0.18	75.9	1.1
90.0	-0.02	0.25	92.5	2.5
95.2	-0.01	0.28	97.5	2.3
100.0	0	0.30	N/A	N/A

Table 4.2 Measured Viscosity Factors for Nitrogen-Argon System at 53°C

$\%N_2$	$B(\mu)_{N2}$	$B(\mu)_{Ar}$	$100Y_{N2P}$	error
0	-0.20	0	N/A	N/A
4.7	-0.187	0.011	5.6	0.9
10.1	-0.187	0.028	13.0	2.9
24.9	-0.160	0.047	22.7	-2.2
49.2	-0.113	0.125	52.5	3.3
75.0	-0.075	0.20	72.7	-2.3
90.7	-0.021	0.269	92.3	1.6
95.5	-0.016	0.292	94.8	-0.7
100.0	0	0.314	N/A	N/A

Table 4.3 Measured Viscosity Factors for Nitrogen-Argon System at 80°C

$\%N_2$	$B(\mu)_{N2}$	$B(\mu)_{Ar}$	$100Y_{N2P}$	error
0	-0.20?	0	N/A	N/A
4.7	-0.188	0.011	5.5	0.8
9.7	-0.183	0.028	13.3	3.6
25.0	-0.167	0.052	23.7	1.3
49.6	-0.127	0.123	49.1	-0.5
75.2	-0.069	0.204	74.7	-0.5
90.0	-0.026	0.274	91.3	1.3
95.3	-0.016	0.290	94.7	-0.6
100.0	0	0.314?	N/A	N/A

Table 4.4 Measured Viscosity Factors for Nitrogen-Helium System at 25°C

$\%N_2$	$B(\mu)_{N2}$	$B(\mu)_{He}$	$100Y_{N2P}$	error
0	0.194	0	N/A	N/A
4.6	0.071	0 ?	N/A	N/A
10.0	0.014	0 ?	N/A	N/A
25.1	-0.071	0.019	21.1	-3.0
50.0	-0.006	0.048	44.4	-5.6
75.3	-0.004	0.075	65.2	-10.1
90.0	-0.016	0.088	84.6	-5.4
95.0	-0.008	0.100	92.6	-2.4
100.0	0	0.100	N/A	N/A

Table 4.5 Measured Viscosity Factors for Helium-Argon System at 25°C

%Ar	$B(\mu)_{Ar}$	$B(\mu)_{He}$	$100Y_{ArP}$	error
0	1.43	0	N/A	N/A
4.9	0.94	-0.04	4.1	-0.8
9.8	0.63	-0.06	8.7	-1.1
25.2	0.16	-0.053	24.9	-0.3
50.4	-0.009	0.008	47.1	-3.3
74.9	-0.013	0.052	80.0	5.1
90.0	-0.007	0.072	91.1	1.1
95.3	0 ?	0.083	95.4	0.1
100.0	0	0.094	N/A	N/A

4.4.2 Findings from Tables

Considering the inherent errors in measuring these viscosity factors, the predictions are surprisingly good. For both nitrogen containing systems, the average deviation is around two percent, whilst for the argon-helium system, the error is around five percent; indeed, for some compositions the factors are too small to even attempt a prediction. However, these apparently "small" errors cover up larger variations in the actual viscosity factors, which are accurately required. Coupled with the problem of the "unobtainable" factors for the helium-argon system, it would seem that alternative ways of obtaining these viscosity factors should be investigated. The next section investigates possible alternatives.

4.5 Gas-Mixture Viscosity Representation

4.5.1 Introduction

From the definitions of these viscosity factors, they involve the mixture viscosity and the gradient of the mixture viscosity-composition curve. Thus the following alternatives will be concerned with *directly* obtaining the *complete* curve.

4.5.2 Direct Graphical Determination

Consider the flow of *carrier gas* from the upstream back pressure regulator to the downstream back pressure regulator. Consider a molar balance over the whole system. Because the system is at steady-state, there can be no change in the moles of carrier gas contained within the system (the *holdup*) with time. Thus, the upstream molar flowrate

must equal the downstream molar flowrate. A molar balance can also be carried out on any element in the system with the same result that the inlet and outlet flowrates are equal. Finally, the molar flowrate of the carrier through the system is the same everywhere and is represented by the following equation;

$$M = \frac{K_S}{\mu_M}(P_U^2 - P_D^2) \qquad 4.18$$

where K_S = overall system constant depending on tubing and column
P_U = fixed upstream pressure
P_D = fixed downstream pressure

Hence, if these pressures can be kept constant, M varies inversely with μ_M. From a smooth graph of inverse M against composition, the mixture viscosity and mixture gradient can be measured and so these viscosity factors can be determined directly. However, if these pressures cannot be kept perfectly constant, the points will have slight vertical deviations and a smooth curve will be more difficult to draw. It is the purpose of the rest of this argument to investigate how a typical change in pressure will affect the drawing of the graph. Consider the derivative of M with respect to P_U:

$$\frac{dM}{dP_U} = \frac{2P_U K_S}{\mu_M} \qquad 4.19$$

Thus the % change in M caused by a small change in P_U is obtained by dividing Equations 4.18 by 4.19:

$$100\frac{dM}{M} = \frac{200P_U}{P_U^2 - P_D^2}dP_U \qquad 4.20$$

Typically P_U = 2.25 bar
P_D = 1.00 bar

Thus for an absolute change of 0.01 bar there would be a 1% change in the molar flowrate. On the mixture viscosity-composition graph, this would give a significant vertical deviation. Experimentally, each time the composition is changed the upstream back pressure regulator is adjusted to obtain the required pressure. Thus, the absolute change mentioned above can be positive or negative leading to *upward* or *downward* vertical deviations on the mixture viscosity-composition graph. When the graph was plotted for the nitrogen-argon system, these deviations made it difficult to draw a smooth curve through the points. Predictions of an accepted theory were plotted and the deviations from the experimental points could ba accounted for by the calculated 1% flowrate variation. To obtain a constant upstream pressure with varying composition, one possibility is to use a pressure gauge with a finer

calibration; at present the minimum scale deviation on the gauge is 0.05 bar and it would be desirable to reduce this to 0.01 bar. Alternatively, an instrument termed a *dead-weight tester* can be employed; this will maintain a constant upstream pressure because the pressure is solely determined by the mass of weights employed rather than observation of a needle on a scale. However, this instrument is cumbersome to use. Anyway, even if a smooth curve can be obtained through the points, it can be difficult to determine the gradients of the curve graphically by drawing tangents.

4.5.3 Predictive Methods

4.5.3.1 Introduction

An alternative way to obtain these viscosity factors is to find an algebraic equation which *adequately* represents the mixture data. Once this is achieved, the gradient and mixture value can be obtained from the relevant algebraic equations and the viscosity factors obtained from Equations 4.4 and 4.5. There have been many predictive equations and these are all of the same form, namely that proposed by Sutherland (1876). Here it is shown in dimensionless form because of previous arguments:

$$\mu_M^* = \frac{Y_A}{Y_A + Y_B\Phi_{AB}} + \frac{Y_B\left(\frac{\mu_{BO}}{\mu_{AO}}\right)}{Y_B + Y_A\Phi_{BA}} \qquad 4.21$$

where μ_{AO} = vscosity of component A at system temperature

μ_{BO} = viscosity of component B at system temperature

Φ_{AB} = Sutherland coefficient for component A

Φ_{BA} = Sutherland coefficient for component B

The gradient of this viscosity curve can then be obtained by differentiating Equation 4.21:

$$\frac{d\mu_M^*}{dY_A} = \frac{\Phi_{AB}}{(Y_A + Y_B\Phi_{AB})^2} - \frac{\Phi_{AB}\left(\frac{\mu_{BO}}{\mu_{AO}}\right)}{(Y_B + Y_A\Phi_{BA})^2} \qquad 4.22$$

The predictive methods differ in the way these Sutherland coefficients are defined. However, all the methods utilise the ratio of the pure-component viscosities and the ratio of the molecular weights. The three main methods will now be dealt with in turn.

4.5.3.2 The Wilke Equation

This was first proposed by Buddenberg and Wilke (1949) although their form contained a density and diffusion term. This was then simplified by Wilke (1950) who proposed the following form for the Sutherland coefficients:

$$\Phi_{AB} = \frac{\left\{1 + \left(\frac{\mu_{BO}}{\mu_{AO}}\right)^{1/2} \left(\frac{M_B}{M_A}\right)^{1/4}\right\}^2}{\left\{8\left(1 + \frac{M_A}{M_B}\right)\right\}^{1/2}} \quad 4.23$$

$$\Phi_{BA} = \frac{\left\{1 + \left(\frac{\mu_{BO}}{\mu_{AO}}\right)^{1/2} \left(\frac{M_A}{M_B}\right)^{1/4}\right\}^2}{\left\{8\left(1 + \frac{M_B}{M_A}\right)\right\}^{1/2}} \quad 4.24$$

where M_A = molecular weight of component A

M_B = molecular weight of component B

4.5.3.3 The Herning-Zipperer Equation

This was proposed by Herning and Zipperer (1936) and the Sutherland coefficients are of a much simpler form:

$$\Phi_{AB} = \left(\frac{M_B}{M_A}\right)^{1/2} \quad 4.25$$

$$\Phi_{BA} = \left(\frac{M_A}{M_B}\right)^{1/2} \quad 4.26$$

4.5.3.4 The Brokaw Approximation

This equation was derived after a rigourous study of gas-mixture viscosities by Brokaw (1968, 1969). The form of the Sutherland coefficients is seen to be simpler:

$$\Phi_{AB} = \left(\frac{\mu_{AO}}{\mu_{BO}}\right)^{1/2} A_{AB} \quad 4.27$$

$$\Phi_{BA} = \left(\frac{\mu_{BO}}{\mu_{AO}}\right)^{1/2} A_{BA} \quad 4.28$$

In these equations, the two functions A_{AB} and A_{BA} are complex functions involving only the ratio of molecular weights. These functions are represented by graphs, but for particular ratios these can be represented by much simpler functions.

4.5.4 Correlative Methods

4.5.4.1 Literature Review

As the name suggests, these methods involve taking the basic Sutherland Equation, and obtaining the coefficients using one or more independently obtained mixture viscosities. Saxena and Naryamen (1967) suggested that these coefficients are independent of

composition and may be determined from any two mixture compositions by solving the two relevant equations. Saxena and Gambhir (1967) suggested that for any system these two coefficients are related by a simple equation and thus only one experimental mixture viscosity is required. Later, Saxena (1970) investigated many systems and discovered that these correlative techniques give different coefficients, and so different mixture predictions depending upon the mixture points selected. Although these coefficients do not vary greatly, this variation may adversely affect the values of *viscosity factors* predicted. The next section presents a novel technique which may provide some improvement.

4.5.4.2 New Correlative Method

This method depends upon treating the two Sutherland coefficients as two independent quantities which must be determined from two mixture points; similar to the method of Saxena and Naryamen (1967). However, instead of measuring actual *viscosity mixture* data, two of the measured *viscosity factors* will be employed. As has been discussed previously, these can be measured more accurately where the perturbation gas is added to a pure carrier of the other component. Of course, from Equations 4.4 and 4.5, these factors involve the gradient of the mixture viscosity curve as well as the mixture viscosity itself. Since at the end-points, the mixture viscosity will be that for one of the pure components (which are well tabulated), this method involves specifying the initial and final *gradients* of the mixture viscosity-composition curve. Equations 4.5 and 4.6 can be re-written for the case of adding perturbation component A to carrier component B ($B(\mu)_{A^*}$) and perturbation component B to carrier component A ($B(\mu)_{B^*}$):

$$B(\mu)_{A^*} = \frac{1}{\left(\frac{\mu_{BO}}{\mu_{AO}}\right)} \frac{d\mu_M^*}{dY_A} \tag{4.29}$$

$$B(\mu)_{B^*} = -\frac{d\mu_M^*}{dY_A} \tag{4.30}$$

Substituting using Equation 4.22, the following two equations are obtained:

$$\frac{1}{\Phi_{AB}} - \Phi_{BA}\left(\frac{\mu_{BO}}{\mu_{AO}}\right) = B(\mu)_{A^*}\left(\frac{\mu_{BO}}{\mu_{AO}}\right) \tag{4.31}$$

$$\Phi_{AB} - \frac{1}{\Phi_{BA}}\left(\frac{\mu_{BO}}{\mu_{A0}}\right) = -B(\mu)_{B^*} \tag{4.32}$$

Substituting to eliminate one of these unknowns, the following quadratic is obtained:

$$B(\mu)_B \cdot \Phi_{BA}^2 + \left\{\frac{\mu_{BO}}{\mu_{AO}} - \frac{\mu_{AO}}{\mu_{BO}} + B(\mu)_A \cdot B(\mu)_B\right\}\Phi_{BA} - B(\mu)_A \cdot \left(\frac{\mu_{BO}}{\mu_{AO}}\right) = 0 \qquad 4.33$$

The roots of this equation can be obtained from the standard quadratic formula. Of course, one implication is that if the solution gives complex roots, the system cannot be represented by the Sutherland form with the specified gradients. For Sutherland representation, the following equality must apply:

$$\left(\frac{\mu_{BO}}{\mu_{A0}} - \frac{\mu_{AO}}{\mu_{BO}} + B(\mu)_A \cdot B(\mu)_B\right)^2 + 4B(\mu)_A \cdot B(\mu)_B \cdot \left(\frac{\mu_{BO}}{\mu_{AO}}\right) \geq 0 \qquad 4.34$$

Immediately, it can be seen that if both viscosity factors are of the same sign, then the inequality will always be satisfied (namely both helium containing systems). This fact makes this correlative method attractive, since the helium containing systems are potentially awkward. For the nitrogen-argon systems, there is no such guarantee.

4.5.4.3 Possible Improvement of Correlative Method

The correlative method uses the end-point viscosity factors because of the relative accuracy with which they can be measured. However, there is also the possibility of using one or more mixture viscosity factors, assuming that they can be measured accurately. For the general mixture case, Equation 4.22 cannot be reduced to a simple form so that it is more difficult to solve the resulting simultaneous equations. One special case involves systems with a maximum: if the position of this maximum can be determined and this is at a composition of Y_{AM} and Y_{BM}, then setting Equation 4.22 to have a zero gradient:

$$\frac{\Phi_{AB}}{(Y_{AM} + Y_{BM}\Phi_{AB})^2} = \Phi_{BA}\frac{\left(\frac{\mu_{BO}}{\mu_{AO}}\right)}{(Y_{BM} + Y_{AM}\Phi_{BA})^2} \qquad 4.35$$

The possible advantage can be seen by considering that the viscosity factors involve the mixture gradient as well as the mixture viscosity itself. Using the original correlative method of Saxena and Naryamen (1967), *only* the two mixture viscosities are specified. However, for the proposed correlative method, as well as specifying two mixture viscosities, the actual gradients at these points are specified; the mixture predictions should be improved. However, when the end-point viscosity factors are specified, only the two gradients are fixed and so any advantage is dependent upon the relative importance of the viscosity mixture curve gradient. This question will be discussed later after the various viscosity graphs have been presented.

4.6 Standard Mixture Viscosity-Composition Graphs

The standard graphical representations are shown in Figures 4.4 to 4.6. For each graph, from the legend it can be seen that four series are plotted. The first series, termed *correlation*, refers to the new correlative method described in Section 4.5.4.2 in which the entire mixture viscosity-composition curve is predicted using only two experimentally determined viscosity factors. The other three methods are purely predictive and require the following information:

Molecular weights from any suitable textbook

$\mu_{N2} = 17.86 \times 10^{-6}$ Ns/m^2

$\mu_{Ar} = 22.72 \times 10^{-6}$ Ns/m^2

$\mu_{He} = 19.89 \times 10^{-6}$ Ns/m^2

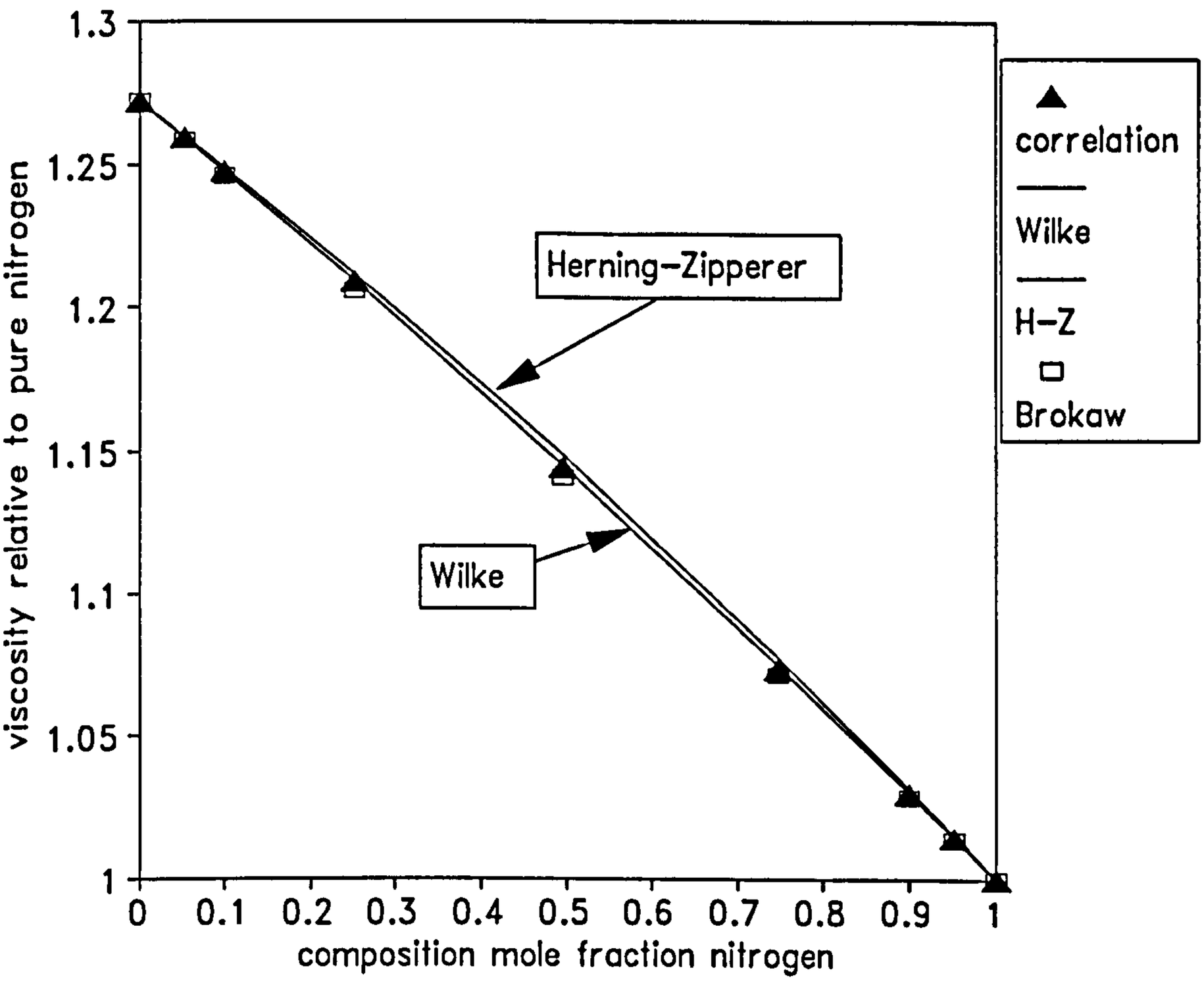

Figure 4.4 Comparison of Methods for Nitrogen-Argon System

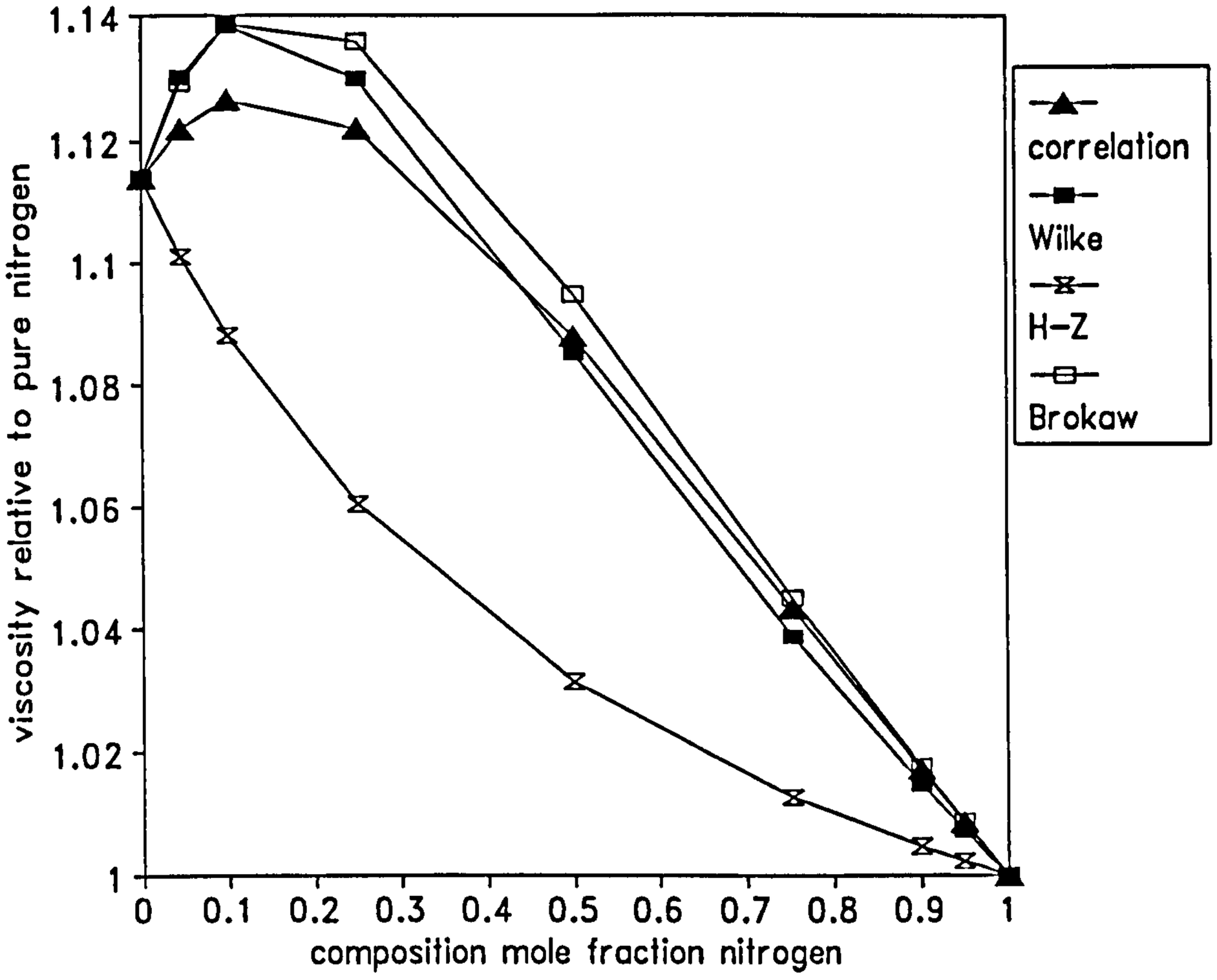

Figure 4.5 Comparison of Methods for Nitrogen-Helium System

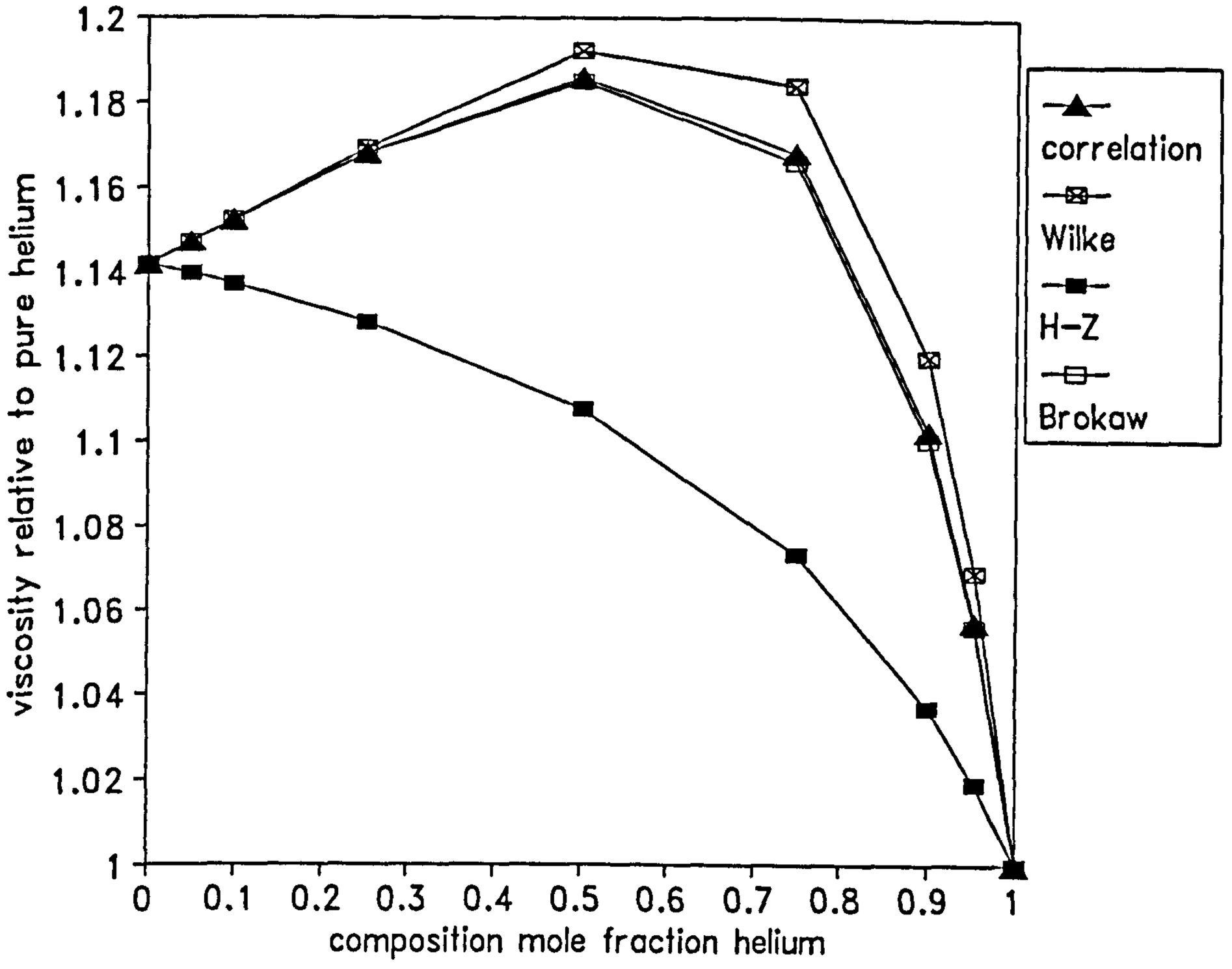

Figure 4.6 Comparison of Methods for Argon-Helium System

4.7 Gradients of Mixture Viscosity-Composition Graphs

The gradient representations are shown in Figures 4.7 to 4.9. As for the standard representations, from the legends it can be seen that four series are plotted.

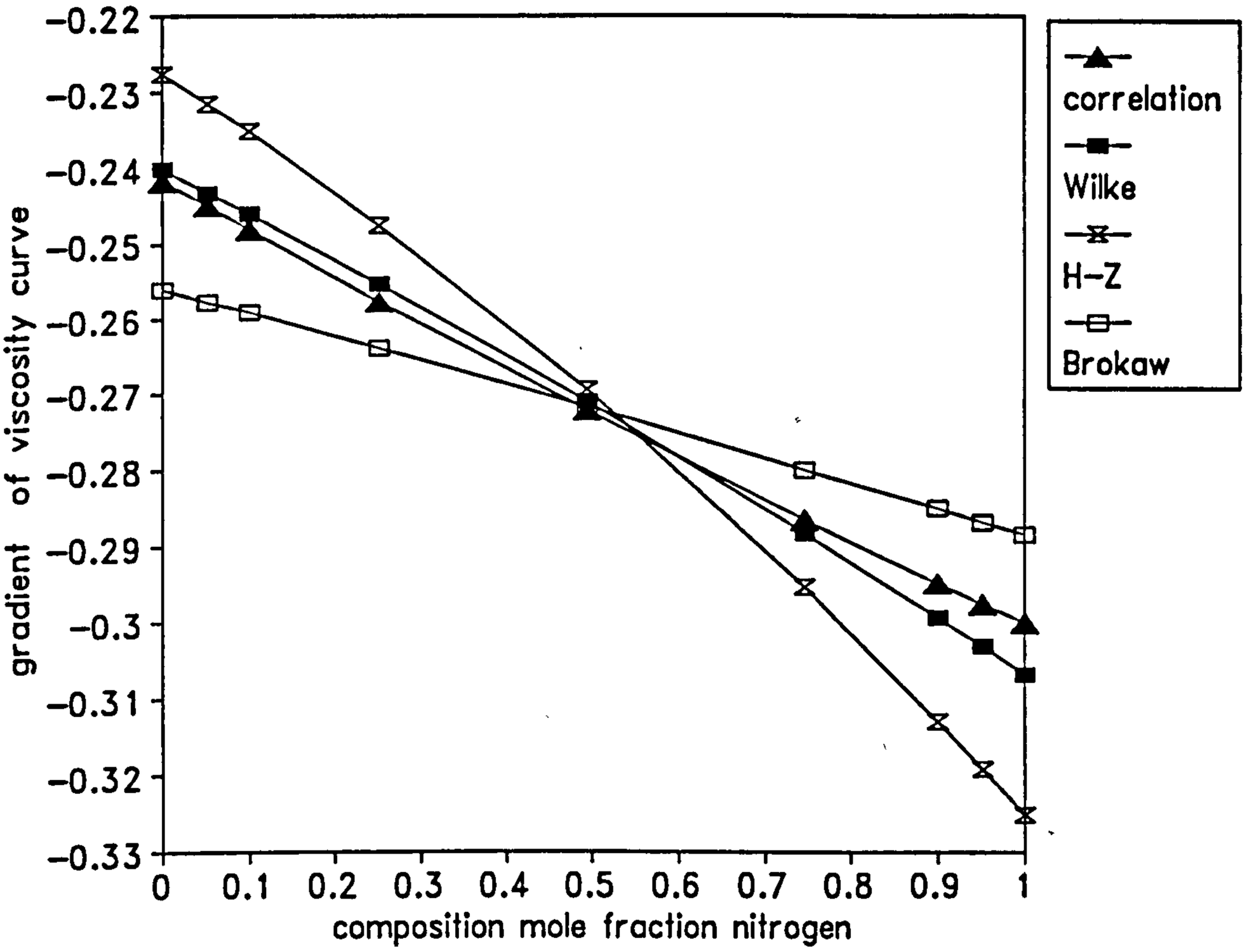

Figure 4.7 Comparison of Gradients for Nitrogen-Argon System

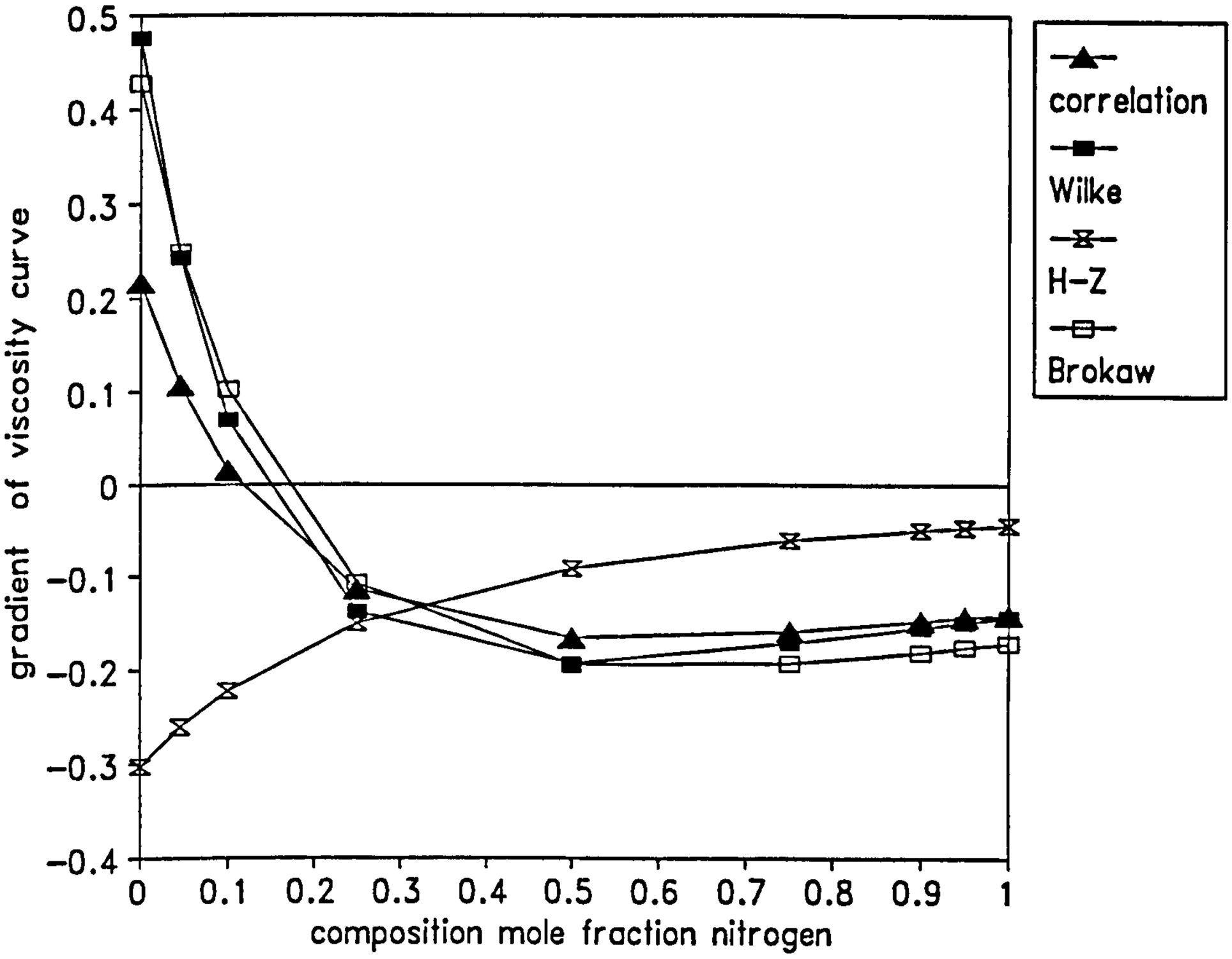

Figure 4.8 Comparison of Gradients for Nitrogen-Helium System

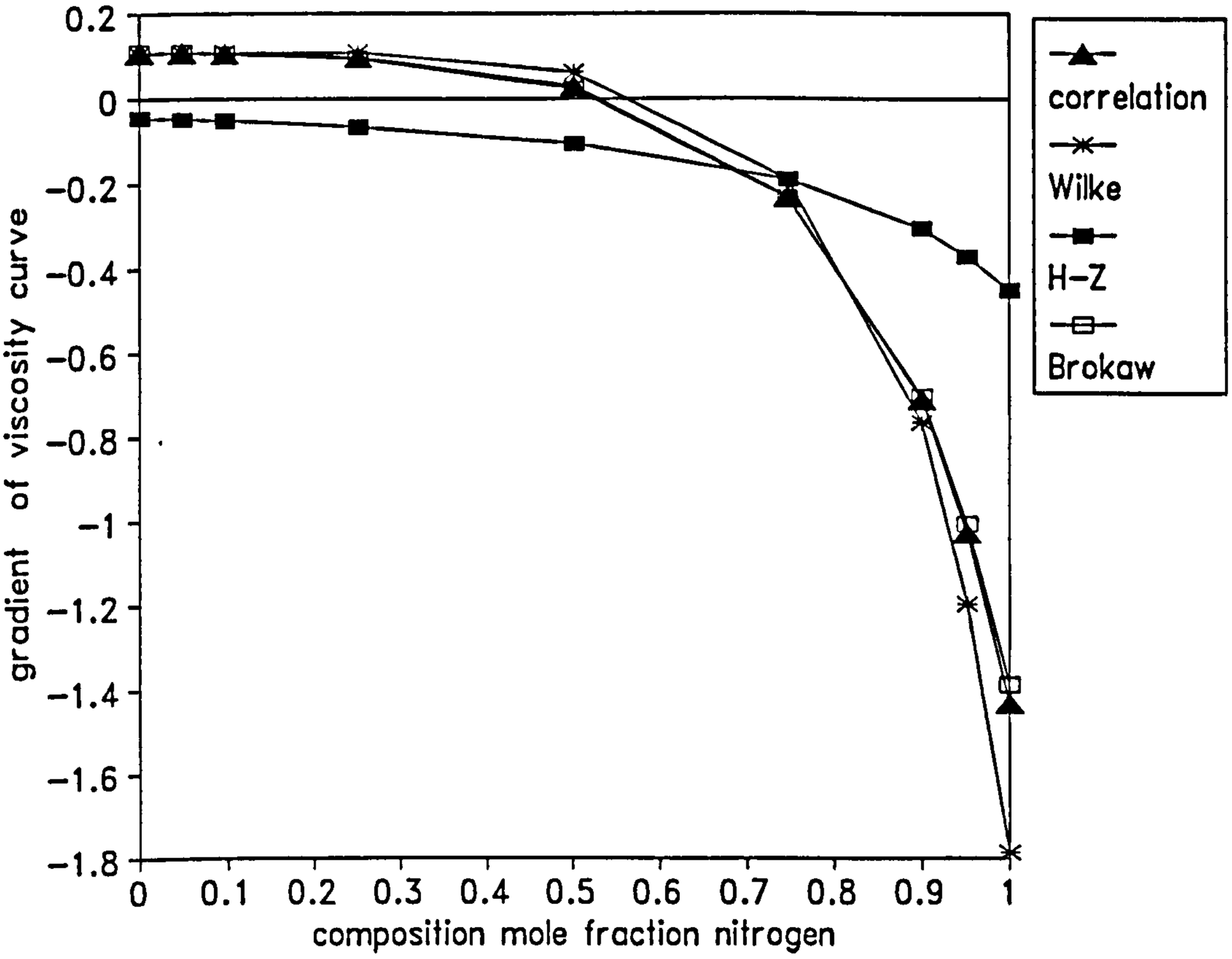

Figure 4.9 Comparison of Gradients for Argon-Helium System

4.8 Viscosity Factor-Composition Graphs

The viscosity factor representations are shown in Figures 4.10 to 4.15. There are two graphs for each of the three systems at room temperature (one for each perturbation gas). Compared to the other representations, there is an extra series corresponding to the measured viscosity factors. From Section 4.2.4, the viscosity factor is obtained by dividing two distances measured on the flowrate chromatogram. Thus, there will be experimental error in measuring the viscosity factors. The denominator is usually in the range 80 to 100 mm, and the numerator is less than 20 mm. The approximate error bar will be around 1/90 = 0.01.

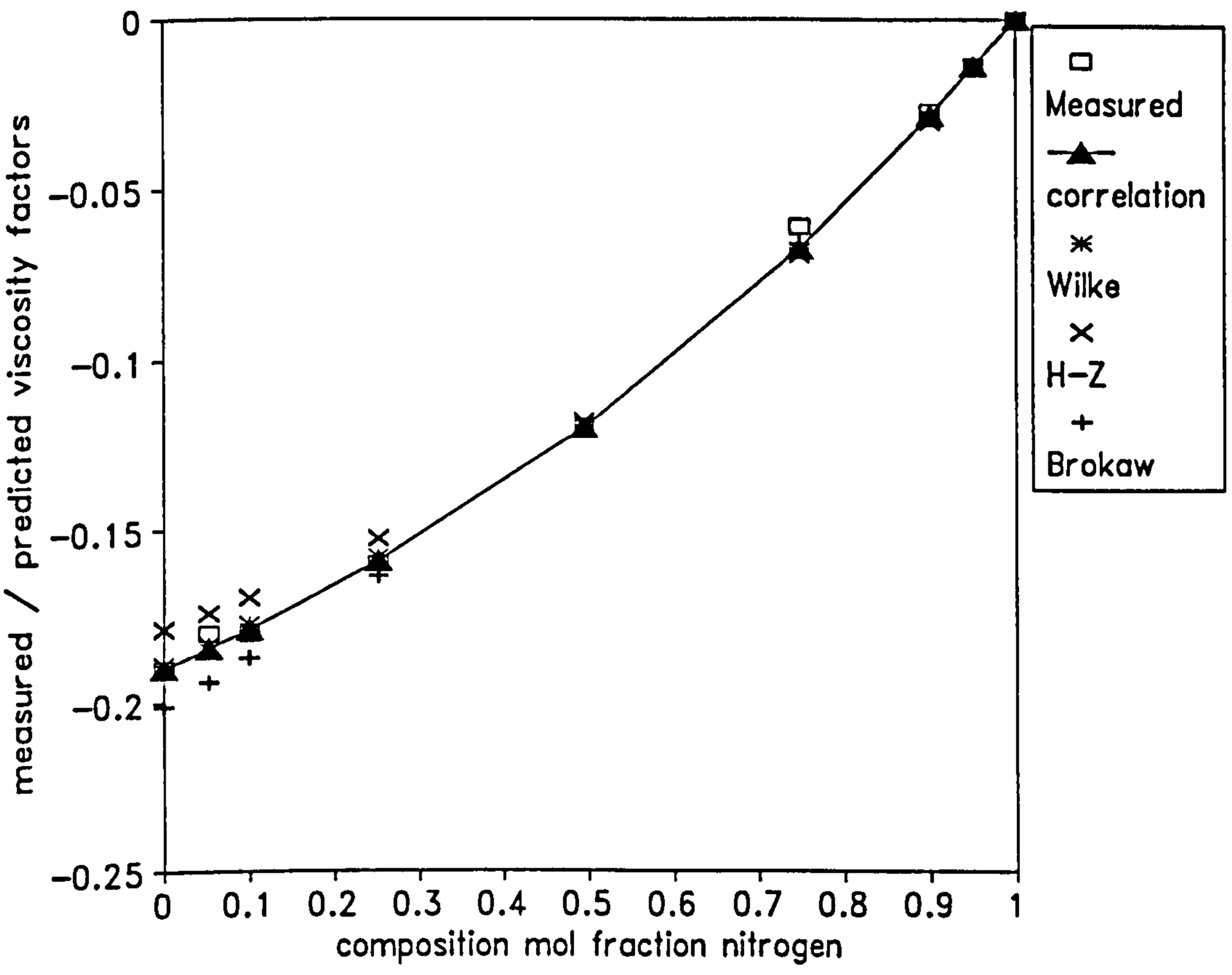

Figure 4.10 $B(\mu)$ Values for Nitrogen Perturbation in Nitrogen-Argon System

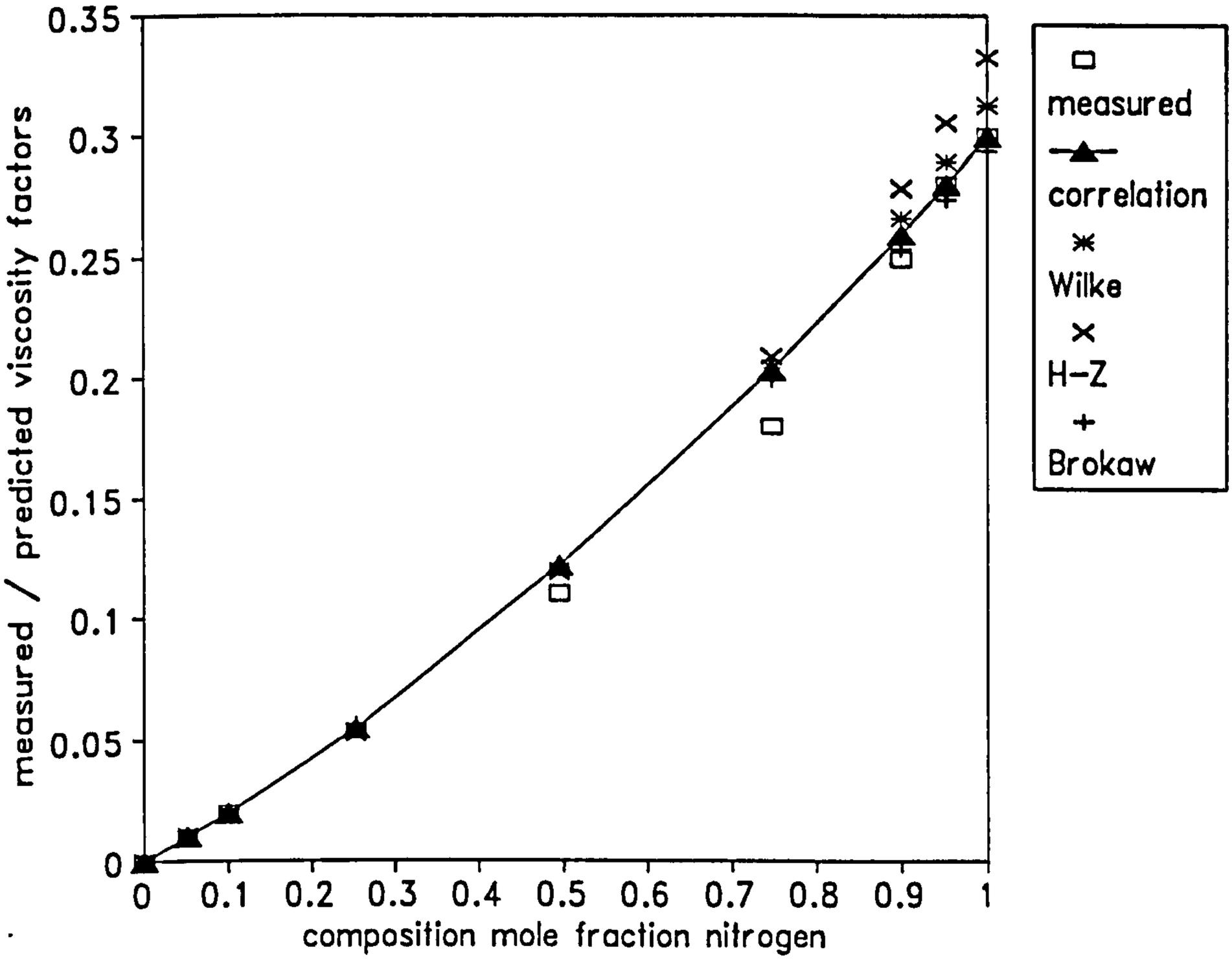

Figure 4.11 $B(\mu)$ for Argon Perturbation in Nitrogen-Argon System

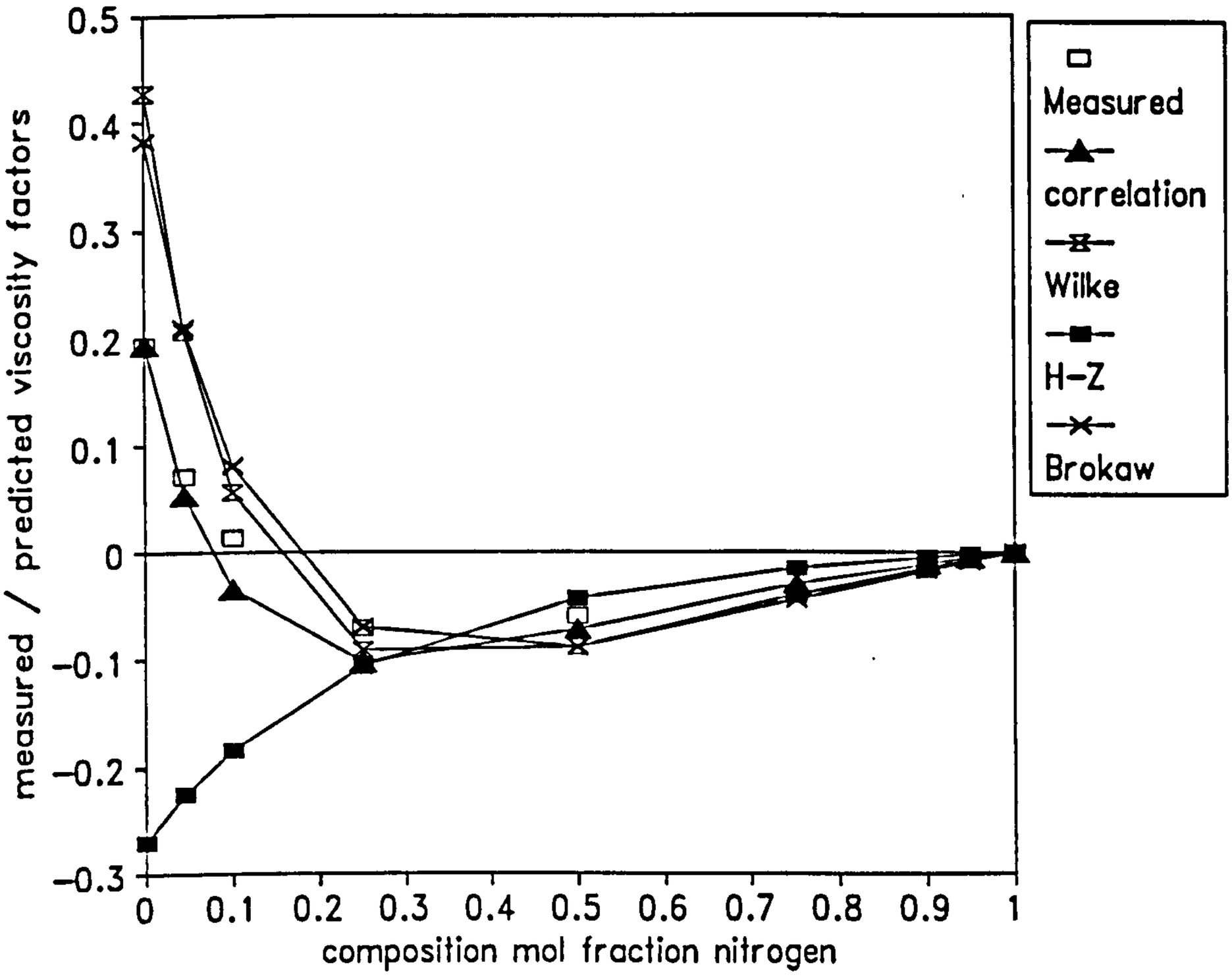

Figure 4.12 $B(\mu)$ for Nitrogen Perturbation in Nitrogen-Helium System

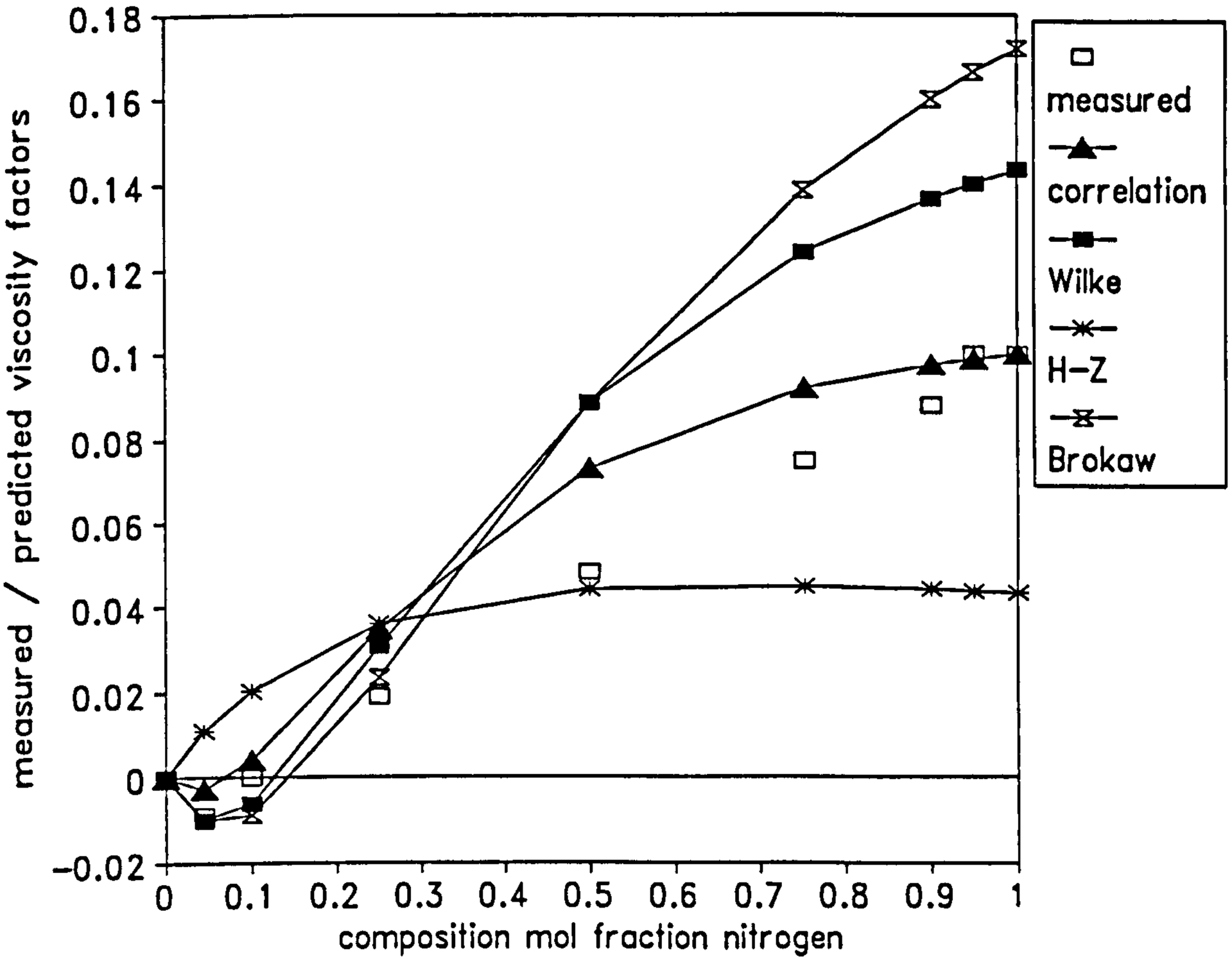

Figure 4.13 $B(\mu)$ for Helium Perturbation in Nitrogen-Helium System

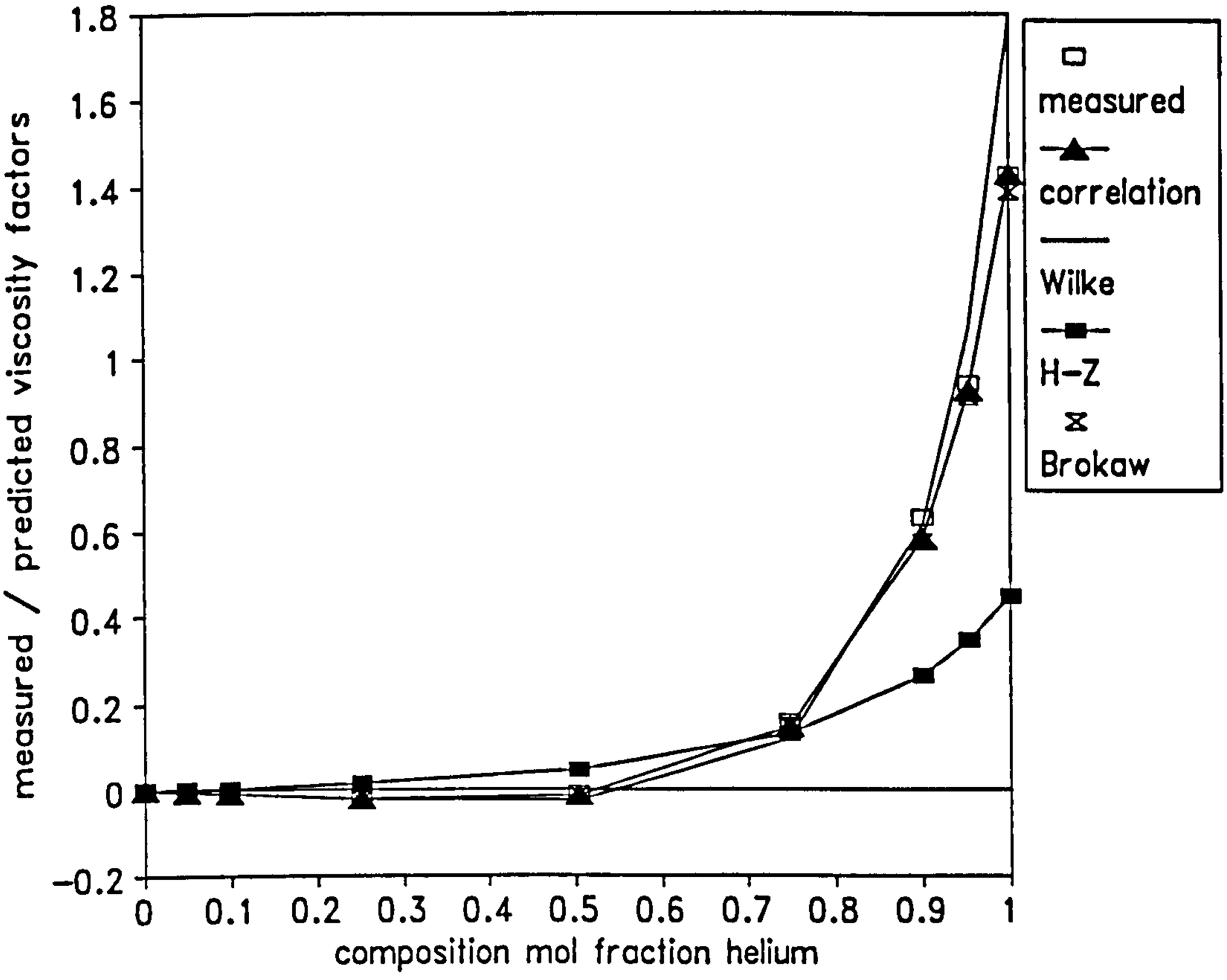

Figure 4.14 $B(\mu)$ for Argon Perturbation in Argon-Helium System

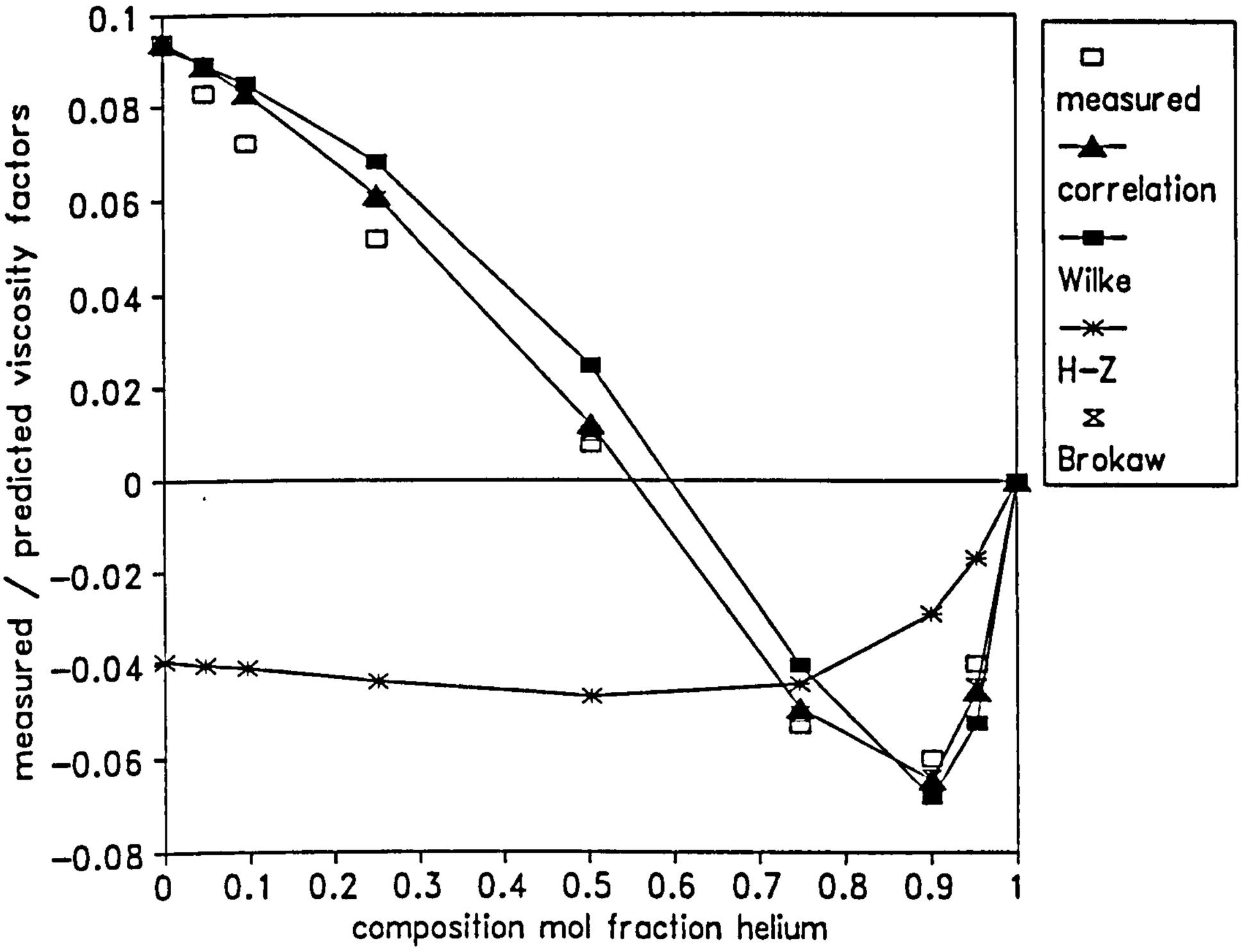

Figure 4.15 $B(\mu)$ for Helium Perturbation in Argon-Helium System

4.9 Findings from Graphs

4.9.1 General Points

Generally, the *gradient representation* is a more severe test of agreement than the *standard representation*. For example, from Figure 4.5 the predictions for the argon-nitrogen system would appear to be very close together; indeed, the predictions do not deviate by more than 1%. However, from Figure 4.8, the gradients deviate by up to 10% at the end points although they are in virtual agreement in the centre region. Thus the possible advantage of this new correlative method can be seen; if the end-point viscosity factors can be measured accurately, then these gradients can be fixed where there is potentially more chance of error. It is hoped that this might lead to a much better viscosity representation across the whole range.

The *standard* and *gradient representations* serve only to compare the predictive and correlative methods. It does not necessarily mean that one of the methods must be good even if the literature states that the predictions are good. From the above arguments "good" literature predictions are not necessarily suitable for this project. However, from the *viscosity factor representations*, if the measured viscosity factors are close enough (within error bar range) to a particular set of predictions, this may help when later investigating the important equation connecting τ_P and τ_N. The suitable predictive method could then show

the probable direction for any adjustment in the measured viscosity factors. Otherwise, only the error bars can be used in making possible adjustments to the measured viscosity factors

4.9.2 Argon-Nitrogen System

As has already been discussed, the gradient representation is required to make a distinction between the predictive methods. It can be seen that only the Wilke method follows the correlation predictions, the other two methods giving distinctively different predictions. Actually, care had to be taken over the initial and final gradient specifications for the correlation. The higher the magnitude of one specified viscosity factor, the smaller the range of the other viscosity factor otherwise complex roots would be formed. This can be qualitatively seen from Equation 4.34. From the roots of this correlation, both sets were positive and it was found that *either* set would give *exactly the same mixture viscosity presentation*. However, at higher temperatures of 54°C and 80°C it was found that the measured viscosity factors resulted in complex roots; a Sutherland representation could not be obtained. For the important viscosity factors, from Figures 4.10 and 4.11 all the methods give virtually identical predictions in certain regions, although further down the composition ranges these predictions separate out. It can be concluded that there should be reasonable confidence in the measured viscosity factors, although for some compositions the measured values are sufficiently apart from the predictions and these may need to be adjusted.

4.9.3 Nitrogen-Helium System

From Figure 4.5, this system is awkward in that neither of the predictions or correlations seem to agree; they are all significantly different. Only the Herning-Zipperer method cannot qualitatively predict a maximum. The correlative method is seen to give a strange kink after it has passed the maximum. This could be caused by the curve not being steep enough at the final point; the specified viscosity factor is not high enough. Actually, it was discovered that this factor was calculated with a very small numerator and so this would lead to a high error. If this viscosity factor is increased to that for the Wilke predictions, the correlative curve looks more realistic and the maximum is positioned between 10 and 25% nitrogen (the same as the other predictions). However, for pure helium, this factor can be measured quite accurately and this gradient is much smaller than that for the Wilke and Brokaw predictions. Thus it seems likely that these latter methods over-predict the mixture viscosities. The correlative predictions are similar to the experimental mixture data reported in a final year project of 1988 with regard to the position and relative value of the maximum. However, Figures 4.12 and 4.13 show that the measured viscosity factors

cannot be adequately fitted by either of the predictive or correlative methods. Hence, when these graphs are used in Chapter Seven, it would seem that only the error bars can be used for possible adjustments.

4.9.4 Argon-Helium System

From Figure 4.6, it can be seen that the predictions of the correlative method and the Brokaw Approximation are virtually co-incident; the gradient representation of Figure 4.9 confirms this. Once again, only the Herning-Zipperer method cannot qualitatively predict a maximum. For this system, Wilke (1950) compares the Wilke predictions with the experimental data; the Wilke method is seen to over-predict the experimental data. Thus, from Figure 4.6 it would seem that the Brokaw and correlative predictions are very close to the experimental data. From Figures 4.14 and 4.15, it can be seen that the measured viscosity factors are very close to the correlative and Brokaw predictions (this further confirms the above findings). Thus it would seem that there should be confidence in the measured viscosity factors.

4.10 Summary of Main Findings

1. From the theory, the employment of downstream delay-lines enables the important viscosity factors to be directly measured from the flowrate chromatogram by simply dividing two offsets. These measured viscosity factors can used in a novel correlative method to try and predict the entire mixture viscosity curve using only two measured factors. The two end-points are a convenient choice because they can be measured the most accurately. Alternatively, one or more *mixture* points can be employed because of the resulting *extra* specification (this may provide better predictions). Actually, using this new method only allows the predictions to be compared.

2. Using the end-points, the novel method has been used to investigate the argon-nitrogen, argon-helium and nitrogen-helium systems at room temperature. At higher temperatures, this novel method cannot be used for the nitrogen-argon system. Good agreement is obtained for the nitrogen-argon system, although this system is roughly linear. Encouragingly, for the argon-helium system, the predictions are almost identical to the Brokaw predictions, despite the presence of a potentially awkward maximum. However, for the nitrogen-helium system, neither of the predictions agree with each other. Although, there is a degree of error in measuring one of the factors.

3. For mixtures rich in the respective perturbation component, the factor numerators become very small and so determination becomes inaccurate. However, from Equation 4.7, both perturbation gas viscosity factors are related to the mixture composition; hence measurement of one factor can be used to determine the other. In Figures 4.10 to 4.15, the

measured factors are plotted along with those predicted by various models. If these measured factors are accurately determined, they allow an absolute rigourous comparison of the various models.

4. In Chapter Seven, reliable values of the viscosity factors are required to test the validity of Equation 4.12. From the required Figure 4.10 to 4.15, observation of the calculated value of $B(\mu)_A$ will show whether any equation discrepancy can be accounted for by an incorrect value of $B(\mu)$ by observing whether both values are within experimental error of each other.

Chapter Five

HEAT EFFECTS IN THE OVEN

5.1 Introduction

This chapter is concerned with all the cases of heat transfer in the oven. In a typical oven there are two *sources* of heat. Firstly, when the oven is switched on, heat will be radiating from the heating elements to the oven walls and oven contents. Secondly, when a composition perturbation is made to the system, there will be net adsorption or desorption in the column and, depending on the sign of the heat of adsorption, this will lead to either the column heating up or cooling down. The *problems* of heat transfer in an oven can be divided into three categories. Firstly, when the oven is switched on, the incoming carrier gas must be heated to reach the oven temperature before the carrier gas reaches the packing. If this is not achieved, the results become meaningless since the equilibrium data is required at the oven temperature; equilibrium data is very sensitive to temperature. Secondly, when the composition front passes through the column, if the adsorption heat causes a significant temperature change, this may cause frontal spreading; from Chapter One, sharp fronts are desirable for retention time measurement. Finally, although the oven is supposed to control at constant temperature, there is the problem of thermal noise which can cause flowrate baseline fluctuations. Although these fluctuations do not have the same drastic effect as the other two factors, reduction of this noise is obviously desirable.

5.2 Oven Heat Load for Bulk Gas

5.2.1 Introduction

Generally, when the oven is switched on and it has reached the desired temperature, heat continues to be radiated from the elements. This is because there will be heat losses from the oven walls and so heat is required to maintain the selected temperature. Similarly, during each experimental run, the carrier gas will be flowing continuously and this gas must be continually heated to the oven temperature; this gives an additional heating load on the oven. It is conventional to have a section of tubing preceding the actual column packing, the purpose of it being to ensure that the gas flow will reach the oven temperature before it reaches the packing. From basic principles, this is more likely to be a problem at higher gas flow-rates. In this section a mathematical model will be developed which will give the variation of bulk-gas temperature with distance along the tubing, and hence the minimum preceding tubing length, in terms of the various operating parameters.

5.2.2 Form of Overall Heat Transfer Coefficient

As the gas flows through the tubing it will heat up and a heat balance can be set up. However, the rate of heat transfer is determined by the *overall heat transfer coefficient* (OHTC) and the problem is to obtain the value. Figure 5.1 shows the cross-section of the tubing preceding the column. The tubing through which the gas flows has an internal radius r_1 and an external radius r_2. If any insulation is placed over this tubing, it will have an internal radius r_2 and an external radius r_3. The oven temperature is considered constant at T_{EN}. The temperature at the surface of the insulation is T_3 and the temperature at the boundary of the insulation and the tube wall is T_2. The average carrier gas temperature is T_B and the temperature at the internal tube wall is T_1. At any position along the length of this tubing, none of the temperatures will vary with time. However, all these temperatures will tend to increase as the carrier gas flows further into the oven.

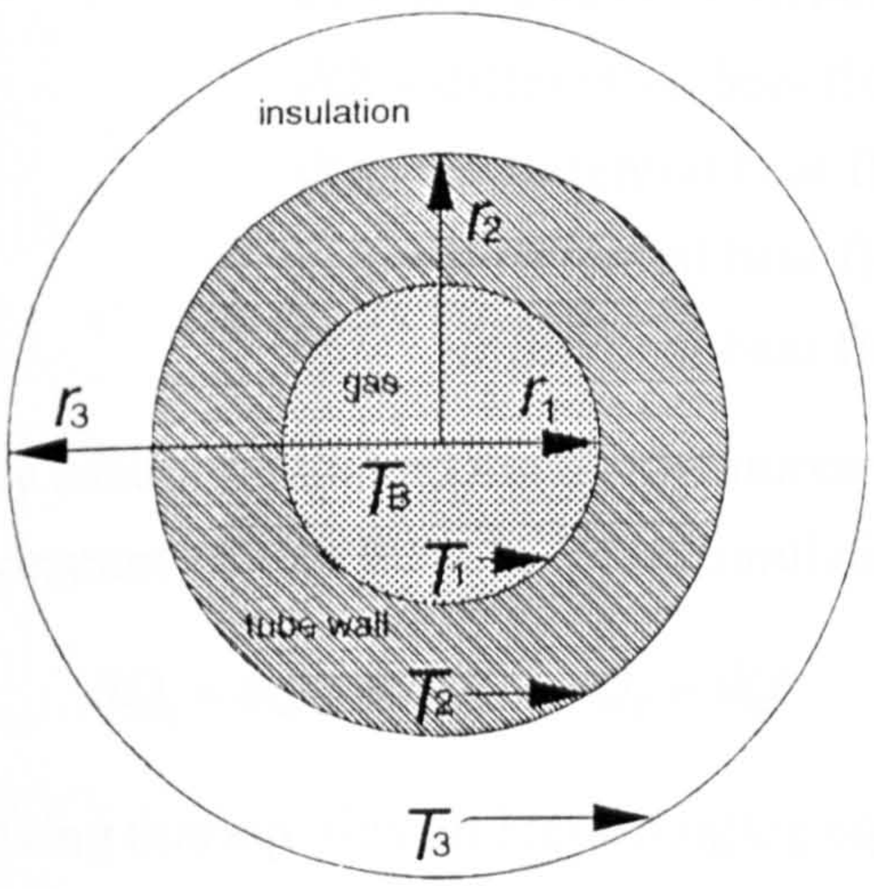

Figure 5.1 Cross Section of Oven Tubing Preceding Column

Consider a heat balance over a length dx during which the bulk temperature rises by dT_B. This allows the following two equations to be written:

$$dQ = MC_P dT_B \qquad 5.1$$

$$dQ = 2\pi r_1 U(T_{EN} - T_B)dx \qquad 5.2$$

where M = molar flowrate of gas

C_P = molar heat capacity of gas

U = overall heat transfer coefficient based on r_1

dQ = differential heat flow from enclosure to bulk gas

To determine the form of the OHTC will necessitate a consideration of the heat flows through each section:

$$dQ_I = 2\pi r_1 h_1 (T_1 - T_B) dx \qquad 5.3$$

$$dQ_W = 2\pi k_W (T_2 - T_1) \frac{dx}{\ln\left(\frac{r_2}{r_1}\right)} \qquad 5.4$$

$$dQ_E = 2\pi r_3 h_2 (T_{EN} - T_3) dx \qquad 5.6$$

$$dQ_N = 2\pi k_N (T_3 - T_2) \frac{dx}{\ln\left(\frac{r_3}{r_2}\right)} \qquad 5.5$$

where h_1 = heat transfer coefficient between internal wall and bulk gas
k_N = thermal conductivity of insulation material
k_W = thermal conductivity of wall material
h_2 = heat transfer coefficient between enclosure and external wall
dQ_I = differential heat flow between internal wall and bulk gas
dQ_W = differential heat flow across wall
dQ_N = differential heat flow across insulation
dQ_E = differential heat flow between enclosure and outside wall

By assuming that all the temperatures will be at steady state (temperature at every position constant so that there is no accumulation) the following equalities apply:

$$dQ_I = dQ_W = dQ_N = dQ_E = dQ \qquad 5.7$$

Using this equality and re-arranging equations 5.2 to 5.6 the following equation is obtained:

$$dQ = \left(\frac{1}{2\pi r_1 h_1} + \ln\frac{\left(\frac{r_2}{r_1}\right)}{2\pi k_W} + \ln\frac{\left(\frac{r_3}{r_2}\right)}{2\pi k_N} + \frac{1}{2\pi r_3 h_2} \right)^{-1} (T_{EN} - T_B) dx \qquad 5.8$$

Making this equation equal to 5.2 the following equation for the overall heat transfer coefficient is obtained:

$$\frac{1}{U} = \frac{1}{h_1} + \frac{r_1}{k_W} \ln\left(\frac{r_2}{r_1}\right) + \frac{r_1}{k_N} \ln\left(\frac{r_3}{r_2}\right) + \frac{r_1}{r_3} h_2^{-1} \qquad 5.9$$

Each one of these terms is the particular contribution to the overall heat transfer resistance. It is useful to know if any of these terms is limiting and so typical values will now be calculated in turn.

5.2.3 Individual Heat Transfer Coefficients

5.2.3.1 Conduction across Tubing Walls

A typical value for this contribution to the overall resistance can be obtained by substituting in the respective values for 1/16 inch large bore stainless steel tubing, for which:

$r_1 = 0.0006$ m

$r_2 = 0.0008$ m

$k_W = 16$ W/mK

for which the particular term from Equation 5.9 is 5.4×10^{-4} m^2K/W

5.2.3.2 Heat Transfer into Bulk Gas Flow

The Reynolds Number is a dimensionless number characterising how turbulent, if at all, is the flow. This well known equation is defined as:

$$Re = \frac{V\rho 2r_1}{\mu} \qquad 5.10$$

where Re = Reynolds number

ρ = gas density

μ = gas viscosity

V = gas velocity

Substituting in typical values of the above quantities for typical tubing diameters gives Reynolds numbers of between 10 and 50. According to Coulson and Richardson (1982a) these values are safely in the laminar region. Because no mixing of the fluid takes place, heat transfer takes place by conduction alone (Knudsen and Katz, 1958). For the general problem of laminar heat transfer in tubes the classical Graetz solution is useful (Graetz, 1885). The practical result of this solution is a graph of the internal Nusselt number against tube distance, where:

$$Nu_1 = 2r_1 \frac{h_1}{k_G} \qquad 5.11$$

where Nu_1 = internal Nusselt number

k_G = gas thermal conductivity

The Graetz solution was derived for constant wall temperature, however later variations were for constant heat flux and a linear variation in wall temperature with tube distance. For all these cases, the limiting value of Nu_1 (as the distance becomes infinite) levels off at values of 3.7, 4.4 and 4.4 respectively. Coulson and Richardson (1982b) obtained a constant temperature value of 4.1 by using a simplified method which approximates the fluid

temperature to a polynomial function. For heat transfer calculations it is useful to have a mean value of Nusselt number and Hausen (1943) proposed a solution for the constant temperature case. The problem with all these solutions is that they are strictly only valid for constant physical properties, whereas the density and the viscosity will vary with temperature. This problem was considered by Deissler (1951) who showed that the value decreased by about 20% at a wall temperature to bulk temperature ratio of about 5.8. Considering the experimental conditions, a value of 4 will be employed. For nitrogen at 25°C, k_G = 0.024 W/mK, for which the respective term from Equation 5.9 is 5.6 x 10^{-3} m^2K/W

5.2.3.3 Heat Transfer in Enclosure

If the tubes were exposed in the oven with hot air flowing over them, the mode of heat transfer would be forced convection. However, as discussed in more detail in Section 5.4., this gives a much increased thermal noise level. The solution is to screen the tubes from direct air flow by placing them in an enclosure. The result is that the mode of heat transfer changes to natural convection, for which the heat transfer coefficients are lower. From Coulson and Richardson (1982c) the general equation for natural convection from the outside of a tube in streamline conditions is:

$$Nu_o = 0.47(PrGr)^{1/4} \qquad 5.12$$

where Pr = dimensionless Prandtl number

Gr = dimensionless Grashoff number

Nu_o = external Nusselt number

For natural convection from air, the same authors have put in the relevant physical properties to obtain the equation:

$$h_2 = 5.18\left(\frac{(T_{EN} - T_3)}{d_3}\right)^{1/4} \qquad 5.13$$

If the enclosure consisted of water instead of air then the coefficient value of 5.18 in Equation 5.13 would become 105 meaning that the heat transfer coefficient would be about 25 times higher. However, experimentally this may be difficult to achieve, and so the present section will be concerned with the air case. Moreover, it is possible that this air coefficient will be limiting and so the overall analysis will be more rigourous with the air enclosure. The analysis will be complicated because the coefficient is temperature dependant and for a temperature difference of 50°C the respective contribution to the overall resistance in Equation 5.9 is 2.5 x 10^{-2} m^2K/W

5.2.3.4 Conduction Across Insulation

The respective contribution to the overall resistance in Equation 5.9 can be obtained by substituting in values for 1/8 inch nylon tubing, for which:

$r_3 = 0.0016$ m

$k_N = 0.24$ W/mK

giving a value of 5.4×10^{-3} m^2K/W

5.2.3.5. Comparing Individual Contributions

Overall, it can be seen that for the air enclosure the natural convection term is the limiting coefficient especially when the respective temperature difference approaches zero. This means that the majority of the overall temperature difference will be from the enclosure to the tube outside wall.

5.2.4 Computer Programme to Determine Temperature-Distance Profiles

Making Equations 5.1 and 5.2 equal the following equation is obtained:

$$\frac{dT_B}{dx} = \frac{2\pi r_1 U(T_{EN} - T_B)}{M C_p} \qquad 5.14$$

However, U is not constant since the natural convection term will include a temperature difference which will decrease with tubing distance downstream. In order to overcome this problem, the individual temperature drops are equated to the overall temperature drop, and using the steady state condition (no change in temperature at any position) the following equation is obtained:

$$(T_{EN} - T_3) + (T_{EN} - T_3)^{5/4}\left(\frac{1}{(2\pi r_1 h_1)} + \frac{\ln\left(\frac{r_2}{r_1}\right)}{(2\pi k_W)} + \frac{\ln\left(\frac{r_3}{r_2}\right)}{(2\pi k_N)}\right) = (T_{EN} - T_B) \qquad 5.15$$

This is a non-linear equation in $(T_{EN}$-$T_3)$ and is solved for values of $(T_{EN}$-$T_B)$ by a Newton-Raphson scheme. This scheme is used in conjunction with a fourth-order Runge-Kutta method for the numerical integration. The program is written in Turbo-Basic and the program listing is contained in Appendix B.

5.2.5 Qualitative Results of Computer Simulation

1. The *required tube distance* is that required to heat the gas to within 0.1°C of the oven temperature.

2. The product MC_p is very important. The higher this product, the greater the distance required. Generally, the variation in the heat capacity is not great so that the molar flow-rate is determining.

3. The internal diameter has no effect on the distance required.

4. Increasing the value of external diameter will lead to a lower value of distance required, even if this is achieved by placing on extra insulation.

5.2.6 Quantitative Results of Computer Simulation

The results of the programme are shown in tabular form in Appendix B for the following five cases:

1. Exposed 1/16 inch stainless-steel tubing at normal flowrate and 50°C
2. Exposed 1/16 inch stainless-steel tubing at increased flowrate and 50°C
3. Insulated 1/16 inch stainless-steel tubing at normal flowrate and 50°C
4. Exposed 1/4 inch glass tubing at normal flowrate and 50°C
5. Exposed 1/16 inch stainless-steel tubing at normal flowrate and 80°C

It can be seen that all the configurations have required tube distances which are not excessive. The gas heats up very quickly in the first two cm where the value of U is relatively high. Even at higher flowrates the required distance is still less than 10 cm. For the normal flowrate, the 1/4 inch glass tubing gives the most rapid rise to oven temperature in less than 2 cm. For narrower tubing, the required distance is less than 8 cm.

5.3 Heat of Adsorption Effects

5.3.1 Introduction

Whenever a perturbation flow of one component is added to a carrier mixture (not having the same composition as the perturbation flow) there will be a net change in composition and this gives rise to a net heat change. This heat will be either absorbed or evolved and the exact amount will depend upon the binary gas mixture-adsorbate system and the amount of perturbation flow. This heat change will cause the gas and packing around the composition front to heat up or cool down. However, any temperature change excursion will be temporary since there is a continual carrier flow behind the composition front. Hence, the effect of this heat would be a "temperature pulse" moving through the column. It is important to point out that, despite the sensitivity of equilibrium data to temperature, any temperature excursion should not affect the equilibrium results; only the front sharpness will be affected. Because any temperature excursion is temporary, the whole column will eventually return to the oven temperature. The theory behind the chromatographic method is only concerned with the initial and final column states after a perturbation has been

initiated; both of these are at the oven temperature. Finally, if the composition and flowrate records of the chart recorder are monitored for long enough, the resulting transients should enable the correct equilibrium data to be obtained.

Generally, it is accepted that small diameter columns coupled with small perturbation flows lead to isothermal situations (Helfferich, 1982). However, for industrial adsorbers where the column diameters and perturbation flows are much larger, the greater amounts of heat are more easily retained by the column leading to significant temperature changes (Leavitt, 1962). The purpose of this section is two-fold. Firstly, it is necessary to investigate the project apparatus with regard to the adsorption of helium, nitrogen and argon on 5A molecular sieve. Secondly, there is the possible problem of future application of the chromatographic method to other binary gas mixture-adsorbent systems more prone to heat effects.

5.3.2 Literature Review of Adsorption Heat Models

There have been many papers produced on this subject but most have been concerned with adiabatic or near-adiabatic columns with only a small heat loss. However, because of the project operating conditions, the present investigation is concerned with near-isothermal operation. One of the first papers was by Ruthven, Garg and Crawford (1975) who produced a constant pattern model for a favourable isotherm neglecting radial temperature gradients. Later, Sircar *et al.* (1983) developed this idea by including proportionate pattern waves as well. The next development was the consideration of the radial temperature gradient by Kaguei *et al.* (1987). Recently, Farooq and Ruthven (1990a, 1990b) compared the one-dimensional and two-dimensional (radial temperature gradient) models. They concluded that for most practical systems, the former model, with all the heat transfer resistance concentrated at the column inside wall, would suffice (basically the assumptions of Ruthven *et al.* (1975)). Another important conclusion from Farooq and Ruthven (1990a) is that *desorption is almost isothermal* and the temperature change is independent of column diameter. This may have implications with regard to future experimental procedure. The perturbation gas will be added to each carrier mixture and then removed; one of these transitions will be isothermal. All these papers have one thing in common; they all involve adding an adsorbate perturbation flow to an inert carrier. These papers do not cover the case when the carrier flow is a mixture.

5.3.3 Model for Computer Simulation

5.3.3.1 Literature Model Chosen

The original model of Ruthven *et al.* (1975) will be chosen since its use of the dimensionless quantities makes comparison, both qualitative and quantitative, much easier. The restriction to constant-pattern systems might appear severe in that this rules out linear systems. However, Garg and Ruthven (1974a) have shown that the apparently linear systems nitrogen-argon-5A zeolite and nitrogen-helium-5A zeolite are slightly curved; the transient obtained when adding nitrogen is always sharper. Moreover, these findings were confirmed by the results of the present project; indeed it is very rare that the adding and leaving transients are mirror images. This might suggest that very few systems are linear and that either adding or leaving transients will lead to constant-pattern formation. The literature model involves three dimensionless parameters:

α characterises the relative rates of heat and mass transfer

β involves the relative heat capacities of adsorbent and gas

γ characterises the isotherm curvature

5.3.3.2 Justifications of Assumptions

As already mentioned, all the literature models involve adding a perturbation flow to a pure inert carrier. With regard to the present project, this will limit the application to the addition of adsorbates to helium carrier and so would seem to preclude the use of mixtures. However, adding a perturbation flow to a mixture will not involve complete saturation, unlike adding a perturbation flow to an inert carrier. Therefore, in the inert carrier case, there is a greater likelihood of heat problems. If it can be shown that there is no problem for the inert carrier case, then it should be safe to assume that it should be likewise for the mixture case. For systems in which neither of the components are inert (the general case), it would seem that the literature models will not apply. However, for the same reasons pertaining to the mixture case, the heat problem will be reduced compared to the inert carrier case and the above assumption will apply. However, justification of this assumption will require that the mass transfer resistance is not unduly increased. This problem is discussed more in Section 5.3.6.

5.3.3.3 Modification to Heat Transfer Assumption

Another assumption which all the literature models have in common is an infinite heat transfer coefficient at the exterior of the column. This allows the assumption that the wall is always at the temperature of the enclosure and so makes the heat balance easier; otherwise a varying wall temperature would necessitate knowledge of the wall heat capacity and make the problem unsteady state. This infinite coefficient is usually obtained by submerging the column in flowing air or a water bath. However, as shown later in 5.4, placing a column

in flowing air would give disastrous noise effects and so it is conventional to place it in a stagnant enclosure. In this case the mode of heat transfer is natural convection for which the heat transfer coefficient is much lower. Using Equation 5.13 and comparing with typical values of the wall heat transfer coefficient in Ruthven *et al.*(1975) would suggest that the natural convection coefficient would be limiting. These wall coefficients can be well correlated by the Leva correlation (Leva, 1952):

$$Nu_C = \frac{h_C d_C}{k_G} = 0.813 Re^{0.19} \exp \frac{-12 R_P}{d_C} \qquad 5.16$$

where Nu_C = Nusselt number for wall coefficient
h_C = wall heat transfer coefficient
d_C = column internal diameter
R_P = pellet radius

The power of the Reynolds number confirms the statement of Yagii and Kunii (1968) that for Reynolds numbers lower than about 50 the coefficient is independent of gas velocity. The variation with d_C would suggest that this dominance would increase as the column diameter decreased. The column diameter in the Ruthven paper is 3.8 cm whereas in the present project the column diameter is no more than about 0.9 cm. The equation for the OHTC for heat transfer between the enclosure and the packing is given by (Ruthven, 1984c):

$$\frac{1}{U_C} = \frac{1}{h_C} + \left(\frac{d_C}{2k_C}\right) \ln\left(\frac{d_E}{d_C}\right) + \frac{d_C}{d_E h_E} \qquad 5.17$$

where U_C = overall heat transfer coefficient based on d_C
d_E = external column diameter
h_E = heat transfer coefficient (same as h_2 for tubing)
k_C = thermal conductivity of column walls

Strictly speaking this, equation can only be applied when there is a steady-state situation so that the temperatures everywhere are constant. However, this problem can be overcome by assuming that one of the resistances is limiting; the two cases are now discussed:

1. For the literature case of an infinite external coefficient, the second and third terms on the right hand side are ignored and $U_C = h_C$.

2. Ignoring the contributions of the first two terms, all the temperature drop is on the outside of the tubing and so the tubing wall is at the same temperature of the packing (for this case $U_C = d_E h_E / d_C$). For this situation, the different conditions will necessitate a change in the form of the two dimensionless parameters α and β. Actually, the former parameter is critical to the temperature rises obtained, whereas the latter only affects the relative position of the

concentration and temperature fronts. To modify α, the h_c is removed from the expression and is replaced with the expression for U_c. For β, the numerator will include an extra positive contribution. If the column wall thickness is very small compared to the internal diameter, and the product of the column density times column specific heat capacity small, then beta will be unchanged.

5.3.4 The Computer Programme

5.3.4.1 Numerical Schemes

Basically, the program obtains the solution of two ordinary differential equations; these are the constant-pattern heat and mass balances. The authors suggest a fourth-order Runge-Kutta scheme and this has been adopted. However, no mention is made of the step length in dimensionless time and so a value of 0.01 time unit has been necessary to deal with typical values of the dimensionless parameters. For extreme values of these dimensionless parameters a step length of 0.001 is employed. However, for this value the programme run time becomes excessive. For very small values of β, there is an alternative using a non-differential scheme. If β is close to zero, the two differential equations are made equivalent and so a non-linear equation is obtained. Firstly, this can be solved to obtain the maximum value of temperature using a Newton-Raphson scheme. Secondly, the program steps up the concentration curve from this maximum temperature using another Newton-Raphson scheme. Thirdly, the program steps down the concentration curve using a third Newton-Raphson scheme.

5.3.4.2 Presentation of Results

1. The print-out states whether the column is thermostatted or if the external heat transfer coefficient is limiting.

2. The basic output of the program consists graphs and tables of the dimensionless concentration and temperature profiles.

3. The dimensionless time for the breakthrough curve is calculated. This can be adjusted by specifying the concentration limits of the breakthrough curve; usually between 1% and 99%.

4. Knowing these limits, an average dimensionless temperature can be calculated for the breakthrough curve.

5.Finally, these dimensionless quantities can be converted to actual times and temperatures knowing the various process parameters.

5.3.5 Application of Model to Project Systems

For the adsorption of gases such as argon, nitrogen and helium on 5A molecular sieve, the isotherms are relatively linear; that is compared to those for gases such as propane and butane (Garg and Ruthven, 1974a). For the former systems, the values of gamma would be close to zero whereas for the latter systems the values approach 0.9. Substituting continually lower values of γ into the model produces maximum values of temperature rise which approach zero. Even by reducing α, this contributes little toward increasing the temperature rise. Hence, by this argument alone, it would seem reasonable to assume that these systems are isothermal. The paper by Garg and Ruthven (1974a) is the only reference to heat effects in the present system. The authors conducted experiments on the effect of nitrogen and ethane perturbation flows on helium and argon carrier flows. Considering all these systems, they state that the maximum temperature rise is no more than 3°C.

For the 5A zeolite systems, the addition and removal transients are similar in shape although the addition transient is always slightly sharper. For the 4A zeolite systems the difference is much more pronounced. Therefore, the model can be applied to perturbation gas addition where heat is evolved. For the 4A zeolite systems, the value of γ is much higher and the value of α is much lower. Therefore, the 3°C rise most likely applies to this system. Moreover, this rise was for a column of diameter 5.3 cm whereas Ruthven *et al.*(1975) used a diameter of 3.8 cm and the present project employs a column diameter of about 0.4 cm. Knowing the variation of α with diameter enables the maximum temperatures to be obtained for these respective diameters. The diameter appears explicitly in the denominator of α and also from Equation 5.16 the heat transfer coefficient is inversely proportional to the diameter. Firstly, the program is run for all these diameters when the column is thermostatted (this is the situation assumed in the literature). Secondly, the program is run for all these diameters when the limiting mode of heat transfer is natural convection from the external tube wall. Table 5.1 summarises the actual results in terms of temperature changes.

Table 5.1 Effect of Column Diameter on Temperature Rise

	thermostatted		insulated	
d_C/cm	θ_{MAX}/K	θ_{AV}/K	θ_{MAX}/K	θ_{AV}/K
0.4	0.4	0.2	5.0	2.5
3.8	5.2	3.0	18.0	15.0
5.3	19.0	10.0	33.0	25.0

The table shows how increasing the column diameter greatly increases both the maximum and average temperature rises. The absence of thermostatting conditions will increase this rise even more. However, the present project utilises much smaller column diameters and the table shows the potentially lower temperature problems. The stated 3°C rise becomes even smaller for the 0.4 cm column case and so for the present project systems, the already insignificant temperature rise will become even smaller. Moreover, this 3°C rise was for perturbation flow 4% of the carrier, this being about 4 times higher than normal. Finally, for the systems reported in this thesis, thermostatting will not be required.

5.3.6 Implications Concerning Other Systems

5.3.6.1 Introduction

Although the binary gas systems employed in the project will not be prone to heat effects, the present research project is concerned with the development of a general method. Binary equilibrium data may be required for other systems more prone to heat effects. Output from the computer programme shows that the breakthrough curves will become more spread out. For these problematic systems, different process conditions may be required in order to reduce these potentially large temperature rises. This section discusses how these process conditions should be chosen for particular systems.

5.3.6.2 The Dimensionless Parameters

From the computer programme, β is relatively unimportant when considering temperature rises. γ is an intrinsic property of the isotherm, and so only α can be varied. As α tends to infinity the system becomes isothermal. In reality, a large enough value of α should be chosen which will make the system isothermal. The higher the value of γ, the higher the value of α required. The dimensionless parameter α consists of many terms and in general the numerator terms should be increased and the denominator terms reduced. Straight away it can be seen that the perturbation flow should be as small as possible and the diameter small; this results in a higher surface area per unit column volume. The problem of mass and heat transfer resistance is more complex and will be dealt with next.

5.3.6.3 Relative Rates of Mass and Heat Transfer

The expression for α contains the ratio of heat transfer coefficient to mass transfer coefficient. In general, adsorption itself is very fast so that the overall rate of adsorption is determined by the overall mass transfer coefficient; the rate at which molecules can travel from the bulk gas to the active sites. The overall heat transfer coefficient must be large enough to conduct the heat away otherwise it would accumulate and cause an undesirable rise in temperature. Obviously a low transfer coefficient would increase this ratio. However,

from basic chromatography theory, this would give more spread out fronts which is undesirable. Therefore, the ideal situation is a large mass transfer coefficient and a very large heat transfer coefficient.

5.3.6.4 Variation of Heat Transfer Coefficient

The equation concerned here is the correlation of Leva (1952) which is listed as Equation 5.16. As long as the pellet diameter is not too large compared to the column diameter, the respective Nusselt number is roughly constant. Thus, the heat transfer coefficient is inversely proportional to the internal diameter. For comparison purposes the h_C can be replaced by another d_C on the denominator and so the expression for alpha now has a d_C^2 on the denominator.

5.3.6.5 Overall Mass Transfer Coefficient

This is the last parameter to be dealt with and unlike the above parameters, it can not be simply reduced to a simple variation. Before considering the variation it is helpful to consider the structure of commercial adsorbents. Most commercial adsorbents consist of very small microporous crystals formed into a macroporous pellet. The crystals cannot be left in their original form since any fluid flow would require an excessive pressure drop. In a composite pellet, there are three contributions to the overall mass transfer resistance as the molecules travel from the bulk gas to the active sites. Two of these are diffusional; firstly the molecule must travel down the macropores and secondly the molecule must travel through the actual crystal. In order to get from the bulk gas into the pellet itself, the molecule must travel through an external film. Figure 5.2 shows the idealised cross-section of the pellet.

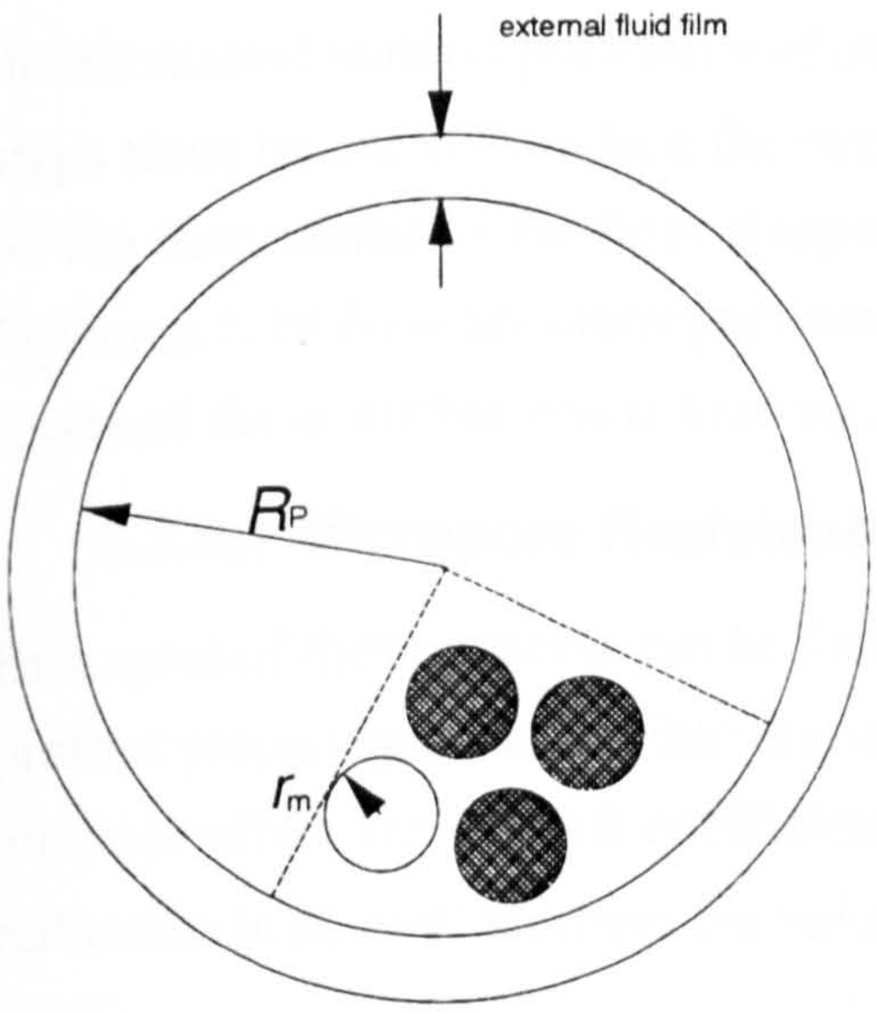

Figure 5.2 Idealised Cross-Section of Composite Pellet (Ruthven, 1984b)

Under certain conditions these resistances are linearly additive (Ruthven, 1984d) and the overall resistance is given by the following equation:

$$\frac{1}{k_A} = \frac{KR_P}{3k_f} + \frac{KR_P^2}{15\varepsilon_P D_P} + \frac{r_m^2}{15D_m} \qquad 5.18$$

where k_A = overall mass transfer coefficient
K = Henry constant
D_P = macropore diffusivity
D_m = micropore diffusivity
r_m = crystal radius
k_f = fluid film mass transfer coefficient
ε_p = pellet voidage

The fluid film mass transfer coefficient may be estimated from the correlation of Petrovic and Thodos (1968):

$$k_f = 0.357 V Re_P^{-0.36} Sc^{-0.67} \qquad 5.20$$

where Re_P = particle Reynolds number
Sc = Schmidt number

5.3.6.6 Variation of Mass Transfer Coefficient

In an ideal isothermal situation the overall mass transfer coefficient should be as high as possible to produce sharp fronts. However, in reality this will need to be limited by the overall heat transfer coefficient. If the temperature rises are prohibitive, and the column is thermostatted with no possibility of an increase in the overall heat transfer coefficient, then steps must be taken to reduce the overall mass transfer coefficient. Actually this may not be too detrimental to the front sharpness if the coefficient is high enough anyway. From Equation 5.19 there are many parameters determining k_A. However, this task is made easier if one of the contributions is limiting. These limiting cases will now be discussed in turn

5.3.6.7 Micropore Resistance Limiting

Examples of these systems can be found in Ruthven and Garg (1974a). Indeed, some of the present project systems fall into this category. For this situation, variation of the pellet size will not effect the overall coefficient. However, from the correlation of Leva (1952) a reduction in R_P will increase the value of the heat transfer coefficient.

5.3.6.8 Macropore Resistance Limiting

Examples of this type of system can be found in Garg and Ruthven (1974b). Increasing R_p will increase the mass transfer resistance and because the term is squared, this increase need not be much to effect a significant change. Of course, this will be offset to some extent by the reduction in the heat transfer coefficient.

5.3.6.9 External Fluid Film Resistance Limiting

In general, this type of limitation is rare and is more likely when the value of γ tends to one, since then the diffusion coefficients will become very large. From the respective term in Equation 5.18 the pellet size is included. From the equation for k_f, it can be seen that the coefficient is proportional to the fluid velocity. However, the fluid velocity is dependent on the volumetric flowrate and the column diameter. This type of variation is more complex than the other two cases since it includes more non-independent parameters. For this type of limitation the value of α needs to be considered overall. If the volumetric flowrate is kept constant, then varying the column diameter will have hardly any effect on the mass transfer coefficient. Ruthven *et al.*(1975) show a good example of the effect of fluid velocity by considering the system butene-helium-5A zeolite. The maximum temperature rise is seen to rise with fluid velocity at a constant column diameter. However, this variation is not quite proportional since the fluid film resistance is not quite limiting.

5.3.6.10 Case Study for Problematic System

Finally, for an example the ideas summarised in the previous sections will be applied to try and reduce the temperature rise of a problematic system from the literature. Considering the paper of Ruthven *et al.*(1975) the largest temperature rise is for Run 18 where a 4% butene perturbation flow is added to the helium carrier. The maximum rise is 47°C for a thermostatted column. The value of alpha is 0.06. From previous considerations, the column must remain well thermostatted.

1. Firstly, the perturbation flow can be reduced to 1% of the carrier flow so that the value of alpha becomes 4 x 0.06 = 0.24. From the programme, this will reduce the maximum temperature rise to 13°C.

2. Secondly, the column diameter can be reduced to 1/4 of the original value. Remembering the variation of the heat transfer coefficient with column diameter as well as the explicit appearance of column diameter, ° will increase by a factor of 4 x 4 = 16. The maximum temperature rise will now additionally reduce to less than 1°C.

Thus it can be seen that the temperature problem has been eradicated without recourse to adjusting the overall mass transfer coefficient. Actually, the fluid film resistance is not totally negligible so that the figure of 1°C is optimistic. This shows the importance of knowing relative values of the individual mass transfer resistances. If fluid film was limiting then changing diameter would have no effect and the fluid velocity would then have to be reduced.

5.4 Thermal Noise Effects

5.4.1 Introduction

The results from Sections 5.2 and 5.3 provide a framework of possibilities within which the thermal noise must be reduced to an acceptable level. These two problems were dealt with firstly because there would be no point in obtaining a noise proof arrangement if it were to be unacceptable according to Sections 5.2 and 5.3. At project commencement there was an arrangement in the oven which had significantly reduced the thermal noise. This was acceptable for runs in which the perturbation flow was around 2% of the carrier flowrate and the chart recorder sensitivity around 0.5 V for full scale deflection (1V corresponds to 10 mm water). However, for perturbation flows less than 1% of the carrier gas flow, and especially for particular mixtures, the noise levels were so significant that they made the retention time measurement difficult. It thus became necessary to obtain an improved oven arrangement. This section will start off with an explanation of thermal noise before carrying out a series of experiments to determine which factors affect the thermal noise levels. Finally, the findings will be applied to the reduction of thermal noise in different column arrangements.

5.4.2 Thermal Noise and Heat Transfer

Noise manifests itself as a non-smooth baseline. When the heater is on, random fluctuations in the oven are transmitted to the carrier gas flow in the tube causing the gas to expand and contract; this partially explains the effect on the flowrate baseline. If a section of the stainless-steel tubing is held between the fingers for some time, the baseline deviates as shown in Figure 5.3. This corresponds to a step change in temperature. The initial increase in flowrate is caused by gas expanding in the section within the fingers. However, as this gas moves out of the heating section, it loses the excess heat and so contracts resulting in a decrease in flowrate. Eventually, a situation is attained in which the rate of gas heating equals the rate of gas cooling and the flowrate returns to the original baseline position. At this steady state, heat is being transferred across the tubing into the gas which means that there is a temperature difference across the tubing and thus the tubing itself has been heated.

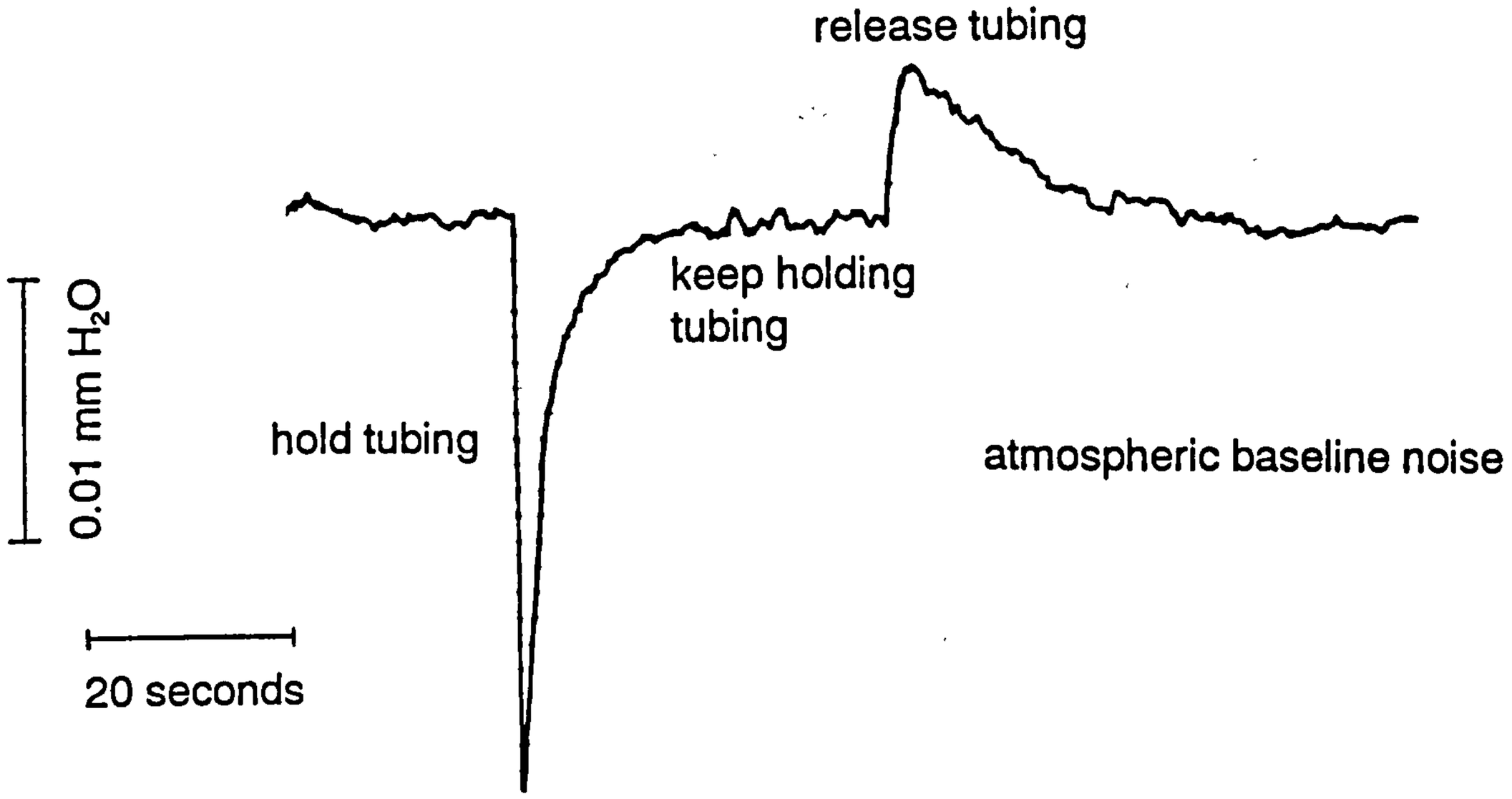

Figure 5.3 Baseline Deviation for Step Temperature Change

If a section of the stainless-steel tubing is only held momentarily, the deviation is represented by Figure 5.4. The negative deviation is due to gas cooling down whilst there is no source heating the gas since the fingers have been removed. This is actually an *impulse* in temperature and basically represents what is happening in the oven since the oven temperature is approximately constant but with small random temperature fluctuations. In reality, there are many of these impulses in temperature at any time in the oven causing the gas to expand and contract at many locations. They all contribute to the baseline noise effect. From these arguments, it would be expected that the thermal baseline noise level will increase with the total tubing length; this will increase the number of locations at which the gas can expand and contract.

However, holding the tubing is not quite representative of reality. When the tubing is held, the temperature change is effected at the tube surface whereas in reality these impulses occur in the oven at the heating coils and have to be transmitted to the tubing surface by a particular mode of heat transfer. When an impulse reaches the tube surface, it has to be transmitted through any insulation, the tube wall and finally into the carrier gas. The quicker this temperature impulse can be transmitted to the carrier gas, the sharper will be the doublet and the greater the thermal noise level. Hence, the value of the overall heat transfer coefficient becomes relevant to the noise level. However, it is not realistic to characterise the noise level solely in terms of the heat transfer coefficient. Before the heat from the impulse reaches the gas, the tubing (and insulation if present) will have partially heated up. Thus thermal noise is a case of *unsteady state heat transfer* since the temperatures will change with time. This brings in the concept of *thermal mass* which depends on the heat capacity and density of both the tubing wall and the insulation (if present). In short, a higher

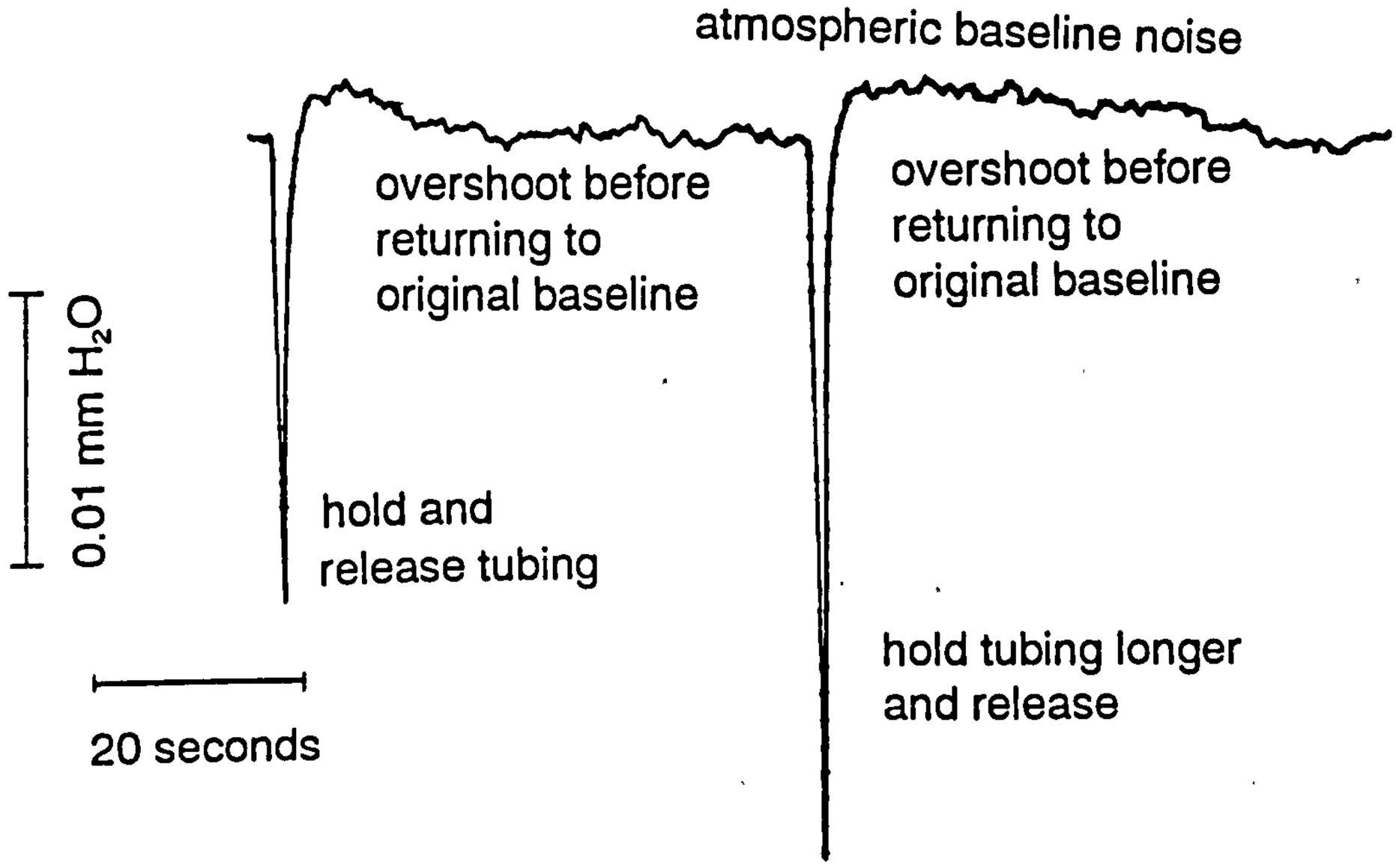

Figure 5.4 Baseline Deviation for Impulse Temperature Change

thermal mass will lead to a reduction in the baseline noise level; more heat will be required to set up the temperature differences and this reduces the sharpness of the doublet. The above concepts can be demonstrated by enclosing the stainless-steel tubing in a nylon insulation layer. When the tubing is subjected to the same temperature impulse with the fingers, the baseline response is flattened out significantly. Adding the insulation layer will have reduced & increased the overall heat transfer coefficient and the thermal mass sufficiently to reduce the thermal baseline noise.

5.4.3 Preliminary Experiments into Noise Factors

In a normal experimental situation there will be a combination of packed column, empty column and stainless-steel tubing. Each will make a contribution to the overall noise level. It seems reasonable to assume that the noise levels will increase with tube lengths. This is analogous to holding the tubing with more fingers, whence the deviation is larger. However, there will always be a minimum length of tubing in the oven so it is necessary to find out which of the components give the noisiest contributions so that these can be minimised. If a packed column with helium flowing is held in the standard way with two fingers as indicated in Figure 5.3, the deviation is about four times larger than that obtained for the stainless-steel tubing. If nitrogen is flowing, this deviation is about forty times larger. Nitrogen is adsorbed to a greater extent than helium and the heat transferred to the packing causes gas to desorb greatly increasing the deviation. When the background thermal noise levels are obtained for these three cases, the relative noise levels are in agreement with the above results. Figures 5.5 to 5.7 show the background noise levels for the three cases.

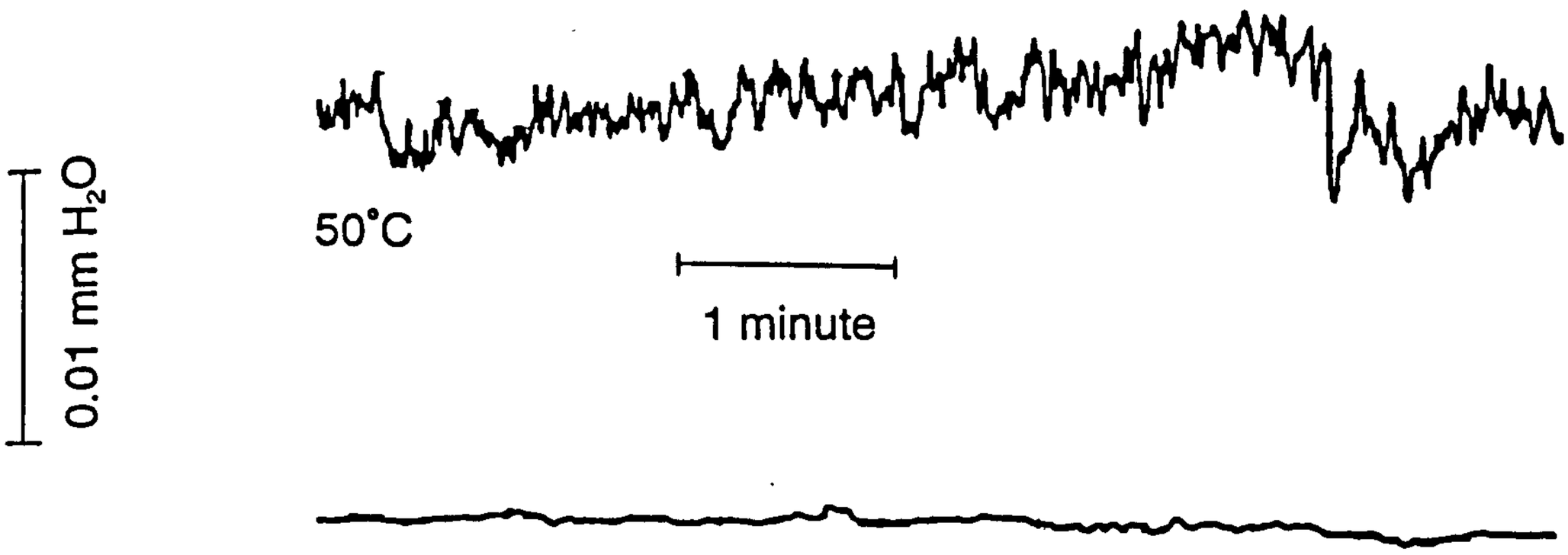

Figure 5.5 Background Noise for 1/16 inch Stainless-Steel Tubing with Oven Fan

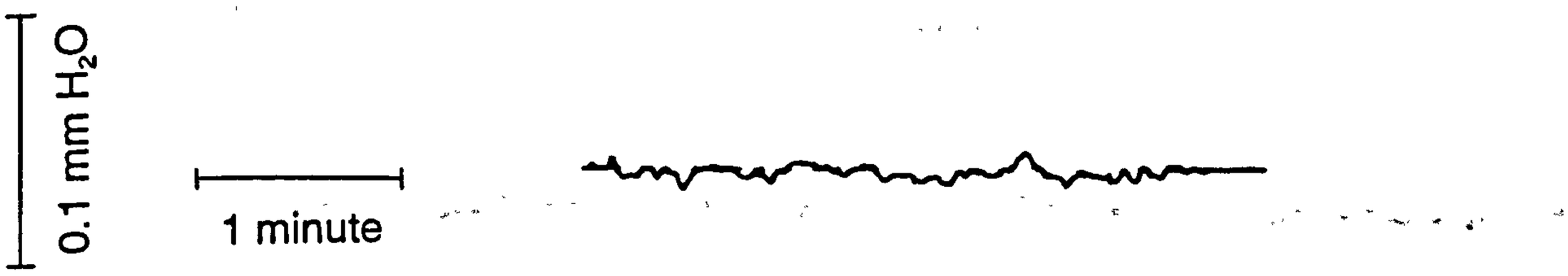

Figure 5.6 Helium Background Noise for Packed Columns at 50°C

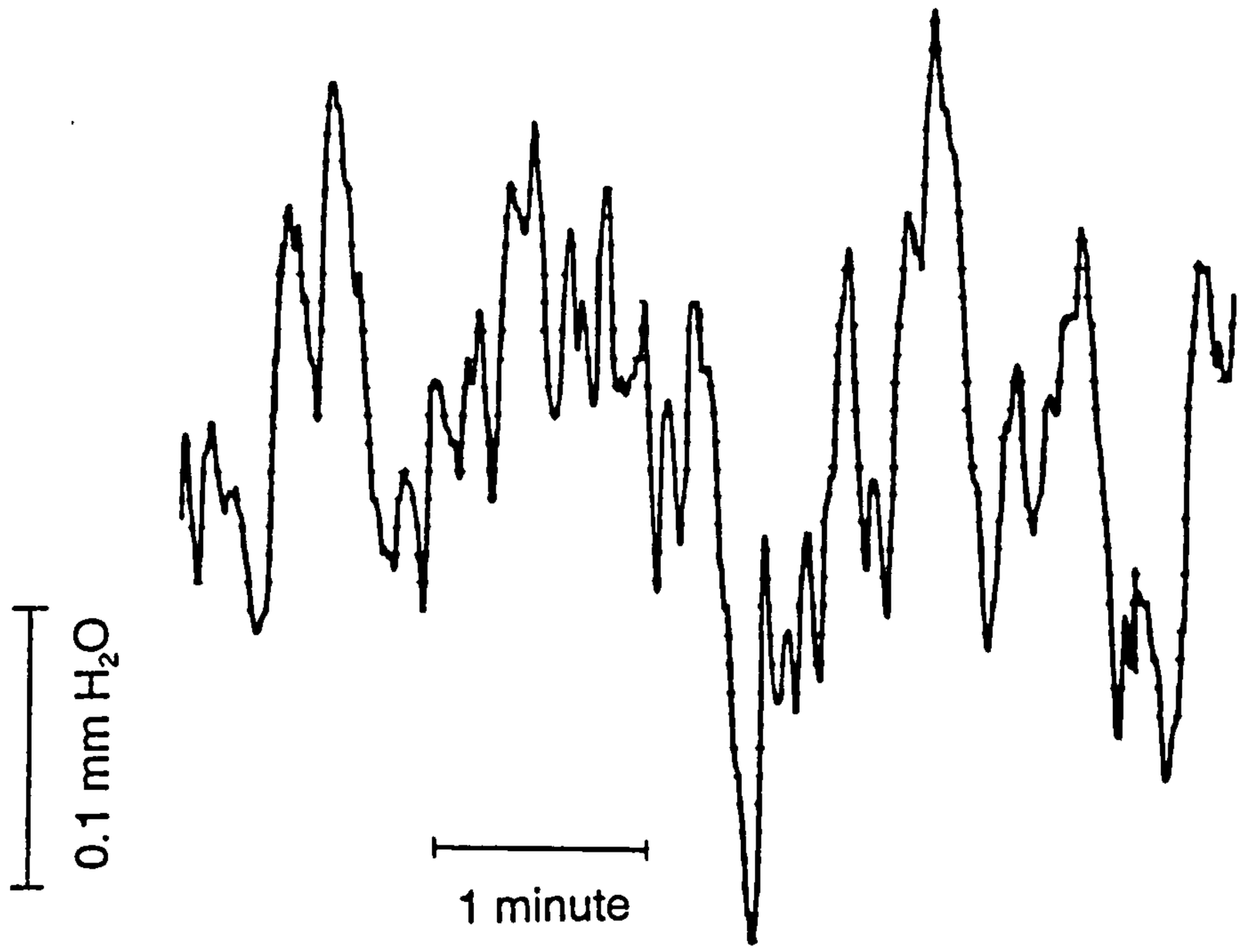

Figure 5.7 Nitrogen Background Noise for Packed Column at 50°C

These findings would suggest that potentially the columns would offer the biggest noise problem. It is obvious that the noise levels in Figures 5.6 and 5.7 are unacceptable, and at the start of the project it was conventional to enclose the columns in a brass container. This resulted in a much improved noise level shown in Figure 5.8.

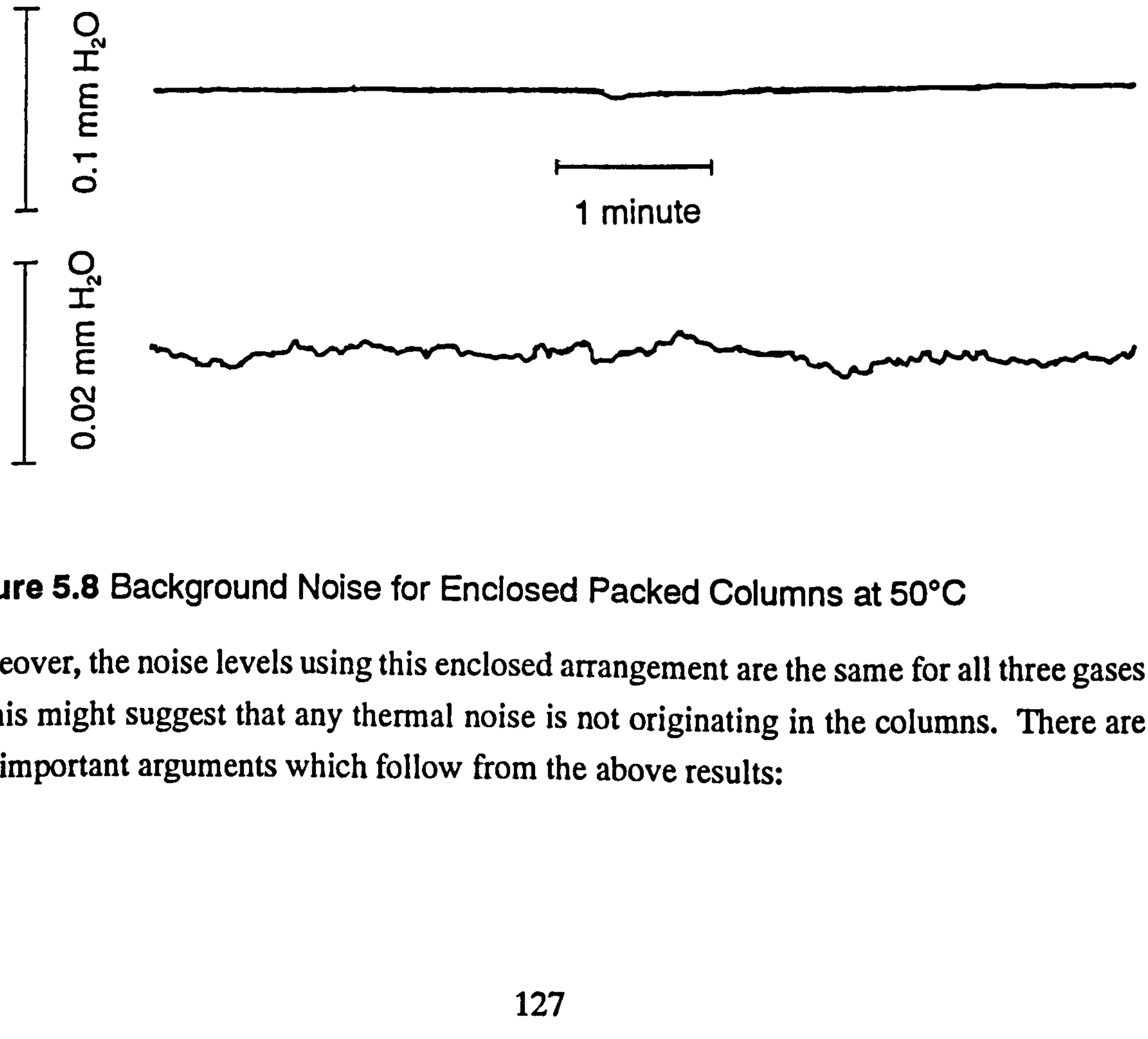

Figure 5.8 Background Noise for Enclosed Packed Columns at 50°C

Moreover, the noise levels using this enclosed arrangement are the same for all three gases so this might suggest that any thermal noise is not originating in the columns. There are two important arguments which follow from the above results:

1. Enclosing the columns gives a great reduction in the noise level, and from Section 5.2 it has been shown that this will change the type of convection greatly reducing the heat transfer coefficient. Hence, the importance of the overall heat transfer coefficient is demonstrated.

2. The noise level in Figure 5.5 is solely due to the gas expanding and contracting. By holding the empty glass column, the deviation is seen to be about four times as great as that for the stainless-steel tubing. Similarly, replacing the stainless-steel tubing in the oven with the empty glass tubing, the noise level is seen to increase. Obviously, this noise level is due to the gas expanding and contracting and does not involve gas adsorbing or desorbing. However, glass has a much lower thermal conductivity than stainless-steel, and moreover, the glass columns have a wall thickness about four times as great as that for the stainless-steel tubing. Obviously, the relative effects cannot be explained in terms of the thermal conductivities. It is thus necessary to consider the mode of heat transfer to the outside of the tubing (forced convection). The equation for forced convection heat transfer to the outside of a single tube is given by (Coulson and Richardson, 1982c):

$$Nu_{OF} = \frac{h_O d_O}{k_G} = 0.24 Re^{0.6} \qquad 5.21$$

For a constant fan speed, the expression on the right remains relatively constant (because of the power less than one) so that the coefficient for glass tubing (h_O) is probably 1/4 that of the stainless-steel tubing. Therefore, this coefficient cannot explain the relative noise levels. Thus, the only other difference between the two situations is the tube internal and external diameters; the glass tubing is about four times wider than the stainless steel tubing. The external surface area (external diameter) determines the total heat rate into the tubing. The internal surface area determines the area with which this heat can contact the gas. Further experiments will thus be necessary to determine the relative importance of these two diameters.

5.4.4 Secondary Experiments into Noise Factors

5.4.4.1 Introduction

From the preliminary results, it is obvious that the problem of noise factor determination is complex and that further investigation is required. Therefore, the oven noise levels were determined for many combinations of tubing arrangements and oven conditions. Packed columns are not utilised here because they would preclude the use of small bore tubing and hence prevent a comprehensive review. Also, it has been seen that the activity of the column packing is critical to the noise level, and so for a proper comparison the tubing would have to be baked out each time; considering the number of arrangements this would lead to an excessive experimental time.

5.4.4.2 Fan Speed

At the start of the project, the oven fan had two speeds. With the later introduction of a Variac, this allowed the column speed to be varied continuously from a very slow speed. For any type of tubing, the noise level will increase with fan speed. In this case the mode of heat transfer is forced convection and from Equation 5.21, the Reynolds number and hence the heat transfer coefficient will increase with fan speed. Hence, in this case the relative noise effects can be determined solely in terms of the relative heat transfer coefficients.

5.4.4.3 Tubing Insulation

By enclosing 1/16 inch stainless-steel tubing inside 1/8 inch nylon insulation, the noise level is seen to decrease significantly decrease. Nylon has a much lower thermal conductivity than stainless-steel and so the noise reduction can be partially explained in terms of the increased heat transfer resistance. Additionally, the presence of the nylon tubing will also increase the thermal mass; when an impulse in temperature arrives at the surface of the insulation, more heat will be required to heat up the material before the impulse can reach the carrier gas. However, adding progressively more insulation seems to make no further reduction in noise level. Possibly, the increase in thermal mass and heat transfer resistance will be countered by an increase in the external surface area. The same effect was qualitatively seen in Section 5.2 where the external diameter was critical to the gas temperature rise regardless of the material with which this diameter is increased.

5.4.4.4 Isolation by Enclosure and Tank

As has been discussed previously, placing the tubing in a water tank or an enclosure for isolation from the direct air flow gives large reductions in the thermal noise level. In the normal situation, there are identical carrier gas flows in each side of the system, passing from choke to column to measuring capillary via any delay lines present. However, if one of these carrier flows is bypassed around the enclosure and column before passing through the measuring capillary, the noise level significantly increases. This disparity is magnified by repeating the experiment for packed columns with a nitrogen carrier gas. Probably, the enclosure achieves noise reduction by effecting a *cancelling out effect*; the effect of a particular impulse will act on both columns at the same time and these effects will cancel out. Finally, insulating columns within an enclosure makes very little difference to the noise level. Probably, the natural convection term is limiting so that the extra insulation makes little difference to the overall heat transfer resistance.

5.4.4.5 Tubing Internal Diameter

The variation in tubing internal diameter was achieved by using 1/16 inch stainless-steel tubing with different bore sizes. As the bore size was reduced, the thermal noise level was seen to decrease significantly. Increasing the thickness of the tubing will increase the overall thermal resistance, but since the natural convection term is limiting, the thickness increase will hardly affect the overall heat transfer resistance. Of course, increasing the thickness of the tubing will increase the thermal mass and this will reduce the thermal noise. Reducing the bore will lead to an increase in fluid velocity. However, experiments conducted on a piece of tubing at varying flowrates did not indicate any variation of the baseline noise level. Of course, reducing the bore will lead to an increased pressure drop across the tubing because of the increased tubing resistance. It must be remembered that thermal noise fluctuations actually appear as pressure changes upstream of the measuring capillaries at the DPT. Thus the fluctuations have to travel through this high resistance tubing to reach the DPT; the actual length of tubing travelled will depend upon the location of the temperature impulse. These fluctuations may not be transmitted as rapidly through this high resistance tubing as they would through larger bore tubing; the tubing may act to damp out the fluctuations.

5.4.4.6 Tubing External Diameter

By increasing the stainless-steel tubing diameter from 1/16 inch to 1/8 inch, the noise level is seen to increase significantly. Figure 5.9 shows the background noise level obtained for 1/8 inch stainless-steel tubing in the oven at 50°C. According to the form of Equation 5.21, the natural convection coefficient should decrease with an increase in external diameter. However, from Section 5.2 it was seen that gas heats up more rapidly when the external diameter is increased; although the overall heat transfer coefficient is reduced, the increase in external tube area more than counteracts this reduction in coefficient. Since the heat transfer coefficient is proportional to $d_C^{-0.4}$ and the surface area is proportional to d_C, then it might be expected that the noise level should be proportional to $d_C^{0.6}$. According to this relation, doubling the external diameter should give a roughly 50% increase in the noise level. However, comparing the baseline noise levels, it would appear that the increase is approaching 100%. This extra contribution might be attributable to the reduction in tubing pressure drop with increasing tubing diameter.

The stainless-steel tubing was removed and replaced with the standard Pye columns each of length 150 cm. These have an external diameter of 1/4 inch and an internal diameter of 4mm. The oven was switched on and the flowrate baseline recorded. This baseline is not directly comparable with those for the stainless-steel tubing because of the differing tube lengths; stainless-steel tubing lengths of 50 cm were employed. From Section 5.4.2 it was

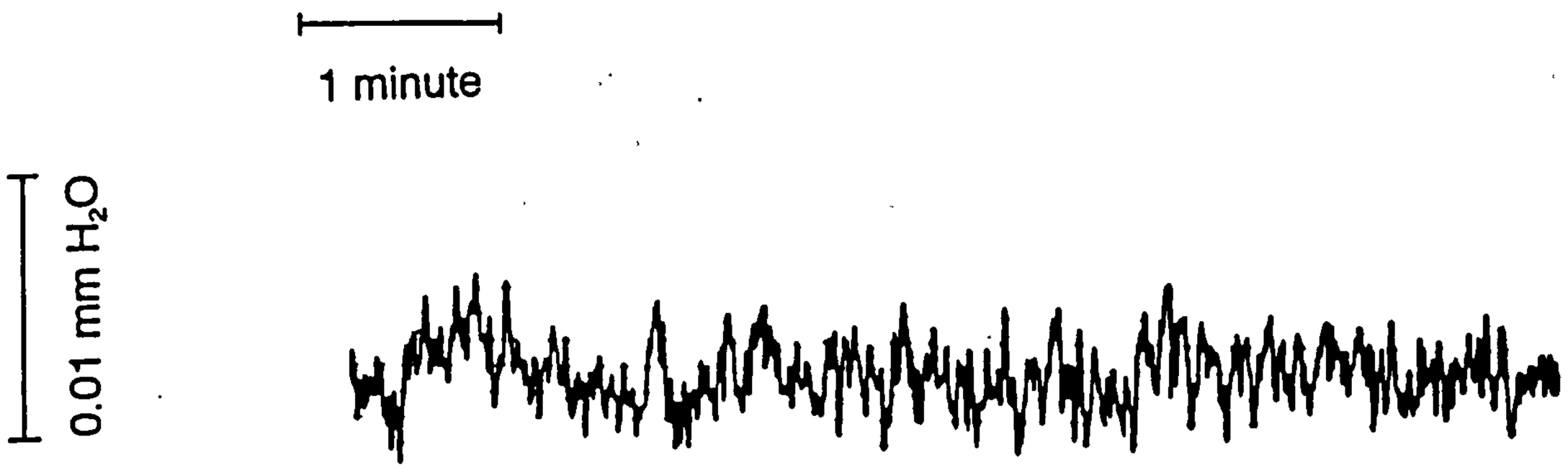

Figure 5.9 Background Noise Level for 1/8 inch Stainless-Steel Tubing

seen how tubing length might affect the noise level; hence the glass tubing noise level might need to be divided by about three to enable direct comparison. From earlier discussion, it might be expected that the (corrected) glass column noise level should be about twice that for the 1/8 inch stainless-steel tubing. However, the noise levels are roughly the same. One reason for this is the increased thickness of the tubing and the reduced thermal conductivity compared to steel. Another reason is the increased thermal mass of the glass tubing. Overall, it would appear that these two factors are enough to cancel out the effect of the increased external tubing surface area.

5.4.5 Tertiary Experiments into Noise Factors

5.4.5.1 Introduction

The secondary section enabled many conclusions to be made about which factors determine noise and so how noise can be reduced. However, these experimental runs were done without the presence of the columns. The column is effectively a buffer volume much larger than the actual empty column volume; the adsorbed concentration is much higher than the gas concentration. Apart from this volume effect, the column may offer finite resistance and affect the noise deviations. Thus a number of experiments were carried out by the standard "holding the tubing" test but including the brass block containing the columns. In each case, the tubing was held until the baseline has reached a steady position.

5.4.5.2 1/16 inch (30 and 43 thou) Stainless-Steel Tubing

Holding a length of 43 thou tubing produced a positive deviation corresponding to an increase in flowrate with gas expansion. After a few seconds, the flowrate will return to the original baseline position; the overall transient shape is pulsed. The transient is the same whether the tubing is upstream or downstream of the column. Moreover, the transient shape and size is independent of the column presence. For the 30 thou tubing, the transient shape is the same as that for the 43 thou tubing, although the size is smaller. With the slightly reduced bore, the actual gas volume to be heated is reduced and this explains the smaller deviations.

5.4.5.3 1/16 inch (20 thou) Stainless-Steel Tubing

As is expected for the 20 thou tubing the deviations are much smaller because of the reduced gas volume. However, eventually the flowrate does not return to the original baseline but is offset corresponding to a reduction in flowrate. The position of the baseline depends upon the molar flowrate through the system which depends upon the total flow resistance throughout the whole system. Before heating, the whole of the test tubing is at room temperature. When a section of the test tubing is heated, the gas in this section heats up *and* its viscosity will increase. This will increase the flow resistance of the test tubing by a *fixed fraction*. For the 43 thou tubing, the flow resistance is a negligible fraction of the total flow resistance so that the *increase* in flow resistance is negligible and the baseline shift invisible. However, for the 20 thou tubing, the change in flow resistance of the tubing caused by heating increases the total flow resistance such that a baseline shift is observed.

5.4.5.4 1/16 inch (10 thou) Stainless-Steel Tubing

For the 10 thou tubing the results of holding this tubing are striking. Firstly, the final baseline deviations are much greater than for the 20 thou tubing; the flow resistance of the 10 thou tubing is greater than that for the 20 thou tubing and so the fractional change in total flow resistance will be greater. However, the overall transient shape will depend upon the tubing position relative to the column. When the tubing is *upstream* of the column, there will be a slow movement to the final baseline position. Conversely, when the tubing is *downstream* of the column, there is a large negative overshoot corresponding to a flow reduction before attainment of the final plateau. In the heating section, the volumetric flowrate and viscosity will increase such that the pressure drop across this tubing will also increase. The extra effects are due to this change in connecting tubing pressure drop changing the average column pressure. For the upstream tubing, the average column pressure will be reduced and so gas will be desorbed from the column giving a temporary increase in flowrate. However, this positive deviation will be opposed by the negative deviation due to the final flowrate reduction; overall these effects partially cancel out leading

to a sluggish approach to the final baseline position. For the downstream tubing, the average column pressure will be increased and so gas will be adsorbed onto the column from the gas phase giving a temporary reduction in flowrate. Coupled with the negative flow deviation due to the overall flowrate reduction, the cumulative effect is an overshoot. Not surprisingly, this effect is greater for nitrogen than it is for helium. Experiments with the 10 thou tubing were repeated but using an empty buffer volume of diameter 3/8 inch but having the same volume as the empty columns. The deviations were qualitatively the same, but the overshoot for the downstream tubing was not as great, and for the upstream tubing the approach to the final baseline was quicker; the packing has a higher equivalent volume and the changes in holdup are greater for a particular change in average column pressure.

5.4.6 Applications to Reduce Column Thermal Noise

5.4.6.1 Introduction

At the start of the project, the arrangement that gave the lowest noise level is shown in Figure 5.8. This section will be devoted to attempts to further reduce the noise levels by employing different arrangements. In each case, the oven temperature is 50°C and the fan speed is low.

5.4.6.2 Brass Block Design

Following on from the *cancelling out effect* of the enclosure, it was decided to take a brass block and simply bore out two holes for the columns. A photograph of the block is shown in Plate 5.1. The logic behind this modification is due to the very high thermal conductivity and heat capacity of brass; any temperature impulse arising on the block should be quickly conducted around the block and so there would be no net column effect. The brass block would always be at the same temperature. The brass block requires connecting tubing, the length of which should be minimised and insulated. Once this is achieved, Figure 5.10 shows a typical background noise recording.

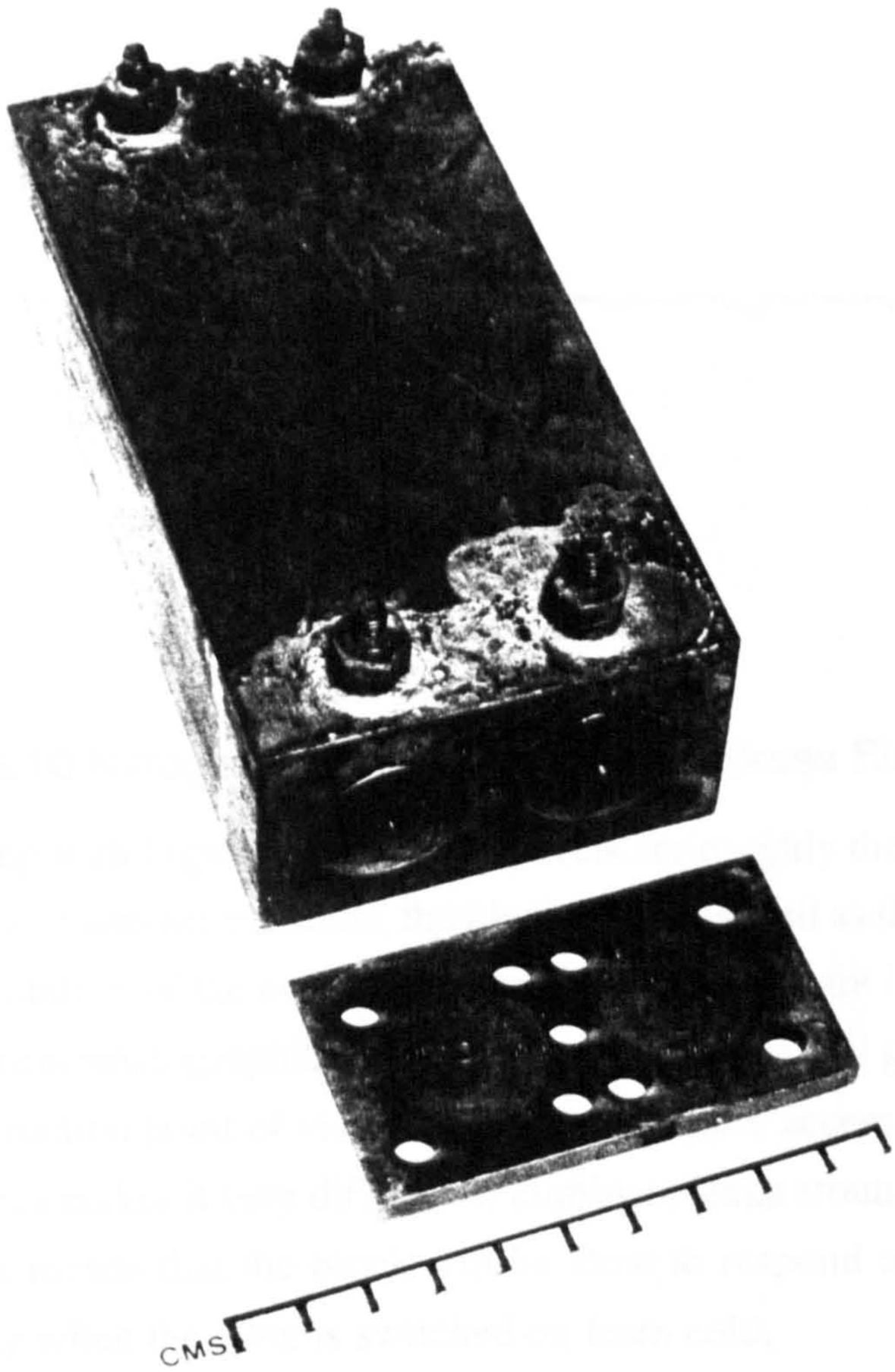

Plate 5.1 Photograph of Brass Block

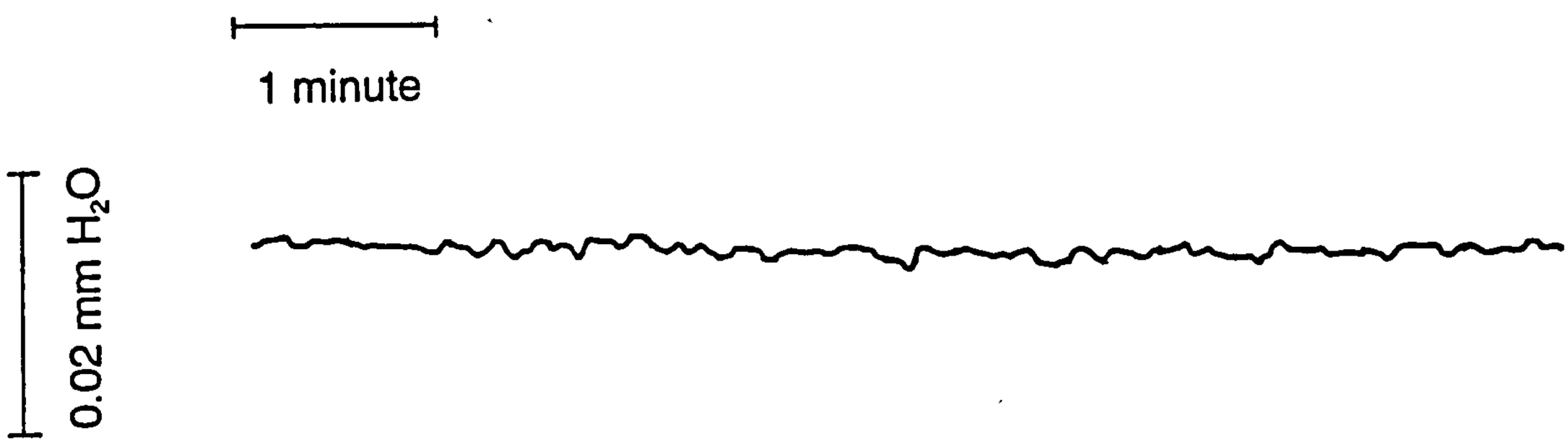

Figure 5.10 Nitrogen Background Noise for Brass Block

Comparing with Figure 5.8, the noise levels are roughly the same. Because the noise levels for all three gases are the same, the block works as well as the enclosure. However, because of the limitation of the oven dimensions, the columns are limited to being rather short and fat. From chromatographic considerations alone, this will give poor front sharpness. From the construction point of view, the columns require access in order to change the packing. This access makes it very difficult to eliminate leaks around the block. The large weight of the block means that the block will be slow to respond to changes in oven temperature, especially when the oven is switched on from cold.

5.4.6.3 Glass Pig Enclosures

The glass "pig" basically consists of standard glass columns which are coiled tightly, and all enclosed within an outer glass casing. These pigs have to be specially made, although it is possible to use a variety of column lengths and diameters. As opposed to the original enclosure these pigs provide complete sealing from the air flow. These pigs also require connecting tubing and so this must be insulated. A photograph of the pig is shown in Plate 5.2.For an air-filled pig, the noise level is roughly the same as that in Figure 5.8. However, for a water-filled pig, the baseline noise level is reduced even more and Figure 5.11 shows the improvement.

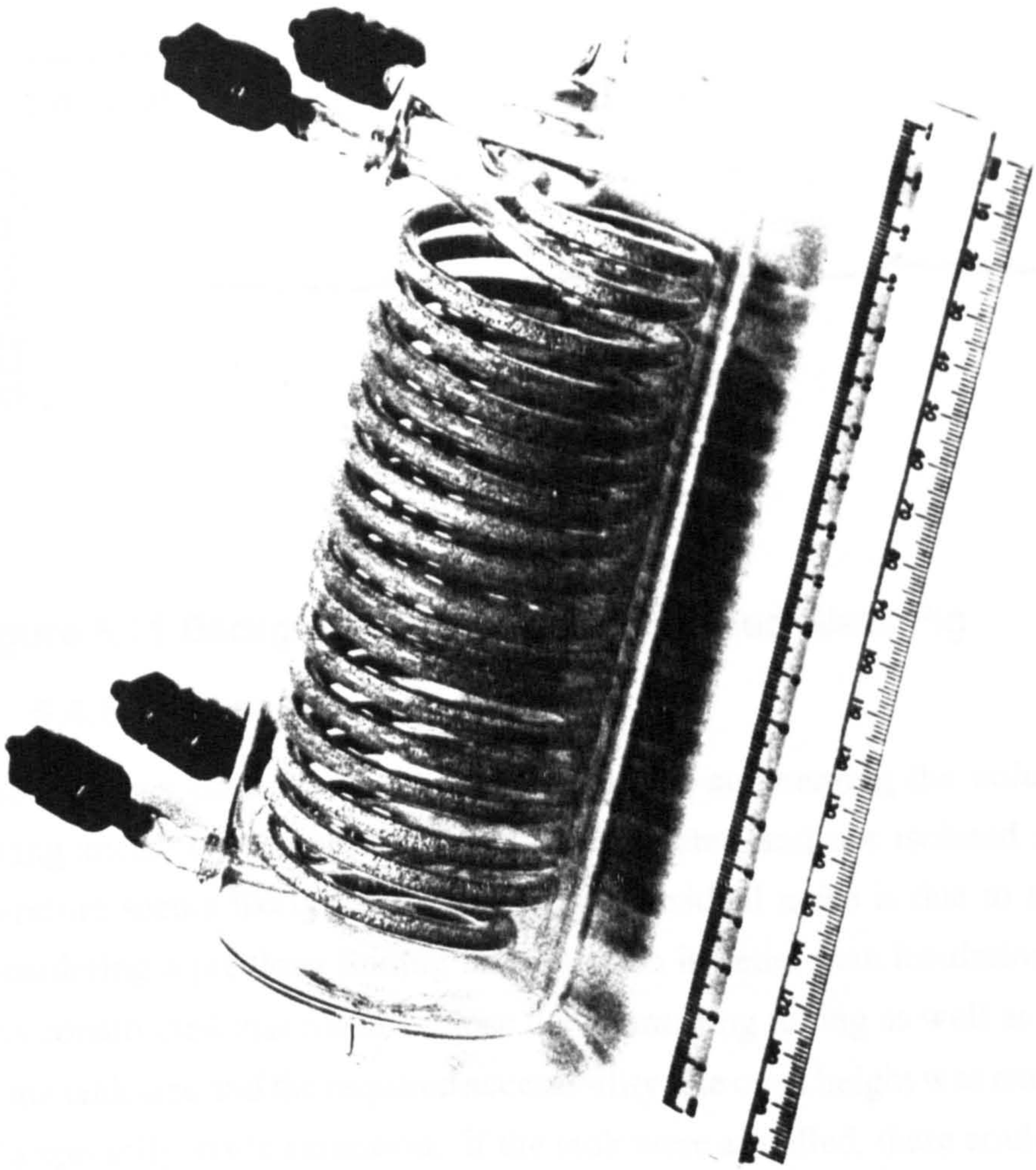

Plate 5.2 Photograph of Chromatography Pig

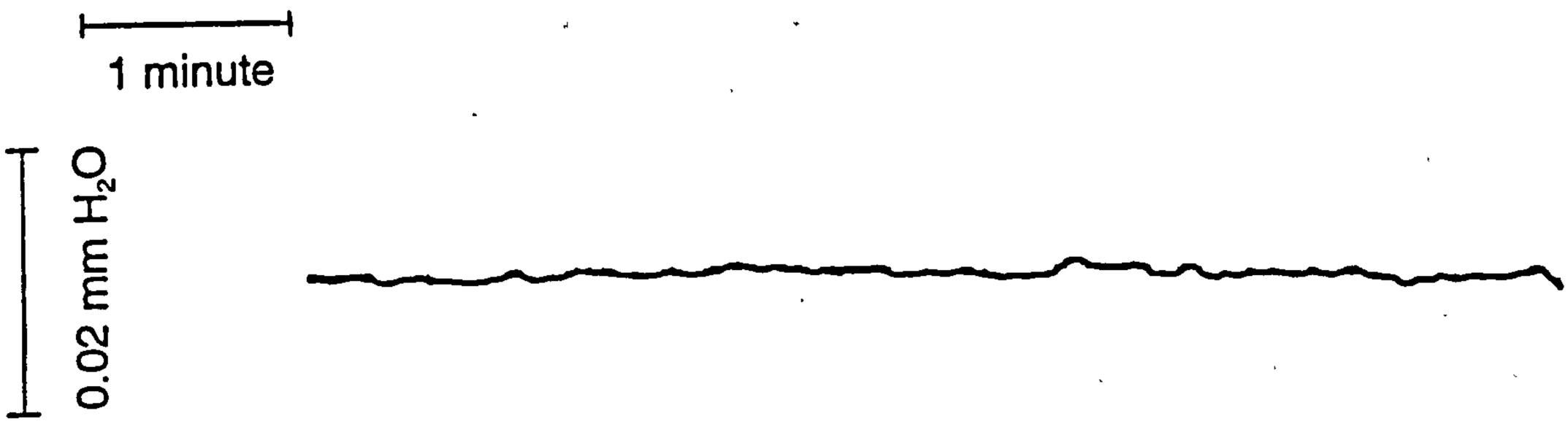

Figure 5.11 Background Noise for Water-Filled Glass Pig

5.4.6.4 Brass Water Tank

The previous case showed the importance of submerging the columns in water. In this arrangement, the connecting tubing is insulated and not isolated from the air flow. It therefore seems likely to assume that the residual noise is due to the connecting tubing, considering a previous finding that isolation is better than insulation. Hence, a water tank was constructed that could enclose the connecting tubing as well as the columns. Because of the tank size and the required accessibility, the oven height was extended by the inclusion of a specially made extension. If the tank were air-filled, there could have been a problem with hot air getting through gaps and flowing over the packed columns. At first, the columns took the form of normal Pye columns cut down in order to fit into the tank. However, the noise was bad for helium gas and very bad for nitrogen gas. This indicated that hot air flow was close to the packing and upon examining the tank this was confirmed. Another problem was that the water level would reduce with time due to evaporation. The remedy was to use one of the glass pigs instead of the Pye columns. This could be placed deeper into the tank and so the previous noise problem was solved. Actually, with this arrangement there was still some connecting tubing and so this was insulated. The resulting background noise was slightly better than that shown in Figure 5.11. The main problem with this arrangement is the many connections and hence possible sources of leaks. Each time the columns need to be baked out, the tank needs emptying and then the fittings need tightening. This can be very time consuming. Additionally, for the same reasons given previously the water tank will take a long time to heat up.

5.5 Summary of Findings

1. The carrier gas reaches the oven temperature usually within a few centimetres of entering the oven. This distance is independent of the tube internal diameter, but decreases with increasing external diameter, even if this increase in external diameter is accomplished using insulation. The reason for this is that the limiting mode of heat transfer is convection to the tube external surface, and increasing this tube surface will greatly increase the rate of heat transfer.

2. For the present system, there are no problems with the heat of adsorption affecting the gas temperature and thus the determined equilibrium properties. Calculations have shown that the best way of reducing any problematic rises is to reduce the column diameter; the variation in the maximum temperature being approximately inversely squared. Most systems described in the literature use columns having diameters of over 3cm. In this project, the column diameter was much smaller and this will effect a significant reduction in temperature rise; even the worse systems will have rises of only around 1°C. Isolating the columns from the direct air flow will significantly reduce the convection heat transfer coefficient and increase any temperature rise. However, this will only be a problem if the temperature rise is significant originally.

3. There is only a problem with thermal noise when the oven is switched on (normal ambient fluctuations do not affect the flowrate signal). The magnitude of the thermal noise is seen to depend upon three main factors: the overall coefficient for heat transfer (OHTC), the heat transfer area and the thermal mass. Since the area is effectively fixed, the best way of reducing the OHTC is to isolate the columns from direct air flow since the limiting mode of heat transfer is the natural convection term. Enclosing the columns in a specially constructed glass pig was found to be the most effective way.

4. Although the above three points have been discussed separately, they are all connected by consideration of the OHTC. Initially, the OHTC should be high enough to ensure that the gas reaches the oven temperature before it reaches the column. As the front passes through the column the OHTC should be high enough so that any heat is dissipated quickly before it causes a temperature rise. At the same time the OHTC should not be too high so that the thermal noise is prohibitive. The solution is not simple because of the problem of *two-way heat flow*. There is thus a range of acceptable values of the OHTC. The problem of adsorption heat is characterised by unusually long tailing. Because none of the chromatograms obtained exhibit this tailing, it might be assumed that OHTC is in the correct range.

Chapter Six

AN INVESTIGATION INTO FURTHER APPLICATIONS OF DELAY-LINES

6.1 Introduction

In Chapter One, it was explained that it was conventional to switch the perturbation flow from one column to the other matched column, so that the composition and flowrate transients obtained were the cumulative effect of a perturbation gas being to one column (advancing transient) and being removed from the other column (retreating transient). This is experimentally easy to attain with a standard five-port valve, which switches the perturbation gas from one side of the system to the other. This standard procedure was repeated with a pair of newly packed columns. However, for this situation it was found that the composition fronts were emerging at slightly different times and so both cumulative transients were distorted as a result. The column masses were re-checked and the columns were baked out again. Despite some improvement, both cumulative composition and flowrate transients were still distorted. It seemed that this was due to some difference in column activity and a potential remedy would be to separate out the transients due to both perturbations so that the rogue column could be identified. Generally, this concept would also allow an investigation into any fundamental differences between advancing transients and retreating transients. This chapter is primarily concerned with how this goal can be achieved. Firstly using the standard five-port valve, separation of the transients is achieved using delay-lines in various locations. Finally, a three-port valve is used which invokes either an advancing or retreating transient in one valve movement. Many results are presented for different gas-mixture systems and different column types all at room temperature, and comparisons made. The use of delay-lines in various locations is also seen to reveal interesting behaviour.

6.2 Comparison of Perturbation Addition and Removal Effects

6.2.1 Front Sharpness and Plate Number

Comparison of fronts is mainly concerned with relative sharpness, since they will have approximately the same shape. From basic chromatographic theory, as a front moves through a column it will become broader (less sharp). The sharpness of the front can be characterised by the two related column properties; *number of theoretical plates* and *theoretical plate height*. There are other factors which determine front sharpness and these will be discussed later. The larger the number of plates, the sharper the front; this is desirable for chromatographic applications. For pulses (elution chromatography), these quantities are well defined in the literature but require measurement of the *peak variance*. This problem

is solved by assuming that the pulse can be represented by a Gaussian distribution in which case the variance can be obtained by simple measurements. This assumption is justified if the column is long enough. However, this project is concerned with using small perturbation flows (frontal chromatography), and so the front can be considered the integral of a Gaussian peak; namely representation by the normal error curve. From Purnell (1967), the following equation represents the breakthrough curve:

$$\frac{c}{c_F} = \frac{1}{2} - A_\varepsilon\left[\sqrt{N}\frac{t_R - t_C}{\sqrt{t_R t_C}}\right] \qquad 6.1$$

where N = number of theoretical plates in column
c = breakthrough concentration at time t_C
c_F = final limiting breakthrough concentration
t_R = residence time to centre of front
A_ε = normal curve of error

The form of Equation 6.1 would suggest that N should be obtained from any part of the breakthrough curve. When the term in brackets is unity, from mathematical tables the area of the error curve is 0.3413 and thus $c/c_F = 0.1587$. Thus, if the time is measured at which the breakthrough curve reaches 15.87% of its maximum deviation, the following equations are used to calculate the number of plates in the column and the theoretical plate height:

$$N = \frac{t_{16\%} t_R}{(t_R - t_{16\%})^2} \qquad 6.2$$

$$H = \frac{L}{N} \qquad 6.3$$

where L = column length
H = theoretical plate height

Indeed, calculating N at different positions should give a consistent set of values, within experimental error, and thus confirm the assumption of a Gaussian distribution. However, it will be seen that some systems have strange shapes, and for these systems it will be futile to try and calculate the plate height. In order to make a distinction, N_A refers to the number of plates for an advancing transient, and N_R refers to the number of plates for a retreating transient. The factors affecting front sharpness can be divided into three categories: column factors, isotherm curvature and perturbation step. These categories will now be dealt with in turn.

6.2.2 Column Factors

If the isotherm is linear, then the analysis is considerably simplified since only these column factors affect the front shape. Both adding and removing the perturbation gas will give exactly the same frontal shape. For this case, the well known Van Deemter equation (Van Deemter *et al.*, 1956) has been applied. The main purpose of this equation has been to help select the carrier gas flowrate which will give the optimum theoretical plate height. This is especially useful in analysis situations, where a low value of the plate height is desirable for separating peaks.

$$H = A + \frac{B}{U} + CU \qquad 6.4$$

where A = eddy diffusion term
B = longitudinal diffusion term
C = mass transfer resistance term
U = interstitial velocity of carrier gas

Each of the above terms in the equation is a contribution to the overall variance of the front. The form of the equation would suggest a minimum in the curve, and it is desirable to operate as close as possible to this minimum. This analysis will apply equally to addition and removal of the perturbation gas. Indeed, the analysis represents *linear non-ideal* chromatography and the form of the equations would suggest that both fronts will become broader the larger the column and still remain mirror-images. Of course, the analysis makes no mention of the column diameter. The exact effect of this has not been quantified, but generally it is assumed that the *column efficiency* varies inversely with column diameter. The column efficiency refers to the ability of a column to separate components and increases with a reduction of plate height.

6.2.3 Isotherm Curvature

The situation is complicated when the isotherm is curved, since the curvature will affect the frontal shapes in one of two ways (Ruthven, 1984d) depending upon the form of *isotherm transition*. The term isotherm transition refers to the change in equilibrium state caused by the perturbation flow; the two categories are *favourable* and *unfavourable*. The term transition is used rather than just isotherm because it is not only the shape of the isotherm which determines the above category but also the direction which the transition takes. If adding a perturbation gas causes a favourable transition, then removing the perturbation gas will give an unfavourable transition. If the transition is favourable, the front will be a *shock transition*, namely a vertical concentration profile (the sharpest possible) if the spreading effects of the column can be ignored. In reality, the front will expand until the

effect of isotherm curvature is cancelled out by the spreading effects of the column; this is defined as *constant pattern formation.* The front then advances with no further change in shape. The final front shape will be sharper the more favourable the transition and the lower the spreading effects of the column. However, if the transition is unfavourable, the effect will be a continually broadening front, even without the spreading effects of the column; this is defined as *dispersive wave formation.* For isotherms only slightly curved, the fronts for both adding and removing the perturbation gas will be similar in shape, and any difference will only become apparent in long columns. Many sorbates exhibit Langmuir-type behaviour, and for these the adsorption transition is favourable.

6.2.4. Perturbation Step

This section includes the effect of perturbation flowrate, and, for breakthrough curves, the sorbate composition in the carrier. A reasonable perturbation step had been assumed; usually around one percent of the carrier flowrate. For non-linear systems, reducing this perturbation step would be expected to reduce any difference between advancing and retreating fronts; the perturbation step would tend to a small length of straight line. The more non-linear the system, the smaller this step should become. However, for linear systems it might be expected that the perturbation step size would not affect the fronts. However, Ruthven (1984d) has shown that the effect of increasing the step is qualitatively similar to that of a curved isotherm. This is due to the increasing concentration giving an increased frontal velocity because of the sorption effect. This means that usually the adsorption front will tend to a constant-pattern formation.

6.3 Separating Composition Transients Using Delay-Lines

6.3.1 Introduction

As indicated in previous chapters, the composition transient is simple in shape and lasts for a short time compared to the flowrate transient. For most of the experiment, the composition record does not move until the front leaves the column and passes through the katharometer. Conversely, the flowrate record moves as soon as the perturbation is effected and finally stops deviating after the front has left the column. Thus the first task is to separate the composition transient of one column from the transient of the other column by ensuring that they appear at sufficiently different times on the composition record; namely that the delayed transient arrives at the katharometer long after the non-delayed transient has left the katharometer.

6.3.3 Use of Single Delay-Line Tubing Length

The simplest way of separating the composition transient of one column from the transient of the other column is to insert a single length of tubing between one column and the corresponding katharometer port. Figure 6.1 gives a schematic representation of the experimental arrangement.

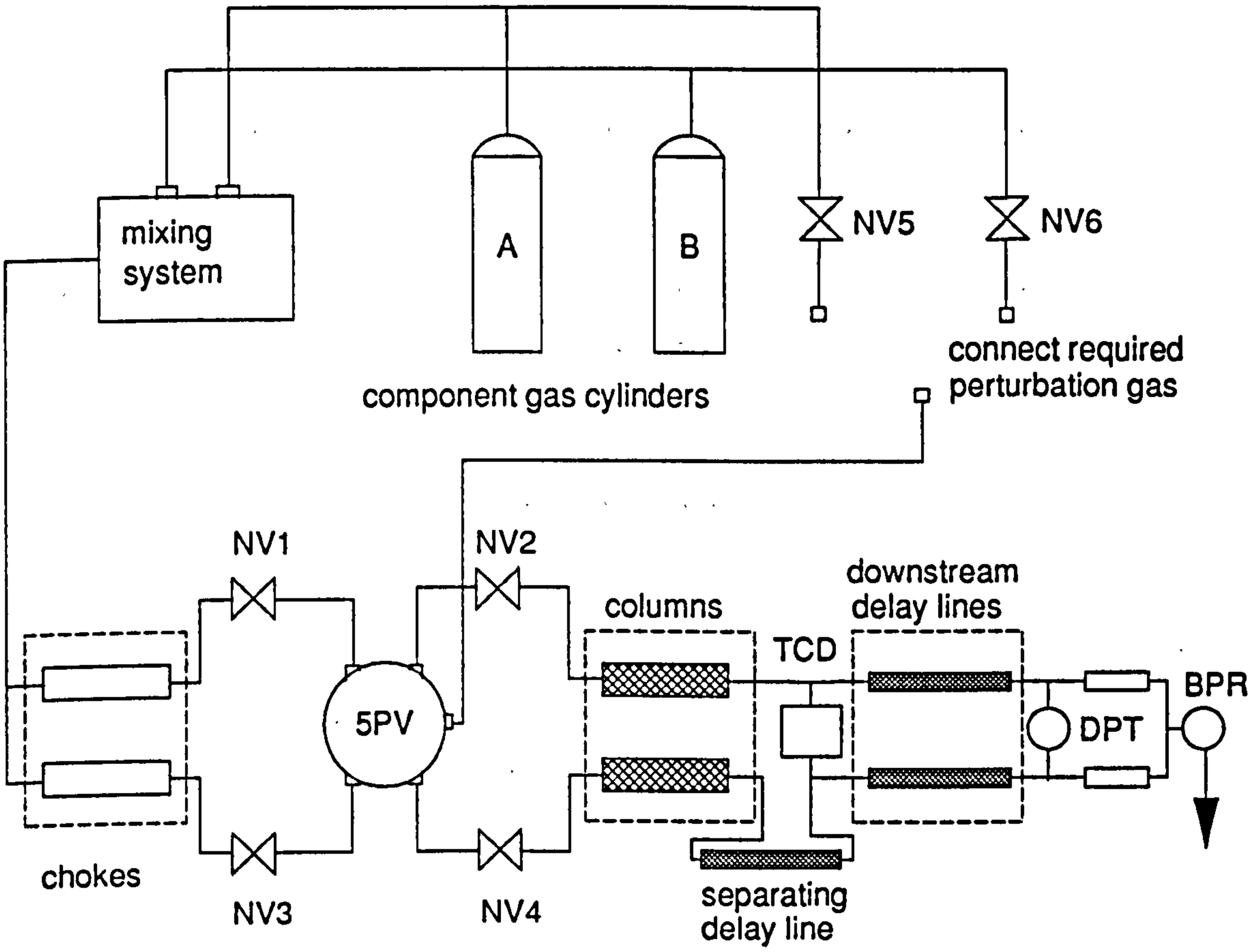

Figure 6.1 Initial Apparatus for Composition Transient Separation

The apparatus is seen to include the previously discussed downstream delay-lines in order to obtain the viscosity effect deviations. Figure 6.2 shows how typical results for switching a nitrogen perturbation gas between argon carrier flows should be affected by the separating delay-line. The bottom chromatogram is the composition record and the top one is the flowrate record. If there was no separating delay-line, the composition fronts would arrive at the TCD at the same time and the composition record would sweep straight from the initial baseline $x(0)$ to the final baseline $x(\infty)$. Because only the one side of the system has

the extra tubing, the composition front will reach the TCD later in this side than the other side (the volume of tubing determining the actual delay time). When the non-delayed composition front arrives, the composition front will sweep from the initial baseline $x(0)$ to the plateau position $x(p)$. When the delayed composition front arrives, thecomposition front will sweep from the plateau position to the final baseline $x(\infty)$. Not surprisingly, the level of $x(p)$ should be halfway between $x(0)$ and $x(\infty)$. The separating delay-line should be long enough so that the non-delayed front has completely passed before the delayed front arrives at the TCD; the broader the front, the longer the required delay-line length. However, the flowrate transients will not be separated because the columns are upstream of the separating tubing. In Chapter One, the general form of the flowrate chromatogram was explained. Because there is a flowrate reduction as the front passes through the column, the perturbation gas must be causing net adsorption. If there was no separating delay-line, both composition fronts would leave the downstream delay-lines and enter the measuring capillaries at the same time; the viscosity effect would be the cumulative effect of both fronts and would consist a direct sweep from the $n(\infty)$ position to the $p(\infty)$ position. Actually, the composition fronts will be separated downstream of the TCD, and so the fronts will arrive at the measuring capillaries at different times. The non-delayed composition front will move the pen from the $n(\infty)$ position to the intermediate plateau position $n(p)$, and the delayed composition front will move the pen from the intermediate $n(p)$ position to the final position $p(\infty)$. As for the composition record, it would be expected that the intermediate position $n(p)$ should be situated halfway between the $n(\infty)$ and $p(\infty)$ positions.

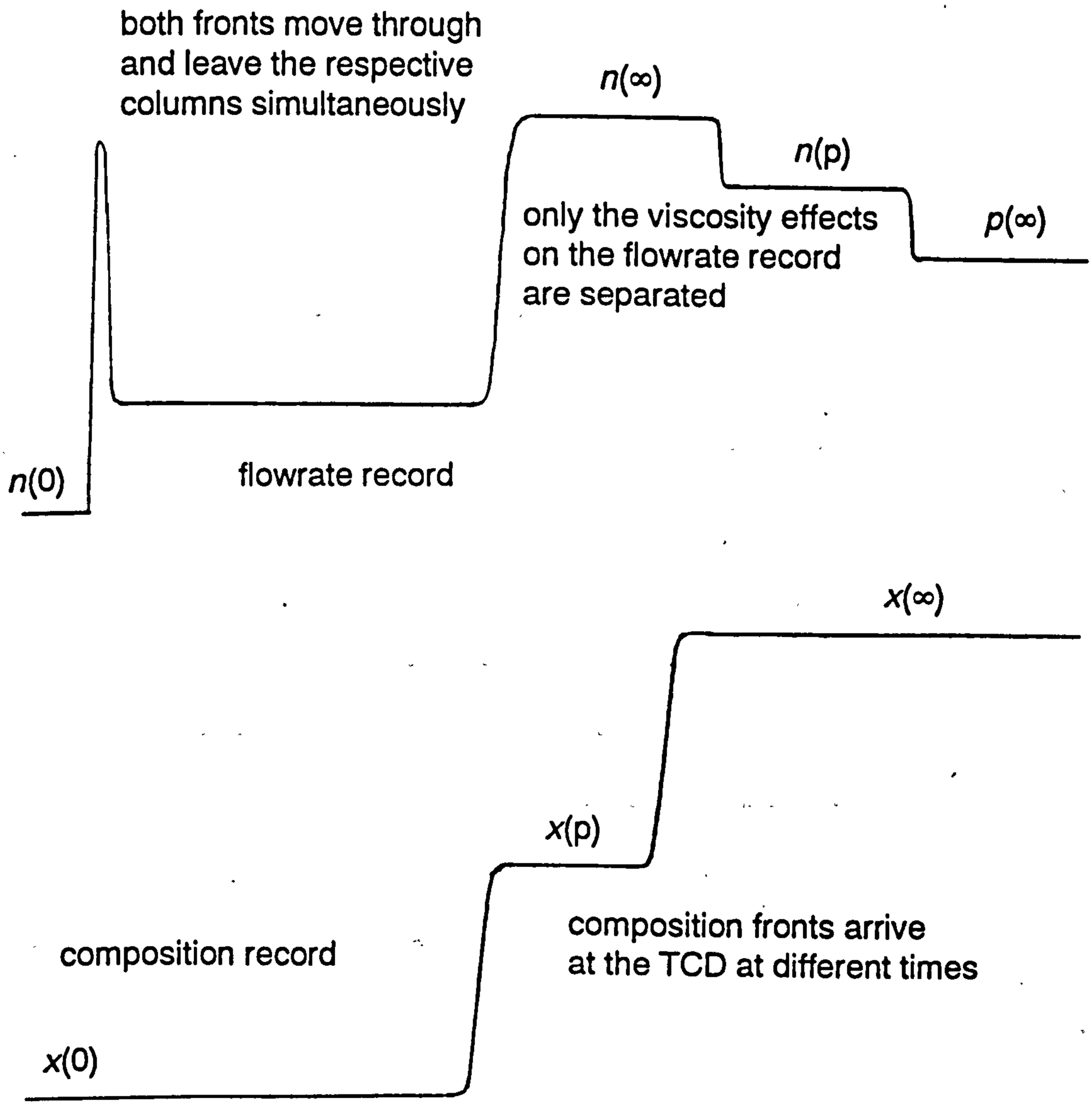

Figure 6.2 Theoretical Effect of Composition Transient Separation

6.3.3 Results Obtained for Composition Transient Separation

Lengths of either 30m or 60m of 1/8 inch tubing were employed so that a plateau could be attained on the composition record before the delayed front arrived. The results can be divided into five categories and a table will be presented for each category. When the carrier is represented by two gases with a slash between, this represents a mixture. Firstly, results

were obtained for the powder (high pressure-drop) columns using an argon carrier and a nitrogen perturbation flow. The carrier gas flowrate was varied using a constant perturbation flowrate. The results are summarised in Table 6.1.

Table 6.1 Results for Powder Columns with Varying Carrier Flowrate

P_U/bar	N_A	N_R	observations
0.7	2400	300	addition much sharper
1.1	2400	650	addition sharper
2.0	1400	1000	addition slightly sharper
2.2	1050	950	both very similar

Secondly, results were obtained for the standard columns (22-30 mesh packing size) using an argon carrier and a nitrogen perturbation flow. The results are contained in Table 6.2.

Table 6.2 Results for Standard Columns with Varying Carrier Flowrate

P_U/bar	N_A	N_R	observations
0.7	1050	380	addition sharper
1.1	600	370	addition slightly sharper
2.0	310	280	both very similar

Thirdly, using a constant P_U of 1.1 bar, many gas-mixture systems were investigated using the standard (22-30 mesh packing size) columns. In come cases, the perturbation flow was varied. The results are summarised in Table 6.3.

Table 6.3 Results for Standard Columns for Many Systems

carrier	pertbn	N_A	N_R	observations
argon	nitrogen	600	370	addition sharper
argon	nitrogen	530	460	reduced prtbn flowrate
nitrogen	argon	550	610	removal slightly sharper
Ar/N_2	nitrogen	420	390	addition slightly sharper
helium	nitrogen	730	380	addition sharper
helium	nitrogen	570	450	reduced prtbn flowrate
helium	argon	540	570	very similar
N_2/He	nitrogen	420	300	addition slightly sharper
N_2/He	helium	390	450	removal slightly sharper
argon	helium	-	-	removal, strange kinking
nitrogen	helium	360	620	removal, strange kinking
nitrogen	helium	450	570	reduced, prtbn flowrate

Fourthly, results were obtained using the powder columns but with a constant value of P_U. Many different gas systems were employed, including some mixtures. The results are summarised in Table 6.4.

Table 6.4 Results for Powder Columns for Many Systems

carrier	pertbn	N_A	N_R	observations
argon	nitrogen	1640	730	addition much sharper
argon	nitrogen	1100	900	reduced trace flowrate
helium	nitrogen	880	350	addition much sharper
nitrogen	argon	800	910	removal slightly sharper
helium	argon	500	480	very similar
argon	helium	-	-	removal, strange kinking
nitrogen	helium	-	-	removal, larger kinking

Finally, results were obtained using the large packing size columns but using a constant value of P_U. One variation was to increase the perturbation flowrate. The results are summarised in Table 6.5.

Table 6.5 Results for Coarse Particle Columns for Many Systems

carrier	pertbn	N_A	N_R	observations
argon	nitrogen	444	284	addition sharper
N_2/Ar	nitrogen	250	210	addition slightly sharper
nitrogen	helium	-	-	removal, slight kinking
nitrogen	argon	333	365	removal slightly sharper
nitrogen	argon	282	361	increased trace flowrate

Figure 6.3 shows how the chromatograms for switching a helium perturbation flow between nitrogen carriers is affected by the inclusion of a separating delay-line. The chromatogram on the left is the composition record and the chromatogram on the right is the flowrate record. For the flowrate record, the viscosity effect for each composition front is seen to occur at different times because of the presence of the intermediate plateau at n(p); this observation confirms the presence of the separating delay-line. For the composition record, it can be seen that the separating delay-line is long enough because the presence of the intermediate plateau at x(p) indicates that the non-delayed front has completely passes before the delayed front arrives at the TCD. The non-delayed transient is due to the retreating front and it can be seen that this is sharper than that due to the advancing front. Interestingly, there is a kink in the composition front as the retreating front moves through the column. This unique behaviour was confirmed by switching the five-port valve again so that the non-delayed transient was due to the advancing front; there was no corresponding kink as the advancing front moved through the column.

6.3.4 Summary of Findings

1. Employment of a single delay-line of sufficient length enables the composition transients to be separated out on the chart recorder. By switching the valve each way, two chromatograms will be obtained in which the non-delayed transient will correspond to adding the perturbation gas and then removing the perturbation gas. The delayed transients will correspond to removing and adding the perturbation gas respectively. Comparison of the chromatograms showed that the delayed composition transient was not distorted.

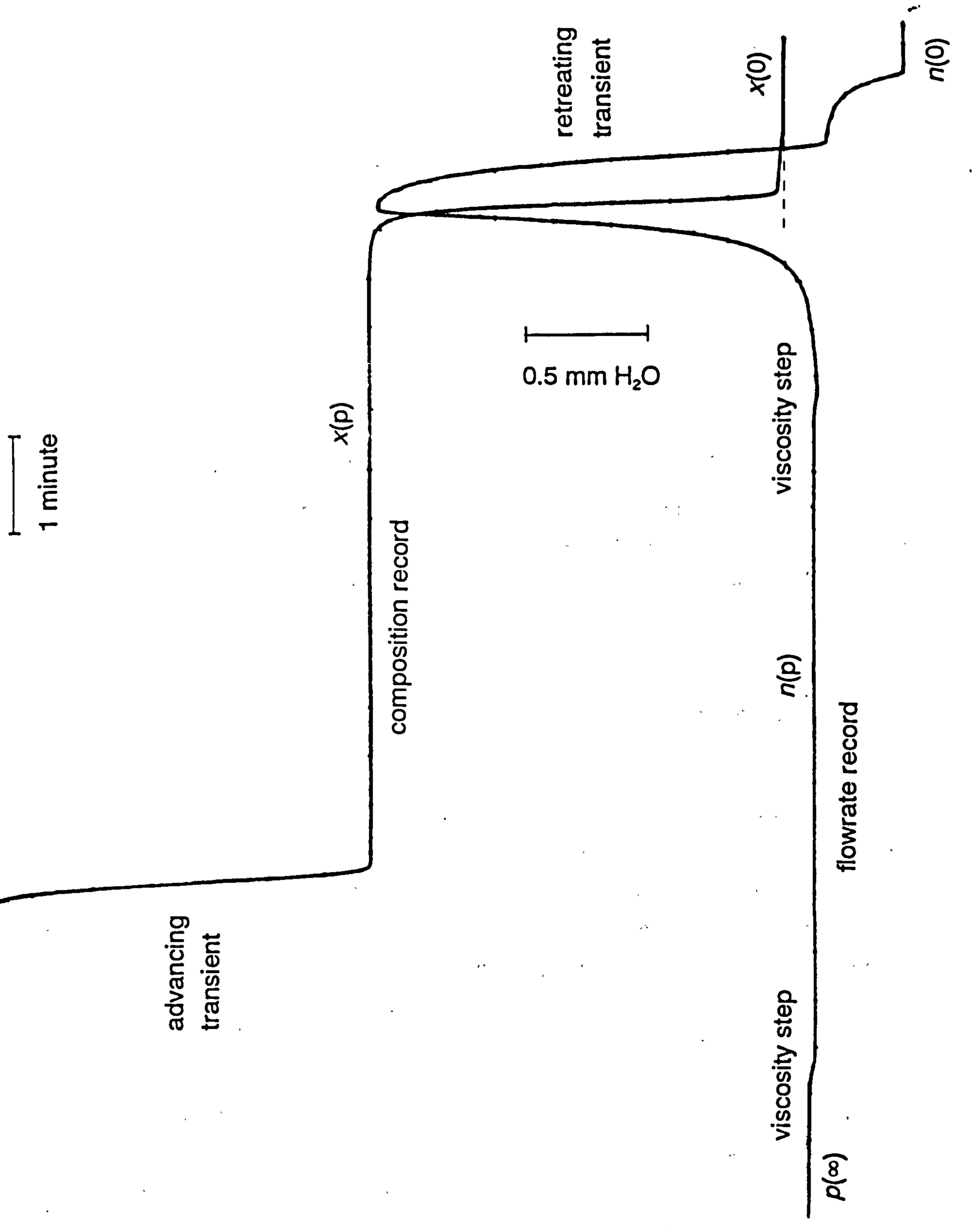

Figure 6.3 Actual Effect of Composition Transient Separation

2. When the problem of baseline thermal noise was discussed in Chapter Five, it was concluded that reduction of this noise was aided by matching the equipment components on each side of the system. Clearly, from Figure 6.1 this is not the case because of the separating delay line. The thermal fluctuations from the room alone were sufficient to impart a significant baseline noise-level on the flowrate record.

3. In general, the previous assumption of mirror-image shapes is incorrect; for some systems there is a significant difference between advancing and retreating transients but for others the difference is negligible. A good example of the latter is a helium carrier and an argon perturbation.

4. Any difference between advancing and retreating transients is increased by three factors: increasing the perturbation flowrate, reducing the carrier flowrate and using a column with a higher pressure-drop. The latter factor involves using a finer packing size.

5. By considering various parts of the composition transient, calculations have shown that the fronts are closely represented by the normal error curve. However, for systems involving a helium perturbation flow, the retreating transients demonstrate a *premature* kink as the front is passing through the column.

6. There seems to be a distinct difference in *column behaviour*; for any system, the larger packing size gives broader fronts and the finer packing size gives sharper fronts.

6.3.5 Experimental Improvements

All experiments were carried out with a single delay-line downstream of one column and no matching delay line downstream of the other column and this imbalance was seen to affect chromatogram quality. An obvious way to improve the flowrate record quality would be to insert a matching length of tubing on the other side of the system downstream of the katharometer. Figure 6.4 shows the subsequent experimental configuration. Figure 6.5 shows how the hypothetical flowrate chromatogram shown in Figure 6.2 would be affected by the balancing arrangement shown in Figure 6.4 The tubing arrangement upstream of the TCD is unchanged, and so the composition fronts will arrive at the TCD at different times and will thus be separated; the composition record will be unchanged from that of Figure 6.2. It can be seen that the total tubing length upstream of each measuring capillary is the same. Hence, each composition front will arrive at the respective measuring capillary at the same time, and the flowrate record will sweep directly from the $n(\infty)$ position to the $p(\infty)$ position with no intermediate plateau. Hence, the viscosity effects will not be separated and will appear as a cumulative effect.

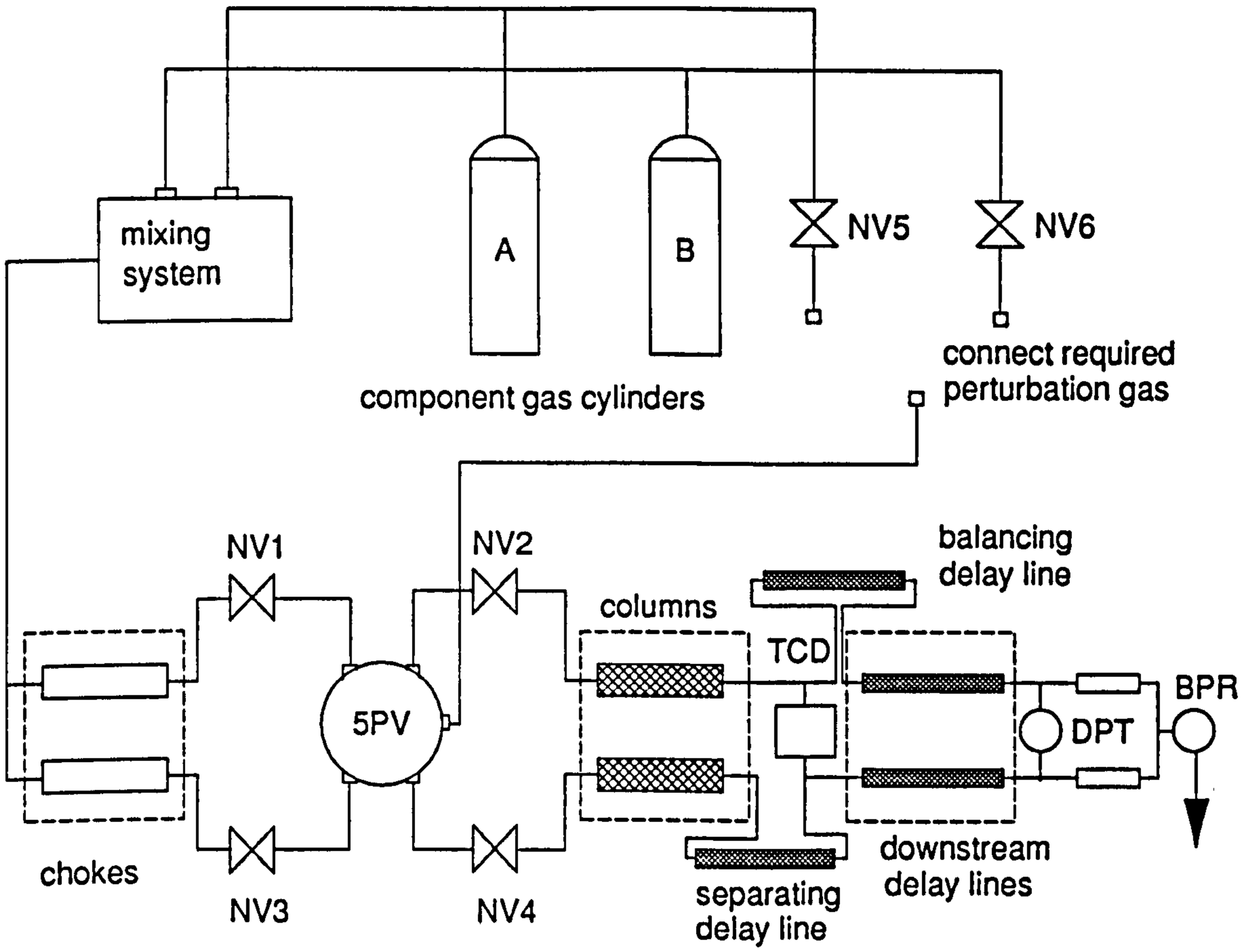

Figure 6.4 Improved Apparatus for Composition Transient Separation I

A further possibility involves using only the original downstream delay-lines and not utilising the original separating delay line. Figure 6.6 shows the subsequent experimental arrangement and it can be seen that the downstream delay-lines stagger the TCD. Similar to Figure 6.4, the tubing arrangement upstream of the TCD is unchanged and so the composition fronts will arrive at the TCD at different times and will thus be separated. The composition will be unchanged from that of Figure 6.2 and Figure 6.4. Similar to Figure 6.4, it can be seen that the total tubing length upstream of each measuring capillary is the same and so the composition fronts will arrive at the DPT at the same time; the flowrate record will sweep directly from $n(\infty)$ to $p(\infty)$ and the viscosity effects will not be separated. However, the total tubing length upstream of each measuring capillary is reduced compared to Figure 6.4 and so each composition front will spend less time in the delay-line tubing; the viscosity step at $n(\infty)$ will be shorter compared to that in Figure 6.5.

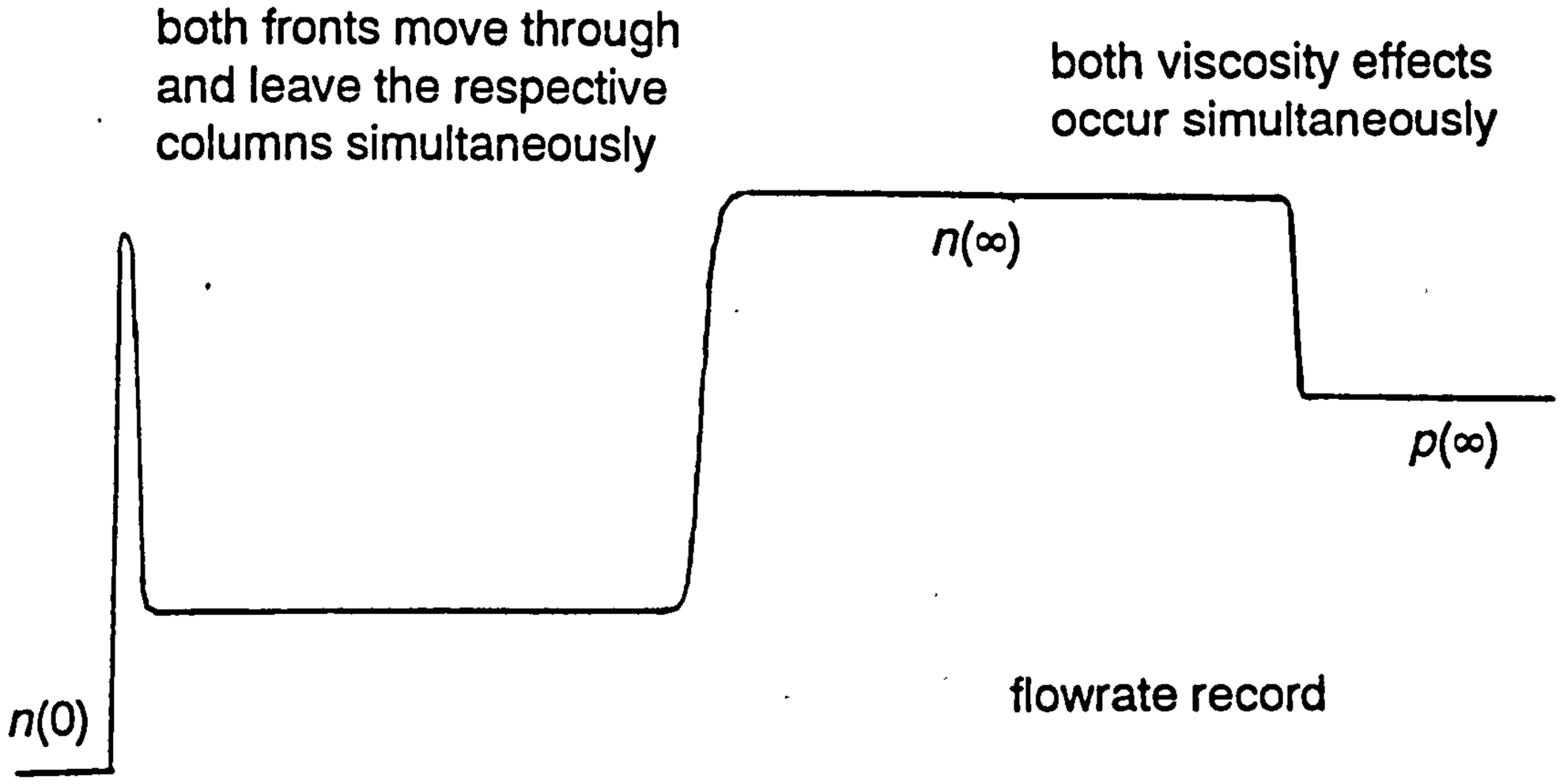

Figure 6.5 Theoretical Effect of Balancing Delay-Line Length I

6.4 Separating Flowrate Transients Using Delay-Lines

6.4.1 Using Single Delay-Line Tubing Length

Comparing with Figure 6.1, the simplest way the flowrate transients can be separated is to move the extra delay-line and place it upstream of the column. Theoretically, this should allow complete separation of both composition and flowrate transients. Figure 6.7 shows a schematic representation of the experimental arrangement. However, this idea is not as simple as it was for the composition transients, because the flowrate transients can take much longer; the system using a helium carrier and a nitrogen perturbation gas would require about 100 metres of the standard 1/8 inch tubing. Not surprisingly, this large imbalance in volume between the two sides of the system caused the flowrate baseline to become poor in quality. The noise on the flowrate record was different from the rapid fluctuations characteristic of the oven shown in Chapter Five. For this chapter, the noise consisted a much slower movement with larger deviations. The pressure drop across this long length of tubing was measured to be larger than the column, and this is undesirable. The logical alternative was to use delay tubing having an increased diameter (namely 1/4 inch tubing).

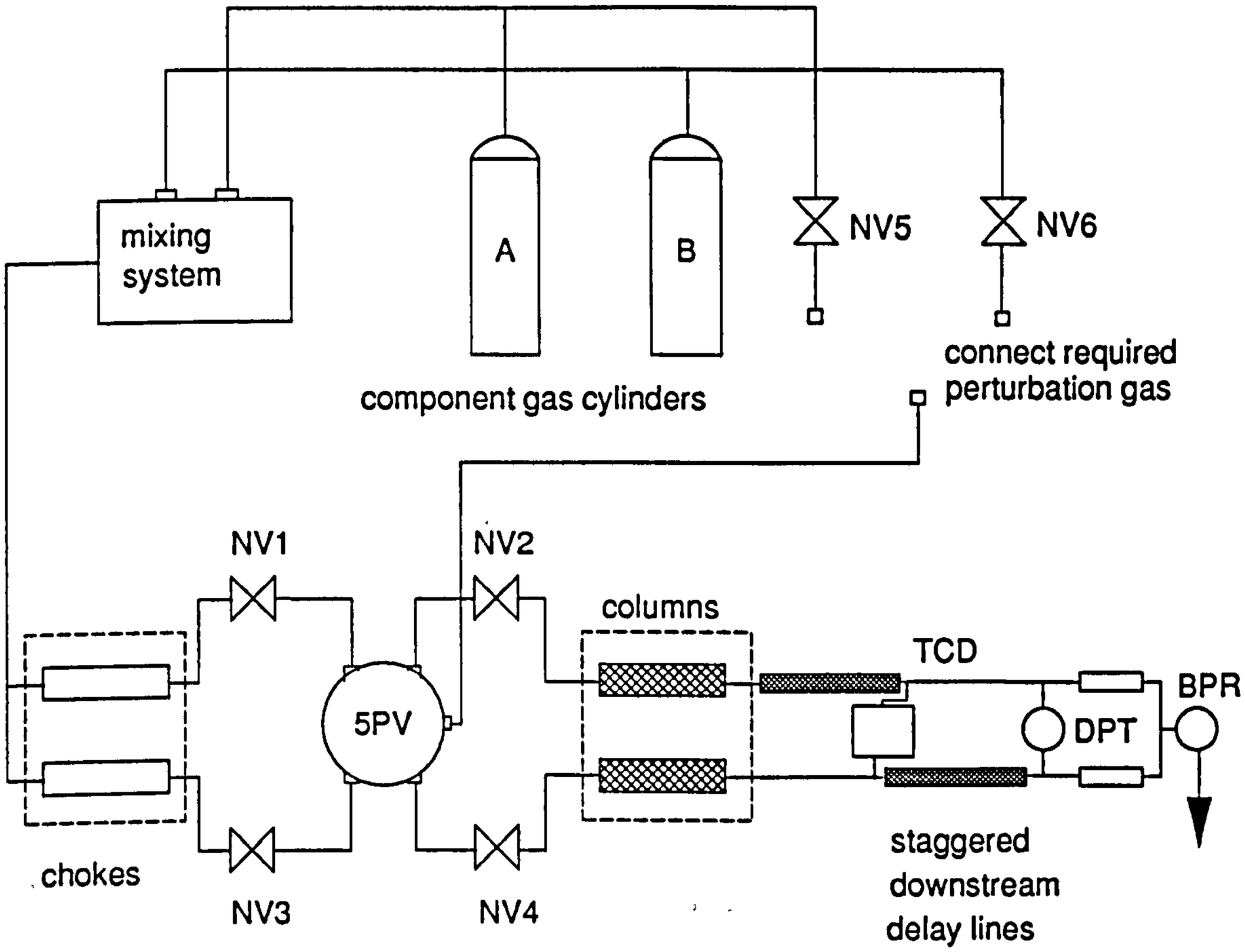

Figure 6.6 Improved Apparatus for Composition Transient Separation II

Because of the increase in tubing diameter, the same delay could be achieved with a much shorter tubing length, and the pressure drop was measured to be negligible. Preliminary results showed a big improvement in the flowrate record quality.

The flowrate transient separation obtained will be divided into two categories; *complete* and *staggered.* An example of the former case is a nitrogen carrier with a helium perturbation gas (shown in Figure 6.3), for which the transients can be completely separated with a relatively short length of tubing. That is, the non-delayed front will enter the respective measuring capillary and the flowrate pen will move from the respective $n(\infty)$ to the $p(\infty)$ positions before the delayed front has left the separating delay-line and entered the column. It is necessary that a reasonable plateau is attained at the $p(\infty)$ position before the delayed front enters the column. The latter case refers to the transients emerging with a particular delay such that while one transient is deviating, the other is moving along a plateau with no vertical deviation. One such candidate for the latter case is the system depicted in Figure 6.2. It is necessary to ensure that the delayed front enters the respective column while the non-delayed front is still passing through the respective column. Once the delayed front enters the column, there is a situation in which both fronts are in the respective columns, albeit in different parts. It is necessary that a reasonable plateau is attained before the

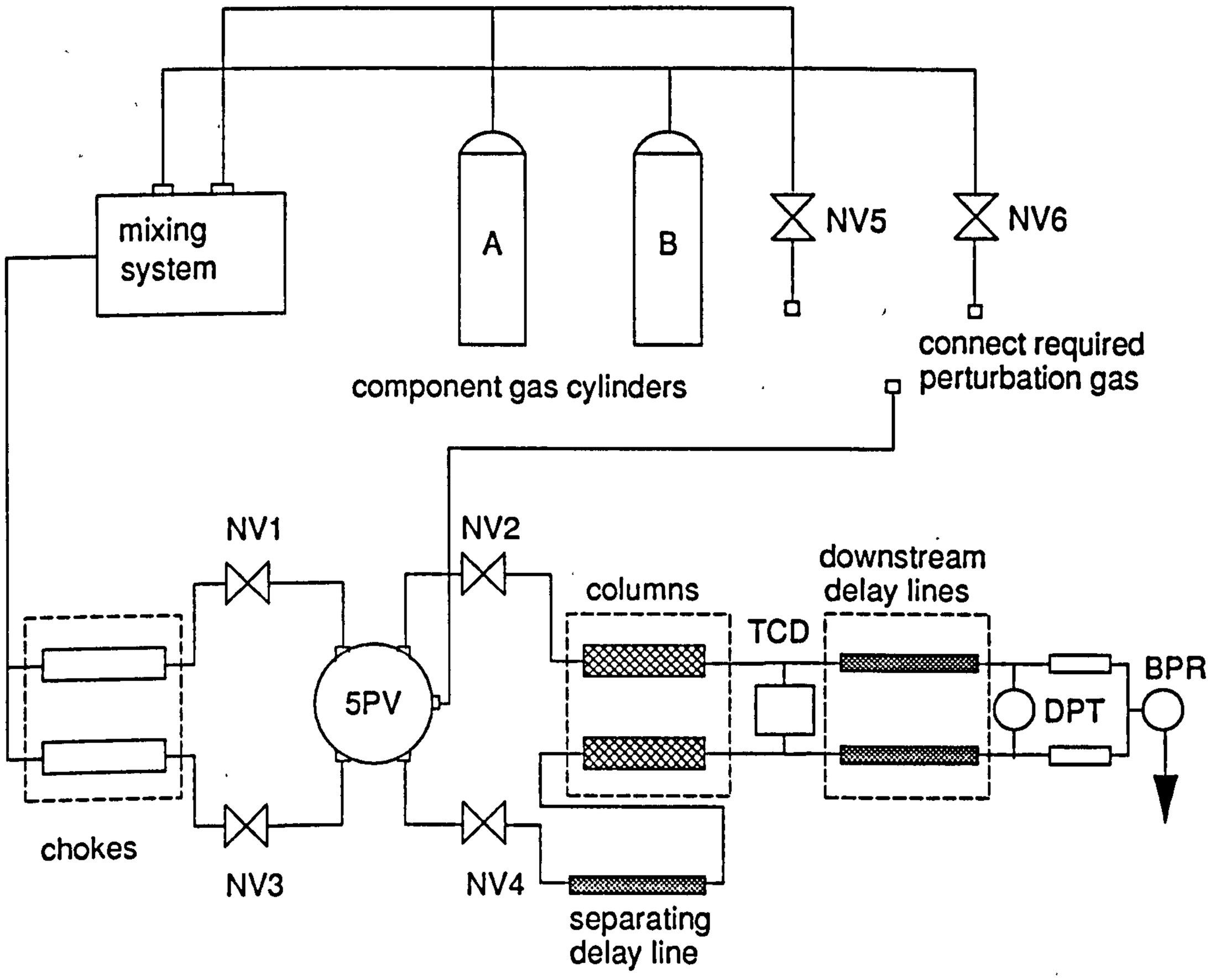

Figure 6.7 Apparatus for Complete Transient Separation

non-delayed front leaves the respective column and the pen moves to the respective $n(\infty)$ position. The subsequent viscosity effect moves the pen to the respective $p(\infty)$ position. It is necessary that a reasonable plateau is attained at this $p(\infty)$ position before the delayed front leaves the column and the pen moves to the respective $n(\infty)$ position. Finally, the viscosity effect for the delayed front will cause the pen to move to the respective $p(\infty)$ position. This type of separation is not always possible. It is more likely when the composition retention time is high (long column plateau) and the fronts are relatively sharp. Otherwise great care must be taken in selecting a suitable length so that the transients will not deviate at the same time.

6.4.2 Additional Employment of Upstream Delay-Lines

This experimental modification will not lead to any actual separation. The idea is to put equal lengths of 1/8 inch tubing upstream of *each* column, such that when the perturbation flow is added, a plateau will be attained in the flowrate record before the non-delayed front reaches the respective column. Figure 6.8 shows the subsequent experimental arrangement. It might be expected that this initial plateau level should be the same as the plateau attained

at $n(\infty)$ when the front leaves the column. The deviation from the initial flowrate baseline $n(0)$ to $n(\infty)$ corresponds to twice the perturbation flow; the same perturbation flow is *added to* one side and *removed from* the other side of the system, and the DPT measures the difference between both sides of the system. The initial plateau can be compared to that at $n(\infty)$ and observations made. By the time the front has left the column and the plateau is attained at $n(\infty)$, although the perturbation flowrate is the same, the viscosity and hence resistance of the column will have changed. This will lead to a slight change in the total molar flowrate through that side of the system. If this change is large enough, there will be a noticeable difference in plateau levels (for most cases this will be undetectable). The length of upstream delay line required to attain the first plateau will be seen to depend upon the column packing; the coarser packed columns require only five metres of tubing but the finer packed columns require at least 20 metres of tubing.

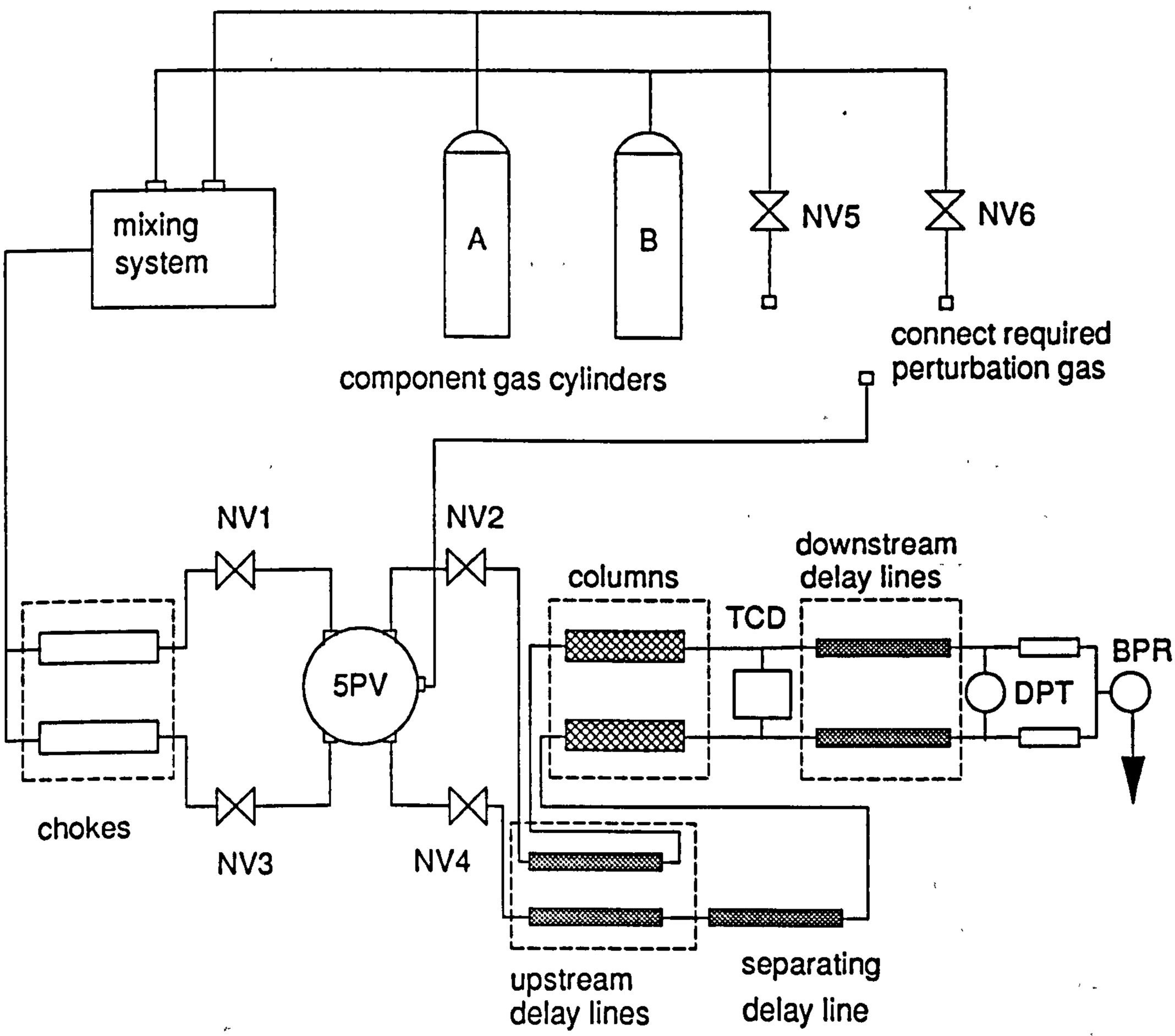

Figure 6.8 Modified Apparatus for Complete Transient Separation

6.4.3 Experimental Results and Descriptions

Experiments were carried out on many gas-mixture systems using the experimental arrangement of Figure 6.8. Also, different column types were employed. Rather than list all the many systems in turn, it has been decided to select three gas-mixture systems and comprehensively discuss the resultant chromatograms. Figure 6.9 shows the chromatograms recorded for switching a helium perturbation flow between argon carriers. The columns are of the standard dimension with the 22-30 mesh packing size. The top chromatogram is the flowrate record and the bottom one is the composition record. From the composition record, it can be seen that the separating delay-line has enabled both composition fronts to arrive at the TCD at different times and be separated; there is a plateau attained at x(p). Comparing the composition fronts would suggest that the non-delayed advancing front is the sharper. The valve was switched again so that the retreating front merged first. However, for this situation the retreating front appeared sharper. This would suggest that the delayed composition front had been distorted in both cases. From the flowrate record, the effect of the upstream delay-lines can be observed; upon switching the perturbation gas, the flowrate pen moves from the initial baseline n(0) and slowly reaches the plateau at n(p1). The distance between the positions n(0) and n(p1) corresponds to *twice* the perturbation flow. When the non-delayed front reaches the column, the helium gas will cause desorption from the column and a large increase in flowrate. When the non-delayed front leaves the column, there is no more net desorption and the pen returns to the n(p1) position as the front moves through the downstream delay-lines. When the non-delayed front enters the respective measuring capillary, the viscosity effect is seen to move the baseline position from n(p1) to n(p2). The delay-line is long enough because there is a sufficient plateau at n(p2) before the delayed front causes the flowrate increase as it passes through the respective column. However, the transient shape is distinctly different from that of the non-delayed front. This delayed "triangular shape" is obtained whether the front is advancing or retreating. The viscosity effect is seen as a shift in baseline position from n(p2) to $p(\infty)$. Finally, the separating delay-line would appear to have distorted both flowrate and composition transients.

Figure 6.10 shows the chromatograms recorded for switching a nitrogen perturbation flow between helium carriers. The columns are of the standard dimension with the 22-30 mesh packing size. The bottom chromatogram is the composition record and the top one is the flowrate record. For the composition record, it can be seen that the separating delay-line has enabled both composition fronts to emerge at different times and be separated; there is a plateau attained at x(p). Comparing the composition transients would suggest that the advancing front is sharper. Moreover, this is the delayed front so this does not appear to be distorted unlike in Figure 6.9. This difference concerns previous findings for the

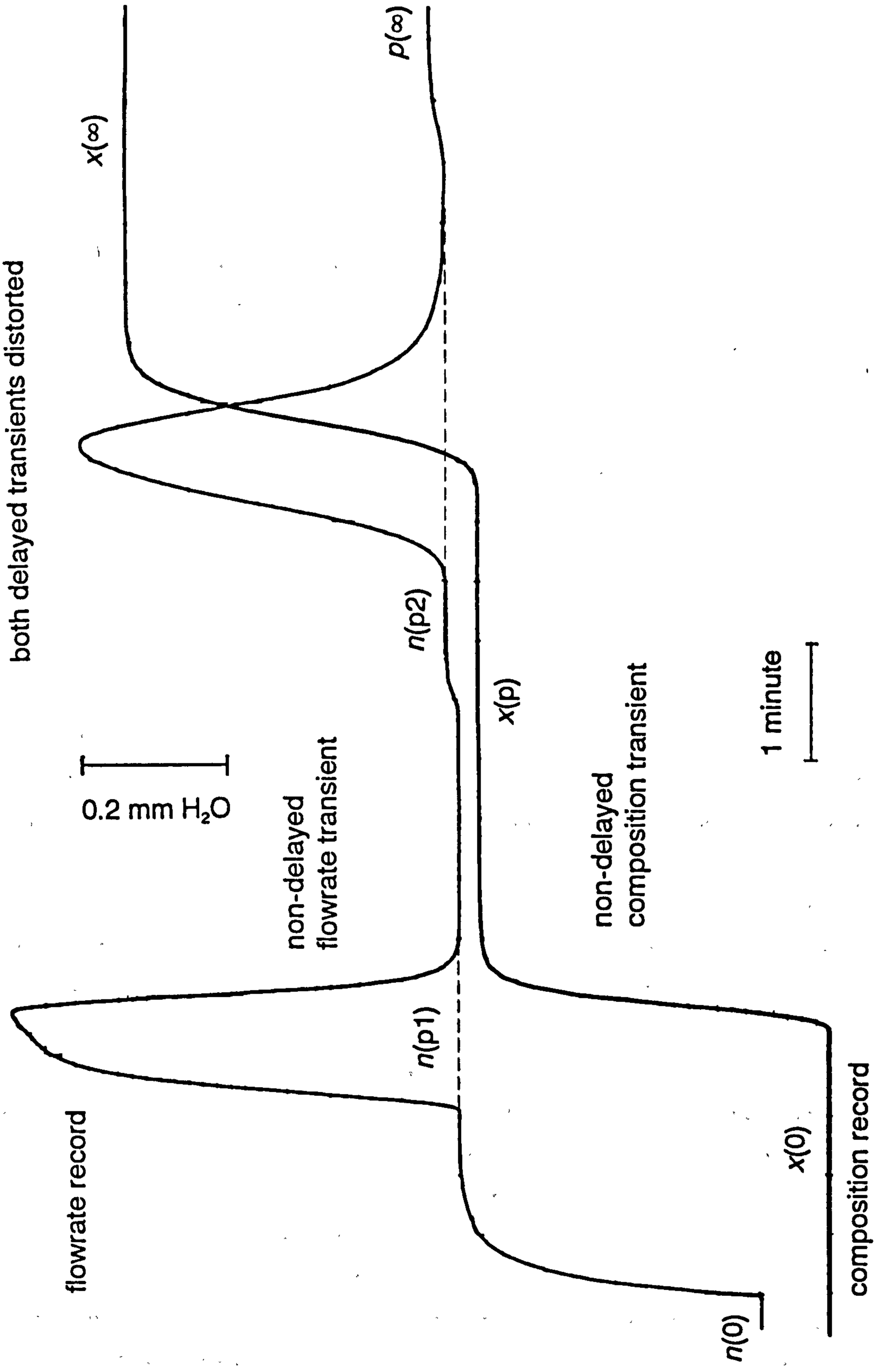

Figure 6.9 Actual Effect of Total Transient Separation

nitrogen-helium system. From the flowrate record, the effect of the upstream delay-lines can be observed; upon switching the valve, the flowrate pen moves from the positions $n(0)$ to $n(p1)$. The distance between these positions corresponds to twice the perturbation flow.

When the non-delayed front reaches the respective column, the nitrogen gas will cause net adsorption and a subsequent reduction in the column flowrate to the position *n*(p2). The next event is the delayed front reaching the respective column; the subsequent change in column flowrate will move the flowrate pen further down to position *n*(p3). When the non-delayed front leaves the respective column, there is no more net adsorption in this column and the flowrate pen moves up to the position *n*(p2). The subsequent viscosity effect as the non-delayed front moves through the respective measuring capillary moves the pen further up to position *n*(p4). The separating delay-line is long enough because a sufficient plateau is attained at position *n*(p4) before the delayed front emerges and the subsequent flowrate increase moves the pen up to position *n*(p5). The final viscosity effect will move the pen up to position $p(\infty)$. It can be seen that the delayed flowrate transient is slightly distorted by the separating delay-line. However, it can be seen that the sharpness of the composition front is mirrored by the sharpness in the flowrate record as the front leaves the column and the viscosity effect deviation. That is, if the retreating front emerges first, the plateau at level *n*(p4) is not so well defined before the delayed front leaves the respective column.

Figure 6.11 shows the chromatograms recorded for switching a nitrogen perturbation flow between helium-nitrogen mixture carriers. The columns are of the standard dimension with the coarser (11-14 mesh) packing size. The top chromatogram is the flowrate record and the bottom one is the composition record. Comparing with Figures 6.9 and 6.10, it can be seen that complete separations of the transients is obtained since the viscosity effect for the non-delayed front occurs before the delayed front reaches the respective column. Observation reveals that the delayed flowrate transient is distorted by the separating delay-line. A close look at the composition record reveals strange behaviour. As soon as the valve is switched, the composition record starts to deviate and the deviation is maintained as the non-delayed front moves through the respective column. After the non-delayed front has left the respective column, there is a slight kink in the composition record until the plateau at x(p) is attained. As the delayed front passes through the respective column, there is an increasing deviation in the composition record. This *increasing* deviation is in the opposite direction to the *maintained* deviation as the non-delayed front passes through the respective column. Finally, when the delayed front leaves the respective column, the final composition record baseline $x(\infty)$ is not attained straight away because of the characteristic kinking

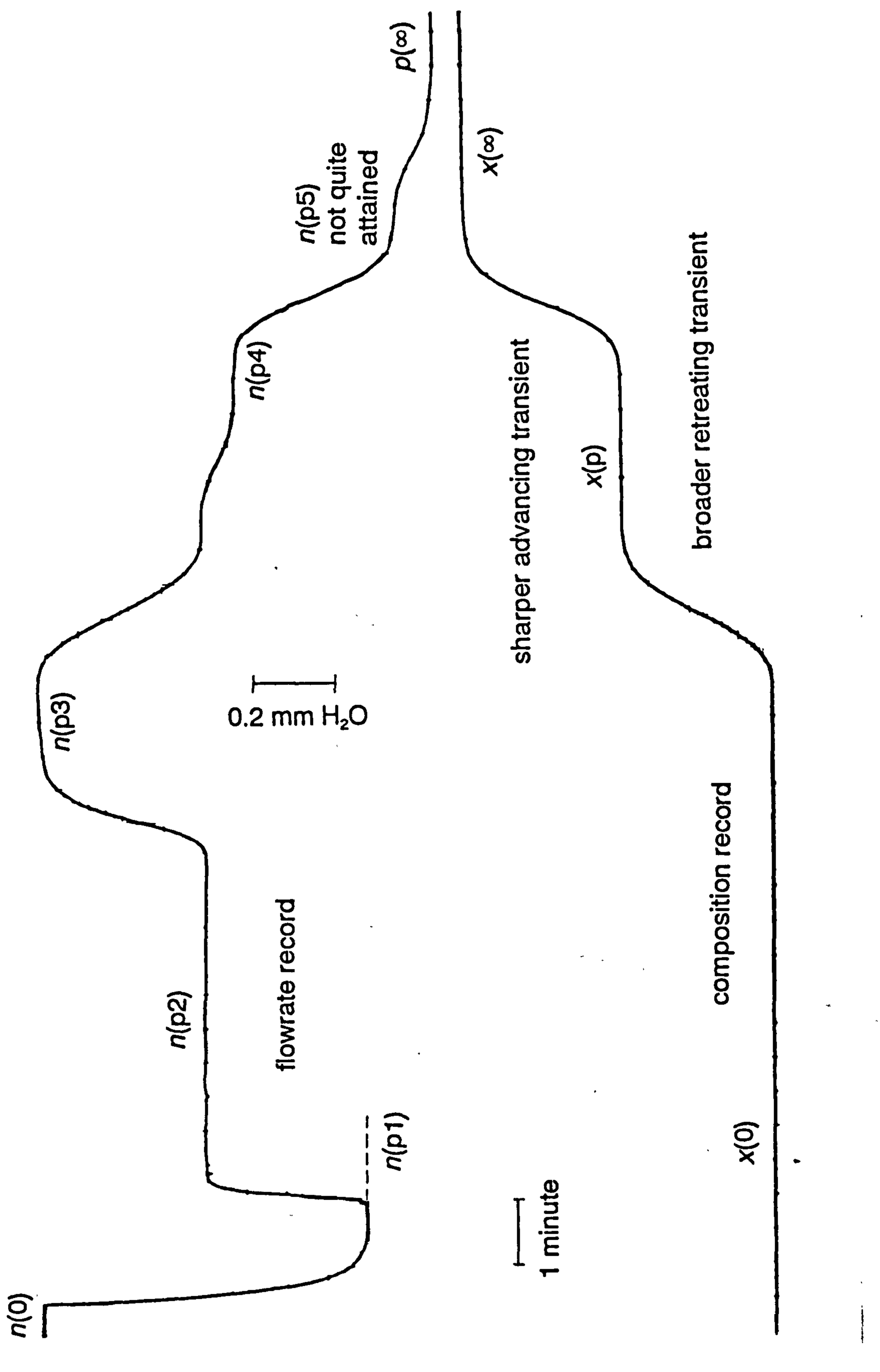

Figure 6.10 Actual Effect of Staggered Transient Separation

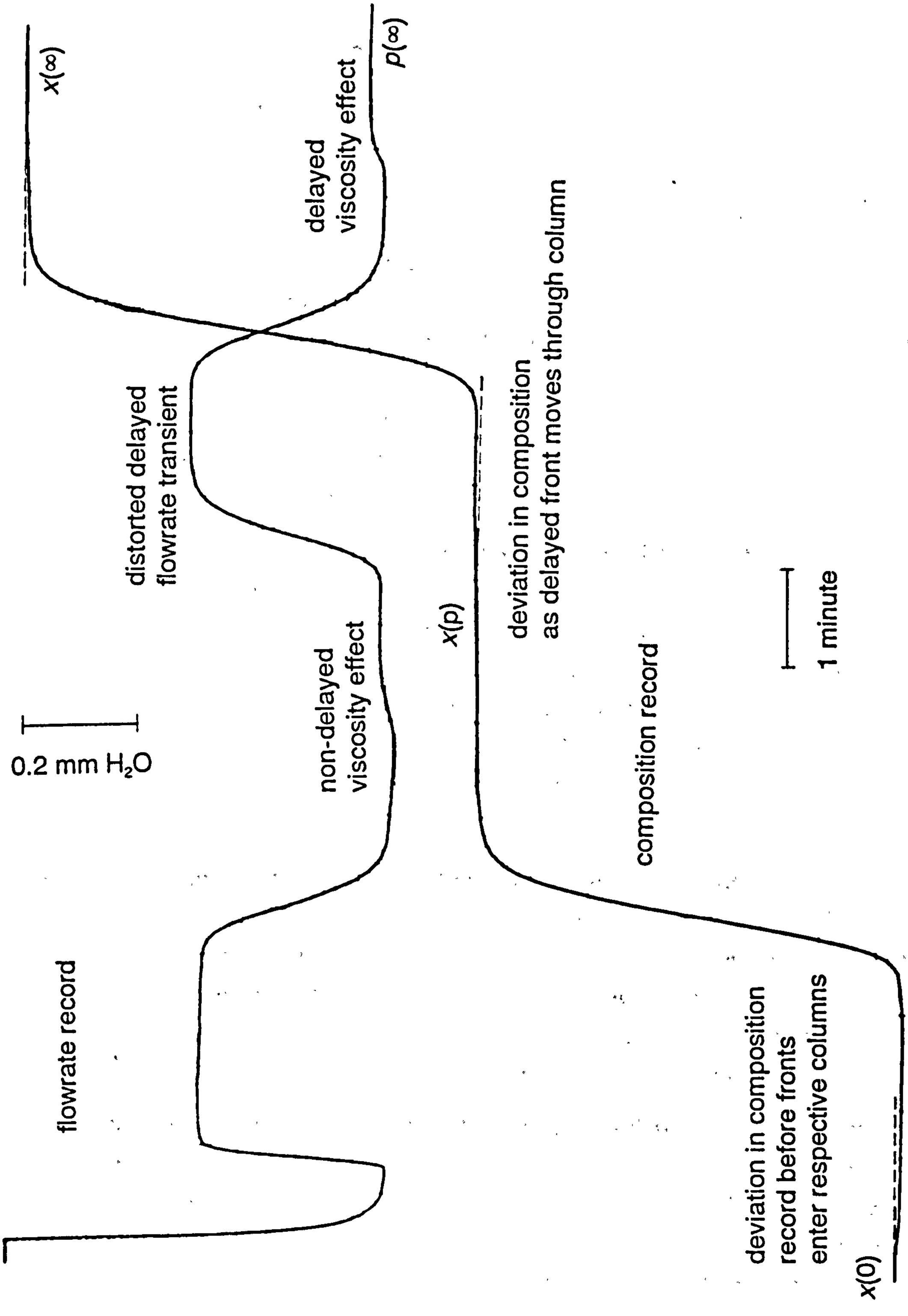

Figure 6.11 Total Transient Separation with Carrier Mixture

6.4.4 Summary of Results for Powder Columns

1. Pure Carrier and Respective Pure Perturbation Gas

Using only the 20 metres of 1/8 inch upstream delay-lines for each column, the flowrate chromatograms were obtained for the nitrogen and helium cases. Because only one component was involved for each case, the TCD was not employed. For this situation, when the perturbation gas was added, the flowrate pen moves slowly (compared to results for lower column pressure drops) from the initial $n(0)$ baseline to the final $n(\infty)$ position. Compared to the general case where the perturbation flow causes a composition change, the flowrate transient is relatively simple in shape. For the nitrogen case, it seemed to take longer for the flowrate pen to attain the final $n(\infty)$ position. The results suggested that the 20 metre length should be sufficient to enable the plateau to be attained at $n(\infty)$ before the non-delayed front could enter the respective column.

2. Helium Carrier and Nitrogen Perturbation - Separated Transients

As well as the standard upstream delay-lines described above, a sufficient length of 1/4 inch separating delay-line was inserted between one upstream delay-line and the respective column. Importantly, it was noticed that the initial plateau at $n(\infty)$ was not attained before the non-delayed front reached the respective column. It would appear that this is due to the separating delay-line. Furthermore, the delayed flowrate transients were distorted. However, the delayed composition transients were unaffected and these confirmed previous findings that for this system, the advancing front gives the sharper transient.

3. Argon Carrier and Nitrogen Perturbation - Separated Transients

The upstream and separating delay-line arrangement described above was employed for this system. Once again, the initial plateau at $n(\infty)$ was not attained before the non-delayed front reached the respective column. Also, the delayed flowrate transient was distorted. However, the delayed composition transient was not distorted and these confirmed previous findings that for this system, the advancing front gives the sharper transient.

4. Helium-Nitrogen Mixture and Nitrogen Perturbation - Separated Transients

The real interest for this system concerned the strange shape of the composition record. As soon as the valve was switched, the composition record started deviating. While the non-delayed front moved through the column, the composition record deviated in a different way. When the non-delayed front left the column, there was a kink in the composition record retarding the attainment of the final baseline position at $x(\infty)$. Qualitatively the same behaviour was noticed for the same gas-mixture system in Figure 6.11. However, for the case of Figure 6.11, columns having a much lower pressure drop were employed. It would

appear that the size of these "strange" composition record deviations is dependent upon the column pressure drop. Interestingly, for a nitrogen-argon mixture, the deviations were not so great.

6.4.5 Summary of General Findings

1. Generally, placing the single separating delay-line upstream of one column has been shown able to separate both composition and flowrate transients for the advancing and retreating fronts. However, the separating delay-line will distort the delayed flowrate transient, and it will sometimes distort the delayed composition transient. Hence, to compare both advancing and retreating fronts necessitates two movements of the five-port valve. The results for the system behaviour of Section 6.3, where only the composition transients were separated, have been confirmed.

2. The sharpness of the composition front is reflected in the sharpness of the flowrate transient as the front leaves the respective column, and the flowrate pen moves to the $n(\infty)$ position. The sharper the front, the better defined the plateau at the $n(\infty)$ position before the front reaches the measuring capillary. Then, the sharper the front, the sharper the viscosity effect as the front enters the measuring capillary and the flowrate pen moves from the $n(\infty)$ position to the final $p(\infty)$ position. This effect is clearly seen when the flowrate transients are staggered: if the non-delayed front is the sharper, a better defined plateau is attained at the respective $p(\infty)$ position before the *delayed front* leaves the respective column and the flowrate record starts to move to the next $n(\infty)$ position.

3. Clearly, placing the standard delay-lines upstream of each column causes the flowrate pen to move slowly when a perturbation flow is added. Furthermore, employing the separating delay-line makes the flowrate response even more sluggish, such that for the powder columns (high pressure drop) the $n(\infty)$ position was not attained before the non-delayed front reached the respective column. Measurement of the flowrate retention time τ_N requires measurement of the particular flowrate transient area, and so caution should be taken when measuring retention times with delay-lines.

6.4.6 Discussion of Composition Record Behaviour

The "strange" composition record behaviour obtained for the helium-nitrogen mixture carriers requires further explanation. This effect is very pronounced for the powder columns and from Figure 6.11 it is still noticeable for low pressure drop columns. It can be seen that as soon as the valve is switched, before the non-delayed front has reached the respective column, the composition of gas in the TCD is changing. Thus, the composition of the gas leaving the column must necessarily be changing. When the perturbation gas is added or removed, the average column pressure will increase or decrease respectively, and so the

amount of gas in the adsorbed phase will increase or decrease respectively. From the results, it would appear that the small change in average column pressure is accompanied by a slight change in the equilibrium adsorbed phase composition. Where the perturbation flow is added, one of the components will preferentially pass from the gas phase to the adsorbed phase leading to a change in the gas phase composition. Both columns are directly upstream of the TCD, and so any change in average column pressure will quickly change the composition of the gas leaving the column and cause a quick response from the TCD regardless of the position of the front in the column.

In Figure 6.11, as the delayed front passes through the respective column, the composition record is seen to deviate increasingly from the intermediate position at $x(p)$. This effect is unlike that noticed for the non-delayed front moving through the respective column; for the latter case, the composition record deviation is constant from the initial baseline at $x(0)$ and in the opposite direction. This difference in behaviour is because for the non-delayed front, the combined effects of the valve being switched (changing *both* average column pressures) *and* the non-delayed front moving through the column are measured. If the upstream delay-lines were long enough, both these effects would be separated out and there would be a "bulge" in the composition record and a subsequent return to the initial baseline position at $x(0)$, before the non-delayed front reached the respective column. When a front reaches the column, there is a change in the column outlet flowrate depending upon whether the perturbation gas causes net adsorption or desorption. The nitrogen perturbation gas causes net adsorption and this will temporarily reduce the column flowrate and hence the average column pressure. From previous arguments, this will cause a change in the adsorbed phase composition, and when it reaches the TCD, a deviation in the composition record. For the delayed front, it would appear that the changing deviation in the composition record is *solely* attributable to the latter effect. This will be further discussed in Section 6.5.

It can be seen that the composition record deviations are greater for the powder columns than for the coarse particle columns. This effect can be explained in terms of the chromatographic theory summarised in Chapter One. For the preliminary results, a pressure correction was employed to allow for the change in average column pressure upon adding the perturbation gas; the change in average column pressure is seen to increase with the column pressure drop. This explains why the deviations for the powder columns are greater. Summarising, for particular gas-mixture systems, changes in the average column pressure will cause unexpected deviations in the composition record. The magnitude of these deviations will depend upon the column pressure drop and gas-mixture system. The direction of these deviations will depend upon the perturbation gas.

6.4.7 Experimental Improvements

One possibility is to place a balancing length of 1/4 inch tubing downstream of the TCD, although this would cause the viscosity effects for each front (movement from the $n(\infty)$ to the $p(\infty)$ positions) to appear in the cumulative form. This is because the *total* length of delay-line upstream of each measuring capillary is the same. A final point concerns the effect of the change in average column pressure and subsequent deviation in the composition record for particular gas-mixtures. When the valve is switched, immediately the average pressure in one column increases and that in the other reduces. For reasons already discussed, because of the subsequent changes in the equilibrium adsorbed phase compositions, there will be simultaneous changes in the gas-mixture composition leaving each column. Because both columns feed directly into the TCD ports, the subsequent deviations in the composition record will arrive at the TCD at the same time and the cumulative effect will be recorded. Strictly speaking, the present delay-line arrangement will not achieve complete separation of the composition record. This can be remedied by putting an extra length of delay tubing between the katharometer and the front column only.

6.5 Complete Transient Separation Using Three-Port Valve

6.5.1 Introduction

The previous section has showed how the advancing and retreating transients can be separated using delay-lines in various arrangements. Conclusions can be made regarding the behaviour of various systems. However, the use of delay-lines can be detrimental to the flowrate record quality. Moreover, it is likely that these delay-lines will affect measurement of retention times. Hence, it is desirable to invoke either perturbation gas addition or removal in one valve movement. This would remove the problem of transient separation. This idea would require the use of a three-port valve, and this section will describe the subsequent development.

6.5.2 Initial Experimental Configuration

The simplest way that this can be achieved requires only a tee-piece where the perturbation flow joins the carrier flow. Figure 6.12 shows the experimental arrangement. The BPR is set to the same pressure as that of the tee-piece, so that there are no undesirable blips upon adding the perturbation gas. To test this arrangement, perturbation gas addition and removal were carried out for three systems using the standard columns with the standard packing.

1. Nitrogen Carrier and Nitrogen Perturbation

For this case, both flowrate transients had exactly the same shape.

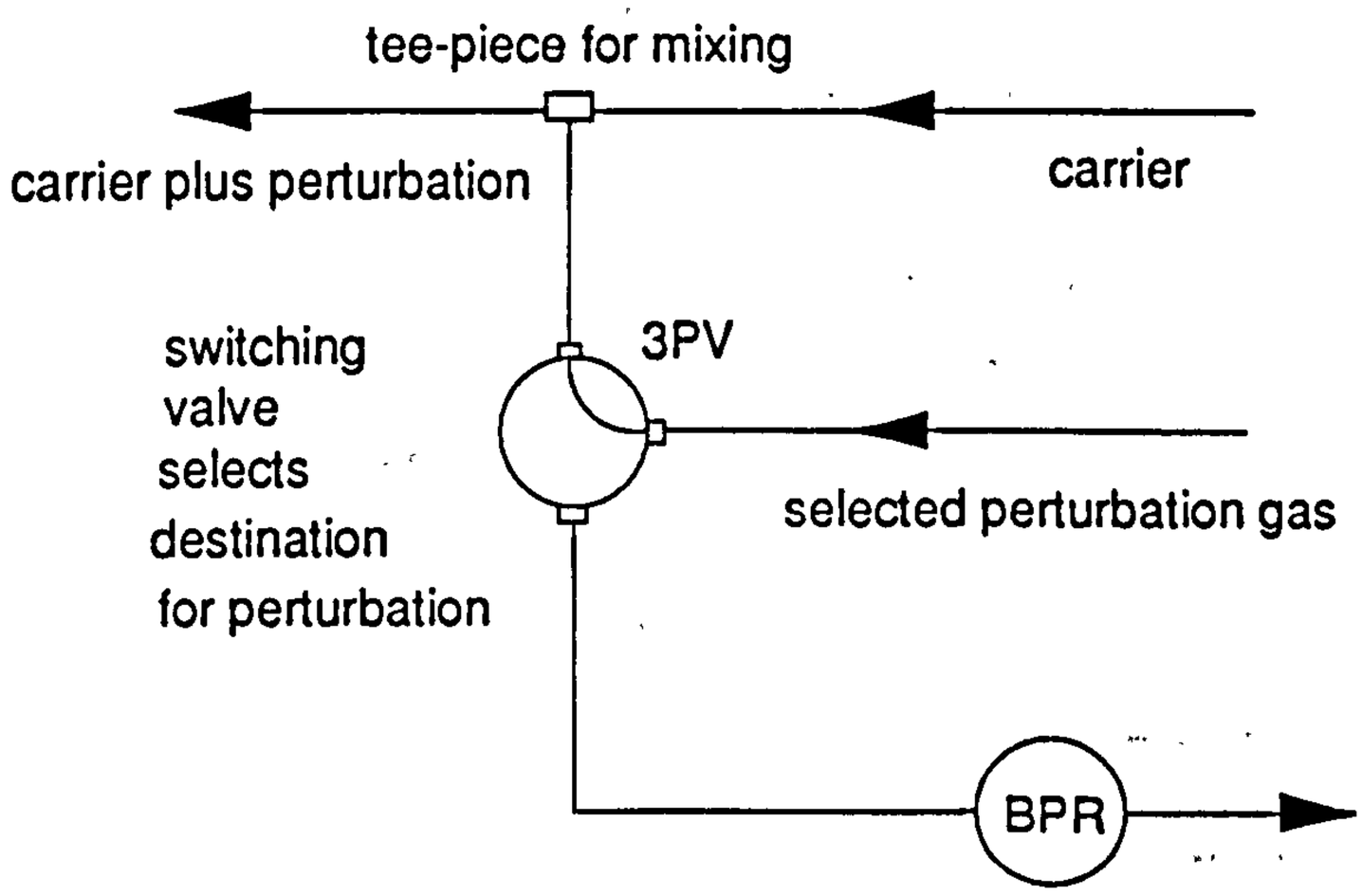

BPR = back pressure regulator
SV = switching valve

Figure 6.12 Simple Experimental Configuration for Three-Port Valve

2. Helium Carrier and Nitrogen Perturbation

For this case, the advancing flowrate transient had a shape similar to that obtained in previous sections (corresponding to a relatively sharp front). This was also echoed by the shape of the corresponding composition transient. However, the retreating transient has a distorted shape; it was more spread out than that obtained previously. For the retreating transient, the pen is unable to attain the plateau at $n(\infty)$ as the front leaves the column and enters the delay-line. Also, it is not possible to distinguish the viscosity step as the front passes into the measuring capillary and the pen moves to the $p(\infty)$ position.

3. Helium Carrier and Argon Perturbation

From previous experiments, the advancing and retreating transients should be virtually identical in shape. Indeed, the advancing transient is similar to that obtained for the previous five-port valve and separating delay-line arrangement. However, once again the retreating transient is distorted; it was more spread out than that obtained previously. Figure 6.13 shows the flowrate chromatogram for the retreating front. For the advancing front, the plateau at $n(\infty)$ is easily attained as the front leaves the column and passes into the delay-line. Then, when the front passes into the measuring capillary, the comparatively large viscosity effect moves the pen sharply to the final $p(\infty)$ position. In Figure 6.13, it can be seen that the plateau at $n(\infty)$ is barely attained as the front leaves the column. Finally, when the front passes into the measuring capillary, there is a long tail as the pen approaches the $p(\infty)$ position.

Generally, the above findings suggest that the advancing transients are consistent with the previous experiments involving transient separation, but the retreating ones are distorted. It seems that when the valve is switched to cut off the perturbation flow, this does not happen immediately. The problem is the amount of tube volume between the cut-off point (valve) and the mixing point (tee-piece). When the perturbation flow is cut off, there is still a finite volume full of the perturbation gas which will then diffuse into the system. If the perturbation and carrier gas have the same composition, then there should not be a problem and this was confirmed for the pure nitrogen case.

6.5.3. Modified Experimental Arrangement

From the results of the initial experimental arrangement, modification is required to reduce this *dead volume* as much as possible. So, a device was constructed which could be screwed into one port of the three-port valve. The carrier gas would then be directed through this device over the external surface of the central tubing to the end of the port where it would be mixed with the perturbation flow. The resultant mixture would then return down the centre of the tubing. This device was developed elsewhere in the laboratory and Figure 6.14 shows a schematic cross-section of the mixing device.

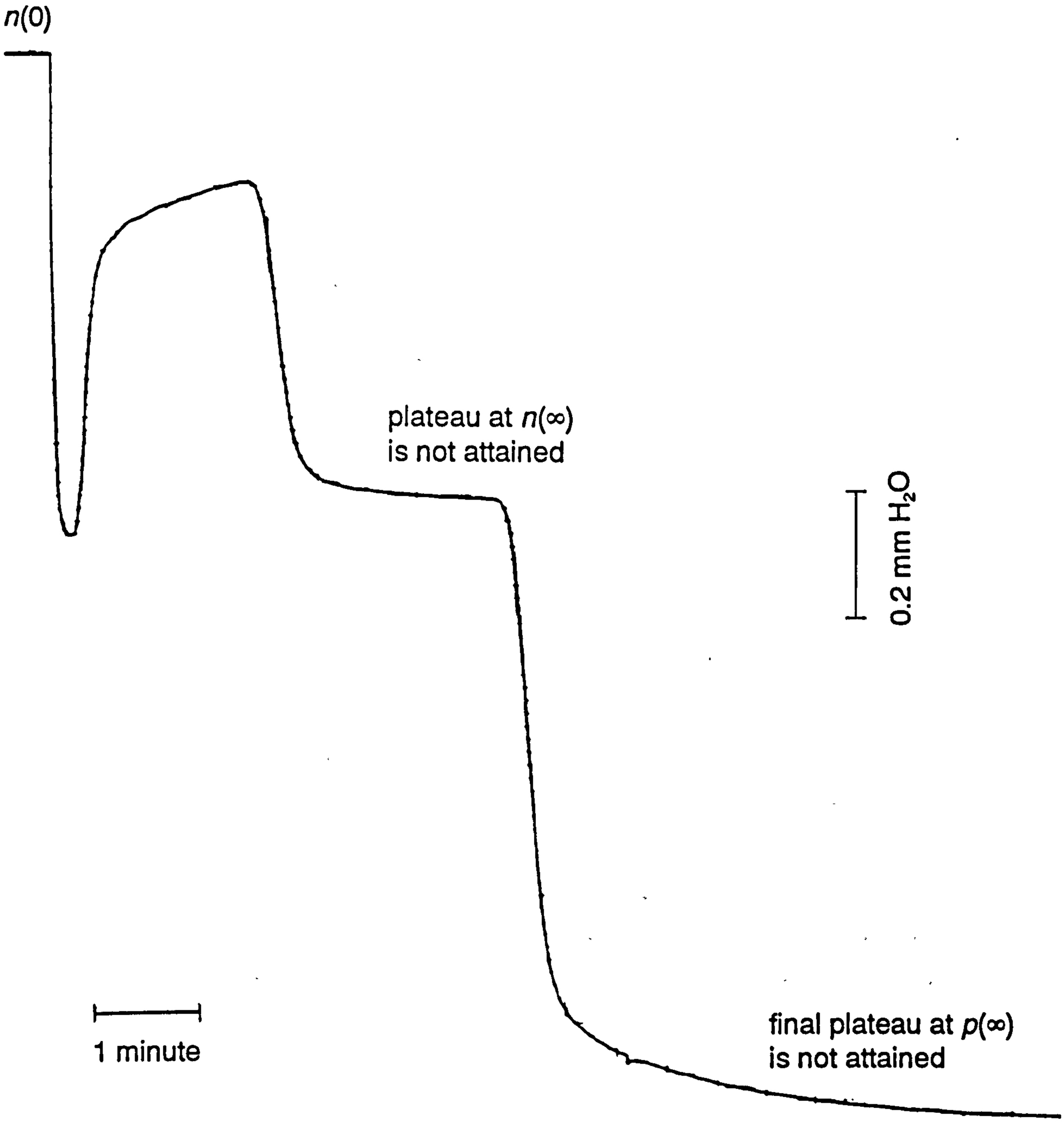

Figure 6.13 Flowrate Transient for Initial Experimental Arrangement

Figure 6.15 shows the chromatograms obtained for *removing* an argon perturbation from a helium carrier, using the standard columns and standard packing. As well as the standard downstream delay-lines, upstream delay-lines of length 20 metres were employed. The top chromatogram is the flowrate record and the bottom one is the composition record. Comparing Figure 6.15 with Figure 6.13, it can be seen that the modified experimental arrangement has realistically improved the shape of the flowrate chromatogram. Indeed, the chromatograms corresponding to *adding* the perturbation gas (not shown here) are

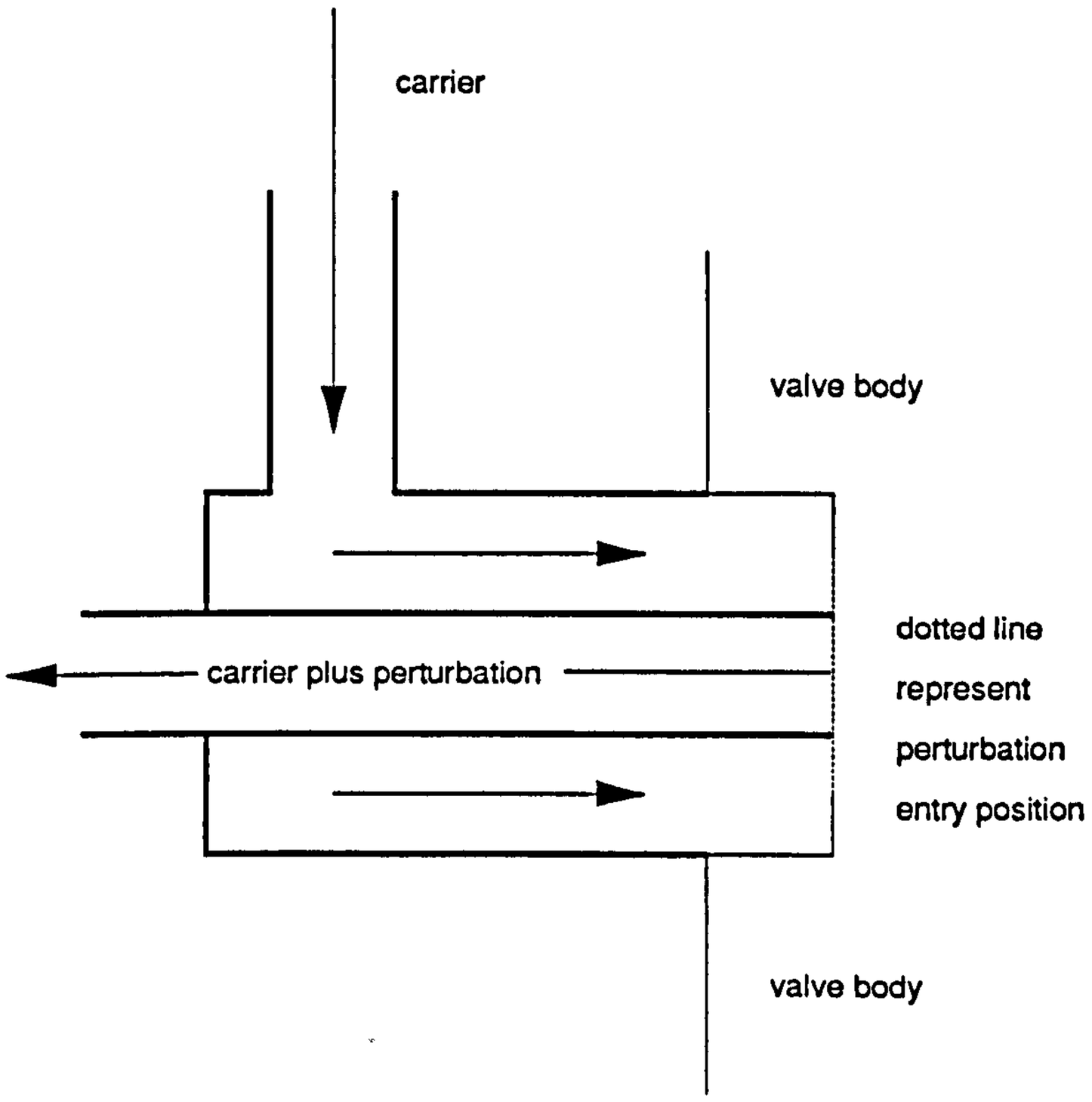

Figure 6.14 Schematic Cross-Section of Mixing Device

virtually identical; these findings would confirm previous findings of this chapter. Once again, the composition record is relatively simple in shape, and the only deviation occurs when the front leaves the column and enters the TCD; the pen sweeps from the $x(0)$ to the $x(\infty)$ positions. When the perturbation flow is removed, the flowrate pen moves from the $n(0)$ to the $n(\infty)$ positions. The vertical deviation from $n(0)$ to $n(\infty)$ corresponds to the perturbation flowrate. When the front enters the column, there will *net desorption* (net adsorption for *adding* the perturbation flow). When the front leaves the column and enters the downstream delay-line, there will be no more net desorption and the pen moves to the $n(\mathrm{p})$ position. The final deviation is the comparatively large viscosity effect when the front leaves the downstream delay-line and enters the measuring capillary; this is represented by the flowrate pen deviation from the $n(\mathrm{p})$ to the $p(\infty)$ positions. Clearly, the level of $n(\mathrm{p})$ is different from that of $n(\infty)$. This would indicate that the movement of the front through the column has significantly changed the column resistance (for adding the argon perturbation the resistance has increased). Previously, $n(\infty)$ was used to specify the flowrate record level attained when the front left the column and entered the downstream delay-line. From Figure 6.15, strictly speaking $n(\infty)$ should be reserved for the flowrate record level attained if sufficient lengths of delay-lines are placed upstream of each column.

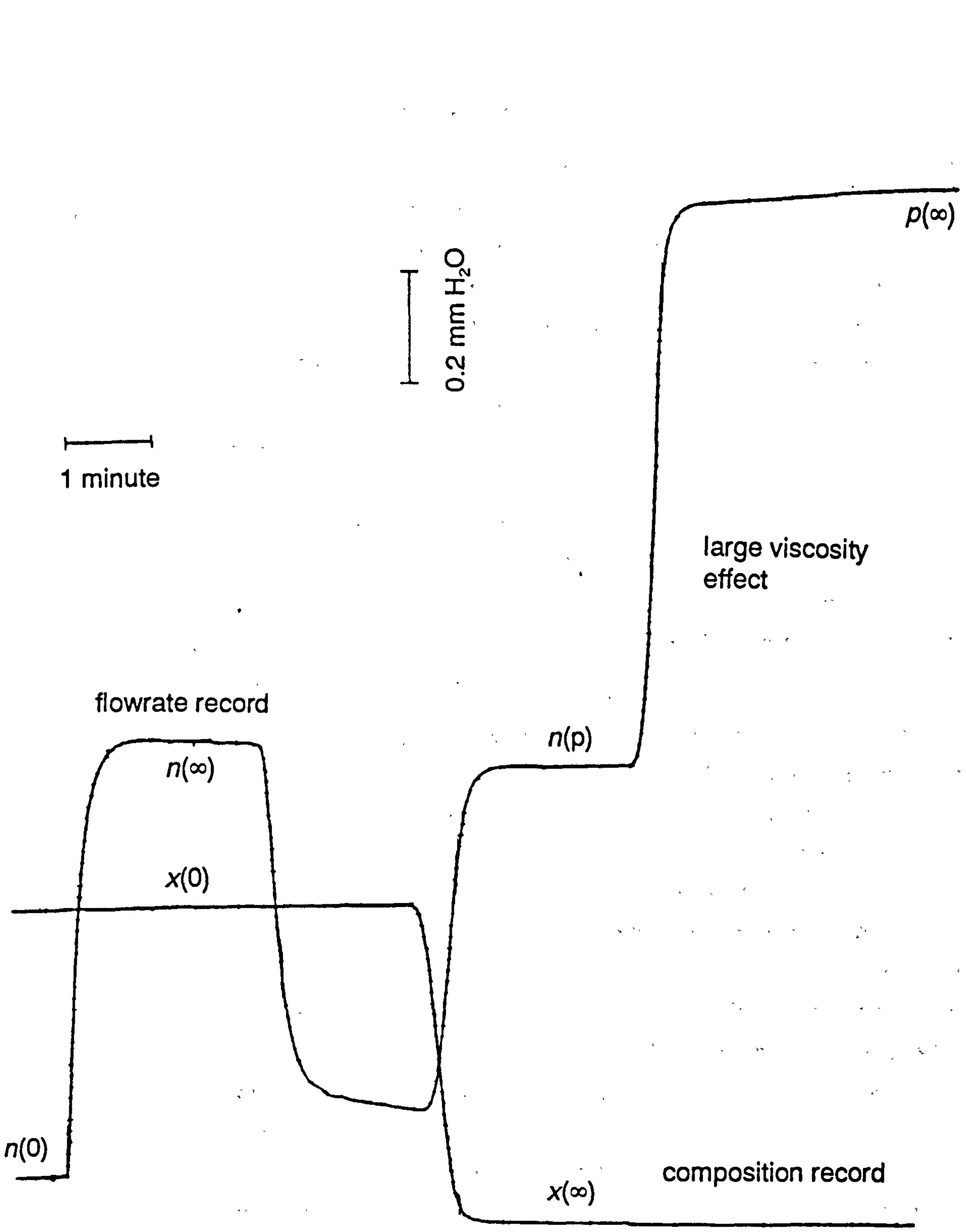

Figure 6.15 Chromatograms Obtained Using Modified Experimental Arrangement

6.5.4 Further Investigation of Composition Record Behaviour

In Figure 6.11, a helium-nitrogen mixture was investigated using columns having a low pressure drop. In this situation, an extra separating delay-line was used to separate the flowrate transients. Also, delay-lines of length five metres were employed upstream of each column. Unexpected deviations were observed in the composition record behaviour before the usual sweep from $x(0)$ to $x(\infty)$ as the front left the column and entered the downstream delay-lines. These deviations were attributed to changes in average column pressure, and it appeared that the magnitude of these deviations increased with column pressure drop. Hence, the investigation was continued with the standard columns and packing which give a higher column pressure drop. Figure 6.16 shows the chromatograms obtained for adding a helium perturbation gas to the same helium-nitrogen mixture, using the modified experimental arrangement. It should be pointed out that the chromatograms obtained for *removing* the perturbation gas are identical; this would help confirm the validity of the modified experimental arrangement. As well as the normal downstream delay-lines, upstream delay-lines of 20 metres were employed.

When the perturbation gas is added, the flowrate pen moves from the initial baseline $n(0)$ to (what appears to be) $n(\infty)$ because of the upstream delay-lines. However, unlike previous situations with upstream delay-lines, the movement is not a smooth sweep because of the small step observed. In the composition record, a significant "bulge" is observed from the initial baseline $x(0)$ while the front is moving through the upstream delay-line. The longer upstream delay-line enables the bulge to be isolated from other movement in the composition record. When the front enters the column, the composition pen deviates from $x(0)$ in the same direction as the initial bulge. From this latter deviation, as the front leaves the column, the standard sweep in the composition record is observed. However, the final $x(\infty)$ position is not attained smoothly in the conventional way; a kink is observed which retards the movement towards $x(\infty)$. This latter kink is mirrored in the shape of the flowrate transient as the front leaves the column; the final $n(\infty)$ position does not appear to be attained before the front enters the measuring capillary and the subsequent viscosity effect moves the pen to the final $p(\infty)$ position.

6.5.5 Further Discussion of Composition and Flowrate Record Behaviour

The purpose of this section is to explain comprehensively the reasons for the unexpected deviations in the composition and flowrate records of Figure 6.16. To help the explanation, Figure 6.17 shows the movement of a front through the system. This representation is simplified because the front is represented as a line, whereas the front will be of finite width. Firstly consider the situation designated as A in which the front is moving through the upstream delay-line. Adding the helium (or nitrogen) perturbation flow will cause an

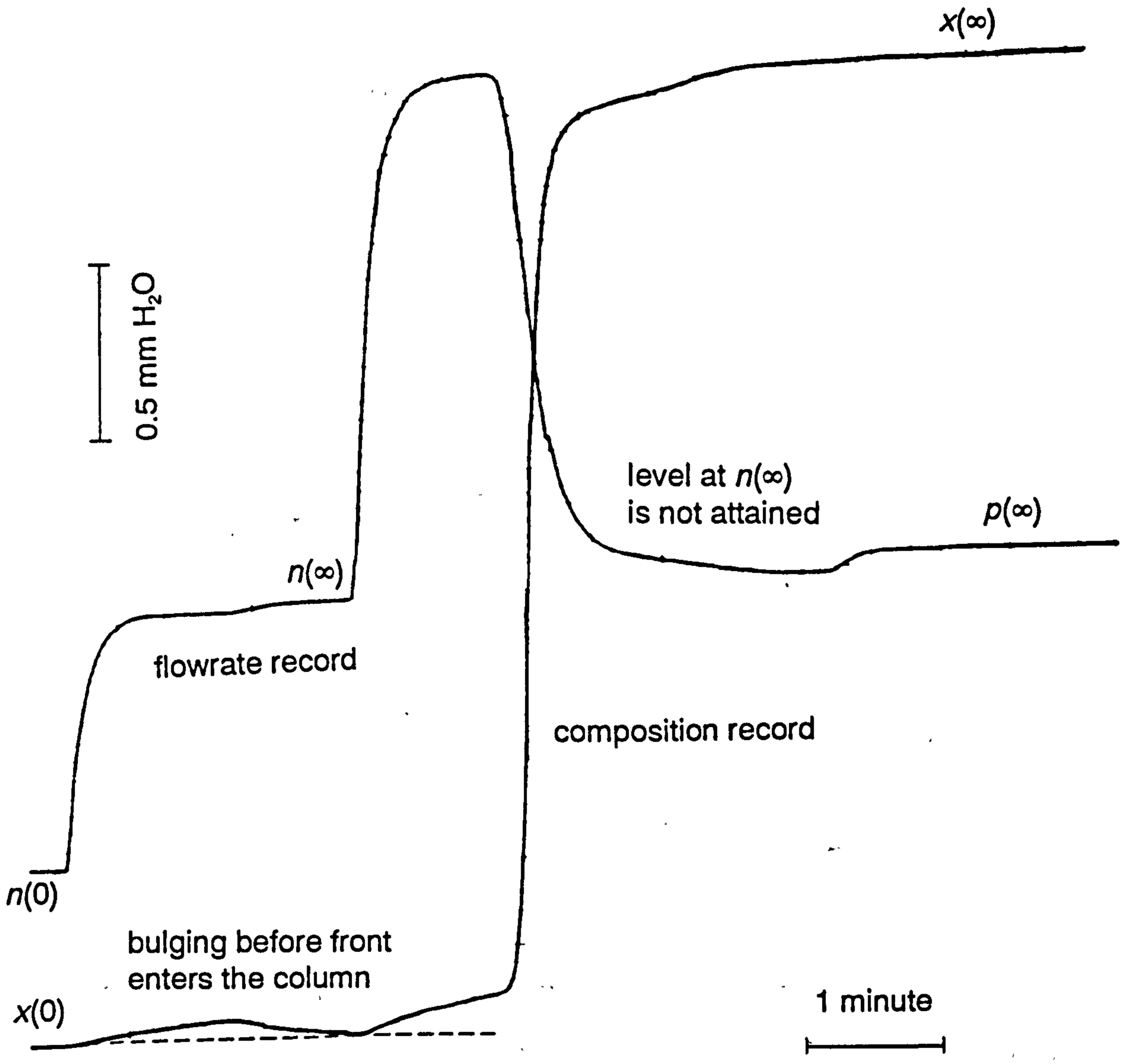

Figure 6.16 Mixture Chromatograms Obtained with Modified Experimental Arrangement

increase in column flowrate *before* the front reaches the column. The increase in column flowrate causes an increase in column pressure drop and an increase in *average column pressure*. At this increased average column pressure, the equilibrium adsorbed amount will increase and this may explain the step in flowrate record before the attainment of $n(\infty)$. Thus, gas will pass from the carrier flowing through the column into the packing (adsorbed phase). It can be seen that the composition record deviates and returns to the initial $x(0)$

baseline position, forming a "bulge". This would suggest that one component preferentially passes out of the gas phase, and there will thus be a deficiency of this component in the carrier gas leaving the column. At the increased average column pressure, it would seem that the equilibrium adsorbed phase composition will also change. Because the TCD is directly downstream of the column, any composition change in the carrier leaving the column will immediately cause a movement in the composition record. Because the composition record returns to the $x(0)$ baseline after the bulge, the carrier has returned to the normal composition before the front reaches the column. It should be pointed out that these initial deviations in both records are independent of the perturbation gas; they are solely dependent on the increase in average column pressure.

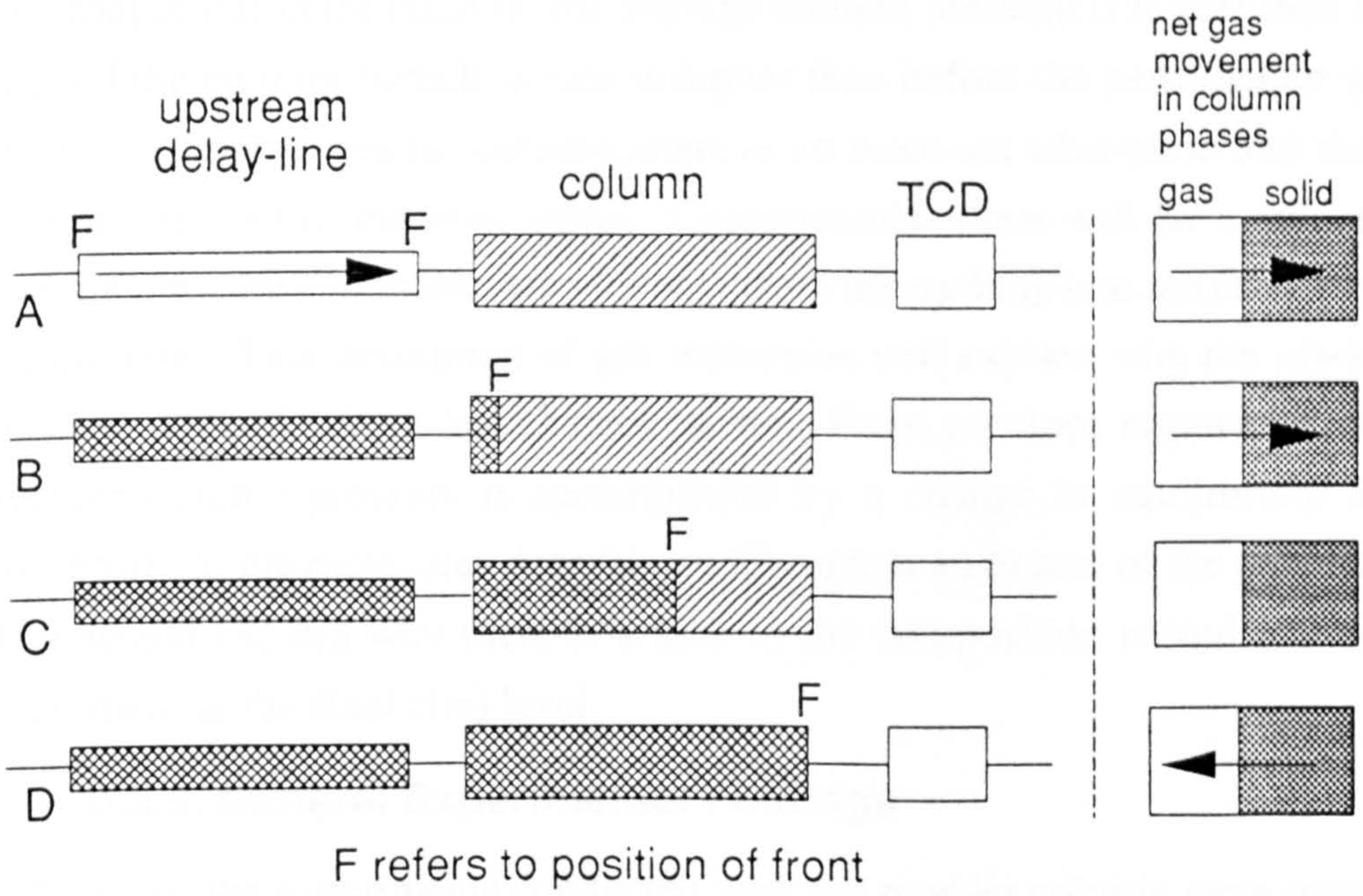

Figure 6.17 Schematic Representation of Front Movement in System

Now consider the situation designated by B in which the front has *just* entered the column. When the front enters the column, there will be an increase in column outlet flowrate due to the net desorption caused by the helium perturbation. Initially, this increase in flowrate will apply throughout the whole column and this will increase the column pressure drop and hence average column pressure. Similar to the situation in A, gas will pass from the carrier into the packing. From the continual deviation in the composition record away from $x(0)$, the same component (as in situation A) will preferentially pass from the carrier into the packing. For the nitrogen perturbation, the deviation away from $x(0)$ is seen to be in the opposite direction. Because the nitrogen perturbation causes net adsorption, there will be a *reduction* in the column outlet flowrate and hence average column pressure. Thus,

gas will pass *from* the packing into the carrier flowing through the column. In this gas movement, there will be an excess of the component already mentioned, and the composition record will deviate in the opposite direction.

Thirdly, consider the situation designated C in which the front is at an intermediate location in the column. Because the front is in the column, there will still be net desorption and the column outlet flowrate will be at the high value. However, this increased flowrate will be flowing through a reduced column length. Meanwhile, the inlet column flowrate will be at the $n(\infty)$ value. The composition record is deviating continuously because it takes time for the carrier gas (depleted in the particular component) to flow out of the column. Finally, consider the situation designated D in which the front is about to leave the column. While the front is still in the column, the average column pressure is higher than before the front entered the column (which in turn is higher than before the perturbation gas was added). When the front leaves the column, there is no more net adsorption and the column outlet flowrate returns to the $n(\infty)$ value. Consequently, there will be a reduction in average column pressure and molecules will pass from the packing into the carrier flowing through the column. This desorption of gas molecules will explain why the $n(\infty)$ level is barely attained when the front leaves the column. From previous arguments, the reduction in average column pressure is accompanied by a change in equilibrium adsorbed phase composition; the molecules desorbing will contain an excess of the particular component. This would explain why there is a kink in the composition record preventing a smooth attainment of the final $x(\infty)$ level.

6.5.6. General Experimental Findings

1. Many of the experiments conducted with the powder column were repeated, including those with varying carrier flowrate and mixture carriers. The respective system characteristics were confirmed, including those having *sharper* retreating transients. This would suggest that the problem of dead volume has been eliminated, or at least significantly reduced. Of course, it is no longer necessary to employ the extra separating delay-line.

2. Since replacing the five-port switching valve, the columns have become deactivated (the composition retention times have been significantly reduced). Also, by employing upstream delay-lines, strange kinks were noticed in the flowrate transient as the front entered the column, the direction being opposite to that of the viscosity effect. In some cases, this effect could be clearly noticed, because the kink was in the opposite direction to the pen movement as the front entered the column. These kinks are due to the column being partially deactivated, and are what would be expected for an inert column. As the front moves through the column, the small change in gas composition causes a small change in gas-mixture viscosity, leading to a change in the column and *overall* system resistance. The

gradient of this kink is proportional to the size of the viscosity deviation as the front enters the measuring capillary and the pen moves from the $n(\infty)$ to the $p(\infty)$ positions. Hence, using an argon perturbation and helium carrier will give the largest kink in the flowrate transient. Overall, the use of upstream delay-lines will reveal any deactivation at the upstream section of the column.

3. Regardless of whether the columns are deactivated, once the front has left the column, there will be a change in column resistance due to the change in gas-mixture viscosity. As discussed previously, when upstream delay-lines are employed, there are *two intermediate* plateaus on the flowrate record: the first is attained with upstream delay-lines when the perturbation flow is added (before the front enters the column) and the second is attained when the front leaves the column and enters the downstream delay-line. Any difference in these plateau levels will indicate a change in column resistance. For a particular system, any change will be greater for the powder columns because of their higher absolute resistance and higher contribution to the overall system resistance. Once again, the direction of any plateau offset will be opposite to that of the standard viscosity deviation as the front enters the measuring capillary. Also for any column pressure drop, the magnitude of the plateau offset will be proportional to the size of the standard viscosity deviation.

4. In Section 6.5.5, a comprehensive explanation was given for the unexpected deviations observed on the composition and flowrate records for the helium-nitrogen mixture. The same deviations were observed for both adding and removing the perturbation gas. It is now helpful to explain the composition record deviations observed for a helium perturbation gas and a nitrogen carrier; for *removing the perturbation gas only*, the composition record was seen to deviate when the front was in the column. Similarly, the deviation can be explained in terms of changes in average column pressure. When the perturbation gas is removed, there is already a 1% helium mixture carrier flowing through the column. However, when the perturbation gas is added, the carrier flowing through the column is pure nitrogen.

6.6 Literature Comparison

The only comparable case in the literature is the investigation by Garg and Ruthven (1974a) on the performance of 5A zeolite adsorption columns with micropore diffusion control. They measured the breakthrough curves for saturation (adsorption) and regeneration (desorption) using small concentrations of various sorbates in argon and helium carriers. The chromatograms were obtained by switching the two carrier flows (one carrier having the small perturbation flow added) between each side of the system. Of course, in the present project, the perturbation flow is added to and removed from *only one side* of the system. For a 3% nitrogen mixture at 50°C, they found the adsorption curve to be slightly

sharper than that for desorption. They accounted for this difference by the small deviation in linearity of the nitrogen isotherm. The authors also considered much stronger adsorbed components (having more curved isotherms) for which the difference in the advancing and retreating transients was much greater.

The authors used a comparatively large particle size of 1/8 inch, much larger than any of the column packings employed in the present project. From the results of the present project, it was found that using a coarser particle size resulted in broader fronts; this would explain why the literature case had a comparatively large breakthrough time of about 10 minutes. The authors also tried runs at higher sorbate concentrations (corresponding to higher perturbation flowrates). At the lower sorbate concentrations, they found the saturation and regeneration curves to be almost mirror images, whereas at higher concentrations the saturation curve became much sharper. These findings have been confirmed by two categories of the experimental runs; increasing the perturbation flowrate at constant carrier flowrate and reducing the carrier flowrate at constant perturbation flowrate.

6.7 Conclusions

1. Previously, experiments were conducted by switching a perturbation flow from one column to the other using a five-port valve, and measuring the cumulative effect. This chapter has shown how, with the same valve, along with lengths of tubing, these effects can be separated. The results have revealed intrinsic characteristics of particular systems. These results have been repeated with the use of a three port valve which only allows perturbation addition or perturbation removal in one valve movement. General findings, as well as the behaviour of the argon-nitrogen system, have been confirmed by the literature.

2. The use of upstream delay-lines has shown how, in certain circumstances, the katharometer trace can be deviating before and after the front has left the column. If the carrier is a mixture, the usual changes in the average column pressure can cause changes in the equilibrium adsorbate composition and hence the unusual deviations. These effects are more extreme the higher the column pressure drop. If not accounted for, they can make a front look broader than in reality.

3. For certain experimental arrangements, the delay-lines will lead to an obvious increase in the composition retention time, although this can easily be accounted for. However, it would appear that on some occasions, the flowrate transient appears "sluggish" and that the flowrate retention time will collect an extra positive contribution. In Chapter Seven, the quantitative effect of delay-lines will be investigated.

Chapter Seven

THE EFFECT OF DELAY-LINES ON RETENTION TIME MEASUREMENTS

7.1 Introduction

In Chapter Four, an equation was derived which related the flowrate retention time to the retention time indicated by the capillary flowmeter by measurement of changing pressure. The *pressure retention time* is thus the measured quantity and the *flowrate retention time* is the quantity required to obtain the isotherm gradients. In Chapter Four, it was then shown how the flowrate retention time could be directly obtained by inserting delay-lines of a suitable length downstream of the columns because, the delay line enables the effects of viscosity and flowrate to be separated in time. In order to determine the validity of the equation which, with certain approximations, links the flowrate and pressure retention times, it was intended to conduct experiments and analyse the results both with and without these delay lines. Results from Chapter Six have shown that inserting delay lines upstream of the columns can make the flowrate response more sluggish, indicating that the respective areas and hence retention times might be affected. Since these retention times are being used to calculate intrinsic quantities, clearly some form of correction might be required. It was not clear how the downstream delay lines would affect the response curves. The basic question arises: Is it better to use delay lines or omit them? Therefore, this chapter will consist a thorough investigation of the effect of delay-lines, both upstream and downstream of the column. Also, columns of differing dimensions and containing differing packing-sizes (thus giving differing pressure-drops) will be considered. The results presented will be divided into two categories: firstly systems in which the perturbation gas causes no composition change and secondly systems in which there is a composition change. For the first category, the analysis is simplified because only one retention time is affected. The findings from this category will be used for the second category, and help confirm the validity of the derived equation relating the flowrate and pressure retention times.

7.2 Useful Terminology

7.2.1 Column Characteristics

In this chapter results will be presented for many column types having differing characteristics. Thus it will be easier to refer to these columns by an identification letter; A to E will be employed for the five column types. The column pressure-drop will also be given for each column type. These were measured with a manometer as well as a precision pressure gauge. For the columns having low pressure drops, a mercury manometer is inaccurate and so a water or paraffin manometer was employed and the distances scaled

down appropriately. Obviously, the column pressure drop will depend upon the bulk flowrate, and so all the pressure drops are presented for $P_U = 1.3$ bar (this is the pressure upstream of the flow restrictors) and room temperature. Table 7.1 summarises the relevant column characteristics.

Table 7.1 Relevant Column Characteristics

column	L_C/cm	d_C/cm	mesh	ΔP_C/mm Hg
Type E	40	1.0	22-30	8
Type B	150	0.4	1100	10
Type A	150	0.4	22-30	35
Type C	150	0.4	30-60	90
Type D	150	0.4	60-80	200

7.2.2 Delay-Line Terminology

In this chapter results will be presented for many delay-line arrangements. Delay-lines will be classified according to their position relative to the column, katharometer and switching valve. There are thus four different classifications and Figure 7.1 gives a schematic representation of the delay-line locations.

1. The original location of the delay line was between the katharometer and the measuring capillaries; this location is defined as *downstream* and the relevant subscript is D.

2. The second location is between the column and the katharometer; this is defined as *intermediate* and the relevant subscript is I.

3. The third location is directly upstream of the column, downstream of the valve position; this is defined as *upstream* and the relevant subscript is U.

4. The final location is directly upstream of the valve. Although the perturbation flow cannot pass through this location, later it will be shown how it can affect the results. This location is defined as *switching* and the relevant subscript is S.

5. When describing a delay line for the general case where the location is of no relevance, the subscript DL is employed.

The above subscripts are applied to variables such as absolute pressure, pressure-drop and volume. For the sake of convenience, the following nomenclature will be used to describe the delay-line location, diameter and length:

$L_{\text{SUBSCRIPT}}$ @ diameter in inches = length in metres

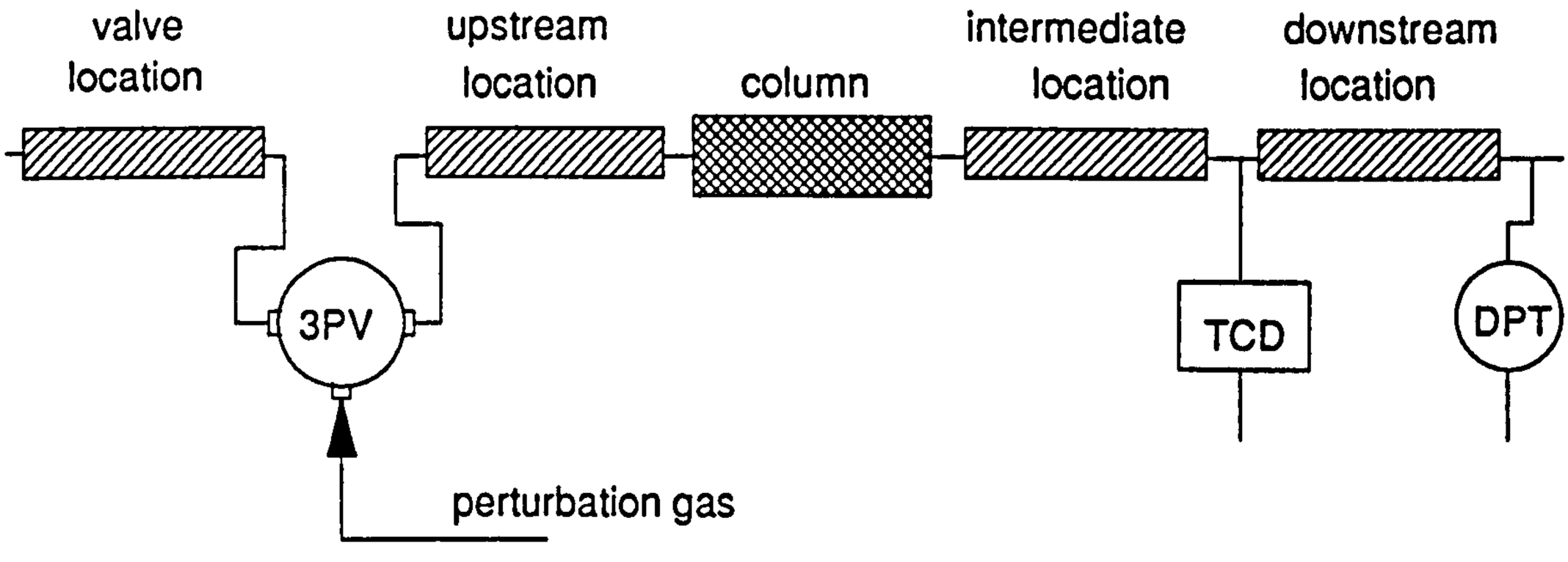

3PV = three port valve
TCD = katharometer
DPT = differential pressure transducer

Figure 7.1 Schematic Representation of Delay-Line Location

d_I = delay-line internal diameter for general case

d_O = delay-line external diameter for general case

Because the delay-line pressure drops are comparatively small, it is more accurate to measure them using a water manometer from which the distances can be scaled down to the equivalent length of mercury. Different 30 metre lengths of tubing were employed, and there was found to be a range in the pressure drop. This is not surprising, since the flow-resistance is proportional to the inverse of the internal diameter squared. Any small variation in extruding the tubing will be reflected in the pressure drop; a 10% change in pressure drop can be caused by a diameter change of 0.1 mm. Table 7.2 summarises the important characteristics.

Table 7.2 Relevant Delay-Line Characteristics

d_O/inch	d_I/mm	L_{DI}/m	ΔP_{DI}/mm Hg	V_{DI}/cc
1/8	1.58	30	11-14	59
1/4	4.32	30	2	440

7.3 Evaluation of Isotherm Gradients for Non-Composition Change Cases

7.3.1 Development of Theory

The basic chromatographic method equations, summarised in Chapter One, enable the two component isotherm gradients to be obtained in terms of the two retention times and the correction factor F_{PVC_i}. This correction factor is required to account for the total change in column gas concentration, which involves the *column pressure drop* as well as the change

in composition caused by the perturbation. Derivation of this correction factor requires that the outlet column pressure remains constant. When the perturbation composition equals the mixture composition, the expression for holdup derivative for each component reduces to:

$$\frac{\Delta H_i}{\delta c_i} = M \int_0^{\infty} \frac{x_i(\infty) - x_i(t)}{\delta c_i} dt + \frac{MRT_C}{\Delta P_C} \left[\frac{1 + \frac{\Delta P_C}{P_{COUT}}}{1 + \frac{\Delta P_C}{P_{COUT}}} \right] \tau_N \qquad 7.1$$

Equation 7.1 refers to the general case where, rather than a pure component perturbation gas, a perturbation gas having the same composition of the carrier can be employed. For cases involving a pure component carrier, the first term can be ignored since the numerator equals zero but the denominator does not equal zero; the former is true since there will be no deviation in the composition record and the latter is ensured because there will be a change in the *total* column concentration due to the increase in column flowrate and hence average column pressure. In this case, the isotherm holdup gradient of the pure component can be obtained without the composition retention time. This can be done because the average column pressure is being varied, thus changing the amount adsorbed. For this case, Equation 7.1 reduces to:

$$\frac{\Delta H_i}{\delta c_i} = \frac{2MRT_C}{\Delta P_C} \left[\frac{1 + \frac{\Delta P_C}{2P_{COUT}}}{1 + \frac{\Delta P_C}{3P_{COUT}}} \right] \tau_N \qquad 7.2$$

Also because the molar flowrate M is the same everywhere, the gas laws give:

$$RM = \frac{P_{COUT} Q_{COUT}}{T_C} = \frac{P_{AT} Q_{AT}}{T_{AT}} \qquad 7.3$$

The subscript AT refers to measurements at ambient conditions. From the form of Equation 7.2, the value of the flowrate retention time should be roughly proportional to the column pressure drop because the term in brackets is roughly constant. Using Equations 7.2 and 7.3, in the next section component gradients will be presented for nitrogen, argon and helium on 5A molecular sieve columns using various column types.

7.3.2 Tables of Results

Table 7.3 Nitrogen Isotherm Gradients for Various Column Types

column type	τ_N/s	$Q_M/\frac{ml}{min}$	$\frac{\Delta H_i}{\delta c_i}/ml$
Type E	6.1	51.6	507
Type B	5.4	55.0	386
Type A	11.4	52.5	164
Type C	19.0	55.0	151
Type D	36.3	45.0	110

Table 7.4 Argon Isotherm Gradients for Various Column Types

column type	τ_N/s	$Q_M/\frac{ml}{min}$	$\frac{\Delta H_i}{\delta c_i}/ml$
Type E	4.5	43.6	309
Type B	4.0	43.2	217
Type A	8.0	42.5	91
Type C	12.5	42.6	76
Type D	26.0	36.3	62

Table 7.5 Helium Isotherm Gradients for Various Column Types

column type	τ_N/s	$Q_M/\frac{ml}{min}$	$\frac{\Delta H_i}{\delta c_i}/ml$
Type E	3	50.9	238
Type B	3	49.0	178
Type A	3.8	47.5	48
Type C	5.0	50.0	35
Type D	9.0	42.6	25

Table 7.6 Removal of Downstream Delay Lines for Column Type A

		delay lines		no delay-lines	
system	T_c/°C	τ_N/s	$\frac{\Delta H_i}{\delta c_i}$/ml	τ_P/s	$\frac{\Delta H_i}{\delta c_i}$/ml
nitrogen	25	11.8	169	6.7	96
argon	25	8.2	93	4.0	45
helium	25	3.2	40	1.4	18
nitrogen	54	8	102	4.7	60
argon	54	5.5	56	3	30
helium	54	3.0	34	1.0	22

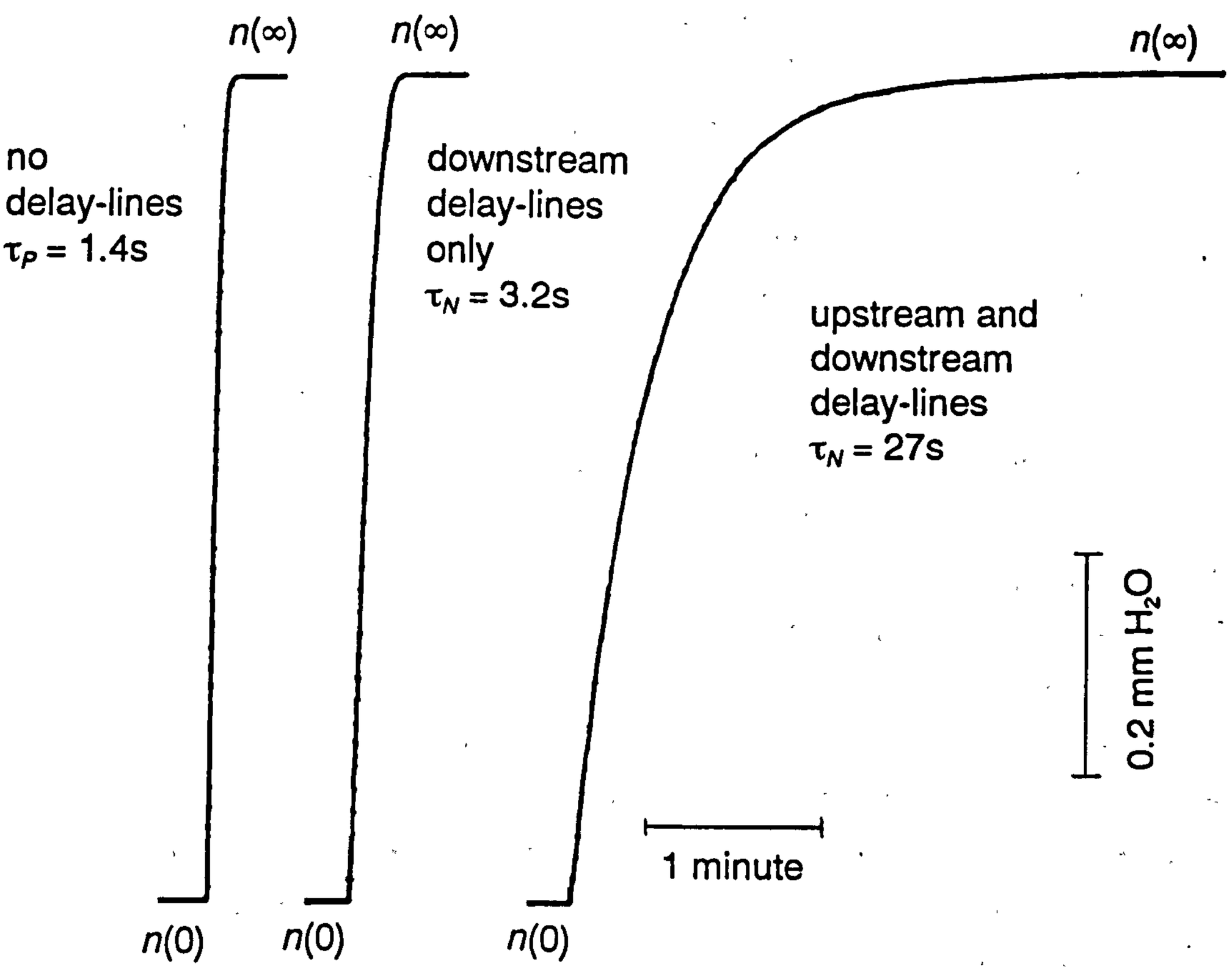

Figure 7.2 Flowrate Chromatograms for Pure Helium System

Figure 7.2 shows the flowrate chromatograms for adding a helium perturbation to a helium carrier at romm temperature. For the chromatogram on the left, there is a complete absence of delay-lines (τ_P is measured). For the centre chromatogram, downstream delay-lines of length 30 metres are employed. For the chromatogram on the right, upstream delay-lines of length 60 metres are employed as well as the downstream delay-lines. The general form of the chromatogram is simple compared to those for which the perturbation causes a composition change. When the perturbation is added, the flowrate record sweeps from the initial baseline at $n(0)$ to the final position at $n(\infty)$. According to the definition of τ_N, the required integral area is shown bordered by the dotted line and the chromatogram. It can be seen that inserting delay-lines gives an increased area, and hence an increased measured flowrate retention time. The measured retention times are not *directly* comparable with Table 7.8, because in Figure 7.2 *both* upstream and downstream delay-lines are used together.

7.3.3 Findings from Results

From Chapter Four, when the concept of delay lines was first considered, they were thought of only as a means of enabling the flowrate retention time to be measured directly. The length was not considered important as long as the delay-line was long enough to separate out the flowrate and viscosity effects. With this attitude in mind, it might have been expected that since the packed columns and voidages are approximately the same, the isotherm holdup gradients should not vary with column type. However, Tables 7.3 to 7.5 show that this expectation is clearly not the case. Although, there seems to be a trend; the lower the column pressure drop, the higher the holdup gradient and so the higher the apparent isotherm gradient. The form of Equation 7.2 would suggest that the flowrate retention time should increase with the column pressure drop and this is roughly the case although the relationship is not linear. From past experience, the values of the holdup gradient for the columns with the lower pressure drops are much too high. The systematic variation would suggest that the theory requires modification. The reason for these discrepancies is seen in Table 7.6 when the downstream delay lines are removed and the holdup gradients are restored back to reasonable values. Of course , there is really no need to employ these delay lines when the carrier and perturbation flows are of the same composition since there is no viscosity effect; these delay lines had been previously installed for the mixture carriers. The change in holdup measured ΔH_t is really the change in holdup of the *whole* system including any delay lines present. It would appear that the delay lines are making a contribution to the measured flowrate retention time, so giving excessive values of the holdup gradient. The next section consists a thorough investigation of delay line length and position on the measured flowrate retention time for perturbations causing no change in composition.

7.4 Variation of τ_N with Delay-Line Arrangement-Constant Composition

7.4.1 Results for Column Type A

Table 7.7 Variation of τ_N for Nitrogen System

L_D@ 1/8"	L_U@ 1/8"	τ_N/s	$\Delta\tau_N/s$
0	0	3.7	-
30	0	6.8	3.1
60	0	11.6	7.9
0	0	5	-
0	20	12	7
0	60	25	20

Table 7.8 Variation of τ_N for Helium System

L_D@ 1/8"	L_U@ 1/8"	τ_N/s	$\Delta\tau_N/s$
0	0	0.9	-
30	0	2.0	1.1
60	0	5.2	4.3
0	0	0.9	-
0	20	7.9	7
0	60	21.0	20.1

7.4.2 Results for Column Type D

Table 7.9 Variation of τ_N for Nitrogen System

L_D@ 1/8"	L_U@ 1/8"	τ_N/s	$\Delta\tau_N/s$
0	0	33.5	-
15	0	34	0.5
30	0	36	2.5
60	0	42	8.5
30	0	36	-
30	20	60.3	24.3
30	40	83.7	47.7
30	60	102	66

Table 7.10 Variation of τ_N for Helium System

L_D@ 1/8"	L_U@ 1/8"	τ_N/s	$\Delta\tau_N/s$
0	0	6.8	-
15	0	6.8	0
30	0	9.0	2.2
60	0	15.0	8.2
30	0	9.0	-
30	20	35.5	26.5
30	40	58.1	49.1
30	60	73.0	64.0

The final table of results consists repeating particular runs for the nitrogen system but using equivalent volumetric lengths of 1/4 inch tubing. From the ratio of tubing diameters, the above lengths will need to be divided by about 7.5. Moreover, the pressure drops become negligible because of the reduction in length.

Table 7.11 Variation of τ_N for Nitrogen System

L_D @1/4"	L_U @1/4"	τ_N/s	$\Delta\tau_N/s$
0	0	33.5	-
8.5	0	34	0.5
0	0	33.5	-
0	8.5	94	60.5

7.4.3 Findings from Results

1. Clearly, the inclusion of delay-lines has a certain, and sometimes drastic, effect on the measured flowrate retention time. Since this quantity is being used to calculate an intrinsic quantity, the isotherm gradient, a quantitative adjustment will be required for the theory.

2. The position of the delay-lines relative to the column is very important; the inclusion of upstream delay-lines leads to a larger increase in the flowrate retention time. For the upstream location, the increase in the retention time is proportional to the length. However, for the downstream location, the relationship is not proportional; adding 15 metres makes little difference but adding 60 metres gives an increase of about eight seconds.

3. The increase in retention time due to the inclusion of upstream delay-lines depends upon the column employed. For Column Type A, adding 20 metres increases the retention time by about six seconds and for Column Type D, the increase is around 25 seconds.

4. For the downstream location, using the equivalent length of 1/4 inch tubing makes very little difference to the retention time; the equivalent length of 60 metres of 1/8 inch tubing gives an increase of about 0.5 seconds compared to about eight seconds.

5. For the upstream location, using the equivalent length of 1/4 inch tubing makes roughly the same contribution as the 1/8 inch tubing. Probably, the increase is not as high as for the 1/8 inch tubing.

6. This is a severe test since it involves measuring the increase in holdup from a small increase in pressure.

7.5 Development of Theory to Allow for Delay Lines

7.5.1 Introduction

The first stage of development concerns the modification to the chromatographic theory summarised in Chapter One. It is helpful to show how the total change in holdup for component *i* is represented by the following equation:

$$\Delta H_i = M \int_0^{\infty} x(\infty) - x(t)dt + Y_{i0} \int_0^{\infty} n(\infty) - n(t)dt \qquad 7.4$$

The two integrals represent what is measured by the composition record and flowrate record respectively. Originally, it was assumed that when the perturbation was initiated, the change in gaseous concentration of component *i* in the column could be represented by the following equation:

$$\delta c_i = c_T dY_i \qquad 7.5$$

Equation 7.5 assumes that the total gaseous concentration in the column c_T remains constant after the perturbation is initiated. However, this assumption was found to give erroneous results and for the next stage the change in average column pressure was considered:

$$\delta c_i = c_T dY_i + Y_i dc_T \qquad 7.6$$

The term dc_T was represented by an expression which assumed that the column outlet pressure remains constant. This assumption is valid if the carrier gas leaving the column flows directly into the measuring capillaries and out to atmosphere. However, if there are delay lines situated *downstream* of the column, the perturbation will change the pressure drop across these delay lines. This will necessarily change the column outlet pressure and thus the dc_T term in Equation 7.6 must be adjusted to incorporate this extra increase in gas concentration. An important part of the theory developed by Mason and Buffham (unpublished) is the relationship between the change in average gas concentration and the pressure drop; this allows the change in average concentration in the downstream delay-lines to be re-stated in terms of the downstream delay-line pressure drop:

$$\delta c_{AD} = \frac{\Delta P_D}{2RT_D}\left[\frac{1+\frac{\Delta P_D}{3P_{DOUT}}}{1+\frac{\Delta P_D}{2P_{DOUT}}}\right]\frac{n}{M} \qquad 7.7$$

Also from the same analysis, the change in downstream delay-line inlet pressure is related to the change in downstream delay-line mean pressure by the following equation;

$$\frac{\Delta P_{DIN}}{\Delta P_{DMEAN}} = \frac{3}{2}\frac{1}{\left[1-\left(\frac{P_{DIN}}{P_{DOUT}}+1\right)^2\right]} = K_{DL} \qquad 7.8$$

For a small delay line pressure drop, the value of K_{DL} will tend to two and for a very large pressure drop, the value will tend to 3/2. This allows Equation 7.6 to be re-stated but with an extra term corresponding to the change in column outlet pressure:

$$\delta c_A = c_T d Y_A + Y_A \left\{ \frac{\Delta P_C}{2RT_C} \left[\frac{1+\frac{\Delta P_C}{3P_{COUT}}}{1+\frac{\Delta P_C}{2P_{COUT}}} \right] \frac{n}{M} + K_{DL} \frac{\Delta P_D}{2RT_D} \left[\frac{1+\frac{\Delta P_D}{3P_{DOUT}}}{1+\frac{\Delta P_D}{2P_{DOUT}}} \right] \frac{n}{M} \right\} \qquad 7.9$$

In order to simplify the form of Equation 7.9 and aid future comparison, it is helpful to define an *equivalent column pressure drop* ΔP_C^* which keeps the equation in the same form as Equation 7.6:

$$\delta c_A = c_T d Y_A + Y_A \left\{ \frac{\Delta P_C^*}{2RT_C} \left[\frac{1+\frac{\Delta P_C}{3P_{COUT}}}{1+\frac{\Delta P_C}{2P_{COUT}}} \right] \frac{n}{M} \right\} \qquad 7.10$$

$$\Delta P_C^* = \Delta P_C + K_{DL} \Delta P_D \frac{T_C}{T_D} \left[\frac{1+\frac{\Delta P_D}{3P_{DOUT}} 1+\frac{\Delta P_C}{2P_{COUT}}}{1+\frac{\Delta P_D}{2P_{DOUT}} 1+\frac{\Delta P_C}{3P_{COUT}}} \right] \qquad 7.11$$

The overall result is that the downstream delay-lines cause the correction factor F_{PVCI} which appears in Equation 1.10 to be re-stated but including the equivalent column pressure drop instead of the actual column pressure drop. For the case of adding a pure perturbation gas to the respective carrier, Equation 7.2 must be re-stated including the equivalent column pressure drop:

$$\frac{\Delta H_i}{\delta c_i} = \frac{2MRT_C}{\Delta P_C^*} \left[\frac{1+\frac{\Delta P_C}{2P_{COUT}}}{1+\frac{\Delta P_C}{3P_{COUT}}} \right] \tau_N \qquad 7.12$$

From Equation 7.12 it is apparent that the effect of using the equivalent pressure drop will be greater for columns having a lower pressure drop. For column type E, the denominator will be effectively increased by four times, whereas for column type D, the denominator will increase by about 10%.

7.5.2 Further Effects of Delay Lines

In Section 7.5.1 it was seen how the presence of *downstream* delay-lines will affect the column gaseous concentration such that the required correction factors need to be re-stated. This section is concerned with the holdup changes in the delay-lines themselves and the subsequent effects on the measured retention times. This is a repeat of the basic analysis summarised in Chapter One but with the inclusion of upstream and downstream delay lines. For perturbations not causing a composition change, there is no distinction between the downstream and intermediate locations; they are both downstream of the column. When a perturbation is made to the system, the molar balance can be written for component A:

$$\Delta H_A = (1-\varepsilon)V_C\delta q_A + \varepsilon V_C\delta c_A + V_U\delta c_{AU} + V_D\delta c_{AD} \qquad 7.13$$

Equation 7.7 shows the change in average concentration for the downstream delay lines. Similar to the argument in Section 7.5.1, it is not possible to represent the corresponding change for the upstream delay-lines in the same simple form; the inlet column pressure will increase and this will necessarily increase the upstream delay-line outlet pressure. Equation 7.14 shows how the change in column inlet pressure is related to the change in average column pressure:

$$\frac{\Delta P_{CIN}}{\Delta P_{CMEAN}} = \frac{3}{2}\frac{1}{\left[1-\left(\frac{P_{CIN}}{P_{COUT}}+1\right)^2\right]} = K_C \qquad 7.14$$

Additionally, if there are any downstream delay-lines present, these will further affect the change in upstream delay-line average concentration; when a perturbation is initiated, the pressure upstream of these downstream delay-lines will increase and this will necessarily increase the column outlet pressure and the pressure throughout the rest of the system. With this argument, δc_{AU} can be represented by Equation 7.15:

$$\delta c_{AU} = \frac{\Delta P_U}{2RT_U}\left[\frac{1+\frac{\Delta P_U}{3P_{UOUT}}}{1+\frac{\Delta P_U}{2P_{UOUT}}}\right]\frac{n}{M} + K_C\frac{\Delta P_C^*}{2RT_C}\left[\frac{1+\frac{\Delta P_C}{3P_{COUT}}}{1+\frac{\Delta P_C}{2P_{COUT}}}\right]\frac{n}{M} \qquad 7.15$$

Re-arranging Equation 7.13 enables the intrinsic isotherm gradient to be obtained explicitly:

$$\frac{\delta q_A}{\delta c_A} = \frac{\frac{\Delta H_A}{\delta c_A} - \varepsilon V_C - V_I\frac{\delta c_{AI}}{\delta c_A}}{(1-\varepsilon)V_C} \qquad 7.16$$

Since the isotherm gradient is independent of the presence of delay lines, the extra terms on the numerator enable the contributions to the measured flowrate retention time of the downstream delay lines τ_{ND} and the upstream delay lines τ_{NU} to be obtained:

$$\tau_{ND} = \frac{V_D\Delta P_D}{2MRT_D}\left[\frac{1+\frac{\Delta P_D}{3P_{DOUT}}}{1+\frac{\Delta P_D}{2P_{DOUT}}}\right] \qquad 7.17$$

$$\tau_{NU} = \frac{V_U\Delta P_U}{2MRT_U}\left[\frac{1+\frac{\Delta P_U}{3P_{UOUT}}}{1+\frac{\Delta P_U}{2P_{UOUT}}}\right] + K_C\frac{V_U\Delta P_C^*}{2MRT_C}\left[\frac{1+\frac{\Delta P_C}{3P_{COUT}}}{1+\frac{\Delta P_C}{2P_{COUT}}}\right] \qquad 7.9$$

The form of Equations 7.17 and 7.18 would suggest that inserting an equivalent delay line upstream of the column will give an increased contribution and that this contribution will increase for columns having a higher pressure drop.

7.5.3 Qualitative Effects of Theory Modification

1. The situation is complicated when downstream delay lines are employed because there are two stages of correction. Two approaches can be adopted depending upon which type of the above tables are investigated. For Tables 7.3 to 7.5, all the systems have the same length of downstream delay line and it is required to correct the initially calculated $\Delta H_i/\delta c_i$ value such that the *required* $\Delta H_i/\delta c_i$ value is obtained which is solely representative of the column. The first stage of correction involves using the equivalent column pressure drop ΔP_C^* rather than the actual column pressure drop ΔP_C. The second stage of correction involves subtracting the τ_{ND} contribution from the measured flowrate retention time

2. The second type of investigation with downstream delay lines concerns Tables 7.6 to 7.12 in which the downstream delay line length is changed and the flowrate retention time measured for each configuration. Consider a hypothetical situation in which the standard downstream delay lines are replaced with tubing having the same pressure drop but zero volume. According to Equation 7.17, the τ_{ND} contribution necessarily becomes zero because V_D becomes zero. However, the measured flowrate retention time will have a contribution due to the increased δc_i caused by the downstream tubing resistance. Consider the situation in which a length of this tubing is added downstream of the column; previously there was no delay line at all and τ_p was the measured retention time by definition. Because V_D is zero, there is no ΔH_i contribution in the resistance tubing. The effective retention time contribution due to the *pressure drop only* of the downstream delay line will be termed τ_{ND}^*. This can be calculated by considering the form of Equation 7.12 for each situation:

$$\frac{\Delta H_i}{\delta c_i} = \frac{2MRT_C}{\Delta P_C}\left[\frac{1+\frac{\Delta P_C}{2P_{COUT}}}{1+\frac{\Delta P_C}{3P_{COUT}}}\right]\tau_p = \frac{2MRT_C}{\Delta P_C^*}\left[\frac{1+\frac{\Delta P_C}{2P_{COUT}}}{1+\frac{\Delta P_C}{3P_{COUT}}}\right](\tau_p + \tau_{ND}^*) \qquad 7.19$$

$$\tau_{ND}^* = \tau_p \frac{\Delta P_C^* - \Delta P_C}{\Delta P_C} \qquad 7.20$$

From the form of Equation 7.20, the τ_{ND}^* contribution will depend upon the value of τ_p. Hence, it would be expected that the contribution for the nitrogen system would be greater than that for the helium system. Consider a situation in which there are no delay-lines present for a particular gas system and column type; τ_p can be directly obtained. If a delay

line of volume V_D and pressure drop ΔP_D is added downstream of the column, it should be possible to predict the measured value of the flowrate retention time

τ_N

by the following equation:

$$\tau_N = \tau_P + \tau_{ND} + \tau^*_{ND} \qquad 7.21$$

3. The situation is simpler if only upstream delay lines are employed because the $\Delta H_i/\delta c_i$ term requires no correction; δc_i is representative of reality. The measured flowrate retention time is corrected by subtracting the τ_{NU} contribution.

7.5.4 Quantitative Effects of Theory Modification

1. From Equation 7.17, the τ_{ND} contribution can be simplified by substituting for M in terms of the volumetric flowrate Q_{AT} measured at atmospheric pressure P_{AT} with the bubble flowmeter:

$$\tau_{ND} = \frac{V_D \Delta P_D}{2 P_{AT} Q_{AT}} \qquad 7.22$$

From the relevant catalogue (Phase Separations, 1990), the internal diameter of 1/8 inch nylon tubing is 0.062 inch; this will give the volume of a 30 metre length of about 58ml. Typically, the measured column flowrate will vary between 20 and 25 ml/min, and considering the ΔP_D variation shown in Table 7.2, the τ_{ND} contribution will vary between about 1.0 and 1.6 seconds. For a 60 metre length of tubing, both ΔP_D and V_D will be doubled and the τ_{ND} contribution will vary between 4.0 and 4.6 seconds. From Table 7.3, it can be seen that for column type E, the calculated $\Delta H_i/\delta c_I$ value is greatly exaggerated by the inclusion of the downstream delay lines. Clearly, even if the highest τ_{ND} contribution of 1.6 seconds is subtracted from the measured retention time, this will not bring the $\Delta H_i/\delta c_I$ to a reasonable value representative of the column. However, from Equation 7.11, the equivalent column pressure drop ΔP^*_C is about 8+(2x11)=30 mmHg. Using this value in Equation 7.14 will reduce the $\Delta H_i/\delta c_I$ from 507 ml to 135 ml. Finally, subtracting the τ_{ND} contribution of 1.3 seconds from the measured flowrate retention time will reduce the $\Delta H_i/\delta c_I$ to 107 ml. This should be the holdup gradient for the column alone. As the column pressure drop increases, both the corrections due to using the equivalent column pressure drop and the τ_{ND} contribution become reduced in significance. This can be seen from the calculated holdup gradients for column type D; since these are close to the expected values, they would appear to require little correction.

2. Table 7.6 shows the effect of a 30 metre length of downstream delay-line on the measured flowrate retention time. It can be seen that the increase in the measured retention time increases going from the helium to the argon to the nitrogen system. Also, these changes are lower for the corresponding systems at the increased oven temperature. Using Equations 7.17 and 7.20, the various contributions can be obtained and the measured flowrate retention time predicted; this will be termed τ_{NP}. This can be compared with the actual measured retention time τ_N and the difference will be termed $\Delta\tau_N$. The results are summarised in Table 7.12 and it can be seen that the actual values are predicted quite well.

Table 7.12 Prediction of Downstream Delay Line Effects

system	T_C/°C	τ_p/s	τ_{ND}/s	τ^*_{ND}/s	τ_{NP}/s	$\Delta\tau_N$/s
nitrogen	25	7.0	1.0	4.3	12.3	0.5
argon	25	4.0	1.3	2.5	7.8	-0.4
helium	25	1.7	1.1	1.1	3.9	0.5
nitrogen	54	4.7	1.0	2.2	7.9	-0.1
argon	54	3.0	1.3	1.4	5.7	0.3
helium	54	1.0	1.1	0.4	2.5	-0.5

3. From Table 7.7, it can be seen that equivalent lengths of upstream delay line give greater contributions than for the downstream location. This is qualitatively predicted by the analysis in Section 7.5.2; furthermore these contributions will depend upon the column pressure drop and it can be seen that those for column type D are much greater than those for column type A. Comparing Tables 7.7 and 7.6 it can be seen that in the former case, the column is partially deactivated. The first change consists of inserting 30 metres of nylon tubing downstream of the column. For this case, $\Delta P^*_C = 35+(2x11) = 57$ mm Hg and the following contributions are calculated:

$\tau_{ND} =$ 1.1 seconds

$\tau^*_{ND} =$ 3.7 x 22 / 35 = 2.3 seconds

$\tau_{NP} =$ 3.7 + 1.1 + 2.3 = 7.1 seconds

This compares very well with the actual value of 6.8 seconds. In Table 7.7, the third change consists of inserting 20 metres of nylon tubing upstream of the column. For this case, V_U = 38 cc and ΔP_D = 7 mm Hg. Since there are no downstream delay lines, then the actual column pressure drop can be employed and the contribution predicted:

$$\tau_{NU} = 0.4 + 5.9 = 6.3 \text{ seconds}$$

This compares very well with the actual value of seven seconds. In Table 7.7, the fourth change consists of inserting 60 metres of nylon tubing upstream of the column. For this case, V_U = 114 ml and ΔP_D = 22 mm Hg. Since there are no downstream delay lines, then the actual column pressure drop can be employed and the contribution predicted:

$$\tau_{NU} = 4.4 + 17.6 = 22.0 \text{ seconds}$$

This compares well with the measured value of 20 seconds.

7.6 Effect of Downstream Delay-Lines for General Mixture Case

7.6.1 Introduction

Results are presented for four systems in Tables 7.13 to 7.20, one for each perturbation gas. It had originally been intended to include these tables in Chapter Four, where they could be used to test the validity of the Equation 4.12 relating the pressure and flowrate retention times. However, because of the possibility of the delay-lines themselves making a contribution to the flowrate retention time, it was decided to include the tables in this chapter, where the effect of the delay-lines *and* the validity of the equation can be checked together. Using Equation 4.12, τ_{NC} refers to the value of flowrate retention time calculated using the measured pressure retention time and the measured viscosity factor. The value of τ_N refers to the directly measured value of flowrate retention time. From Chapter Four, it was stated that accurate values of the viscosity factor are required to check the validity of Equation 4.12. Because of this, one of the table columns contains the value of viscosity factor required for Equation 4.12 to give perfect predictions; this is termed the *agreement viscosity factor* and is termed $B(\mu)_A$. The actual and agreement viscosity factors are then used in conjunction with the relevant graph from Figure 4.7 to 4.12. In some cases, it may be that an apparent failure of Equation 4.12 to give a good prediction can be accounted for by an inaccurate value of viscosity factor. There will be a fair amount of error involved in compiling these tables. Firstly, there is the usual error in measuring the areas and dividing by the offsets. However, any differences in flowrate require the pressure retention time to be multiplied by a particular factor; this factor can be obtained by comparing either the composition retention times or comparing the flowrates. Thus, for each comparison the cumulative error may be very high.

7.6.2 Perturbation Addition and Removal

For each carrier mixture, there are two runs corresponding to adding (A) and then removing (L) the perturbation flow. This is the first time that results have been presented in this manner, rather than by the cumulative effect. It will be seen that there are certain trends

with regard to the relative magnitude of both the flowrate and composition retention times. This might not appear surprising for two reasons. Firstly, the total flowrate for perturbation addition will be higher and, secondly, the starting composition will be slightly different. Any small difference in the composition factor can lead to a larger difference in the multiplication factor for the flowrate retention time. These implications will be discussed later. This section, however, is only concerned with obtaining *reliable* values of the retention times. Separating the effects of adding and removing the perturbation gas has two advantages. Firstly, it provides twice the amount of data and, secondly, overall trends can be used to spot rogue points.

7.6.3 Tables of Results

Table 7.13 Nitrogen Perturbation Results for Nitrogen-Argon System

$\%N_2$	$B(\mu)$	τ_p/s	τ_{NC}/s	τ_N/s	$\Delta\tau_N$/s	$B(\mu)_A$	τ_X/s
0-A	-0.190	268	306	306	0	-	470
0-L	-0.190	264	304	302	-2	-0.183	472
10-A	-0.175	230	265	266	1	-0.182	429
10-L	-0.175	224	260	260	0	-	431
25-A	-0.155	167.3	196.1	198.7	2.6	-0.170	353
25-L	-0.155	164.8	193.4	192.1	-1.3	-0.148	349
50-A	-0.121	94.1	113.7	116.1	2.4	-0.135	257
50-L	-0.121	91.9	111.5	112.8	1.3	-0.127	257
75-A	-0.057	43.0	51.1	50.3	-0.8	-0.052	185
75-L	-0.057	42.6	50.9	52.3	1.4	-0.067	188
90-A	-0.022	17.3	20.0	25.2	5.1	-0.062	144
90-L	-0.022	18.6	21.2	24.8	3.6	-0.049	145

Table 7.14 Argon Perturbation Results for Nitrogen-Argon System

$\%N_2$	$B(\mu)$	τ_p/s	τ_{NC}/s	τ_N/s	$\Delta\tau_N$/s	$B(\mu)_A$	τ_X/s
10-A	0.016	-18.0	-25.3	-18.7	6.6	0.002	425
10-L	0.016	-15.1	-22.3	-18.5	3.8	0.008	429
25-A	0.057	-38.8	-61.0	-52.2	8.8	0.034	351
25-L	0.057	-35.5	-57.8	-53.7	4.1	0.047	355
50-A	0.106	-68	-102	-90.5	11.5	0.070	254
50-L	0.106	-62.6	-96	-89.6	6.4	0.083	261
75-A	0.180	-82.3	-129.5	-122	7.5	0.151	180
75-L	0.180	-80.4	-128.4	-119	9.4	0.144	186
90-A	0.247	-82.8	-139	-126	13	0.190	144
90-L	0.247	-84.3	-143	-130	13	0.200	148
100-A	0.308	-88.1	-153	-141	12	0.251	123
100-L	0.308	-83.7	-148.6	-139	9.6	0.262	127

Table 7.15 Nitrogen Perturbation Results for Nitrogen-Argon System

$\%N_2$	$B(\mu)$	τ_p/s	τ_{NC}/s	τ_N/s	$\Delta\tau_N$/s	$B(\mu)_A$	τ_X/s
0-A	-0.200	97.3	126.5	131	4.5	-0.231	243
0-L	-0.200	98.1	128	128	0	-	246
25-A	-0.160	66.6	89	91.3	2.3	-0.176	207
25-L	-0.160	66.6	89.3	92.2	2.9	-0.180	209
50-A	-0.113	39.9	53.5	57	3.5	-0.143	160
50-L	-0.113	39.8	54.0	57.5	3.0	-0.141	165
75-A	-0.075	18.1	25.7	28.4	2.7	-0.102	119
75-L	-0.075	18.4	26.3	29.6	3.3	-0.107	123

Table 7.16 Argon Perturbation Results for Nitrogen-Argon System

$\%N_2$	$B(\mu)$	τ_P/s	τ_{NC}/s	τ_N/s	$\Delta\tau_N/s$	$B(\mu)_A$	τ_X/s
25-A	0.047	-13.7	-24	-24.3	-0.3	0.048	206
25-L	0.047	-10.9	-21.4	-20.4	1.2	0.042	213
50-A	0.125	-23	-45.9	-48.4	-2.5	0.139	160
50-L	0.125	-23.3	-47	-44	3	0.110	166
75-A	0.200	-29.6	-59.5	-61	-1.5	0.210	120
75-L	0.200	-30.7	-61/7	-61	0.7	0.195	125
100-A	0.314	-36.9	-77.7	-80	-2.3	0.334	92
100-L	0.314	-36.5	-78.4	-77	1.4	0.306	96

Table 7.17 Argon Perturbation Results for Argon-Helium System

%Ar	$B(\mu)$	τ_P/s	τ_{NC}/s	τ_N/s	$\Delta\tau_N/s$	$B(\mu)_A$	τ_X/s
0-A	1.43	128.5	100.6	90	-10.6	1.974	148
0-L	1.43	127.1	97	98	1	1.392	148
10-A	0.63	114.9	95.3	91.7	-3.6	0.746	146
10-L	0.63	113.9	93.7	95.1	1.4	0.586	146
25-A	0.16	90.5	82.7	82.8	0.1	0.159	139
25-L	0.16	91.6	83.5	85.0	1.5	0.131	142
50-A	-0.009	53.5	54.0	55.3	1.3	-0.030	113
50-L	-0.009	54.3	54.9	58.3	3.4	-0.064	117
75-A	-0.013	27.4	28.2	30.7	2.5	-0.053	89
75-L	-0.013	28.1	28.9	33.0	4.1	-0.080	90
90-A	-0.007	13.0	13.4	17.2	3.8	-0.068	75
90-L	-0.007	13.3	13.7	17.2	3.5	-0.062	76

Table 7.18 Helium Perturbation Results for Argon-Helium System

%Ar	$B(\mu)$	τ_p/s	τ_{NC}/s	τ_N/s	$\Delta\tau_N$/s	$B(\mu)_A$	τ_X/s
10-A	-0.06	-16.9	-7.3	-5.4	1.9	-0.070	143
10-L	-0.06	-15.9	-6.1	-2.9	3.2	-0.080	147
25-A	-0.053	-33.7	-24.7	-22.1	2.6	-0.068	137
25-L	-0.053	-31.2	-22.2	-19.1	3.0	-0.071	140
50-A	0.008	-47.9	-49.2	-47.4	1.8	-0.063	113
50-L	0.008	-48.1	-49.4	-46.0	3.4	-0.013	117
75-A	0.050	-65.1	-72.8	-71.3	1.5	0.041	88
75-L	0.050	-62.8	-70.6	-69.4	1.2	0.042	94
90-A	0.072	-79.3	-90.3	-85.4	4.9	0.040	72
90-L	0.072	-76.9	-87.7	-83.1	4.6	0.041	75
100-A	0.094	-81.5	-94.8	-92.4	2.4	0.077	60
100-L	0.094	-79.8	-93.2	-92.6	0.6	0.089	64

Table 7.19 Nitrogen Perturbation Results for Nitrogen-Helium System

$\%N_2$	$B(\mu)$	τ_p/s	τ_{NC}/s	τ_N/s	$\Delta\tau_N$/s	$B(\mu)_\Lambda$	τ_X/s
0-A	0.194	391	384	386.1	2.1	0.129	429
0-L	0.194	392	384	385.9	1.9	0.149	433
10-A	0.014	319	318.5	319	0.5	0.000	360
10-L	0.014	314.5	313.8	318.5	4.7	-0.086	361
25-A	-0.071	251.7	255	251.5	-3.5	0.004	298
25-L	-0.071	246.7	250.4	250.5	0.1	-	300
50-A	-0.060	144.6	147.5	147	-0.5	-0.050	193
50-L	-0.060	143.2	146.5	144	-2.5	-0.015	198
75-A	-0.040	60.8	62.7	66	3.3	-0.110	108
75-L	-0.040	61.7	64.1	68.1	4.0	-0.127	112
90-A	-0.016	25.3	26.1	30.2	4.1	-0.105	72
90-L	-0.016	26.7	27.4	31	3.6	-0.089	75

Table 7.20 Helium Perturbation Results for Nitrogen-Helium System

$\%N_2$	$B(\mu)$	τ_P/s	τ_{NC}/s	τ_N/s	$\Delta\tau_N$/s	$B(\mu)_A$	τ_X/s
10-A	0	-32.8	-32.8	-26.4	6.4	-0.016	366
10-L	0	-30.5	-30.5	-25.3	5.2	-0.013	372
25-A	0.019	-68.8	-75.6	-68.9	6.7	0	290
25-L	0.019	-67.8	-74.7	-67.2	7.4	-0.001	294
50-A	0.048	-120.5	-135.2	-119.7	15.5	-0.002	186
50-L	0.048	-122	-137.1	-123.7	13.4	0.005	192
75-A	0.075	-146.5	-165.0	-153.6	11.4	0.029	100
75-L	0.075	-147.6	-166.7	-156.0	10.7	0.033	105
90-A	0.088	-163.6	-183.9	-182.2	1.7	0.081	67
90-L	0.088	-160.9	-181.2	-171.0	10.2	0.044	70
100-A	0.100	-172.8	-194.1	-180	14	0.035	46
100-L	0.100	-167.4	-189.1	-177	12	0.044	50

7.6.4 Interpretation of Tables

7.6.4.1 Nitrogen-Argon System at Room Temperature

1. Generally, for the nitrogen perturbation gas it can be seen that Equation 4.12 predicts the flowrate retention times very well. It can be seen that most of the differences are positive; the few negative values can be explained as rogue points. The differences vary from about one to five seconds. From Figure 4.10, up to 25% nitrogen it can be seen that there is some flexibility in the value of viscosity factor employed; the perfect values are within experimental range. However, in the rest of the composition range, the predictions are virtually co-incident. This might suggest that the measured values should be co-incident with the predictions, in which case the 75% point should be moved downwards making the predictions worse. The largest deviations are at 90% nitrogen, but the measured value is co-incident with the predictions; the required value for agreement is out of reach.

2. Generally, for the argon perturbation gas it can be seen that Equation 4.12 does not give good predictions. Once again, the differences are positive and they increase with the nitrogen

mixture composition. From Figure 4.11, the required viscosity factors are far removed from the predictions and the measured values; reasonable adjustments in these factors will not help equation agreement.

7.6.4.2 Nitrogen-Argon System at 54°C

1. For the nitrogen perturbation gas, similar to the room temperature case, it can be seen that Equation 4.12 predicts the measured values quite well and the discrepancies are all positive. Generally, the differences are between two and four seconds.

2. For the argon perturbation gas, the predictions of Equation 4.12 are much better than for the room temperature case. The results are not so good because the changing sign makes spotting a trend more difficult.

7.6.4.3 Nitrogen-Helium System at Room Temperature

1. For the nitrogen perturbation gas, the trend is similar to the nitrogen-argon system in that the predictions are good; the differences are generally positive and generally increase from about one to four seconds. Generally, it can be seen that each set of pressure and flowrate retention times is similar; the effect of Equation 4.12 being to add on and remove roughly the same amount so that there is little overall change. For the pure helium case, it can be seen that a comparatively large change in viscosity factor (0.06) would be required to correct by two seconds. Thus, the system is comparatively insensitive to the value of viscosity factor employed. This can be explained by the form of Equation 4.12. As the value of the composition retention time approaches that of the pressure retention time, the viscosity factor term tends to disappear from the equation. Comparing, for the nitrogen-argon system, a two second correction would require a change of 0.007.

2. For the helium perturbation gas, Equation 4.12 generally gives poor predictions. The differences are all positive and vary from about five seconds at 10% nitrogen to twelve seconds at 100% nitrogen. From Figure 4.13, there is no way that these differences can be significantly improved by adjustment of the viscosity factors.

7.6.4.4 Argon-Helium System at Room Temperature

1. For the argon perturbation gas, the trend is similar to the previous nitrogen perturbation results in that Equation 4.12 gives good predictions. Apart from a few rogue points, the positive deviations increase from about one to four seconds as the argon mixture composition increases. From Figure 4.14, the predictions of the viscosity factors are very close to the measured values and so the differences for the argon-rich mixtures cannot be reduced further.

2. Unlike the previous system, for the helium perturbation gas Equation 4.12 gives good predictions of the measured values. Once again, the deviations are positive and increase from about one to five seconds. From Figure 4.15, it would appear that the helium-rich viscosity factors are accurate, although there may be slight adjustments made for the argon-rich mixtures, which will have an adverse effect on the predictions.

7.6.5 Discussion of Results

From Section 7.5, it was seen that putting in downstream delay-lines imposed a positive contribution on the measured flowrate retention times; the value being roughly fixed for a particular system arrangement. From this conclusion, it might be expected that for the general case, when the perturbation causes a composition change, the behaviour should be the same. However, the general case causes a problem, because measurement of the flowrate retention time requires that the flowrate pen reaches the plateau at $n(\infty)$ as the front leaves the column and enters the downstream delay-line. This must be attained before the front enters the measuring capillary and the pen moves to the final $p(\infty)$ position. From Chapter Four, without the downstream delay-lines, the flowrate pen moves directly to the $p(\infty)$ position as the front leaves the column and passes directly into the measuring capillary. There is no such problem when the perturbation and carrier have the same composition; as soon as the perturbation gas is added, the flowrate pen will sweep directly from the initial baseline $n(0)$ to the final position $n(\infty)$ (the latter position will always be attained). The problem for the general case is the *changing* column outlet flowrate. From Chapter Six, any change in column outlet flowrate will change the column *and* downstream delay-line average pressures. The change in equipment average pressure will cause a change in equipment *holdup*; this is the instantaneous amount (moles) of total gas contained in the equipment. When the average pressure increases, there will be a pause in the outlet flowrate to enable the required increase in holdup to be attained. Conversely, when the average pressure decreases, there will be an increase in the outlet flowrate to enable the excess holdup to be expelled. Overall on the flowrate record, the effect of these holdup changes will be to slow down the movement of the flowrate pen. These holdup changes *may* effect the τ_N measurement in two ways, and these will now be discussed in turn:

1. Net Adsorption As soon as the perturbation gas is added, the flowrate pen will move from the initial baseline $n(0)$ towards the position $n(\infty)$; the latter position would be attained if upstream delay-lines were employed. However, when the front reaches the column, the net adsorption will move the flowrate pen to a position below the level $n(\infty)$; the extent of the reduction will depend upon the system. As the front moves through the column, the average pressure in both the column and downstream delay-lines will be reduced. When the front reaches the end of the column, there will be no more net adsorption and the flowrate

pen will move towards the $n(\infty)$ position. The required increase in holdup for both column and delay-line will slow down the attainment of the $n(\infty)$ position. However, despite the temporary changes, as long as the plateau at $n(\infty)$ is attained, the measured flowrate retention time should contain a fixed contribution. From the relevant tables, this would appear to be the case. However, if the plateau at $n(\infty)$ is not attained as the front leaves the column, the measured area *and* the measured offset on the flowrate record will both be reduced from the correct values. From a typical flowrate chromatogram, since there is proportionally more area for τ_N close to $n(\infty)$, the overall effect might be to *reduce* the measured flowrate retention time.

2. Net Desorption Similarly, when the perturbation gas is added, the flowrate pen will move from the initial baseline $n(0)$ towards the position $n(\infty)$. However, when the front reaches the column, the net desorption will increase the column outlet flowrate and this will move the flowrate pen to a position above the level $n(\infty)$. As the front moves through the column, the average pressure in both the column and delay-line will be increased. When the front reaches the end of the column, there will be no more net desorption and the flowrate pen will move back to the $n(\infty)$ position. The required reduction in holdup for both the column and delay-line as the front leaves the column, means that all the excess gas will exit through the downstream delay-line. This temporary increase in flowrate will retard the movement of the pen towards the required $n(\infty)$ position. The required area for τ_N measurement consists a "negative" area above the $n(\infty)$ level and a smaller "positive" area below the $n(\infty)$ level. If the plateau is not attained, the measured offset will be increased and the negative area reduced leading to a reduction in the flowrate retention time magnitude (τ_N is negative). This might explain the discrepancies noted for using the helium perturbation in the nitrogen-helium system, and using the argon perturbation in the nitrogen-argon system.

7.7 Problem of Column Deactivation

In the following section, results are presented using various columns and upstream delay-lines. However, in certain cases the columns were found to be partially deactivated; a cursory inspection of the chromatogram shapes revealed this problem. This is not really surprising since changing the upstream delay-line arrangement will necessarily involve cutting of the column inlet flowrate. Actually, because of this problem, the apparatus was later modified and this modification is described in Chapter Three. From Chapter One, column deactivation is characterised by a general reduction in the *magnitudes* of all the retention times. This will cause problems since the point of this chapter is to investigate the effect of the delay-line employment *alone* on the measured retention times. One solution is to try and separate out the effects of column deactivation, so that the delay-line effects

can be studied alone. An attempt was made at this problem by taking the chromatographic equations described in Chapter One and making finite changes in each of the *four* retention times (two for each perturbation gas). These correspond to the two flowrate retention times (τ_{NA} and τ_{NB}) and the two composition retention times (τ_{XA} and τ_{XB}) for each perturbation gas. Two equations are formulated since the changes must be related so that each perturbation gas gives isotherm gradient agreement for each component:

$$\Delta\tau_{XA}+\left(\frac{Y_{AO}}{1-Y_{AO}}\right)\Delta\tau_{NA}=\left[\frac{1+\left(\frac{Y_{AO}}{1-Y_{AO}}\right)P_{CR}}{1-P_{CR}}\right](\Delta\tau_{XB}-\Delta\tau_{NB}) \qquad 7.23$$

$$\Delta\tau_{XA}-\Delta\tau_{NA}=\left[\frac{1-P_{CR}}{1+\left(\frac{Y_{BO}}{1-Y_{BO}}\right)P_{CR}}\right]\left[\Delta\tau_{XB}+\left(\frac{Y_{BO}}{1-Y_{BO}}\right)\Delta\tau_{NB}\right] \qquad 7.24$$

$$P_{CR}=\frac{\Delta P_C}{2P_{COUT}}\left(\frac{1+\frac{\Delta P_C}{2P_{COUT}}}{1+\frac{\Delta P_C}{3P_{COUT}}}\right) \qquad 7.25$$

These equations can be re-arranged so that both composition retention time terms are on the right side. It is necessary to treat these separately because according to the theory, they do not have the same value although the difference is reduced as the column pressure drop is reduced. This is an important part of the method development and is significant for other chromatographic methods since the choice of perturbation gas will determine the retention time. Finally, the equations were incorporated into a simple computer program and the following points summarise the main results:

1. As P_{CR} tends to zero, both equations become equivalent and require the solution:

$$\Delta\tau_{XA}=\Delta\tau_{XB} \qquad 7.26$$

The changes in the flowrate retention times are independent of the composition retention time and any changes are represented by the following equation:

$$\frac{-\Delta\tau_{NA}}{\Delta\tau_{NB}}=\frac{1-Y_{AO}}{Y_{AO}} \qquad 7.27$$

The negative sign is present, since although the negative retention time decreases in magnitude, it becomes more positive. For a 50% mixture the changes are the same but at the extreme ends of the composition range, one of the changes will be much larger.

2. Using a finite value of the pressure ratio P_{CR}, the changes in each composition retention time must be specified separately. Interestingly, if the same values are specified, the results are trivial and independent of the values. It became clear that for the program to generate realistic results, the specified values must be different. Moreover, a larger reduction is required for the more strongly adsorbed component, that is the perturbation component generating the positive flowrate retention time.

3. From the simulations, the results are independent of the composition retention time changes, but dependent upon the difference of these changes. From the simulations, the following equation is representative:

$$\overline{\Delta\tau_{NA}} + \overline{\Delta\tau_{NB}} = \frac{\Delta\tau_{XA} - \Delta\tau_{XB}}{P_{CR}} \qquad 7.28$$

As the pressure ratio P_{CR} tends to zero, the changes in both flowrate retention times are related by Equation 7.27. For finite values of the pressure ratio, the ratio of the two retention times will also depend upon the difference in the changes in the composition retention times.

4. The useful part of the simulation is to show the relationship between the reduction in each flowrate retention time when the columns become deactivated. To obtain the absolute changes would require a knowledge of the change in each composition retention time. Considering the sensitivity of Equation 7.28, these are very difficult to obtain. By knowing the *ratio* of these two reductions, one possibility would be to set up two simultaneous equations with the other unknown being the delay-line contribution to the measured retention time.

7.8 Effect of Delay-Lines for Mixture Carrier

7.8.1 Introduction

From Section 7.5.1, it was seen that employment of downstream delay-lines affected the theory by giving an increased value of δc_i in the column. The original theory required that the column outlet pressure remained constant during the perturbation, whereas the presence of the downstream delay-lines violates this requirement. The conclusion was that the ΔP_C term employed in the F_{PVCi} term should be replaced with the ΔP_C^* term which takes account of the downstream delay-line pressure drop. The effect of using the ΔP_C^* term is more complex for the mixture carrier, since the perturbation gas will also cause a composition change. The quantitative effect of this modification will depend upon which perturbation gas is employed to calculate the $\Delta H_i/\delta c_i$ value; if the perturbation gas is component *i* then the initially calculated $\Delta H_i/\delta c_i$ value will be reduced, whereas if it is not component *i* the value will be increased.

In Section 7.5.3, an analysis was carried out which predicted an equivalent contribution to the measured flowrate retention time due solely to the downstream delay-line pressure drop. This was relatively easy to obtain for two reasons. Firstly, the $\Delta H_i/\delta c_i$ equation is characterised solely by the flowrate retention time; there is no composition retention time to consider. Secondly, because there is no viscosity effect, the pressure and flowrate retention times are equivalent. To carry out a similar analysis for the binary mixture is complicated for two reasons. Firstly, the expression for $\Delta H_i/\delta c_i$ involves *both* flowrate and composition retention times. Secondly, direct measurement of the flowrate retention time requires sufficient delay volume to separate out the viscosity and flow effects; it is not equivalent to the pressure retention time.

7.8.2 Modification to Original Theory

Consider a situation in which there are no downstream delay lines present. In this case, when a perturbation is made, the change in concentration of any component in the column is represented in the standard way by Equation 7.6. The two measured composition and flowrate retention times will be τ_χ and τ_p respectively. Now, consider a hypothetical situation in which a delay line of sufficient volume and zero pressure drop is placed in the downstream location. From this arrangement, it should be possible to measure the flowrate retention time directly. Moreover, because the column outlet pressure will remain constant, the change in column concentration is the same as in Equation 7.6 and thus the measured flowrate retention time will purely representative of the column and there will be no other contributions. It should be possible to calculate directly the intrinsic isotherm gradients directly with no corrections; this hypothetical value will be termed τ_{NH}. From Equation 4.12, it should be possible to relate τ_{NH}, τ_p and τ_χ by the following equation:

$$\tau_{NH} = (1 + B(\mu))\tau_p - \tau_\chi B(\mu) \qquad 7.29$$

Now consider a hypothetical situation in which a zero volume flow resistance is placed in the downstream location with no delay lines present. Because there is not a sufficient delay volume, a pressure retention time will be measured on the flowrate record. However, from previous arguments, the change in column concentration will now be represented by Equation 7.9 which involves the equivalent column pressure drop. Hence, it might be expected that the measured pressure retention time will include an extra contribution and will increase to $\tau_p + \tau^*_{pD}$. In a typical situation, the downstream delay-lines will have sufficient volume and a finite pressure drop. From Section 7.5.2, it was seen that the measured flowrate retention time τ_N will include a contribution τ_{ND} which will depend upon the delay line pressure drop and volume. Thus it would be expected that the measured flowrate retention time would be greater than τ_{NH} because of two contributions and Equation 7.24 shows how these contributions *should* be related:

$$\tau_N = \tau_{NH} + \tau^*_{ND} + \tau_{ND} \qquad 7.30$$

In order to equate the expressions for $\Delta H_i/\delta c_i$ it will be necessary to do this for both components. This will lead to two simultaneous equations and it will thus be necessary to consider a contribution to the measured composition retention time, and this will be termed τ^*_{XD}.

$$\frac{\Delta H_i}{\delta c_i} = \frac{Q_{CAV}}{F_{PVCi}}\left[\tau_X + \frac{Y_{iO}}{Y_{iT} - Y_{iO}}\tau_{NH}\right] \qquad 7.31$$

$$\frac{\Delta H_i}{\delta c_i} = \frac{Q_{CAV}}{F^*_{PVCi}}\left[(\tau_X + \tau^*_{XD}) + \frac{Y_{iO}}{Y_{iT} - Y_{iO}}(\tau_{NH} + \tau^*_{ND})\right] \qquad 7.32$$

Equations 7.31 and 7.32 must be equated for Y_{iT}=0 and Y_{iT}=1 and this will give the two simultaneous equations from which the required contributions τ^*_{ND} and τ^*_{XD} can be deduced.

$$\frac{1 - \frac{\Delta P^*_C}{2P_{COUT}}\left[\frac{1 + \frac{\Delta P_C}{2P_{COUT}}}{1 + \frac{\Delta P_C}{3P_{COUT}}}\right](1 + B(\mu))}{1 - \frac{\Delta P_C}{2P_{COUT}}\left[\frac{1 + \frac{\Delta P_C}{2P_{COUT}}}{1 + \frac{\Delta P_C}{3P_{COUT}}}\right](1 + B(\mu))} = \frac{\tau_X + \tau^*_{XD} - \tau_{NH} - \tau^*_{ND}}{\tau_X - \tau_{NH}} \qquad 7.33$$

$$\frac{1 + \frac{\Delta P^*_C}{2P_{COUT}}\frac{Y_{iO}}{Y_{iT} - Y_{iO}}\left[\frac{1 + \frac{\Delta P_C}{2P_{COUT}}}{1 + \frac{\Delta P_C}{3P_{COUT}}}\right](1 + B(\mu))}{1 + \frac{\Delta P_C}{2P_{COUT}}\frac{Y_{iO}}{Y_{iT} - Y_{iO}}\left[\frac{1 + \frac{\Delta P_C}{2P_{COUT}}}{1 + \frac{\Delta P_C}{3P_{COUT}}}\right](1 + B(\mu))} = \frac{\tau_X + \tau^*_{XD} + \frac{Y_{iO}}{Y_{iT} - Y_{iO}}\tau_{NH} + \frac{Y_{iO}}{Y_{iT} - Y_{iO}}\tau^*_{ND}}{\tau_X + \frac{Y_{iO}}{Y_{iT} - Y_{iO}}\tau_{NH}} \qquad 7.34$$

For convenience, the ratio of the correction factors in Equation 7.33 will be termed F_0 and the ratio of the correction factors in Equation 7.34 will be termed F_1. As is expected from the form of both equations, as ΔP^*_C tends to ΔP_C both contributions tend to zero.

7.8.3 Quantitative Effects and Further Implications

It is instructive to calculate typical contributions for a standard column with the usual 30 metre length of downstream delay-line. Table 7.21 summarises the calculated contributions for a number of hypothetical situations.

Table 7.21 Retention Time Contributions for Hypothetical Situations

τ_X/s	τ_{NH}/s	Y_{iO}	F_O	F_1	τ^*_{XD}/s	τ^*_{ND}/s
50	-200	0	0.986	1	0	3.5
200	100	0.5	0.986	1.014	1.4	2.8
200	100	0.25	0.986	1.005	0.6	2.0
200	100	0.75	0.986	1.038	3.7	5.1
200	-100	0.5	0.986	1.014	-1.4	2.8

Summarising, the results for the hypothetical situations would indicate that the downstream delay line pressure drop makes contributions to both the measured composition and flowrate retention times. The actual values of these contributions will depend upon the gas mixture composition and the values of τ_X and τ_{NH}. Interestingly, when the τ_{NH} becomes negative the composition contribution becomes negative. This has implications regarding the measurement of τ_X for either perturbation gas. Usually, it is assumed that they have the same value. When downstream delay lines are employed, the τ_X measured for the less adsorbed perturbation gas will be reduced, and the measured τ_X for the more adsorbed perturbation gas will be increased.

The τ^*_{XD} effect will also have implications with regard to Tables 7.13 to 7.20 where measured values of pressure and flowrate retention time are used to validate Equation 4.12. When compiling these tables, it was assumed that τ_X was intrinsically the same, namely that it would only depend upon the carrier flowrate which may vary from system to system. Because the carrier flowrates can be measured accurately, the ratio of these flowrates was used to bring the measured retention times to the same basis. However, the τ^*_{XD} contribution would violate this assumption and it might be necessary to normalise the measured composition retention times for a better comparison. Consider Table 7.14 where an argon perturbation gas is used for the argon-nitrogen system. From this table, Equation 4.12 was seen to give the worst predictions; positive $\Delta\tau_N$ deviations varied from about four to twelve seconds. Consider the case of adding the argon perturbation gas to the 50% mixture. Solving Equations 7.33 and 7.34 gives the following contributions:

$\tau^*_{XD} =$ -1.4 seconds

$\tau^*_{ND} =$ 3.6 seconds

Firstly, the τ^*_{ND} contribution would mean that the best prediction of Equation 4.12 would be around four seconds. The negative τ^*_{XD} contribution would mean that the comparison was taking place at different values of τ_X, the difference being about 1%. This might require τ_N to be increased by 1% and this would give an extra effective contribution of around one second. Thus, the overall effect of these contributions would mean that the best prediction of Equation 4.12 would be around five seconds greater than the predicted value τ_{NC}. If Equations 7.33 and 7.34 are solved for the whole composition range in Table 7.14, the τ^*_{ND} contribution would increase up to about five seconds. These are certainly significant and will explain *partially* the deviations in Table 7.14. In the next section, the contributions of the delay-lines themselves will be investigated.

7.8.4 Employment of Intermediate Delay Lines

Previously, the intermediate location was defined to be between the column and the TCD. Hence, the measured composition retention time will be significantly increased since the composition front will be physically delayed in the delay lines. Of course, it is possible to correct this obvious error by comparing chromatograms and estimating the time spent in the tubing. However, it is better to start from first principles and consider the total change in holdup for each component when a perturbation is effected. Equation 7.35 shows the molar balance for component A:

$$\Delta H_A = (1-\varepsilon)V_C\delta q_A + \varepsilon V_C\delta c_A + V_I\delta c_{AI} \qquad 7.35$$

The subscript I refers to properties in the intermediate delay lines. The equation can thus be re-arranged in the standard way to obtain the isotherm gradient explicitly:

$$\frac{\delta q_A}{\delta c_A} = \frac{\frac{\Delta H_A}{\delta c_A} - \varepsilon V_C - V_I\frac{\delta c_{AI}}{\delta c_A}}{(1-\varepsilon)V_C} \qquad 7.36$$

Since the isotherm gradient is independent of the presence of delay lines, the extra term on the numerator enables the contributions to the measured flowrate retention time τ_{NI} and the measured composition retention time τ_{XI} to be obtained. Similar to the analysis of Mason and Buffham (unpublished) for the change in *column* concentration, the concentration change in the *intermediate delay-line* concentrations can be represented by the following equations:

$$\delta c_{iI} = \frac{P_{IMEAN}}{RT_I} dY_i F_{PVI} \qquad 7.37$$

$$F_{PVIi} = 1 + \left(\frac{Y_{iO}}{Y_{iT} - Y_{iO}} \right) \frac{\Delta P_I}{2P_{IMEAN}} \left[\frac{1 + \frac{\Delta P_I}{3P_{IOUT}}}{1 + \frac{\Delta P_I}{2P_{IOUT}}} \right] (1 + B(\mu)) \qquad 7.38$$

Substituting Equations 7.37 and 7.38 into Equation 7.36 the required contributions are obtained;

$$\tau_{XI} = \frac{V_I}{Q_{IMEAN}} \qquad 7.39$$

$$\tau_{NI} = \frac{V_I}{Q_{IMEAN}} \frac{\Delta P_I}{2P_{IMEAN}} \left[\frac{1 + \frac{\Delta P_I}{3P_{IOUT}}}{1 + \frac{\Delta P_I}{2P_{IOUT}}} \right] (1 + B(\mu)) \qquad 7.40$$

The contribution to the composition retention time is, not surprisingly, the delay time in the intermediate tubing. The contribution to the flowrate retention time is similar to that in Section 7.5.2 except for the additional presence of the viscosity term. For systems in which the viscosity factor is small, the contributions will be roughly the same as those calculated in Section 7.5.3.

7.8.5 Employment of Downstream Delay Lines

Because this location is downstream of the TCD, there will be no effect on the composition retention time and $\tau_{XD} = 0$. The form of τ_{ND} will be the same as that for the intermediate case except for the relevant subscript.

7.8.6 Employment of Upstream Delay-Lines

Similar to the analysis of Section 7.8.4, when a perturbation is made to the system, Equation 7.41 gives the molar balance for component A:

$$\Delta H_A = (1 - \varepsilon) V_C \delta q_A + \varepsilon V_C \delta c_A + V_U \delta c_{AU} \qquad 7.41$$

The subscript U refers to the properties in the upstream delay lines. Equation 7.41 can be rearranged to obtain the isotherm gradient explicitly:

$$\frac{\delta q_A}{\delta c_A} = \frac{\frac{\Delta H_A}{\delta c_A} - \varepsilon V_C - V_U \frac{\delta c_{AU}}{\delta c_A}}{(1 - \varepsilon) V_C} \qquad 7.42$$

Since the isotherm gradient is independent of the presence of the delay lines, the extra term on the numerator enables the contributions of the upstream delay-lines to the measured composition retention time τ_{XU} and the measured flowrate retention time τ_{NU} to be obtained.

From the analysis of Section 7.5.2, the change in upstream delay line concentration δc_{iU} will depend upon the column pressure drop, and from the analysis of Mason and Buffham this can be represented by the following equations:

$$\delta c_{iU} = \frac{P_{UMEAN}}{RT_U} dY_i F_{PViU} \qquad 7.43$$

$$F_{PVUi} = 1 + \left(\frac{Y_{iO}}{Y_{iT} - Y_{iO}} \right) \left\{ \frac{\Delta P_U}{2P_{UMEAN}} \left[\frac{1 + \frac{\Delta P_U}{3P_{UOUT}}}{1 + \frac{\Delta P_U}{2P_{UOUT}}} \right] + K_C \frac{T_U}{T_C} \frac{\Delta P_C^*}{2P_{CMEAN}} \left[\frac{1 + \frac{\Delta P_C}{3P_{COUT}}}{1 + \frac{\Delta P_C}{2P_{COUT}}} \right] \right\} (1 + B(\mu)) \qquad 7.44$$

Substituting Equations 7.43 and 7.44 into Equation 7.42 and simplifying, the relevant upstream contributions are obtained:

$$\tau_{XU} = \frac{V_U}{Q_{UMEAN}} \qquad 7.45$$

$$\tau_{NU} = \left\{ \frac{V_U \Delta P_U}{2MRT_U} \left[\frac{1 + \frac{\Delta P_U}{3P_{UOUT}}}{1 + \frac{\Delta P_U}{2P_{UOUT}}} \right] + \frac{K_C V_U \Delta P_C^*}{2MRT_C} \left[\frac{1 + \frac{\Delta P_C}{3P_{COUT}}}{1 + \frac{\Delta P_C}{2P_{COUT}}} \right] \right\} (1 + B(\mu)) \qquad 7.46$$

The contribution to the measured composition retention time is of the same form as the intermediate case. In reality, because the absolute pressure in the upstream delay lines will be higher and the volumetric flowrate lower, the contribution will be greater. The contribution to the flowrate retention time consists of two terms. The equation is similar in form to that for the non-composition change case except for the additional presence of the characteristic viscosity term. The conclusion from Equation 7.46 is that the contribution will be significant for a high column pressure drop.

7.8.7 Employment of Switching Valve Delay Lines

As the perturbation gas cannot physically pass through this location, it might appear that it has no practical use. Indeed, this location is included for the sake of completeness. Thus, there will be no contribution to the measured composition retention time. Although the flowrate through this delay line location will not increase, the pressure downstream of this delay line will necessarily increase due to all the increases in pressure downstream of this delay line location. As the flowrate increases through each component of equipment, the average pressure in this component will increase; the increase depending upon the component pressure drop. However, the change in the inlet pressure of each component is important since this will directly affect the outlet pressure of equipment component directly upstream. It has already been seen that the increase in the inlet pressure can be twice as

high as the increase in the average pressure. Now, similar to the analysis of Section 7.8.4, consider a molar balance on component A with δc_{AS} the concentration change in the delay line of interest:

$$\Delta H_A = (1-\varepsilon)V_C \delta q_A + \varepsilon V_C \delta c_A + V_S \delta c_{AS} \qquad 7.47$$

However, for this location, there is *no* composition change caused by the perturbation and δc_{AS} is represented by Equation 7.48:

$$\delta c_{AS} = Y_{AO}\delta c_T = Y_{AO}\frac{K_C \Delta P_C}{2RT_C}\left[\frac{1+\frac{\Delta P_C}{3P_{COUT}}}{1+\frac{\Delta P_C}{2P_{COUT}}}\right]\frac{n}{M} \qquad 7.48$$

Once again, if Equation 7.48 is re-arranged to obtain the isotherm gradient explicitly, the extra term on the numerator enables the flowrate retention time contribution τ_{NS} to be obtained:

$$\tau_{NS} = \frac{V_S K_C \Delta P_C}{2MRT_S}\left[\frac{1+\frac{\Delta P_C}{3P_{COUT}}}{1+\frac{\Delta P_C}{2P_{COUT}}}\right] \qquad 7.49$$

Hence, for an equivalent delay-line, the τ_{NU} contribution will be greater than the τ_{NS} contribution. This is not really surprising since there is no flowrate change (only the average pressure) through a delay line in this location.

7.8.8 Typical Correction Values

Using the above derived equations, it is instructive to work out typical contributions for the flowrate retention times. The contributions for the composition retention times are self-explanatory and so will not be attempted; they simply involve dividing the relevant delay volume by the corresponding volumetric flowrate. The required information can be found in Tables 7.1 and 7.2.

1. Downstream/Intermediate Location

   For L_{DL}=20 metres τ_{ND}= 0.8-1.2 seconds

   For L_{DL}=30 metres τ_{ND}= 1.0-1.6 seconds

2. Upstream Location With ΔP_C = 40 mmHg

   For L_{DL}=20 metres τ_{NU} = 5-7 seconds

3. Upstream Location With ΔP_C = 200 mmHg

   For L_{DL}=20 metres τ_{NU} = 23-26 seconds

In Section 7.8.3, it was shown that the predictions of Equation 4.12, which relates the measured flowrate and composition retention times, could never give perfect agreement because of the τ^{*}_{ND} contribution. The range of values of τ_{ND} calculated above mean that when downstream delay lines are employed, there will be an additional significant contribution. The values calculated above are approximate because the volumes are estimated by taking the nominal inside diameter and assuming a cylindrical volume.

7.9 Results for Upstream Delay-Line Employment

7.9.1 Introduction

Tables of results will be presented for different systems and for different columns. In some cases, comparison will be difficult because of a difference in column activity. Following each table, a discussion will be presented on the changes in both retention times. For each carrier, there will be results for adding (A) and removing (L) the perturbation gas. The "normal" table heading refers to use of downstream delay-lines only.

7.9.2 Mixture Results for Column Type A

Table 7.22 Comparisons for 50% Nitrogen-Argon Mixture

	normal		L_U@1/8"= 20m		difference	
prtbn	τ_X/s	τ_N/s	τ_X/s	τ_N/s	$\Delta\tau_X$/s	$\Delta\tau_N$/s
N_2-A	195.8	83.9	300.1	89.5	104.3	5.6
N_2-L	199.1	85.1	301.4	89.6	102.3	4.5
Ar-A	197.4	-66.8	302.4	-61.0	105.0	5.8
Ar-L	200.8	-65.9	307.6	-62.2	106.8	3.7

In Table 7.21, for both arrangements the columns are partially deactivated; the retention times are lower when comparing with other results. Not surprisingly, inserting upstream delay-lines leads to a fixed increase in the composition retention time; this should be the delay volume divided by the delay-line volumetric flowrate. The increase in the flowrate retention time is consistent with the equations previously derived. Because the viscosity factors are small, the contributions are roughly the same for each perturbation gas.

Table 7.23 Comparisons for 75% Nitrogen-Helium Mixture

	normal		L_U@1/8"= 20m		difference	
prtbn	τ_X/s	τ_N/s	τ_X/s	τ_N/s	$\Delta\tau_X$/s	$\Delta\tau_N$/s
N_2-A	94	51.0	218	60.2	124	9.2
N_2-L	98	51.8	222.8	61.3	124.8	9.5
He-A	91	-128.0	213.9	-137.4	122	-9.4
He-L	94	-127.0	217.4	-134.4	123	-7.4

After inserting the upstream delay-lines, the columns were baked out. However, the columns are seen to have a higher activity after baking for two reasons. Firstly, the increase in the nitrogen perturbation composition retention time is higher than that for helium. Secondly, for the nitrogen perturbation it would appear that activation has increased the flowrate retention time by about four seconds. From the deactivation simulation, considering the column type and mixture composition, the corresponding change for helium perturbation gas will be about three times greater, roughly minus twelve seconds. Adding this to the positive delay-line contribution, this would confirm an overall change of about minus eight seconds.

7.9.3 Mixture Results for Column Type E

Table 7.24 Comparisons for 75% Nitrogen-Helium Mixture

	normal		L_U@1/8"= 20m		difference	
prtbn	τ_X/s	τ_N/s	τ_X/s	τ_N/s	$\Delta\tau_X$/s	$\Delta\tau_N$/s
N_2-A	106	58.1	213.1	58.5	107.1	0.4
N_2-L	105.3	58.0	213.4	56.7	108.1	-1.3
He-A	100.9	-160.0	210.6	-147.4	110	12.6
He-L	106.9	-162.1	216.5	-143.2	110	18.8

For this column type, the pressure drop is much lower than for previous cases. From the developed theory, the upstream delay-line contributions should be much smaller, probably around three seconds. From the respective increases in the composition retention times, the columns have become deactivated upon inserting the upstream delay-lines. For the nitrogen perturbation gas, the effect of the column deactivation would appear to have cancelled out the delay-line contribution. From the deactivation simulation, for a low

column pressure drop, the ratio of the changes of the flowrate retention times should be in proportion to the respective compositions; that is, for the 75% nitrogen mixture, the helium perturbation gas contribution should be three times that for nitrogen perturbation gas. Thus, the overall change should be around twelve seconds, and this compares well with Table 7.24.

7.9.4 Mixture Results for Column Type C

Table 7.25 Comparisons for 75% Nitrogen-Helium Mixture

	normal		L_U1/8"= 20m		difference	
prtbn	τ_X/s	τ_N/s	τ_X/s	τ_X/s	$\Delta\tau_X$/s	$\Delta\tau_N$/s
N_2-A	123.8	83.6	237.7	91.8	113.9	8.2
N_2-L	123.9	83.3	241.3	87.0	117.4	4.0
He-A	108.7	-180	224.8	-156.0	116.1	24
He-L	111.4	-179.4	230.2	-156.0	118.8	23.4

For this column type, the pressure drop is about double that of the standard column. From the theory, the upstream contribution to the flowrate retention times should be around twelve seconds. From the respective increases in the composition retention times, the column has become deactivated upon inserting the upstream delay-lines. For the nitrogen perturbation gas, the expected delay-line contribution would appear to have been offset by around six seconds due to deactivation. From the deactivation simulation, for a higher column pressure drop, the ratio of the helium to nitrogen contributions will be much less than three; probably around 1.5 times. This would give an expected overall helium change of around 1.5 times six plus twelve which equals 21. This compares well with the values from Table 7.25.

7.9.5 Results for Argon-Helium System

7.9.5.1 Introduction

This system will be treated separately for two reasons. Firstly, unlike the nitrogen perturbation gas systems, deactivation has less effect on the retention times; argon and helium are not adsorbed as strongly as nitrogen. This allows better comparisons to be made without the problem of column deactivation. Secondly, at one end of the composition range (helium carrier and argon perturbation), the viscosity factor is large and this will allow the effects of viscosity factor $B(\mu)$ as predicted by the theory to be rigourously tested.

7.9.5.2 Measurement of Flowrate Retention Time

When adding an argon perturbation flow to the helium carrier, it was noticed that there was an offset between the flowrate record positions attained when the front entered the upstream delay-lines and when the front left the column and entered the downstream delay-lines. Figure 7.3 shows the flowrate chromatograms obtained for adding an argon perturbation to a helium carrier using column type D. The top chromatogram is the composition record and the bottom one is the flowrate record. As seen before, the composition record is relatively simple in shape and the only deviation occurs when the front leaves the column and enters the TCD and the pen sweeps from the initial baseline $x(0)$ to the final position $x(\infty)$. When the perturbation flow is added, the flowrate pen moves from the initial baseline $n(0)$ towards the position $n(\infty)$; the latter position would be attained if upstream delay-lines were employed. When the front leaves the column, the net adsorption causes a reduction in column outlet flowrate. Indeed, the flowrate pen moves below the initial baseline $n(0)$. When the front leaves the column, there is no more net adsorption and the flowrate pen moves up to the level $n(\mathrm{p})$. Finally, when the front enters the measuring capillary, the subsequent large viscosity effect moves the pen to the $p(\infty)$ position.

The striking thing about the chromatogram concerns the level attained upon leaving the column $n(\mathrm{p})$. Although there were no upstream delay lines present, it can be seen the level $n(\mathrm{p})$ is well below that which would be obtained with upstream delay lines; indeed $n(\infty)$ shows the upstream delay line level. This *plateau offset* is due to a reduction in the overall column flowrate due to an increase in the column resistance. This offset will depend upon the viscosity factor. For a non-zero viscosity factor, there will always be a plateau offset, although for most systems it will be too small to be detected. This observation was first made in Chapter Six. This observation raises implications regarding the measurement of the flowrate retention time. The problem concerns the $n(\infty)$ term. If this is taken literally, this will be at the plateau after the column. However, if a line is drawn through this level, this will cut through the delay-line section and cause unwanted negative area. Actually, initially $n(\infty)$ will be at the upstream delay-line plateau level. This will allow the denominator or offset to be measured. However, once the front reaches the column, then $n(t)$ position will be moved downwards additionally because of the gradual change in column resistance. If this is not allowed for, the measured retention time will be unrealistically too high. Indeed, it is helpful to consider a hypothetical system in which the viscosity factor is so large that $n(\mathrm{p})$ was the same level as $n(0)$; in this case, according to previous interpretation of the definition the denominator of τ_N will be zero. This problem was solved by assuming a sloping value of $n(\infty)$ as the front passes through the column from the initial plateau to the second plateau. The linear variation of $n(\infty)$ assumes that the front moves at constant speed through the column. Strictly speaking, the volumetric flowrate is higher

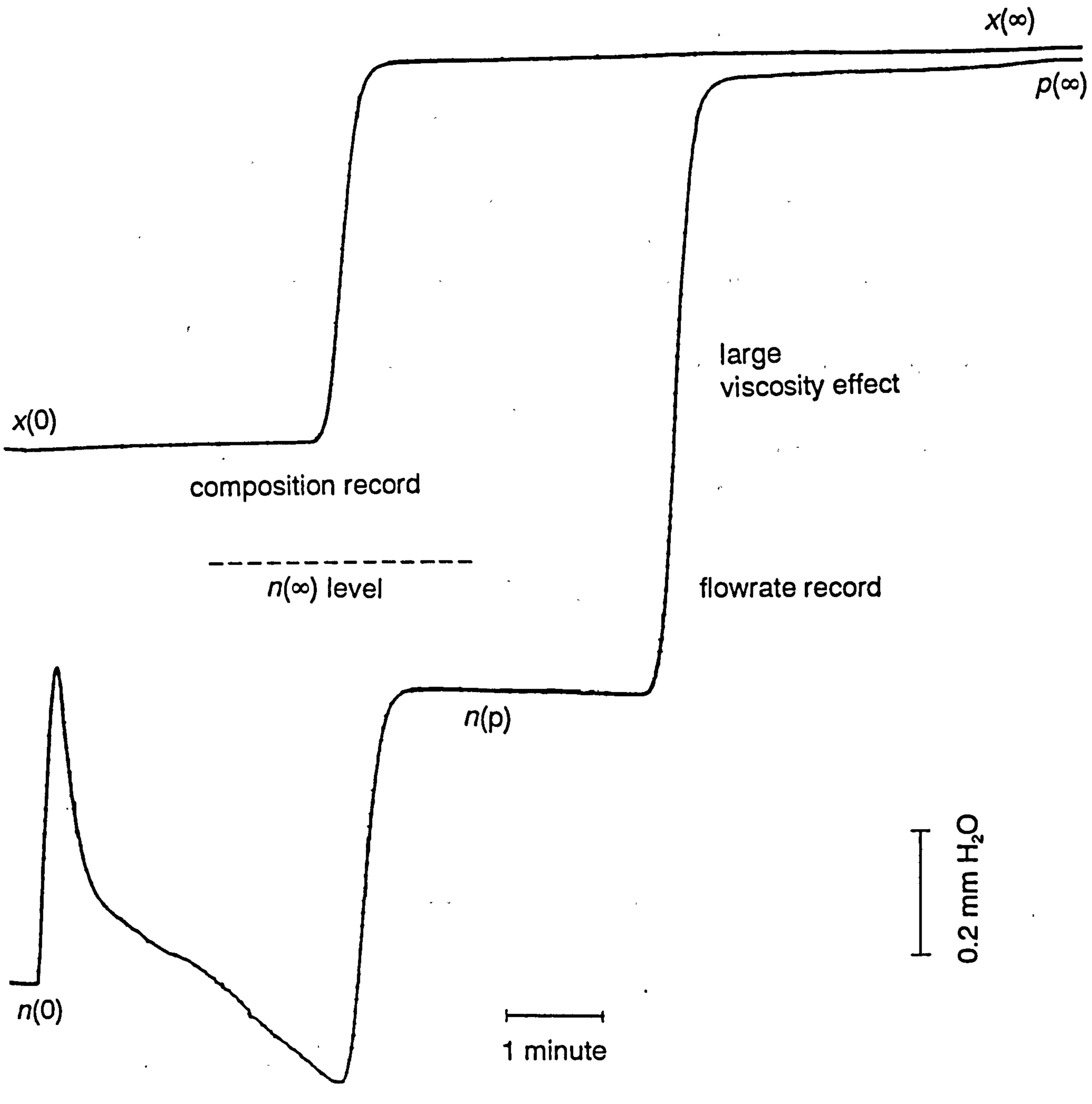

Figure 7.3 Chromatograms for Helium Carrier and Argon Perturbation

downstream and so the $n(\infty)$ variation should be slightly curved. Thus, for some systems, the correct determination of the flowrate residence time will require an initial run with upstream delay-lines to obtain the initial $n(\infty)$ level and hence the correct denominator.

7.9.5.3 Further Implications of Plateau Difference

The first implication concerns the direct measurement of the viscosity factors, previously described in Chapter Four. This consisted of measuring two offsets from the chart-recorder and their subsequent division. The above observations would suggest that upstream delay-lines should be employed for correct determination of both offsets. For example, if this were not done for the problematic argon-helium system, the measured value of the viscosity factor would be to large, since the measured denominator would be unrealistically too small. The second implication concerns the measurement of the pressure retention time. In the derivation of Equation 4.12, the pressure retention time was obtained by dividing an area by the sum of the two required offsets. However, any plateau offset will either increase or decrease this total. Because of this problem, it is necessary to re-consider the derivation of Equation 4.12. Figure 7.4 shows a hypothetical flowrate chromatogram obtained for a system with a positive viscosity factor such that the plateau offset (p) is negative.

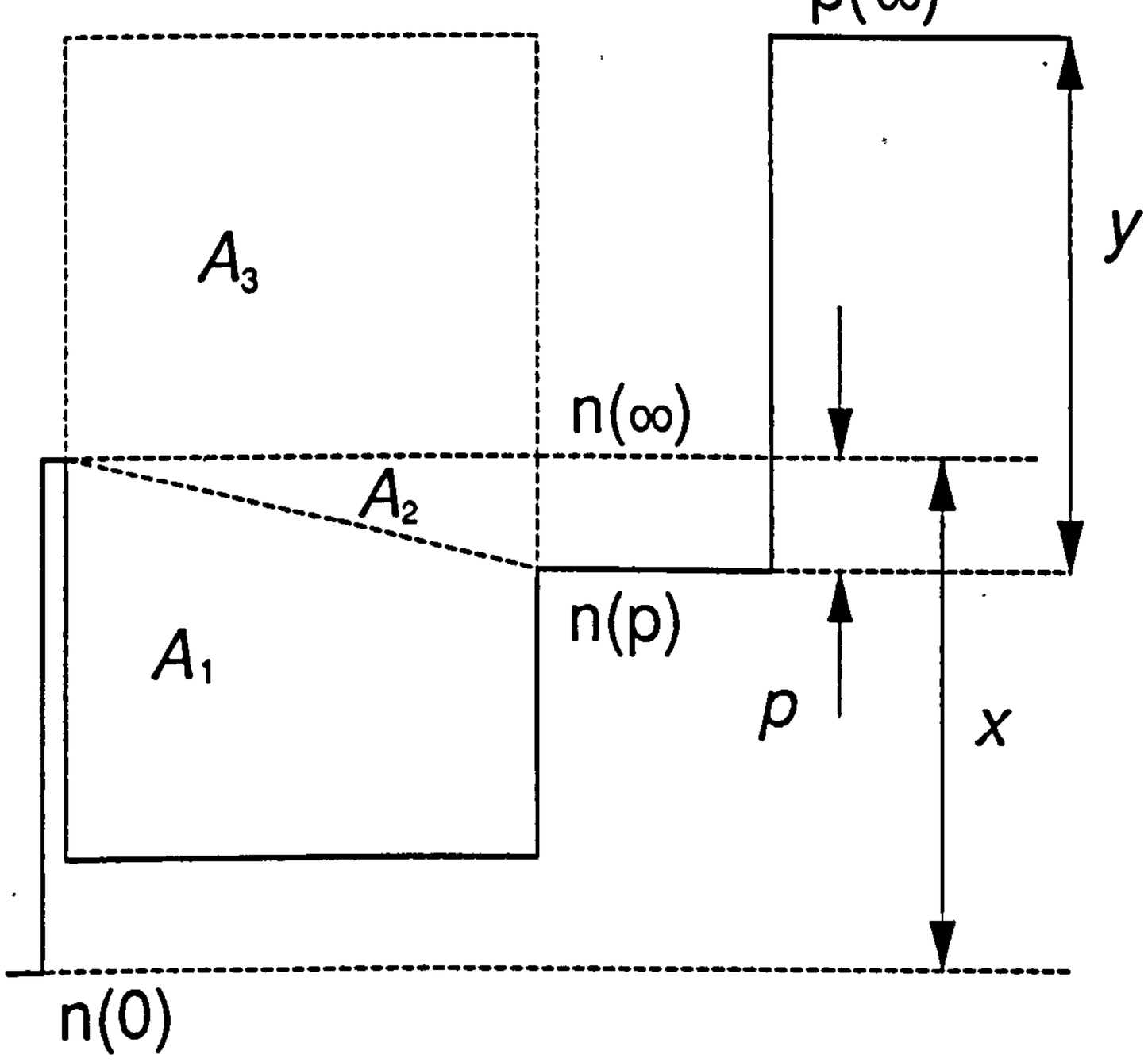

Figure 7.4 Retention Times for Idealised Chromatogram

This analysis can equally be applied to a system with a negative viscosity factor such that the plateau offset is positive. According to Chapter Four, the actual viscosity factor $B(\mu)$ does not depend upon any change in column resistance; it depends only upon the perturbation flowrate and the viscosity change as the front passes through the measuring capillaries. From Figure 7.4, as well as the actual viscosity factor, two further dimensionless viscosity factors can be stated in terms of the relevant offsets:

$$B(\mu)=\frac{y}{x} \qquad 7.50$$

$$B(\mu)_M=\frac{y}{x-p} \qquad 7.51$$

$$C(\mu)=-\frac{p}{x} \qquad 7.52$$

$B(\mu)_M$ is the measured viscosity factor which does not take account of any plateau offset. If the plateau offset tends to zero, the measured value tends to the true value. $C(\mu)$ is the plateau offset divided by the initial offset from $n(0)$ to $n(\infty)$; this is termed the *plateau viscosity factor*. For the above case it is negative. Its value depends upon the true viscosity factor and the column characteristics. For columns with a low pressure-drop, the value tends to zero regardless of the true viscosity factor. Now, from the above definitions, the various viscosity factors can be related:

$$B(\mu)_M=B(\mu)\frac{1}{1+C(\mu)} \qquad 7.53$$

Now consider the measurement of τ_N with downstream delay-lines. Because of the plateau offset, the flowrate record will be at the lower level $n(p)$ whereas the perturbation flowrate is proportional to the difference in levels $n(\infty)-n(0)$. From previous arguments, the required integral area is shown on the diagram by A_1. Now consider the measurement of τ_p without the downstream delay lines. Without these delay lines, the flowrate record will move directly to $p(\infty)$ as the front leaves the column. The required integral area is simply $A_1+A_2+A_2$ and the actual offset is $y+x-p$. The retention times can be stated in terms of the relevant areas and offsets:

$$\tau_N=\frac{A_1}{x} \qquad 7.54$$

$$\tau_p=\frac{A_1+A_2+A_3}{y+x-p} \qquad 7.55$$

$$\tau_X = \frac{2A_1}{p} = \frac{A_3}{y-p} \qquad 7.56$$

This allows Equation 4.12 to be re-stated allowing for the plateau offset:

$$\tau_N = \tau_P(1 + B(\mu) + C(\mu)) - \tau_X\left(B(\mu) + \frac{C(\mu)}{2}\right) \qquad 7.57$$

As the plateau viscosity factor tends to zero, Equation 7.57 tends to Equation 4.12.

7.9.5.4 Results for Column Type A

Table 7.26 Argon Carrier and Helium Perturbation System

	normal		L_U@1/8"= 20m		difference	
prtbn	τ_X/s	τ_N/s	τ_X/s	τ_N/s	$\Delta\tau_X$/s	$\Delta\tau_N$/s
He-A	61	-86	207	-78.7	146	7.3
He-L	67	-82	212.7	-78.8	145.7	3.2

Table 7.27 Helium Carrier and Argon Perturbation System

	normal		L_U@1/8"= 20m		difference	
prtbn	τ_X/s	τ_N/s	τ_X/s	τ_N/s	$\Delta\tau_X$/s	$\Delta\tau_N$/s
Ar-A	134	85.4	263	101.7	129	16.3
Ar-L	137	86.2	268	102.5	131	16.3

The flowrate contributions for Table 7.27 are much higher than those for Table 7.26. This difference is consistent with the theory since the viscosity factor is significantly higher when adding an argon perturbation gas to the helium carrier.

7.9.5.5 Results for Column Type D

Table 7.28 Argon Carrier and Helium Perturbation System

	normal		L_U@1/8"= 20m		difference	
prtbn	τ_X/s	τ_N/s	τ_X/s	τ_N/s	$\Delta\tau_X$/s	$\Delta\tau_N$/s
He-A	71.4	-146.0	262	-109.5	190.6	36.5
He-L	73.1	145.5	268.6	-110.5	194.9	35.0

Table 7.29 Helium Carrier and Argon Perturbation System

	normal		L_U@1/8"= 20m		difference	
prtbn	τ_X/s	τ_N/s	τ_X/s	τ_N/s	$\Delta\tau_X$/s	$\Delta\tau_N$/s
Ar-A	204.5	169.2	379.5	231	175.0	61.8
Ar-L	207.0	173.0	382.1	235.8	175.1	62.8

As expected, compared to Column Type A, the upstream contributions are much larger for column type D. Furthermore, the importance of the viscosity factor is seen in nearly doubling the contribution for the argon carrier-helium perturbation system. Column type D is useful, because the larger delay-line contributions will reduce the significance of any deactivation effects.

7.9.5.6 Caution from Column Observations

So far, it has been seen that placing delay-lines anywhere in the system leads to corrections to the measured retention times. By the same principle, any dead volume in the glass columns will also require corrections. A close look at the Column Type D reveals that there is dead length of about 15 cm which is equivalent to about 1 metre of 1/8 inch nylon tubing. This will require a small correction to the flowrate retention time, but will require corrections of around eight to ten seconds to the composition retention times. Strictly speaking, it is necessary to take into account dead-volume anywhere in the system.

7.10 Further Discussion of Delay-Line Effects

Earlier in this chapter, contributions to the measured flowrate and composition retention times were derived for a variety of delay-line locations. For the mixture carrier, the main requirement for these contributions to apply is that the plateau at $n(\infty)$ should be attained as the front leaves the column and enters the downstream delay-line. This section is concerned with the effect of the varying column outlet flowrate on the delay-line holdups and the subsequent effect on the shape of the flowrate record. This was already discussed in Section 7.6.5 for the downstream delay-lines. In this section, the additional effect of upstream delay-lines will be considered. From Figure 7.3, it can be seen that the plateau at n(p) is clearly attained when the front leaves the column and enters the downstream delay-lines. The experiment was then repeated but including 20 metre lengths of upstream delay-line. For the new arrangement, the composition record was of the *same shape*, except for the obvious dealy in the upstream section. When the perturbation gas was added, the flowrate pen moved comparatively slowly from the initial baseline at $n(0)$ towards $n(\infty)$. This is not surprising in view of the high τ_{NU} contribution for column type D. However,

when the front entered the column, the shape of the flowrate record was comparatively more spread out. Similarly, when the front reached the end of the column and there was no more net adsorption, the flowrate pen moved comparatively slowly towards the n(p) level. This was just attained before the front entered the measuring capillary and the pen moved to the final $p(\infty)$ position. From Section 7.6.5, it would appear that the variation in column outlet flowrate (due to changes in adsorption) also affects the average pressure and holdup in the upstream delay-line, thus affecting the shape of the flowrate record.

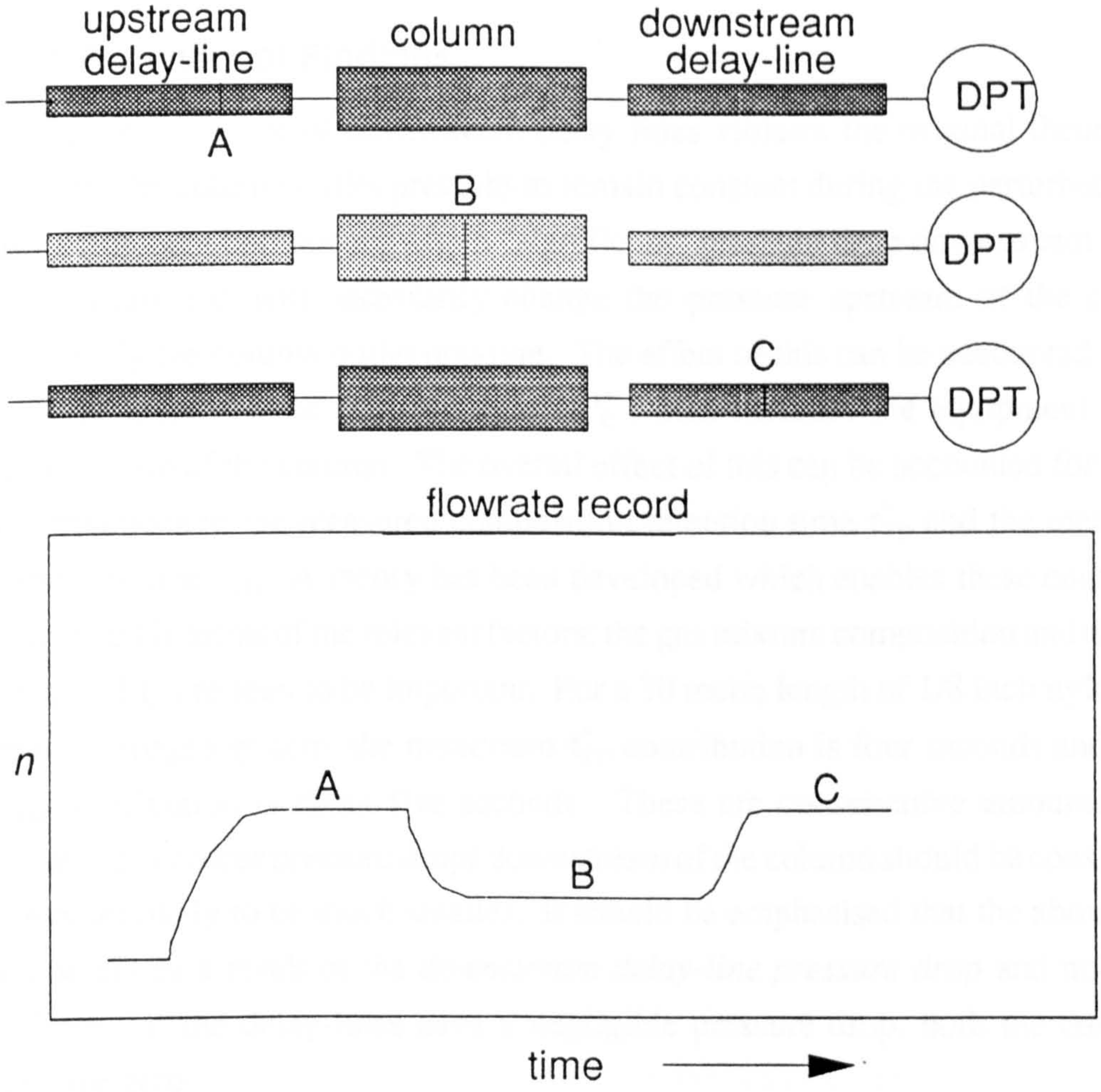

Figure 7.5 Representation of Front and Corresponding Flowrate Record

To help the discussion, Figure 7.5 shows the movement of a front through a system with downstream and upstream delay-lines. From the shape of the flowrate record, the perturbation gas causes net adsorption. When the perturbation gas is added, the flowrate pen moves from the initial baseline $n(0)$ to $n(\infty)$; the difference in levels corresponds to the perturbation flowrate. For position A, the flowrate through both delay-lines and column is increased. While the front is at any position B in the column, the net adsorption reduces the column outlet flowrate. This reduces the average pressure and holdup in the downstream delay-line. Although the flowrate *upstream* of position B is at the $n(\infty)$ level, the subsequent

reduction of pressure at position B will reduce the entire column pressure profile. This will necessarily reduce the pressure downstream of the upstream delay-line, and thus the average upstream delay-line pressure. Thus, the shape of the flowrate record in the movement from A to B will be affected by the temporary reduction in holdup of column and *both* delay-lines. When the front reaches the end of the column, there will be no more net adsorption and the column outlet flowrate will increase to the $n(\infty)$ level. Thus the shape of the flowrate record in the movement from position B to C will be affected by the increase in holdup of column and delay-lines.

7.11 Summary of Findings

1. The employment of downstream delay lines violates the original theory because this requires the column outlet pressure to remain constant during the perturbation. If there is any equipment component with a "significant" pressure drop downstream of the column, the perturbation will necessarily change the pressure upstream of the component and eventually the column outlet pressure. The effect of this can be accounted for by defining an equivalent column pressure drop ΔP_C^* which includes the equipment pressure drops downstream of the column. The overall effect of this can be accounted for by considering contributions to the measured composition retention time τ_{XD}^* and the measured flowrate retention time τ_{ND}^*. A theory has been developed which enables these contributions to be calculated in terms of the relevant factors; the gas mixture composition and the actual values of τ_X and τ_N are seen to be important. For a 30 metre length of 1/8 inch nylon tubing in the argon-nitrogen system, the maximum τ_{XD}^* contribution is four seconds and the maximum τ_{ND}^* contribution is about five seconds. These are conservative amounts, since strictly speaking, *all* other pressure drops downstream of the column should be considered although these are likely to be much smaller. It should be emphasised that the above contributions are solely as a result of the *downstream delay-line pressure drop* and not the delay-line volume. If the delay-lines have a negligible pressure drop, both the contributions will become zero.

2. Additionally, the location of delay-lines will give further contributions to both the measured composition and flowrate retention times due to the change in holdup of the delay-lines themselves. A theory has been developed which enables these contributions to be obtained for a variety of locations. The flowrate contributions will depend upon the internal delay-line volume as well as the delay-line pressure drop. For the upstream location, the flowrate contribution will also depend upon the column pressure drop and this can be very significant. Not surprisingly, the composition retention time contribution will be significant if the location is upstream of the TCD since the front will be physically delayed in such a location

3. For certain gas-mixture systems, the use of upstream delay-lines is necessary for correct determination of both the viscosity factor and the flowrate retention time. This situation arises when there is a significant change in column resistance after the front has passed through the column; this requires a high column pressure drop *and* a large viscosity factor and is termed a *plateau offset.*

4. Equation 4.12, which relates the measured flowrate and composition retention times to the viscosity factor, is shown to give generally good predictions. This equation can also be derived by considering areas on a chromatogram for which there is no plateau offset. However, for systems in which there is a plateau offset, the equation requires modification and the analysis is aided by defining a dimensionless *plateau viscosity factor.* As this factor tends to zero, the modified equation tends to Equation 4.12. Actually, for most systems, this viscosity factor is close to zero.

5. In six out of eight cases, Equation 4.12 gives satisfactory predictions of the measured flowrate retention times from the measured pressure retention times. However, direct measurement of the flowrate retention time requires downstream delay-lines and from previous arguments these will give two positive contributions to the measured flowrate retention time. At best, it might be expected that the measured values of the flowrate retention time should be the predicted value plus the two relevant contributions. To support this case, most of the predictions deviate by some positive contribution although this deviation varies from system to system. However, a "proper" direct measurement of τ_N requires that the flowrate record should reach the $n(\infty)$ position as the front leaves the column and enters the downstream delay-lines. This position must be attained before the front enters the measuring capillary and the pen moves to the final $p(\infty)$ position. The flowrate chromatogram represents the variation in the flowrate *leaving* the column and thus the flowrate through the downstream delay lines. Any change in column outlet flowrate will affect the column and downstream delay-line average pressures and hence the holdups, albeit in a temporary way. It may be that these holdup changes in the column and delay-line and the subsequent flowrate changes will prevent the flowrate record reaching the required position at $n(\infty)$. For the more adsorbed perturbation gas (positive τ_N), the flowrate record increases as the front leaves the column. The changing holdup in the downstream delay-lines might be to reduce the measured τ_N. For the least adsorbed perturbation gas (negative τ_N), the flowrate record decreases as the front leaves the column and the changing holdup of these delay-lines might also be to reduce the magnitude of the measured τ_N. The overall effect of these *transient* (changing holdup) and *calculated* contributions might explain how Equation 4.12 seems to give better predictions when the perturbation gas is the more adsorbed component. Finally, caution will be used when employing these directly measured flowrate retention times to determine isotherm gradients in Chapter Eight.

Chapter Eight

EXPERIMENTAL DETERMINATION OF BINARY GAS-MIXTURE EQUILIBRIA ON 5A ZEOLITE

8.1 Introduction and Previous Investigation

In Chapter One, preliminary results were obtained for the adsorption of argon-nitrogen mixtures on molecular sieve 5A at 54°C and a total pressure of 1.25 bar. These results were obtained by switching a perturbation flow from one column to the other and measuring the cumulative effect. With the preliminary oven arrangement, the thermal noise level was significant on the flowrate record and this made the flowrate retention time difficult for some compositions. From the summarised theory in Chapter One, it should be possible to calculate the isotherm gradient for each component using either perturbation gas. Then, from the relevant equations in Chapter One, both perturbation gases were used to obtain these gradients. The agreement was fairly good except where the perturbation gas was added to a mixture rich in that component; then the respective component isotherm gradient was too high. At that time, this disparity was thought to be caused by error in measuring the column pressure drop; a higher value would help agreement. However, in Chapter Seven, it was shown that the use of delay lines in any location requires corrections to the measured retention times. These corrections have qualitatively the same effect as a higher column pressure drop. From these findings, determination of the isotherm gradient for any component using the *other* component as the perturbation gas requires much smaller corrections. Despite the disparities in the composition ranges described above, integration of both sets of gradients seemed to help agreement. The final results confirmed previous findings that the nitrogen isotherm is curved and the argon isotherm is very nearly straight.

In this chapter, results are presented for the nitrogen-argon, argon-helium and the nitrogen-helium systems obtained using certain experimental modifications. First, the glass pig arrangement of Chapter Five will be employed to reduce the thermal noise. Second, in view of the findings of Chapter Six, the perturbation gas was added to and removed from a particular column. All the experimental modifications are shown in Chapter Three. These were carried out to reduce all the thermal causes of flowrate fluctuations and to enable the required perturbation component to be selected quickly without any chance of column deactivation. In the final section, the use of a perturbation gas having the same composition of the carrier is investigated. The summarised theory in Chapter One is extended to deal with the case when the perturbation gas causes no composition change and hence no baseline shift in the composition record.

8.2 Program to Process Mixture Retention Times

In the following sections, investigations are reported for various systems across the whole composition range. A program has been written to carry out all the required calculations including integration of the isotherm gradients to obtain the mixture isotherms. The program is written in *Turbo Basic* and a listing of a program is contained in Appendix D. The program consists of three parts:

1. First, each set of component holdups is presented for each perturbation gas according to the equations presented in Chapter One. In the program, it is possible to present the calculated isotherm holdups without the important correction factor due to the column pressure drop. In this case, the agreement between the calculations for each perturbation gas will be poor and this will help demonstrate the importance of this pressure correction. Additionally, the concept of *apparent* and *actual* perturbation gas composition is included. When the perturbation flow is added, the increase in the pressure at that point leads to a reduction in the bulk flow passing through the upstream chokes. This leads to slight reductions in the multiplication factor for the flowrate retention time. This becomes more important as the column pressure drop increases.

2. Using the column parameters, these holdups are converted into isotherm gradients. Using a polynomial-fitting subroutine, each set of gradients is shown with the best fitting polynomial of specified order. The polynomial-fitting subroutine was modified from a *BBC Basic* program written by C.R.G. Treasure in the Chemical Engineering Department in 1983. The polynomial should be of reasonable order; if there are rogue deviations, a higher-order polynomial would be required to fit the rogue set, although this makes the whole procedure less meaningful. Then, the four polynomials are integrated to obtain each mixture isotherm as an integrated polynomial. For convenience, the calculated isotherm points are presented at 10% intervals. The most suitable set of isotherm points is then exported into a spreadsheet package for graph plotting.

3. The calculated gradients are also integrated by using the trapezoidal rule. Another method of integration is Simpson's Rule, although this has not been employed because it requires a constant step length in composition and this has not been achieved experimentally. Unlike the polynomial method described above, the trapezoidal rule requires isotherm gradients for each component across the whole composition range. However, when the carrier is a pure component, using the same component as the perturbation gas only allows the pure component gradient to be obtained; it is not possible to obtain both mixture gradients because the other component is not present. In this case, it is necessary to use the isotherm gradients calculated using the other perturbation gas.

8.3 Investigation of Nitrogen-Argon System at 25°C

8.3.1 Initial Calculation of Isotherm Holdups

The retention times and other relevant data are contained in Table C.1 in Appendix C. For simplicity, only the retention times corresponding to adding the perturbation gas will be considered although the same results should be obtainable from the retention times obtained by removing the perturbation gas. Actually, in most cases, a choice of two composition retention times was available. This is because the composition retention time can usually be obtained by two methods; trapezoidal estimation and area determination using a planimeter. Strictly speaking, from the definition of the composition retention time in Chapter Four, the area is required. However, in some cases, this area must be divided by a small offset. In these cases, it is better to use trapezoidal estimation. For most cases, a choice of two *reliable* retention times is available. Although the difference is rarely more than three seconds, the choice is important since it can affect agreement between each perturbation gas and the overall trend with respect to composition down the relevant table in the column. From the nitrogen-lean mixtures, it would appear that the composition retention times should be close; values will be chosen to conform with this trend. At 25°C, the column pressure drop was measured to be 35 mmHg. The program was run in the basic way, without any pressure corrections. Similar to the findings of Chapter One, there were large systematic differences in agreement between each perturbation gas at either end of the composition range. The table of isotherm holdups will not be shown since these values cannot be used. Table 8.1 shows the isotherm holdups calculated applying all the corrections.

Table 8.1 Isotherm Holdups Using Pressure and Viscosity Corrections

	nitrogen component			argon component		
% N_2	G_{N2p}/ml	G_{Arp}/ml	ΔG/ml	G_{N2p}/ml	G_{Arp}/ml	ΔG/ml
0	158.5	-	-	58.9	99.1	-40.2
5	155.4	155.6	-0.2	57.9	88.0	-30.1
10	155.5	155.1	0.4	57.7	75.1	-17.4
25	146.2	143.9	2.3	56.5	65.9	-9.4
50	130.5	126.1	4.4	52.7	58.0	-5.3
75	118.0	117.8	0.2	51.4	53.3	-1.9
90	125.4	111.4	14.0	49.7	53.3	-3.6
95	125.4	111.6	13.8	49.6	52.0	-2.4
100	156.9	109.1	47.8	-	50.0	

From Table 8.1 it can be seen that applying the pressure and viscosity corrections has made a drastic improvement to the agreement between each perturbation gas, although agreement is far from satisfactory. The differences are qualitatively the same as before; they are greater ar either end of the composition range. At first it was thought that substituting a higher value of the column pressure drop would help agreement increasing the correction terms; there is error associated with measuring the column pressure drop. However, it was then discovered that different values of column pressure drop would be required for agreement at each composition.

8.3.2 Discussion of Holdup Differences

Assuming that the theory is correct, there are three reasons why, for some compositions, each perturbation gas may give different isotherm holdup values.

1. There may be errors in the composition retention times employed. At the standard chart recorder speed, 1mm corresponds to three seconds. For some compositions small changes would help agreement, but for other compositions much larger changes would be required.

2. There may be measurement errors in the gas mixture composition in the experiments. A mixing system was used to supply the gas mixture of the required composition. This required calibration of a rotameter for each component. From Chapter Three, this has since been replaced by a mixing system based on the linearity of mass flow controllers. Looking down the ΔG columns in Table 8.3, it can be seen that the differences between the calculated

holdups for each perturbation gas follow the same trend except for the 75% nitrogen values. A 1% increase in the nitrogen composition would fit in with the column trends; the nitrogen component holdup for the nitrogen perturbation gas would increase to 121 ml. This example shows the importance of measuring the gas mixture composition accurately. Furthermore, this sensitivity to composition is even more important for mixtures rich in the gas; a 1% increase in composition from 95 to 96% would increase the multiplication factor from 19 to 24.

3. There may be errors in the flowrate retention times employed. Although the second reason may explain differences in component holdup agreement for mixtures rich in the respective perturbation component, it cannot explain differences in component holdup agreement for mixtures lean in the respective perturbation component because of the diminishing multiplication factor for the flowrate retention time. From a cursory glance, it can be seen that more negative values of the argon perturbation flowrate retention times would greatly help argon component agreement across the whole composition range.

In Chapter Four, the direct measurement of the flowrate retention time by using downstream delay-lines was described. If these delay-lines are not employed, the pressure retention time is directly obtained. An equation was derived (Equation 4.12) relating the flowrate and pressure retention time to other factors. In Chapter Seven, sets of pressure and flowrate retention times were measured directly and used to try and confirm the validity of Equation 4.12. The results are contained in Tables 7.13 and 7.14. For the nitrogen perturbation gas, the predictions were very close to the measured values although the differences were all positive. However, for the argon perturbation gas, Equation 4.12 predicted more negative values of the flowrate retention time, these differences being from five to thirteen seconds. This range of values will correspond to holdup corrections from about two to five ml. This would be the order of magnitude required to aid agreement. In Chapter Seven, doubts were cast over either Equation 4.12 or the directly measured flowrate retention times. In the light of the results for the argon-nitrogen system, it would appear that the validity of Equation 4.12 has been confirmed whilst doubt has been cast over the direct measurement of the flowrate retention time using downstream delay-lines.

8.3.3 Secondary Calculation of Isotherm Holdups

In this section, the isotherm holdups are recalculated using predicted values of the flowrate retention times. The discussion in Chapter Seven shows that there can be great error while compiling the comparison tables. Hence the adjustments made to the measured retention times will only be approximate.

Table 8.2 Isotherm Holdups Using Predicted Flowrate Retention Times

	nitrogen component			argon component		
% N_2	G_{N2p}/ml	G_{Arp}/ml	ΔG/ml	G_{N2p}/ml	G_{Arp}/ml	ΔG/ml
0	158.5	-	-	58.9	99.1	-40.2
5	155.4	157.6	-2.2	57.9	62.6	-4.7
10	155.5	157.1	-1.6	57.7	60.0	-2.3
25	146.0	146.0	0.0	57.2	60.3	-3.1
50	129.5	129.0	0.5	53.8	55.2	-1.4
75	118.0	120.5	-2.5	51.4	52.4	-1.0
90	116.3	116.6	-0.3	50.9	52.7	-1.8
95	114.2	116.5	-2.3	50.4	51.7	-1.3
100	157.0	113.2	43.8	-	50.0	-

From Table 8.2, it can be seen that using predictions of τ_N from Equation 4.12, rather than direct measurements, results in significant agreement in holdup gradients across the whole composition range. From Chapter Seven, these same holdups should be obtainable by using the *equivalent column pressure drop* ΔP_C^* and subtracting the τ_{ND} contribution from the measured value of τ_N. Although, this assumption requires that flowrate record reaches the $n(\infty)$ position before the front reaches the measuring capillary and the subsequent viscosity effect. It can be seen that at 100% nitrogen and 100% argon, the G values obtained using the respective carrier component as the perturbation gas are excessive. From Chapter Seven, it is required to use the equivalent column pressure drop and subtract the τ_{ND} contribution. This was done in Chapter Seven, and G values were obtained of 45ml and 65ml for argon and nitrogen respectively. The reason that these values seem low is that they correspond to the gradients of the *pure-component* isotherms. The pure-component isotherms will be different (and have different gradients) from the binary isotherms in the argon-nitrogen mixture.

Table 8.3 Isotherms Obtained by Trapezoidal Integration

	all concentrations in mole per cubic metre					
	nitrogen component			argon component		
% N_2	q_{N2p}	q_{Arp}	Δq	q_{N2p}	q_{Arp}	Δq
0	0	0	0	187.5	194.9	-7.4
10	59.1	59.7	-1.6	167.2	173.5	-6.3
20	116.8	117.8	-1.0	147.1	152.4	-5.3
30	171.9	173.0	-1.0	127.2	131.3	-4.1
40	224.4	225.3	-0.8	107.8	111.0	-3.2
50	274.2	275.0	-1.0	88.9	91.4	-2.5
60	321.8	322.6	-0.8	70.5	72.5	-2.0
70	367.6	368.9	-1.4	52.5	54.0	-1.5
80	411.8	414.0	-2.2	34.8	35.9	-1.1
90	455.3	457.9	-2.6	17.3	17.7	-0.4
100	497.9	501.0	-3.1	0	0	0

From Table 8.3, it can be seen that the improved holdup agreement has resulted in much improved isotherm agreement. At the end-points, converting the differences to percentages gives a nitrogen value of 0.6 and an argon value of 3. The error in the argon value is due to holdup differences in the argon-rich mixtures. Integrating by fitting third-order polynomials, the results are exactly the same as those above; the differences being less than 0.2 mole/cubic metre. For each system, three graphs will be presented. The first graph will be the actual *mixture binaries*, and from Chapter One, this is the absolute presentation. In this graph, the total amount adsorbed is also shown. The second graph will be the *phase diagram* which gives the adsorbed phase molar composition as a function of the gaseous phase composition. The final graph is the *selectivity chart*; from Chapter One, this allows more rigourous comparisons than the phase diagram.

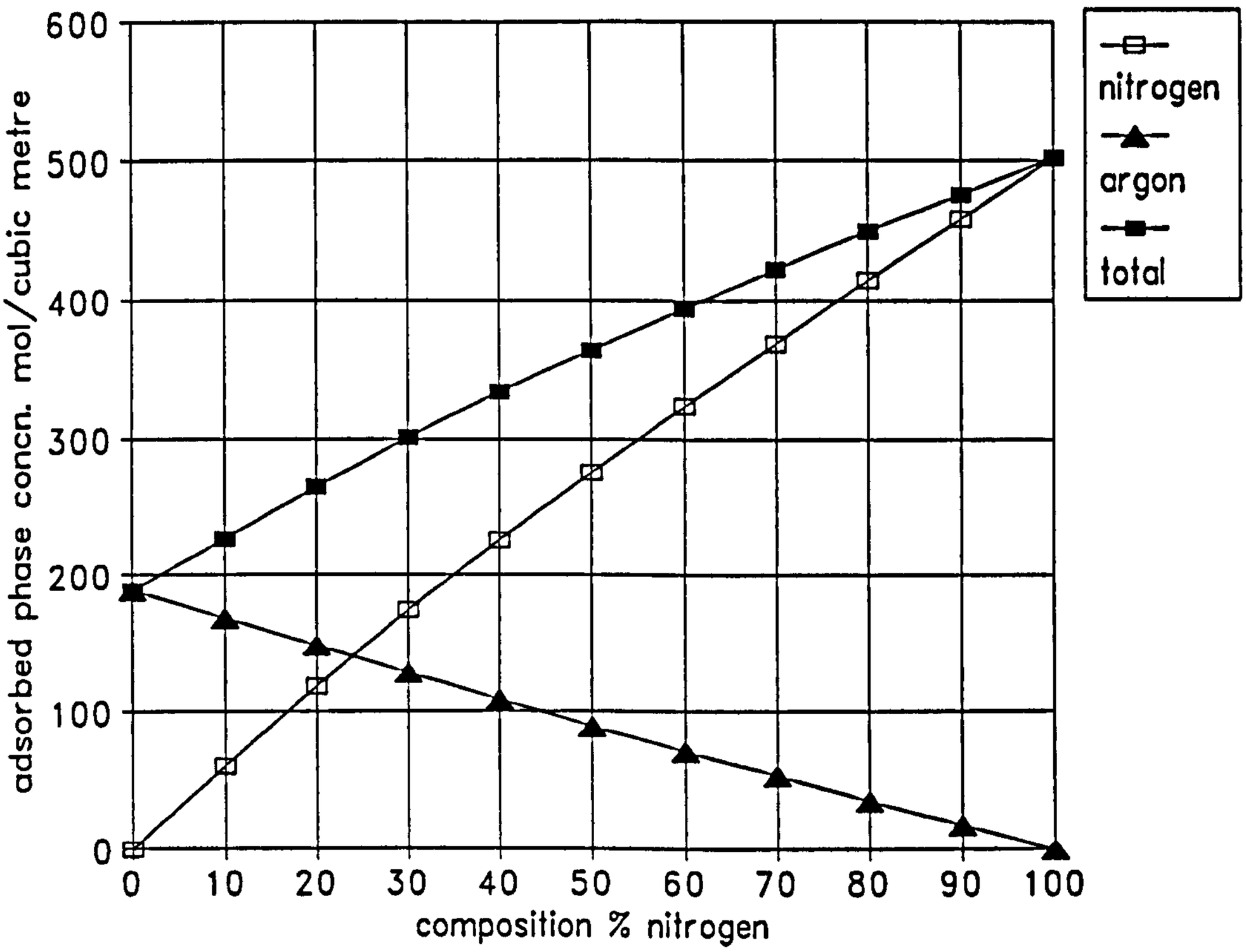

Figure 8.1 Nitrogen-Argon System Binaries at 25°C

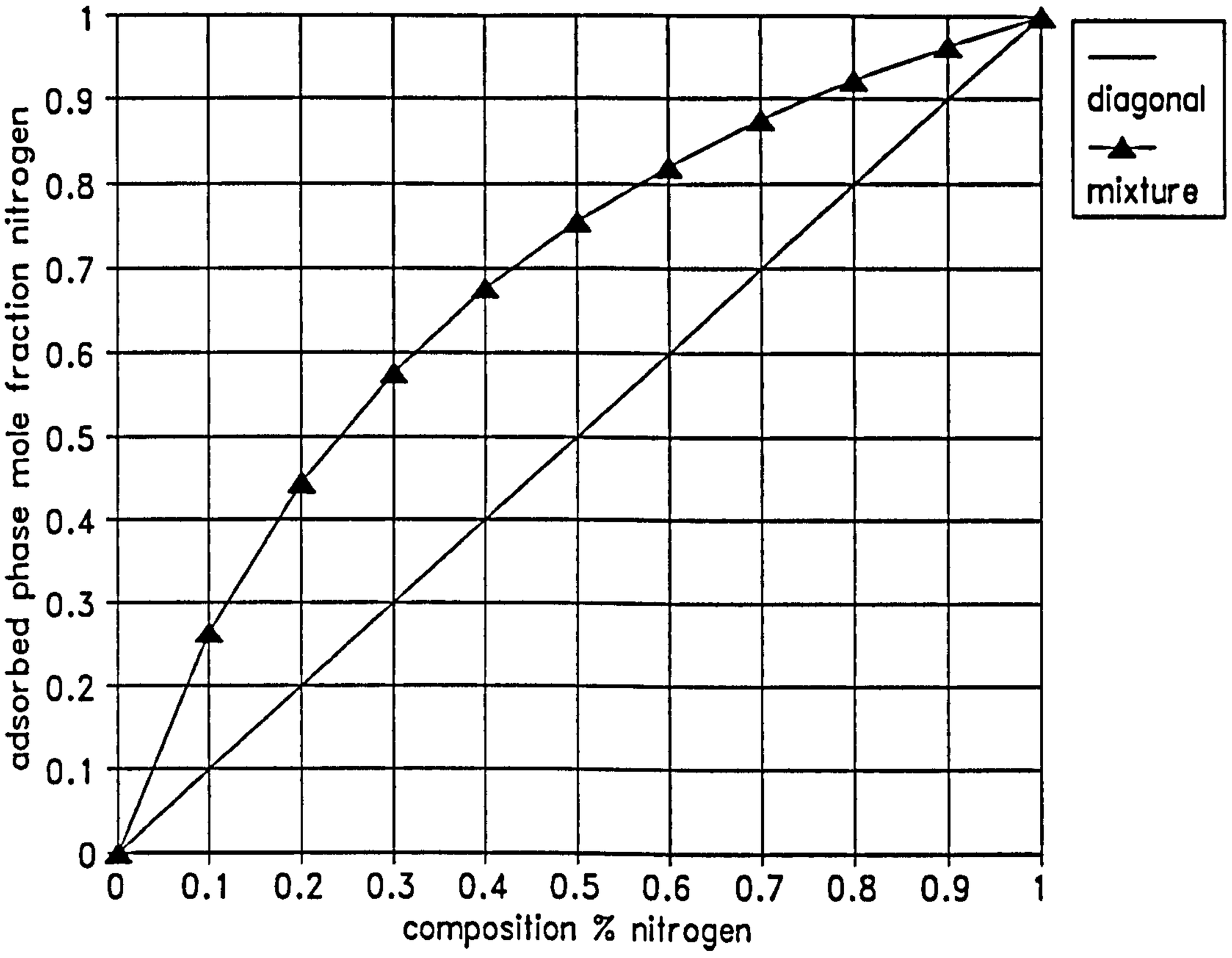

Figure 8.2 Nitrogen-Argon Phase Diagram at 25°C

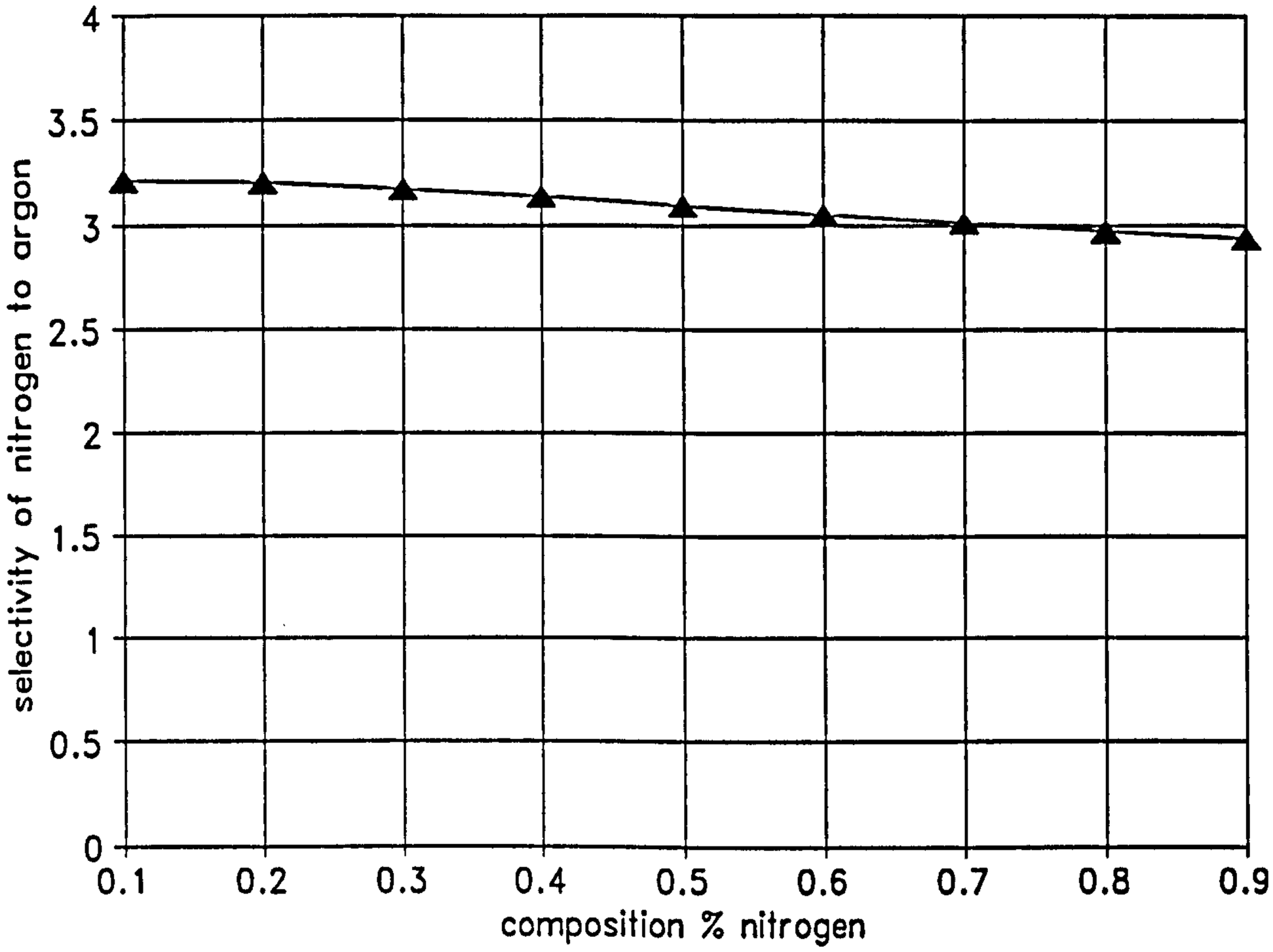

Figure 8.13 Nitrogen-Argon Selectivity Chart at 25°C

8.4 Investigation of Nitrogen-Helium System at 25°C

The retention times and other relevant data are contained in Table C.2 of Appendix C. The program was executed in the standard way using all the corrections and with a column pressure drop of 35 mmHg. Table 8.4 contains the resultant isotherm holdup gradients.

Table 8.4 Isotherm Holdups Using Pressure and Viscosity Corrections

	nitrogen component			helium component		
% N_2	G_{N2p}/ml	G_{Hep}/ml	ΔG/ml	G_{N2p}/ml	G_{Hep}/ml	ΔG/ml
0	161.1	-	-	21.0	67.2	-46.2
5	156.7	157.7	-1.0	21.2	48.2	-27.0
10	153.5	155.2	-1.7	21.3	44.6	-23.3
25	145.5	139.4	6.1	21.2	33.0	-11.8
50	127.4	120.1	7.3	19.6	25.7	-6.1
75	118.2	106.7	11.5	18.6	20.7	-2.1
90	121.1	105.4	15.7	18.6	19.3	-0.7
95	128.1	100.3	27.8	18.3	18.8	-0.5
100	156.2	92.6	63.6	-	18.8	-

Table 8.4 shows that using the pressure and viscosity corrections, agreement generally improves between the isotherm holdups calculated using each perturbation gas. However, it can be seen by looking down the columns that there is still a systematic disagreement between the isotherm holdups calculated for each perturbation gas. The general behaviour is close to that observed for the argon-nitrogen system. From Table 7.17, for the nitrogen perturbation gas the measured values are relatively close to the predicted values, although there is an underlying positive difference. From Table 7.18, for the helium perturbation gas these positive differences are much larger; they vary from about five to twenty seconds. Using these tables, approximate corrections can be made and the isotherm holdups recalculated. The corrected isotherm holdups are contained in Table 8.5.

Table 8.5 Isotherm Holdups Using Predicted Flowrate Retention Times

	nitrogen component			helium component		
% N_2	G_{N2p}/ml	G_{Hep}/ml	ΔG/ml	G_{N2p}/ml	G_{Hep}/ml	ΔG/ml
0	161.1	-	-	21.8	67.2	-45.4
5	156.6	159.1	-2.5	21.6	28.7	-7.1
10	153.5	157.5	-4.0	21.7	27.5	-5.8
25	145.5	142.3	3.2	21.2	25.3	-4.1
50	127.4	125.9	1.5	19.6	20.1	-0.5
75	114.2	111.5	2.7	20.1	19.2	0.9
90	108.5	106.1	2.4	20.3	19.3	1.0
95	104.9	104.5	0.4	20.0	18.6	1.4
100	156.2	99.9	56.3	-	18.8	-

This is similar to the situation for the argon-nitrogen system. From Chapter Seven, the same holdup values *should* be obtained by consideration of the equivalent column pressure drop ΔP_C^* and the τ_{ND} contribution. Once again, pure carrier values of 156.2 and 67.2 require the above corrections to obtain the pure-component holdup gradients. From Chapter Seven, for helium a G value was obtained of 18 ml. However, because of the smaller initial τ_N value, there will be more error in using the τ_{ND} contribution.

Table 8.6 Isotherms Obtained by Trapezoidal Integration

	all concentrations in mole per cubic metre					
	nitrogen component			helium component		
% N_2	q_{N2p}	q_{Hep}	Δq	q_{N2p}	q_{Hep}	Δq
0	0	0	0	54.1	60.1	-6.0
10	59.5	60.3	-0.9	48.2	52.3	-4.0
20	116.5	118.0	-1.5	42.4	44.3	-1.9
30	171.3	171.9	-0.6	36.7	37.0	-0.3
40	223.4	222.9	0.4	31.2	30.5	0.7
50	272.4	271.3	1.1	26.0	24.9	1.2
60	319.0	317.2	1.8	20.9	19.7	1.2
70	363.6	360.9	2.7	15.7	14.6	1.1
80	406.1	402.4	3.8	10.5	9.7	0.8
90	447.1	442.4	4.7	5.2	4.8	0.4
100	485.9	480.8	5.1	0	0	0

From Table 8.6, it can be seen that the improved agreement between the isotherm holdups calculated for each perturbation gas has resulted in much improved isotherm agreement. Once again, integrating the gradient sets by fitting third-order polynomials gives almost exactly the same results. As for the previous case, this data is best represented in Figures 8.4 to 8.5.

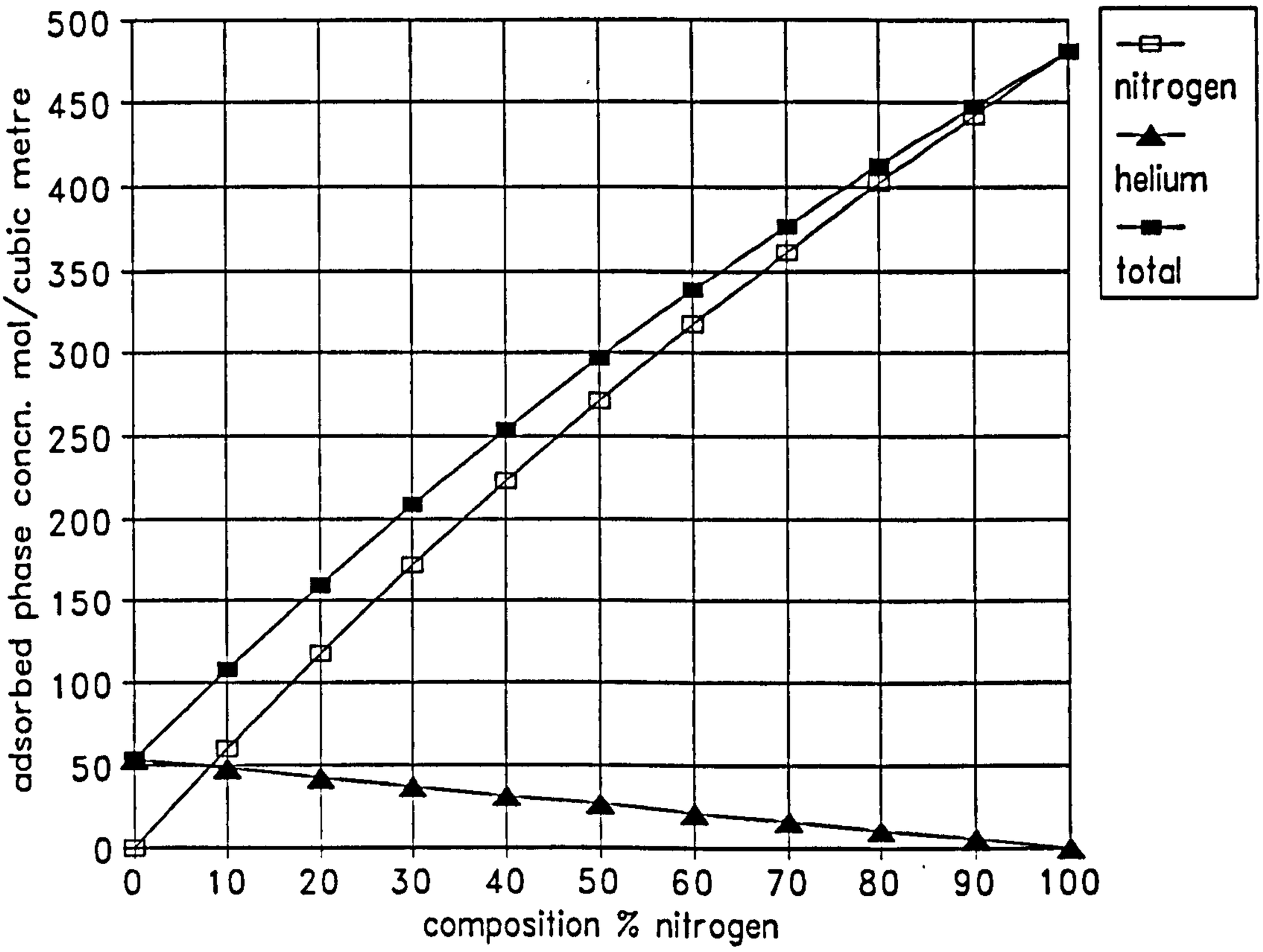

Figure 8.4 Nitrogen-Helium System Binaries at 25°C

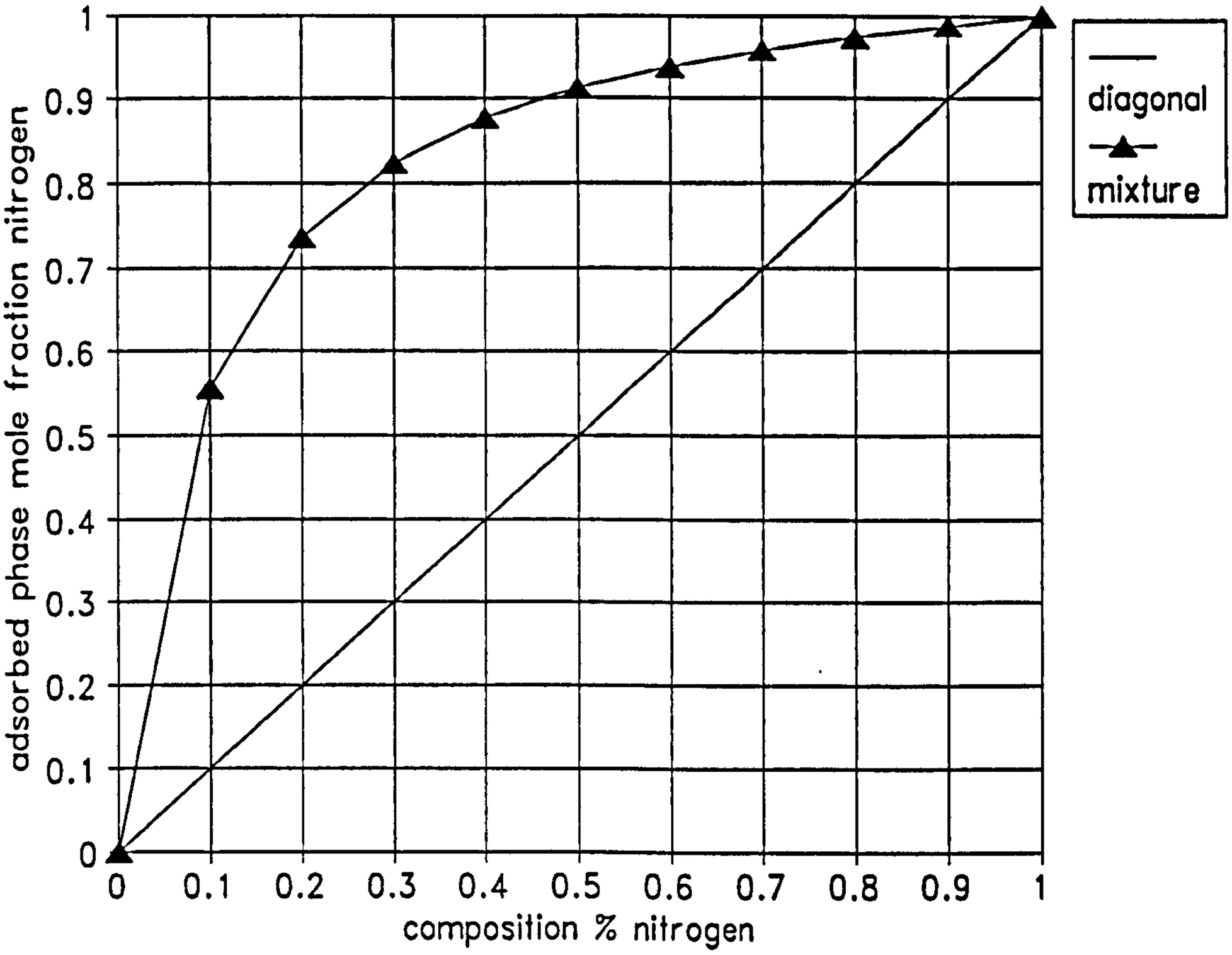

Figure 8.5 Nitrogen-Helium System Phase Diagram at 25°C

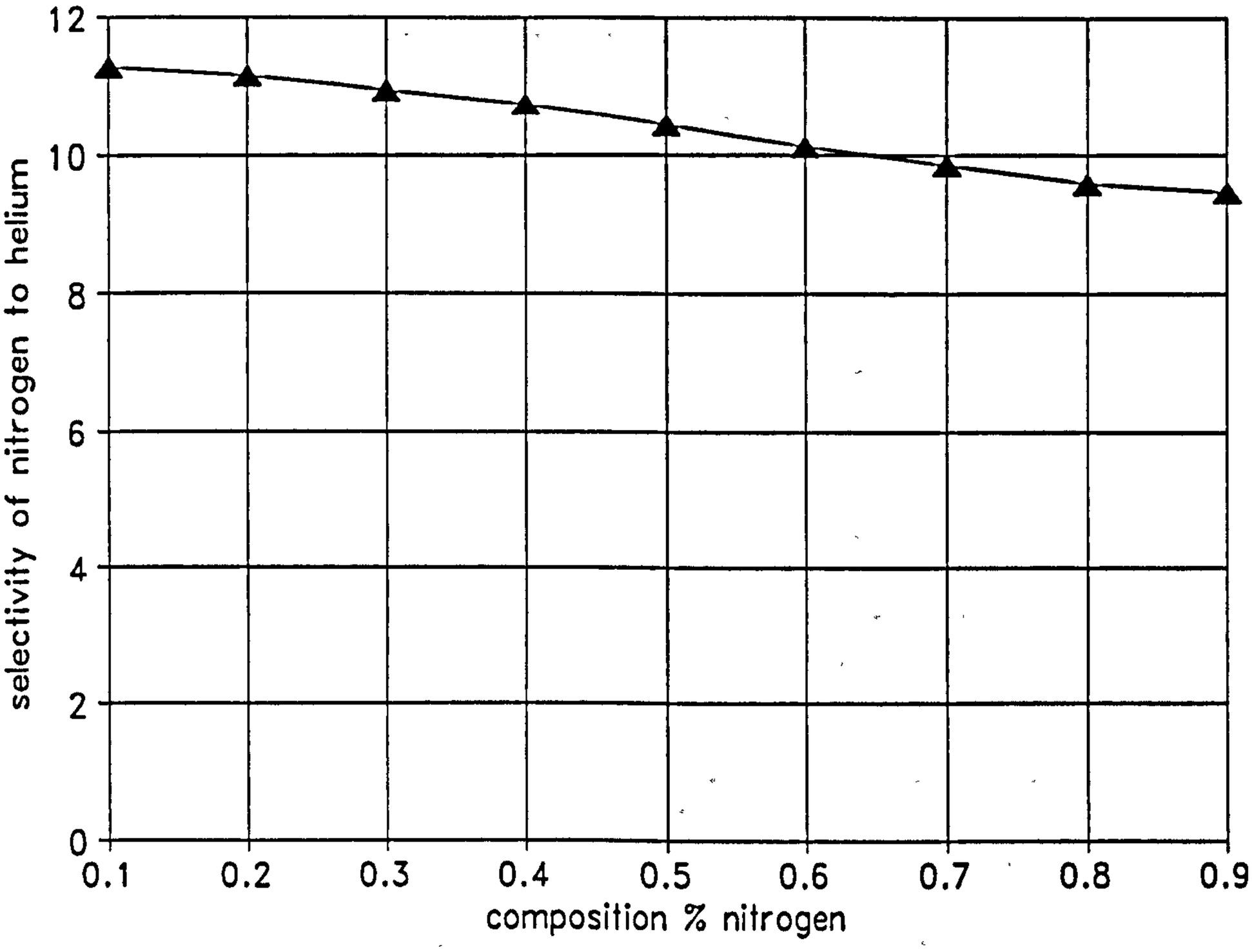

Figure 8.6 Nitrogen-Helium System Selectivity Chart at 25°C

8.5 Investigation of Argon-Helium System at 25°C

The retention times and other relevant data are contained in Table C.3 in Appendix C. The program was executed in the standard way with all the corrections and with the column pressure drop of 35 mmHg. Table 8.7 contains the resultant isotherm holdups.

Table 8.7 Isotherm Holdups Using Pressure and Viscosity Corrections

	argon component			helium component		
% Ar	G_{Arp}/ml	G_{Hep}/ml	ΔG/ml	G_{Arp}/ml	G_{Hep}/ml	ΔG/ml
0	52.7	-	-	20.9	51.1	-30.2
5	54.5	50.0	4.5	19.8	32.6	-12.8
10	54.0	50.5	3.5	20.0	26.1	-6.1
25	53.6	52.5	1.1	19.3	22.3	-3.0
50	52.3	51.2	1.1	19.4	19.8	-0.4
75	53.9	50.7	3.2	19.3	19.6	-0.2
90	60.1	50.0	10.0	17.8	19.3	-1.5
95	72.7	51.5	21.2	18.7	19.6	-0.9
100	99.9	51.1	48.8	-	19.6	-

Using the pressure and viscosity corrections, agreement between the isotherm holdups calculated for each perturbation gas is seen to be generally good apart from the usual combinations where the component isotherm holdup is obtained for a mixture rich in the respective perturbation gas component. Agreement is much better than the previous systems. This better agreement is mirrored by the fact that from Tables 7.19 and 7.20, the predictions from Equation 4.12 are relatively close to the measured values. However, from the trends of these tables, the measured flowrate retention times all contain certain positive contributions. Because the isotherm holdups are generally smaller for this system, these "small" contributions will have a greater proportional effect.

Table 8.8 Isotherm Holdups Using Predicted Flowrate Retention Times

	argon component			helium component		
% Ar	G_{Arp}/ml	G_{Hep}/ml	ΔG/ml	G_{Arp}/ml	G_{Hep}/ml	ΔG/ml
0	55.0	-	-	22.6	51.1	-28.5
5	54.5	53.0	1.50	20.2	24.7	-4.5
10	54.0	53.4	0.7	20.0	22.5	-2.5
25	53.4	53.3	0.1	19.8	20.1	-0.3
50	51.9	51.8	0.1	19.8	19.2	0.6
75	51.7	51.2	0.5	20.1	19.4	0.7
90	51.0	51.6	-0.6	19.0	19.1	-0.1
95	54.2	52.5	1.7	20.1	19.6	0.5
100	99.9	52.6	47.3	-	20.3	-

From Table 8.8, it can be seen that using predictions from Equation 4.12, rather than direct measurements, results in better agreement between the isotherm holdups calculated for each perturbation gas across the whole composition range.

Table 8.9 Isotherms Obtained by Trapezoidal Integration

	all concentrations in mole per cubic metre					
	argon component			helium component		
% Ar	q_{Arp}	q_{Hep}	Δq	q_{Arp}	q_{Hep}	Δq
0	0	0	0	52.0	53.0	-1.0
10	18.9	18.5	0.4	46.4	46.3	0.1
20	37.5	37.0	0.5	41.2	40.4	0.9
30	56.0	55.4	0.6	36.1	35.0	1.1
40	74.2	73.5	0.7	30.9	29.9	1.0
50	92.2	91.5	0.7	25.8	24.9	0.9
60	110.0	109.2	0.8	20.6	20.0	0.6
70	127.8	126.9	0.9	15.4	15.0	0.4
80	145.6	144.5	1.1	10.1	10.0	0.1
90	163.2	162.2	1.0	5.2	5.1	0.1
100	181.5	180.2	1.3	0	0	0

Table 8.9 shows the isotherms obtained by trapezoidal integration. Once again, the polynomial-fitting method gives almost exactly the same results. As in the previous systems, the integrated data is best represented by Figures 8.7 to 8.9.

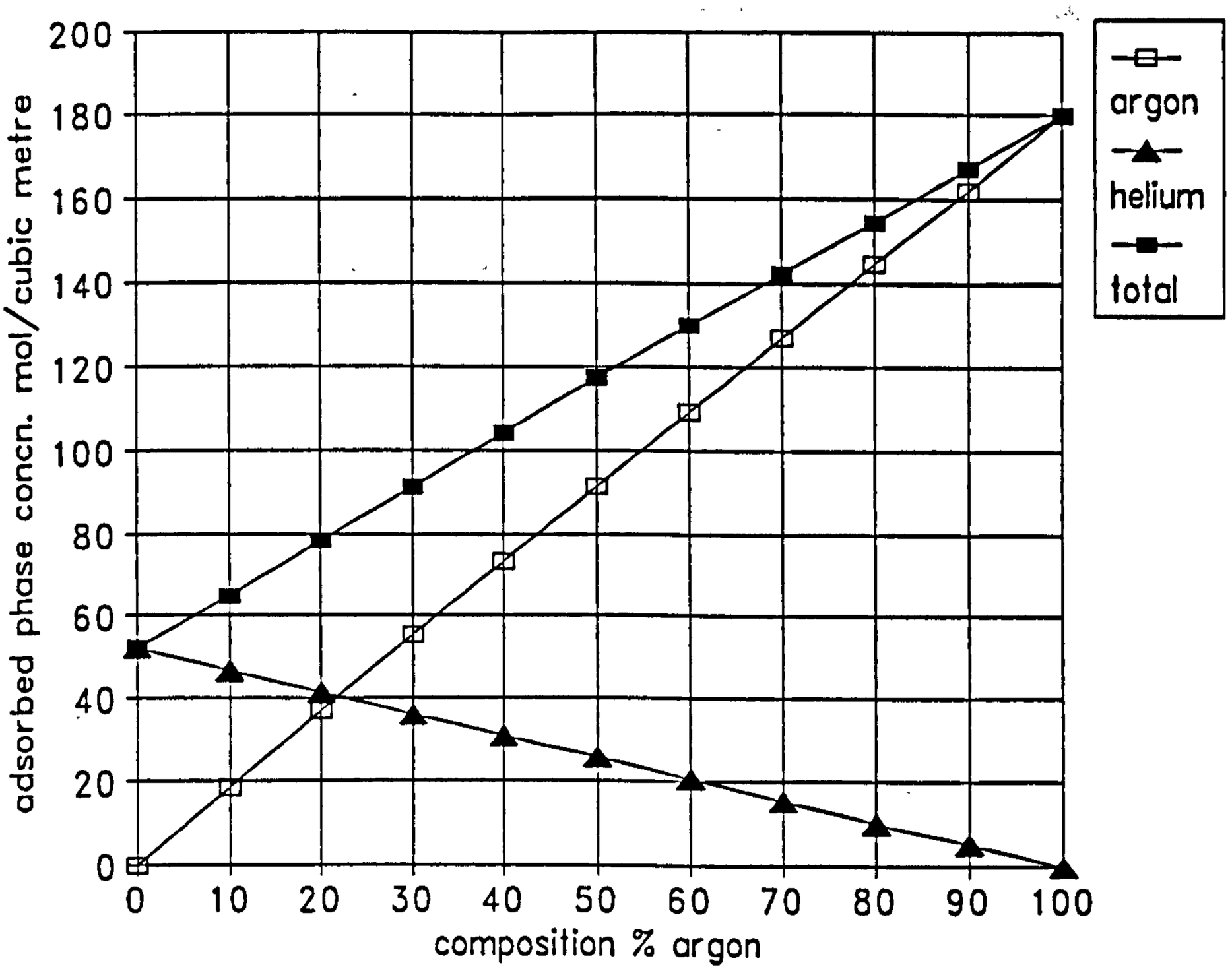

Figure 8.7 Argon-Helium System Binaries at 25°C

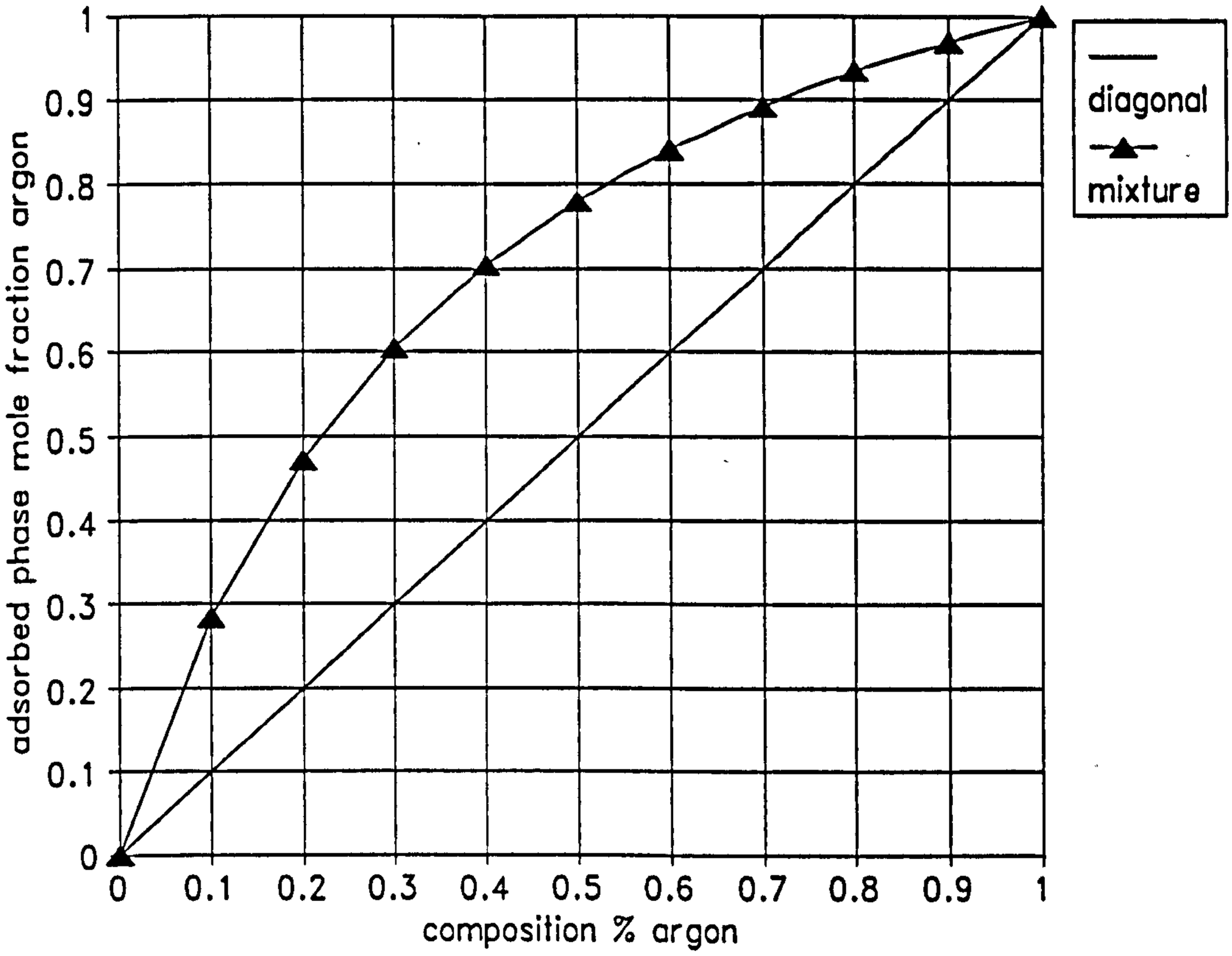

Figure 8.8 Argon-Helium System Phase Diagram at 25°C

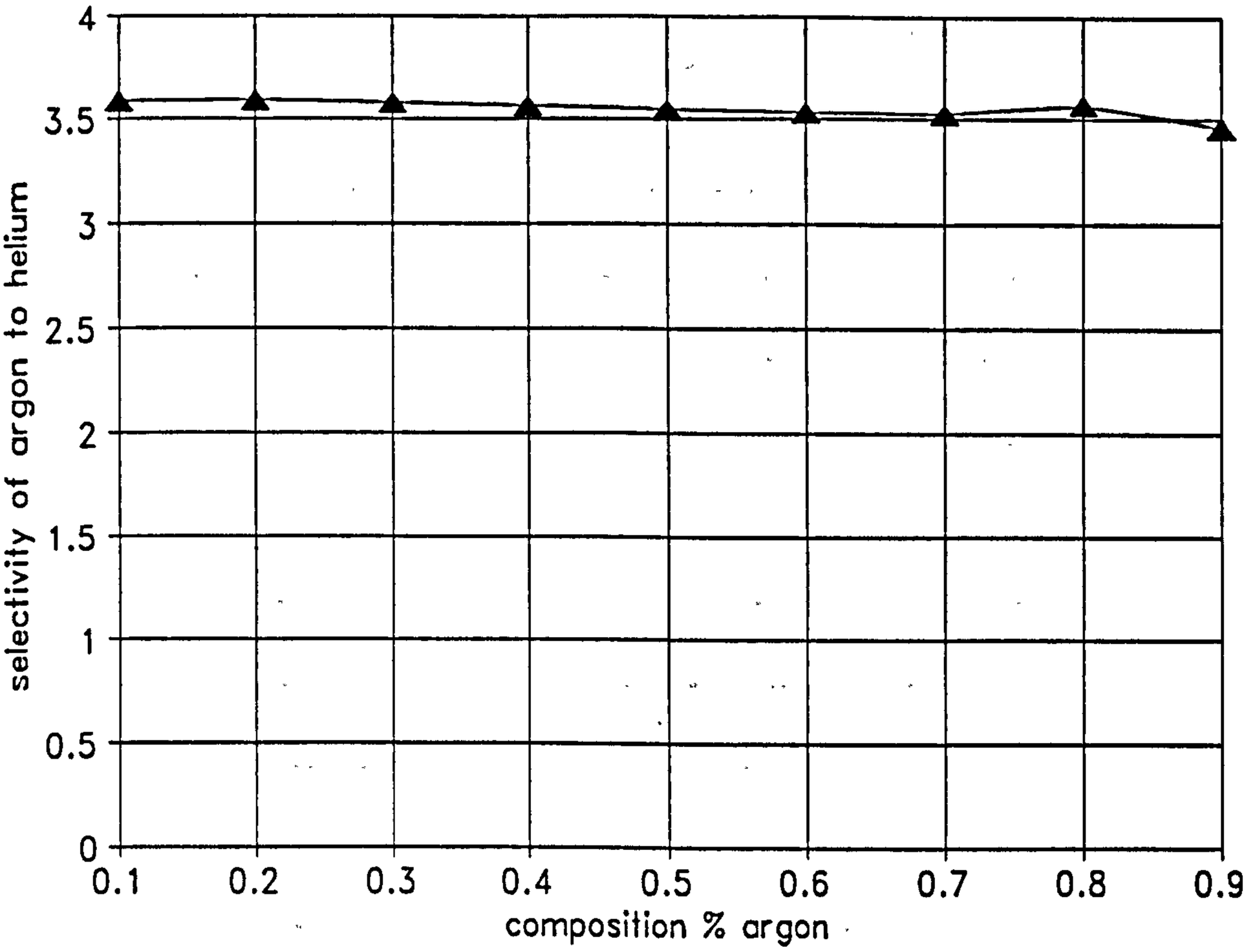

Figure 8.9 Argon-Helium Selectivity Chart at 25°C

8.6 Investigation of Nitrogen-Argon System at 54°C

The retention times and other relevant data are contained in Table C.4 in Appendix C. For the higher temperature, the column pressure drop was measured to be 42 mmHg. The program was executed in the standard way with all the corrections and the isotherm holdups are contained in Table 8.10.

Table 8.10 Isotherm Holdups Using Pressure and Viscosity Corrections

	nitrogen component			argon component		
% N_2	G_{N2p}/ml	G_{Arp}/ml	ΔG/ml	G_{N2p}/ml	G_{Arp}/ml	ΔG/ml
0	89.2	-	-	43.2	65.1	-21.9
5	89.3	89.9	-0.6	43.4	59.9	-16.5
10	90.9	90.9	0.0	43.8	44.0	-0.2
25	85.2	85.5	-0.3	43.7	45.5	-1.8
50	80.9	82.2	-1.3	41.1	41.8	-0.7
75	80.1	77.7	2.4	39.5	41.6	-2.1
90	77.0	76.5	0.5	40.2	41.2	-1.0
95	85.7	79.3	6.4	39.2	40.7	-1.5
100	123.5	77.8	45.7	-	40.9	-

Using the pressure and viscosity corrections, agreement between the isotherm holdups calculated for each perturbation gas is seen to increase generally, apart from the usual combinations of mixtures rich in the respective perturbation component; it can be seen that corrections would certainly be required at 5% and 95% nitrogen. Indeed, agreement would be effected by small changes in these compositions. In view of these problems, it may be better to ignore these columns containing the rogue values of 85.65 and 59.88. Once again, any disagreement between the isotherm holdups calculated for each perturbation gas can be explained in terms of the value of flowrate retention time employed. Tables 7.15 and 7.16 indicate that the required corrections are not as great as those for the room temperature system. Hence, using these corrections makes very little difference to the final isotherms which are contained in Table 8.11.

Table 8.11 Isotherms Obtained by Trapezoidal Integration

	all concentrations in mole per cubic metre					
	nitrogen component			argon component		
% N_2	q_{N2p}	q_{Arp}	Δq	q_{N2p}	q_{Arp}	Δq
0	0	0	0	127.5	132.9	-5.4
10	29.7	29.8	-0.1	114.2	116.7	-2.4
20	59.2	59.4	-0.2	100.9	103.1	-2.3
30	87.3	87.7	-0.4	87.4	89.4	-2.0
40	114.5	115.2	-0.7	74.1	75.9	-1.8
50	141.0	142.2	-1.2	61.2	62.8	-1.6
60	166.9	168.5	-1.6	48.6	50.0	-1.4
70	192.4	194.3	-1.9	36.2	37.3	-1.1
80	217.7	219.6	-1.9	24.0	24.7	-0.8
90	242.8	244.6	-1.8	11.9	12.3	-0.4
100	269.6	270.3	-0.7	0	0	0

As in the previous cases, the above data are best represented by the following Figures 8.10 to 8.12. Compared with Figures 8.1 to 8.3, it can be seen that the amounts adsorbed, isotherm curvatures and the selectivity are reduced at the higher temperature.

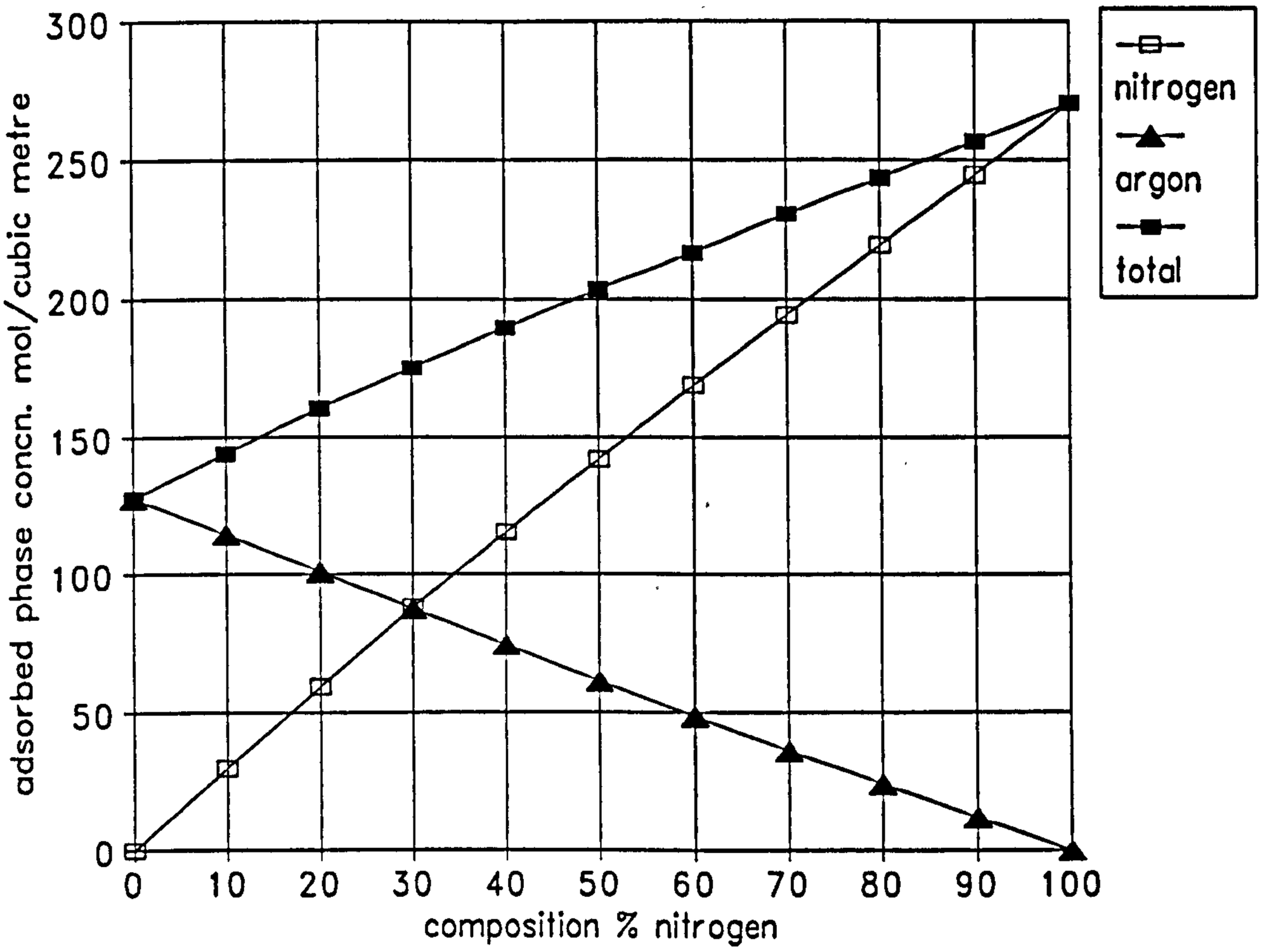

Figure 8.10 Nitrogen-Argon System Binaries at 54°C

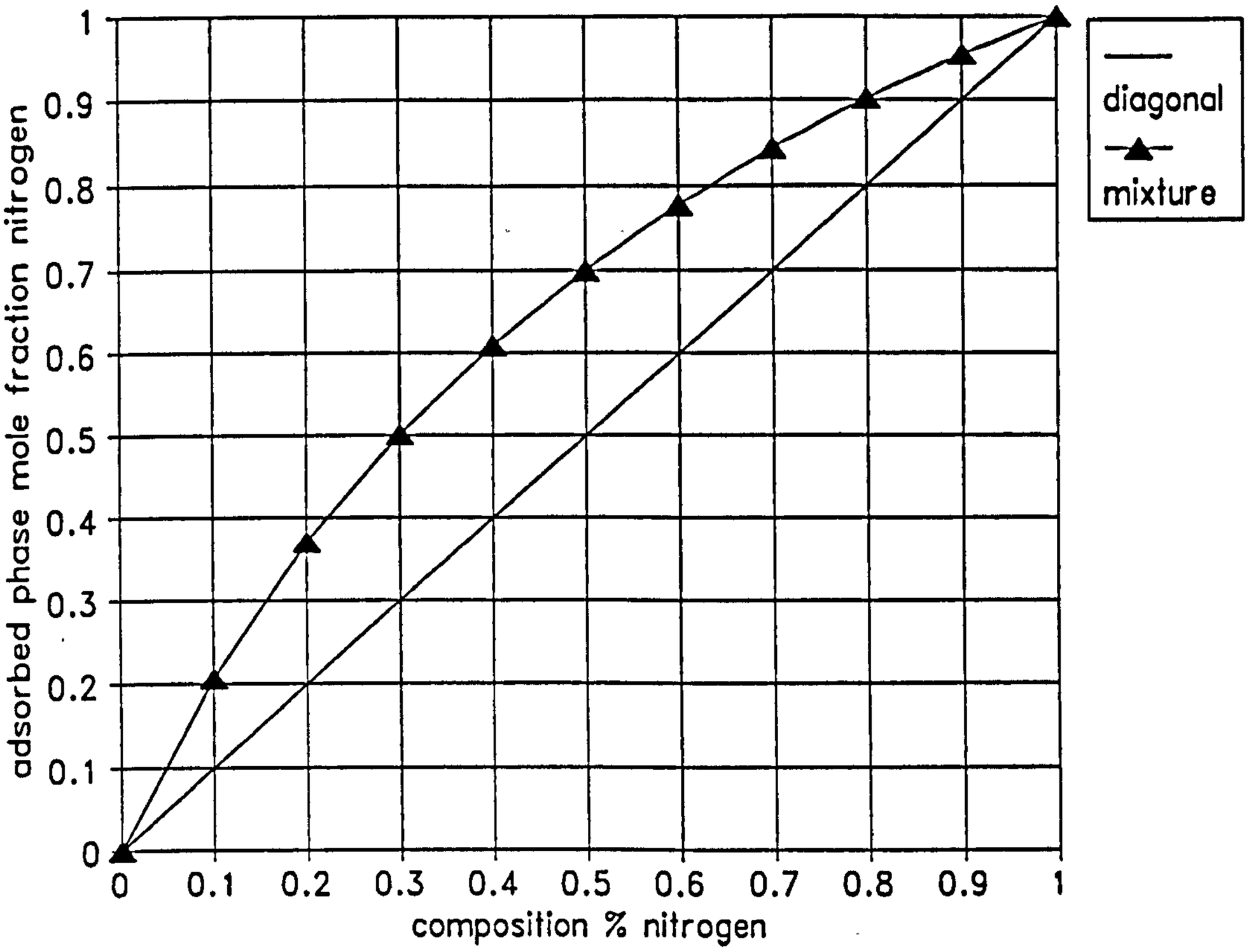

Figure 8.11 Nitrogen-Argon System Phase Diagram at 54°C

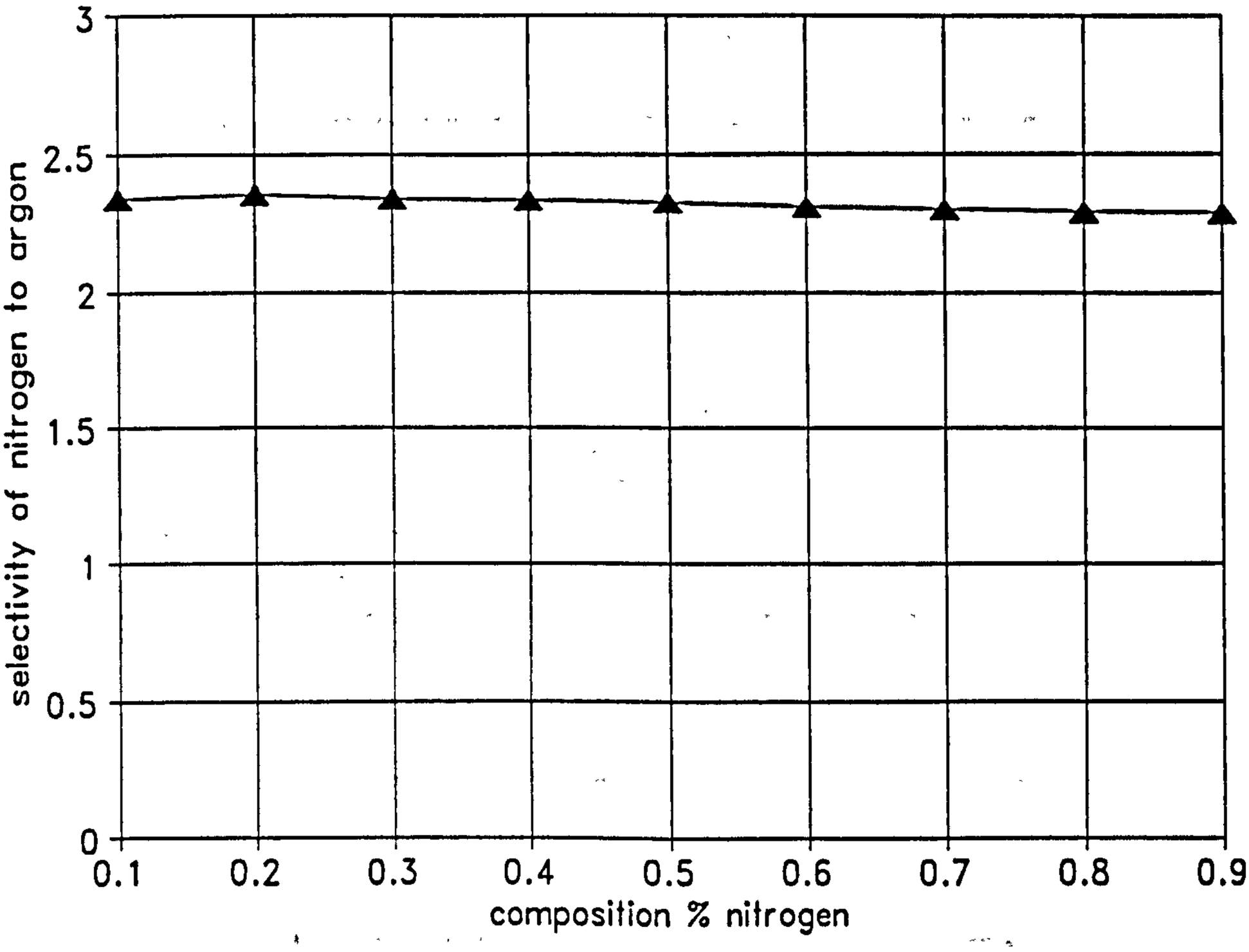

Figure 8.12 Nitrogen-Argon Selectivity Chart at 54°C

8.7 Investigation of Nitrogen-Argon System at 81°C

The retention times and other relevant data are contained in Table C.5 in Appendix C. At this higher temperature, the column pressure drop was measured to be 48 mmHg. The program was executed in the normal way with all the corrections and the isotherm holdups are contained in Table 8.12

Table 8.12 Isotherm Holdups Using Pressure and Viscosity Corrections

	nitrogen component			argon component		
% N_2	G_{N2p}/ml	G_{Arp}/ml	ΔG/ml	G_{N2p}/ml	G_{Arp}/ml	ΔG/ml
0	60.2	-	-	35.9	59.4	-23.5
5	60.1	61.7	-1.6	36.2	32.9	3.3
10	60.8	59.6	1.2	36.3	40.6	-4.3
25	59.4	59.1	0.3	35.8	38.9	-3.1
50	59.4	58.5	0.9	34.7	38.3	-3.6
75	61.0	57.8	3.2	34.5	35.6	-1.1
90	62.2	57.2	5.0	34.7	35.3	-0.6
95	78.3	57.6	20.7	33.6	36.0	-2.4
100	91.9	57.4	34.5	-	36.3	-

Using the pressure and viscosity corrections, agreement between the isotherm holdups calculated for each perturbation gas is seen to be generally good, apart from the usual combinations of carrier mixture rich in the respective perturbation component. Not surprisingly, at this higher temperature, the amounts adsorbed are lower and both isotherms have been flattened out. Table 8.13 shows the final isotherms obtained by trapezoidal integration. Once again, integrating the gradient sets by fitting third-order polynomials gives almost exactly the same results.

Table 8.13 Mixture Isotherms Obtained by Trapezoidal Integration

	all concentrations in mole per cubic metre					
	nitrogen component			argon component		
% N_2	q_{N2p}	q_{Arp}	Δq	q_{N2p}	q_{Arp}	Δq
0	0	0	0	94.3	101.5	-7.2
10	17.8	18.0	-0.2	84.6	91.9	-7.4
20	35.6	35.5	0.1	74.8	80.9	-6.1
30	53.1	52.9	0.2	65.2	70.1	-5.0
40	70.6	70.2	0.4	55.7	59.5	-3.9
50	88.1	87.5	0.7	46.3	49.0	-2.7
60	105.8	104.6	1.1	37.0	38.8	-1.8
70	123.6	121.7	1.9	27.7	28.8	-1.1
80	141.7	138.7	3.0	18.5	19.2	-0.7
90	160.0	155.5	4.4	9.2	9.7	-0.4
100	180.7	172.4	8.3	0	0	0

The columns corresponding to component isotherm holdups using the *other* component as the perturbation gas are probably more reliable, and so these are used to obtain the following graphs shown in Figures 8.13 to 8.15.

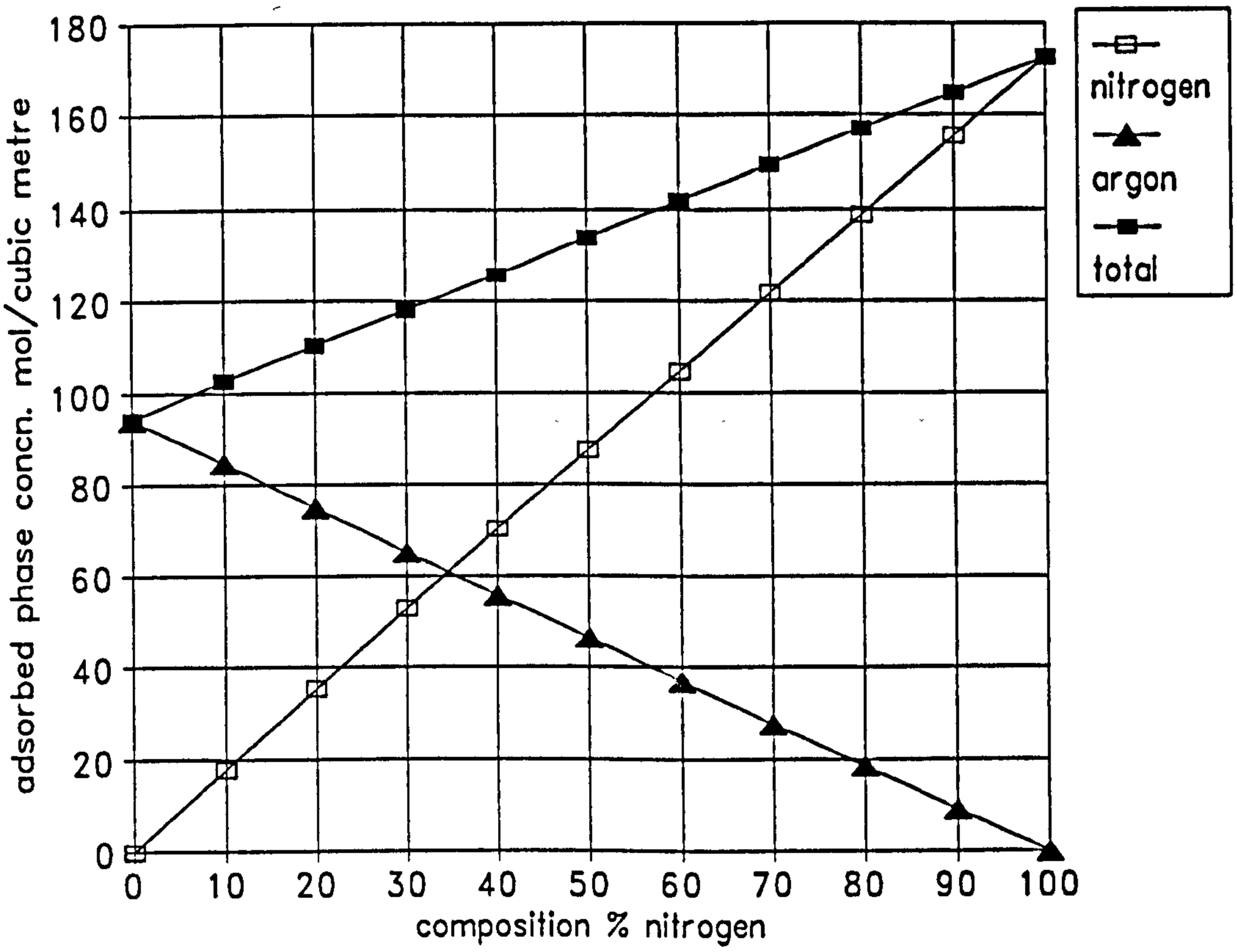

Figure 8.13 Nitrogen-Argon System Binaries at 81°C

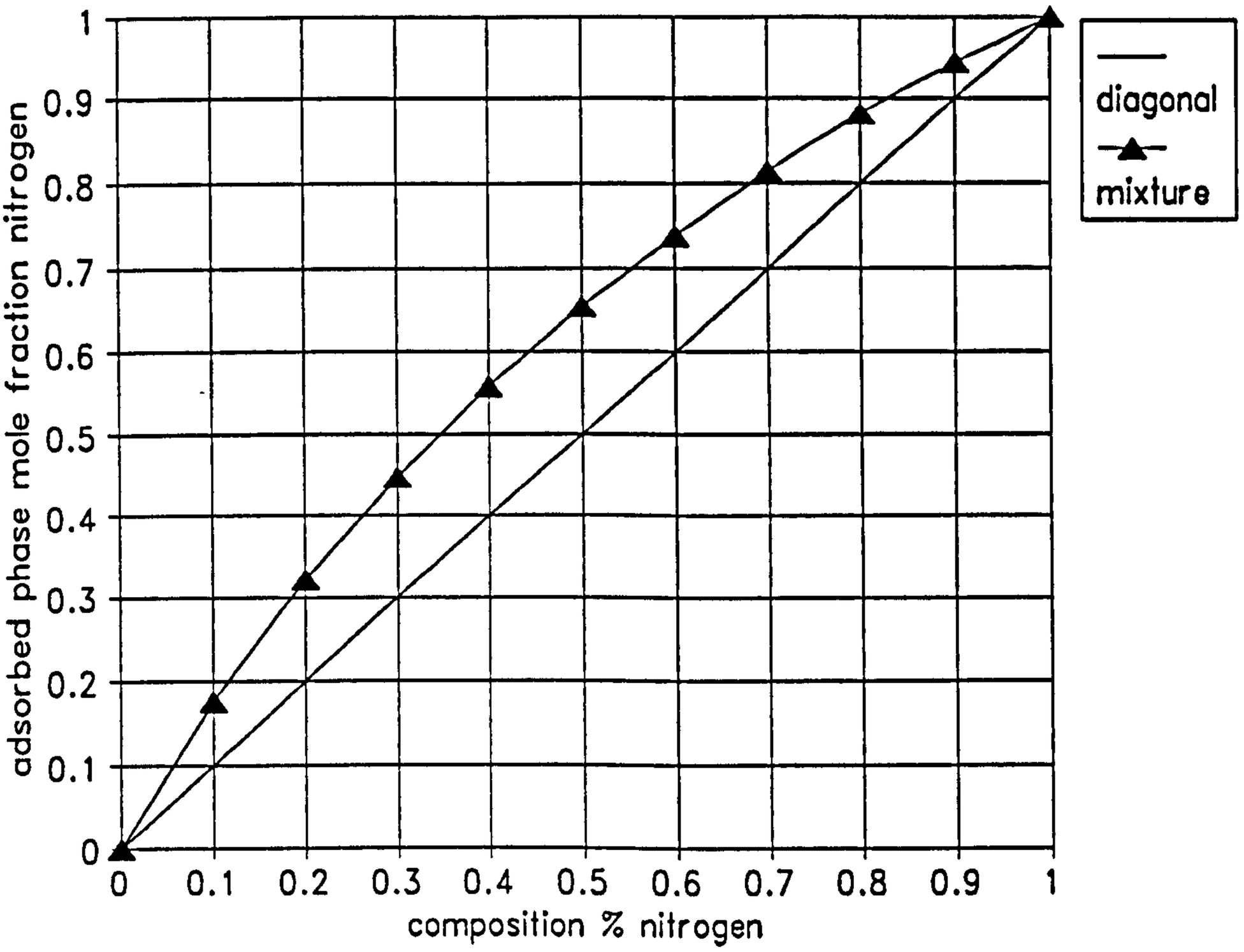

Figure 8.14 Nitrogen-Argon System Phase Diagram at 81°C

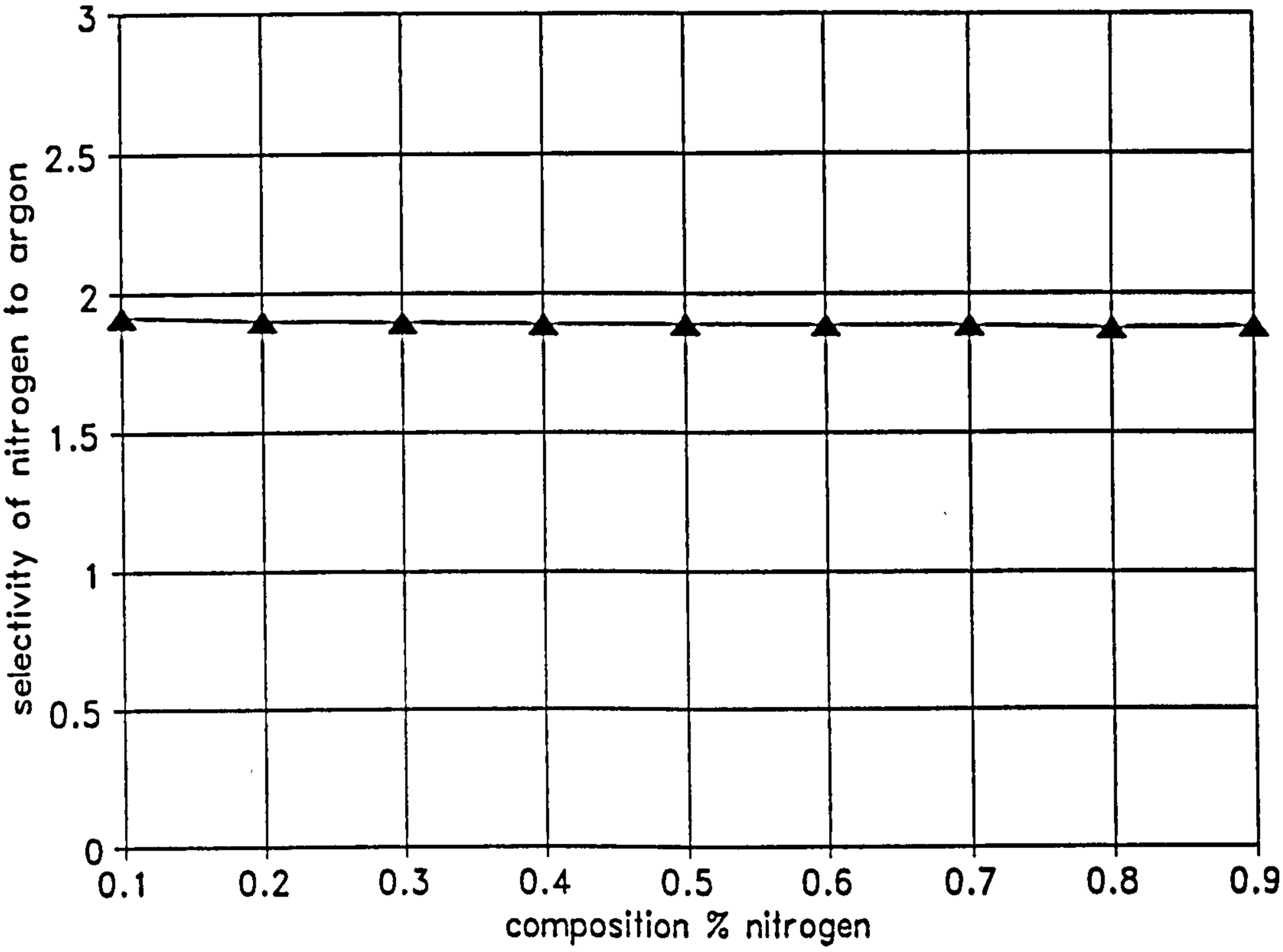

Figure 8.15 Nitrogen-Argon System Selectivity Chart at 81°C

8.8 Employment of Mixture Perturbation Gas

8.8.1 Extension of Project Theory to Incorporate Mixture Perturbation

From Chapter Seven, it was shown that the chromatographic theory summarised in Chapter One reduces to a special form if the perturbation gas has the same composition as the carrier:

$$\frac{\Delta H_i}{\delta c_i} = M \int_0^{\infty} \frac{x(\infty) - x(t)}{\delta c_i} dt + \frac{2MRT_C}{\Delta P_C} \left[\frac{1 + \frac{\Delta P_C}{2P_{COUT}}}{1 + \frac{\Delta P_C}{3P_{COUT}}} \right] \tau_N \qquad 8.1$$

The equation consists of two terms; the first term corresponds to the composition record and the second term corresponds to the flowrate record. When the carrier consists of only one component, there is no movement in the composition record and the first term disappears. The resultant equation can then be employed to evaluate the isotherm gradients at 100% composition. For the general case, when a mixture carrier is employed, both terms must be considered. Because there is no change in composition, there is no offset in the composition record and so this requires calibration. This can be obtained by considering the addition of one of the pure component perturbation gases to the mixture. Consider adding a flow n_T of composition Y_{iT} which changes the carrier composition by dY_i such that

the composition deviation on the chart recorder is S_X cm and the flowrate deviation on the chart recorder is S_{NT} cm. From these deviations, scaling constants can be defined relating chart recorder deviation at fixed sensitivity to the actual perturbation:

$$S_{NT} = k_N n_T \qquad 8.2$$

$$S_X = k_X d Y_i \qquad 8.3$$

where k_N = flowrate record scaling factor

k_X = composition record scaling factor

When adding a mixture perturbation gas of flowrate n to the carrier of the same composition, the term δc_i in Equation 8.1 is solely due to the change in average column pressure and this is represented by Equation 8.4:

$$\delta c_i = Y_{i0}\delta c_T = Y_{iO}\frac{\Delta P_C}{2RT_C}\left[\frac{1+\frac{\Delta P_C}{2P_{COUT}}}{1+\frac{\Delta P_C}{3P_{COUT}}}\right]\frac{n}{M} \qquad 8.4$$

The measurement from the composition record *should* consist a bulging area A_X without an offset. The shape of the flowrate record should be the same shape as adding a pure perturbation gas to the respective carrier; a gradual movement from the initial baseline $n(0)$ to the eventual position $n(\infty)$ (the difference in positions corresponding to the perturbation flowrate). The distance moved by the flowrate record will be R_N. Dividing the sweeping area by the distance R_N should enable the flowrate retention time τ_N to be obtained. A final consideration is the chart recorder speed; the faster this speed the greater the measured area; thus a scaling factor is required for the chart recorder speed. If the chart recorder moves a distance dV in a time dt, the following equation can be written:

$$dV = k_V dt \qquad 8.5$$

where k_V = chart speed dependant factor

Combining all the above equations, Equation 8.1 can be re-written as:

$$\frac{\Delta H_i}{\delta c_i} = \frac{2MRT_C}{\Delta P_C}\left[\frac{1+\frac{\Delta P_C}{2P_{COUT}}}{1+\frac{\Delta P_C}{3P_{COUT}}}\right]\left\{\frac{S_{NT}}{R_N}\frac{Y_{iT}-Y_{iO}}{Y_{iO}}\frac{A_X}{S_X k_V}+\tau_N\right\} \qquad 8.6$$

For the above equation, great care must be taken to ensure that the area and offsets are standardised to the same chart recorder sensitivities.

8.8.2 Preliminary Experiments

Experimentally, a mixture perturbation gas was obtained by directing a flow from the carrier upstream of the flow setting chokes and passing it through a mass flow controller to select a suitable small flowrate. The perturbation gas system is described schematically in Chapter Three and the mixture perturbation gas can be selected by appropriate action at the main valve panel. The first carrier selected was a 50% nitrogen-argon mixture at room temperature using the standard column type. However, even using the highest composition record sensitivity (to increase the actual distances on the chart recorder) no bulge in the composition record could be detected. From the findings of Chapter Six, it was decided to change gas system; a 75% nitrogen-helium mixture was selected. Also, because this system has already been investigated in Section 8.4, it can provide comparison for the calculated isotherm holdups.

The results of the preliminary experiments were unexpected. Although there was significant bulging, the composition record did not return to its expected baseline position. This suggested that the perturbation gas and carrier mixture were of slightly different compositions. This problem was also noticed for the same gas system using the fine packing columns. However, this problem was not noticed when using a nitrogen-argon mixture with the fine packing columns. The likely explanation is that helium is preferentially diffusing out of the perturbation flow tubing; the perturbation flow is much lower and the tubing residence time much longer. To try and alleviate this problem, a low-volume stainless steel tubing was employed. This seemed to help somewhat, but did not entirely cure the problem.

8.8.3 Upstream Delay-Line Employment

When the perturbation gas has the same composition as the carrier, because there is no change in composition any composition record deviation is caused by the change in mean column pressure. From the preliminary experiments, the pressure effect is partially obscured by a small composition change. From the findings of Chapter Six, these effects can be separated by the employment of upstream delay lines so that the pressure bulge appears on the composition record before the composition front reaches the column. Figure 8.16 shows the chromatograms obtained for adding a nitrogen perturbation flow to a 75% nitrogen-helium mixture. The column type is A and standard downstream delay-lines of length 30 metres are employed. Additionally, upstream delay-lines of length 20 metres are employed. The top chromatogram is the composition record and the bottom one is the flowrate record. From the composition record, it can be seen that the upstream delay lines are long enough to separate out the initial bulging due to the increase in column pressure; the composition record has enough time to return to the $x(0)$ level before the front reaches

the column and the composition record deviates in the opposite direction as the front moves through the column. This system was dealt with in Chapter Seven and an explanation was given for the kinks in the composition record as the front moved through *and* as the front left the column. This is the bulge area described above which would be obtained if an *exact* mixture perturbation gas could be employed, since it is solely due to the change in average column pressure.

When the nitrogen perturbation is added, the flowrate pen moves from $n(0)$ and there is a slight kink before the $n(\infty)$ position is attained. When the perturbation reaches the column, the net adsorption causes a reduction in column outlet flowrate. The initial part of the flowrate record is the same regardless of the perturbation gas; it is solely due to the change in average column pressure. On Figure 8.16, the dotted arrows show the expected movement in the flowrate record for the helium and *exact* mixture perturbations. For the helium case, the net desorption will cause the flowrate to increase and for the mixture case, there should be no more deviation in the composition record. Hence, the area shown bounded by the dotted line and the chromatogram is that which would be obtained if an exact mixture perturbation gas was employed, and this can be used to calculate τ_N. The advantage of using this experimental arrangement with upstream delay-lines is that it is not necessary to carry out another experiment for calibration purposes; the required composition record deviation S_X is shown, and the two flowrate record deviations S_{NT} and R_N are equal to each other thus simplifying somewhat the form of Equation 8.6.

8.8.4 Evaluation of Isotherm Holdups

1. For column type A, 20 metres of 1/8 inch nylon tubing was placed upstream of each column. For this case, the nitrogen perturbation gas was used for calibration and some of the relevant quantities are:

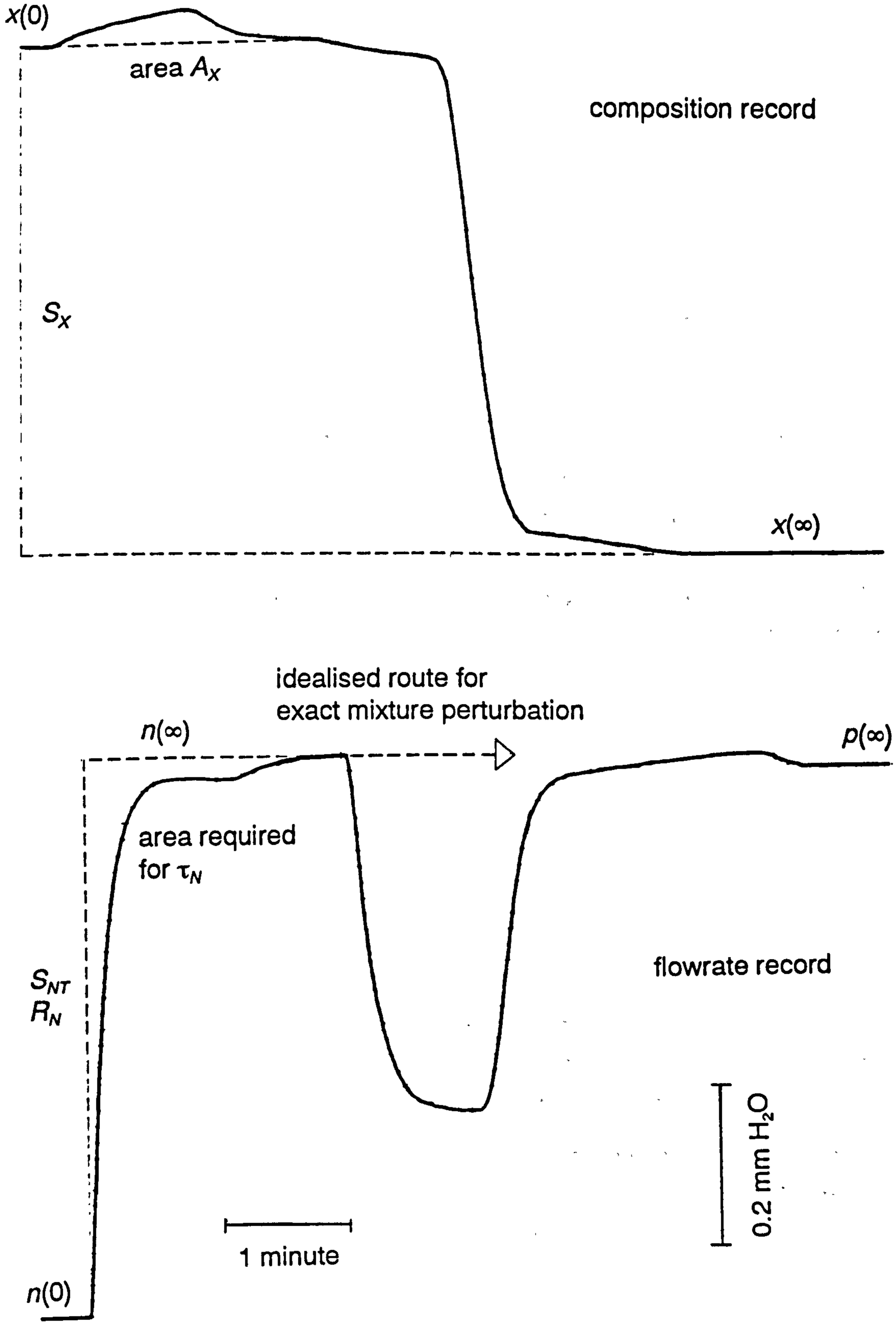

Figure 8.16 Chromatograms Affected by Upstream Delay Lines

$\Delta P_C = 35$ mmHg

$\tau_N = 12.4$ seconds

$A_X = 2.5$ cm^2 at 2mV and 20 mm/min

$S_X = 8$cm at 5mV composition record sensitivity

$S_{NT} = 8.8$ cm at 0.2V flowrate record sensitivity

$R_N = 8.25$ cm at 0.2V flowrate record sensitivity

From the discussion of Chapter Seven, when downstream delay lines are employed the column concentration change is more than that predicted by the original theory and so the equivalent column pressure drop ΔP_C^* must be used. The value of ΔP_C^* required will be 35+(2x11)=57 mmHg. Also, from the theory of Chapter Seven, the use of upstream delay lines will give a significant contribution to the measured flowrate retention time τ_{NU} and this must be subtracted from the above measured value. Strictly speaking, the exact form of Equation 7.44 is not applicable to this situation since the initial part of the flowrate chromatogram concerns the composition front *before* it reaches the column. Hence, there will be no viscosity change in the column and the viscosity factor $1+B(\mu)$ should only be multiplied by the first term in brackets. This contribution will be probably be between five and seven seconds. Using both stages of correction, the isotherm holdups can be calculated for each component:

$$\frac{\Delta H_{N2}}{\delta c_{N2}} = 90 \text{ ml}$$

$$\frac{\Delta H_{He}}{\delta c_{He}} = 27 \text{ ml}$$

Comparing these holdups with Table 8.5, it can be seen that the nitrogen value is too low and the helium value is too high. For this case, the error will be much greater for the helium isotherm holdup because it is more sensitive to the value of upstream contribution employed.

2. For column type B, the 20 metres length is not long enough to separate out the two composition effects, and so the length is increased to 40 metres. Using the nitrogen perturbation gas for calibration, the following important data is obtained:

$\Delta P_C = 90$ mmHg

$\tau_N = 45.4$ seconds

$A_X = 2.9$ cm^2 at 5 mV and 20 mm/min

Once again, it is necessary to correct for the equivalent column pressure drop ΔP_C^* due to the presence of the downstream delay lines. The value of ΔP_C^* required will be 90+(2x11)=112 mmHg. Also, the τ_{NU} contribution will be higher than that for column type A because of the increased column pressure drop and the increased length of delay-line tubing; this will be roughly around 30 seconds. Using both stages of correction, the isotherm holdups can be calculated for each component:

$$\frac{\Delta H_{N2}}{\delta c_{N2}} = 110 \text{ ml}$$

$$\frac{\Delta H_{He}}{\delta c_{He}} = 24 \text{ ml}$$

Actually, despite the larger corrections, the calculated isotherm holdups are in better agreement with Table 8.5 than the corresponding holdups calculated for column type A.

3. For column type D, 40 metre upstream delay-lines are employed. However, this length is only just long enough to separate out the bulge in the composition record before the composition step occurs. Using the nitrogen perturbation gas for calibration, the following data is obtained:

$\Delta P_C = 200$mmHg

$\tau_N = 76.7$ seconds

$A_X = 17.4$ cm^2 at 2 mV and 20 mm/min

As is expected from Equation 8.6, the composition bulge area is increased because of the column pressure drop. The area is roughly double that measured for column type B corresponding to a double in the column pressure drop. Once again, it is necessary to correct for the effect of the downstream delay-lines by considering the equivalent column pressure drop. However, because of the increased column pressure drop, this has a lower proportional effect. The τ_{NU} contribution will be very large and from Equation 7.44 this will be between 40 and 50 seconds.

8.8.5 Discussion

The importance of the upstream delay lines is seen in separating out the important bulge in the composition record from the effects as the front passes through the column. If an *exact* mixture perturbation gas can be obtained, then it is better to use column type D since all the measured areas will be greater. If an exact mixture perturbation gas cannot be obtained and upstream delay-lines are required, then the mixture perturbation gas becomes unnecessary; all the required information can be obtained by using either of the pure

perturbation gases, since the initial bulging in the composition record is independent of the perturbation gas selected, only upon the actual perturbation flow. The results for each column type will give approximately correct holdups, although the retention time corrections will reduce their reliability. Hence, it would be beneficial to develop the method experimentally to obtain a true mixture perturbation.

8.9 Possible Experimental Improvement

8.9.1 Introduction

From the basic theory summarised in Chapter One, the total change in holdup caused by adding a particular perturbation gas is characterised by the two measured retention times. At the time, the total holdup change for each component *i* was thought to consist of two contributions; the packing and voidage contributions. The latter was subtracted in order to obtain the change in packing holdup and hence both isotherm gradients. Furthermore, from Chapter Seven, it was shown that the presence of delay lines would make extra contributions to the measured isotherm holdups and would thus require extra corrections. From Section 8.8, when using a mixture perturbation gas it was seen that upstream delay-lines are essential, but these require large corrections to the measured flowrate retention times making the method especially inaccurate. In view of this discussion, this section considers a possible experimental configuration which would eliminate the need for *any* correction by obtaining only the holdup of interest. It should be stressed that no results have been obtained; the arrangement is just hypothetical.

8.9.2 Description of Experimental Configuration

Figure 8.17 shows a schematic representation of the experimental configuration. The major development is that a perturbation flow is added to each side of the system; this is achieved by the valve 6PV-1. The rear carrier will always pass through the molecular sieve column. The valve 8PV enables the front carrier to pass through either the molecular sieve column or the ballotini column. This brings up a potential problem; the columns should be identical with regard to dimensions and packing size and pressure drop. If this is not achieved, the whole design is rendered useless. The column not in action is purged continuously with carrier; this is important for the molecular sieve column because of the danger of deactivation.

The valves 6PV-2 AND 6PV-3 are always switched together, otherwise the column flow will be switched off. The purpose of these valves is to determine whether the front perturbation gas is being added to the auxiliary flow or the carrier flow. When these valves are switched to the *zero baseline shift* position, switching 6PV-1 will add or remove both perturbation gases together so that the chart recorder registers no change in the flowrate

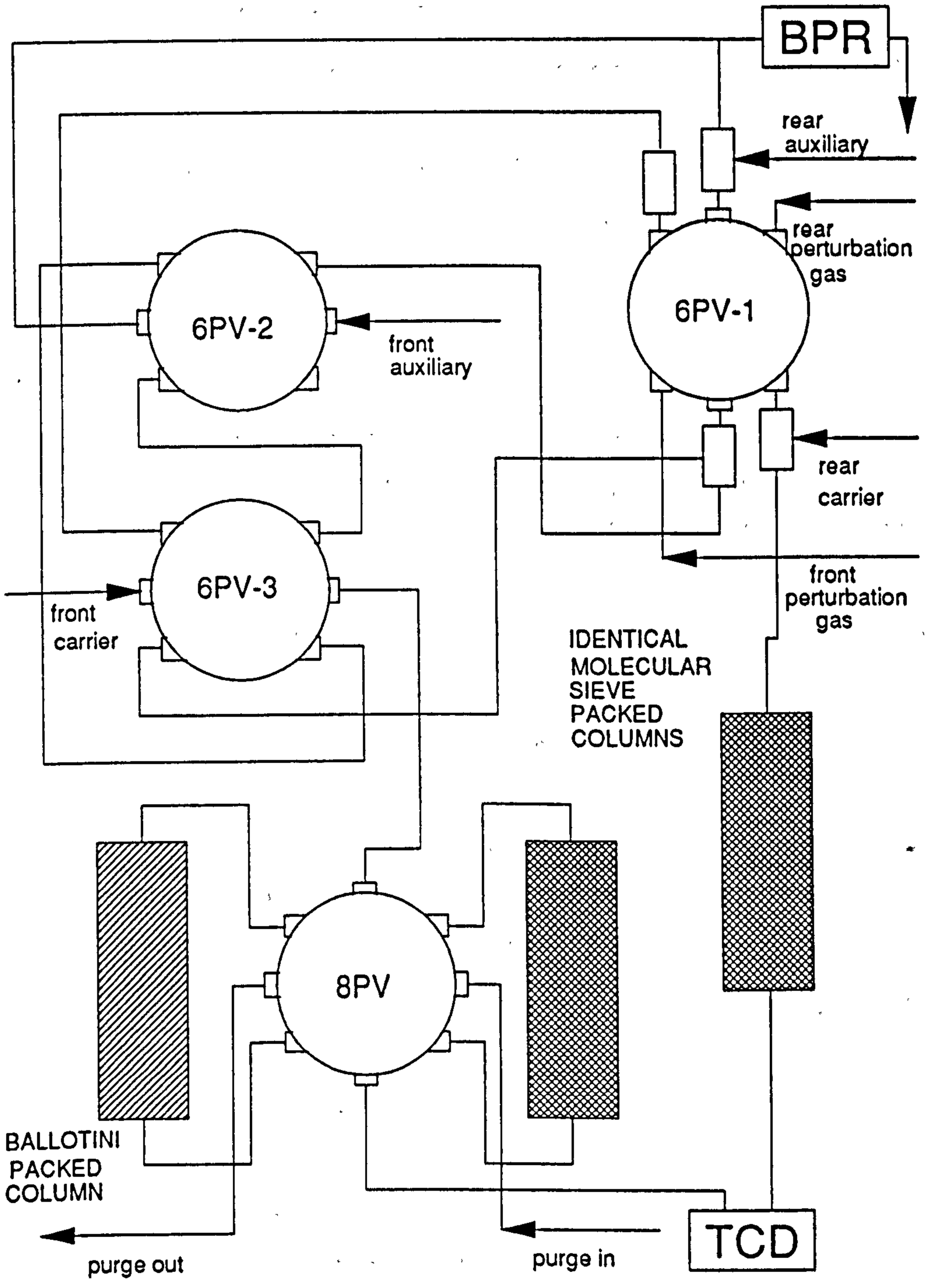

Figure 8.17 Schematic Representation of Experimental Configuration

baseline, since it works differentially. Conversely, if valves 6PV-2 and 6PV-3 are switched to the *opposite change* position, switching 6PV-1 will add one perturbation flow while removing the other perturbation flow. Thus for the same perturbation flowrates, the chart recorder chromatograms are twice as large as those which would be obtained with just one perturbation flow.

8.9.3 New Experimental Procedure

For each carrier mixture, three experiments will be required to obtain the isotherm gradients using a mixture perturbation flow. For the experiments of Section 8.8, this compares with two experiments, and it will be shown how the extra measurement is very useful.

1. For the first experiment, the following operational parameters are selected:

mixture perturbation gas selected
[8PV-1] molecular sieve column
[6PV-2/3] opposite change

This is what was achieved in Section 8.9, except that because two perturbation flows are employed, the measured flowrate offset will be $2R_N$ and the measured composition bulge will be $2A_X$. However, because of the previous problems, the flowrate retention time will not be obtained from this experiment.

2. For the second experiment, the following operational parameters are selected:

a pure perturbation gas selected
[8PV-1] molecular sieve column
[6PV-2/3] opposite change

Once again, this was achieved in Section 8.9 for the purpose of calibrating the composition bulge area. Because two perturbation flows are employed, the flowrate and composition offsets measured will be $2S_{NT}$ and $2S_X$ respectively.

3. For the third experiment, the following operational parameters are selected:

mixture perturbation gas selected
[8PV-1] ballotini column
[6PV-2/3] zero baseline shift

This experiment is used to determine the flowrate retention time. Because a perturbation gas is simultaneously added to each column, there will be no chart recorder offset. Indeed only a bulging should be observed in the composition record assuming the perturbation flows are identical. The novel thing about this experiment is that, since the pressure is increased in each side of the system, all significant corrections due to delay lines and other volumes should cancel out. Of course, this requires identical column pressure drops. The concept is desirable since the bulging area A_N is solely a result of the increased holdup due to the packing adsorption, and does not include even the increased column voidage holdup. The corrected retention time τ_N^* can be obtained by the following equation:

$$\tau_N^* = \frac{A_N}{R_N k_V} \qquad 8.7$$

As before, care must be taken that A_N and R_N are normalised , if necessary, to the same sensitivities.

8.10 Summary of Main Findings

1. At any one temperature, the results for the three binary systems are not totally independent, despite the interaction being different in each system. At the maximum end-points, the component is pure and the adsorbed value depends only on the pure component isotherm. Hence, for each of the three components, the two relevant maximum end-points from the two relevant systems should agree. This requirement will thus provide three additional tests for the results. Considering all the potential sources of error, agreement for each component is fairly good.

2. Generally, the results confirm that on molecular sieve zeolite 5A, the nitrogen, argon and helium are adsorbed in decreasing order. As the temperature is increased, the individual amounts adsorbed are seen to decrease. Also, as the temperature is increased, the greatest reduction is for the more adsorbed component and this means that the selectivity is reduced. The results would tend to suggest that design of an industrial adsorber to separate any of the two components is more desirable at lower temperatures, for reasons of selectivity as well as capacity.

3. The nitrogen isotherm appears to be more concave with respect to the composition axis when the other component is helium; the presence of argon seems to flatten it out somewhat. In the argon-helium system, the argon isotherm is virtually straight. Upon replacing the helium with nitrogen, the argon isotherm becomes convex with respect to the composition axis. In the argon-helium system, the helium isotherm is slightly convex. When the argon is replaced with nitrogen, the curvature of the helium isotherm becomes greater.

4. In Chapter Seven, an investigation was carried out to try and establish the validity of Equation 4.12 which gives the relationship between the pressure and flowrate retention times. The predictions were mixed, but indicated that the measured flowrate retention time would always contain some positive contribution. From the summarised theory of Chapter One, it should be possible to calculate the same component isotherm holdup using either perturbation gas. From the findings of this chapter, this agreement between the calculated isotherm holdups for each perturbation gas was found to be significantly greater when the *predicted* values of the flowrate retention time were employed rather than the directly

measured values. These findings would appear to confirm the validity of Equation 4.12 whilst casting doubt on the direct measurement of the flowrate retention time with downstream delay-lines.

5. Preliminary experiments have demonstrated a novel way for obtaining the isotherm holdups for the nitrogen-helium system using the standard column type A and upstream delay-lines. Basically, this method works by measuring the change in adsorption caused *solely* by the change in average column pressure when the perturbation gas is added. The change in average column pressure is accompanied by a change in the adsorbed phase composition and this causes the composition record to deviate before returning to the original baseline. Ideally, the perturbation gas should have the same composition as the carrier but this was found difficult to achieve and so upstream delay lines were employed to separate out the effects of the pressure change from the effects due to the composition change. Ideally, this method is better suited to columns having a higher pressure drop since the required bulge area in the composition record will be necessarily higher. The applicability of the method is also dependent on the gas system employed; using an argon-nitrogen carrier with the standard columns, a measurable bulge in the composition record could not be detected. The solution was to employ columns having a higher pressure drop.

Chapter Nine

AN APPLICATION OF THE CHROMATOGRAPHIC METHOD TO SPECIFIED BINARY GAS-MIXTURE SYSTEMS

9.1 Introduction

As has been discussed previously, the aim of this project method has been to develop and test a method for the rapid determination of isotherms of binary gas mixtures. Experimentally, a small perturbation flow is added to the particular mixture and the composition and flowrate retention times are measured by recording the chromatographic response. These two retention times are substituted into the basic equations of the method and both binary gradients are obtained. The two binary isotherms are obtained by integrating the respective sets of gradients.

This chapter considers the method working in reverse. One *starts* with the binary isotherms. These can be specified in different ways and a separate section will be devoted to these ways. From these isotherms, the gradients can be obtained and these can be substituted into the basic equations of the method. Working back, these two simultaneous equations are solved to obtain the composition and flowrate retention times. This procedure is ideal for a computer and this novel way is powerful since perfect flowrate and composition retention times can be generated for any binary system.

Although the flowrate retention time is not used in any conventional chromatographic methods, the composition retention time has many applications. One such application is the main chromatographic rival to the method used here; namely, the concentration-pulse polynomial fitting method proposed by Van der Vlist and Van der Meijden (1973). The calculated composition retention times can be used to rigourously analyse this curve-fitting method by trying to obtain the binary isotherms which were assumed at the start. Of course, the chromatographic method requires integration of the respective binary gradients and this can be attempted in many ways; the integration results can then be compared to the specified binary isotherms. Concluding, this chapter will consist a thorough investigation of both methods for a range of binary systems.

9.2 Generation of Retention Times

9.2.1 Main Chromatographic Equations

The equations used for relating isotherm gradients to the flowrate and composition retention times are critical to this chapter and are taken from Mason and Buffham (1991). The two equations, one for each component, are:

$$\frac{F_{PVCA}}{Q_{CAV}}\left[\frac{dq_A}{dc_A}(1-\varepsilon)V_C+\varepsilon V_C\right]=\tau_X+\frac{Y_{AO}}{Y_{AT}-Y_{AO}}\tau_N \qquad 9.1$$

$$\frac{F_{PVCB}}{Q_{CAV}}\left[\frac{dq_B}{dc_B}(1-\varepsilon)V_C+\varepsilon V_C\right]=\tau_X+\frac{Y_{BO}}{Y_{BT}-Y_{BO}}\tau_N \qquad 9.2$$

$$Y_{BO}+Y_{AO}=Y_{AT}+Y_{BT}=1 \qquad 9.3$$

where Q_{CAV} = average gas volumetric flowrate in column

F_{PVCA} = column correction factor for component A

F_{PVCB} = column correction factor for component B

V_C = total column volume

dq_A/dc_A = dimensionless binary gradient for component A

dq_B/dc_B = dimensionless binary gradient for component B

ε = column voidage

τ_X = composition retention time

τ_N = flowrate retention time

Y_{AO} = carrier gas composition

Y_{AT} = perturbation gas composition

The values chosen for the carrier gas flowrate, column volume and column voidage are not critical to this chapter; for convenience, values are chosen representative of the conditions in Chapter Eight.

9.2.2 Column Correction Factors

The values of the correction factors stated above depend upon the column dimensions and the particle size, and ultimately, the column pressure drop. For negligible column pressure drops these correction factors tend to unity and so can be omitted. However, if these factors cannot be neglected, the whole analysis is complicated because the important composition retention times will be different for each perturbation gas.

$$F_{PVCA}=1+\frac{Y_{AO}}{Y_{AT}-Y_{AO}}\frac{1}{2}\frac{\Delta P_C}{P_{CMEAN}}\left[\frac{1+\frac{\Delta P_C}{3P_{COUT}}}{1+\frac{\Delta P_C}{2P_{COUT}}}\right](1+B(\mu)) \qquad 9.4$$

$$F_{PVCB}=1+\frac{Y_{BO}}{Y_{BT}-Y_{BO}}\frac{1}{2}\frac{\Delta P_C}{P_{CMEAN}}\left[\frac{1+\frac{\Delta P_C}{3P_{COUT}}}{1+\frac{\Delta P_C}{2P_{COUT}}}\right](1+B(\mu)) \qquad 9.5$$

where ΔP_C = column pressure drop

P_{COUT} = column outlet pressure

P_{CMEAN} = column mean pressure

$B(\mu)$ = mixture viscosity factor

The set of composition retention times obtained for each perturbation gas will be different and this difference will increase with the column pressure drop. Each set of composition retention times will not extend over the whole composition range, since there will be no composition retention time measured when a perturbation gas of a particular component is added to a pure carrier of the same component. Hence, for a finite column pressure drop, it is not possible to present consistent values of the composition retention time across the *whole* composition range on a single graph. Thus, it was necessary to investigate all the papers citing the original Van der Vlist method. Actually, Van der Vlist and Van der Meijden (1973) recorded a significant column pressure drop of 10 cmHg. However, all the citing authors either state or imply that the column pressure drop is negligible. Hence, for the majority of this chapter, the correction factors will be assumed to be unity and can thus be neglected. This will enable the two simultaneous equations to be solved to obtain a consistent set composition retention times across the whole concentration range. The next section shows how these composition retention times are processed by the polynomial-fitting method.

9.3 The Polynomial-Fitting Method

9.3.1 The Important Equations

The method is based on the original equation of Martin and Synge (1953) which was further developed by Haydel and Kobayashi (1967) to relate the retention volume of the concentration perturbation in a mixture to the slopes of the individual component isotherms. For simplicity, this original equation is converted to a form which uses retention times instead of volumes, and which uses dimensionless isotherm gradients:

$$K = \left(\frac{\varepsilon}{1-\varepsilon}\right)\left[\frac{\tau_X}{\tau_U} - 1\right] \qquad 9.6$$

$$K = (1 - Y_{AO})\frac{dq_A}{dc_A} + Y_{AO}\frac{dq_B}{dc_B} \qquad 9.7$$

where K = effective equilibrium constant for mixture

τ_U = retention time for unretained pulse

Generally, both component isotherm gradients will vary with composition. Substitution of the set of composition retention times generated previously will thus give a range of K values. From the polynomial-fitting method point of view, both of the gradients are unknown and Sections 9.3.2 and 9.3.3 will show how the method is applied to this problem.

9.3.2 Determination of Single-Component Isotherms

The single-component isotherm for component A can be evaluated when component B is inert, or negligibly adsorbed compared to component A. To obtain the single-component isotherm for component A, the component B isotherm gradient is assumed to be constant across the whole composition range at the Henry's law value. From Equation 9.7, the Henry's law constant is the value of K at Y_{AO}=1. Although this gradient is small compared to that of component A, assumption of a zero gradient for component B will cause error as Y_{AO} tends to one (Ruthven and Kumar, 1980). Thus, the values of component A gradient can be directly obtained from the K values. This set of gradients must then be integrated to obtain the single-component isotherm. This can be accomplished in a number of ways:

1. The *trapezoidal rule* is the simplest way and this approximates the area by connecting each consecutive pair of points by a straight line. The advantage of this method is that the interval length need not be fixed. Obviously, the smaller the interval length the more accurate the integration.

2. *Simpsons's rule* approximates the area by fitting a polynomial to each set of consecutive three points. However, this rule requires a fixed interval.

3. If a polynomial of high enough order can be fitted through each set of gradients, the isotherm can be represented by the integrated form of the polynomial. Obviously, the polynomial is required to give a good fit and so the polynomial order required will depend upon the system.

Although this chapter is primarily concerned with binary systems this section concerned with single-component isotherms is included because of the connection with the project method; both cases involve the direct integration of the isotherm gradients and the problem is to find a suitable integration method.

9.3.3 Determination of Binary-Mixture Isotherms

A different approach is required for binary systems since in this case both gradients will be unknown. It is normal practice to fit a third-order polynomial to the range of K values using a fitting subroutine (Ruthven and Kumar, 1980):

$$K = A_0 + A_1 Y_{AO} + A_2 Y_{AO}^2 + A_3 Y_{AO}^3 \qquad 9.8$$

where A_0, A_1, A_2 and A_3 are the determined best fit coefficients

It is not necessary to use a third-order polynomial and a discussion of different order fittings is presented later. The next step is to represent the slopes of the equilibrium curves by second order polynomials:

$$\frac{dq_A}{dc_A} = B_0 + B_1 Y_{AO} + B_2 Y_{AO}^2 \qquad 9.9$$

$$\frac{dq_B}{dc_B} = C_0 + C_1 Y_{AO} + C_2 Y_{AO}^2 \qquad 9.10$$

where B_0, B_1, B_2, C_0, C_1 and C_2 are unknown coefficients

There are now six unknowns but only four known fitting coefficients. The extra two pieces of information are obtained by specifying the isotherm end-points, that is, the amounts of pure component adsorbed at the total system pressure. Substituting Equations 9.9 and 9.10 into 9.7 and equating coefficients using Equation 9.8 enables the six unknowns to be determined:

$$B_0 = A_0 \qquad 9.11$$

$$B_2 = 6\left[\frac{q_{AM} + q_{BM}}{100}\right] - 12A_0 - 6A_1 - 3A_2 - 2A_3 \qquad 9.12$$

$$B_1 = \frac{1}{3}\left[6\frac{q_{AM}}{100} - 6A_0 - 2B_2\right] \qquad 9.13$$

$$C_0 = A_1 + A_0 - B_1 \qquad 9.14$$

$$C_1 = A_2 + B_1 - B_2 \qquad 9.15$$

$$C_2 = A_3 + B_2 \qquad 9.16$$

where q_{AM} = amount of pure A adsorbed at total system pressure

q_{BM} = amount of pure B adsorbed at total system pressure

The binaries are thus represented by the integrated forms of Equations 9.9 and 9.10, namely:

$$q_A = c_T\left[B_0 Y_{AO} + \frac{B_1 Y_{AO}^2}{2} + \frac{B_2 Y_{AO}^3}{3}\right] \qquad 9.17$$

$$q_A = c_T\left[C_0(1 - Y_{AO}) + \frac{C_1(1 - Y_{AO}^2)}{2} + \frac{C_2(1 - Y_{AO}^3)}{3}\right] \qquad 9.17$$

$$c_T = c_A + c_B \qquad 9.19$$

where q_A = mixture adsorbed concentration of A

q_B = mixture adsorbed concentration of B

c_A = gaseous concentration of A

c_B = gaseous concentration of B

c_T = total gaseous concentration which is fixed

Ideally, the isotherms obtained by the above method should be the same as those specified initially since the retention times being used are from these initial binaries. The agreement between these two sets is an indication of the effectiveness of the method. Obviously, a major requirement is that the set of K values can be properly fitted with a third-order polynomial. Different binary systems will give different variations in K values, and so some binary systems will be better represented by a third-order polynomial. The rest of this chapter will be concerned with starting off with different binary systems and observing how well the K values can be fitted with a polynomial and ultimately how well the specified binary system can be re-generated. It should then be possible to make conclusions regarding the suitability of the polynomial-fitting method for different binary systems.

9.4 The Implications of the Polynomial-Order

9.4.1 Third-Order Polynomial

The great majority of citations of this method use a third-order polynomial. It is particularly convenient since only two pieces of independent information are required and these are the pure-component data. Thus, the final predictions of the isotherms will give agreement at the end-points. This "pinning" of the isotherms can sometimes give peculiar shapes.

9.4.2 Second-Order Polynomial

This is obviously less useful because using a second-order polynomial will preclude many systems which require a higher order. Additionally, because of the number of unknowns, only one piece of independent information can be specified; one of the pure-component end points. Thus, in the final predictions agreement may only be obtained at one end-point. Moreover, this order is less useful since if one end-point is required it seems logical to use the other end-point and utilise a more flexible polynomial order.

9.4.3 Fourth-Order Polynomial

Mathematically, although this case involves just one more unknown this set of simultaneous equations is much more difficult to solve. For the third-order case, the coefficients are of a form such that the unknowns can be easily be explicitly obtained. For the fourth-order case, the coefficients can vary and can involve difficult fractions. Originally, it was intended to solve the matrix of equations iteratively, but the solution would not converge. Consequently, the matrix was solved by a Gaussian elimination subroutine. A fourth-order

polynomial will be able to fit many systems which a third-order cannot. However, the drawback is that an extra piece of independent information is required in addition to the pure-component end-points; that is, a mixture data point is required. Although the original authors of this method mention the possibility of higher order fitting, they do not go into any more detail. In reality, this mixture point can be specified in three ways:

1. Fixing the total amount adsorbed
2. Fixing the amount of A adsorbed in the mixture
3. Fixing the amount of B adsorbed in the mixture

From a practical point of view, the first case is more convenient since it does not require any composition measurements and can be achieved with the same equipment used to determine the pure-component end-points. Thus the predictions can be pinned to agree with the specified isotherms at any composition using any of the above three cases. Obviously, the question arises as to whether there is an optimum specification to improve the predictions; possibly this specification is determined by the particular system. Indeed, some specifications may not be possible or may cause large deviations at other compositions. Results for this idea will be shown at a later stage, although the above discussion will help with the literature review.

9.4.4 Higher-Order Polynomial

Obviously, the higher the order of polynomial, the better the chance of fitting particularly awkward K data. Although, for many systems this is not necessary. However, each time the order is increased, an additional mixture point must be specified. It might be thought that specifying these points at regular spacings would result in much improved predictions. Once again, there are many ways of specifying two points with three different cases and the question arises as to a possible optimum specification. Mathematically, the matrix could still be quickly solved by Gaussian elimination.

9.5 Literature Review of Polynomial-Fitting Method

9.5.1 Van der Vlist and Van der Meijden (1973)

As already stated, this was the original paper. Experimentally, the authors used a long narrow column with a comparatively small packing size; consequently, the pressure drop was as high as 10 cmHg. The only system considered was nitrogen-oxygen on 5A zeolite at atmospheric pressure and around 27°C. The results were not compared with independently obtained data. From Equations 9.4 and 9.5, the correction factors would be significant and the retention times different for each perturbation gas. This might explain why the retention times for both perturbation gases were averaged.

9.5.2 Ruthven and Kumar (1979)

The column diameter was such that there would have been a negligible pressure drop. The system studied was nitrogen-methane on 4A zeolite at atmospheric pressure. As well as binary data, single-component isotherms were obtained using helium as the inert carrier. The results were not compared with independently obtained data.

9.5.3 Ruthven and Kumar (1980)

The experimental set-up is the same as above. Many systems were investigated including argon-nitrogen and nitrogen-oxygen on 5A zeolite and others on 4A zeolite. As well as the mixtures, single-component isotherms were obtained using helium as the inert carrier. There was no comparison with static data only with predictions by Ruthven's statistical model (Ruthven 1976, 1984e). The attitude seemed to be that the chromatographic method was absolute and the *statistical predictions* were being tested.

9.5.4 Hyun and Danner (1982)

This was the first paper to try and critically analyse the polynomial-fitting method. It did not present new experimental data but used other literature and thesis data determined by static methods. The authors used basically the same principle of this chapter. Using this static mixture data, they determined the binary gradients graphically and substituting into the equation they obtained a set of K values. These K values were then used to try and obtain the static data. The authors considered three systems:

1. CO-CH_4 on activated carbon at 25°C and 9.5 bar. For this system a third-order polynomial fitted the K data very well and so the final predictions were very good.

2. i-C_4H_{10}-C_2H_4 on 13X zeolite at 25°C and 1.4 bar. Once again a third-order polynomial fitted the K data very well although the predictions were not so good. However, this system has an azeotrope.

3. C_2H_6-C_2H_4 on 13X zeolite at 25°C and 1.4 bar. The third-order polynomial fitted the respective K data poorly and so the predictions were poor.

The authors concluded that while the method should always work well for single-component determination, the method did not work well for all binary systems.

9.5.5 Hyun and Danner (1985)

This paper continued the critical theme of the previous while extolling the virtues of the rival tracer-pulse method. The authors focused on just the azeotropic system of the previous paper but this time determined the retention volumes experimentally by injecting pulses of radioactive tracer molecules. With modified equipment, both tracer-pulse and

concentration-pulse retention times were evaluated. Somewhat surprisingly, the same system then gave very poor predictions again using a third-order polynomial. The authors then used a fourth-order polynomial and despite this giving a much improved fitting, the final isotherms were just as bad. Actually, the authors did not state the required mixture specification for this higher order. Also, the authors considered a second-order fitting as well. However, with this order they obtained agreement at both end-points and it has just been shown that only one end-point can be specified with a second-order polynomial. Thus there are areas of doubt over some of the results in this paper. Finally, the authors advocated combining both rival methods to obtain good predictions. This is necessary when an isotope can only be obtained for one of the components.

9.5.6 Shah (1988)

The experimental set-up was such that there would have been a negligible column pressure-drop. Three systems were investigated on 5A zeolite. In each case both binary isotherms and single isotherms were obtained using helium as carrier. The predictions were not compared with static data but with the Ruthven statistical method (Ruthven, 1976 and 1984e). However, the author was concerned with a critical analysis of the chromatographic method. For the oxygen-nitrogen system, the statistical method gave predictions in good agreement with the chromatographic method. However, for the other systems there are visible differences in the predictions. For the more strongly adsorbed component, there is a strong kink towards the high mole fraction region and the other component is continually over predicted. Analysis of these findings is made difficult since the retention time data and subsequent polynomial fitting are not shown. Shah concludes that the polynomial-fitting method is well suited to the determination of pure-component isotherms but is not suitable for all binary systems. Furthermore, the strong kinking mentioned above was further analysed: "this kinking being characteristic of non-ideal systems but since this is an ideal system the actual method is causing the kinking". Actually, this same behaviour is noticed in the third system described in Section 9.5.4.

9.5.7 Tezel *et.al* (1992)

The most recent citation involves the investigation of the krypton-nitrogen system over dealuminated H-mordenite and silicalite. These systems were investigated at atmospheric pressure and temperatures of 226K and 298K. To initiate the perturbations, pulses were used rather than flows. The polynomial method was used to obtain both pure and binary isotherms. Using the pure-component isotherms, the IAST and statistical methods were used to try and predict the binary isotherms. There was no comparison with independently obtained mixture data. It can be seen that the third-order polynomials gave adequate fits for two of the systems and poor fits for the other two systems.

9.6 Specification of Binaries

9.6.1 Direct Algebraic Specification

The calculations are carried out by a computer program and this is fully described in Section 9.7. The first version of the program involves specifying the form of each *binary isotherm* directly in algebraic form. After looking through the literature at many systems, it can be seen that there are many shapes of *binary isotherm*. Some are virtually straight lines, while others have only a slight concave or convex curvature. Alternatively, some isotherms have a highly concave or convex curvature. A less common category is the binary isotherm having a point of inflexion; sometimes the isotherm can appear as a "s" shape curve, but the isotherm can also appear as a concave or convex curve with a kink towards one end of the curve (see Figure 9.11B). Eventually after many modifications, it was decided that Equations 9.20 and 9.21 can represent many isotherm shapes. Each of the three terms is relevant because they are all used to represent pure-component isotherm data. Obviously, a linear binary can be specified by making both M and R both zero. A Langmuir binary can be specified by making both H and M zero. It has not been thought suitable to have just a Langmuir-Freundlich contribution because this involves a zero initial gradient and this is thermodynamically inconsistent (Talu and Myers, 1988).

$$q_A = H_A c_A + \frac{R_A c_A}{T_A + c_A} + \frac{M_A c_A^{FA}}{N_A + c_A^{FA}} \qquad 9.20$$

$$q_B = H_B c_B + \frac{R_B c_B}{T_B + c_B} + \frac{M_B c_B^{FB}}{N_B + c_B^{FB}} \qquad 9.21$$

where H is linear contribution

R and T are coefficients for Langmuir contributions

M, N and F are coefficients for Langmuir-Freundlich contributions

In order to obtain the more "peculiar shapes" of binary, H is made zero and the other two terms are added together in varying proportions. It has been found convenient to define a % Langmuir contribution: this is defined at the end-point as the % of the total amount adsorbed due to the Langmuir term. A final modification is to allow the initial and final gradients to be specified. This saves time when the choice of gradients is important and is especially useful when requiring azeotropic systems. A partial listing of this program is contained in Appendix F.

9.6.2 The Binary-Langmuir Theory

This theory was first proposed by Markham and Benton (1931). The main requirement is that both pure-component isotherms can be fitted to the conventional Langmuir isotherm. Once this is established, the theory then takes these pure-component parameters and uses them to form two coupled equations to predict the mixture isotherms:

$$q_A = \frac{R_A c_A}{T_A + c_A + \left(\frac{T_A}{T_B}\right) c_B} \qquad 9.22$$

$$q_B = \frac{R_B c_B}{T_B + c_B + \left(\frac{T_B}{T_A}\right) c_A} \qquad 9.23$$

The characteristic shape of the predicted binaries is shown in Figure 9.1. As shown, the isotherms will always have opposite curvatures. However, if the pure-component parameters are specified in such a way, then the system reduces to a linear one.

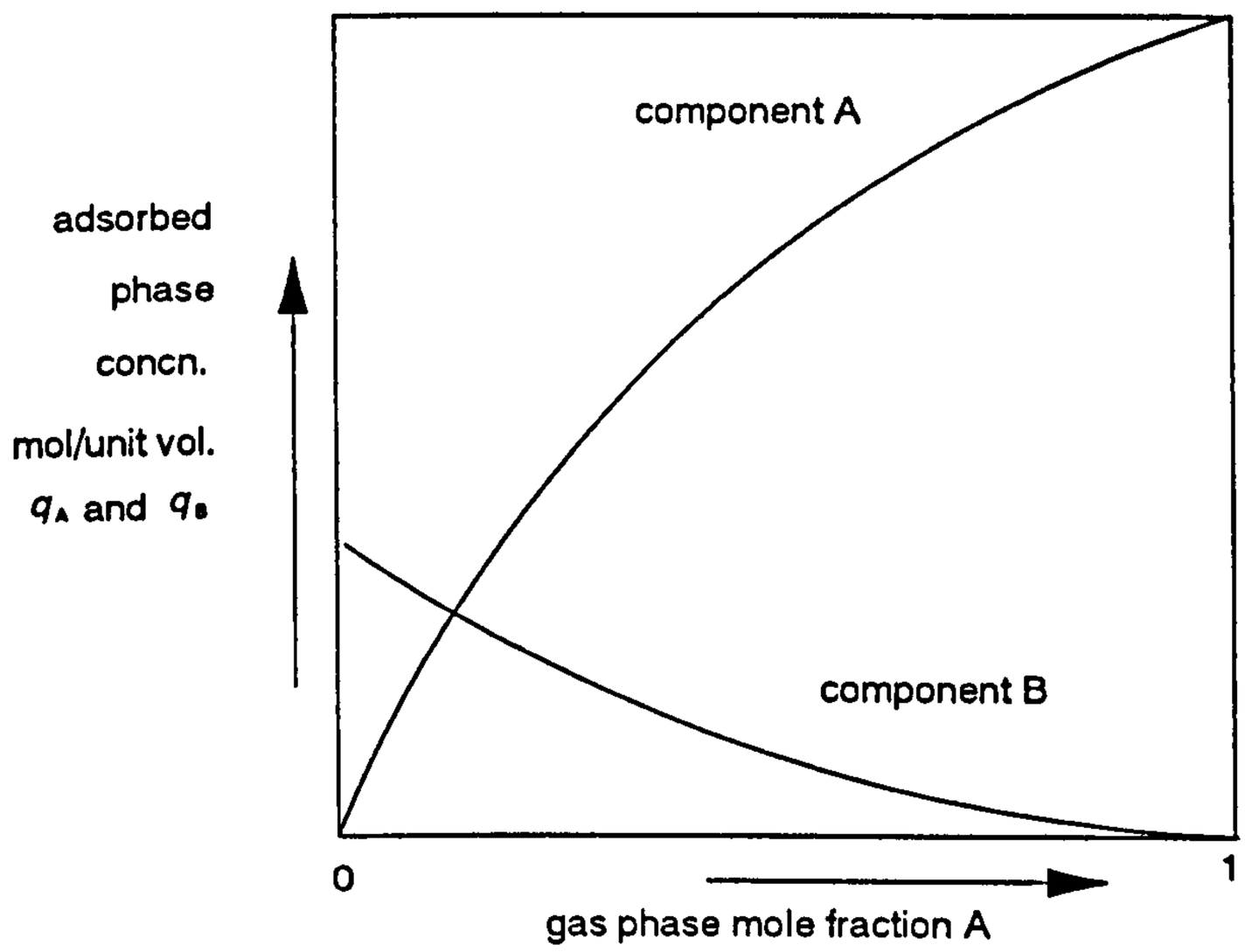

Figure 9.1 Characteristic Shape of Binary-Langmuir Predictions

This method has received much criticism from the literature although some systems have exhibited such behaviour. Indeed, looking through the literature, many systems have roughly the same shape as above. A complete listing of the program is contained in Appendix E.

9.6.3 The Ideal Adsorbed Solution Theory (IAST)

This theory was first proposed by Myers and Prausnitz (1965) and has received over 200 citations. Like the previous theory the IAST requires the pure-component isotherms to be specified in an algebraic form. This can be in the Langmuir form, although the greater

flexibility of this method means that the algebraic form can be that which best fits the data. The main requirement for this method is that the adsorbed phase should be ideal; the activity coefficients should be unity. Although this may seem a severe requirement, surprisingly many systems have been shown to exhibit such behaviour. Ideality is usually guarantied by the components having similar molecular properties. The IAST theory introduces the necessary concept of *spreading pressure*. This is obtained from the *pure-component data* and for component A is defined by:

$$\pi(c_{AO}) = \int_0^{c_{AO}} \frac{q_A}{c_{AO}} dc_{AO} \qquad 9.24$$

where q_A = function (c_{AO}) is pure component isotherm for A

$\pi(c_{AO})$ = spreading pressure for component A

Likewise, the spreading pressure for component B involves just the pure-component isotherm for B. The variables c_{AO} and c_{BO} are analogous to the quantities used in vapour-liquid equilibrium. The fundamental requirement for the theory is that in the mixture the spreading pressure of each component should be equal and the same as that of the mixture:

$$\pi(c_{AO}) = \pi(c_{BO}) \qquad 9.25$$

For an ideal adsorbed solution both activity coefficients are unity and thus:

$$c_A = c_{AO} x_A \qquad 9.26$$

$$c_B = c_{BO} x_B \qquad 9.27$$

where x_A = mole fraction of A in adsorbed phase

x_B = mole fraction of B in adsorbed phase

Because the sum of these mole fractions is one, an expression can be found connecting c_{AO} and c_{BO}:

$$c_{BO} = \frac{c_{AO} c_B}{c_{AO} - c_A} \qquad 9.28$$

Because the pure-component isotherms are specified algebraically, the expressions for the spreading pressure can be obtained algebraically :

$$\pi_A(c_{AO}) = H_A c_{AO} + \left(\frac{M_A}{F_A}\right) \log\left(\frac{N_A + c_{AO}^{FA}}{N_A}\right) \qquad 9.29$$

$$\pi_B(c_{BO}) = H_B c_{BO} + \left(\frac{M_B}{F_B}\right) \log\left(\frac{N_B + c_{BO}^{FB}}{N_B}\right) \qquad 9.30$$

Considering the spreading pressure equality, Equations 9.29 and 9.30 are made equal and using Equation 9.28 an expression is obtained in which the only unknowns are c_{AO} and the gas phase composition. When the latter is specified, the whole expression becomes an implicit expression in c_{AO} and this must be solved by an iterative procedure which requires guesses of c_{AO} until convergence. Once this is obtained, c_{BO} and the adsorbed phase composition can be easily calculated and the total amounts adsorbed can be obtained from:

$$\frac{1}{q_T} = \frac{x_A}{q_{AO}} + \frac{x_B}{q_{BO}} \qquad 9.31$$

$$q_A = q_T x_A \qquad 9.32$$

$$q_B = q_T x_B \qquad 9.33$$

where q_T = total amount adsorbed

q_{AO} = amount of pure A adsorbed at c_{AO}

q_{BO} = amount of pure B adsorbed at c_{BO}

9.6.4 Real Adsorbed Solution Theory (RAST)

While many systems do exhibit ideal behaviour, many do not and so the final category of binary specification involves non-unity activity coefficients. This theory was first proposed by Costa *et al.* (1981, 1989). This theory uses activity coefficient equations based on vapour-liquid equilibrium and these equations do not include the necessary spreading-pressure variation. Thus care should be taken with its application (Talu and Zweibel, 1988). Firstly, Equations 9.26 and 9.27 are re-stated but including the activity coefficients:

$$c_A = c_{AO} x_A \lambda_A \qquad 9.34$$

$$c_B = c_{BO} x_B \lambda_B \qquad 9.35$$

where λ_A = activity coefficient for component A

λ_B = activity coefficient for component B

These activity coefficients can be represented by the classic Wilson equation (Wilson, 1964). Presumably any solution of the Gibbs-Duhem equation could be employed. For example, the two-constant Margules equation has already been demonstrated by Glessner and Myers (1969) to apply to the butane-carbon dioxide system on 5A zeolite:

$$\ln\lambda_A = (2B - A)x_B^2 + 2(A - B)x_B^3 \qquad 9.36$$

$$\ln\lambda_B = (2B - A)x_A^2 + 2(B - A)x_A^3 \qquad 9.37$$

A and B are the mixture coefficients defining activity coefficient variation. The situation is more complicated than before because the activity coefficients are functions of the adsorbed phase composition which is unknown. Thus it is not possible to obtain a simple relationship between c_{AO} and c_{BO}. Instead, c_{AO} and c_{BO} must be replaced by the complicated expressions involving x_A. Using the spreading-pressure equality, a complex expression is obtained in which the only unknowns are the gas phase composition Y_{AO} and the adsorbed phase composition x_A. After the former has been specified, an implicit expression in x_A is obtained which must be solved iteratively. Because of the comparative complexity of the expression, convergence is difficult to achieve and depends upon the values of A and B as well as the isotherm parameters. For linear isotherms, convergence is easily attained but with isotherm curvature, the initial guess is important. A partial listing of the program is contained in Appendix H.

9.6.5 Individual Perturbation Gas Treatment

A final possibility for developing the program structure involves dealing with each perturbation gas individually: perturbation gas A with the carrier composition varying from 0% to 95% component A, and perturbation gas B with the carrier composition varying from 5% to 100% component A. Obviously, the respective end-points are omitted because adding a perturbation gas of the same composition of the carrier will not produce a composition retention time. The reason for this program development is that the effect of a *significant column pressure-drop* can be investigated. As discussed previously, if the column pressure-drop is negligible, from Equations 9.4 and 9.5 the factors F_{PVCA} and F_{PVCB} are unity; solving Equations 9.1 and 9.2 gives the same set of composition retention times for each perturbation gas. Otherwise, each perturbation gas will give a different set of composition retention times and hence a different set of *binary isotherm predictions*.

9.7 Structure of Program

9.7.1 Number of Data Points

It has been decided to do the calculations at an interval of 5% composition. Thus, there will be 21 composition points including the two pure carriers. A smaller interval is used (rather than say 10 %) because some binaries have initial steep gradients which this larger interval would not cover. For computing purposes, a constant interval is desirable.

9.7.2 Units Employed

The units of both gas-phase and adsorbed-phase compositions are *mole per unit volume.* This enables dimensionless gradients to be employed and makes simulation much easier. The total gas phase concentration is constant at 100 mole per unit volume.

9.7.3 Viscosity Variation with Composition

Despite the system pressures remaining constant, in reality the carrier gas flowrate will vary with composition because of the viscosity variation. This has been crudely simulated by assuming a straight-line viscosity variation with composition; there is an option in the program to define this gradient. Thus, the unretained pulse time will vary with composition and this time appears in the expression for K. Actually, the value of viscosity variation does not affect the fitting of K values, but is included for reality.

9.7.4 Number of Data Points for *K* Fitting

Although the *calculations* will be carried out at a 5% composition interval across the whole range, it is unlikely that each worker will investigate 21 compositions. Indeed, it is usual to only use a 10% composition interval. Removing any point(s) from condsideration will affect the best fitting polynomial curve for the remaining K values, unless the K variation is a straight line. Since the parameters of this fitting curve are used directly to obtain the binaries, any removal of K values will affect the final binary predictions. In the normal case, the weighting factor for each K value is unity. In the program, the weighting factors are contained in the third column of the main matrix $X(N,2)$, where N ranges from 1 to 21. An extra development is to include a subroutine in the program to enable any K value to be discounted from the polynomial fitting by setting the respective weighting to zero. The K value graph will only show the K values used for fitting. This flexibility is important, since it allows the theoretical effect of omitting particular K values to be instantly seen on the subsequent fitting curve and binary isotherm predictions.

9.7.5 Random Error Options

So far, the generated retention times have been perfect; those which would have been obtained if there were no experimental error. In reality, these will need to be measured and a further possibility is to impose a random error on these retention times. As well as the composition retention time, the unretained pulse retention time will need to be measured for each mixture. Thus, it is possible to adjust the set of K values by this error imposition and it could be interesting to see the quality of subsequent fitting and prediction of binary isotherms. This option uses a random number generator which generates random numbers between zero and one. Before the K values can be adjusted, the % random error (+/-) must be specified and this determines the value of *VL*:

$$VL = \frac{50}{\%Error} \tag{9.38}$$

$$Factor = \frac{VL - \frac{1}{2} + RandomNumber(0-1)}{VL} \tag{9.40}$$

Thus each K value will be multiplied by the value of *Factor*. The use of the 1/2 term allows an equal chance of positive and negative errors. Finally, the random number generator will need to be re-seeded each time the program is run so that the same sequence of random numbers is generated.

9.7.6 Presentation of Results-Generation of Binaries

This section only applies to the cases where the pure-component isotherms are specified and the particular theory predicts the binary isotherms. For this graph, the pure-component isotherms are shown as continuous lines and the mixture predictions shown as points every 5 % interval.

9.7.7 Presentation of Results-Effectiveness of Polynomial Method

1. Firstly, a graph is presented showing the actual discrete K values and the subsequent best fitting polynomial order employed.

2. The *absolute* way of presenting adsorption data is to show each component isotherm on the same graph. Hence, for clarity, the *actual isotherms* are shown as solid lines and the *predicted isotherms* are shown as discrete points. For the following parts 3 to 5, this will be the terminology.

3. From the literature, the information is often re-stated as total amount adsorbed. This is especially useful if using higher-order polynomial fitting (greater than 3) when the mixture data point specified is a total amount. This graph will confirm that the mixture point has been attained. Additionally, maxima or minima in this graph demonstrate the presence of non-idealities.

4. Sometimes, the adsorption data can be re-stated as a *phase diagram*. This form of presentation is especially useful when there is the possibility of azeotropes; on a phase diagram an azeotrope is obtained when the phase line crosses the diagonal.

5. Finally, it is possible to re-state the adsorption data as a *selectivity chart*; this demonstrates the ease of separation of the two components. An azeotrope is demonstrated by a unity selectivity. This type of presentation is dealt with in Chapter One.

9.7.8 Presentation of Results-Integration of Binary Gradients

For clarity, the integrations for each component are shown can be shown in two graphs:

1. For the *absolute* presentation, the actual isotherm is shown as a smooth line along with the trapezoidal integration as discrete points. Also shown is the integration due to a first-order polynomial fitting of the gradients.

2. For the *integration error* presentation, the absolute concentration errors are shown for the four cases; the two methods mentioned above plus Simpson's rule and a higher order polynomial fitting.

9.7.9 Source of Polynomial Fitting Subroutine

The programs are written in *Turbo Basic*. The polynomial fitting subroutine is modified from a *BBC Basic* program written by C.R.G Treasure in the Department of Chemical Engineering in 1983.

9.8 Application of the Program to Hypothetical Situations

9.8.1 Specifying Linear Isotherms

For this case the linear isotherms are specified by the following end-points:

q_{AM}= 800 mole per unit volume
q_{BM}= 400 mole per unit volume

The results of the polynomial simulation are shown in the following Figures 9.2A and 9.2B. As can be seen, the K values form a straight line and can be perfectly fitted by a first-order polynomial. The binary isotherms are then predicted perfectly. This may seem a trivial case, but it shows that the program is working correctly since perfect polynomial-fitting gives perfect predictions of the isotherms. Each set of gradients consists constant set of values. Thus, it would be trivial to compare the integration methods since they will all give perfect results.

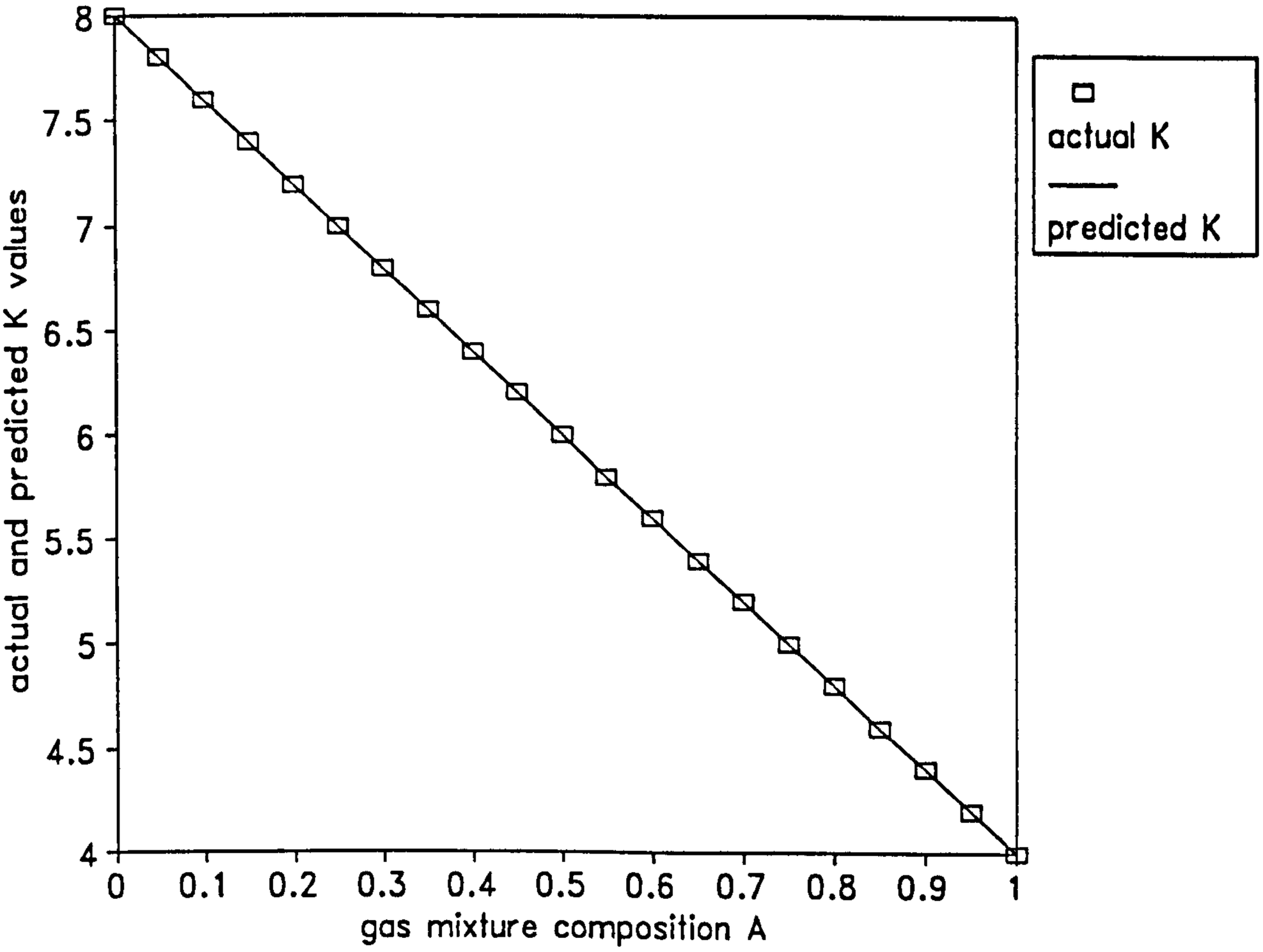

Figure 9.2A Actual and Fitted Values of *K* for Linear System

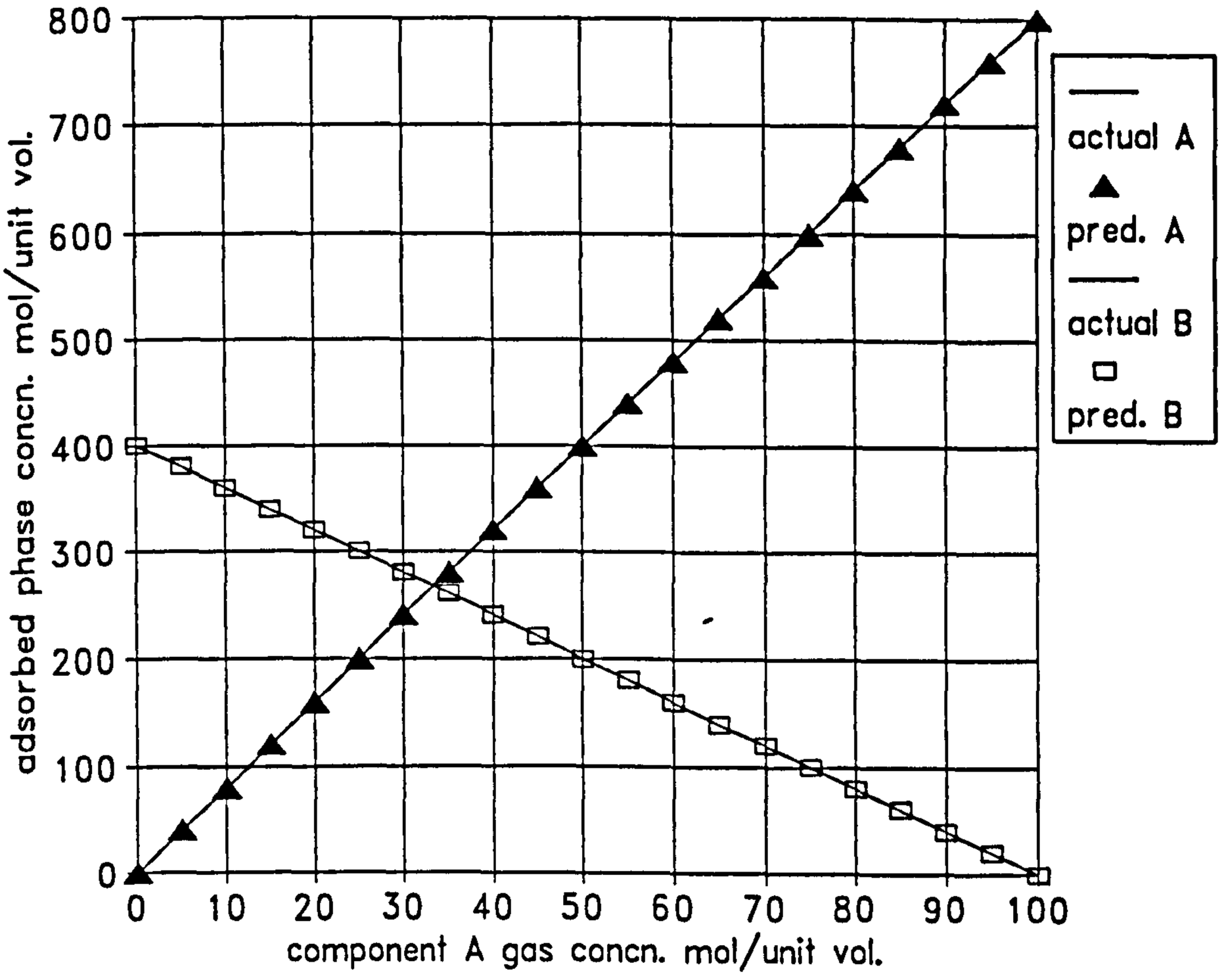

Figure 9.2B Actual and Predicted Binaries for Linear System

9.8.2 Using IAS Predictions

For this case the pure-component isotherms are specified to be of the Langmuir form with the following parameters:

q_{AM} = 800 mole per unit volume
q_{BM} = 400 mole per unit volume
M_A = 1000
M_B = 2000

The IAST predictions for the mixture are shown in Figure 9.3A. From this graph it can be seen that the IAST predictions give binaries with opposite curvatures, with actual adsorbed amounts less than the respective pure-component values. The results of the polynomial simulation are shown in Figures 9.3B and 9.3C. From the first graph, the polynomial fitting of the K values is mediocre since a third-order polynomial cannot cope with the steep gradient and subsequent plateau. Consequently, component B is seen to be over-predicted across the whole range. The predictions for component A show a large under-predicting kink at high mole fraction but fairly good predictions elsewhere.

Figures 9.3D and 9.3E show the errors involved in each integration method. It can be seen that a first-order polynomial is not sufficient to fit either set of gradients and the subsequent integrations are poor. It can be seen that fourth-order polynomials give much improvement over first-order polynomials, although a higher order would be required to attain the same accuracy level as the trapezoidal and Simpson integrations. For component A, the trapezoidal error is seen to occur at the beginning of the isotherm where the steep gradient is located. Also, the Simpson error shows a curious zigzag effect and this may be due to the weighting factors characteristic of this method.

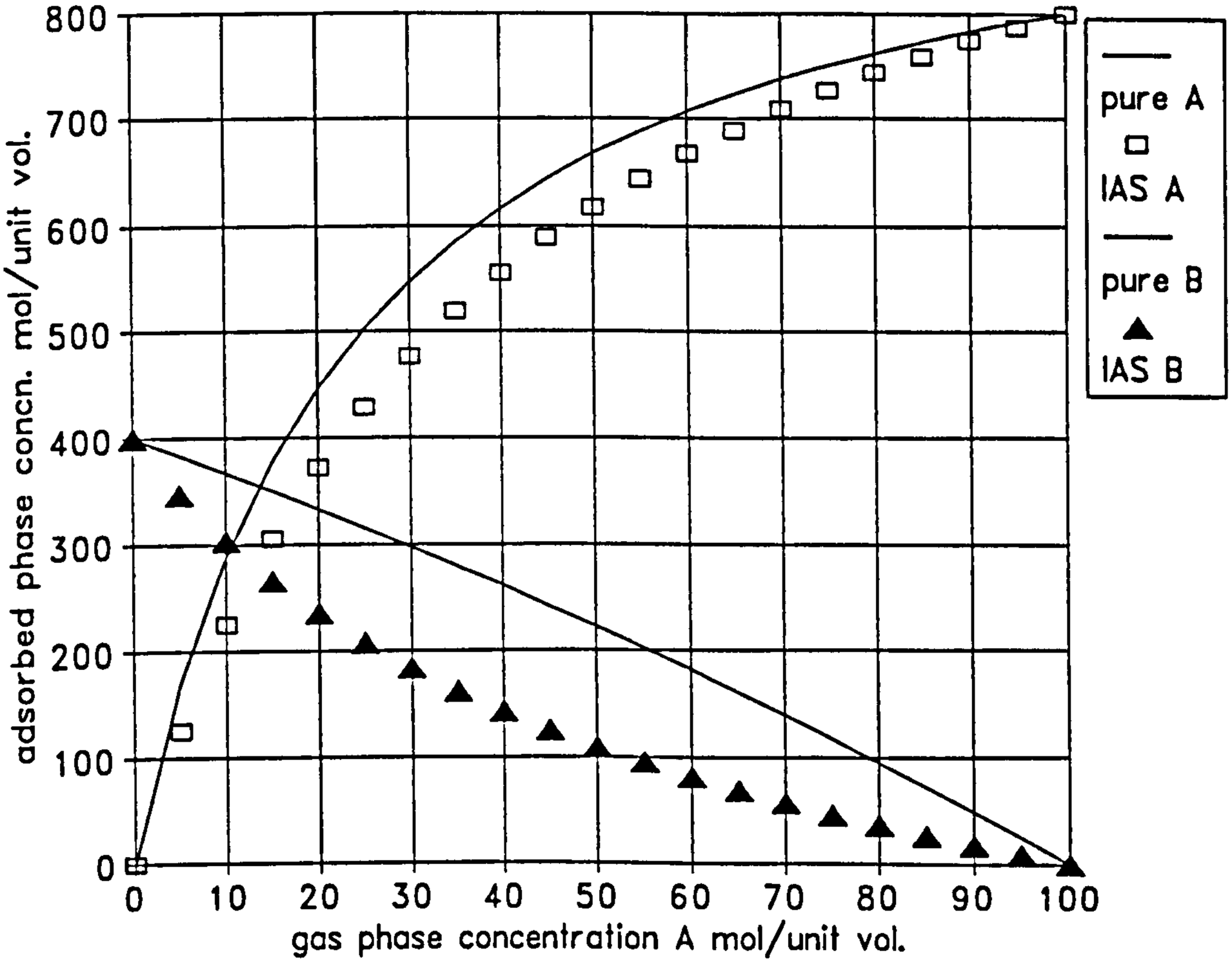

Figure 9.3A Pure-Component and IAST Predictions

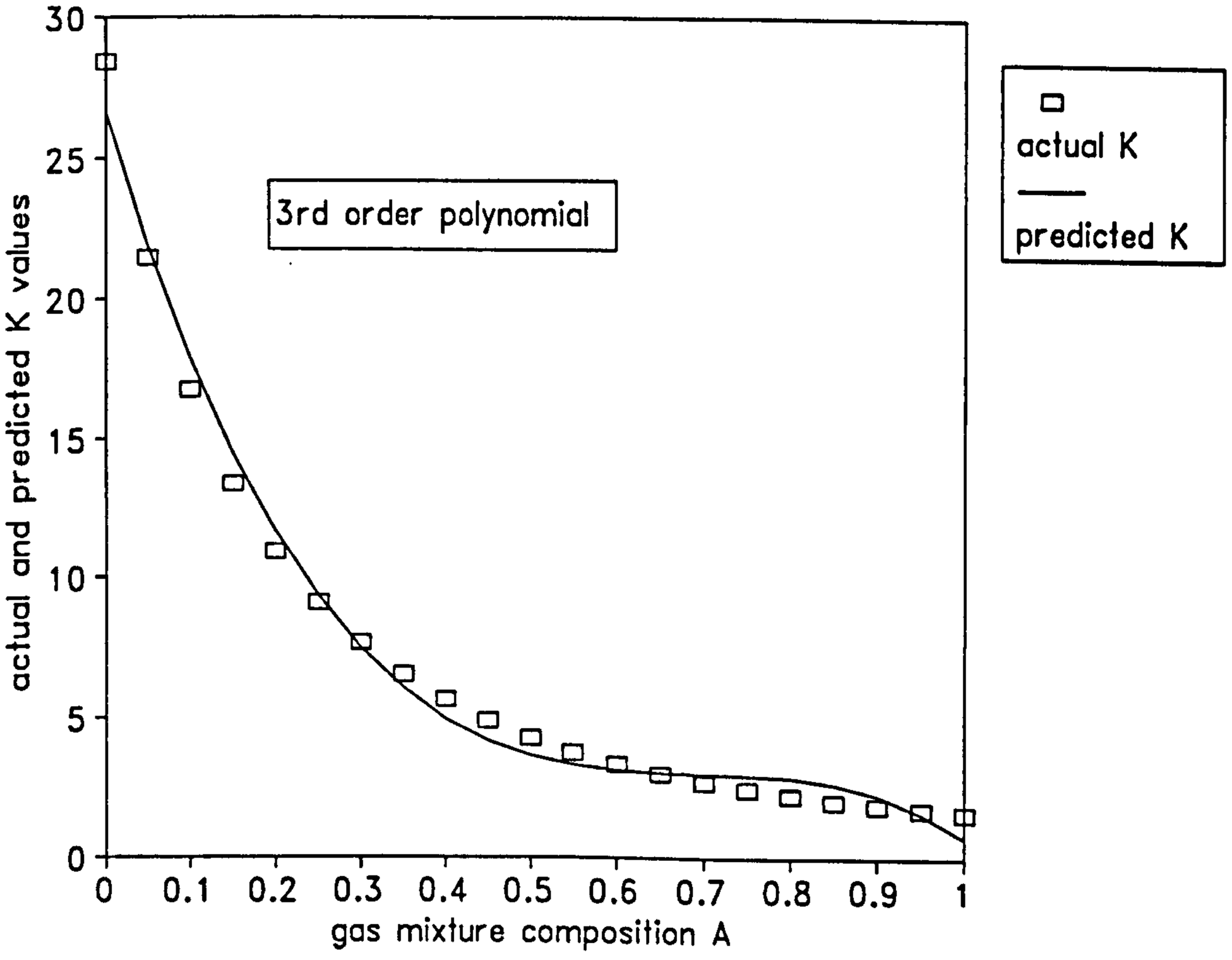

Figure 9.3B Actual and Fitted Values of *K* for IAST System

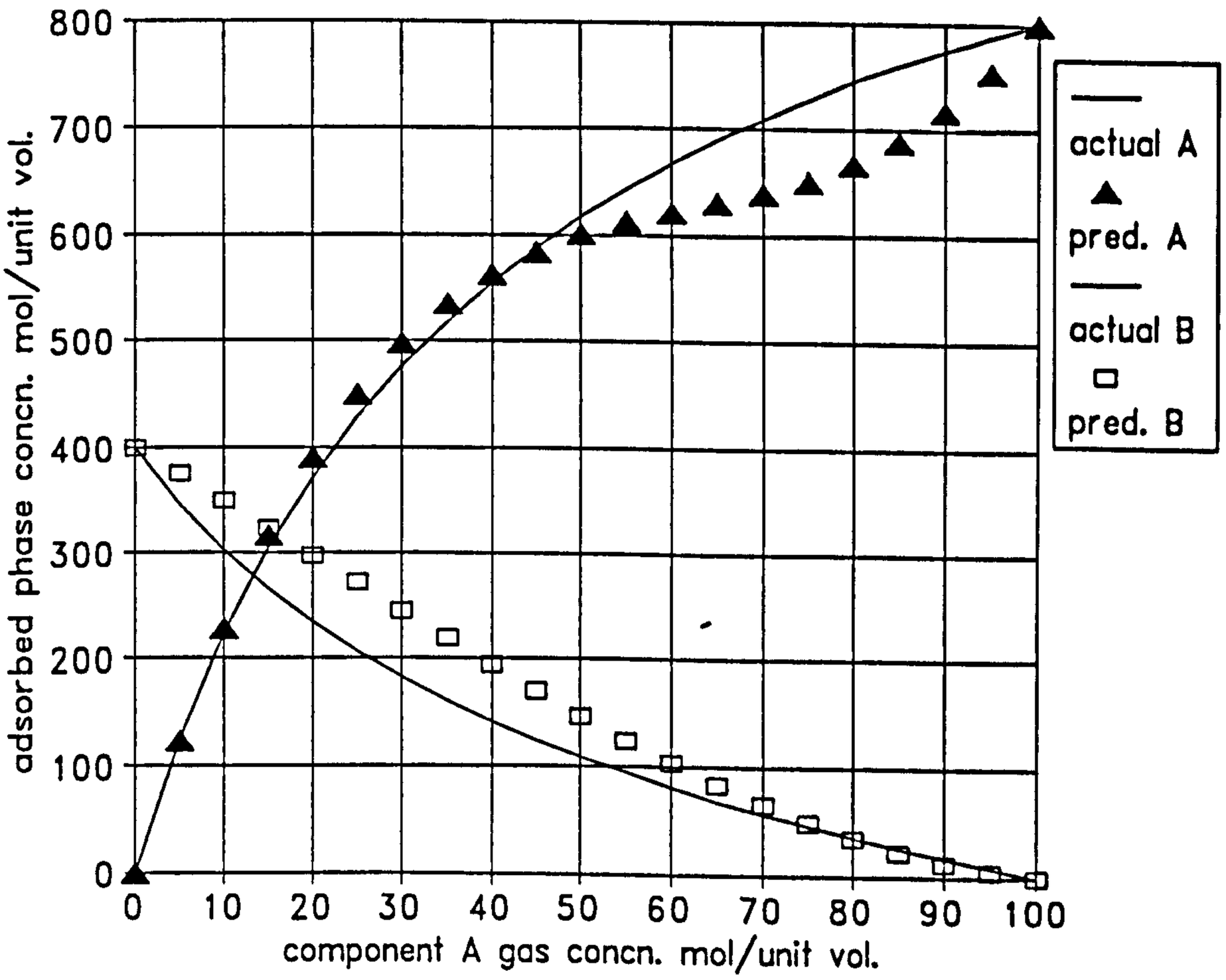

Figure 9.3C Actual and Predicted Binaries for IAST System

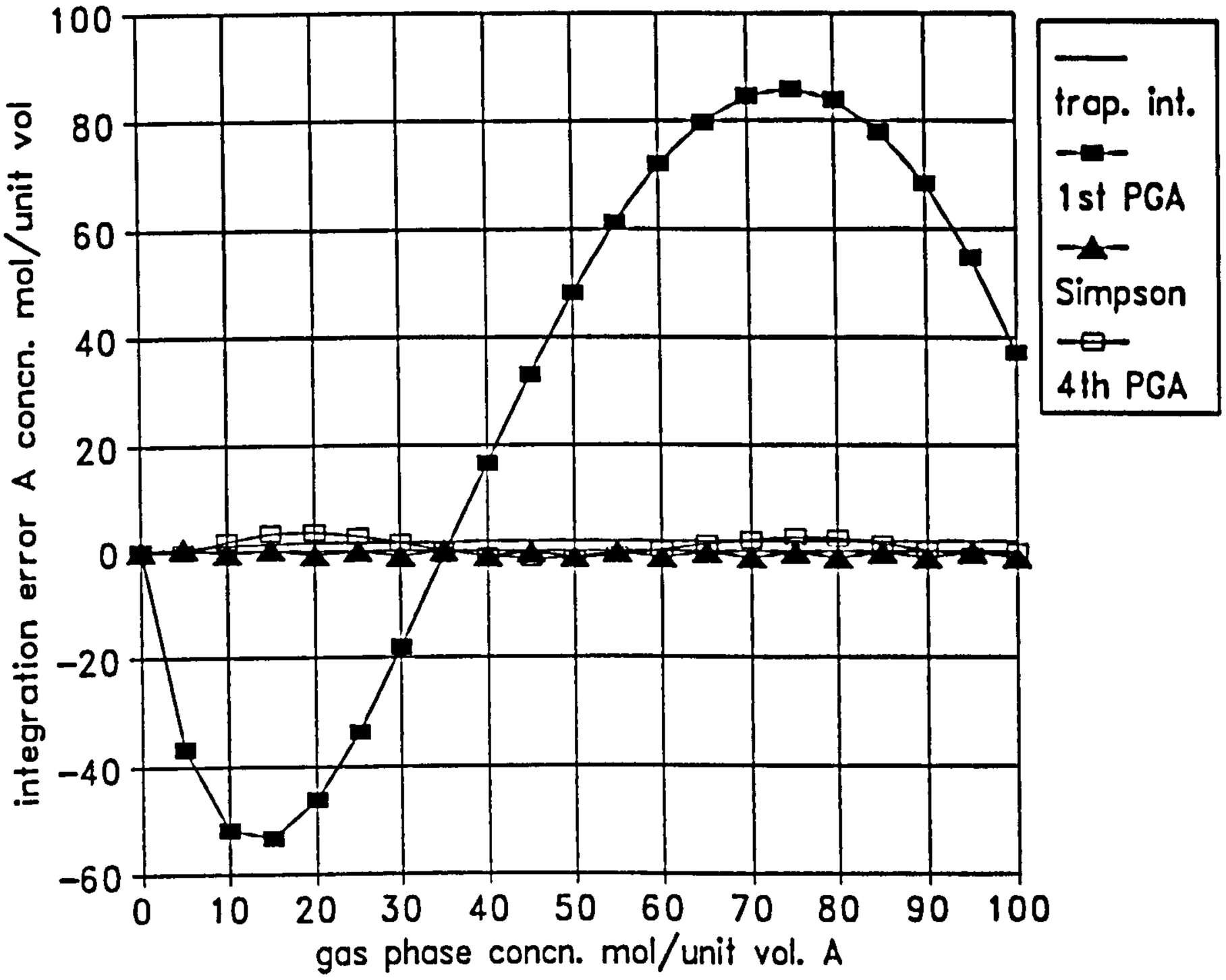

Figure 9.3D Comparison of Methods for Component A Gradient Integration

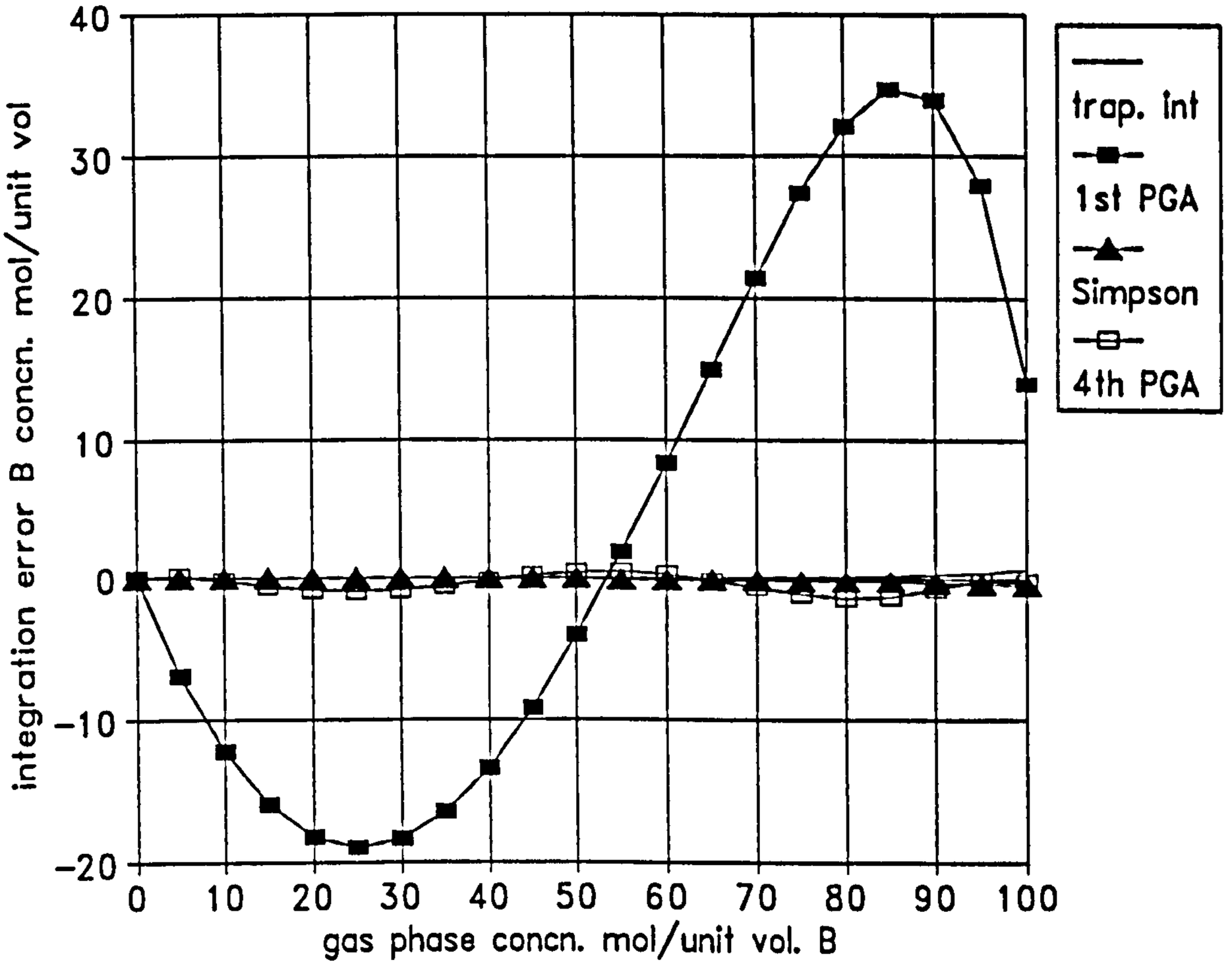

Figure 9.3E Comparison of Methods for Component B Gradient Integration

9.8.3 Binary-Langmuir Theory with Third-Order Fitting I

For this case, the pure-component isotherms must be of the Langmuir form and the following parameters are selected:

q_{AM} = 800 mole per unit volume
q_{BM} = 400 mole per unit volume
M_A = 1500
M_B = 2000

The Binary-Langmuir predictions for the mixture are shown in Figure 9.4A. From this graph, it can be seen that the predictions give binaries of opposite curvature with actual amounts adsorbed less than the respective pure-component values. The more strongly adsorbed component (lower M) gives the concave isotherm shape. The results of the simulation are shown in Figure 9.4B and 9.3C. As can be seen, the third-order polynomial fits the K value much better because of the relatively small curvatures. Consequently, the predictions for both components are very good; the maximum error being around 0.5%. Looking very closely, the predictions for component A show a kink similar in form to that for the IAST case, but much smaller in magnitude. The graphs are not shown, but because

of the small deviation from linearity, trapezoidal integration is sufficiently accurate to obtain both isotherms. Compared to the previous case, a first-order polynomial will give much better gradient fits and subsequent integrations. The Simpson integration is close to perfect.

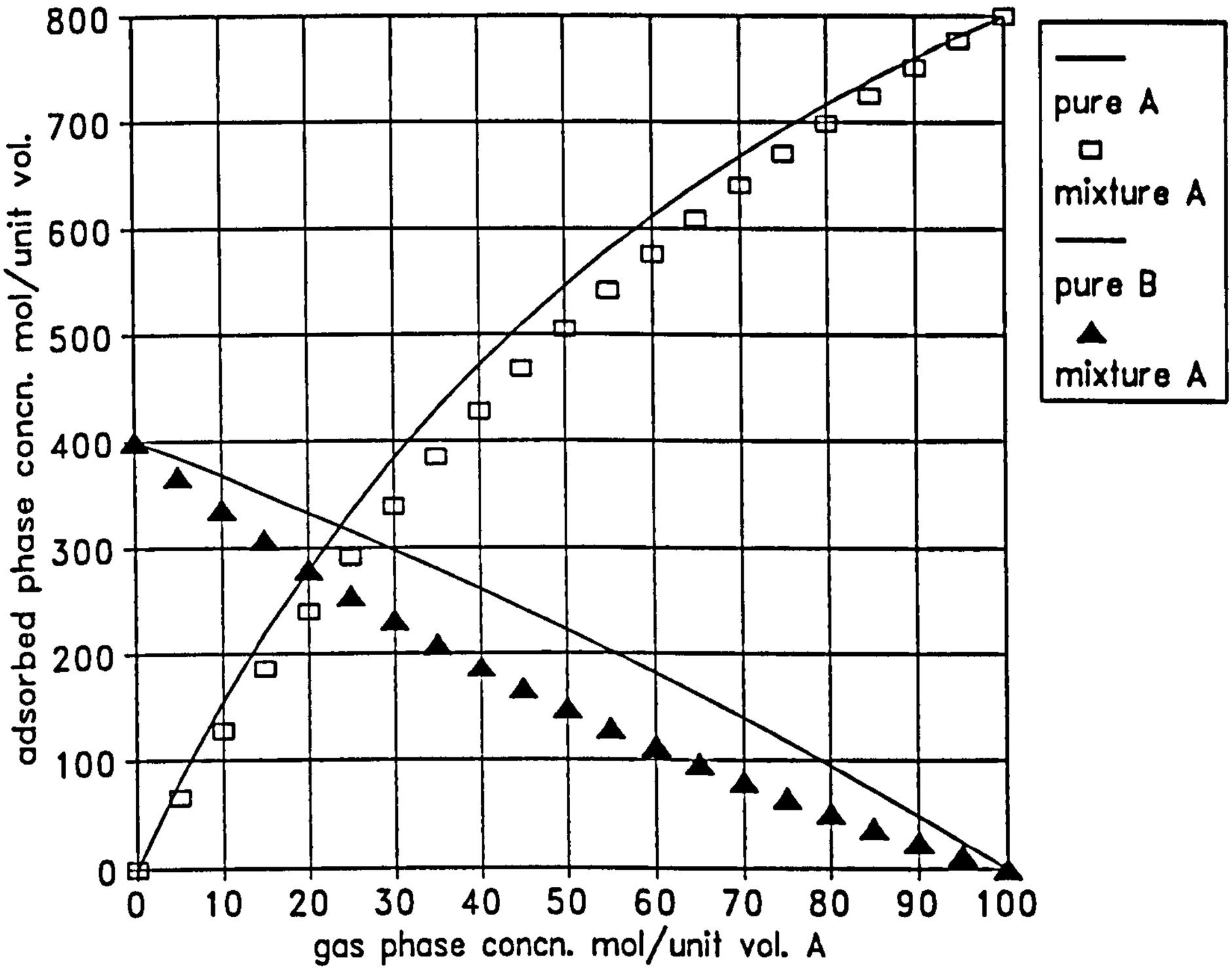

Figure 9.4A Pure-Component and Binary-Langmuir Predictions

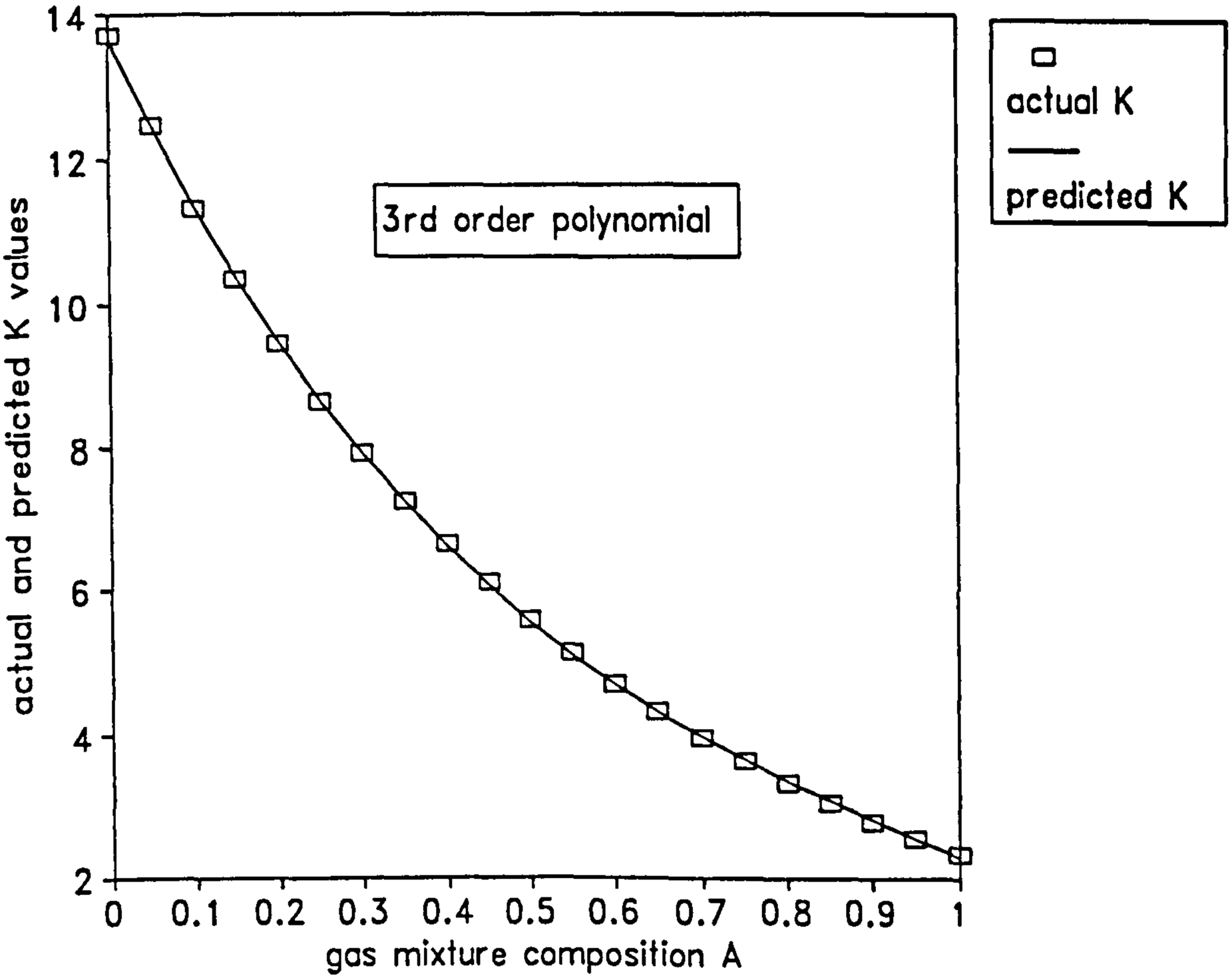

Figure 9.4B Actual and Fitted Values of *K* for Binary-Langmuir System

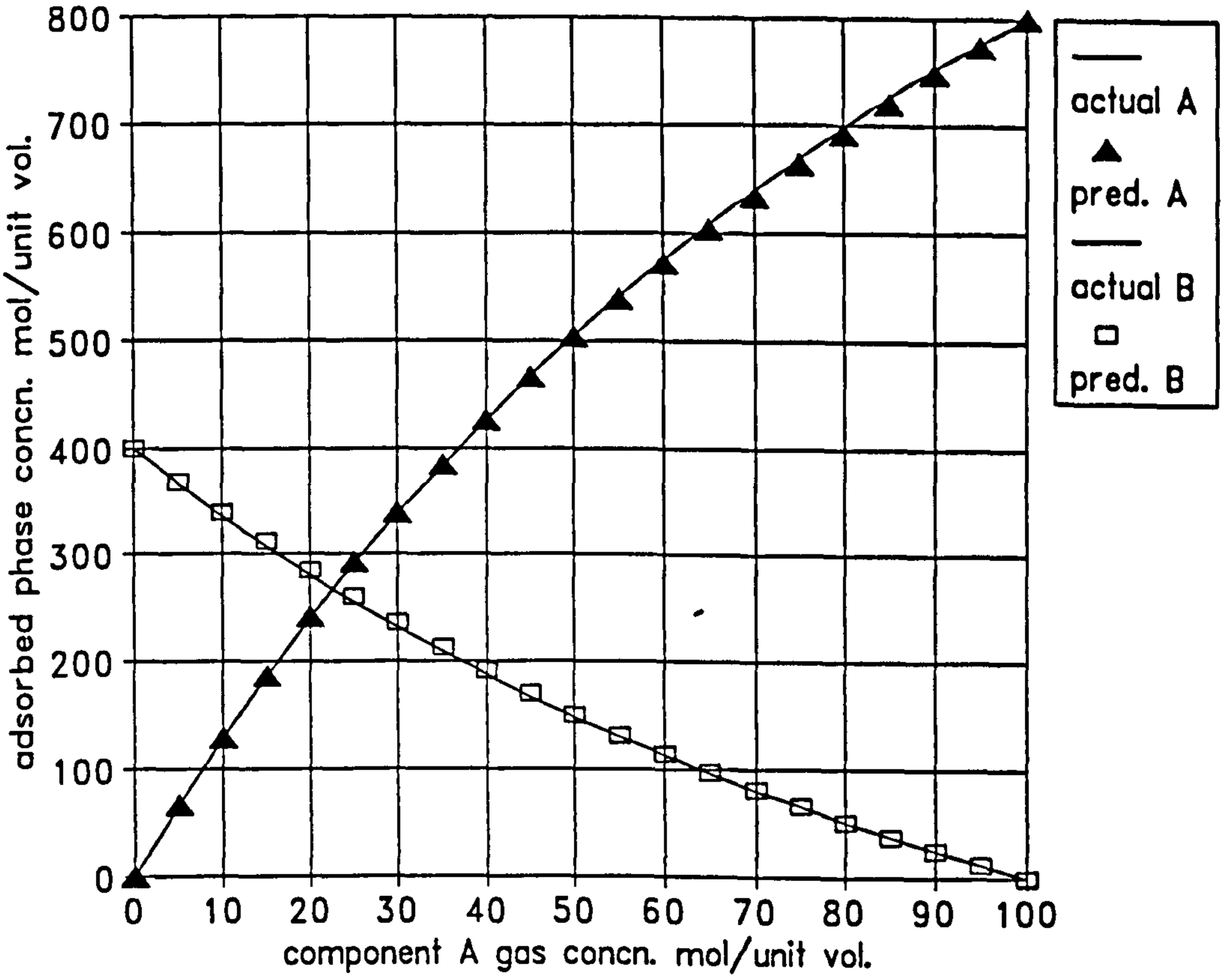

Figure 9.4C Actual and Predicted Binaries for Binary-Langmuir System

9.8.4 Binary-Langmuir Theory with Third-Order Fitting II

Once again, the pure-components must be of the Langmuir form and the following parameters are selected:

q_{AM}= 800 mole per unit volume
q_{BM}= 400 mole per unit volume
M_A = 1000
M_B = 2000

The Binary-Langmuir predictions for the mixture are shown in Figure 9.5A. The mixture predictions are of opposite curvature, although the curvatures are more prominent than the previous case. The pure-component parameters given above are the same as those used for the IAST case, and so the diagrams can be used to compare the theories. The predictions of both theories are similar although there are subtle differences; the binary-Langmuir theory gives higher predictions for component A and lower predictions for component B. Visually, the binary-Langmuir predictions exhibit higher curvatures with the isotherms further apart.

The results of the polynomial simulation are shown in Figures 9.5B and 9.5C. As for the IAST case, the third-order polynomial cannot cope with the steep ascent and subsequent plateau of the variation in K values. Again, component B is over-predicted across the entire range whilst component A demonstrates the kink at high mole fraction. The magnitudes of these deviations are slightly smaller for the IAST case; possibly due to the IAST giving mixture binaries with lower curvatures. The graphs showing the gradient integration for each component are not presented, but because of the increased curvatures, a first-order polynomial is not sufficient to fit either set of gradients. Using a fourth-order polynomial will give much better integrations approaching those of the trapezoidal rule. Once again, the Simpson integration gives the best predictions.

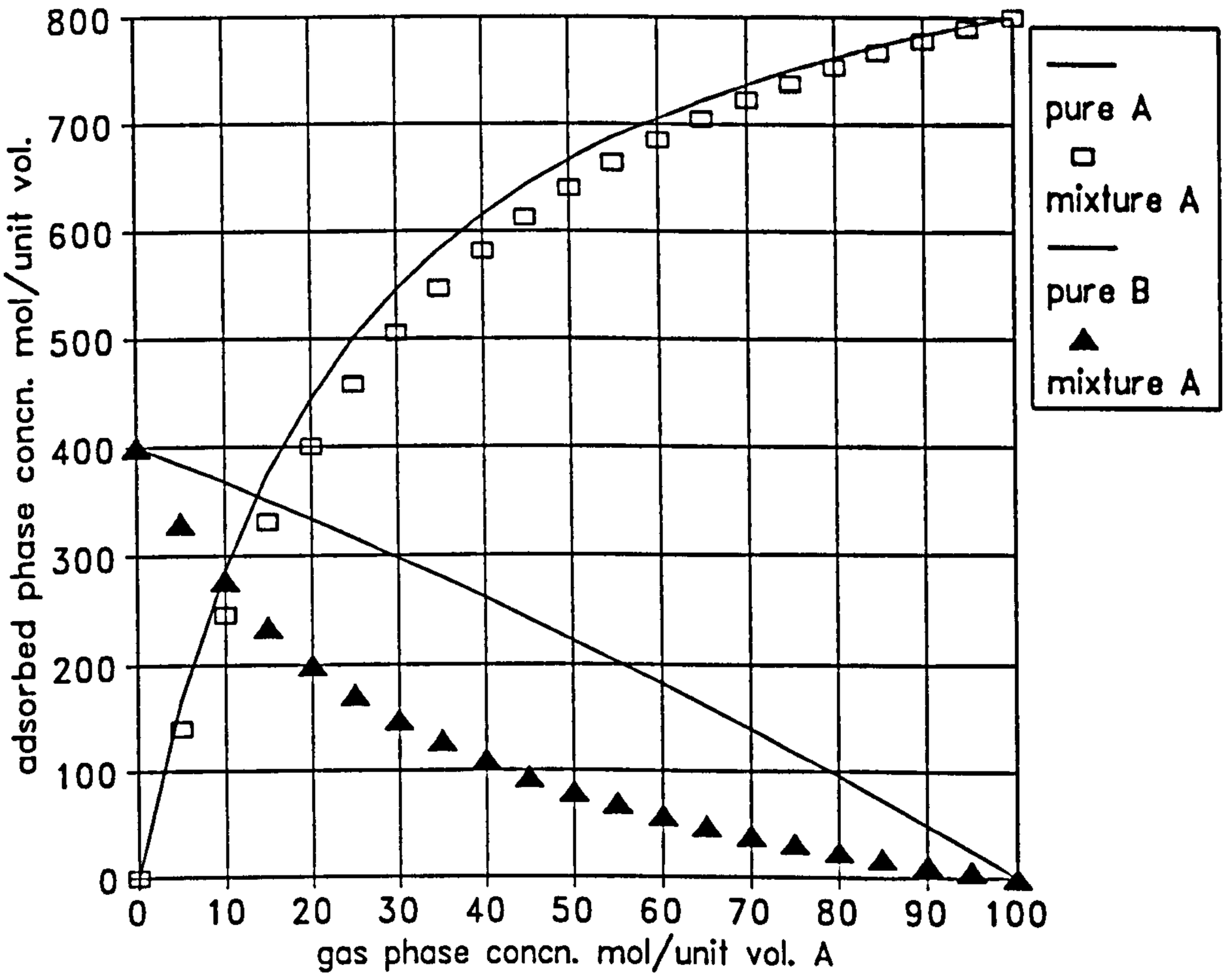

Figure 9.5A Pure-Component and Binary-Langmuir Predictions

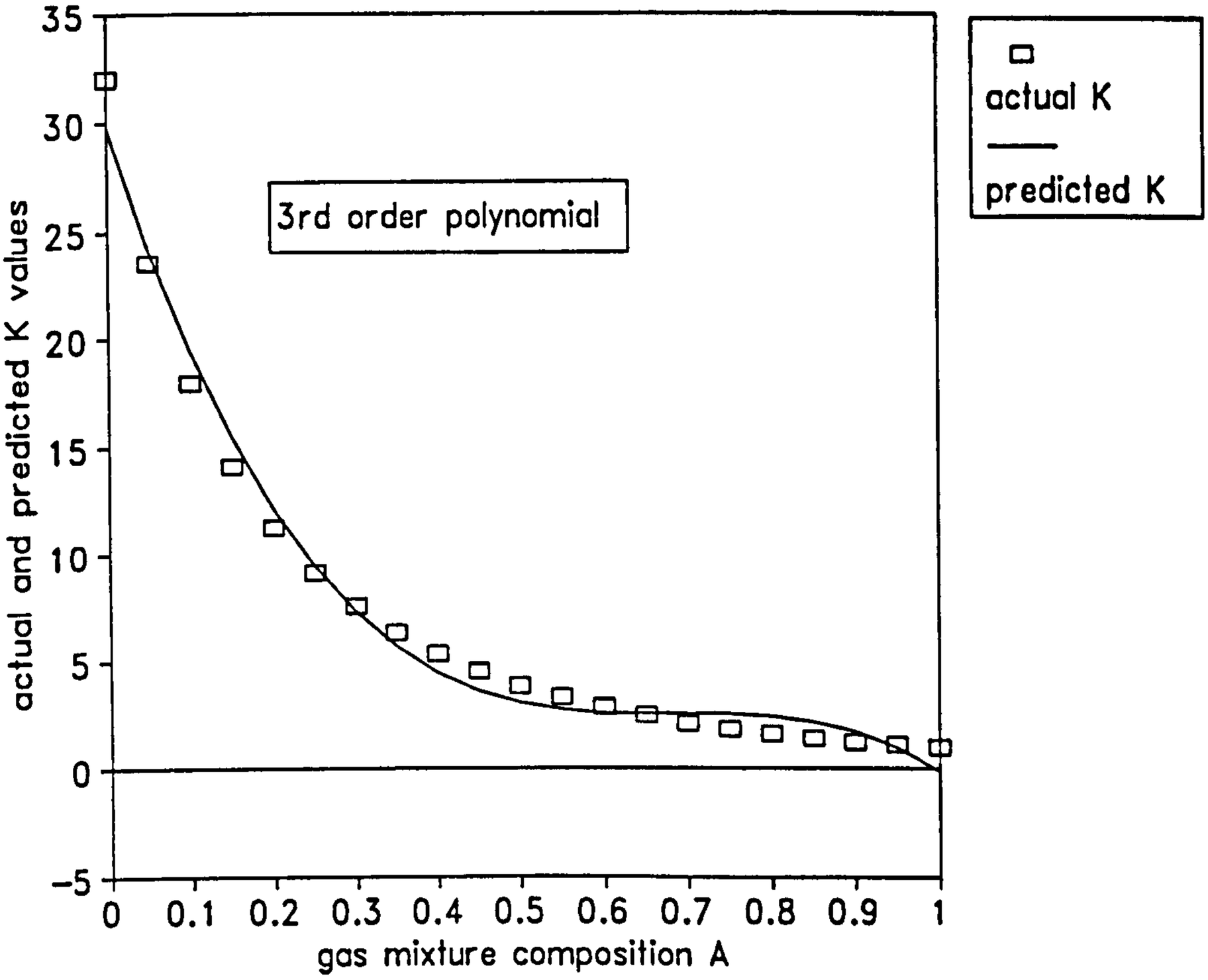

Figure 9.5B Actual and Fitted Values of *K* for Binary-Langmuir System

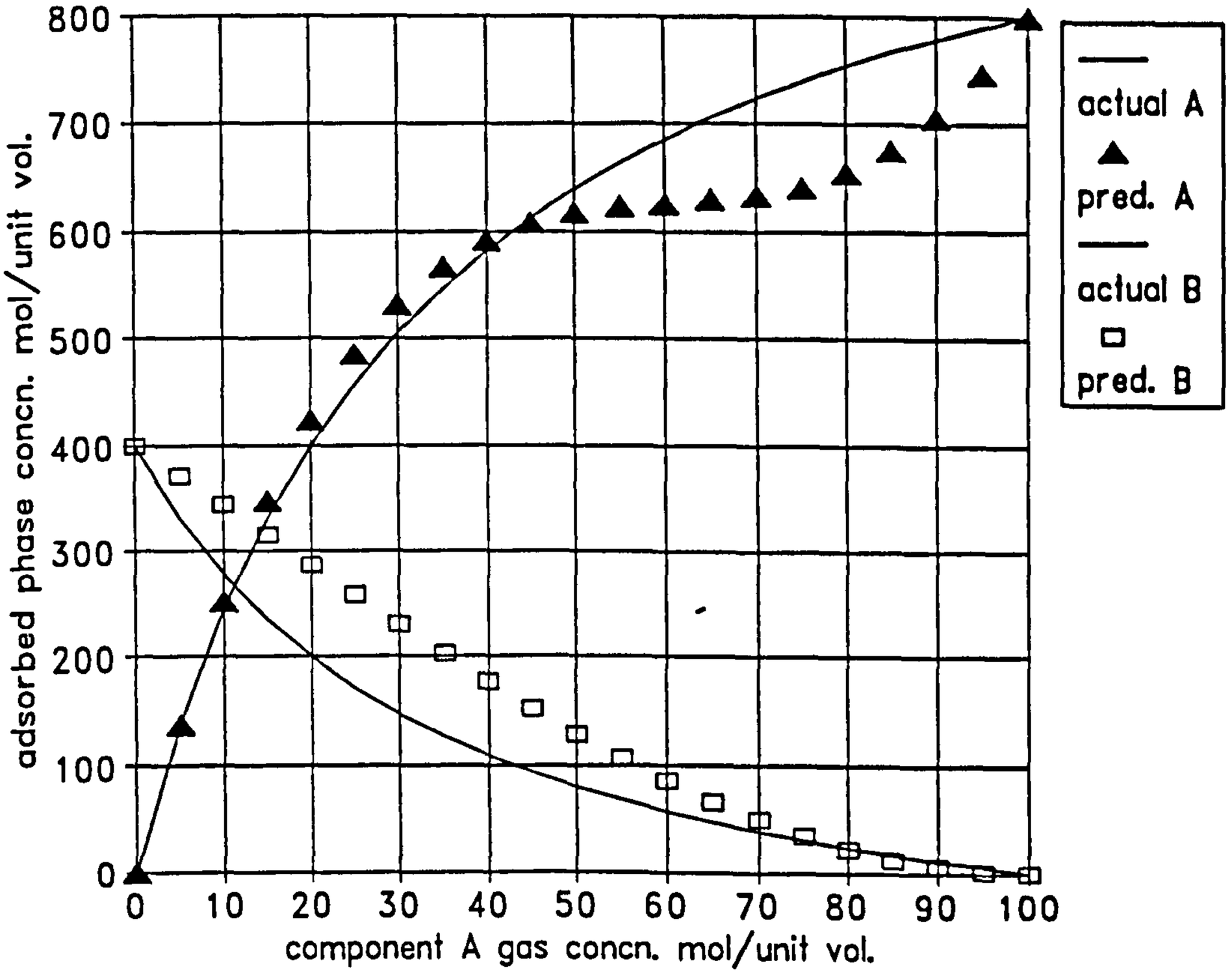

Figure 9.5C Actual and Predicted Binaries for Binary-Langmuir System

9.8.5 Binary-Langmuir Theory with Fourth-Order Fitting

Using the same parameters as Section 9.8.4, Figure 9.6A shows that a fourth-order polynomial gives a much better fitting of the *K* values. From previous discussion on the fourth-order fitting, a *total mixture amount constraint* was employed. The composition specified was 80% component A and the subsequent polynomial predictions are shown in Figure 9.6B and 9.6C. Indeed, Figure 9.6C confirms agreement at the specified 80% composition. The predictions are much better than before. Before using a composition of 80% component A, it seemed logical to employ a composition of 50% component A. However, the predictions were very bad; as the matrix was solved, large values of the unknowns were obtained giving ridiculous isotherm values. Obviously, the system found it unreasonable to have this constraint at 50% and this caused bad predictions elsewhere. This problem was not noticed at any other compositions. Also the simulations were repeated but with the *component A amount constraint*. For this case, there was no problem at 50% composition. Specifying at a high composition was useful in eliminating the characteristic kink for component A. Thus, although in principle a fourth-order fitting can improve the predictions great care must be taken with the choice of constraint. From the above case, a *total* constraint can cause problems although this may be specific to the system type. Further investigation should be carried out before making any conclusions.

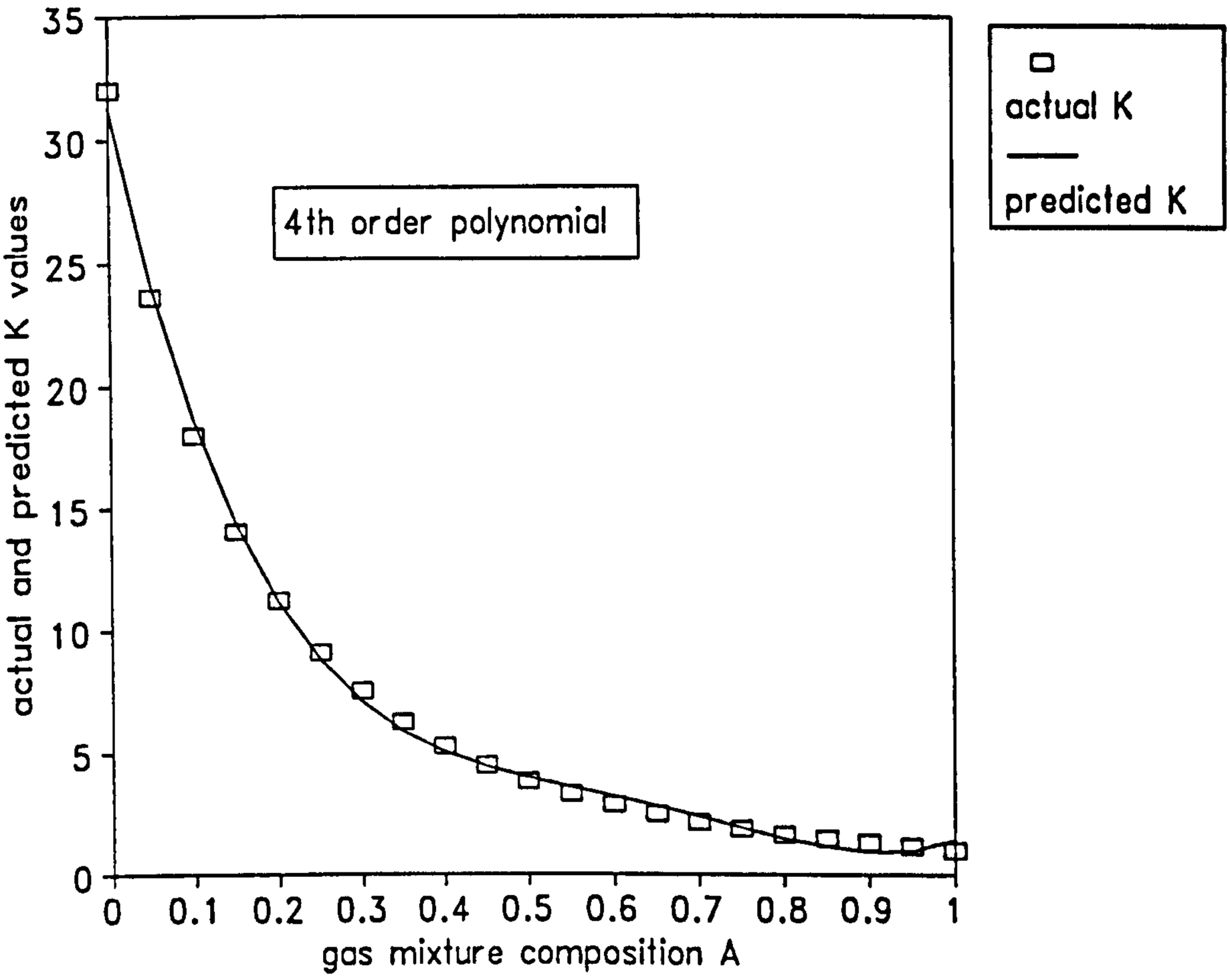

Figure 9.6A Actual and Fitted *K* Values for Binary-Langmuir System

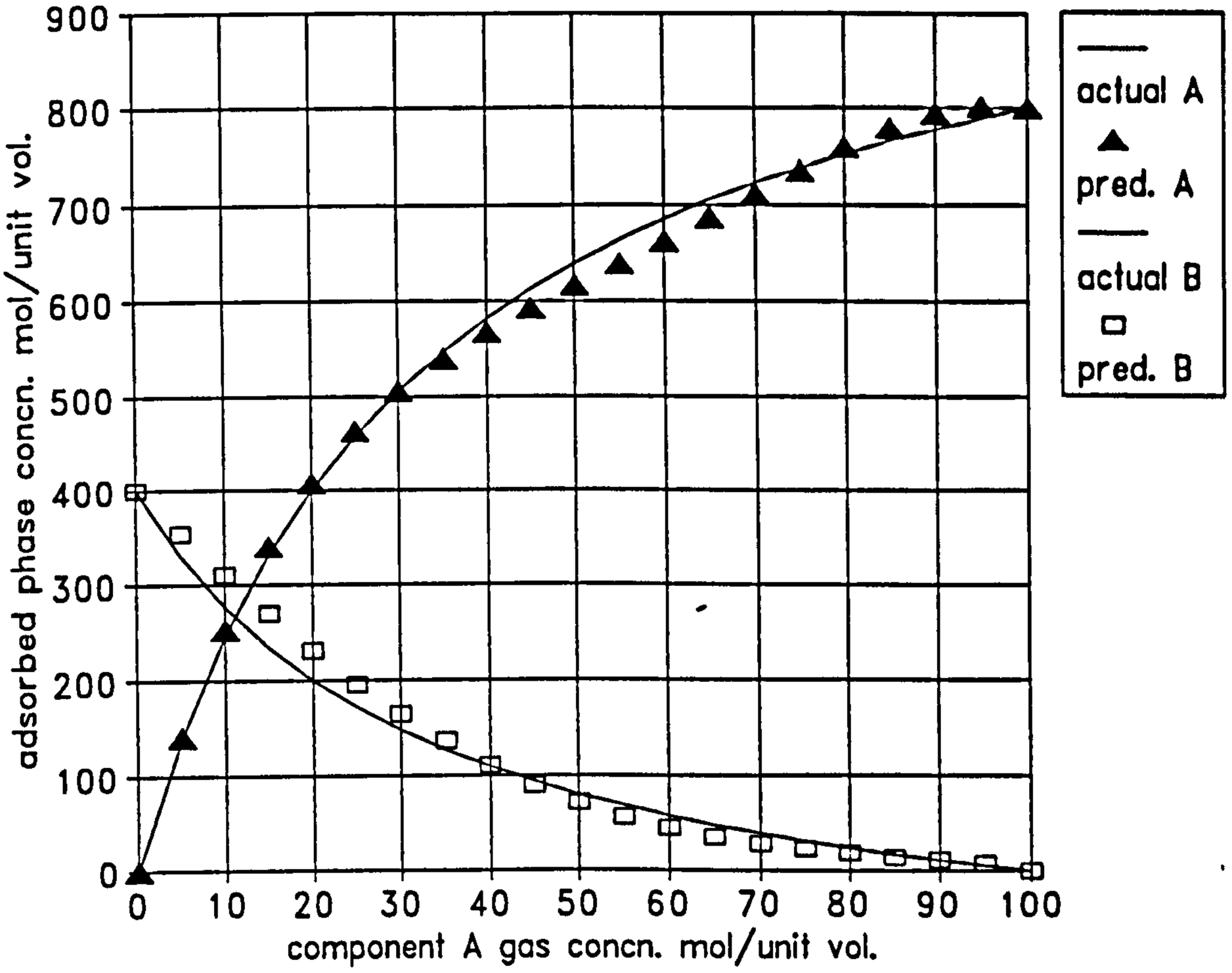

Figure 9.6B Actual and Fitted Binaries for Binary-Langmuir System

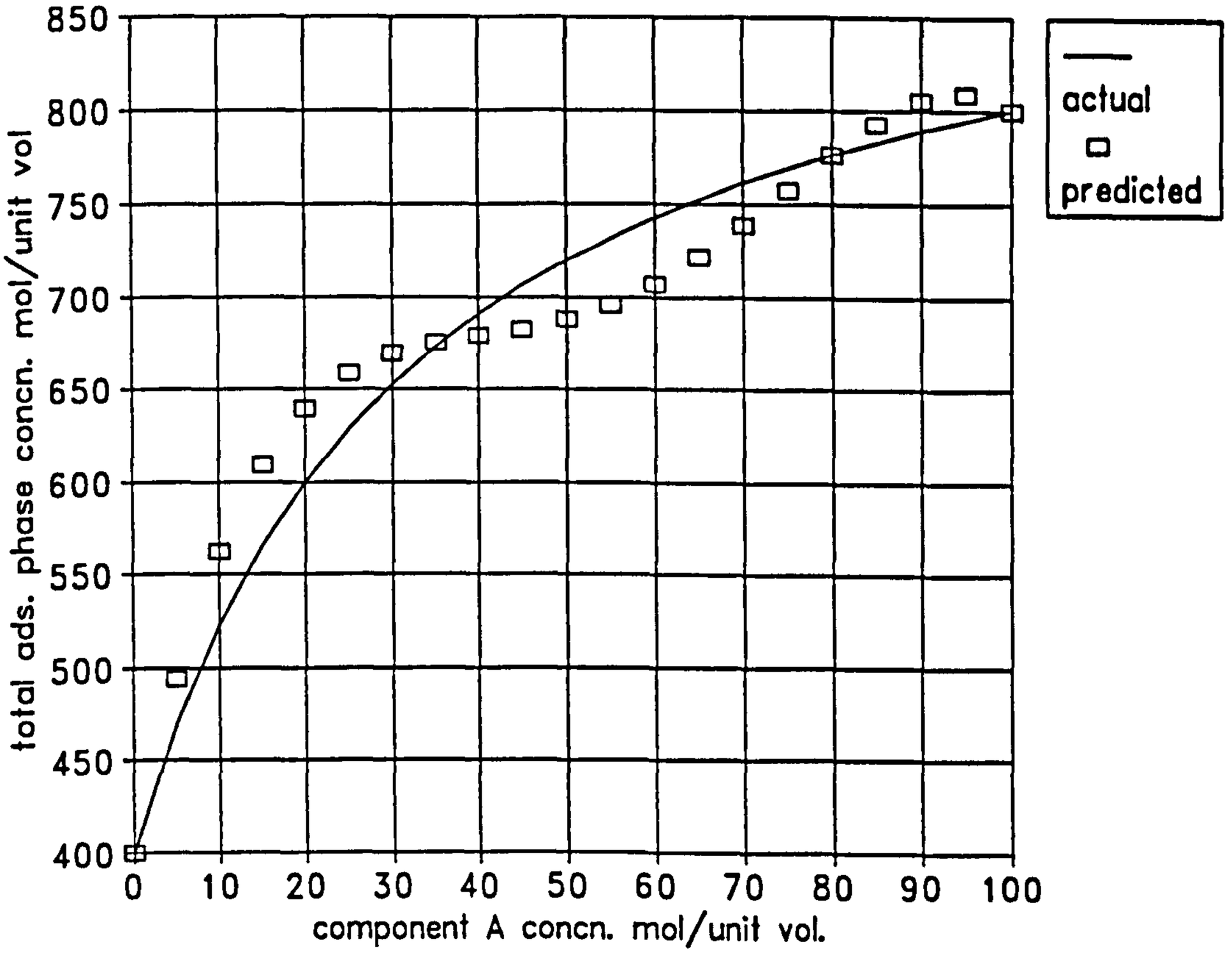

Figure 9.6C Actual and Predicted Total Amounts for Binary-Langmuir System

9.8.6 Using RAST Predictions

This case will show how non-ideality in the adsorbed phase can affect the predictions of the polynomial method. The pure-component isotherms will be the linear system discussed previously. The Margules coefficients are chosen to be:

$A = -0.5$

$B = -0.5$

Choice of these values will give a symmetrical variation of activity coefficient with composition. Values such as above will give moderate degrees of non-ideality. From previous simulations, when the values of A and B go beyond unity, the RAST predictions take unrealistic shapes and azeotropes can be formed. The activity-coefficient variations can be represented by Figure 9.7. The RAST predictions are shown in Figure 9.8A and it can be seen that both isotherms are predicted to be concave to the composition axis; that is the RAST gives higher predictions than the IAST. This is qualitatively the same result reported by Glessner and Myers (1969), although they did not have linear pure-component isotherms.

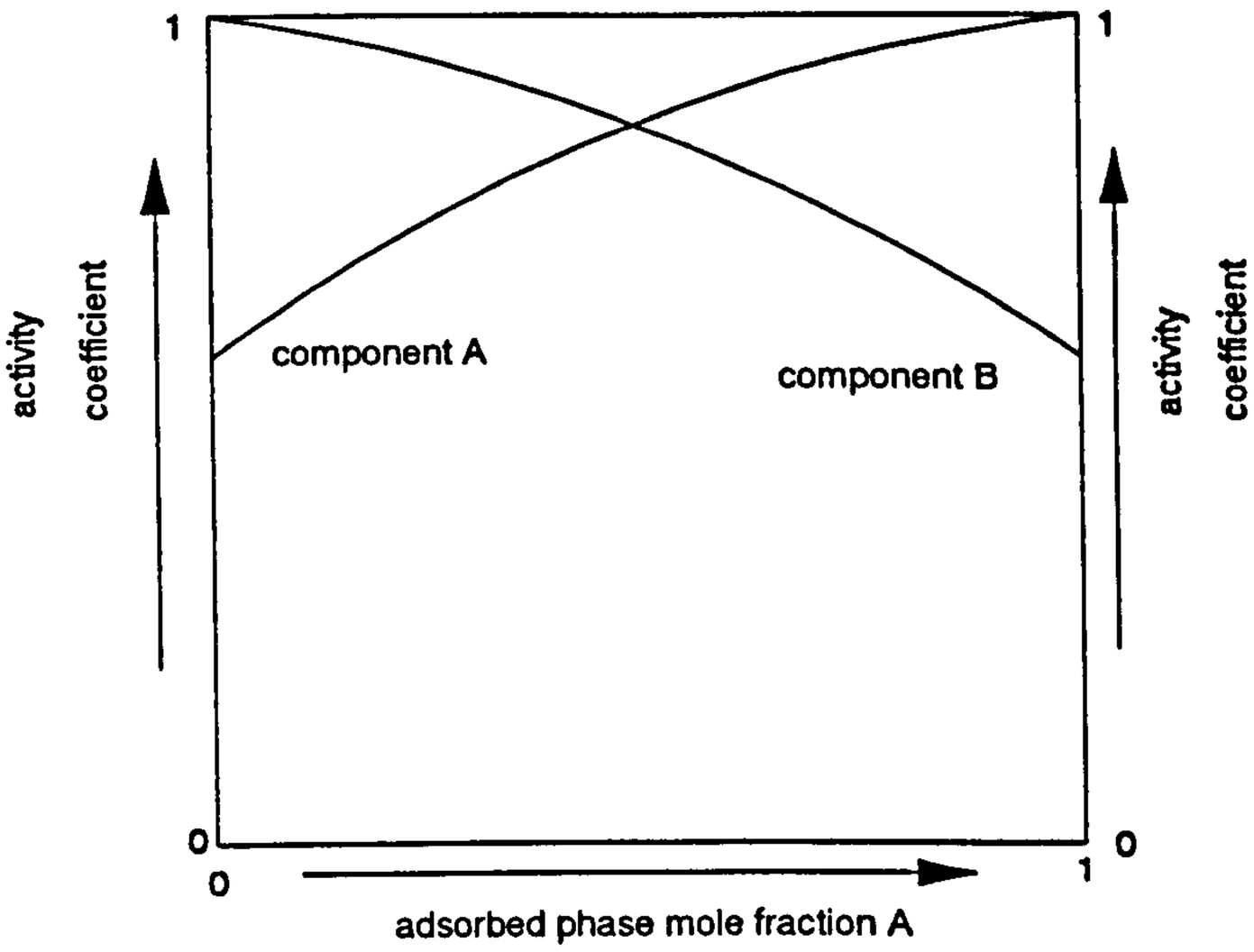

Figure 9.7 Activity Coefficient Variation for A = B = -0.5

The results of the simulation are shown in Figures 9.8B and 9.8C. As can be seen, the set of K values has a minimum and the third-order polynomial only gives an average fitting. Despite this average fitting, the binary predictions are really quite good; component B is slightly over-predicted whilst component A demonstrates the small characteristic kink towards high mole fraction region. The graphs showing the gradient integration of each component are not presented, but once again a first-order polynomial is not sufficient to fit either set of gradients; the non-idealities cause initial isotherm steepness. Both the trapezoidal and Simpson integrations are good. To obtain the same agreement, a fifth-order polynomial would be required.

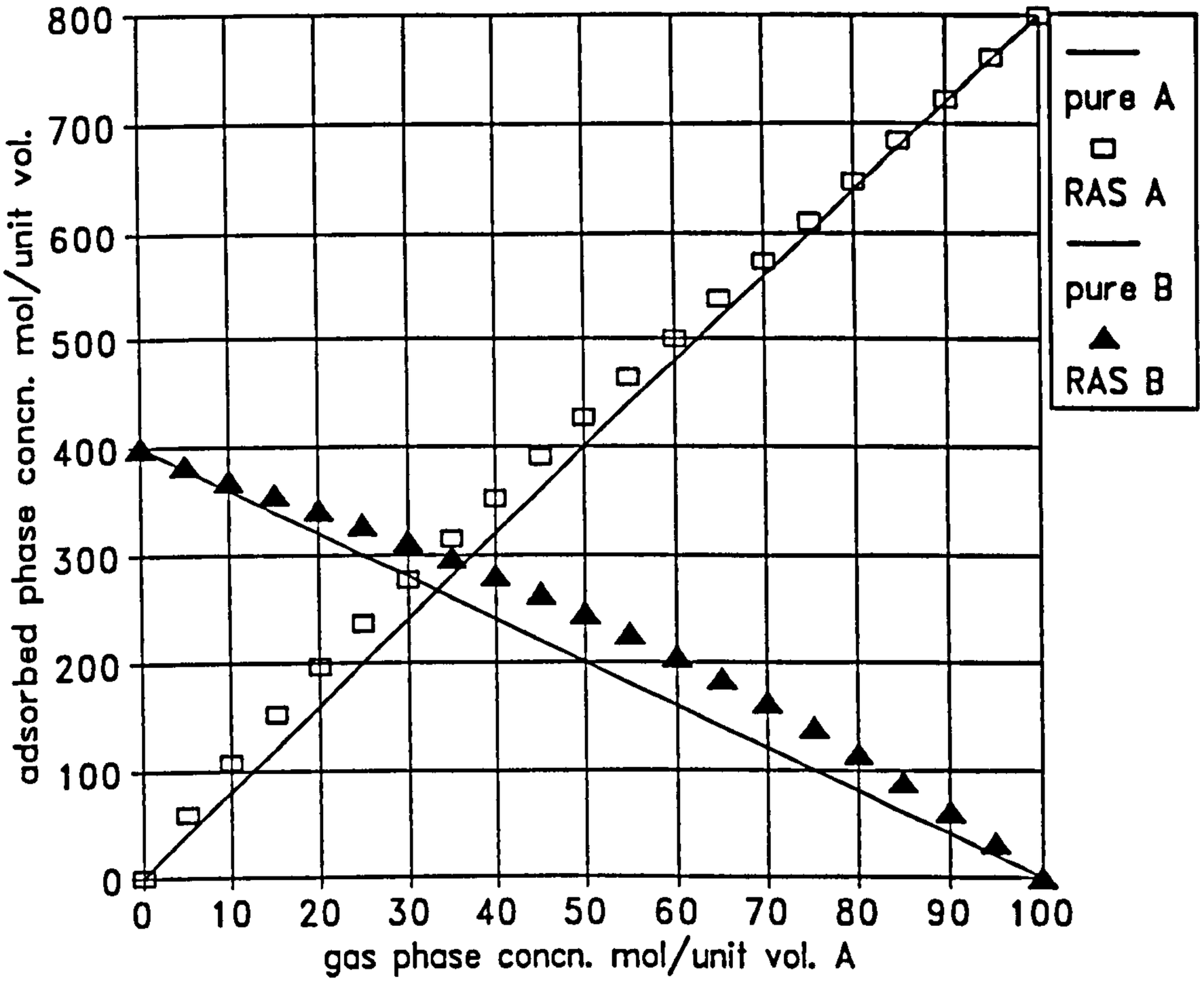

Figure 9.8A Pure-Component Isotherms and RAST Predictions

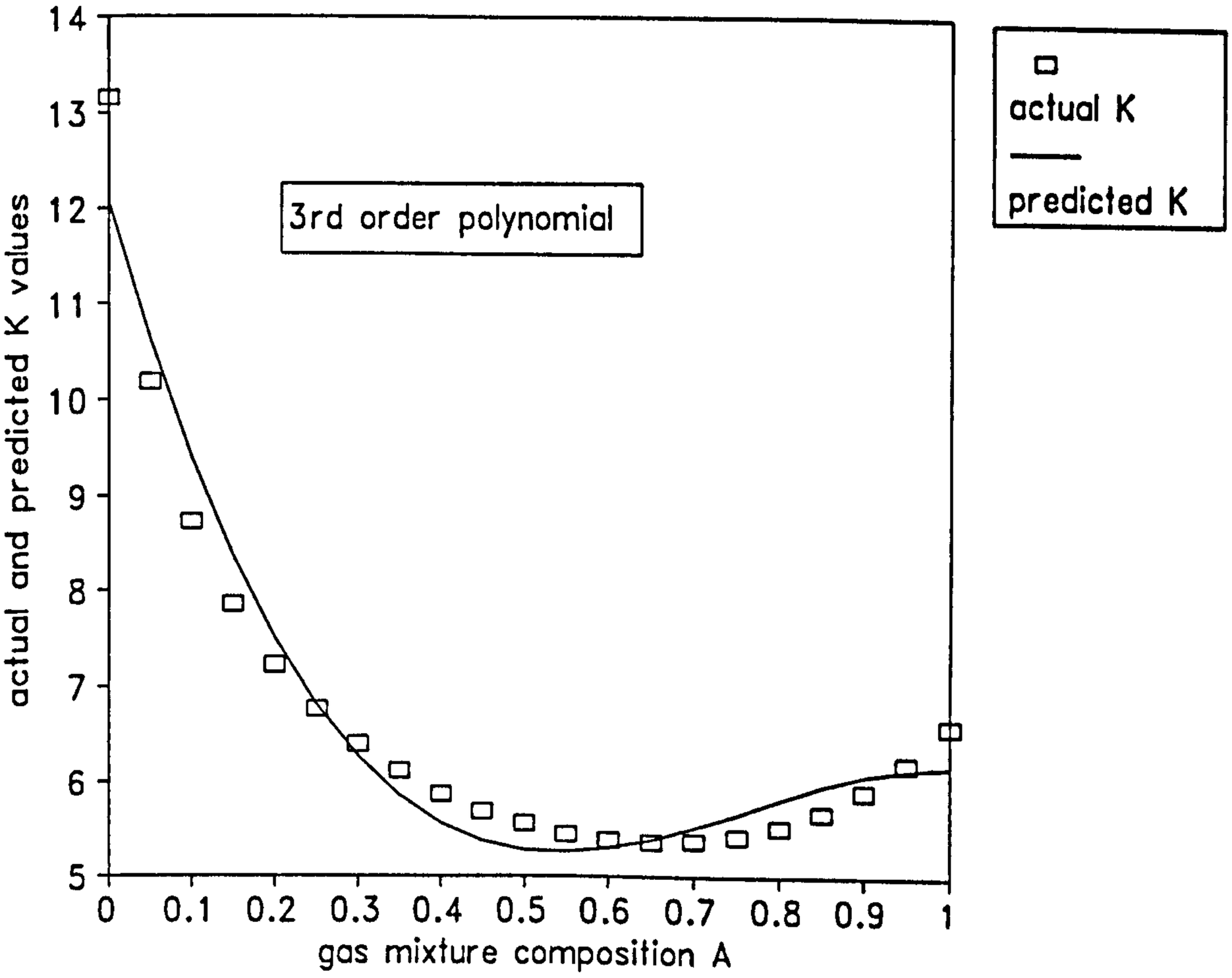

Figure 9.8B Actual and Fitted Values of *K* for RAST System

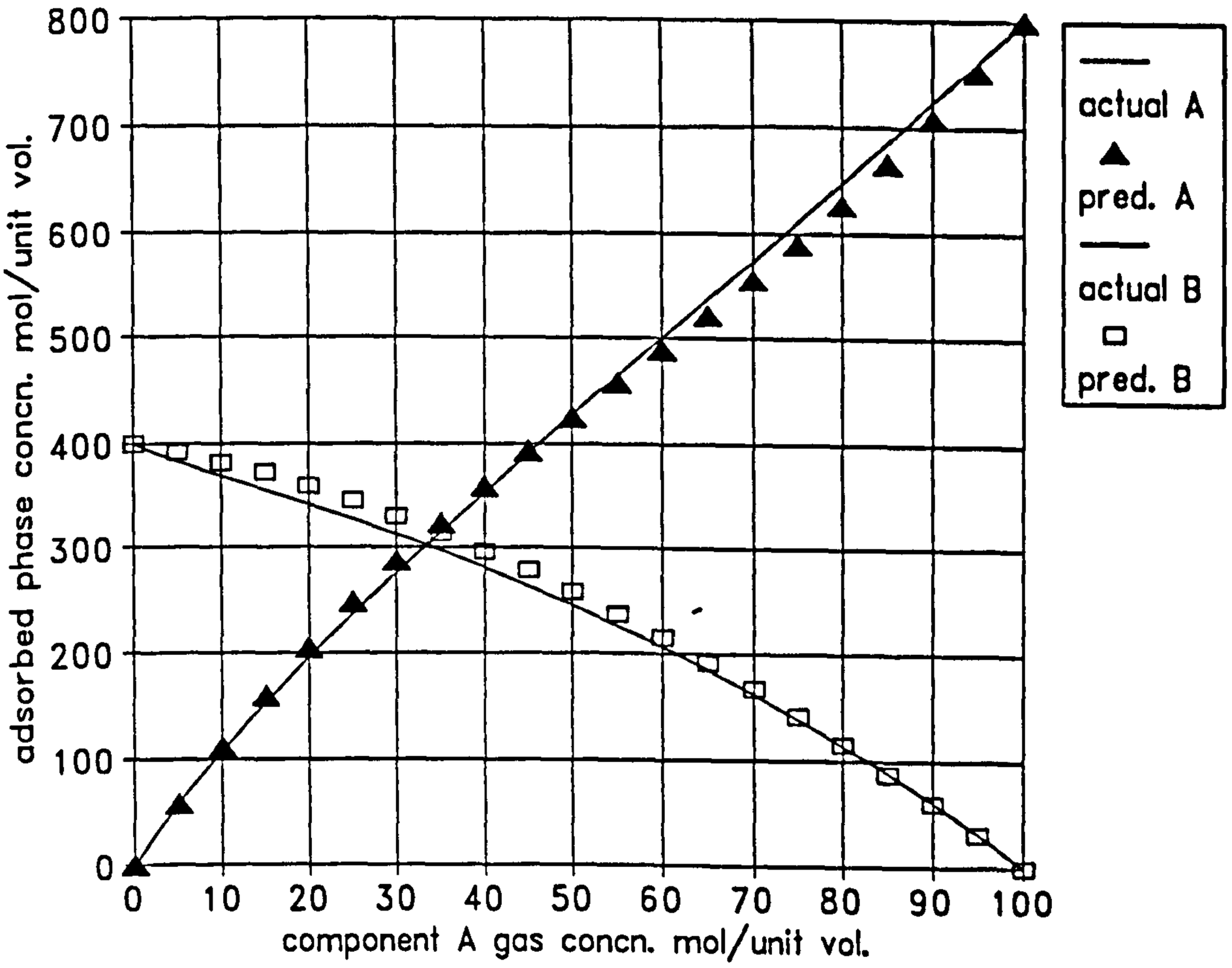

Figure 9.8C Actual and Predicted Binaries for RAST System

9.8.7 Significant Column Pressure Drop

This case utilises the linear system previously employed and the relevant pressure ratio used is:

$$\frac{\Delta P_C}{P_{COUT}} = 0.05$$

This is a reasonable value and is roughly that obtained in the project equipment. For perturbation gas A the resulting set of K values is fitted perfectly, and those for perturbation gas B are fitted to from 1-2%. The final isotherm predictions can be represented by the following table:

Table 9.1 Effect of Column Pressure on Final Predictions

	component A		component B	
prtbn	min%	max%	min%	max%
A	+0.2	+1.3	+0.5	+6.0
B	-0.5	-9.0	-0.4	-2.0
mean	-0.1	-0.6	+0.2	+2.0

As can be seen, a significant column pressure-drop will impose positive errors for perturbation gas A and negative errors for perturbation gas B. As the name suggests, the *averaged* column values are formed by obtaining the mean of the values calculated using each perturbation gas. An experimenter might conceivably use an average upon noticing disparities of up to 7%. Interestingly, the table shows that using perturbation gas averages reduces but does not eliminate these systematic errors.

9.8.8 Conclusions from Hypothetical Results

The success of this method requires the polynomial to adequately fit the set of K values. For some systems this is possible with a third order polynomial, but for others a higher-order polynomial is required, and then care must be taken to select a suitable mixture constraint. Thus, systems having binaries closer to linearity will always be better predicted. Alternatively, systems with smaller binary-gradient ranges will be more amenable to the method. Thus, there may be some correlation between the first derivative of the gradient and the success of the method. For a straight line, the first derivative of the gradient will be zero.

9.9 Application of Program to Literature Cases

9.9.1 CO-CH_4 on BPL Activated Carbon

This case has already been discussed in the literature review in Section 9.5.4. Not unexpectedly, the data is presented in a dimensional form and to convert the gradients to a dimensionless form would require a knowledge of the pellet density and the voidage. The general shape of the binaries is shown in Figure 9.9. From the general shape, comparison with the hypothetical results would suggest that this system could be represented by the binary-Langmuir theory; the isotherms have opposite curvatures. However, because of the relatively small curvatures, relatively large values of M_A and M_B should be employed. The subsequent range of K values can easily be fitted by a third-order polynomial, and thus the program simulation confirms the literature conclusion that this system is well suited to the polynomial method.

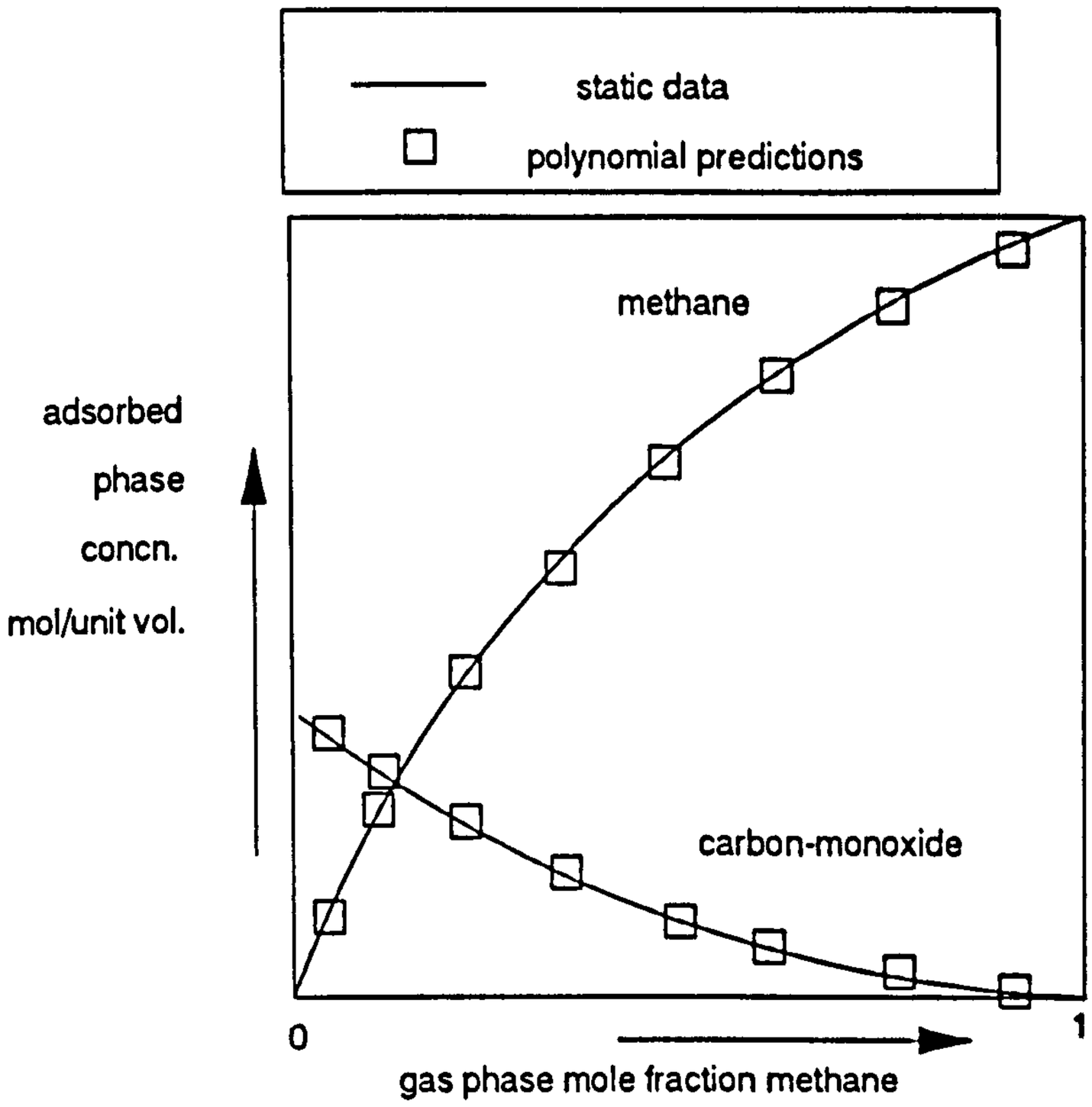

Figure 9.9 General Shape of Literature System Binaries

9.9.2 $iC_{10}H_4$-C_2H_4 on 13X Zeolite

Once again, this case has already been discussed in the literature review in Section 9.5.4. Again, to convert the data to the dimensionless form would require a knowledge of the pellet density and voidage. The general shape of the binaries is shown in Figure 9.10. From the peculiar shape of the isotherms, it is evident that these could not be predicted with either the Binary-Langmuir or IAST theories; indeed, the system has an azeotrope. It is much easier if the binaries are specified directly. Both binaries have points of inflexion and non-zero initial gradients. The binaries can be represented by adding a Langmuir term to a Langmuir-Freundlich term. For the ethylene term the behaviour is predominantly Langmuir-Freundlich whilst for the other it is predominantly Langmuir. Then, the program option allows the initial and final gradients to be specified. Inputting these parameters produced a good representation with an azeotrope close to the specified position.

From the program simulation, the set of K values are of the correct shape and the fitting is average. The fitting of the K values is shown in Figure 9.11A and Figure 9.11B shows the polynomial prediction of the binary system. Figure 9.11B agrees with the literature in that the polynomial predictions are fairly good considering the presence of an azeotrope. However, there are differences regarding the directions of these deviations between the actual and predicted isotherms. From Figure 9.11B, the predictions for component A are

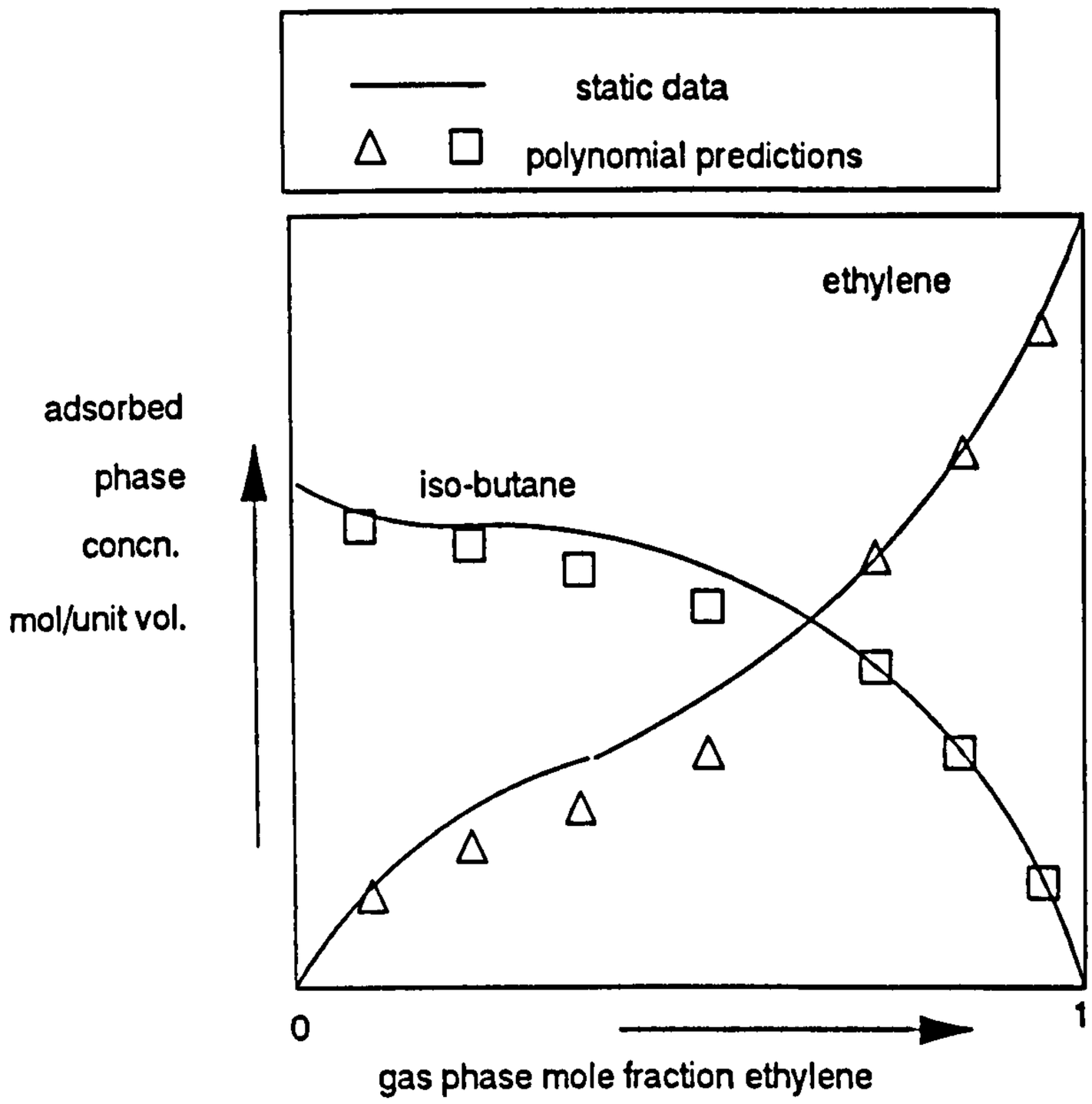

Figure 9.10 General Shape of Literature System Binaries

average up to about the 45% A mixture, and for component B the predictions are good up to about the 40% B mixture. For component A, above the 45% A mixture the polynomial method *under-predicts* the actual isotherm. For component B, above the 40% B mixture the polynomial method *over-predicts* the actual isotherm. For comparison purposes, component A is i-C_4H_{10}. Conversely, the authors show a graph in which the predictions are good for *both* isotherms up to 40% A (the *initial* part of isotherm A and the *final* part of isotherm B). In the composition region above 45% A, the polynomial method is seen to *over-predict* both isotherms. Figure 9.11C shows the phase diagram, and it can be seen the actual set of adsorbed phase composition x_A values crosses the $x_A=Y_{AO}$ diagonal at 65% A; this indicates the presence of an azeotrope. Hence, by independently specifying the binary mixture isotherms, it is possible to define azeotropic systems. The simulation would suggest that for the *defined system*, the polynomial method is able to predict an azeotrope, albeit at a reduced composition of 55% A.

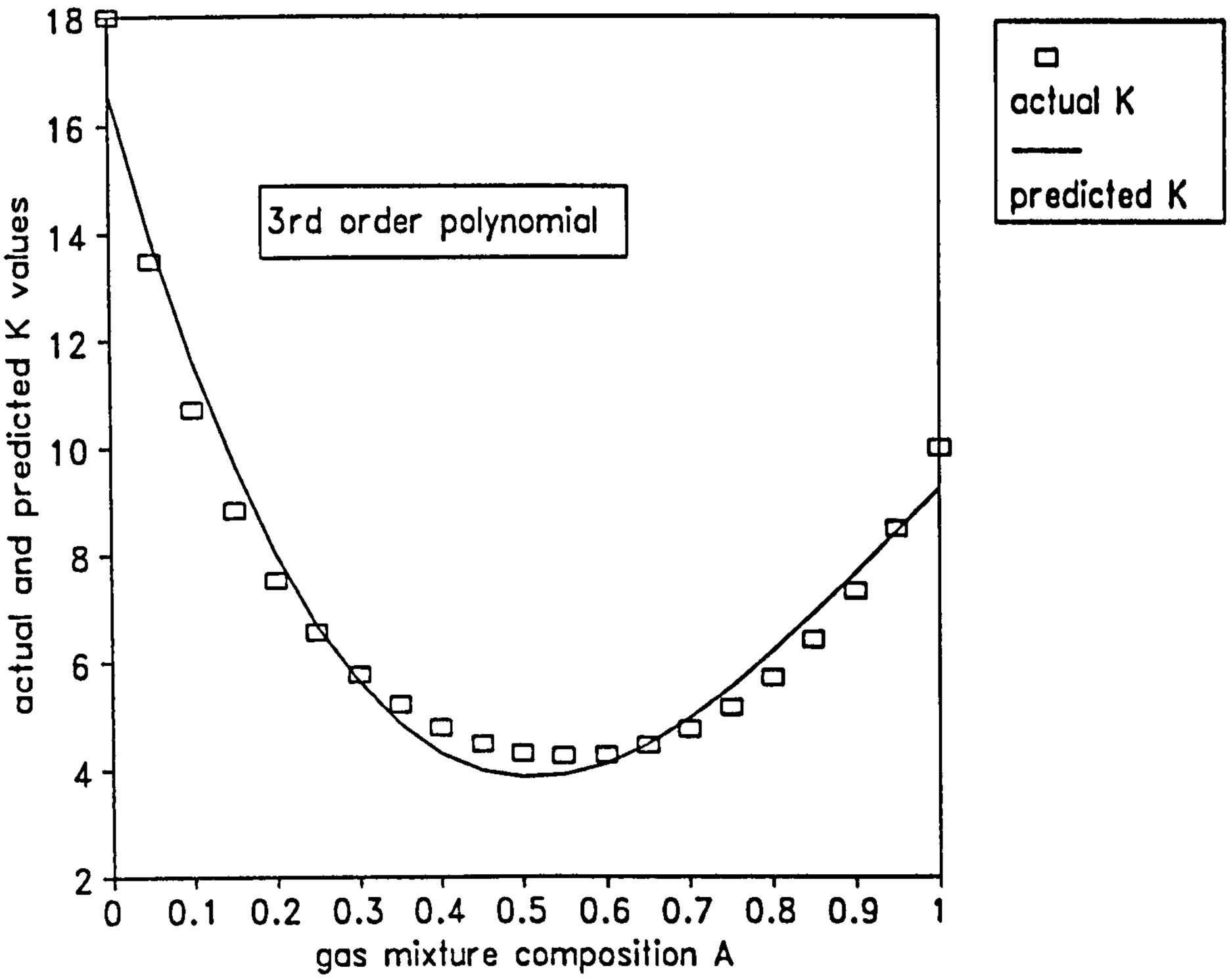

Figure 9.11A Actual and Fitted *K* Values for Literature Simulation

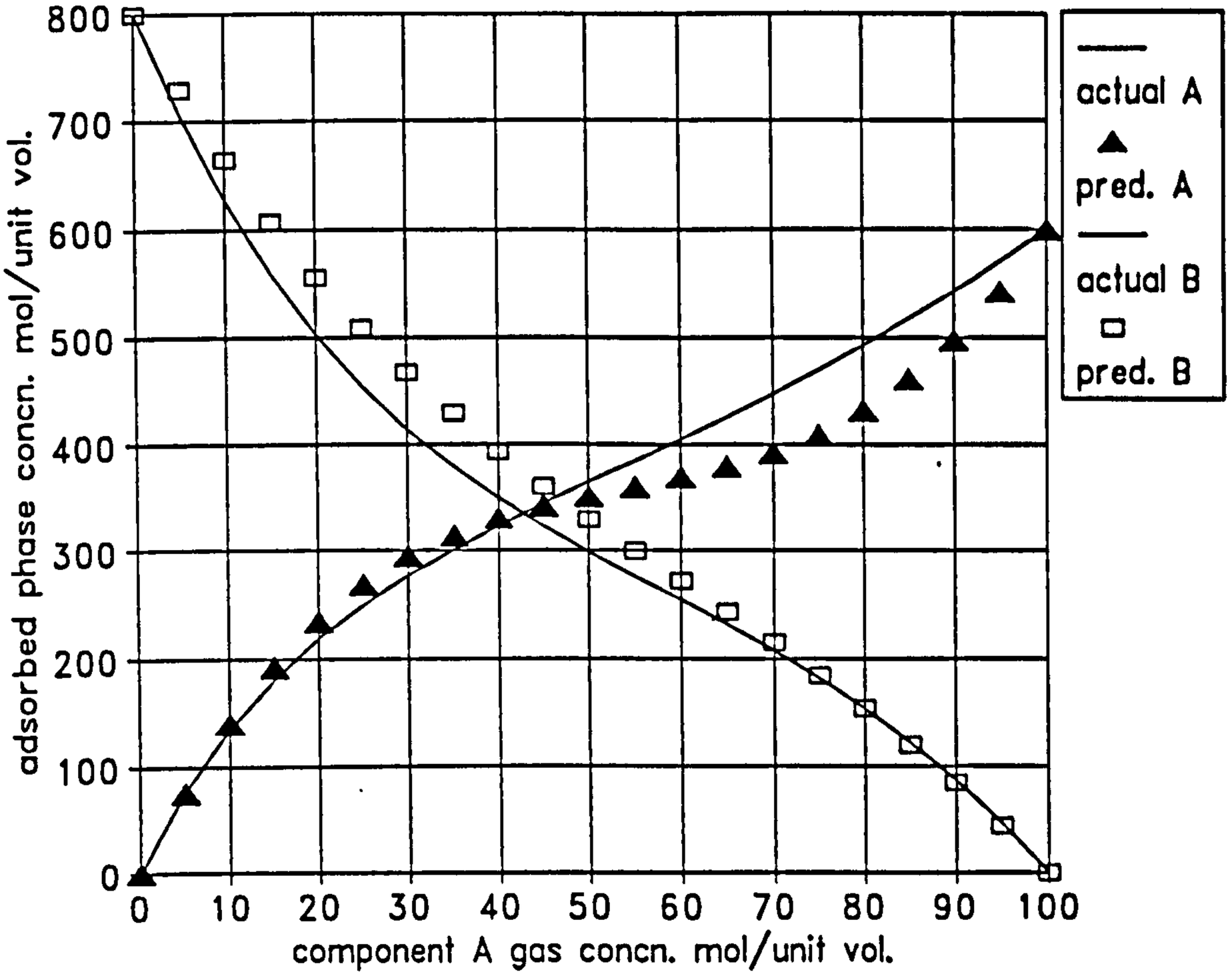

Figure 9.11B Actual and Predicted Binaries for Literature Simulation

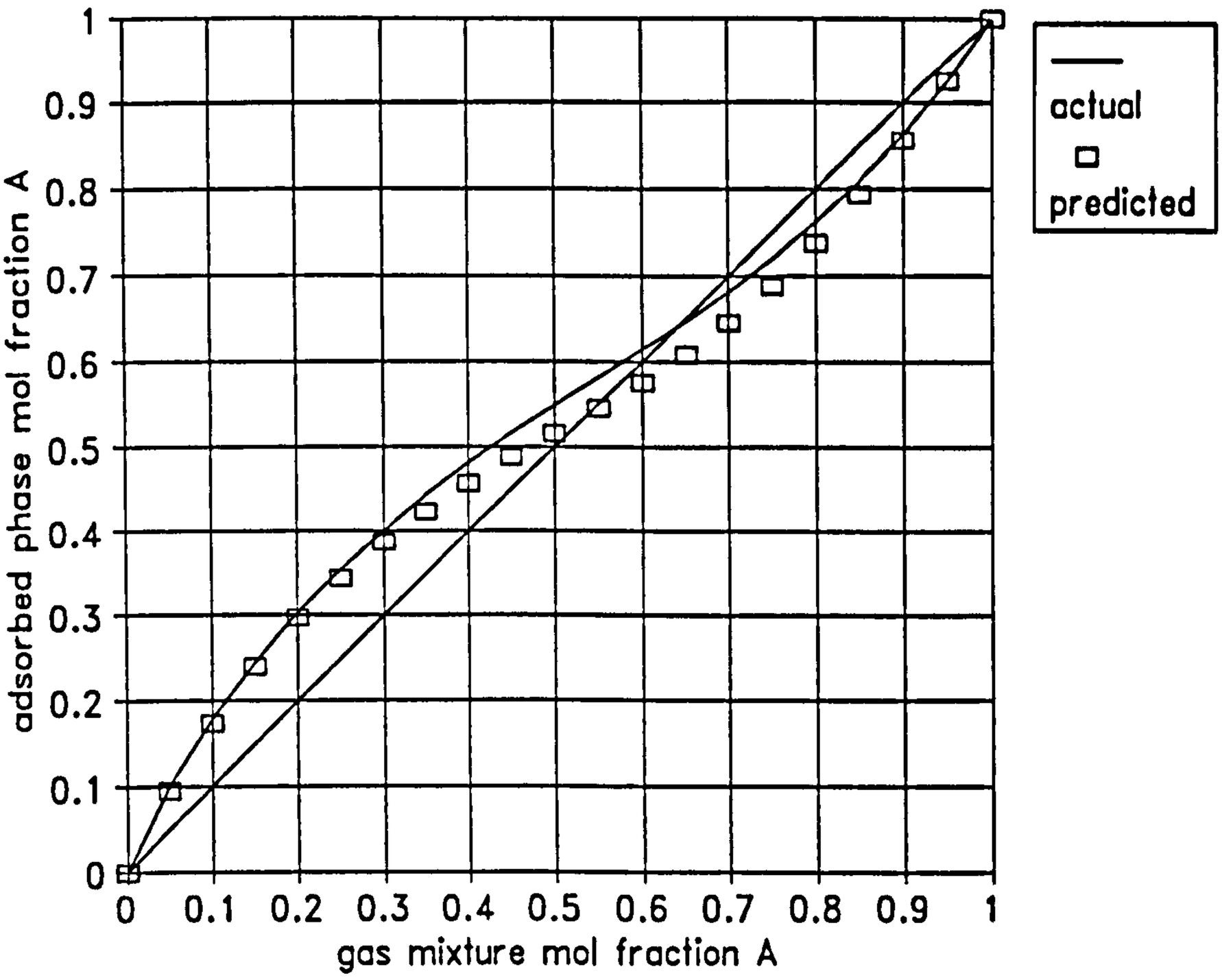

Figure 9.11C Actual and Predicted Phase Diagram for Literature Simulation

9.9.3 C_2H_6-C_2H_4 on 13X Zeolite

This case has already been discussed in the literature review in Section 9.5.4, and to convert the isotherms to the dimensionless form requires knowledge of the pellet density and voidage. Figure 9.12 shows the general shape of the system. This can be seen to be roughly the same shape as the system in Section 9.9.1, regarding the opposite curvatures of each isotherm. Thus, it can be represented by the binary-Langmuir theory or by using the IAST theory with Langmuir shape pure-component isotherms. However, because of the higher curvatures, the program simulation requires a much lower value of M for ethylene. The results from the computer simulation are in very good agreement with the literature. The range of K values has an initial steep descent followed by a plateau which the third-order polynomial cannot fit. Consequently, the amount of ethane adsorption is over-predicted for the whole range and ethylene, the stronger component, develops the characteristic kink towards the high mole fraction region. The only difference between the literature and simulation concerns the initial part of the ethylene isotherm; the literature suggests that the polynomial method will *under-predict* the actual isotherm, whilst the simulation suggests that the polynomial method will *over-predict* the actual isotherm resulting in a point where the actual and predicted isotherms cross each other.

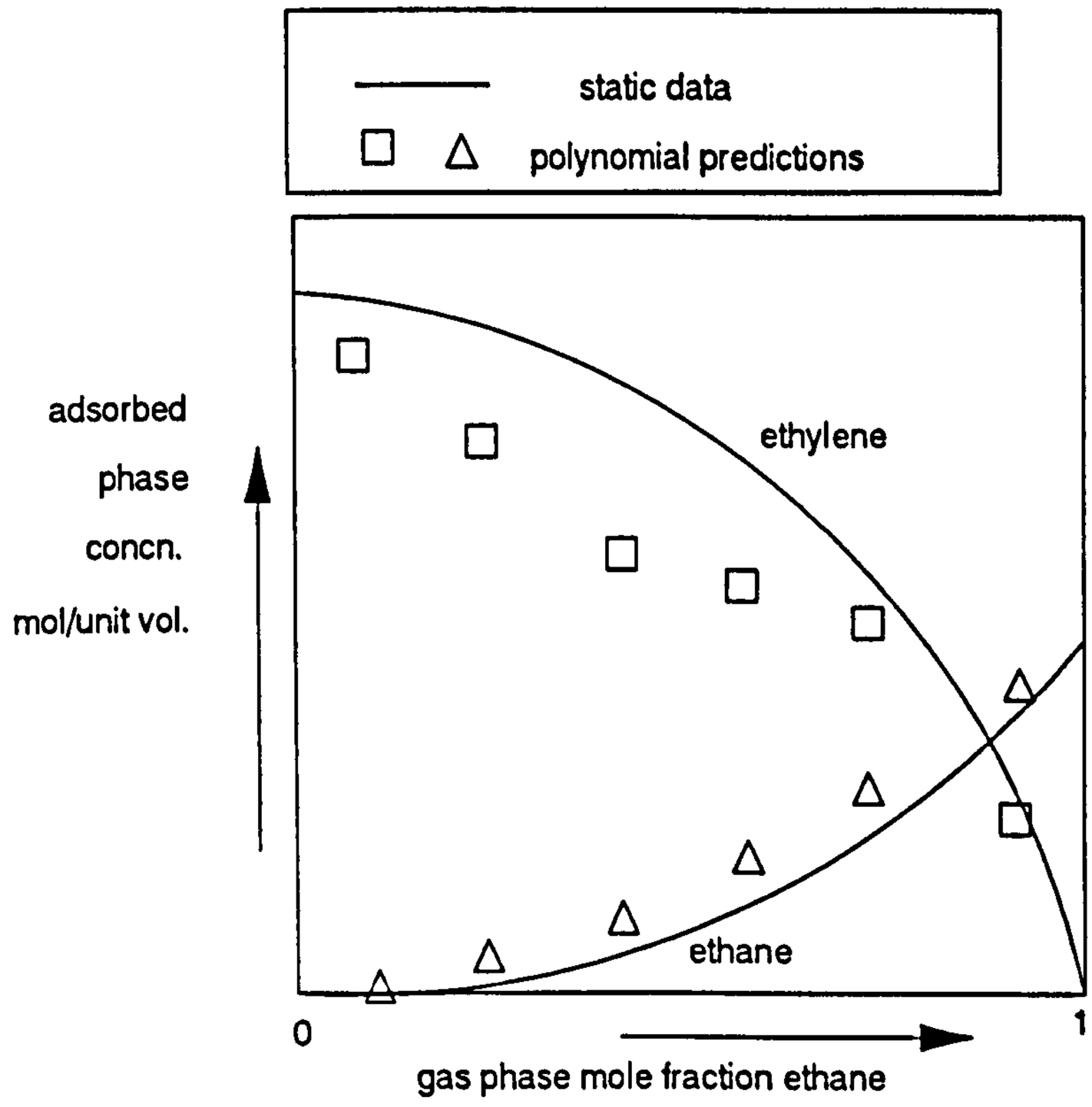

Figure 9.12 General Shape of System Binaries

9.10 Summary of Findings

1. In this chapter, binary gas-mixture systems have been *defined* and using the *chromatographic method*, the predictions of the originally defined system are presented which would be obtained for the polynomial-fitting method. The four versions of the program enable binary gas-mixture systems of any type and specification to be investigated. These include ideal systems, non-ideal systems and even systems with azeotropes; an extreme case of non-ideality.

2. In general, the closer the binaries are to linearity, the better the predictions by the method. Isotherms with rapidly changing gradients give variations in K which are difficult to fit with a third-order polynomial, and subsequently result in poor predictions. The method has been theoretically extended to fourth-order fitting, and although this often leads to better predictions, care must be taken over the choice of mixture constraint. It may be unrealistic for the method to be made to agree at a certain composition such that the predictions would be poor elsewhere. Overall, it is reasonable to use the polynomial method if the isotherms are close to linear, and this may be the advantage of using the new chromatographic method which involves the extra measurement of the flowrate retention time.

3. Under this section is also included the new chromatographic method which uses the flowrate retention time, because both cases involve obtaining directly the isotherm gradients. Hence, the requirement is an effective method of integration. For all systems investigated, the trapezoidal rule will give excellent predictions of the binaries. With this small step-length, 21 mixtures would be required. This seemingly small step-length is unnecessasry if the isotherms are close to linear, but small intervals are required where the gradient is changing quickly; often at the beginning at the isotherm. For programming purposes, a regular step-length is desirable although in practice a larger step-length would be employed in the middle ranges. Using a polynomial to fit the gradients can also give very good results as well. However, the order required will depend upon the system; some systems can be represented by a first-order polynomial but most require a higher order. It was found that a fifth-order polynomial could represent even the most non-linear system investigated.

4. Most of the simulations have been carried out for columns with a negligible pressure-drop. This has been justified because most of the literature cases employ such a column pressure-drop. The situation is complicated when the column pressure drop is significant, because the fitting curve and hence *binary isotherm* predictions will depend upon the perturbation gas.

Chapter Ten

FINAL SUMMARY

1. The objective of this research has been to apply the novel technique of *sorption-effect chromatography* to help determine binary gas-mixture equilibria on various adsorbents. The actual development of sorption-effect chromatography as an analytical tool is described in the thesis of Meacham (1990). Basically, the main characteristic is that the total column inventory is continuously measured because any *net* adsorption/desorption results in instantaneous flowrate deviations. From the chromatograph, these flowrate deviations are monitored by a special detector which consists of two matched pieces of capillary tubing, with a differential pressure transducer (DPT) upstream of this tubing. Any flowrate fluctuations will cause pressure fluctuations and this signal is amplified to give the flowrate chromatogram. From this chromatogram, the novel *flowrate retention time* (τ_N) can be measured. The standard chromatographic measurement is the *composition retention time* (τ_X) which is obtained using a thermal conductivity detector (TCD). The extra measurement enables both mixture isotherm gradients to be calculated directly. The experimental time required to make measurements for each mixture composition is of the order of minutes. Hence, the complete composition range for a particular temperature can be investigated in a few hours. The actual mixture isotherms are obtained by integration of the gradients. The number of compositions at which measurements have to be made will depend upon the system. A computer simulation has shown that highly non-linear systems require more investigation at the end-points of the composition range in order to cope with the extra curvature.

2. From the literature, the alternative methods of measuring binary isotherms can be divided into four categories. Firstly, there are many *direct* methods; these basically involve adding the required gas-mixture to the required adsorbent and waiting for equilibrium to be attained before performing a molar balance. Because the adsorbed phase composition is unknown, an extra measurement is required; this is the gas phase composition which must be determined analytically by gas chromatography. Secondly, there are many *predictive methods* which only require the respective pure-component data at the specified temperature; this is normally readily available. However, their main requirement is an *ideal mixture*, so many systems are precluded. An advance has been the *predictive-correlative* methods which require a number of independently determined mixture points. However, this defeats the object somewhat. Thirdly, there is another chromatographic method which requires the range of mixture composition retention times to be fitted to a third-order polynomial. Using the chromatographic equations of this project to generate perfect data,

a computer simulation has shown that this method is limited to near-linear systems. Also, this method requires the pure-component adsorbed amounts at the system pressure to be determined independently. The simulation has also shown that higher-order polynomials will fit non-linear systems, but these require one or more independently determined mixture points and so this somewhat defeats the object. Finally, there is the *tracer chromatography* method in which the perturbation gas is a radio-isotope of one component. The great advantage of this method is that the actual mixture isotherm point can be directly obtained from the retention time. However, a radio-isotope would be required for each component and the cost would be prohibitive, if indeed a radio-isotope was available for each component.

3. Binary mixture isotherms depend upon the system pressure and temperature. Equilibrium behaviour is very sensitive to temperature, and so it is important that the column and gas are always at the oven temperature. There are two reasons why this may not be achieved and so precautions must be taken in chromatograph design. Firstly, there is a section of tubing preceding the column to ensure that the incoming carrier gas reaches the oven temperature before it reaches the packing. Heat transfer calculations reveal that using 1/4 inch tubing, the carrier gas reaches the oven temperature in a short distance and that the limiting mode of heat transfer is natural convection from the enclosure to the column wall. Secondly, there is the problem of adsorption heat. It must be ensured that any adsorption heat is dissipated. There are many papers in the literature which deal with the effects of the heat of adsorption. However, all of these models assume that the adsorption heat is lost from the column external wall by forced convection. This situation is easy to attain by blowing air over the columns or by enclosing the columns in a jacket with water flowing continuously. For forced convection, the heat transfer coefficient is very high and this helps simplify the analysis since all the heat transfer resistance (and all the temperature drop) is considered to be across the column itself; there is no temperature difference between the column external wall and the enclosure. One such literature model was modified to account for natural convection from the column external wall rather than the "standard" forced convection; that is, a reduced convection coefficient. Even then, calculations suggest that there should be no problematic temperature rises for the 5A gas-mixture systems used in this project; the significant reason is the relatively small column diameter.

4. When the oven is on, the flowrate record is susceptible to thermal fluctuations reducing the smoothness of the flowrate record and making area determination and retention time measurement difficult. Preliminary investigations showed that, rather than coating the column with insulation, the most effective way of reducing these fluctuations was to hide the columns from direct air flow. From the previous section, this corresponded to a reduction in the convection heat transfer coefficient and so a connection seems likely between the

overall heat transfer coefficient (OHTC) and thermal noise. Experimentally, the columns were formed in a small spiral and enclosed within a glass envelope; this is termed the *chromatography pig*. Employment of the pig reduced the noise to such an extent that the baseline noise levels for nitrogen and helium became indistinguishable; previously the noise level for the more highly adsorbed nitrogen was very high. Actually, the findings of parts 3 and 4 are not independent; the OHTC should be large enough that the carrier gas reaches the oven temperature and that any adsorption heat can be quickly dissipated. If the adsorption heat cannot be dissipated, the gas temperature will necessarily rise and the composition front will become broader; this can make determination of both retention times difficult. However, the OHTC should be low enough so that thermal noise is not prohibitive. Overall, there should be a range of acceptable OHTC values.

5. Much of the project has been concerned with the effects of delay-lines (empty lengths of tubing) in various locations. In all, four locations have been defined, although only two can be considered useful. The original location was between the TCD and the DPT; this is termed *downstream*. The main purpose of this location is to allow direct determination of the flowrate retention time; otherwise the pressure retention time (τ_p) is obtained. Delay-lines situated downstream of the column maintain a constant gas composition in the measuring capillary so that the pressure variation at the DPT is solely a result of *flowrate* changes. An equation is derived relating both retention times to the *viscosity factor*, which is a function of the mixture viscosity-composition curve. The viscosity factor can be simply measured from the chromatogram with downstream delay-lines by simply dividing two offsets. However, care should be taken in particular situations where there is a *column plateau offset*; this is a significant change in the column resistance due to a change in the mixture viscosity (this depends upon the viscosity factor) and is more pronounced for columns with a higher pressure drop because of the increased flow resistance. For columns with a high pressure drop, it is safer to use *upstream* delay-lines as well as downstream delay-lines since these will give the correct initial offset. Once obtained, these measured factors can be used in a novel correlative method to predict binary mixture viscosities. Using this method, realistic predictions were obtained for the three binary systems investigated in this project; argon-nitrogen, argon-helium and nitrogen-helium.

6. The *upstream* delay-line location refers to the position directly upstream of the columns. Originally, when the perturbation flow was switched from one column to the other, only one upstream delay-line was employed. This was done to separate both flowrate and composition transients for both adding and removing the removing the perturbation flow, although the delayed transients were distorted. Comparisons revealed slight differences in sharpness, and sometimes differences in shape, of both transients. These differences were increased by reducing the bulk flow or by increasing the perturbation flowrate. Later on,

experimental development allowed a perturbation gas to be either added to or removed from a single column, and the same system behaviour was noted. These findings were partially confirmed by the literature.

For systems in which there is a significant column plateau offset (high pressure drop and high viscosity factor), employment of upstream delay-lines is essential to calculate the flowrate retention time. This is confirmed by considering a hypothetical system for which the viscosity factor causes there to be a zero overall offset between the baseline positions *before* the perturbation is added and *after* the front leaves the column; from the standard theory this would give an infinite flowrate retention time since the denominator becomes zero and this is clearly not realistic. Employment of delay-lines in the upstream location allows the correct value of $n(\infty) - n(0)$ (the denominator of τ_N) to be obtained. The effective position of $n(\infty)$ is then assumed to vary linearly with time until the front leaves the column.

Using upstream delay-lines for certain systems, it was noticed that a peculiar bulging in the composition transient was obtained prior to the front leaving the column. This was more pronounced for columns having a higher pressure drop. This bulging is caused by the increase in mean column pressure when the perturbation flow is added; the basic theory confirms that the increase is higher for columns having a higher pressure drop. Without the upstream delay-lines, the bulging would be superimposed upon the normal frontal variation. This forms the basis for a modification to the chromatographic method of this project and this will be discussed in part 9.

7. It has been shown theoretically and experimentally that the presence of delay-lines affects the measured retention times. The situation is more complicated when downstream delay-lines are employed; in the original theory, it was assumed that the column outlet pressure remained constant but this is invalid if the downstream delay lines have a finite pressure drop. This problem can be accounted for by using an equivalent column pressure drop (ΔP_C^*) instead of the standard column pressure drop (ΔP_C). The ΔP_C^* term includes the effect of the downstream delay-line pressure drop. Consideration of the ΔP_C^* term enables the contributions to the measured composition retention time (τ_{XD}^*) and the flowrate retention time (τ_{ND}^*) to be determined. It should be stressed that these two contributions are solely due to the effect of the downstream delay-line pressure drop, and are not attributable to any holdup changes in the downstream delay-lines. For systems in which the carrier and perturbation gas are the same pure component, there is only the τ_{ND}^* contribution to consider.

Also, there will be the contributions to the measured composition and flowrate retention times due to the holdup changes in the delay-lines themselves. The composition retention time contribution is simply the time spent in the delay volume and this can be significant for a typical delay-line length. Obviously, there will only be a contribution if the delay line

location is upstream of the TCD. The flowrate retention time contribution is much more interesting. If the location of the delay-line is downstream of the column, the contribution will depend mainly upon the delay-line volume and the delay-line pressure drop. For 1/4 inch tubing the contribution will be very small. For a 30 metres length of 1/8 inch tubing, the contribution is around one to three seconds. However, when the location is upstream of the column, the contribution depends mainly upon the *column pressure drop* and the delay-line volume. The effect of upstream delay-lines is generally greater than that for downstream delay-lines because the increase in column pressure increases the delay-line outlet pressure. The column pressure-drop has a large influence on the magnitude of the effect. For column type A, inserting 20 metres of 1/8 tubing gives a contribution of around five to seven seconds. However, for column type D, the contribution is around 24 to 30 seconds.

The theory has been extended so that it should be possible to calculate the intrinsic isotherm gradients for a particular mixture regardless of delay-line location, type and volume. However, this requires an accurate value of the delay line volume and this can be difficult to determine because the specifications are nominal. Overall, it is good practice to use as little delay-line length as possible.

8. An investigation was carried out on the three binaries from the nitrogen-argon-helium system at a range of temperatures on 5A molecular sieve. Overall, the amount of adsorption of the components increases in the order helium-argon-nitrogen. A degree of component interaction is observed; the isotherm shape changes slightly when the second component is changed. With helium, which is relatively non-adsorbed, the nitrogen isotherm is concave to the composition axis and the argon isotherm is relatively linear. Comparing the nitrogen and argon pure-component isotherms with those in the nitrogen-argon system, the nitrogen isotherm becomes less concave and the argon isotherm becomes slightly convex to the composition axis. The behaviour is qualitatively similar to the predictions of the binary-Langmuir theory; one isotherm is concave and the other isotherm is convex. However, this theory predicts a constant selectivity whereas the selectivity decreases as the nitrogen composition increases. As the temperature increases, the isotherms become less curved and the amounts adsorbed become less. The component reductions are such that the selectivities generally become smaller and this usually happens in distillation as well. At any temperature for the three binary systems, each respective pair of pure-component end points should agree since these correspond to the respective pure component amounts adsorbed at the total system pressure; these agree to within two to five per cent.

For each system, initially the isotherm holdups were calculated using the directly measured values of τ_N; these required the presence of downstream delay-lines. The agreement between the isotherm holdups calculated using each perturbation gas was satisfactory for most carriers. However, for systems in which the perturbation gas is added to a carrier rich in that component, the agreement for the respective component holdup is poor. This is not surprising since the multiplication factor for τ_N will be higher for this combination; any error in the value of τ_N will have a proportionately higher effect on the calculated isotherm holdup. Then the holdups were recalculated but using the *predicted* τ_N values from an equation (described in part 5) requiring measured values of the pressure retention time. Using these predicted values resulted in much improved agreement across the composition range for all the systems.

In the light of the holdup calculations, it might be more reliable to *indirectly* obtain the values of τ_N using values of τ_P and the equation described in part 5. The τ_P values can be measured with more confidence, since the flowrate record will *always* attain the final plateau at $p(\infty)$. One project aim was to carry out experiments with and without downstream delay-lines to directly obtain sets of τ_N and τ_P respectively. It was intended to use these to test the validity of the connecting equation. In the end, the situation has been reversed in that the equation has been used to determine the reliability of using downstream delay-lines to directly determine values of τ_N.

9. An original project aim was to obtain both isotherm holdups for each mixture composition using both perturbation gases; the idea was that both values should agree and provide a reliability check. For this case, it is necessary to wait until the composition front had passed through the column, TCD and the DPT so that both composition and flowrate retention times could be evaluated. A major development has been to employ a perturbation gas having the same composition of the carrier such that it is not necessary for the composition front to even *reach* the column. The relevant adsorption information can be obtained from the average column pressure increase caused by simply adding the perturbation gas, although one of the pure perturbation gases is required for calibration purposes. A mixture in the nitrogen-helium system was investigated. Because an *exact* mixture composition could not be obtained, it was necessary to use upstream delay-lines to separate out the required bulge in the composition record from the deviation obtained as the front moves through the column. Of course, this required significant contributions to be removed from the measured τ_N. The preliminary results were reasonable considering that the τ_N corrections were large. Finally, a hypothetical arrangement was proposed in which delay-lines could be used without major corrections. This involved adding an identical perturbation flow to each side of the system; bulging areas without offsets would be obtained for both composition and flowrate records. One column is packed with the

required adsorbent and the other is packed with geometrically identical deactivated adsorbent such that the column pressure drops are identical. Thus, the troublesome delay-line contributions would cancel out and the bulging flowrate transient area would be solely due to the change in packing holdup.

NOMENCLATURE

The following list is of the main symbols used in this thesis. Symbols which only appear locally, or for which the relevant equation is only referred to qualitatively, have been excluded from the nomencalture. The number in brackets after the symbol refers to the first chapter in which the symbol is situated. The general practice is to use *italics* for variables. If the subscript is a variable, then it appears in *italics*; otherwise it appears in Roman. After using any of the *condition subscripts* (OUT, IN or MEAN), it is necessary to state the relevant piece of equipment to which the condition applies: For example, Q_{UMEAN} refers to the average volumetric flowrate in the upstream delay-lines.

ROMAN SYMBOLS

A_{AB}	first Brokaw function (4)
A_{BA}	second Brokaw function (4)
A_X	composition record bulging area (8)
A_0	first polynomial-fitting coefficient (9)
A_1	second polynomial-fitting coefficient (9)
A_2	third polynomial-fitting coefficient (9)
A_3	fourth polynomial-fitting coefficient (9)
B_0	first coefficient for isotherm A gradient (9)
B_1	second coefficient for isotherm A gradient (9)
B_2	third coefficient for isotherm A gradient (9)
$B(\mu)$	true viscosity factor (4)
$B(\mu)_M$	measured viscosity factor (4)
$B(\mu)_A$	viscosity factor for Equation 4.12 agreement (4)
c_i	gaseous concentration of component *i* in mixture (1)
c_{iO}	gaseous concentration of *pure-component i* (9)
C_P	molar heat capacity of carrier gas (5)
c_T	total gaseous concentration in mixture (1)
C_0	first coefficient for isotherm B gradient (9)
C_1	second coefficient for isotherm B gradient (9)
C_2	third coefficient for isotherm B gradient (9)
$C(\mu)$	column plateau difference viscosity factor (7)
d_E	column external diameter (5)
d_I	general delay-line internal diameter (7)
d_C	column internal diameter (5)
d_O	general delay-line external diameter (7)
d_P	packing pellet diameter (3)
F_{PVCi}	column correction factor (1)
F_{PVIi}	intermediate delay-line correction factor (7)
F_{PVUi}	upstream delay-line correction factor (7)
F_0	first ratio of column correction factors (7)
F_1	first ratio of column correction factors (7)
G	isotherm holdup gradient (1)
H_i	holdup for component *i* (1)
H_A	linear component for binary A (9)
H_B	linear component for binary B (9)
h_C	internal wall heat transfer coefficient for packed column (5)
h_1	internal wall heat transfer coefficient for empty tubing (5)
h_2	external wall heat transfer coefficient to enclosure (5)
K	effective equilibrium constant for binary gas mixture (9)
K_C	column pressure profile function (7)
K_{DL}	delay-line pressure profile function (7)
k_G	thermal conductivity of carrier gas (5)
k_N	thermal conductivity of tubing insulation (5)
k_W	thermal conductivity tubing wall (5)
L_C	length of column (7)
L	general length used with relevant subscript
M	molar flowrate of carrier (1)

M_A molecualr weight of component A (4)
M_A first Langmuir-Freundlich coefficient for binary A (9)
M_B molecular weight of component B (4)
M_B first Langmuir-Freundlich coefficient for binary B
n molar flowrate of perturbation (1)
n_T molar flowrate of pure perturbation (8)
$n(t)$ flowrate record position with downstream delay-lines (1)
N_A number of plates for perturbation addition (6)
N_A second Langmuir-Freundlich coefficient for binary A (9)
N_B second Langmuir-Freundlich coefficient for binary B (9)
N_R number of plates for perturbation removal (6)
P general pressure used with relevant subscript
$p(t)$ flowrate record deviation with no downstream delay-lines (4)
P_{AT} atmospheric pressure (1)
P_{CAV} average column pressure (1)
P_U upstream system pressure (4)
P_D downstream system pressure (4)
Q heat flow (5)
Q general flowrate used with relevant subscript
q_{AM} adsorbed concentration of component A at system pressure (9)
q_{BM} adsorbed concentration of component B at system pressure (9)
Q_{CAV} average volumetric flowrate in column (1)
q_i adsorbed concentration of component i in mixture (1)
q_{iO} adsorbed concentration of pure-component i (9)
Q_M measured volumetric flowrate of carrier (1)
R ideal gas constant (1)
R_A first Langmuir coefficient for component A (9)
R_B first Langmuir coefficient for component B (9)
r_1 carrier gas internal tubing radius (5)
r_2 carrier gas external tubing radius (5)
r_3 insulation external tubing radius (5)
S_{AB} selectivity of component A to component B (1)
S_{NT} flowrate record deviation on chart recorder (8)
S_X composition record deviation on chart recorder (8)
T general temperature used with relevant subscript
T_A second Langmuir coefficient for binary A (9)
T_B second Langmuir coefficient for binary B (9)
T_B carrier gas temperature (5)
T_C temperature of column (1)
T_{EN} temperature of oven (5)
T_1 temperature at tubing internal radius (5)
T_2 temperature at tubing external radius (5)
T_3 temperature at insulation external radius (5)
U overall heat transfer coefficient from tubing to enclosure based on r_1 (5)
U_C overall heat transfer coefficient from column to enclosure based on d_C (5)
V interstitial gas velocity in column (6)
V general volume used with relevant subscript
x_i adsorbed phase mole fraction for component i (1)
$x(t)$ composition record position (1)
Y_i gaseous phase mole fraction of component i (1)
Y_{iO} carrier mole fraction of component i (1)
Y_{iT} perturbation mole fraction of component i (1)

DIMENSIONLESS GROUPS

Gr Grashoff number
Nu_C column internal Nusselt number
Nu_I normal tubing internal Nusselt number
Nu_O external insulation Nusselt number
Pr Prandtl number
Re Reynolds number

GREEK SYMBOLS

ΔP_C	actual column pressure drop (1)
ΔP_C^*	equivalent column pressure drop (7)
ΔP	general equiupment pressure drop used with relevant subscript
ε	packed column voidage (1)
Θ_{AV}	average temperature rise of front due to adsorption heat (5)
Θ_{MAX}	maximum temperature rise of front due to adsorption heat (5)
λ_A	adsorbed phase activity coefficient for component A (9)
λ_B	adsorbed phase activity coefficient for component B (9)
μ_{AO}	viscosity of pure-component A (4)
μ_{BO}	viscosity of pure-component B (4)
μ_M	viscosity of binary mixture (4)
μ_M^*	dimensionless viscosity of binary mixture (4)
$\pi(c_{iO})$	spreading pressure for component *i* (9)
τ_N	measured flowrate retention time with downstream delay-lines (1)
τ_{NC}	calculated flowrate retention time using Equation 4.12 (7)
τ_{ND}	downstream delay-line contribution to measured flowrate retention time (7)
τ_{ND}^*	contribution of equivalent column pressure-drop to measured flowrate retention time (7)
τ_{NH}	hypothetical measured flowrate retention time (7)
τ_{NI}	intermediate delay-line contribution to measured flowrate retention time (7)
τ_{NP}	predicted flowrate retention time (7)
τ_{NS}	switching valve delay-line contribution to measured flowrate retention time (7)
τ_{NU}	upstream delay-line contribution to measured flowrate retention time (7)
τ_P	measured pressure retention time (4)
τ_U	unretained pulse retention time (9)
τ_X	measured composition retention time (1)
τ_{XD}^*	contribution of equivalent column pressure-drop to measured composition retention time (7)
τ_{XI}	intermediate delay-line contribution to measured composition retention time (7)
τ_{XD}	downstream delay-line contribution to measured composition retention time (7)
τ_{XU}	upstream delay-line contribution to measured composition retention time (7)
Φ_{AB}	first Sutherland correlation coefficient (4)
Φ_{BA}	second Sutherland correlation coefficient (4)

SUBSCRIPTS FOR RELEVANT VARIABLES

A	component A
Ar	argon component
Arp	argon perturbation
B	component B
C	column
D	downstream delay-line
DL	general delay-line
He	helium component
Hep	helium perturbation
i	general component
I	intermediate delay-line
IN	*upstream* value in the equipment component
MEAN	*average* value in the equipment component
N2	nitrogen component
N2p	nitrogen perturbation
OUT	*downstream* value in the equipment component
S	switching valve delay-line
U	upstream delay-line

BIBLIOGRAPHY

Abdul-Rehman, H.B., M.A. Hassanin and K.F. Loughlin (1990), Quarternary, Ternary, Binary and Pure Component Adsorption on Zeolites 1. Light Alkanes on Linde S-115 Silicalite at Moderate to High Pressures, *Ind. Eng. Chem. Res.*, **29**, 1525-1535

Al-Ameeri, R.S and R.P Danner (1984), An Improved Tracer-Pulse Method for the Measurement of Gas-Adsorption Equilibria, *Chem. Eng. Communication*, **26**, 11-20

Arnold, J.R. (1949), Adsorption of Gas Mixtures - Nitrogen and Oxygen on Anatase, *J. American Chemical Society.*, **71**, 104-110

Barrer, R.M., *Zeolites and Clay Minerals as Sorbents and Molecular Sieves*; Academic Press:1978

Brokaw, R.S. (1968), *NASA Technical Note D-4496*

Brokaw, R.S. (1969), Predicting Transport Properties of Dilute Gases, *Ind. Eng. Chem. Process Des. Dev.*, **8**, 240-253

Broughton, D.B. (1948), Adsorption Isotherms for Binary Gas Mixtures, *Ind. Eng. Chem.*, **40**, 1506-1512

Buddenberg, J.W. and C.R. Wilke (1949), Calculation of Gas-Mixture Viscosities, *Ind. Eng. Chem.*, **41**, 1345-1347

Buffham, B.A. (1973), Model-Independent Properties of Tracer Chromatography, *Proc. R. Soc. London Series A.*, **333**, 89-98

Buffham, B.A. (1978), Model-Independent Properties of Perturbation Chromatography, *Proc. R. Soc. London Series A.*, **364**, 443-455

Buffham, B.A., G. Mason and G. Yadav (1985), Retention Volumes and Retention Times in Binary Chromatography, *J. Chem. Soc. Faraday Trans I*, **81**, 161-170

Buffham, B.A. (1986), *SERC Grant Report No. GR/C/59970*

Chen, Y.D., J.A. Ritter and R.T. Yang (1990), Non-Ideal Adsorption of Multicomponent Gas Mixtures on a 5A Molecular Sieve, *Chem. Eng. Sci.*, **45**, 2877-2894

Cochran, T.W., R.L. Kabel and R.P. Danner (1985), The Vacancy Solution Model of Adsorption-Improvements and Recommendations, *AIChEJ*, **31**, 2075-2088

Cook, W.H. and D. Basmadjian (1965), The Prediction of Binary Adsorption Equilibria from Pure Component Isotherms, *Canadian J. Chem. Eng*, **43**, 78-83

Costa, E., G. Calleja, A. Jimenez and J. Pau (1989), Equilibrium Adsorption of Methane, Ethane, Ethylene and Propylene and their Mixtures on Activated Carbon, *J. Chem. Eng. Data*, **34**, 156-160

Costa, E., G. Calleja, A. Jimenez and J. Pau (1991), Adsorption Equilibrium of Ethylene, Propylene, Propane and their Mixtures on 13X Zeolite, *J. Chem. Eng. Data*, **36**, 218-224

Costa, E., J.L. Sotelo, G. Calleja and C. Marron (1981), Adsorption of Binary and Ternary Hydrocarbon Gas Mixtures on Activated Carbon, *AIChEJ*, **27**, 5-12

Coulson, J.M. and J.F. Richardson, *Chemical Engineering Volume 1*; Chapter 3; Pergamon:1982a

Coulson, J.M. and J.F. Richardson, *Chemical Engineering Volume 1*; Chapter 9; Pergamon:1982b

Coulson, J.M. and J.F. Richardson, *Chemical Engineering Volume 1*; Chapter 7; Pergamon:1982c

Coulson, J.M. and J.F. Richardson, *Chemical Engineering Volume 1*; Chapter 5; Pergamon:1982d

Crosser, O.K. and B.V. Hong (1980), Propane-Carbon Dioxide and Propylene-Carbon Dioxide Mixture Adsorption on 5A Molecular Sieve, *J. Chem. Eng. Data*, **25**, 339-340

Danner, R.P., M.P. Nicoletti and R.S. Al-Ameeri (1980), Determination of Gas-Mixture Adsorption Equilibria by the Tracer-Pulse Technique, *Chem. Eng. Sci.*, **35**, 2129-2133

Danner, R.P. and L.A. Wenzel (1969), Adsorption of Carbon Monoxide + Nitrogen, Carbon Monoxide + Oxygen and Oxygen + Nitrogen Mixtures on Synthetic Zeolites, *AIChEJ*, **15**, 515-520

Deissler, R.G. (1951), *NASA Technical Note 2410*

Dorfman, L.R. and R.P Danner (1975), Equilibrium Adsorption of Nitrogen-Oxygen-Carbon Monoxide Mixtures on Molecular Sieve 10X, *AIChEJ Symp. Ser.*, **71**, 30-39

Farooq, S. and D.M. Ruthven (1990a), Heat Effects in Adsotption Column Dynamics 1. Comparisons of One and Two Dimensional Models, *Ind. Eng. Chem. Res.*, **29**, 1076-1084

Farooq, S. and D.M. Ruthven (1990b), Heat Effects in Adsorption Column Dynamics 2. Experimnetal Validation of One Dimensional Model, *Ind. Eng. Chem. Res.*, **29**, 1084-1090

Garg, D.R. and D.M. Ruthven (1974a), The Performance of Molecular Sieve Adsorption Columns: Systems with Micropore Diffusion Control, *Chem. Eng. Sci.*, **29**, 571-581

Garg, D.R. and D.M. Ruthven (1974b), The Performance of Molecular Sieve Adsorption Columns: Systems with Macropore Diffusion Control, *Chem. Eng. Sci.*, **29**, 1961-1967

Glessner, A.J. and A.L Myers (1969), The Sorption of Gas Mixtures in Molecular Sieves, *AIChE Symp. Ser.*, **65**, 73-79

Grant, R.J. and M. Manes (1966), Adsorption of Binary Hydrocarbon Gas Mixtures on Activated Carbon, *Ind. Eng. Chem. Fund.*, **5**, 490-498

Graetz, L. (1885), *Ann. Phys. u. Chem.*, **25**, 337

Hausen, H. (1943), *Verfahrenstechnik Beith. Z. Ver. deut. Ing.*, **4**, 91

Haydel, J.J and R. Kobayashi (1967), Adsorption Equilibria in the Methane-Propane-Silica System at High Pressures, *Ind. Eng. Chem. Fund.*, **6**, 546-554

Helfferich, F. (1964), Travel of Molecules and Disturbances in Chromatographic Columns, *J. Chem. Education*, **41**, 410-413

Helfferich, F. (1982), Non-Isothermal Behaviour of Fixed Bed-Adsorbers, *J. Chem. Education*, **59**, 646-648

Herning, F. and L. Zipperer (1936), *Gas Wasserfach*, **79**, 49

Holbrow, K.A. and K.F. Loughlin (1977), Multicomponent Sorption Equilibria of Hydrocarbon Gases on 5A Zeolite, *ACS Symposium Series*, **40**, 379-392

Huang, J.C. and R. Madey (1982), Application of Potential Theory to Adsorption of Binary Gas Mixtures on Activated Carbon, *Carbon*, **20**, 118-120

Hyun, S.H. and R.P Danner (1982), Determination of Gas Adsorption Equilibria by the Concentration Pulse Technique, *AIChEJ Symp. Ser.*, **78**, 19-28

Hyun, S.H. and R.P Danner (1985), Gas Adsorption Isotherms by Use of Perturbation Chromatography, *Ind. Eng. Chem. Fund.*, **24**, 95-101

Kaguei, S., M. Nishio and N. Wakao (1987), Parameter Estimation from Constant Pattern Thermal Waves in an Adsorption Column, *Chem. Eng. Sci.*, **42**, 2964-2966

Kapoor, A. and R.T Yang (1989), Kinetic Separation of Methane - Carbon Dioxide Mixture by Adsorption on Carbon Molecular Sieve, *Chem. Eng. Sci.*, **44**, 1723-1727

Kaul, B.K. (1984), Correlation and Prediction of Adsorption Isotherm Data for Pure and Mixed Gases, *Ind. Eng. Chem. Process Res. Dev.*, **23**, 711-716

Kidnay, A.J. and A.L Myers (1966), A Simplified Method for the Prediction of Multicomponent Adsorption Equilibria from Single Gas Isotherms, *AIChEJ* , **5**, 981-986

Kluge, G., Th. Franke, R. Schollner and R. Nagel (1991), Estimation of Component Loadings in Fixed Bed Adsorption from Breakthrough Curves of Binary Gas Mixtures in Non-Trace Systems, *Chem. Eng. Sci.*, **46**, 368-371

Knudsen, J.G. and D.L Katz, *Fluid Dynamics and Heat Transfer*; Chapter 13; Mc-Graw Hill:1958

Langmuir, I. (1918), The Adsorption of Gases on Plane Surfaces of Glass, Mica and Platinum, *J. American Chemical Society*, **40**, 1361-1402

Leavitt, F.W. (1962), Non-Isothermal Adsorption in Large Fixed Beds, *Chemical Engineering Progress*, **58**, 54-59

Lederman, P.B. and B. Williams (1964), The Adsorption of Methane and Nitrogen on Molecular Sieves, *AIChEJ*, **10**, 30-34

Lee, T.V., J.C. Huang and R. Madey (1984), A Separation Factor Method for the Analysis of Ideal Binary Gas Mixtures in Gas-Solid Adsorption, *Separation Science and Technology*, **19**, 157-172

Le Van, D.M. and T. Vermuelen (1981), Binary Langmuir and Freundlich Isotherms for Ideal Adsorbed Solutions, *J. Physical Chemistry*, **85**, 3247-3250

Leva, M. (1947), Heat Transfer to Gases through Packed Tubes - General Correlation for Smooth Spherical Particles, *Ind. Eng. Chem.*, **39**, 857-862

Lewis, W.K., E.R. Gilliland, B. Chertow and W.P. Cadogan (1950), Adsorption Equilibria: Hydrocarbon Gas Mixtures, *Ind. Eng. Chem.*, **42**, 1319-1325

Loughlin, K.F., M.A. Hassanin and H.B Abdul-Rehman (1990), Quarternary, Ternary, Binary and Pure Component Adsorption on Zeolites 2. Light Alkanes on Linde 5A and 13X Zeolites at Moderate to High Pressures, *Ind. Eng. Chem. Res.*, 1535-1546

Loughlin, K.F., K.A. Holborow and D.M. Ruthven (1976), Multicomponent Sorption Equilibria of Light Hydrocarbons on 5A Zeolite, *AIChE Symp. Ser.*, **71**, 24-29

Markham, E.C. and A.F. Benton (1931), The Adsorption of Gas Mixtures by Silica, *J. American Chemical Society*, **53**, 497-507

Martin, A.J.P. and R.L.M. Synge (1941), *Biochem. J.*, A New Form of Chromatography Employing Two Liquid Phases, **35**, 1358-1366

Mason, G. and B.A. Buffham, Paper in *Fundamentals of Adsorption*; Mersmann,A.B. and S.E. Scholl,Eds.; United Engineering Trustees:1991

Meacham, R.I. (1990), Ph.D. thesis, *Sorption-Effect Chromatography*, Loughborough University of Technology

Miller, G.W. (1987), Adsorption of Nitrogen, Oxygen, Argon and Ternary Mixtures of these Gases on 13X Molecular Sieve, *AIChE Symposium Series*, **83**, 28-39

Miller, G.W., Knaebel, K.S. and K.G. Ikels (1987), Equilibria of Nitrogen, Oxygen, Argon and Air on Molecular Sieve 5A, *AIChEJ*, **33**, 194-201

Minkoff, J.G. (1964), Binary Equilibrium Data from Single-Component Isotherms, *Ind. Eng. Chem. Process. Res. Dev.*, **3**, 409-410

Myers, A.L. (1983), Activity Coeffeicients of Mixtures Adsorbed on Heterogeneous Surfaces, *AIChEJ*, **29**, 691-693

Myers, A.L., Paper presented at *World Congress III of Chemical Engineering*, Tokyo, 1986

Myers, A.L. and J.M. Prausnitz (1965), Thermodynamics of Mixed Gas Adsorption, *AIChEJ*, **11**, 121-127

Nandi, S.P. and P.L. Walker (1976), Separation of Oxygen and Nitrogen using 5A Zeolite and Carbon Molecular Sieves, *Separation Science*, **11**, 441-453

Persichini, C. and A. Mersmann (1988), Breakthrough Behaviour of a Binary Gas Mixture with Azeotropic Adsorption, *Chem. Eng. Technology*, **13**, 8-14

Peterson, D.L. and F. Helfferich (1965), Towards a Generalised Theory of Gas Chromatography at High Solute Concentrations, *J. Phys. Chem.*, **69**, 1283-1293

Peterson, D.L. and O. Redlich (1963), Sorption of Normal Paraffins by Molecular Sieve Type 5A, *J. Chem. Eng. Data*, **8**, 570-573

Petrovic, L.J. and G. Thodos (1968), Mass Transfer in the Flow of Gases through Packed Beds, *Ind. Eng. Chem. Fund.*, **7**, 274-280

Purnell, H., *Gas Chromatography*; Chapter 7; Wiley;1962

Richter, E., W. Schultz and A.L. Myers (1989), Effect of Adsorption Equation on Prediction of Multicomponent Adsorption Equilibria by the Ideal Adsorbed Solution Theory, *Chem. Eng. Sci.*, **44**, 1609-1616

Ritter, J.A. and R.T. Yang (1987), Equilibrium Adsorption of Multicomponent Gas Mixtures at Elevated Pressures, *Ind. Eng. Chem. Res.*, **26**, 1679-1686

Ritter, J.A. and R.T. Yang (1989), Thermodynamic Analysis of Rapid Measurments of Equilibrium Adsorption from Binary Gas Mixtures, *Ind. Eng. Chem. Res.*, **28**, 599-608

Robinson, K.S. and W.J. Thomas (1980), The Adsorption of Methane/Ethane Mixtures on a Molecular Sieve, *Trans. Inst. Chem. Engrs*, **58**, 219-227

Ruthven, D.M. (1976), Sorption of Oxygen, Nitrogen, Carbon Monoxide, Methane and Binary Mixtures of these Gases on 5A Molecular Sieve, *AIChEJ*, **22**, 753-759

Ruthven, D.M., *Principles of Adsorption and Adsorption Processes*; Chapter 1; Wiley:1984a

Ruthven, D.M., *Principles of Adsorption and Adsorption Processes*; Chapter 6; Wiley:1984b

Ruthven, D.M., *Principles of Adsorption and Adsorption Processes*; Chapter 7; Wiley:1984c

Ruthven, D.M., *Principles of Adsorption and Adsorption Processes*; Chapter 8; Wiley:1984d

Ruthven, D.M., *Principles of Adsorption and Adsorption Processes*; Chapter 4; Wiley:1984e

Ruthven, D.M., D.R. Garg and R.M. Crawford (1975), The Performance of Molecular Sieve Adsorption Columns; Non-Isothermal Systems, *Chem. Eng. Sci.*, **30**, 803-810

Ruthven, D.M. and R. Kumar (1979), A Chromatographic Study of the Diffusion of N_2, CH_4 and Binary N_2-CH_4 Mixtures on 4A Molecular Sieve, *Canadian J. Chem. Eng.*, **57**, 342-348

Ruthven, D.M. and R. Kumar (1980), An Experimental Study of Single Component and Binary Adsotprtion Equilibria by a Chromatographic Method, *Ind. Eng. Chem. Fund.*, **19**, 27-32

Ruthven, D.M., K.F. Loughlin and K.A. Holborow (1973), Multicomponent Sorption Equilibrium in Molecular Sieve Zeolites, *Chem. Eng. Sci.*, **28**, 701-709

Ruthven, D.M. and F. Wong (1985), Generalised Statistical Model for the Prediction of Binary Adsorption Equilibria in Zeolites, *Ind. Eng. Chem. Fund.*, **24**, 27-32

Saxena, S.C., Paper in *Proceedings of the Sixth A.S.M.E. Symposium on Thermophysical Properties*, 1973

Saxena, S.C. and R.S. Gambhir (1963), A Semi-Empirical Formula for the Viscosity of Multicomponent Gas Mixtures, *Indian J. Pure Applied Physics*, 1, 208-218

Saxena, S.C. and T.K.S. Narayamen (1962), Multicomponent Viscosities of Gaseous Mixtures at High Temperatures, *Ind. Eng. Chem. Fund.*, 1, 191-198

Schalles,P.G. and R.P. Danner (1988), Adsorption of Oxygen and Nitrogen on Carbon Molecular Sieve Type 3A, *AIChE Symp. Ser.*, **84**, 83-88

Shah, D.B (1988), Binary Sorption Equilibria by Pulse Chromatography, *ACS Symposium Series*, **358**, 409-420

Sips, R. (1948), On the Structure of a Catalyst Surface, *J. Chem. Physics*, **16**, 490-498

Sircar, S., R. Kumar and K.J. Anselmo (1983), Effect of Column Non-Isothermality or Non-Adiabacity on the Adsorption Breakthrough Curves, *Ind. Eng. Chem. Process Res. Dev.*, **22**, 10-15

Sircar, S. and A.L. Myers (1973), Surface Potential Theory of Multilayer Adsorption from Gas Mixtures, *Chem. Eng. Sci.*, **28**, 489-499

Sorial, G.A., W.H. Granville and W.O. Daly (1983), Adsorption Equilibrium for Oxygen and Nitrogen Gas Mixtures on 5A Molecular Sieve, *Chem. Eng. Sci.*, **38**, 1517-1523

Stalkup, F.I. and R. Kabayashi (1963), High-Pressure Phase Equilibrium Studies by Gas-Liquid Partition Chromatography, *AIChEJ*, **9**, 121-128

Suwanayuen, S. and R.P. Danner (1980), Vacancy Solution Theory of Adsorption from Gas Mixtures, *AIChEJ*, **26**, 76-87

Sutherland, W. (1895), *Phil. Magazine*, **40**, 421

Talu, O. and A.L. Myers (1988), Rigorous Thermodynamic Treatment of Adsorption, *AIChEJ*, **34**, 1887-1893

Talu, O. and I. Zweibel (1986), Multicomponent Adsorption Equilibria of Non-Ideal Mixtures, *AIChEJ*, **32**, 1263-1276

Tezel, F.H., H.O. Tezel and D.M. Ruthven (1992), Determination of Pure and Binary Isotherms for Nitrogen and Krypton, *J. Colloid and Interface Science*, **149**, 197-207

Touloukian, Y.S., Saxena, S.C. and P. Hestermans, *Thermophysical Properties of Matter Volume 11: Viscosity*; IFI Plenum:1975

Valanzuela, D.P., A.L. Myers, O. Talu and I. Zweibel (1988), Adsorption of Gas Mixtures: Effect on Energetic Heterogeneity, *AIChEJ*, **34**, 397-402

Valanzuela, D.P. and A.L. Myers (1984), Gas Adsorption Equilibria, *Separation and Purification Methods*, **13**, 157-183

Van Deemter, J.J., F.J. Zuiderwerg and A. Klinkenberg (1956), Longitudinal Diffusion and Resistance to Mass Transfer as Causes of Nonideality in Chromatography, *Chem. Eng. Sci.*, **5**, 271-289

Van der Vlist, E. and J. Van der Meijden (1973), Determination of Adsorption Isotherms of the Components of Binary Gas Mixtures by Gas Chromatography, *J. Chromatography*, **79**, 1-13

Van Ness, H.C. (1969), Adsorption of Gases on Solids, *Ind. Eng. Chem.*, **8**, 464-473

Verelst, H. and G. Barron (1985), Adsorption of Nitrogen, Oxygen and Argon on 5A Molecular Sieve, *J. Chem. Eng. Data*, **30**, 66-70

Veyssiere, M.-C. and C. Christianet (1981), Adsorption of Methane + Ethane and Methane + Carbon Dioxide Mixtures on Molecular Sieves, *J. Chem. Soc. Faraday Trans. I*, **77**, 1417-1424

Wilke, C.R. (1950), A Viscosity Equation for Gas Mixtures, *J. Chem. Phys.*, **18**, 517-519

Wilson, G.M. (1964) , Vapour-Liquid Equilibrium. XI A New Expression for the Excess Free Energy of Mixing, *J. American Chemical Society*, **86**, 127-133

Yagi, S. and D. Kunii (1960), Studies on Heat Transfer Near Wall Surface in Packed Columns, *AIChEJ*, **6**, 97-104

Yon, C.M. and P.H. Turnock (1971), Multicomponent Adsorption Equilibria on Molecular Sieves, *AIChEJ Symposium Series*, **67**, 75-83

Appendix A

ROTAMETER CALIBRATION CHARTS

The following graphs are obtained for each of the three gas components at P_{AT}=755 mmHg and T_{AM}=25°C. Each calibration graph is obtained by directing the output from the rotameter into a bubble flow meter which discharges into the atmosphere; subsequent timing of the bubble will give the actual volumetric flowrate. The required gas mixture composition is obtained by setting the respective gas flowrates to the required ratio. For example, if the nitrogen rotameter position is at 10.2 cm (Q_{N_2}=30 ml/min) and the argon rotameter position is at 11.4 cm (Q_{Ar}=30 ml/min), a 50% argon-nitrogen mixture will be obtained. Obviously, for a particular mixture there is an infinite number of combinations of rotameter positions. However there are lower limits for the rotameter positions; the rotameter positions must be high enough so that a finite flowrate is registered by the venting rotameter.

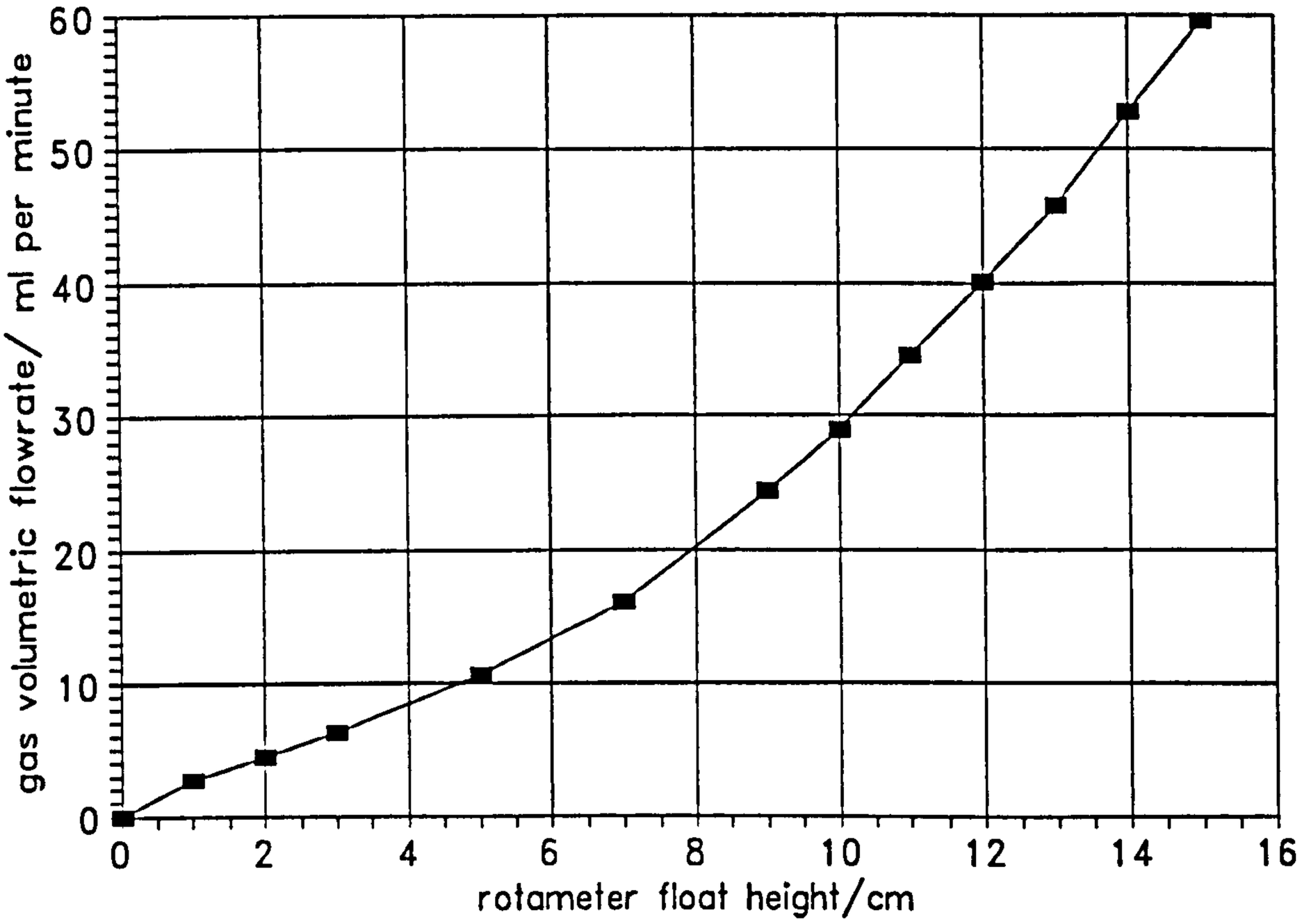

Figure A.1 Calibration Graph for Nitrogen

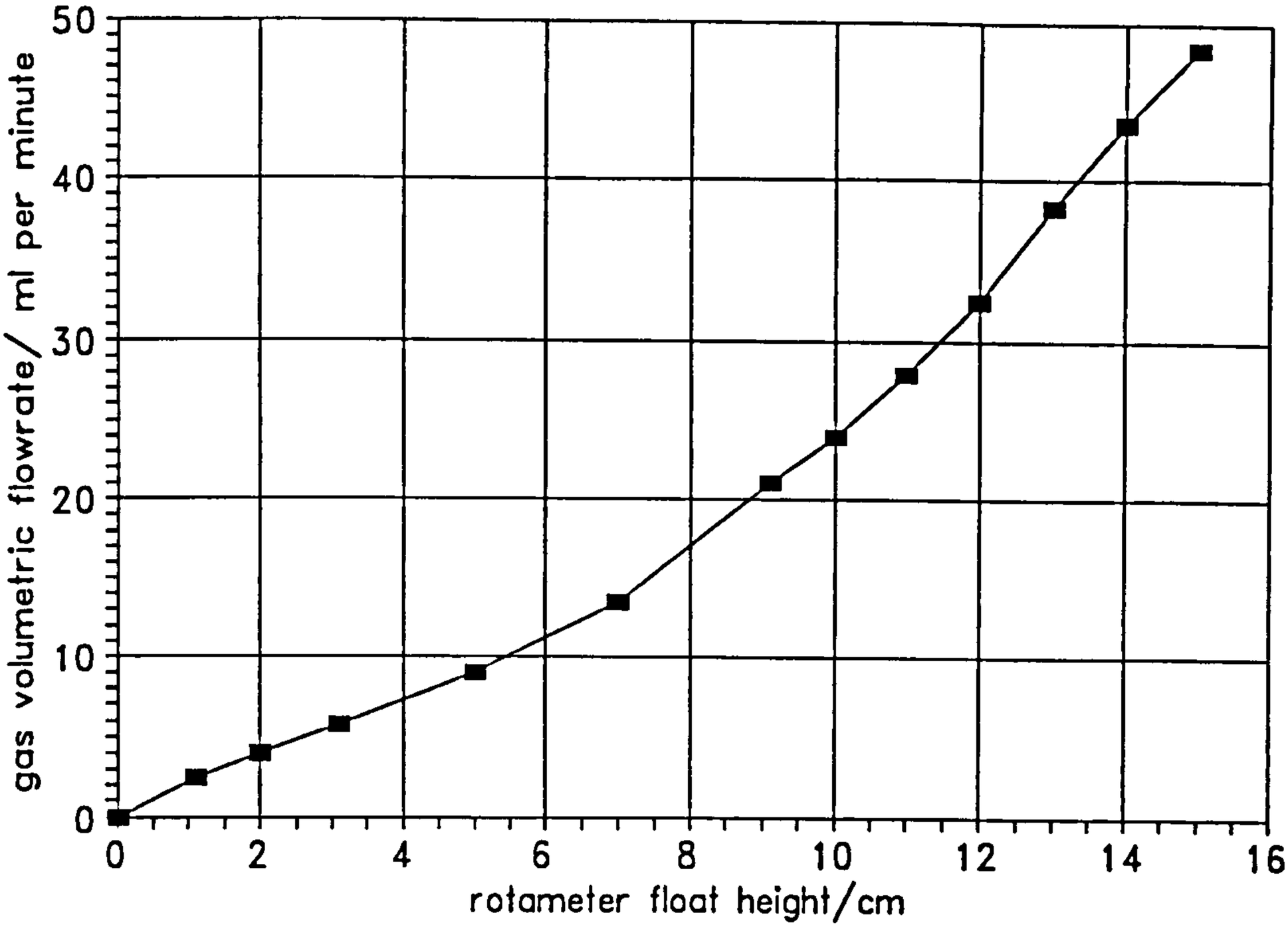

Figure A.2 Calibration Graph for Argon

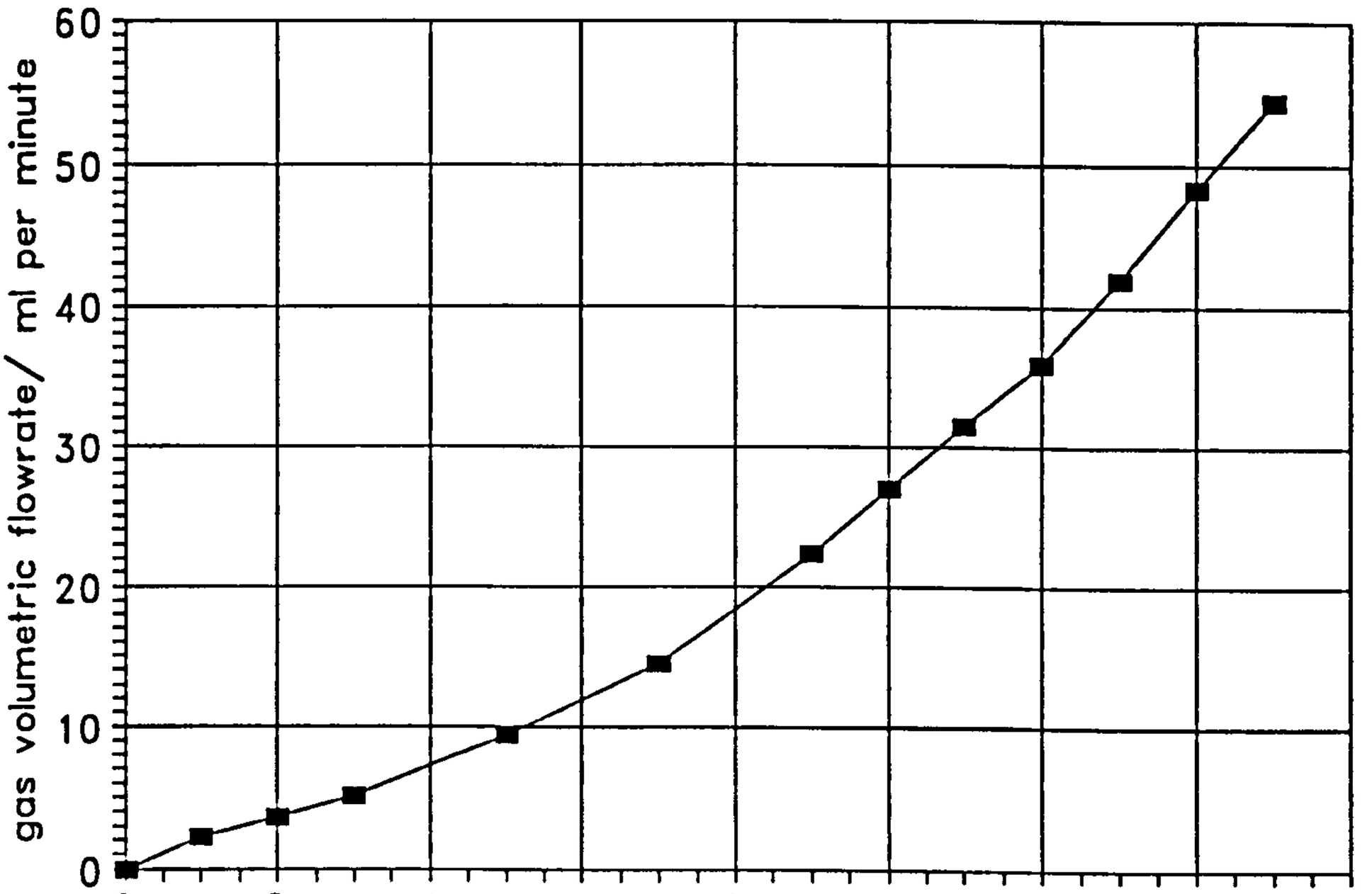

Figure A.3 Calibration Graph for Helium

Appendix B

HEAT EFFECTS IN OVEN

PROGRAM LISTING FOR TEMPERATURE VARIATION IN PRECEEDING TUBING

```
REM This programme uses a fourth-order Runge-Kutta routine together
REM with a Newton-Raphson routine to determine the variation of temperature
REM with time along the tubing preceeding the column.
CLS
INPUT " Final distance in cm ";XFINCM:XFIN=XFINCM/100
DEF FNTemp(D2,D1,TEN,TB,M,CP,HI,K,Z)
A=3.14*D1*(TEN-TB)/(M*CP)
C1=1/HI:C2=D1*LOG(D2/D1)/(2*KT):C3=D1*LOG(D3/D2)/(2*KI):C4=D1/(D3^0.75*
1.18*Z^0.25)
INVU=C1+C2+C3+C4
FNTemp=A/INVU
END DEF
TEN=80:TB=20:Z=TEN-TB:DX=0.001
KT=16:KI=0.24:KF=0.025
D3=0.0016:D2=0.0016:D1=0.0011
NU=4:FL=20:CP=29.4
M=FL/1440000:HI=NU*KF/D1
AZ=1.18*D3^0.75*((1/(D1*HI))+LOG(D2/D1)/(2*KT)+LOG(D3/D2)/(2*KI))
LPRINT "   FL=   ";:LPRINT USING "##.#";FL
LPRINT "   D1=   ";:LPRINT USING "#.####";D1
LPRINT "   D2=   ";:LPRINT USING "#.####";D2
LPRINT "   D3=   ";:LPRINT USING "#.####";D3
LPRINT "   KF=   ";:LPRINT USING "#.###";KF
LPRINT "Distance/cm   Temp./C    U/(W/sq.m C)   (TEN-T3)   Ratio"
COUNT=0
FOR X=0 TO XFIN STEP DX
REM Firstly must obtain the unknown value of Z by the Newton-Raphson method
FOR I=1 TO 10 STEP 1
GZ=AZ*Z^1.25+Z-TEN+TB
HZ=1.25*AZ*Z^0.25+1
ZN=Z-(GZ/HZ):Z=ZN
NEXT I
K1=FNTemp(D2,D1,TEN,TB,M,CP,HI,K,Z)*DX
K2=FNTemp(D2,D1,TEN,TB+K1/2,M,CP,HI,K,Z)*DX
K3=FNTemp(D2,D1,TEN,TB+K2/2,M,CP,HI,K,Z)*DX
K4=FNTemp(D2,D1,TEN,TB+K3,M,CP,HI,K,Z)*DX
DTB=(K1+2*K2+2*K3+K4)/6
CN=COUNT/10
IF CN=INT(CN) THEN LPRINT USING "      ##.#";100*X;:_
LPRINT USING "   #####.####";TB;:LPRINT USING "     ###.##";1/INVU;:__
LPRINT USING "        ##.###";Z;:RA=Z/(TEN-TB):LPRINT USING "    #.###";RA
COUNT=COUNT+1:TB=TB+DTB
NEXT X
LPRINT "  Distance along tubing is ";:LPRINT USING "##.#";XFINCM;:LPRINT
" cm"
LPRINT "  Value of TB is ";:LPRINT USING " ##.####";TB
STOP
```

Table B.1 Normal Flowrate: Exposed 1/16 (43 thou) inch Tubing

L/cm	T_B/°C	$U/\frac{W}{m^2°C}$	$\frac{T_{EN}-T_3}{°C}$	$\frac{T_{EN}-T_3}{T_{EN}-T_B}$
0	20.00	15.81	24.78	0.826
1	40.94	12.39	7.83	0.864
2	46.52	10.12	3.10	0.889
3	48.42	8.51	1.43	0.906
4	49.19	7.32	0.74	0.919
5	49.55	6.41	0.42	0.929
6	49.73	5.7	0.25	0.937
7	49.83	5.12	0.16	0.944
8	49.89	4.65	0.11	0.949
9	49.92	4.26	0.07	0.953

Table B.2 Normal Flowrate: Insulated 1/16 (43 thou) inch Stainless Steel Tubing

L/cm	T_B/°C	$U/\frac{W}{m^2°C}$	$\frac{T_{EN}-T_3}{°C}$	$\frac{T_{EN}-T_3}{T_{EN}-T_B}$
0	20.00	21.70	21.89	0.730
1	44.00	16.23	4.79	0.798
2	48.25	12.75	1.48	0.841
3	49.34	10.41	0.57	0.870
4	49.71	8.74	0.20	0.891
5	49.85	7.52	0.13	0.908
6	49.92	6.58	0.07	0.918
7	49.95	5.84	0.04	0.927
8	49.97	5.24	0.03	0.935
9	49.98	4.74	0.02	0.941

Table B.3 Normal Flowrate: Exposed 1/8 (1/16) inch Stainless Steel Tubing

L/cm	T_B/°C	$U/\frac{W}{m^2°C}$	$\frac{T_{EN}-T_3}{°C}$	$\frac{T_{EN}-T_3}{T_{EN}-T_B}$
0	20.00	15.49	22.55	0.752
1	44.27	11.37	4.68	0.818
2	48.36	8.84	1.41	0.858
3	49.39	7.18	0.54	0.885
4	49.73	6.01	0.25	0.904
5	49.86	5.15	0.13	0.917
6	49.93	4.50	0.07	0.928
7	49.96	3.99	0.04	0.936
8	49.97	3.58	0.03	0.943
9	49.98	3.25	0.02	0.948

Table B.4 Normal Flowrate: Exposed 1/4 inch (4mm) Glass Tubing

L/cm	T_B/°C	$U/\frac{W}{m^2°C}$	$\frac{T_{EN}-T_3}{°C}$	$\frac{T_{EN}-T_3}{T_{EN}-T_B}$
0	20.00	8.71	19.54	0.651
1	46.88	6.00	2.37	0.700
2	49.38	4.43	0.51	0.823
3	49.82	3.46	0.16	0.861
4	49.93	2.82	0.06	0.887
5	49.97	2.37	0.03	0.905
6	49.98	2.03	0.02	0.919
7	49.99	1.78	0.01	0.929
8	49.995	1.58	0.005	0.937
9	49.997	1.42	0.003	0.943

Table B.5 Increased Flowrate: Exposed 1/16 (x0.043) inch Stainless Steel Tubing

L/cm	T_B/°C	$U/\frac{W}{m^2°C}$
0	20.00	15.81
1	28.32	14.82
2	34.01	13.93
3	38.00	13.14
4	40.85	12.42
5	42.92	11.77
6	44.45	11.18
7	45.59	10.64
8	46.46	10.15
9	47.14	9.70

PROGRAM LISTING FOR EFFECT OF ADSORPTION HEAT ON FRONTAL TEMPERATURE RISE

```
REM Programme to determine dimensionless concentration and temperature
REM profiles with respect to dimensionless time. For BETA=0 the programme
REM employs an iterative procedure whereas for BETA not zero a Runge-Kutta
REM method is employed using a step-length of 0.01 time unit
DEF FNP(L,PHI,THETA)=PHI*(1-PHI)/(PHI+(1-L)*EXP(THETA)/L)
DEF  FNT(A,B,L,PHI,THETA,CF)=((PHI*(1-PHI)/(PHI+(1-L)*EXP(THETA)/L))-A*T
HETA^CF)/B
INPUT "  Value of Alpha  ",AL
INPUT "  Value of Beta   ",B
INPUT "  Value of Lamda  ",L
DHA=40000
TSU=300
RG=8.314
MF=DHA/(RG*TSU^2)
NCM=0.000118
D0=0.038:D1=0.038
HW=0.002*(0.038/D1)
ALN=(AL*NCM*(D0^0.75))/(HW*D1*(MF^0.25))
PRINT "  Thermostatted column Y/N?":I$=INPUT$(1):_
IF I$= "Y" THEN CF=1:A=AL ELSE CF=1.25:A=ALN
IF B=0 THEN GOSUB NRM ELSE GOSUB RKM
REM To plot out the generated curves in graphical form
SCREEN 9:COLOR 4,3
LOCATE 6,4:PRINT "1.0"
LOCATE 15,4:PRINT "0.5"
LOCATE 23,4:PRINT "0.0"
LOCATE 10,3:PRINT "Psi":COLOR 1,3
REM Fixing the theta scale
IF THETAM< 2.1 THEN
MSV=2.0
ELSE
SF=LOG10(THETAM)/LOG10(2):MSV=2^(1+INT(SF))
END IF
LOCATE 6,73:PRINT USING " ##.#";MSV
LOCATE 15,73:PRINT USING " ##.#";MSV/2
LOCATE 23,75:PRINT "0.0"
LOCATE 10,75:PRINT " Theta"
```

```
COLOR 5,3:LOCATE 25,20:PRINT "Dimensionless Time"
LINE (50,60)-(590,310),,B
FOR M=104 TO 536 STEP 54
LINE (M,60)-(M,310),8
NEXT M
FOR K=85 TO 285 STEP 25
LINE (50,K)-(590,K),7
NEXT K
COLOR 4,3: LOCATE 1,1:PRINT " Psi is dimensionless concenctration"
COLOR 1,3: LOCATE 2,1:PRINT " Theta is dimensionless temperature"
COLOR 6,3: LOCATE 1,40:PRINT "Alpha1= ";:PRINT USING "##.###";A
COLOR 13,3:LOCATE 1,55:PRINT "Beta= ";:PRINT USING "##.###";B
COLOR 10,3:LOCATE 2,40:PRINT "Lamda= ";:PRINT USING "#.###";L
COLOR 14,3
LOCATE 2,55:PRINT "Theta max.= ";:PRINT USING "##.###";THETAM
LOCATE 3,32:PRINT "Time front= ";:PRINT USING "##.#";TIMEFR
LOCATE 3,55:PRINT "Theta avge.= ";:PRINT USING "##.###";AFTHETA
IF B=0 THEN GOSUB NRPLOT ELSE GOSUB RKPLOT
STOP
RK4:
K1=FNP(L,PHIS,THETAS)*DT
LI=FNT(A,B,L,PHIS,THETAS,CF)*DT
K2=FNP(L,PHIS+K1/2,THETAS+L1/2)*DT
L2=FNT(A,B,L,PHIS+K1/2,THETAS+L1/2,CF)*DT
K3=FNP(L,PHIS+K2/2,THETAS+L2/2)*DT
L3=FNT(A,B,L,PHIS+K2/2,THETAS+L2/2,CF)*DT
K4=FNP(L,PHIS+K3,THETAS+L3)*DT
L4=FNT(A,B,L,PHIS+K3,THETAS+L3,CF)*DT
DELPHI=(K1+2*K2+2*K3+K4)/6
DELTHE=(L1+2*L2+2*L3+L4)/6
RETURN
RKM:
INPUT "   Time of integration  ",TIMET
IF B<0 THEN PHI1=0.999:DR=-1 ELSE PHI1=0.0001:DR=1
THETAS=0.001:TIME=0:TIMEFR=0:DTF=0.1
DELTHEP=0.01:TAREAR=0:TAREAF=0
SPHI=0.01:EPHI=1-SPHI
PRINT "   Time    PHI          Theta"
PHIS=PHI1:DT=DR*0.01
IFINAL=TIMET*100
FOR I=1 TO IFINAL STEP 1
GOSUB RK4
IF PHIS>EPHI THEN LAL1=1
IF PHIS<SPHI THEN LAL2=1
IF SGN (DELTHE/DELTHEP)= -1 THEN_
THETAM=THETAS:TIMEM=TIME
AREAR=DT*THETAS:TAREAR=TAREAR+AREAR
IF PHIS<SPHI OR PHIS>EPHI THEN DTF=0 ELSE DTF=0.01
AREAF=DTF*THETAS:TAREAF=TAREAF+AREAF
TIME=TIME+DT:TIMEFR=TIMEFR+DTF
PHIS=PHIS+DELPHI
THETAS=THETAS+DELTHE
IT=I/100:IF IT=INT(IT) THEN_
PRINT USING " ###.##";TIME;:PRINT USING " ####.######";PHIS,THETAS
DELTHEP=DELTHE
NEXT I
IF CF=1 THEN LPRINT " Thermostatted Column Conditions" ELSE_
LPRINT " Limiting Heat Transfer at Column Surface"
LPRINT "  Value of Alpha is  ";:LPRINT USING " ##.###";A
LPRINT "  Value of Beta is   ";:LPRINT USING " ###.###";B
LPRINT "  Value of Lamda is  ";:LPRINT USING " #.###";L
LPRINT "  Maximum value of theta is ";:LPRINT USING " ##.###";THETAM
LPRINT "  Time for maximum is ";:LPRINT USING " ###.#";TIMEM
AVTHETA=TAREAR/TIME
PRINT "Average value of theta over whole interval is";
PRINT USING " #.###"; AVTHETA:
AFTHETA=TAREAF/TIMEFR
```

```
LPRINT "   Average value of theta over front is ";:LPRINT USING
"#.###";AFTHETA
LPRINT "  Time interval for front is ";:LPRINT USING " ###.#";TIMEFR
IF B<>0 THEN LPRINT "  Time of integration is ";:LPRINT USING " ##.#";TIMET
LALT=LAL1+LAL2:IF LALT <>2 THEN LPRINT " Integration time not large enough
"
PRINT "  Ready for graphics Y/N? ":I$=INPUT$(1):IF I$= "Y" THEN GOTO 200
200 RETURN
NRM:
REM First stage of calculation is to obtain peak value of theta
100 INPUT "   Starting value of theta is  ",THETA
FOR I=1 TO 10 STEP 1:THETAP=THETA
M=A*THETA^CF:K=((1-L)/L)*EXP(THETA)
FTHETA=(M-1)^2-(4*M*K)
GTHETA=(2*A*(M-1)*CF*THETA^(CF-1))-4*A*K*(THETA^CF+CF*THETA^(CF-1))
THETAN=THETA-(FTHETA/GTHETA):THETA=THETAN
NEXT I
RATIO=THETAP/THETA
IF RATIO<1.001 AND RATIO>0.999 THEN
PRINT "  Iteration successful ":THETAM=THETA:PHIM=(1-M)/2
PRINT "  Maximum value of theta is  ";:PRINT USING " ##.###";THETAM
PRINT "  Corresponding psi point is  ";:PRINT USING " #.###";PHIM
ELSE
PRINT "  Require another iteration with higher starting theta value "
GOTO 100
END IF
REM Second stage is to use the method to step down
STP=0.001:PHI3=PHIM-STP:THETA=THETAM:TIMED=0:TAREAFD=0:TIMEDF=0
PRINT "    Time          Psi       Theta ":C=0
FOR PSI=PHI3 TO 0.005 STEP -STP
FOR I=1 TO 10 STEP 1:THETAP=THETA
N=PSI*(1-PSI):HTHETA=N-A*THETA^CF*(PSI+(1-L)*EXP(THETA)/L)
JTHETA=-A*CF*THETA^(CF-1)*(PSI+(1-L)*EXP(THETA)/L)-(A*THETA^CF*(I-L)*EX
P(THETA)/L)
THETAN=THETA-(HTHETA/JTHETA):THETA=THETAN
NEXT I
RATIO=THETA/THETAP
IF RATIO<1.001 AND RATIO>0.999 THEN
DTD=STP/(A*THETA^CF):TIMED=TIMED+DTD
ELSE
PRINT "  Iteration not convergent ":STOP
END IF
IF PSI<0.01 THEN DTD=0
AREAFD=THETA*DTD:TAREAFD=TAREAFD+AREAFD:TIMEDF=TIMEDF+DTD
C=C+1:CN=C/50:IF CN=INT(CN) OR PSI=0.01_
THEN PRINT USING "  ###.###";TIMED,PSI,THETA
NEXT PSI:TIMEDS=TIMED
REM Third stage is to use the method to step down the phi curve
PHI4=PHIM+STP:THETA=THETAM:TIMEU=0:TAREAFU=0:TIMEUF=0
PRINT "    Time          Psi       Theta ":C=0
FOR PSI=PHI4 TO 0.995 STEP STP
FOR I=1 TO 10 STEP 1:THETAP=THETA
N=PSI*(1-PSI):HTHETA=N-A*THETA^CF*(PSI+(1-L)*EXP(THETA)/L)
JTHETA=-A*CF*THETA^(CF-1)*(PSI+(1-L)*EXP(THETA)/L)-(A*THETA^CF*(I-L)*EX
P(THETA)/L)
THETAN=THETA-(HTHETA/JTHETA):THETA=THETAN
NEXT I
RATIO=THETA/THETAP
IF RATIO<1.001 AND RATIO>0.999 THEN
DTU=STP/(A*THETA^CF):TIMEU=TIMEU+DTU
ELSE
PRINT "  Iteration not convergent ":STOP
END IF
IF PSI>0.99 THEN DTU=0
AREAFU=THETA*DTU:TAREAFU=TAREAFU+AREAFU:TIMEUF=TIMEUF+DTU
C=C+1:CN=C/50:IF CN=INT(CN) OR PSI=0.01_
THEN PRINT USING "  ###.###";TIMEU,PSI,THETA
```

```
NEXT PSI:TIMEUS=TIMEU:TIMES=TIMEDS+TIMEUS
PRINT    "  Time taken from maximum down to psi= 0.005 is  ";:
PRINT USING "##.###";TIMEDS
PRINT    "  Time taken from maximum up to psi= 0.995 is  ";:
PRINT USING "##.###";TIMEUS
TIMEFR=TIMEUF+TIMEDF
PRINT "  Total front time is  ";:PRINT USING " ##.###";TIMEFR
AFTHETA=(TAREAFU+TAREAFD)/TIMEFR
PRINT "  Theta front average is  ";:PRINT USING " ##.###";AFTHETA
ZEPIX=(TIMEDS/(TIMES))*540+50
PRINT " Ready for graphics Y/N? ":I$=INPUT$(1):IF I$= "Y" THEN GOTO 300
300 RETURN
RKPLOT:
REM Now to generate points for the graph
THETAS=0.001:TIME=0:DT=DR*0.01
PHIS=PHI1:JFINAL=TIMET*100
FOR J=1 TO JFINAL STEP 1
GOSUB RK4
TIME=TIME+DT
PHIS=PHIS+DELPHI
THETAS=THETAS+DELTHE
IF B>0 THEN XPIX=(TIME/TIMET)*540+50 ELSE XPIX=(TIME/TIMET)*540+590
YPIX=PHIS*(-250)+310
ZPIX=(THETAS/MSV)*(-250)+310
PSET (XPIX,YPIX),4
PSET (XPIX,ZPIX),1
NEXT J:COLOR 5,3
IF B<0 THEN HW=-1:ZW=-1:FW=0 ELSE HW=1:ZW=0:FW=1
LOCATE 23,38:PRINT USING "###.#";HW*TIMET/2
LOCATE 23,71:PRINT USING "###.#";FW*TIMET
LOCATE 23,3:PRINT USING "###.#";ZW*TIMET
RETURN
NRPLOT:
THETA=THETAM:TIMED=0
FOR PSI=PHI3 TO 0.005 STEP -STP
FOR I=1 TO 10 STEP 1
N=PSI*(1-PSI):HTHETA=N-A*THETA^CF*(PSI+(1-L)*EXP(THETA)/L)
JTHETA=-A*CF*THETA^(CF-1)*(PSI+(1-L)*EXP(THETA)/L)-(A*THETA^CF*(I-L)*EX
P(THETA)/L)
THETAN=THETA-(HTHETA/JTHETA):THETA=THETAN
NEXT I
DTD=STP/(A*THETA^CF):TIMED=TIMED+DTD
XPIX=ZEPIX-(TIMED*540)/TIMES
YPIX=PSI*(-250)+310:ZPIX=(THETA/MSV)*(-250)+310
PSET (XPIX,YPIX),4:PSET (XPIX,ZPIX),1
NEXT PSI
THETA=THETAM:TIMEU=0
FOR PSI=PHI4 TO 0.995 STEP STP
FOR I=1 TO 10 STEP 1
N=PSI*(1-PSI):HTHETA=N-A*THETA^CF*(PSI+(1-L)*EXP(THETA)/L)
JTHETA=-A*CF*THETA^(CF-1)*(PSI+(1-L)*EXP(THETA)/L)-(A*THETA^CF*(I-L)*EX
P(THETA)/L)
THETAN=THETA-(HTHETA/JTHETA):THETA=THETAN
NEXT I
DTU=STP/(A*THETA^CF):TIMEU=TIMEU+DTU
XPIX=ZEPIX+(TIMEU*540)/TIMES
YPIX=PSI*(-250)+310:ZPIX=(THETA/MSV)*(-250)+310
PSET (XPIX,YPIX),4:PSET (XPIX,ZPIX),1
NEXT PSI:COLOR 5,3
Z=((ZEPIX-50)/540)*68+5
LINE (ZEPIX,60)-(ZEPIX,310),5
LOCATE 23,Z:PRINT "ZERO"
LOCATE 23,71:PRINT USING "###.#";TIMEUS
LOCATE 23,3:PRINT USING "###.#";-TIMEDS
RETURN
```

Table B.6 Summary of Hypothetical Adsorption Heat Runs

		dimensionless variables				
Run	HT Mode	α	β	λ	θ_{MAX}	θ_{MEAN}
1A	T	0.220	0.2	0.8	0.933	0.523
1B	L	0.061	0.2	0.8	1.626	1.156
2A	T	2.000	0.2	0.8	0.178	0.069
2B	L	0.242	0.2	0.8	0.907	0.528
3A	T	18.00	0.2	0.8	0.021	0.008
3B	L	5.00	0.2	0.8	0.122	0.054
4A	T	18.00	0.2	0.1	0.002	0.000
4B	L	5.00	0.2	0.1	0.001	0.000
5A	T	0.05	0.2	0.67	1.504	1.049
5B	L	0.014	0.2	0.67	2.129	1.685

Appendix C

DATA REQUIRED FOR CHAPTER EIGHT

Table C.1 Summary of Data for Nitrogen-Argon System at 25°C

		nitrogen prtbn		argon prtbn	
% N_2	Q_M/$\frac{ml}{min}$	τ_X/s	τ_N/s	τ_X/s	τ_N/s
0	42.6	474	307	-	6.3
5.3	42.6	455	285	458	-5.1
10.0	43.6	426	266	425	-18.7
25.3	44.7	353	199	352	-52.2
49.6	45.9	257	116	254	-90.5
74.8	48.7	180	50.3	181	-123.5
90.0	51.9	141	25.1	142	-125.7
95.2	52.1	130.5	15	132	-136.4
100.0	52.5	-	8.1	122	-141.0

Table C.2 Summary of Data for Nitrogen-Helium System at 25°C

		nitrogen prtbn		helium prtbn	
% N_2	$Q_M/\frac{ml}{min}$	τ_X/s	τ_N/s	τ_X/s	τ_N/s
0	47.9	430	386	-	2.8
4.6	48.7	392	347	392	-12.0
10.0	49.1	365	319	366	-26.4
25.1	48.7	300	252	290	-68.9
50.0	49.5	193	147.1	186.1	-119.7
75.3	53.4	108	66	100	-153.6
90.0	54.2	72.3	30.2	65.3	-182.2
95.0	54.0	60.9	18.9	53.4	-183.3
100.0	52.3	-	8.1	45.8	-180.0

Table C.3 Summary of Data for Argon-Helium System at 25°C

		argon prtbn		helium prtbn	
% Ar	$Q_M/\frac{ml}{min}$	τ_X/s	τ_N/s	τ_X/s	τ_N/s
0	49.4	144	94.3	-	2.8
4.9	47.3	141	95.3	131	-0.7
9.8	45.5	141	91.7	133	-5.4
25.2	41.6	138	82.8	135.9	-22.1
50.4	40.9	112.9	55.3	109.7	-47.4
74.9	41.0	88	30.7	84.6	-71.3
90.0	40.8	71	17.2	69.4	-85.4
95.3	42.9	66.4	12.3	62.7	-89.2
100.0	42.9	-	6.3	58.2	-92.4

Table C.4 Summary of Data for Nitrogen-Argon System at 54°C

		nitrogen prtbn		argon prtbn	
% N_2	$Q_M/\frac{ml}{min}$	τ_X/s	τ_N/s	τ_X/s	τ_N/s
0	42.3	242	130.9	-	4.5
4.7	44.7	225	118.1	227	0.3
10.1	44.3	225	115.9	222	-9.3
24.9	41.8	207	91.3	206	-24.3
49.7	44.8	159	57	159	-48.4
75.0	49.1	118.5	28.4	118	-61
90.7	50.3	102	12.3	102	-71
95.5	51.0	96	9.6	96	-81
100	51.7	-	7	92	-80

Table C.5 Summary of Data for Nitrogen-Argon System at 81°C

		nitrogen prtbn		argon prtbn	
% N_2	$Q_M/\frac{ml}{min}$	τ_X/s	τ_N/s	τ_X/s	τ_N/s
0	39.7	162	69.6	-	4.7
5	40.8	155	63.6	156	-1.0
10	41.2	151.5	61.3	148.5	-1.8
25	43.0	133.5	47.9	133.5	-9.6
50	45.9	111	33	112.5	-20.5
75	49.6	90	18	88.5	-33.6
90	52.4	78	9.3	76.5	-37.9
95	49.9	79.5	9.7	79.5	-41.7
100	50.8	-	5.7	76.5	-42.1

Appendix D

PROGRAM LISTING FOR CHAPTER EIGHT

PROGRAM LISTING FOR ARGON-NITROGEN SYSTEM

```
5 NP=8:ND=5:VOID=0.376:VOL=18:SH=349:SW=639:NX=4:DTN=0
10 DIM XNF(9,2):DIM AN(9,3):DIM NA(9,3):DIM EN(9,2):DIM EA(9,2)
12 DIM P(NP):DIM T(NP):DIM U(NP):DIM V(NP):DIM X(NP,NX)
15 DIM A(ND):DIM B(ND):DIM C(ND):DIM D(ND+1):DIM F(ND):DIM G(ND)
18 DIM L(ND):DIM Q(ND):DIM S(ND)
19 DIM PQNN(11):DIM PQAN(11):DIM PQNA(11):DIM PQAA(11)
20 DIM HNN(9):DIM HNA(9):DIM HAN(9):DIM HAA(9)
30 DIM FPVNN(9):DIM FPVNA(9):DIM FPVAN(9):DIM FPVAA(9)
40 PD=35:POUTG=38:PAT=762:T=295:TAT=295:PDC=860
50 DIM CNN(5):DIM CNA(5):DIM CAN(5):DIM CAA(5)
70 FOR J=1 TO 9 STEP 1
80 READ XNF(J,1):READ XNF(J,2):READ NA(J,1):READ NA(J,2):READ NA(J,3)
90 READ AN(J,1):READ AN(J,2):READ AN(J,3):NEXT J
100 POUTA=POUTG+PAT:PRT=PD/POUTA:PFN1=(1+PRT+(PRT^2)/3)/(1+PRT/2)
110 PMEAN=POUTA*PFN1:PFN2=(PAT*T)/(TAT*PMEAN*120)
120 PFN3=(1+PRT/3)/(1+PRT/2):PFN4=(PDC*(PAT+PD+PDC/2))/(PD*(PAT+PD/2))
125 CTOT=PMEAN*273*1000/(22.4*T*760)
130 T1=0:T2=0:DTN=0.0:SUMA=0.00:SUMN=0.00
140 PRINT"No correction factor Y/N?":I$=INPUT$(1):IF I$="Y" THEN GOTO 180
150 T1=1:PRINT"Just Fp correction Y/N?":I$=INPUT$(1):IF I$="N" THEN T2=1
160 PRINT"Reductions in TN values Y/N?":I$=INPUT$(1):IF I$="N" THEN GOTO
180
180 INPUT "Nitrogen trace flow in ml/min",TRFN
190 INPUT "Argon trace flow in ml/min",TRAN
200 CLS:IF T1+T2=0THEN PRINT"No correction factors":GOTO 230
210 IF T2=0 THEN LPRINT "Pressure correction only": GOTO 230
220 LPRINT "Pressure and viscosity corrections employed"
230 PRINT "Value of nitrogen trace flow is  ";TRFN;"  ml/min"
240 PRINT "Value of argon trace flow is  ";TRAN;"  ml/min"
260 LPRINT "  XN    (HN)Ntr  (HN)Atr  (HA)Ntr  (HA)Atr"
270 FOR I=1 TO 9 STEP 1:NA(I,3)=NA(I,3)-DTN:AN(I,3)=AN(I,3)-DTN
280 XNT=1.0:FLOW=(XNF(I,2)+TRFN)*PFN2:IF I=9 THEN GOSUB 1000:GOTO 350
290 CFFN=XNF(I,1)/(XNT-XNF(I,1)):CFFA=(1-XNF(I,1))/(XNF(I,1)-XNT)
300 FPVNN(I)=1+(T1*CFFN*PD*PFN3*(1+T2*NA(I,1))/(2*PMEAN))
310 FPVAN(I)=1+(T1*CFFA*PD*PFN3*(1+T2*NA(I,1))/(2*PMEAN))
320 FCORRN=(XNF(I,2)+TRFN)/XNF(I,2)
330 HNN(I)=(FLOW/FPVNN(I))*(NA(I,2)+CFFN*NA(I,3))
340 HAN(I)=(FLOW/FPVAN(I))*(NA(I,2)+CFFA*NA(I,3))
350 XNT=0.0:FLOW=(XNF(I,2)+TRAN)*PFN2:IF I=1 THEN GOSUB 1000:GOTO 420
360 CFFN=XNF(I,1)/(XNT-XNF(I,1)):CFFA=(1-XNF(I,1))/(XNF(I,1)-XNT)
370 FPVNA(I)=1+(T1*CFFN*PD*PFN3*(1+T2*AN(I,1))/(2*PMEAN))
380 FPVAA(I)=1+(T1*CFFA*PD*PFN3*(1+T2*AN(I,1))/(2*PMEAN))
390 FCORRA=(XNF(I,2)+TRAN)/XNF(I,2)
400 HNA(I)=(FLOW/FPVNA(I))*(AN(I,2)+CFFN*AN(I,3))
410 HAA(I)=(FLOW/FPVAA(I))*(AN(I,2)+CFFA*AN(I,3))
420 IF I=1 THEN GOTO 430 ELSE GOTO 470
430 IF T1+T2=0 THEN GOTO 440 ELSE GOTO 450
440 LPRINT USING "#.###";XNF(I,1);:LPRINT USING "    ###.##";HNN(I);
LPRINT "  No value";:LPRINT USING "  ###.##";HAN(I);
LPRINT "   No value":GOTO 550
450 LPRINT USING "#.###";XNF(I,1);:LPRINT USING "    ###.##";HNN(I);
LPRINT "  No value";:LPRINT USING "  ###.##";HAN(I);
LPRINT USING "    ###.##";HAA(I)
460 EA(I,1)=HAN(I)-HAA(I):EA(I,2)=EA(I,1)/(HAN(I)+HAA(I)):GOTO 550
470 IF I=9 THEN GOTO 480 ELSE GOTO 520
480 IF T1+T2=0 THEN GOTO 490 ELSE GOTO 500
490 LPRINT USING "#.###";XNF(I,1);:LPRINT"  No value";
LPRINT USING "  ###.##";HNA(I);:LPRINT"   No value";
LPRINT USING " ###.##";HAA(I):GOTO 550
500 LPRINT USING "#.###";XNF(I,1);:LPRINT USING"   ###.##";HNN(I),HNA(I);
```

```
LPRINT"   No value";:LPRINT USING " ###.##";HAA(I)
510 EN(I,1)=HNN(I)-HNA(I):EN(I,2)=EN(I,1)/(HNN(I)+HNA(I)):GOTO 550
520  EN(I,1)=HNN(I)-HNA(I):EN(I,2)=EN(I,1)/(HNN(I)+HNA(I)):SUMN=SUMN+EN(
I,2)^2
530  EA(I,1)=HAN(I)-HAA(I):EA(I,2)=EA(I,1)/(HAN(I)+HAA(I)):SUMA=SUMA+EA(
I,2)^2
540 LPRINT USING "#.###";XNF(I,1);
LPRINT USING "   ###.##";HNN(I),HNA(I),HAN(I),HAA(I)
550 NEXT I
560 LPRINT "Sum of HN errors squared is ";:LPRINT USING "#.###^^^^";SUMN
570 LPRINT "Sum of HA errors squared is ";:LPRINT USING "#.###^^^^";SUMA
580 PRINT "Look at Fpv values Y/N?":I$=INPUT$(1):IF I$="Y" THEN GOSUB 1100
590  PRINT "Try another run Y/N?":I$=INPUT$(1):IF I$="Y" THEN GOTO 130
600  PRINT "Print out comparisons Y/N?":I$=INPUT$(1):IF I$= "Y" THEN GOTO
700
700 LPRINT "  XN     DiffHN   %Error   DiffHA   %Error"
710 IF T1+T2=0 THEN GOTO 720 ELSE GOTO 730
720 LPRINT USING "#.###";XNF(1,1);
LPRINT" No comparisons possible for HA or HN"
GOTO 735
730 LPRINT USING "#.###";XNF(I,1);:LPRINT"      No comp.(HN)";
LPRINT USING "   ###.##";EA(1,1),100*EA(1,2)
735 FOR I=2 TO 8 STEP 1
738 LPRINT USING "#.###";XNF(I,1);
740 LPRINT USING "   ###.##";EN(I,1),100*EN(I,2),EA(I,1),100*EA(I,2)
750 NEXT I
760 IF T1+T2=0 THEN GOTO 770 ELSE GOTO 780
770 LPRINT USING "#.###";XNF(9,1);
LPRINT" No comparisons possible for HA or HN"
GOTO 790
780 LPRINT USING "#.###";XNF(9,1);
LPRINT USING "   ###.##";EN(9,1),100*EN(9,2);:LPRINT"     No comp.(HA)"
790 IF T1=0 THEN GOTO 820
800  LPRINT" At pure nitrogen, HN error is ";:LPRINT USING
"#.###^^^^";EN(9,2)^2
810 LPRINT" At pure argon, HA error is ";:LPRINT USING "#.###^^^^";EA(1,2)^2
820 LPRINT "Sum of HN errors squared is ";:LPRINT USING "#.###^^^^";SUMN
830 LPRINT "Sum of HA errors squared is ";:LPRINT USING "#.###^^^^";SUMA
840 PRINT "Try composition prediction Y/N?":I$=INPUT$(1)
IF I$="Y" THEN GOSUB 1300
850 PRINT "Go to fitting programme Y/N?":I$=INPUT$(1):IF I$="Y" THEN GOTO
1800
855 PRINT "Try another run Y/N?":I$=INPUT$(1):IF I$="Y" THEN GOTO 130
860 STOP
1000 REM Subroutine to deal with cases for adding pure trace to pure bulk.
1005 IF T1+T2=0 THEN GOTO 1050
1010 IF I=1 THEN GOTO 1040
1020 HNN(9)=FLOW*PFN1*2*POUTA*NA(I,3)/(PD*PFN3):GOTO 1050
1040 HAA(1)=FLOW*PFN1*2*POUTA*AN(I,3)/(PD*PFN3)
1050 RETURN
1100 REM Subroutine to show all values of Fpv terms
1110 IF T1=0 THEN LPRINT "All terms unity for simple case":GOTO 1130
1120 IF T2=1 THEN LPRINT "Pressure and viscosity terms":GOTO 1130
1125 LPRINT "Pressure only correction terms"
1130 LPRINT "  XN    FPVNN   FPVNA   FPVAN   FPVAA"
1140 LPRINT USING "#.###";XNF(1,1);
LPRINT USING "   #.###";FPVNN(1);:LPRINT"  No value ";
LPRINT USING "#.###";FPVAN(1);:LPRINT"  No value"
1150 FOR J=2 TO 8 STEP 1
1160 LPRINT USING "#.###";XNF(J,1);
LPRINT USING "   #.###";FPVNN(J),FPVNA(J),FPVAN(J),FPVAA(J):NEXT J
1170 LPRINT USING "#.###";XNF(9,1);:LPRINT "  No value ";
LPRINT USING "#.###";FPVNA(9);:LPRINT"  No value ";
LPRINT USING "#.###";FPVAA(9)
1180 PRINT "Are you ready to go on Y/N?":I$=INPUT$(1):IF I$="Y" THEN GOTO
1190
1190 RETURN
1300 REM Subroutine to try and predict compositions
1310 IF T1=0 THEN GOTO 1410
1320 IF T2=1 THEN PRINT "Pressure and viscosity terms":GOTO 1340
```

```
1330 PRINT "Pressure only correction terms"
1340 PRINT"XNCab  CFFA   CFFAP   XNP1   CFFN   CFFNP   XNP2"
1350          FOR          I=2          TO          8          STEP
1:FLOW=XNF(I,2)*PFN2:B=PD*PFN3*(1+T2*AN(I,1))/(2*PMEAN)
1360 C=PD*PFN3*(1+T2*NA(I,1))/(2*PMEAN)
1370 CFFAP=(HAN(I)-FLOW*AN(I,2))/(FLOW*AN(I,3)-B*HAN(I))
1380 CFFNP=(HNA(I)-FLOW*NA(I,2))/(FLOW*NA(I,3)-C*HNA(I))
1390 XNP1=1/(1+CFFAP):XNP2=CFFNP/(1+CFFNP)
1395 CFFA=(1-XNF(I,1))/XNF(I,1):CFFN=XNF(I,1)/(1-XNF(I,1))
1400 PRINT USING "#.###";XNF(I,1);
PRINT USING"  ##.##";CFFA,CFFAP;
PRINT USING"   #.###";XNP1;
PRINT USING"  ##.##";CFFN,CFFNP;
PRINT USING"   #.###";XNP2:NEXT I
1405 PRINT "Are you ready to go on Y/N?":I$=INPUT$(1):IF I$="Y" THEN GOTO
1410
1410 RETURN
1800 TAG=1:REM This part of the programme will fit all four sets of dQ/dC
1805 FOR N=1 TO 8 STEP 1:NT=N+1:X(N,2)=1:X(N,3)=0
IF TAG=1 THEN
X(N,0)=XNF(N,1):X(N,1)=(HNN(N)-VOID*VOL)/((1-VOID)*VOL)
ELSEIF TAG=2 THEN
X(N,0)=XNF(NT,1):X(N,1)=(HNA(NT)-VOID*VOL)/((1-VOID)*VOL)
ELSEIF TAG=3 THEN
X(N,0)=XNF(N,1):X(N,1)=(HAN(N)-VOID*VOL)/((1-VOID)*VOL)
ELSE
X(N,0)=XNF(NT,1):X(N,1)=(HAA(NT)-VOID*VOL)/((1-VOID)*VOL)
END IF
NEXT N:N=N-1:N9=N-2:IF N9>ND-1 THEN N9=ND-1
CLS:PRINT " O gives the best order"
PRINT " The highest allowable order is ";N9
INPUT " Polynomial order  ",L
M1=ND:IF L<>0 THEN M1=L+1
IF M1>N-1 THEN M1=N-1
GOSUB 3000
M2=M1-1:PRINT
IF L<>0 THEN
PRINT "Specified polynomial order is ";N2:GOTO 1810
ELSE
PRINT "Maximum order tested is  ";M2_
:PRINT "Order of best polynomial found is  ";N2
END IF
1810 PRINT "      Order     Goodness of fit"
FOR I=1 TO M1:PRINT I-1;"     ";G(I):NEXT:PRINT
PRINT "Coefficients of selected order"
PRINT "   Polynomial order   ";N2
PRINT "Y= ";F(1):IF N2=0 THEN GOTO 1820
PRINT "    + X * ";F(2):IF N2=1 THEN GOTO 1815
FOR I=2 TO N2:PRINT"    +X^";I;" *  ";F(I+1):NEXT
1815 PRINT "Are residuals needed Y/N?":I$=INPUT$(1):IF I$="Y" THEN GOSUB
4200
1818 PRINT "Are plotted points needed":I$=INPUT$(1):IF I$="Y" THEN GOSUB
4300
1820 PRINT "Is a plot needed Y/N?":I$=INPUT$(1):IF I$<>"Y" THEN GOTO 1830
CLS:PRINT "Polynomial order  ";N2:GOSUB 3800
PRINT "Are you ready to go on Y/N?":I$=INPUT$(1):IF I$="Y" THEN CLS
1830 PRINT "   Comp.XN     X(N,1)"
FOR N=1 TO 8
PRINT USING"    #.###";X(N,0);:PRINT USING"      ##.###";X(N,1)
NEXT N
PRINT " XN=   ";XN
PRINT " XM=   ";XM
PRINT " YN=   ";YN
PRINT " YM=   ";YM
PRINT "F(1)=  ";F(1)
PRINT "F(2)=  ";F(2)
PRINT "F(3)=  ";F(3)
PRINT "F(4)=  ";F(4)
PRINT "F(5)=  ";F(5)
PRINT "Ready to go on Y/N?":I$=INPUT$(1):IF I$="Y" THEN GOTO 1835
```

```
1835 FOR KK=1 TO 5 STEP 1
IF TAG=1 THEN
CNN(KK)=F(KK)
ELSEIF TAG=2 THEN
CNA(KK)=F(KK)
ELSEIF TAG=3 THEN
CAN(KK)=F(KK)
ELSE
CAA(KK)=F(KK)
END IF
NEXT KK
TAG=TAG+1
IF TAG=5 THEN GOTO 1850 ELSE GOTO 1805
1850 PRINT "Print out isotherms Y/N?":I$=INPUT$(1):IF I$="Y" THEN GOSUB
4100
PRINT "Try another run with different parameters Y/N?":I$=INPUT$(1)
IF I$="Y" THEN GOTO 130
STOP
3000 REM Subroutine to obtain fitting coefficients
3010 M3=M1-1:N2=M3:FOR I=1 TO M1:C(I)=0:NEXT
3020 Q(1)=0:D(1)=0:D(2)=0:A(1)=1:D2=0:P1=0:G1=0:I2=0
3030 S1=X(1,2):XN=X(1,0):XM=XN:YN=X(1,1):YM=YN
3040 FOR I=2 TO N:X=X(I,0):Y=X(I,1):IF X<XN THEN XN=X
3050 IF X>XM THEN XM=X
3060 IF Y<YN THEN YN=Y
3070 IF Y>YM THEN YM=Y
3080 S1=S1+X(I,2):NEXT
3090 Y3=(YM+YN)/2:Y4=(YM-YN)/2:IF Y4<=0 THEN F(1)=Y:N2=0:GOTO 3450
3100 FOR I=1 TO N:V=(X(I,1)-Y3)/Y4:V(I)=V:VW=V*X(I,2)
3110 P1=P1+VW:D2=D2+V*VW:P(I)=1:T(I)=0
3120 NEXT
3130 S2=P1/S1:S(1)=S2:C(1)=S2:D2=D2-S2*P1:G(1)=ABS(D2/(N-1))
3140 A1=4/(XM-XN):B1=-2-A1*XN
3150 FOR I= 1 TO N:U(I)=A1*X(I,0)+B1:NEXT I
3160 FOR I= 1 TO M3:I1=I+1:D1=0
3170 FOR J= 1 TO N:D1=D1+X(J,2)*U(J)*P(J)*P(J):NEXT J
3180 L(I1)=D1/S1:W2=S1:S1=0:P1=0
3190 FOR J=1 TO N:D1=Q(I)*T(J):T(J)=P(J)
3200 P(J)=(U(J)-L(I1))*P(J)-D1:V=X(J,2)*P(J):S1=S1+V*P(J):P1=P1+V*V(J)
3210 NEXT J:Q(I1)=S1/W2:S(I1)=P1/S1:D2=D2-S(I1)*P1
3220 G(I1)=ABS(D2/(N-1-I)):IF L>0 THEN GOTO 3290
3230 IF I2=1 THEN GOTO 3270
3240 IF G(I1)<G(I) THEN GOTO 3290
3250 N2=I-1:I2=1:G1=G(I)
3260 FOR J=1 TO M1:B(J)=C(J):NEXT:GOTO 3290
3270 IF G(I1)> = .6*G1 THEN GOTO 3290
3280 I2=0:N2=M3
3290 FOR J=1 TO I:D1=D(J+1)*Q(I):D(J+1)=A(J):A(J)=D(J)-L(I1)*A(J)-D1
3300 C(J)=C(J)+S(I1)*A(J):NEXT
3310 C(I1)=S(I1):A(I1)=1:D(I+2)=0:IF I2=0 OR I<>M3 THEN GOTO 3330
3320 FOR J=1 TO M1:C(J)=B(J):NEXT
3330 NEXT:D(1)=1:B(1)=1:F(1)=C(1)
3340 FOR I=2 TO M1:D(I)=1:B(I)=B1*B(I-1):F(1)=F(1)+C(I)*B(I):NEXT
3350 FOR J=2 TO M1:D(1)=D(1)*A1:F(J)=C(J)*D(1):K1=2:J1=J+1
3360 IF J1>M1 THEN J=M1:GOTO 3390
3370 FOR I=J1 TO M1:D(K1)=A1*D(K1)+D(K1-1)
3380 F(J)=F(J)+C(I)*D(K1)*B(K1):K1=K1+1:NEXT
3390 NEXT
3400 REM Calculate residuals
3410 FOR I=1 TO N:J=N2+1:Y5=F(J):IF N2=0 THEN GOTO 3430
3420 FOR K=1 TO N2:Y5=F(J-1)+X(I,0)*Y5:J=J-1:NEXT
3430 X(I,3)=Y5*Y4+Y3:X(I,4)=(V(I)-Y5)*Y4:NEXT
3440 FOR I=1 TO M1:F(I)=F(I)*Y4:NEXT:F(1)=F(1)+Y3
3450 RETURN
3800 REM Subroutine to plot points and curves
SCREEN 9
COLOR 3,1
LINE (30,30)-(610,320),10,B
FOR N=1 TO 8
XPIX=(580*(X(N,0)-XN)/(XM-XN))+30
```

```
YPIX=(290*(YN-X(N,1))/(YM-YN))+320
LINE (XPIX-3,YPIX-2.5)-(XPIX+3,YPIX+2.5),12,B
NEXT N
FOR XPIXS= 30 TO 610 STEP 2:SUMT=0
XNS=((XPIXS-30)*(XM-XN)/580)+XN
FOR K= 1 TO (N2+1) STEP 1
YTERM=F(K)*XNS^(K-1):SUMT=SUMT+YTERM
NEXT K
YPIXS=(290*(YN-SUMT)/(YM-YN))+320
IF XPIXS=30 THEN LINE (30,30)-(XPIXS,YPIXS),10_
ELSE LINE-(XPIXS,YPIXS),14
REM PSET (XPIXS,YPIXS),14
NEXT XPIXS
PRINT "Ready to go on Y/N?":I$=INPUT$(1):IF I$="Y" THEN GOTO 4000
4000 RETURN
4100 REM Subroutine to calculate actual isotherms for each trace
COLOR 7,0:JK1=1
LPRINT "Table of calculated isotherm points"
LPRINT "Concentrations in mol/cubic metre":PRINT
LPRINT "                    Nitrogen isotherm              Argon isotherm"
LPRINT "  XNitr.  (QN)N     (QN)A     Diff    (QA)N     (QA)A    Diff"
FOR XSP=0 TO 1.1 STEP 0.1
PQNN(JK1)=0:PQNA(JK1)=0:PQAN(JK1)=0:PQAA(JK1)=0
FOR JK2=1 TO 5 STEP 1
NNTM=CTOT*(CNN(JK2)*XSP^JK2)/JK2:PQNN(JK1)=PQNN(JK1)+NNTM
NATM=CTOT*(CNA(JK2)*XSP^JK2)/JK2:PQNA(JK1)=PQNA(JK1)+NATM
ANTM=CTOT*(CAN(JK2)*(1-XSP^JK2))/JK2:PQAN(JK1)=PQAN(JK1)+ANTM
AATM=CTOT*(CAA(JK2)*(1-XSP^JK2))/JK2:PQAA(JK1)=PQAA(JK1)+AATM
NEXT JK2
DIFFN=PQNN(JK1)-PQNA(JK1):DIFFA=PQAN(JK1)-PQAA(JK1)
LPRINT USING  "  #.###";XSP;
LPRINT                                  USING                                "
####";PQNN(JK1),PQNA(JK1),DIFFN,PQAN(JK1),PQAA(JK1),DIFFA
JK1=JK1+1:NEXT XSP
LPRINT:LPRINT"    Comparison of total amounts adsorbed"
LPRINT"   XNitr.      Nitr.trace tot.     Ar.trace total       Diff."
FOR JK1=1 TO 11 STEP 1
NTTOT=PQNN(JK1)+PQAN(JK1):ARTOT=PQNA(JK1)+PQAA(JK1):DIFF=NTTOT-ARTOT
LPRINT USING  "   #.###";(JK1-1)/10;
LPRINT USING "              #####";NTTOT,ARTOT,DIFF
NEXT JK1
RETURN
4200 REM Subroutine to calculate residuals
COLOR 7,0:R2=0:CLS:PRINT "Table of residuals"
PRINT "   XNitr.     Actual Y   Predicted Y   Difference"
FOR K=1 TO 8 STEP 1:R2=R2+X(K,4)^2
PRINT USING" #.###";X(K,0);:PRINT USING"     ##.##";X(K,1),X(K,3),X(K,4)
NEXT K:PRINT"Sum of errors squared is  ";R2
RETURN
4300 REM Subroutine to check plotted points
COLOR 7,0:CLS:RANG=XM-XN:XST=RANG/10
PRINT "   Table of plotted points for the graph"
PRINT "   XNitr.     Predicted Y"
FOR XSP=XN TO XM STEP XST:SUMT=0
FOR K=1 TO (N2+1) STEP 1
YTERM=F(K)*XSP^(K-1):SUMT=SUMT+YTERM
NEXT K
PRINT USING"   #.###";XSP;:PRINT USING"         ##.##";SUMT
NEXT XSP
RETURN
5000 DATA 0.00,42.55,-0.19,474,307,0.00,0,6.3
5010 DATA 0.053,42.6,-0.18,449,285,0.01,450,-5.1
5020 DATA 0.1,43.6,-0.18,426,266,0.02,425,-18.7
5030 DATA 0.253,44.7,-0.16,353,199,0.06,350,-52.2
5040 DATA 0.496,45.9,-0.12,257,116.1,0.11,254,-90.5
5050 DATA 0.748,48.7,-0.06,181,50.3,0.18,181,-123.5
5060 DATA 0.900,51.9,-0.02,144,25.1,0.25,144.8,-125.7
5070 DATA 0.952,52.1,-0.01,134,15.4,0.28,134,-136.4
5080 DATA 1.000,52.5,0.00,0,11.4,0.31,121.5,-141
```

Appendix E

CHAPTER NINE PROGRAM STRUCTURE FOR NEGLIGIBLE COLUMN PRESSURE DROP

All the programs have basically the same structure apart from the initial binary system specification. Thus, it would be pointless to show each complete version. Hence, the complete program is shown for the Binary-Langmuir specification, but with the specific Binary-Langmuir part marked out. For the complete listing, the particular specification will be shown bold enclosed in a box. The partial listing will obviously be much smaller. Some of the partial listings will consist of separate parts (at different locations in the program). For ease of reading, boxes will be used to separate out these parts.

COMPLETE PROGRAM LISTING FOR BINARY-LANGMUIR SPECIFICATION

```
NA=100:NB=100:FA=1:FB=1:MA=0:MB=0:NX=4
NP=21:ND=7:DIM KC(21,24):DIM IA(6):DIM IB(6)
KC(1,9)=0:KC(1,11)=0:KC(1,13)=0:KC(21,10)=0:KC(21,12)=0:KC(21,14)=0
DIM VS(8,7):DIM VL(7)
DIM P(NP):DIM T(NP):DIM U(NP):DIM V(NP):DIM X(NP,NX)
DIM A(ND):DIM B(ND):DIM C(ND):DIM D(ND+1):DIM F(ND):DIM G(ND)
DIM L(ND):DIM Q(ND):DIM S(ND)
VOID=0.376:VOL=20
REM Read in matrix data
 FOR ROW=1 TO 6 STEP 1
  FOR COLUMN=1 TO 7 STEP 1
  READ VS(COLUMN,ROW)
 NEXT COLUMN
NEXT ROW
```

```
REM For this case the binaries will be coupled
10 INPUT " Value of QAM ",QAM
PRINT " Value of MA chosen must be greater than ",QAM
INPUT " Value of MA ",MA
INPUT " Value of QBM ",QBM
PRINT " Value of MB chosen must be greater than ",QBM
INPUT " Value of MB ",MB
NA=(MA*100/QAM)-100:NB=(MB*100/QBM)-100
DA1=NA+(100*NA/NB):DA2=1-(NA/NB)
DB1=NB+(100*NB/NA):DB2=1-(NB/NA)
```

```
REM Using selected binaries print out corresponding residence times
200 PRINT "  Data for whole range"
PRINT " Mol.FractA     TN/S     TI/S          TUR/S        K"
I=1
FOR CA=0 TO 100 STEP 5
XAT=1.0:IF CA=100 THEN XAT=0.0
GOSUB ResTE
KC(I,1)=XA:KC(I,2)=K:KC(I,3)=QA:KC(I,4)=QB:KC(I,7)=GRADA:KC(I,8)=GRADB
KC(I,22)=PUQA:KC(I,23)=PUQB
IF CA=0 THEN GRADAM=KC(I,7):GRADBM=KC(I,8)
IF KC(I,7) > GRADAM THEN GRADAM=KC(I,7)
IF KC(I,8) > GRADBM THEN GRADBM=KC(I,8)
I=I+1:NEXT CA
PRINT " Ready to go on Y/N?":I$=INPUT$(1):IF I$="Y" THEN CLS
REM Read values of K and XA into arrays for the polynomial fitting
FOR N=1 TO NP
X(N,0)=KC(N,1):X(N,1)=KC(N,2):X(N,2)=1:X(N,3)=0
NEXT N
N=N-1:N9=N-2:IF N9>ND-1 THEN N9=ND-1
```

```
250 PRINT " Polynomial Order Selection"
PRINT " Highest order allowable is ",N9
PRINT " Selecting '0' gives the best order after a search"
INPUT " Selected order ",L
M1=ND:IF L<>0 THEN M1=L+1
IF M1>N-1 THEN M1=N-1
GOSUB PolFit:REM This subroutine will obtain particular fitting
coefficients
M2=M1-1
IF L<>0 THEN
PRINT " Specified polynomial order is ",N2
ELSE
PRINT " Order of best polynomial order found is ",N2
END IF
REM Now show how well the various polynomials fit the data
PRINT "  Order    Goodness of Fit"
FOR I=1 TO M1 STEP 1
PRINT I-1;:PRINT USING "######.######";G(I)
NEXT I:PRINT
PRINT " Coefficients of selected order"
PRINT " Data for whole range"
PRINT " Polynomial order ",N2
PRINT " K= ";F(1):IF N2=0 THEN GOTO 150
PRINT "     + XA* ";F(2):IF N2=1 THEN GOTO 150
FOR I=2 TO N2
PRINT "     + XA^ ";I;" * ";F(I+1)
NEXT I
150 REM Print list of predicted and actual vaues of K
PRINT " No.     Wt.      XA       True K      Fitted K    Diff.   %Error"
FOR I=1 TO 21 STEP 1:KC(I,16)=X(I,3)
PRINT USING "###";I,X(I,2);:PRINT USING "###.##";X(I,0);
PRINT USING "###.####";X(I,1),X(I,3),X(I,4);
PRINT USING "###.###";-100*X(I,4)/X(I,1)
R2=R2+X(I,4)^2
NEXT I
PRINT " The sum of the errors squared is ";R2
CLS
REM Can now ask whether a plot is required
PRINT " Is a plot required Y/N?":I$=INPUT$(1):IF I$="Y" THEN GOSUB Plot
PRINT " Ready to go on Y/N?":I$=INPUT$(1):IF I$="Y" THEN CLS
REM
PRINT " Try another order Y/N?":I$=INPUT$(1):IF I$="Y" THEN GOTO 250
PRINT " Change any parameters Y/N?":I$=INPUT$(1):IF I$="Y" THEN GOTO 10
PRINT " Print out predictions Y/N?":I$=INPUT$(1):IF I$="N" THEN STOP
REM This section will compare actual and predicted binary isotherms
REM First must consider the order of thr polynomial fitting
IF L=2 THEN
B2=0:B3=0:C2=0:C3=0
PRINT " Fitting at QAmax Y/N? ":I$=INPUT$(1):IF I$= "N" THEN GOTO 555
B0=F(1):B1=((QAM/100)-B0)*2:C0=F(2)+B0-B1:C1=F(3)+B1:GOTO 580
555 B0=F(1):C1=2*(F(1)+F(2)+F(3)-(QBM/100)):B1=C1-F(3):C0=F(2)+F(1)-B1
580 REM Next section is for standard third order fitting
ELSEIF L=3 THEN
B0=F(1):B2=(6*(QAM+QBM)/100)-12*F(1)-6*F(2)-3*F(3)-2*F(4)
B1=((6*QAM/100)-6*F(1)-2*B2)/3
C0=F(2)+F(1)-B1:C1=F(3)+B1-B2:C2=F(4)+B2:B3=0:C3=0
ELSEIF L=4 THEN
VS(8,1)=F(1)+F(2):VS(8,2)=F(3):VS(8,3)=F(4):VS(8,4)=F(5)
VS(8,5)=(QAM/100)-F(1):VS(8,6)=QBM/100
INPUT "  Fixing column (2-20) ",CF:XS=KC(CF,1)
PRINT "  Fixing total amount Y/N?":I$=INPUT$(1):IF I$="Y" THEN GOTO 700
PRINT " Fixing using the A isotherm Y/N?":I$=INPUT$(1):IF I$="N" THEN GOTO
650
VS(1,7)=(XS^2)/2:VS(2,7)=(XS^3)/3:VS(3,7)=(XS^4)/4
VS(4,7)=0:VS(5,7)=0:VS(6,7)=0:VS(7,7)=0:VS(8,7)=(KC(CF,3)/100)-F(1)*XS
GOTO 800
650 VS(1,7)=0:VS(2,7)=0:VS(3,7)=0:VS(4,7)=1-XS:VS(5,7)=(1-XS^2)/2
VS(6,7)=(1-XS^3)/3:VS(7,7)=(1-XS^4)/4:VS(8,7)=KC(CF,4)/100
GOTO 800
700 VS(1,7)=(XS^2)/2:VS(2,7)=(XS^3)/3:VS(3,7)=(XS^4)/4
VS(4,7)=1-XS:VS(5,7)=(1-XS^2)/2:VS(6,7)=(1-XS^3)/3:VS(7,7)=(1-XS^4)/4
```

```
VS(8,7)=((KC(CF,3)+KC(CF,4))/100)-F(1)*XS
800 GOSUB Veiwmat
REM Gaussian Elimination of matrix
FOR C=1 TO 7 STEP 1
REM Obtain maximum coefficient for respective column
CMAX=VS(C,C):RMAX=C
 FOR R=(C+1) TO 7 STEP 1
 IF ABS(VS(C,R)) > ABS(CMAX) THEN CMAX=VS(C,R):RMAX=R
 NEXT R
REM Swap over rows if necessary
IF R<> C THEN
FOR RS=C TO 8 STEP 1
A=VS(RS,RMAX):B=VS(RS,C):VS(RS,RMAX)=B:VS(RS,C)=A
NEXT RS
END IF
REM Modify rows by adding multiples of the pivotal row
FOR RM=(C+1) TO 7 STEP 1
RATIO=-VS(C,RM)/CMAX
 FOR D=C TO 8 STEP 1
 VS(D,RM)=VS(D,RM)+RATIO*VS(D,C)
 NEXT D
NEXT RM
NEXT C
GOSUB Veiwmat
REM Obtain values by back multiplying
FOR L=7 TO 1 STEP -1
SUMT=0
 FOR CN=(L+1) TO 7 STEP 1
 T=VS(CN,L)*VL(CN):SUMT=SUMT+T
 NEXT CN
VL(L)=(VS(8,L)-SUMT)/VS(L,L)
REM IF VS(8,L)<0.0005 THEN VL(L)=0
NEXT L:PRINT USING "####.####";F(1)
FOR L=1 TO 7 STEP 1:PRINT USING "####.####";VL(L):NEXT L
B0=F(1):B1=VL(1):B2=VL(2):B3=VL(3):C0=VL(4):C1=VL(5):C2=VL(6):C3=VL(7)
ELSE
PRINT " Value of L not suitable for isotherm prediction ":STOP
END IF
CLS:PRINT " Actual comparison of the binaries"
PRINT "     True QA   Pred.QA   %ErrorQA    True QB    Pred.QB   %ErrorQB"
FOR I=1 TO 21 STEP 1
SU=KC(I,1):SV=KC(I,3):SY=KC(I,4)
GOSUB Integrate
NEXT I
PRINT " Ready to go on Y/N?":I$=INPUT$(1):IF I$="Y" THEN CLS
PRINT " Comparison of total amounts adsorbed"
PRINT "     TrueTOT    Pred.TOT    %Error.TOT"
FOR I=1 TO 21 STEP 1
TT=KC(I,3)+KC(I,4):PT=KC(I,5)+KC(I,6):PERRT=100*(PT-TT)/TT
PRINT USING "########.##";TT,PT,PERRT
NEXT I
PRINT " Ready to go on Y/N?":I$=INPUT$(1):IF I$="Y" THEN CLS
PRINT " Phase diagram comparison"
PRINT "   XA         TrueYA      Pred.YA     TrueSla     Pred.Sla"
FOR I=2 TO 20 STEP 1
TYA=KC(I,3)/(KC(I,3)+KC(I,4)):PYA=KC(I,5)/(KC(I,5)+KC(I,6))
TSA=KC(I,3)*(1-KC(I,1))/(KC(I,4)*KC(I,1))
PSA=KC(I,5)*(1-KC(I,1))/(KC(I,6)*KC(I,1))
IF I=2 THEN TMAX=TSA:PMAX=PSA
IF TSA>TMAX THEN TMAX=TSA:IF PSA>PMAX THEN PMAX=PSA
PRINT USING "###.##";KC(I,1);:PRINT USING "########.###";TYA,PYA,TSA,PSA
NEXT I:IF TMAX>=PMAX THEN MAXS=TMAX ELSE MAXS=PMAX
PRINT " Observe binaries in graphical form Y/N?":I$=INPUT$(1):IF I$="Y"
THEN GOSUB Bplot
PRINT " Observe total amounts graphically Y/N?":I$=INPUT$(1):IF I$="Y"
THEN GOSUB Tplot
PRINT " Observe phase diagram Y/N?":I$=INPUT$(1):IF I$="Y" THEN GOSUB
Phplot
PRINT " Observe selectivity diagram Y/N?":I$=INPUT$(1):IF I$="Y" THEN
GOSUB SEplot
PRINT " Ready to go on Y/N?":I$=INPUT$(1):IF I$="Y" THEN CLS
```

```
REM The following section is concerned with integrating actual gradients
GOSUB GRAB:PRINT " Ready Y/N?":I$=INPUT$(1):IF I$="Y" THEN CLS
REM Firstly use trapezoidal determination
REM For A isotherm
FOR I=2 TO 21 STEP 1
SUMTM=0
 FOR J=2 TO (I-1) STEP 1
 TERM=KC(J,7):SUMTM=SUMTM+2*TERM
 NEXT J
QAINT=0.5*5*(KC(1,7)+KC(I,7)+SUMTM):KC(I,9)=QAINT
NEXT I
REM For B isotherm
FOR I=20 TO 1 STEP -1
SUMTM=0
 FOR J=20 TO (I+1) STEP -1
 TERM=KC(J,8):SUMTM=SUMTM+2*TERM
 NEXT J
QBINT=0.5*5*(KC(21,8)+KC(I,8)+SUMTM):KC(I,10)=QBINT
NEXT I
REM Secondly use Simpsons rule
REM For A isotherm
TAREA=0
FOR I=1 TO 19 STEP 2
AREA=(10/6)*(KC(I,7)+4*KC(I+1,7)+KC(I+2,7))
KC(I+1,11)=TAREA+0.5*5*(KC(I,7)+KC(I+1,7))
TAREA=TAREA+AREA:KC(I+2,11)=TAREA
NEXT I
REM For B isotherm
TAREA=0
FOR I=21 TO 3 STEP -2
AREA=(10/6)*(KC(I,8)+4*KC(I-1,8)+KC(I-2,8))
KC(I-1,12)=TAREA+0.5*5*(KC(I,8)+KC(I-1,8))
TAREA=TAREA+AREA:KC(I-2,12)=TAREA
NEXT I
REM Thirdly try and fit gradient values to a polynomial
REM For A isotherm
1000 FOR N=1 TO NP STEP 1
CA=100*KC(N,1):X(N,0)=CA:X(N,1)=KC(N,7):X(N,2)=1:X(N,3)=0:NEXT N
N=N-1:N9=N-2:IF N9>ND-1 THEN N9=ND-1
INPUT " Selected order for A gradients ",L:LA=L:M1=ND:IF L<>0 THEN M1=L+1
IF M1>N-1 THEN M1=N-1
FOR J=1 TO (LA+1) STEP 1:F(J)=0:NEXT J
GOSUB PolFit:M2=M1-1
FOR J=1 TO (LA+1) STEP 1:IA(J)=F(J):PRINT IA(J):NEXT J
REM See how well polynomial fits gradients
GOSUB Setup:LOCATE 3,7:PRINT " Fitting of A isotherm gradients"
FOR I=1 TO 21 STEP 1
XPIX=KC(I,1)*540+50:YPIX=(-KC(I,7)/GRADAM)*250+310
LINE (XPIX-4,YPIX-4)-(XPIX+4,YPIX+4),8,B
NEXT I
FOR CA=0 TO 100 STEP 0.1
SUMT=0
 FOR M=1 TO (LA+1) STEP 1
 TERM=IA(M)*CA^(M-1):SUMT=SUMT+TERM
 NEXT M
XPIX=(CA/100)*540+50:YPIX=(-SUMT/GRADAM)*250+310
PSET (XPIX,YPIX),4
NEXT CA
PRINT " Another order Y/N? ":I$=INPUT$(1):IF I$="Y" THEN GOTO 1000
PRINT " Ready to go on Y/N? ":I$=INPUT$(1):IF I$="Y" THEN CLS
REM For B isotherm
1500 FOR N=1 TO 21 STEP 1
CB=100*(1-KC(N,1)):X(N,0)=CB:X(N,1)=KC(N,8):X(N,2)=1:X(N,3)=0:NEXT N
N=N-1:N9=N-2:IF N9>ND-1 THEN N9=ND-1
INPUT " Selected order for B gradients ",L:LB=L:M1=ND:IF L<>0 THEN M1=L+1
IF M1>N-1 THEN M1=N-1
FOR J=1 TO (LA+1) STEP 1:F(J)=0:NEXT J
GOSUB PolFit:M2=M1-1
FOR J=1 TO (LB+1) STEP 1:IB(J)=F(J):NEXT J
GOSUB Setup:LOCATE 3,7:PRINT " Fitting of B isotherm gradients "
FOR I=1 TO 21 STEP 1
```

```
XPIX=KC(I,1)*540+50:YPIX=(-KC(I,8)/GRADBM)*250+310
LINE (XPIX-4,YPIX-4)-(XPIX+4,YPIX+4),8,B
NEXT I
FOR CB=0 TO 100 STEP 0.1:CA=100-CB
SUMT=0
 FOR M=1 TO (LB+1) STEP 1
 TERM=IB(M)*CB^(M-1):SUMT=SUMT+TERM
 NEXT M
XPIX=(CA/100)*540+50:YPIX=(-SUMT/GRADBM)*250+310
PSET (XPIX,YPIX),4
NEXT CB
PRINT " Another order Y/N? ":I$=INPUT$(1):IF I$="Y" THEN GOTO 1500
PRINT " Ready to go on Y/N?":I$=INPUT$(1):IF I$="Y" THEN CLS
REM Integrate to obtain binaries
I=1
FOR CA=0 TO 100 STEP 5
SUMT=0
FOR J=1 TO (LA+1) STEP 1
TERM=IA(J)*(CA^J)/J:SUMT=SUMT+TERM
NEXT J
KC(I,13)=SUMT:I=I+1
NEXT CA
I=1
FOR CB=0 TO 100 STEP 5
SUMT=0
FOR J=1 TO (LB+1) STEP 1
TERM=IB(J)*(CB^J)/J:SUMT=SUMT+TERM
NEXT J
KC(I,14)=SUMT:I=I+1
NEXT CB
GOSUB Polplot:PRINT " Ready Y/N?":I$=INPUT$(1):IF I$="Y" THEN CLS
GOSUB Compare
PRINT " Consider another polynomial plotting Y/N?":I$=INPUT$(1):IF I$="Y"
THEN GOTO 1000
PRINT " Open files for quatro-pro plotting Y/N? ":I$=INPUT$(1):IF I$="N"
THEN STOP
REM Open files to store data for quatro-pro plotting
OPEN "BIN1.BAS" FOR OUTPUT AS #1
FOR I=1 TO 21 STEP 1:KC(I,19)=100*KC(I,1)
PRINT #1,USING "####.##";KC(I,19),KC(I,3),KC(I,5),KC(I,4),KC(I,6)
NEXT I
CLOSE #1
OPEN "TOT1.BAS" FOR OUTPUT AS #2
FOR I=1 TO 21 STEP 1:KC(I,17)=KC(I,3)+KC(I,4):KC(I,18)=KC(I,5)+KC(I,6)
PRINT #2,USING "####.##";KC(I,19),KC(I,17),KC(I,18)
NEXT I
CLOSE #2
OPEN "PD1.BAS" FOR OUTPUT AS #3
FOR I=1 TO 21 STEP 1
IF I=1 THEN
KC(I,20)=0:KC(I,21)=0
ELSEIF I=21 THEN
KC(I,20)=1:KC(I,21)=1
ELSE
KC(I,20)=KC(I,3)/KC(I,17):KC(I,21)=KC(I,5)/KC(I,18)
END IF
PRINT #3,USING "##.###";KC(I,1),KC(I,1),KC(I,20),KC(I,21)
NEXT I
CLOSE #3
OPEN "KFT1.BAS" FOR OUTPUT AS #4
FOR I=1 TO 21 STEP 1
PRINT #4,USING "###.##";KC(I,1),KC(I,2),KC(I,16)
NEXT I
CLOSE #4
OPEN "GRADA1.BAS" FOR OUTPUT AS #5
FOR I=1 TO 21 STEP 1
PRINT #5,USING "#####.##";KC(I,19),KC(I,3),KC(I,9),KC(I,13)
NEXT I
CLOSE #5
OPEN "GRADB1.BAS" FOR OUTPUT AS #6
FOR I=21 TO 1 STEP -1:II=22-I:AAA=KC(I,19)
```

```
PRINT #6,USING "#####.##";AAA,KC(I,4),KC(I,10),KC(II,14)
NEXT I
CLOSE #6
OPEN "BLP.BAS" FOR OUTPUT AS #7
FOR I=1 TO 21 STEP 1
PRINT #7,USING "####.##";KC(I,19),KC(I,22),KC(I,3),KC(I,23),KC(I,4)
NEXT I
CLOSE #7
STOP
REM Now will list all the subroutines
ResTE:
REM Using binary parameters will obtain residence times
CB=100-CA:XA=CA/100:XB=1-XA:XBT=1-XAT:P=1.2
COEFFA=XA/(XAT-XA):COEFFB=XB/(XBT-XB):DIFF=COEFFA-COEFFB:VRATIO=XA*(1-P
)+P
FC=0.5/VRATIO
```

```
QA=(MA*CA)/(DA1+DA2*CA):QB=(MB*CB)/(DB1+DB2*CB)
GRADA=(MA*DA1)/(DA1+DA2*CA)^2:GRADB=(MB*DB1)/(DB1+DB2*CB)^2
PUQA=MA*CA/(NA+CA):PUQB=MB*CB/(NB+CB)
```

```
HA=(1-VOID)*VOL*GRADA+VOID*VOL:HB=(1-VOID)*VOL*GRADB+VOID*VOL
TN=(HA-HB)/(DIFF*FC):TI=(HA/FC)-(COEFFA*TN)
TUR=VOL*VOID/FC:K=(TI/TUR-1)*VOID/(1-VOID)
PRINT USING "#####.##";XA;:PRINT USING "########.###";TN,TI,TUR,K
RETURN
PolFit:
REM Fit value of K to selected polynomial
REM Weighted least squares fit by Forsythes Orthogonal Polynomials
REM Adapted from Lee and Lee
M3=M1-1:N2=M3:FOR I=1 TO M1: C(I)=0:NEXT I
Q(1)=0:D(1)=0:D(2)=0:A(1)=1:D2=0:P1=0:G1=0:I2=0
S1=X(1,2):XN=X(1,0):XM=XN:YN=X(1,1):YM=YN
FOR I=2 TO N:X=X(I,0):Y=X(I,1):IF X<XN THEN XN=X
IF X>XM THEN XM=X
IF Y<YN THEN YN=Y
IF Y>YM THEN YM=Y
S1=S1+X(I,2):NEXT I
REM
Y3=(YM+YN)/2:Y4=(YM-YN)/2:IF Y4<=0 THEN F(1)=Y:N2=0:GOTO 500
REM Scaling the data
FOR I=1 TO N:V=(X(I,1)-Y3)/Y4:V(I)=V:VW=V*X(I,2)
P1=P1+VW:D2=D2+V*VW:P(I)=1:T(I)=0
NEXT:S2=P1/S1:S(1)=S2:C(1)=S2:D2=D2-S2*P1:G(1)=ABS(D2/(N-1))
A1=4/(XM-XN):B1=-2-A1*XN
FOR I=1 TO N:U(I)=A1*X(I,0)+B1:NEXT
FOR I=1 TO M3:I1=I+1:D1=0
FOR J=1 TO N:D1=D1+X(J,2)*U(J)*P(J)*P(J):NEXT J
L(I1)=D1/S1:W2=S1:S1=0:P1=0
FOR J=1 TO N:D1=Q(I)*T(J):T(J)=P(J)
P(J)=(U(J)-L(I1))*P(J)-D1:V=X(J,2)*P(J):S1=S1+V*P(J):P1=P1+V*V(J)
NEXT J:Q(I1)=S1/W2:S(I1)=P1/S1:D2=D2-S(I1)*P1
G(I1)=ABS(D2/(N-1-I)):IF L>0 THEN GOTO 420
IF I2=1 THEN GOTO 400
IF G(I1)<G(I) THEN GOTO 420
N2=I-1:I2=1:G1=G(I)
FOR J=1 TO M1:B(J)=C(J):NEXT:GOTO 420
400 IF G(I1)>=0.6*G1 THEN GOTO 420
I2=0:N2=M3
420 FOR J=1 TO I:D1=D(J+1)*Q(I):D(J+1)=A(J):A(J)=D(J)-L(I1)*A(J)-D1
C(J)=C(J)+S(I1)*A(J):NEXT
C(I1)=S(I1):A(I1)=1:D(I+2)=0:IF I2=0 OR I<>M3 THEN GOTO 440
FOR J=1 TO M1:C(J)=B(J):NEXT
440 NEXT:D(1)=1:B(1)=1:F(1)=C(1)
REM
FOR I=2 TO M1:D(I)=1:B(I)=B1*B(I-1):F(1)=F(1)+C(I)*B(I):NEXT
FOR J=2 TO M1:D(1)=D(1)*A1:F(J)=C(J)*D(1):K1=2:J1=J+1
IF J1>M1 THEN J=M1:GOTO 460
FOR I=J1 TO M1:D(K1)=A1*D(K1)+D(K1-1)
```

```
F(J)=F(J)+C(I)*D(K1)*B(K1):K1=K1+1:NEXT
460 NEXT
REM Calculate residuals
FOR I=1 TO N:J=N2+1:Y5=F(J):IF N2=0 THEN GOTO 480
FOR K=1 TO N2:Y5=F(J-1)+X(I,0)*Y5:J=J-1:NEXT
480 X(I,3)=Y5*Y4+Y3:X(I,4)=(V(I)-Y5)*Y4:NEXT
REM Rescale F()
FOR I=1 TO M1:F(I)=F(I)*Y4:NEXT:F(1)=F(1)+Y3
500 RETURN
Plot:
REM Plot out actual and fitted values of K
SCREEN 9:COLOR 1,3
LINE (50,60)-(590,310),,B
FOR M=104 TO 536 STEP 54
LINE (M,60)-(M,310),8
NEXT M
LOCATE 3,7:PRINT " Graph showing fitting of actual K values "
FOR I=1 TO 21 STEP 1
XPIX=X(I,0)*540+50:YPIX=(-X(I,1)/YM)*250+310
LINE (XPIX-4,YPIX-4)-(XPIX+4,YPIX+4),8,B
NEXT I
FOR XA=0 TO 1.0 STEP 0.001
SUMT=0
FOR J=1 TO (L+1) STEP 1
TERM=F(J)*XA^(J-1):SUMT=SUMT+TERM
NEXT J
XPIX=XA*540+50:YPIX=(-SUMT/YM)*250+310
PSET (XPIX,YPIX),4
NEXT XA
RETURN
Integrate:
REM Firstly the individual binary coefficients will be obtained from
REM the coefficients from K
REM Then the predicted isotherms will be obtained by integration
QAP=100*((B0*SU)+(B1*SU^2)/2+(B2*SU^3)/3+(B3*SU^4)/4)
QBP=100*((C0*(1-SU))+(C1*(1-SU^2))/2+(C2*(1-SU^3))/3+(C3*(1-SU^4))/4)
KC(I,5)=QAP:KC(I,6)=QBP
IF SV=0 THEN PERRA=0:GOTO 600
PERRA=100*(QAP-SV)/SV
IF SY=0 THEN PERRB=0:GOTO 600
PERRB=100*(QBP-SY)/SY
600 PRINT USING "########.##";SV,QAP,PERRA,SY,QBP,PERRB
RETURN
Bplot:
CLS:SCREEN 9:COLOR 5,3
LINE (50,60)-(490,310),8,B
FOR M=94 TO 446 STEP 44
LINE (M,60)-(M,310),8
NEXT M
FOR K=85 TO 285 STEP 25
LINE (50,K)-(490,K),7
NEXT K
LOCATE 3,7:PRINT " Graph showing actual and predicted binaries":LOCATE
1,1
FOR I=1 TO 21 STEP 1
XPIX=X(I,0)*440+50:YPIX=(-KC(I,3)/QAM)*250+310
ZPIX=(-KC(I,4)/QAM)*250+310:WPIX=(-KC(I,5)/QAM)*250+310
VPIX=(-KC(I,6)/QAM)*250+310
LINE (XPIX-4,YPIX-4)-(XPIX+4,YPIX+4),4,B
LINE (XPIX-4,ZPIX-4)-(XPIX+4,ZPIX+4),1,B
LINE (XPIX-2,WPIX-2)-(XPIX+2,WPIX+2),5,B
LINE (XPIX-2,VPIX-2)-(XPIX+2,VPIX+2),14,B
NEXT I
RETURN
Tplot:
CLS:SCREEN 9:COLOR 5,10
LINE (50,60)-(490,310),8,B
FOR M=94 TO 446 STEP 44
LINE (M,60)-(M,310),8
NEXT M
FOR K=85 TO 285 STEP 25
```

```
LINE (50,K)-(490,K),7
NEXT K
LOCATE 3,7:PRINT " Graph showing total actual and predicted total amounts
adsorbed"
LOCATE 1,1
FOR I=1 TO 21 STEP 1
XPIX=X(I,0)*440+50
TT=KC(I,3)+KC(I,4):PT=KC(I,5)+KC(I,6)
YPIX=(-TT/QAM)*250+310
ZPIX=(-PT/QAM)*250+310
LINE (XPIX-4,YPIX-4)-(XPIX+4,YPIX+4),4,B
LINE (XPIX-2,ZPIX-2)-(XPIX+2,ZPIX+2),14,B
NEXT I
RETURN
PHplot:
CLS:SCREEN 9:COLOR 5,11
LINE (50,60)-(490,310),,B
FOR M=94 TO 446 STEP 44
LINE (M,60)-(M,310),8
NEXT M
FOR K=85 TO 285 STEP 25
LINE (50,K)-(490,K),7
NEXT K
LINE (50,310)-(490,60),8
LOCATE 3,7:PRINT " Graph showing phase diagram"
FOR I=1 TO 21 STEP 1
XPIX=X(I,0)*440+50
COMPA=KC(I,3)/(KC(I,4)+KC(I,3)):COMPP=KC(I,5)/(KC(I,5)+KC(I,6))
YPIX=(-COMPA)*250+310:ZPIX=(-COMPP)*250+310
LINE (XPIX-4,YPIX-4)-(XPIX+4,YPIX+4),4,B
LINE (XPIX-2,ZPIX-2)-(XPIX+2,ZPIX+2),14,B
NEXT I
RETURN
SEplot:
CLS:SCREEN 9:COLOR 5,3
LINE (50,60)-(490,310),8,B
LOCATE 3,7:PRINT " Graph showing selectivity"
EXNT=LOG10(MAXS)/LOG10(2):YMAX=2^(INT(EXNT)+1)
ZEROPIX=(-1/YMAX)*250+310:LINE (50,ZEROPIX)-(490,ZEROPIX),8
FOR I=2 TO 20 STEP 1
TSA=KC(I,3)*(1-KC(I,1))/(KC(I,4)*KC(I,1))
PSA=KC(I,5)*(1-KC(I,1))/(KC(I,6)*KC(I,1))
XPIX=X(I,0)*440+50
YPIX=(-TSA/YMAX)*250+310
ZPIX=(-PSA/YMAX)*250+310
LINE (XPIX-4,YPIX-4)-(XPIX+4,YPIX+4),4,B
LINE (XPIX-2,ZPIX-2)-(XPIX+2,ZPIX+2),14,B
NEXT I
RETURN
Veiwmat:
PRINT "     B1      B2      B3      C0      C1      C2      C3      Value"
FOR ROWP=1 TO 7 STEP 1
FOR COLUMNP=1 TO 8 STEP 1
IF COLUMNP=8 THEN PRINT USING "####.####";VS(COLUMNP,ROWP)_
ELSE PRINT USING "####.####";VS(COLUMNP,ROWP);
NEXT COLUMNP
NEXT ROWP
RETURN
Setup:
CLS:SCREEN 9:COLOR 5,11
LINE (50,60)-(590,310),,B
FOR M=104 TO 536 STEP 54
LINE (M,60)-(M,310),8
NEXT M
FOR K=85 TO 285 STEP 25
LINE (50,K)-(590,K),7
NEXT K
RETURN
GRAB:
PRINT "  Grad.A     Grad.B "
FOR I=1 TO 21 STEP 1
```

```
PRINT USING "######.##";KC(I,7),KC(I,8)
NEXT I
RETURN
Polplot:
PRINT "   Poly.IA     Poly.IB"
FOR I=1 TO 21 STEP 1
PRINT USING "#########.##";KC(I,13),KC(I,14)
NEXT I
RETURN
Compare:
PRINT " Comparisons for component A"
PRINT "    Actual QA   Pol.F.K.QA  Trap.Int.QA   Simpson QA    Poly.F.QA"
FOR I=1 TO 21 STEP 1
PRINT USING "##########.##";KC(I,3),KC(I,5),KC(I,9),KC(I,11),KC(I,13)
NEXT I:PRINT " Ready Y/N?":I$=INPUT$(1):IF I$="Y" THEN CLS
PRINT "    Actual QB   Pol.F.K.QB  Trap.Int.QB   Simpson QB    Poly.F.QB"
FOR I=21 TO 1 STEP -1:II=22-I
PRINT USING "##########.##";KC(I,4),KC(I,6),KC(I,10),KC(I,12),KC(II,14)
NEXT I
RETURN
DATA 1,0,0,1,0,0,0
DATA -1,1,0,0,1,0,0
DATA 0,-1,1,0,0,1,0
DATA 0,0,-1,0,0,0,1
DATA 0.5,0.3333333,0.25,0,0,0,0
DATA 0,0,0,1,0.5,0.3333333,0.25
```

PARTIAL PROGRAM LISTING FOR INDEPENDENT BINARY ISOTHERM SPECIFICATION

```
REM First input A binary data
10 INPUT " Value of QAM  ",QAM:HEAM=QAM/100:HEA=QAM/100
20 PRINT " Is isotherm linear Y/N?":I$=INPUT$(1):IF I$="Y" THEN GOTO 100
30 PRINT " Is isotherm of Langmuir form Y/N?":I$=INPUT$(1):IF I$="N" THEN
GOTO 75
40 PRINT " Value of HEA must be less than ",HEAM
45 INPUT " Value of HEA ",HEA
50 RAMIN=QAM-HEA*100:PRINT " Value of RA chosen must be greater than
",RAMIN
60 INPUT " Value of RA ",RA:
TA=100*((RA/(QAM-HEA*100))-1):GOTO 100
REM Firstly must input the Langmuir contribution
75 INPUT " % Langmuir contribution ",PLN:LQAM=PLN*QAM/100:FQAM=QAM-LQAM
80 PRINT " Magnitude of RA chosen must be greater than ",LQAM
INPUT " Value of RA ",RA:TA=100*((RA/LQAM)-1)
REM Now consider the Langmuir-Freundlich contribution
PRINT " Value of MA chosen must be greater than ",FQAM
INPUT " Value of MA ",MA:INPUT " Value of FA ",FA
NA=100^FA*((MA/FQAM)-1):HEA=0:PRINT NA
REM Input binary for B
100 INPUT " Value of QBM  ",QBM:HEBM=QBM/100:HEB=QBM/100
110 PRINT " Is isotherm linear Y/N?":I$=INPUT$(1):IF I$="Y" THEN GOTO 200
120 PRINT " Is isotherm of Langmuir form Y/N?":I$=INPUT$(1):IF I$="N" THEN
GOTO 160
130 PRINT " Value of HEB must be less than ",HEBM
135 INPUT " Value of HEB ",HEB
140 MBMIN=QBM-HEB*100:PRINT " Value of MB chosen must be greater than
",MBMIN
150 INPUT " Value of MB ",MB:NB=100*((MB/(QBM-HEB*100))-1):GOTO 200
REM Firstly must input Langmuir contribution
160 INPUT " % Langmuir contribution ",PLN:LQBM=PLN*QBM/100:FQBM=QBM-LQBM
170 PRINT " Magnitude of RB chosen must be greater than ",LQBM
INPUT " Value of RB ",RB:TB=100*((RB/LQBM)-1)
REM Now consider Langmuir-Freundlich contribution
PRINT " Value of MB chosen must be greater than ",FQBM
INPUT " Value of MB ",MB:INPUT " Value of FB ",FB
NB=100^FB*((MB/FQBM)-1):HEB=0
```

PARTIAL PROGRAM LISTING FOR IAS BINARY SPECIFICATION

```
DEF FNQA(HEA,MA,NA,CA0,FA)=HEA*CA0+(MA*CA0^FA)/(NA+CA0^FA)
DEF FNQB(HEB,MB,NB,CB0,FB)=HEB*CB0+(MB*CB0^FB)/(NB+CB0^FB)
DEF FNGA(HEA,MA,NA,CA0,FA)=HEA*CA0+(MA*CA0^FA)/(NA+CA0^FA)
DEF FNGB(HEB,MB,NB,CB0,FB)=HEB*CB0+(MB*CB0^FB)/(NB+CB0^FB)
DEF FNPIA(HEA,MA,NA,CA0,FA)=HEA*CA0+(MA/FA)*LOG((NA+CA0^FA)/NA)
DEF FNPIB(HEB,MB,NB,CB0,FB)=HEB*CB0+(MB/FB)*LOG((NB+CB0^FB)/NB)
```

```
REM First input A binary data
100 INPUT " Value of QAM ",QAM:HEAM=QAM/100:HEA=QAM/100
PRINT " Is isotherm linear Y/N?":I$=INPUT$(1):IF I$="Y" THEN GOTO 200
PRINT " Value of HEA chosen must be less than ",HEAM:INPUT " Value of HEA
",HEA
INPUT " Value of MA ",MA:INPUT " Value of FA ",FA
NA=100^FA*((MA/(QAM-HEA*100))-1):PRINT " Value of NA is ";
PRINT USING "########.##";NA
REM Now input B binary data
200 INPUT " Value of QBM ",QBM:HEBM=QBM/100:HEB=QBM/100
PRINT " Is isotherm linear Y/N?":I$=INPUT$(1):IF I$="Y" THEN GOTO 300
PRINT " Value of HEB chosen must be less than ",HEBM:INPUT " Value of HEB
",HEB
INPUT " Value of MB ",MB:INPUT " Value of FB ",FB
NB=100^FB*((MB/(QBM-HEB*100))-1):PRINT " Value of NB is ";
PRINT USING "########.##";NB
300 KC(21,1)=1.00:KC(21,4)=0:CA0=100:KC(21,3)=FNQA(HEA,MA,NA,CA0,FA)
KC(21,22)=KC(21,3):KC(1,22)=0:KC(21,23)=0
KC(1,1)=0:KC(1,3)=0:CB0=100:KC(1,4)=FNQB(HEB,MB,NB,CB0,FB):KC(1,23)=KC(
1,4)
CA0=100:KC(21,15)=FNPIA(HEA,MA,NA,CA0,FA)
CB0=100:KC(1,15)=FNPIB(HEB,MB,NB,CB0,FB)
REM Determine the end points
CA=0.1:SP=0.5:GOSUB IAS
GRADA=QA/0.1:GRADB=(KC(1,4)-QB)/0.1:KC(1,7)=GRADA:KC(1,8)=GRADB
CA=99.9:SP=0.02:GOSUB IAS
GRADA=(KC(21,3)-QA)/0.1:GRADB=QB/0.1:KC(21,7)=GRADA:KC(21,8)=GRADB
REM Determine the mixture points
N=2:SP=0.5
FOR CA=5 TO 95 STEP 5:KC(N,1)=CA/100
GOSUB  IAS:KC(N,3)=QA:KC(N,4)=QB:KC(N,15)=G1:KC(N,16)=SA:KC(N,22)=ASUB:K
C(N,23)=BSUB
CA=CA+0.1:GOSUB IAS:CA=CA-0.1
GRADA=(QA-KC(N,3))/0.1:GRADB=(KC(N,4)-QB)/0.1
KC(N,7)=GRADA:KC(N,8)=GRADB
N=N+1:NEXT CA
```

```
IAS:
CB=100-CA:CA0=CA+SP
CA0=CA:CB0=100-CA:ASUB=FNQA(HEA,MA,NA,CA0,FA)
BSUB=FNQB(HEB,MB,NB,CB0,FB):CA0=CA+SP
FOR M=1 TO 20 STEP 1
CB0=CA0*CB/(CA0-CA)
G1=FNPIA(HEA,MA,NA,CA0,FA):G2=FNPIB(HEB,MB,NB,CB0,FB):G=G1-G2
V1=HEA:V2=(MA*CA0^(FA-1))/(NA+CA0^FA)
V3=HEB*CB*CA/(CA0-CA)^2
V4=(MB*CB^FB*CA*CA0^(FB-1))/(CA0-CA)^(FB+1)
V5=NB+(CB*CA0/(CA0-CA))^FB:V6=V4/V5
H=V1+V2+V3+V6
CAN=CA0-(G/H)
CA0=CAN
NEXT M
CB0=CB*CA0/(CA0-CA):QA0=FNQA(HEA,MA,NA,CA0,FA):QB0=FNQB(HEB,MB,NB,CB0
,FB)
XA=CA/CA0:XB=CB/CB0:QT=(XA/QA0+XB/QB0)^-1:QA=QT*XA:QB=QT*XB:YA=CA/100
PIA=FNPIA(HEA,MA,NA,CA0,FA):PIB=FNPIB(HEB,MB,NB,CB0,FB):SA=XA*(1-YA)/
((1-XA)*YA)RETURN
```

PARTIAL PROGRAM LISTING FOR RAS BINARY SPECIFICATION

```
DEF FNQA(HEA,MA,NA,CA0,FA)=HEA*CA0+(MA*CA0^FA)/(NA+CA0^FA)
DEF FNQB(HEB,MB,NB,CB0,FB)=HEB*CB0+(MB*CB0^FB)/(NB+CB0^FB)
DEF FNGA(HEA,MA,NA,CA0,FA)=HEA*CA0+(MA*CA0^FA)/(NA+CA0^FA)
DEF FNGB(HEB,MB,NB,CB0,FB)=HEB*CB0+(MB*CB0^FB)/(NB+CB0^FB)
DEF FNPIA(HEA,MA,NA,CA0,FA)=HEA*CA0+(MA/FA)*LOG((NA+CA0^FA)/NA)
DEF FNPIB(HEB,MB,NB,CB0,FB)=HEB*CB0+(MB/FB)*LOG((NB+CB0^FB)/NB)
DEF FNCASUB(CA,XA)=CA/(XA*EXP(C*(1-XA)^2+D*(1-XA)^3))
DEF FNCBSUB(CB,XA)=CB/((1-XA)*EXP(E*XA^2+F*XA^3))
DEF FNASUB(CA,XA)
A1=XA*(2*C*(1-XA)+3*D*(1-XA)^2):A2=1:A3=XA^2*EXP(C*(1-XA)^2+D*(1-XA)^3)
A4=CA*(A1-A2)/A3
FNASUB=A4
END DEF
DEF FNBSUB(CB,XA)
B1=(XA-1)*(2*E*XA+3*F*XA^2):B2=1:B3=(1-XA)^2*EXP(E*XA^2+F*XA^3)
B4=CB*(B1+B2)/B3
FNBSUB=B4
END DEF
```

```
REM Input parameters to determine activity coefficient variation
INPUT " Value of A ",A:INPUT " Value of B ",B
C=2*B-A:E=2*A-B:D=2*(A-B):F=2*(B-A)
```

```
RAS:
CB=100-CA:YA=CA/100:XA=YA+SP
CA0=CA:CB0=100-CA0:PUQA=FNQA(HEA,MA,NA,CA0,FA)
PUQB=FNQB(HEB,MB,NB,CB0,FB)
FOR M=1 TO 10 STEP 1
CAS=FNCASUB(CA,XA):G1=FNPIA(HEA,MA,NA,CAS,FA)
CBS=FNCBSUB(CB,XA):G2=FNPIB(HEB,MB,NB,CBS,FB):G=G1-G2
S=FNASUB(CA,XA):BS=FNBSUB(CB,XA)
T1=HEA*S:T2=HEB*BS:T3=MA*FA*CAS^(FA-1)*S/(NA+CAS^FA)
T4=MB*FB*CBS^(FB-1)*BS/(NB+CBS^FB)
H=T1+T3-T2-T4
XAN=XA-(G/H):XA=XAN
NEXT M
QA0=FNQA(HEA,MA,NA,CAS,FA):QB0=FNQB(HEB,MB,NB,CBS,FB)
XB=1-XA:QT=(XA/QA0+XB/QB0)^-1:QA=XA*QT:QB=XB*QT
SA=XA*(1-YA)/((1-XA)*YA)
RETURN
```

Appendix F

PUBLISHED WORK

The following abstract is of a paper accepted by the *Journal of Chromatographic Science* for publication in the autumn of 1993. This paper has relevance to the work described in Chapter Five.

CAUSES AND ELIMINATION OF NOISE IN SORPTION-EFFECT CHROMATOGRAPHY II. THERMAL NOISE

By R.I. Meacham, M.J. Heslop, B.A. Buffham and G. Mason

ABSTRACT

In sorption-effect chromatography small changes in gas flowrate are measured. These changes indicate the amount sorbed when a sample enters a column and the amounts desorbed when resolved bands leave. We have used a differential capillary meter to measure these changes. Random temperature fluctuations in the apparatus can also cause small changes in flowrate. This "thermal noise" tends to hide the signal. We have investigated the causes and effects of thermal noise. Temperature fluctuations affect the flowrate by causing expansion and contraction of the apparatus and flowing gases and also by changing the viscosity of the flowing gases. A greater effect is the fluctuation in the amount of gas adsorbed in the columns with temperature fluctuation. In the columns the effect is magnified because the temperature changes cause adsorption and desorption. Advice is given on the minimization of thermal noise and design modifications that reduce thermal noise are described.

Appendix G

CHROMATOGRAMS OBTAINED WITH OVEN PIG ARRANGEMENT

In the final appendix, a selection of flowrate and composition chromatograms will be presented for a variety of experimental runs which are relevant to Chapters Seven and Eight. For each case, the flowrate retention time τ_N, the composition retention time τ_P and the viscosity factor $B(\mu)$ will be stated. Figure G.1 shows the chromatograms obtained for switching a nitrogen perturbation between helium carriers at 50°C. This was one of the first experimental runs carried out with the pig arrangement and was part of a preliminary investigation of the end-point gradients of the three binary systems; the end-point gradients allow only a qualitative determination of the shape of the binary isotherms. From the flowrate record, it can be seen that the thermal noise has been greatly reduced by the new oven arrangement. From the diagram, because the composition record is of a simple form, it can be approximated by a trapezium and τ_X = 255 seconds. Because the perturbation causes net adsorption, τ_N was measured to have a positive value of 208 seconds. Finally, because the viscosity step from $n(\infty)$ to $p(\infty)$ is in the direction of *increasing flowrate*, $B(\mu)$ has a *positive value* of 0.20.

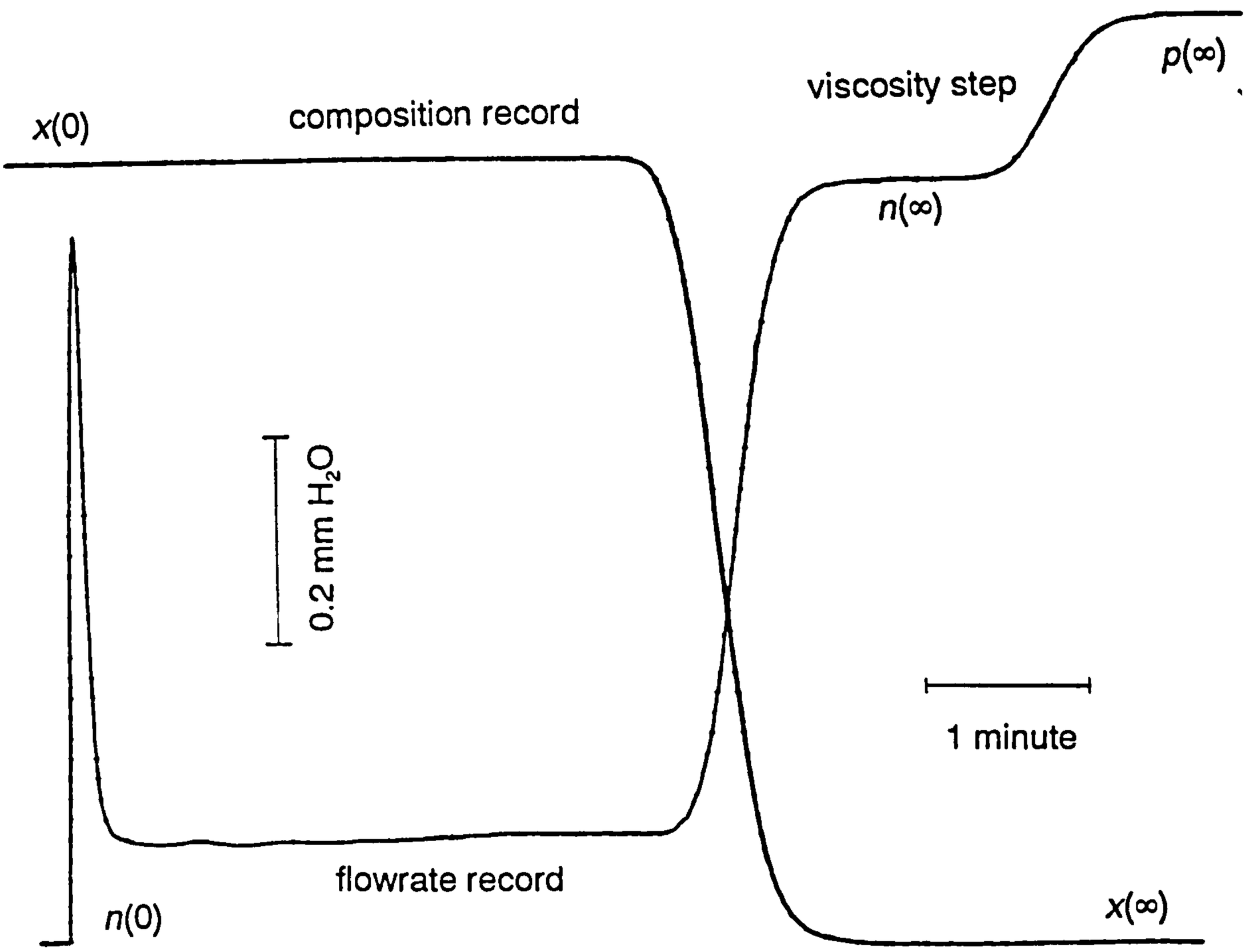

Figure G.1 Chromatograms Obtained for Switching a Nitrogen Perturbation between Helium Carriers at 50°C

Figure G.2 shows the chromatograms obtained for adding a nitrogen perturbation to a helium carrier at 25°C. For the corresponding *perturbation removal* case, the composition front is broader and the plateau at $n(\infty)$ is not so well defined before the viscosity step movement to $p(\infty)$. From the composition record, $\tau_X = 429$ seconds. From the flowrate record, $\tau_N = 386$ seconds and $B(\mu) = 0.194$.

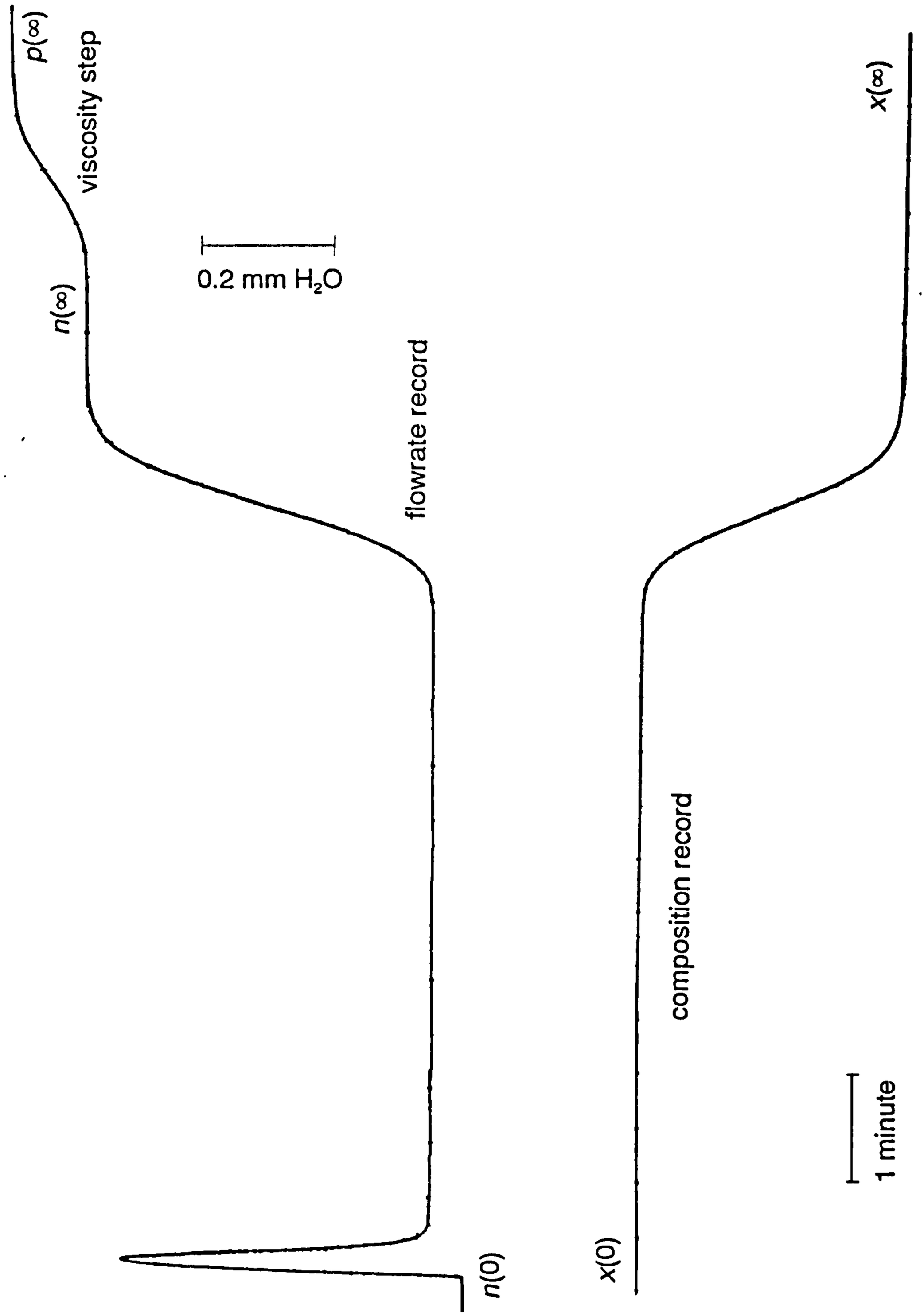

Figure G.2 Chromatograms Obtained for Adding a Nitrogen Perturbation to a Helium Carrier at 25°C

Figure G.3 shows the chromatograms obtained for adding a helium perturbation to a nitrogen carrier at 25°C. For the corresponding *perturbation removal* case, the composition record has a different shape; there is an increasing deviation as the front moves through the column *and* the final position at $x(\infty)$ is quickly attained without an overshoot. From the composition record, $\tau_x = 45.8$ seconds. From the flowrate record $\tau_N = -180$ seconds (net desorption) and from the viscosity step $B(\mu) = 0.1$

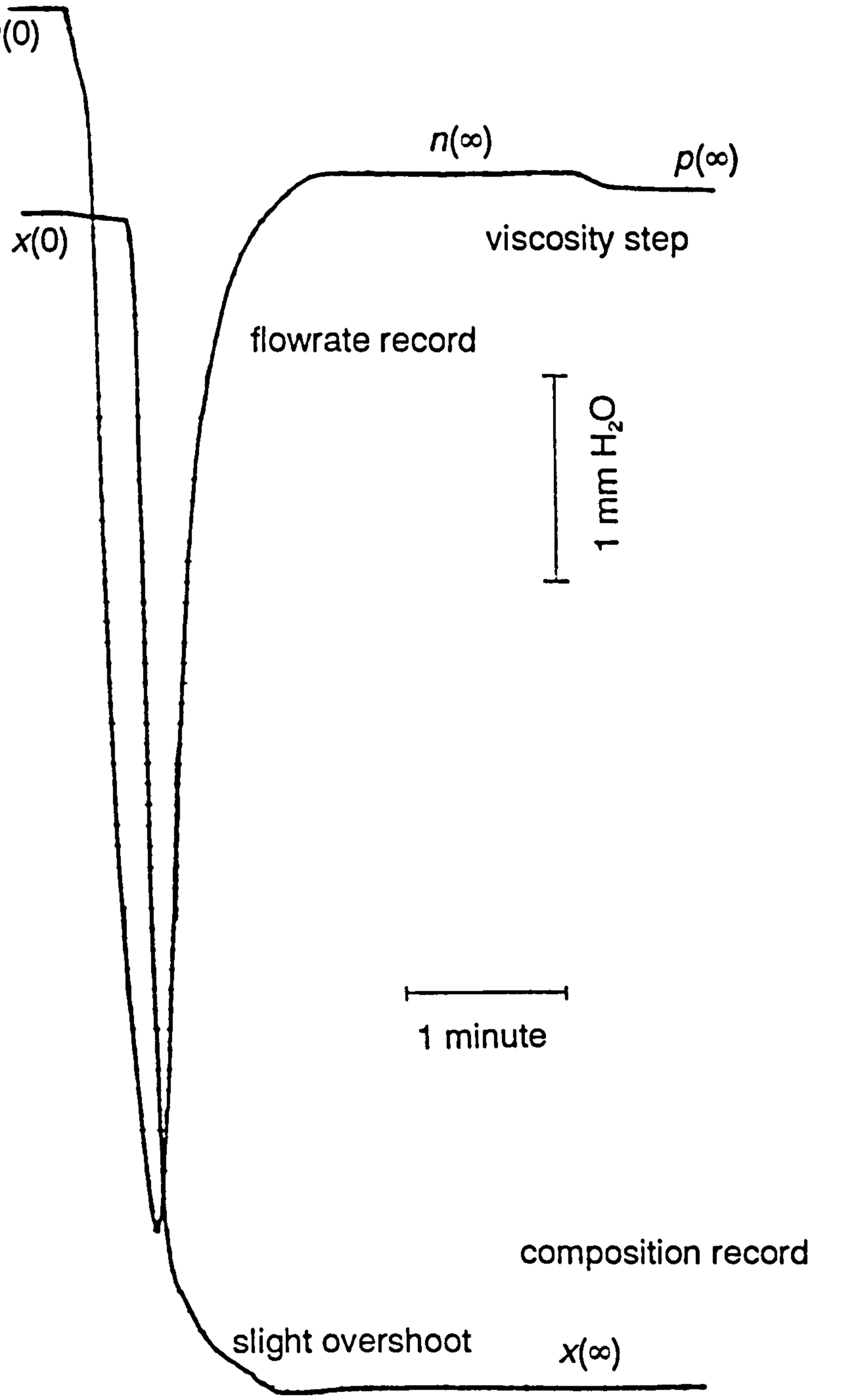

Figure G.3 Chromatograms Obtained for Adding a Helium Perturbation to a Nitrogen Carrier at 25°C

Figure G.4 shows the chromatograms obtained for removing a nitrogen perturbation from an argon carrier at 54°C. From the flowrate record, it can be seen that the thermal noise has been greatly reduced by the new oven arrangement. From the composition record, τ_x = 246 seconds and from the flowrate record τ_N = 128 seconds. Also, from the flowrate record $B(\mu) = -0.2$; because the viscosity step is in the direction of *decreasing* flowrate, the viscosity factor will be *negative*.

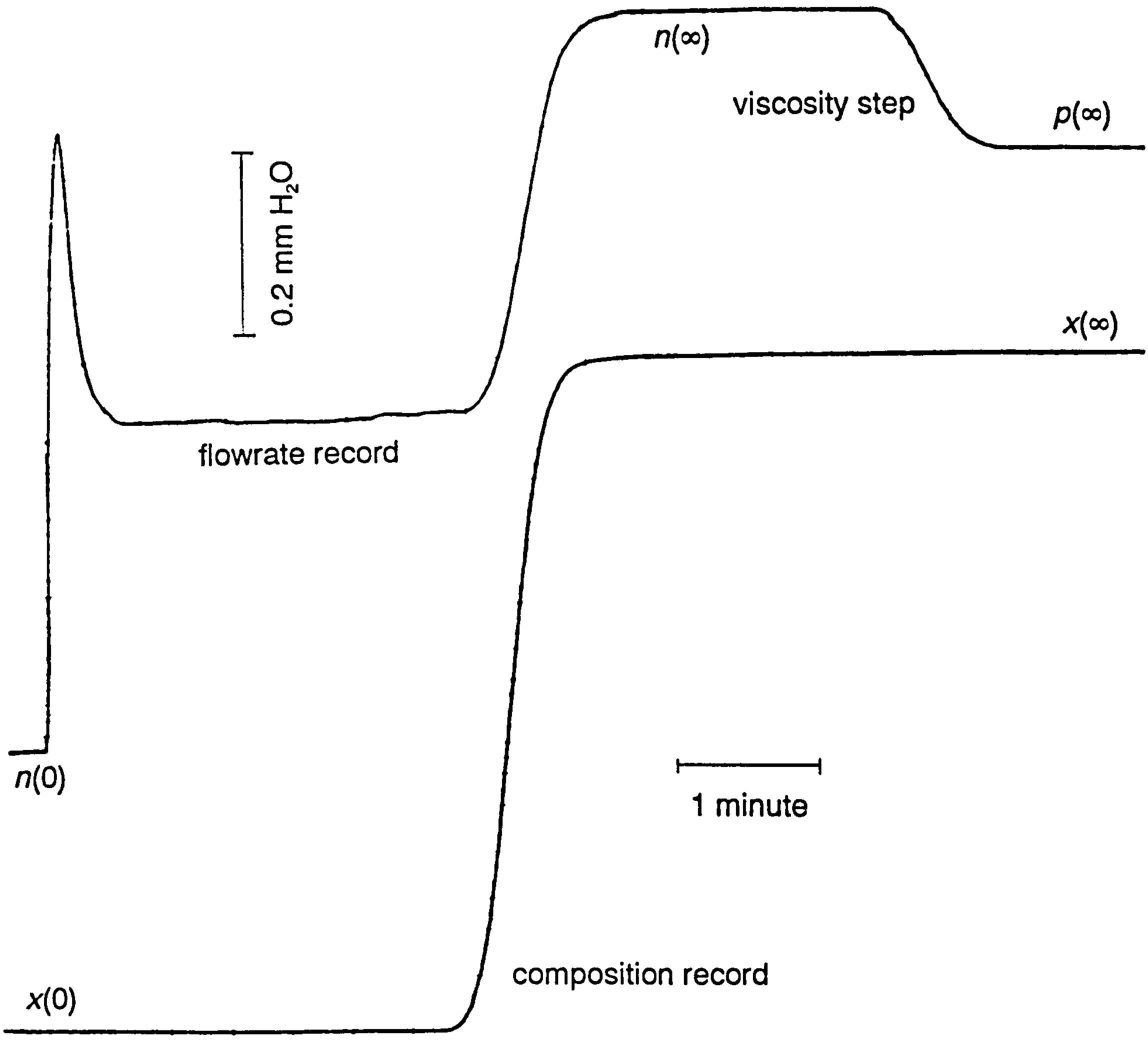

Figure G.4 Chromatograms Obtained for Removing a Nitrogen Perturbation from an Argon Carrier at 54°C

Figure G.5 shows the chromatograms obtained for adding a helium perturbation to an argon carrier at 25°C. Likewise for the nitrogen carrier depicted in Figure G.3, for the corresponding *perturbation removal* case the composition record has a different shape (although the magnitude of the deviations is reduced with the nitrogen carrier). From the flowrate record τ_N = -92.4 seconds (net desorption) and from the viscosity step $B(\mu) = 0.1$. From the composition record τ_X = 58.2 seconds.

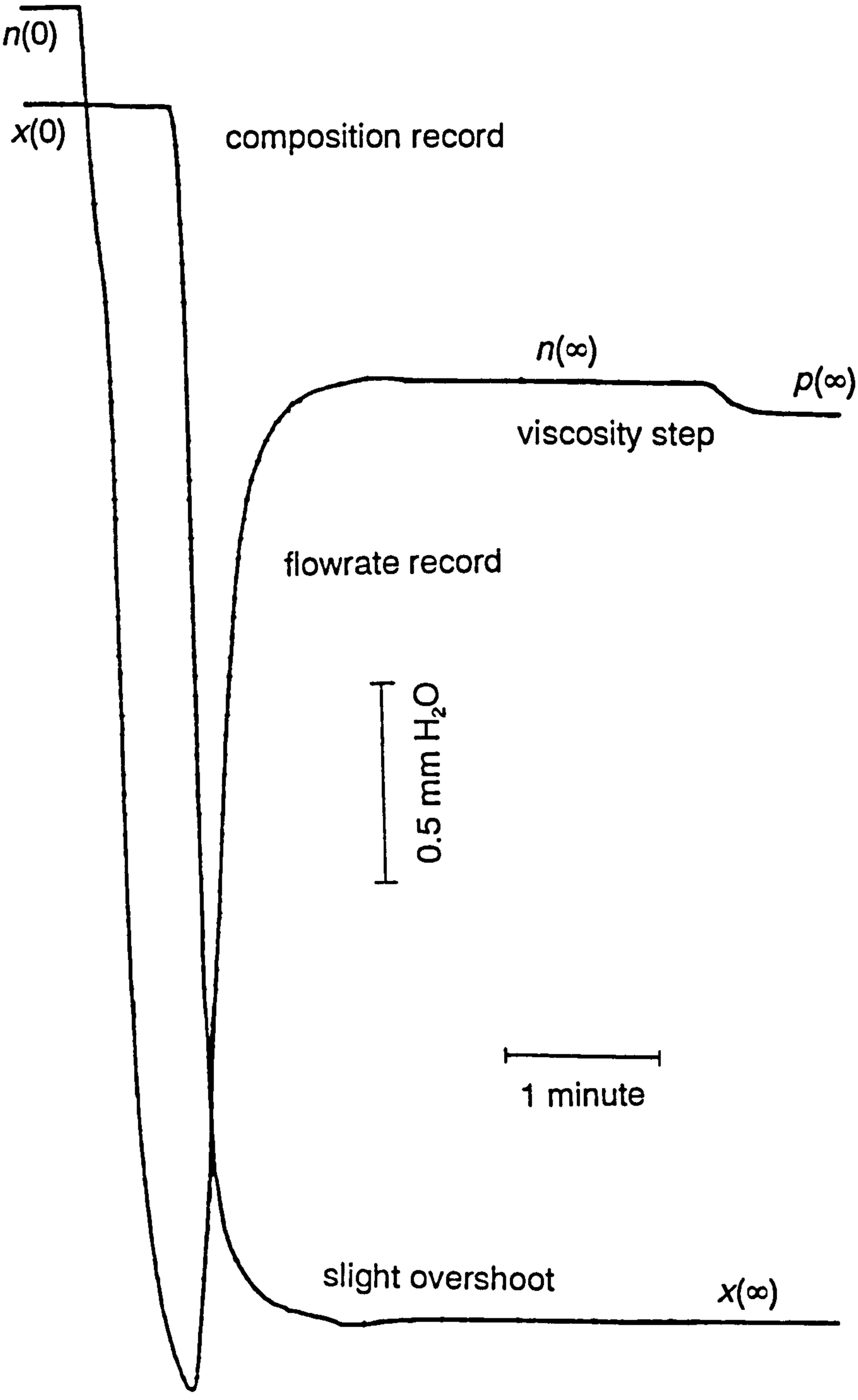

Figure G.5 Chromatograms Obtained for Adding a Helium Perturbation to an Argon Carrier at 25°C

Figure G.6 shows the chromatograms obtained for adding a helium perturbation to a 75% argon-helium carrier at 25°C. For the corresponding *perturbation removal* case, both chromatograms have the same shape as Figure G.5. From the composition record, τ_x = 84.6 seconds. From the flowrate record τ_N = -71.3 seconds (net desorption) and from the viscosity step $B(\mu) = 0.05$. From the flowrate record it can be seen that the plateau at $n(\infty)$ is clearly attained before the viscosity step movement to $p(\infty)$ (this is not observed for the helium-nitrogen system). This may explain why Equation 4.12 appears to give better predictions for the argon-helium system.

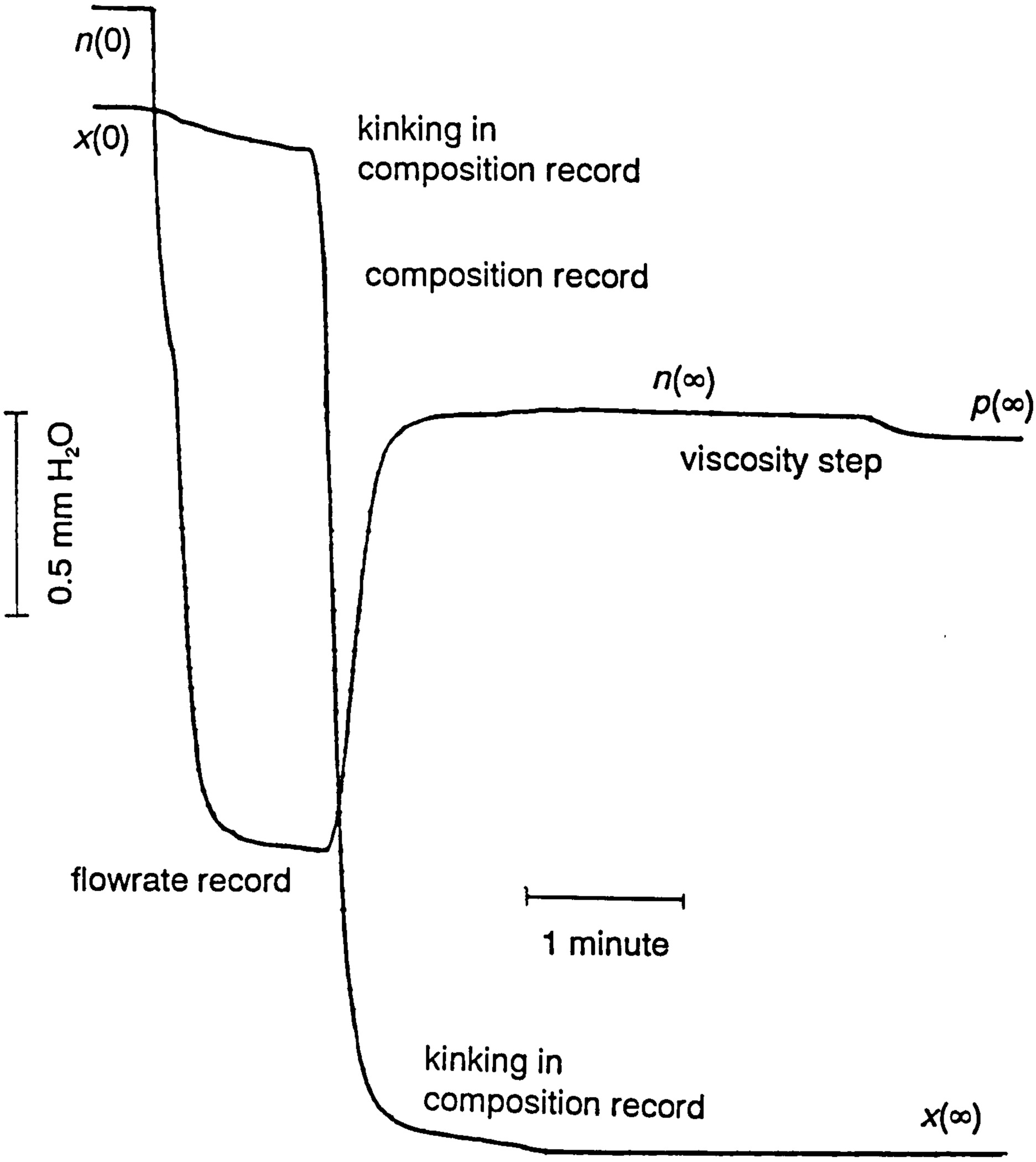

Figure G.6 Chromatograms Obtained for Adding a Helium Perturbation to a 75% argon-helium carrier at 25°C

Figure G.7 shows the chromatograms obtained for removing an argon perturbation from a nitrogen carrier at 25°C. It can be seen that there is a small constant deviation in the composition record while the front is moving through the column; this is not observed for the corresponding *perturbation addition* case. From the composition record, τ_X = 120 seconds. From the flowrate record τ_N = -139 seconds (net desorption) and from the viscosity step $B(\mu)$ = 0.3. From the flowrate record, it can be seen that the plateau at $n(\infty)$ is hardly attained before the viscosity step movement to $p(\infty)$. This may be the reason for the *apparent* poor predictions of Equation 4.12 for this case.

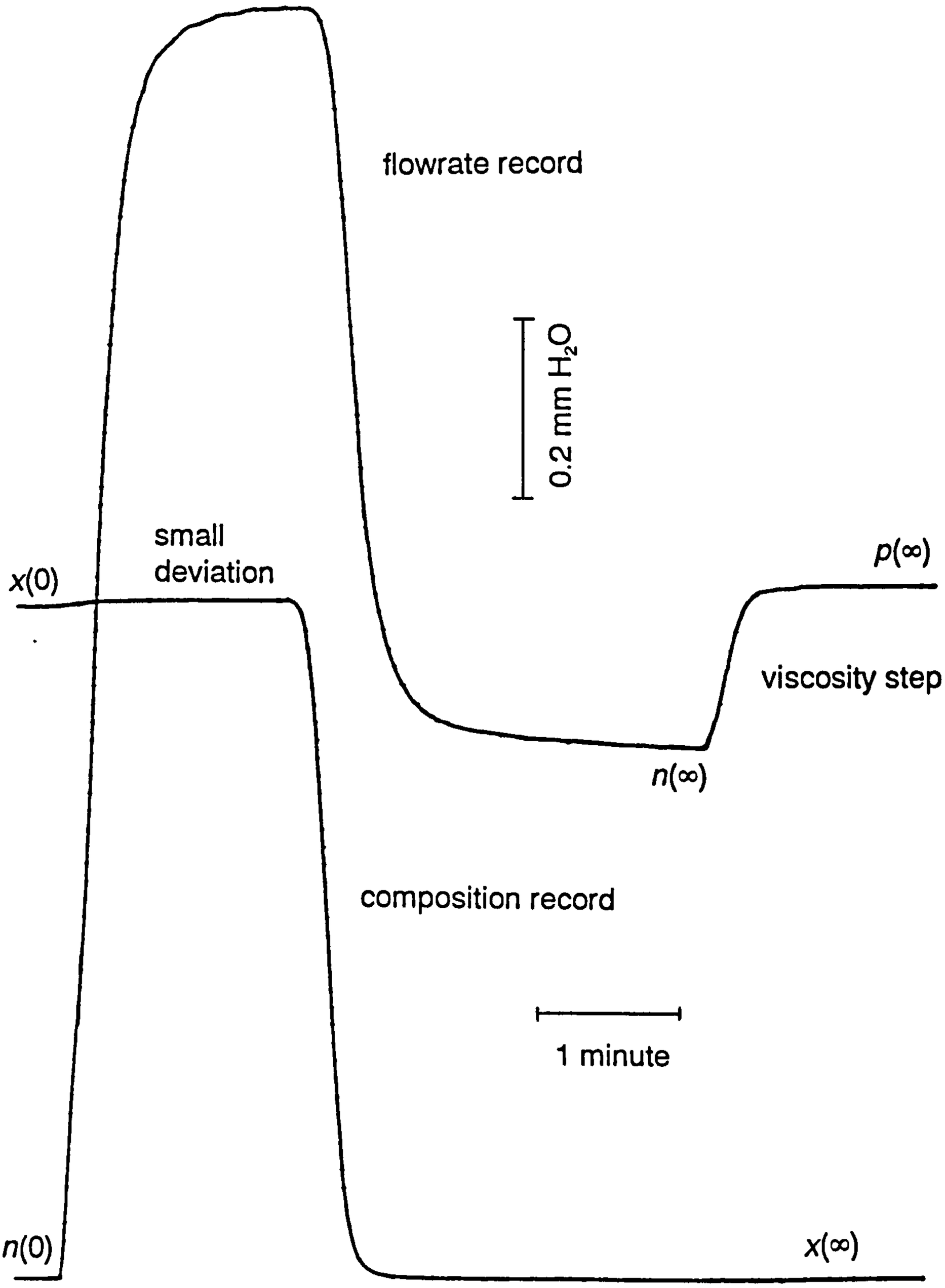

Figure G.7 Chromatograms Obtained for Removing an Argon Perturbation from a Nitrogen Carrier at 25°C

Figure G.8 shows the chromatograms obtained for removing an argon perturbation from a nitrogen carrier at 54°C. From the flowrate record, it can be seen that the thermal noise has been greatly reduced by the new oven arrangement. As for Figure G.7, it can be seen that there is a small constant deviation in the composition record while the front is moving through the column. From the composition record, τ_x = 96 seconds. From the flowrate record τ_N = -77 seconds and from the viscosity step $B(\mu)$ = 0.3. Compared to Figure G.7, it can be seen that the plateau at $n(\infty)$ is well defined before the viscosity step movement to $p(\infty)$. This may be the reason for the *apparent* satisfactory predictions of Equation 4.12 for this case.

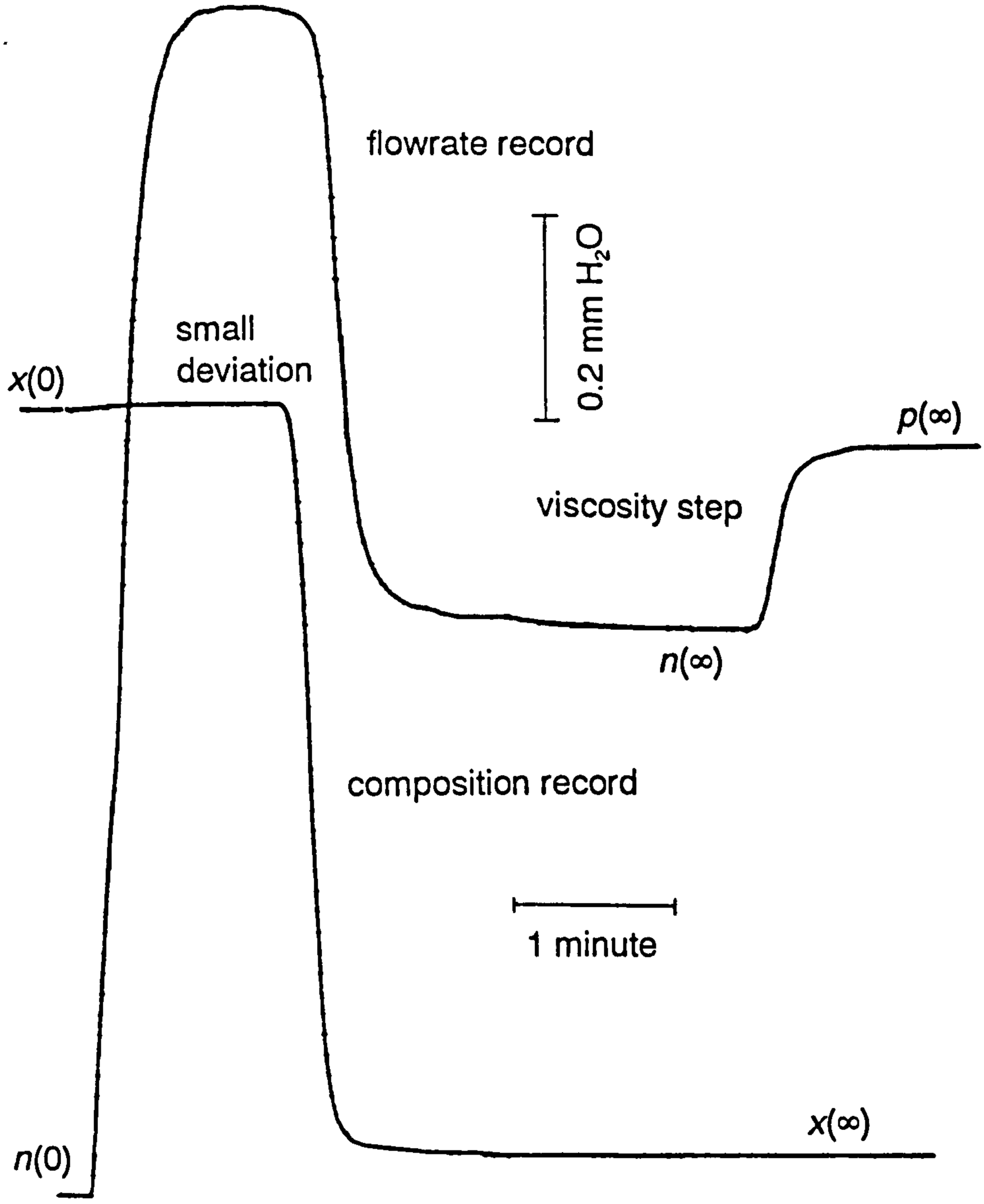

Figure G.8 Chromatograms Obtained for Removing an Argon Perturbation from a Nitrogen Carrier at 54°C .

Figure G.9 shows the chromatograms obtained for removing an argon perturbation from a nitrogen carrier at 81°C. As for Figures G.7 and G.8, it can be seen that there is a small constant deviation in the composition record while the front is moving through the column. From the composition record $\tau_x = 79$ seconds. From the flowrate record $\tau_N = -42.4$ seconds and from the viscosity step $B(\mu) = 0.3$. At the higher oven temperature, the thermal noise is seen to be slightly worse; this problem can be alleviated by using a water-filled pig.

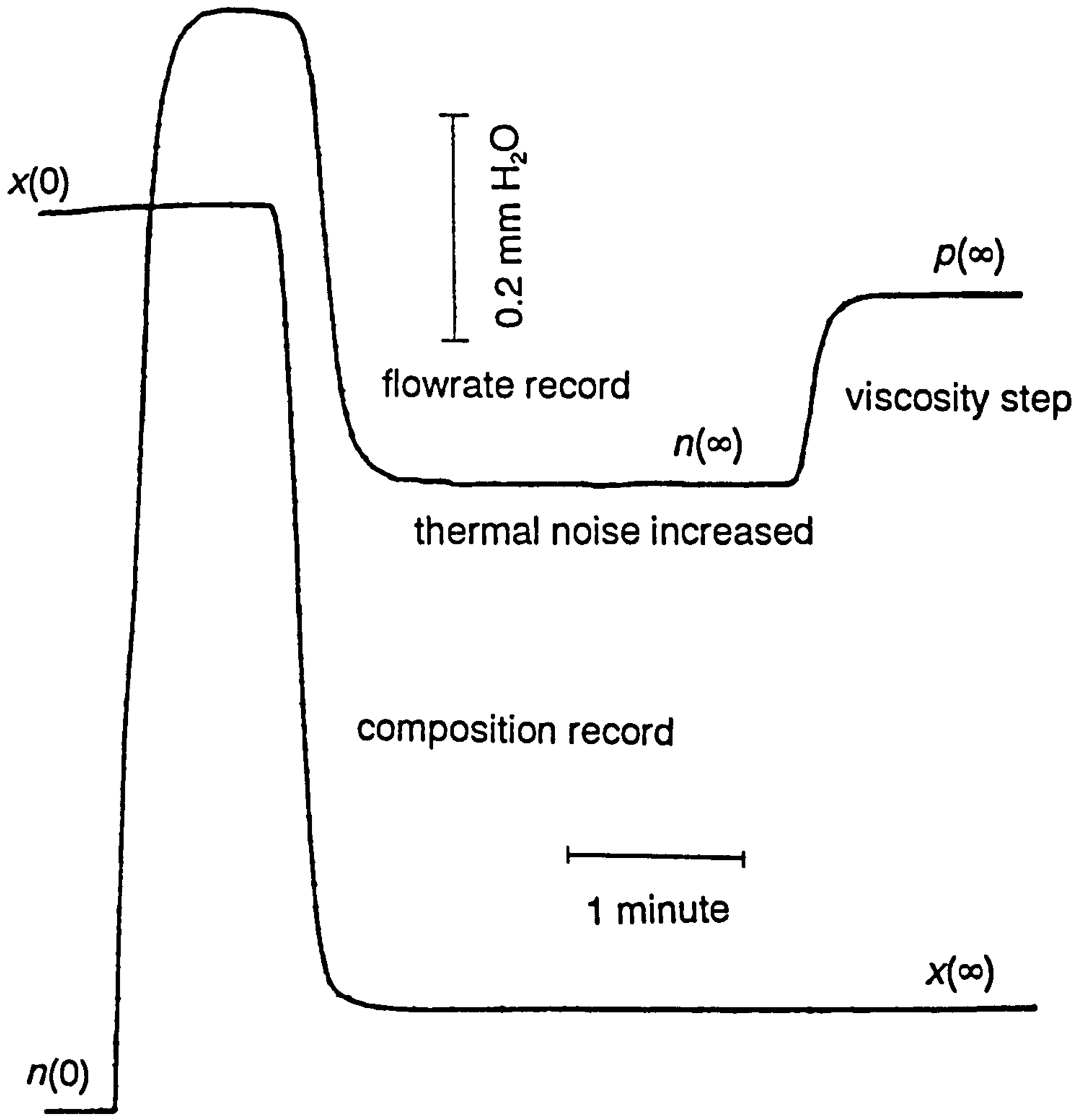

Figure G.9 Chromatograms Obtained for Removing an Argon Perturbation from a Nitrogen Carrier at 81°C

Figure G.10 shows the chromatograms obtained for adding a nitrogen perturbation to a 90% nitrogen-argon carrier at 25°C. For the corresponding *perturbation removal* case, both chromatograms are of the same shape to those of Figure G.10. From the composition record, $\tau_x = 141$ seconds. From the flowrate record $\tau_N = 25.1$ seconds and from the viscosity step $B(\mu) = 0.03$.

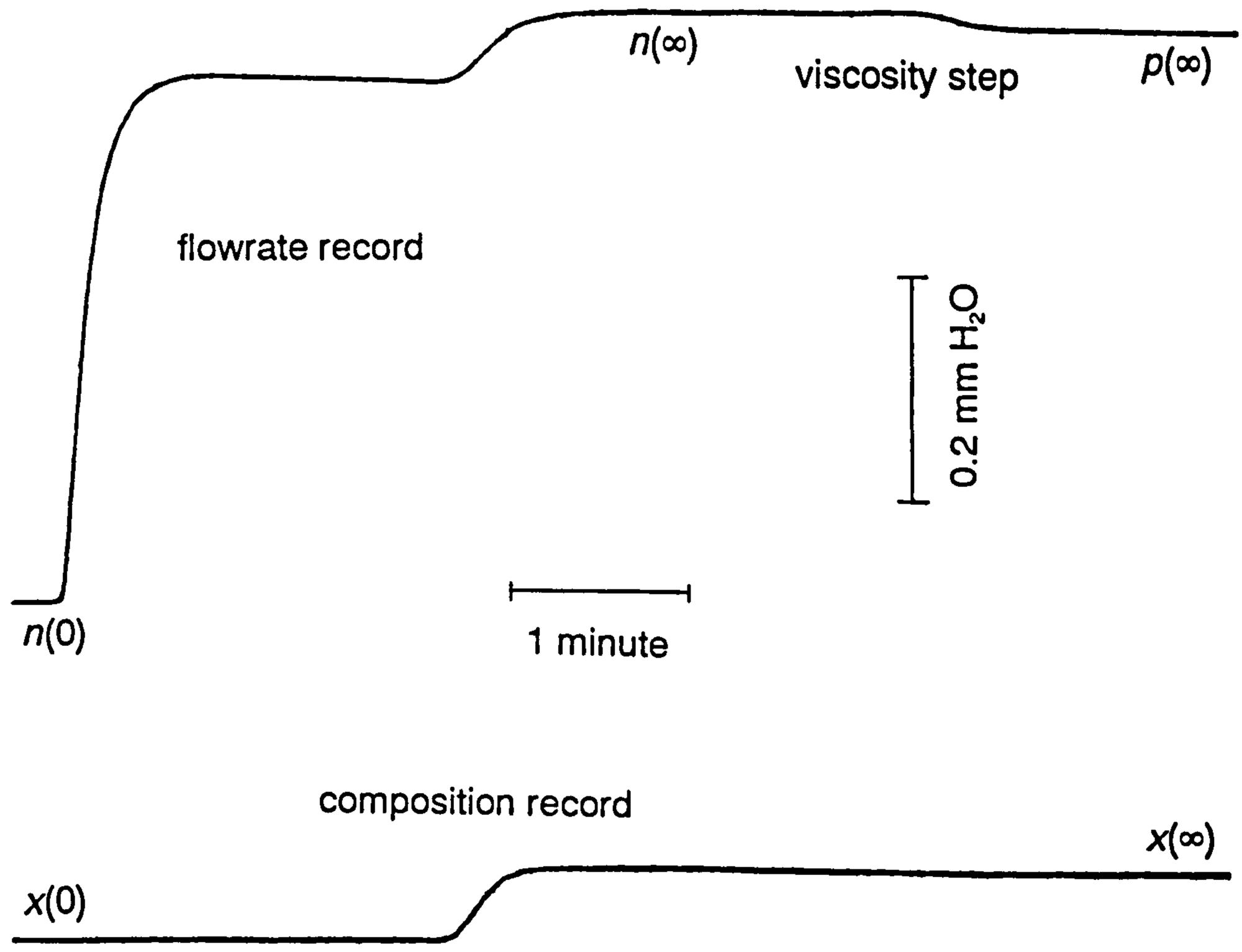

Figure G.10 Chromatograms Obtained for Adding a Nitrogen Perturbation to a 90% Nitrogen-Argon Carrier at 25°C

Figure G.11 shows the chromatograms obtained for adding an argon perturbation to a 25% nitrogen-argon carrier at 25°C. For the corresponding perturbation removal case, both chromatograms are of the same shape to those of Figure G.11. From the composition record, τ_x = 352 seconds. From the flowrate record τ_N = -52.2 seconds and from the viscosity step $B(\mu)$ = 0.06.

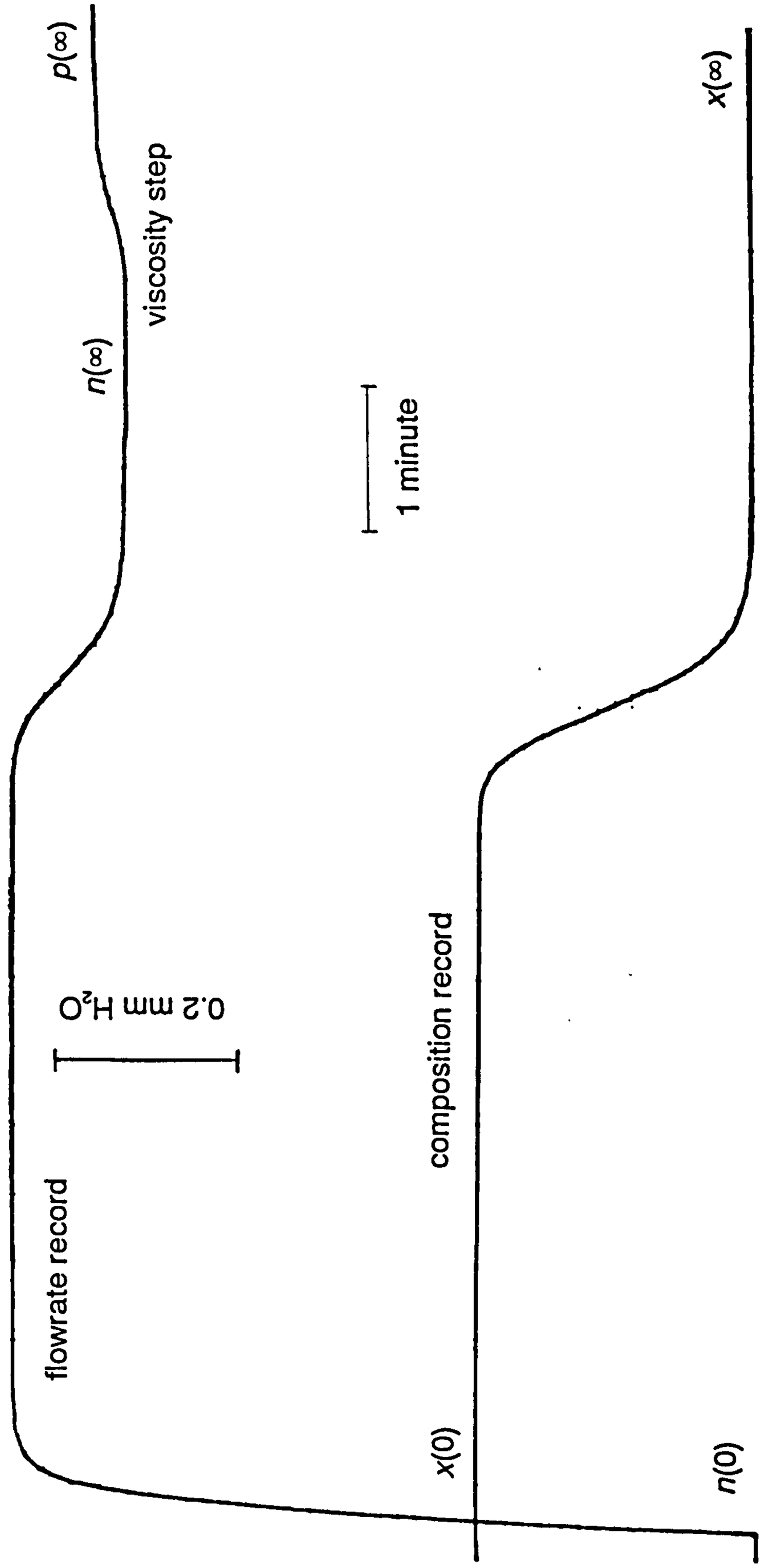

Figure G.11 Chromatograms Obtained for Adding an Argon Perturbation to a 25% nitrogen-argon mixture at 25 °C